Proceedings of the 11th International Probabilistic Workshop

6–8 November 2013
Brno, Czech Republic

Edited by

Drahomír Novák & Miroslav Vořechovský

Published by

Ing. Vladislav Pokorný – LITERA
Tábor 43a, 612 00 Brno, Czech Republic
e-mail: vopelkova@literabrno.cz

11th INTERNATIONAL PROBABILISTIC WORKSHOP (IPW11)

Editors: Drahomír Novák & Miroslav Vořechovský

Liability
The Workshop Organizer, which term includes the Organizing Committee or the Publisher, is not liable for personal accidents or loss/damage of private property during the Workshop. Delegates are encouraged to make their own arrangements for personal insurance.

Disclaimer
Whilst every attempt will be made to ensure that all aspects of the Workshop mentioned will be as scheduled, the Workshop Organizer reserves the right to make any changes should the need arise. The Workshop Organizer is not responsible for any personal expenses incurred or any loss suffered by any Workshop Delegates or his/her guests during or in connection with the event. All statements, opinions (whether of a technical nature or not), evidence, conclusions, exhibits, demonstrations, expressions, issues debated, which are said, made or expressed either orally or in writing and in any form or manner whatsoever including papers, paper prints, discussion material, articles, materials, notes, presentational slides, discussions or speeches are solely the views and opinions of the individual and not that of the Workshop Organizer or the Publisher. The Workshop Organizer will not be responsible whatsoever for the accuracy, correctness or representations of any statements or documents presented or discussed in this Workshop.

ISBN 978-80-214-4800-1

Preface

These proceedings contain papers presented at the 11th International Probabilistic Workshop (IPW11). The workshop is hosted by the Faculty of Civil Engineering at Brno University of Technology, Czech Republic, and is organized by the Institute of Structural Mechanics.

Safety, reliability and risk are key issues in a world of increasingly complex engineering facilities and infrastructure. The existence of natural hazards calls for the consideration of safety and risk in both the design and the assessment stages. IPW11 is focusing on providing solutions for practical applications and dealing with the practical challenges involved in incorporating structural safety and reliability in engineering practice. While there is an underlying theoretical framework in the areas of structural safety and reliability, translation from theory to practice in engineering is still urgently needed. The workshop combines computer science, mathematics, and engineering analysis and design, providing a common forum to facilitate the continuation of the cross-disciplinary exchange of ideas in the field. The stochastic computer analysis of concrete structures has become an important method to investigate the behavior, resistance, and reliability of concrete and reinforced concrete structures in long-term and life-cycle contexts, including deterioration aspects. The main topic of IPW11 is the reliability and risk assessment of concrete structures (mainly bridges and tunnels). One of the intentions is to show recent progress and achievements in the development of advanced simulation methods for the modeling of concrete structures, and in the evolution of software tools and their practical applications.

The first of the IPW series of probabilistic workshops on safety and risk in civil engineering were organized in Dresden in 2003 and 2004. These were followed by workshops held in Vienna (2005), Berlin (2006), Ghent (2007), Darmstadt (2008), Delft (2009), Szczecin (2010), Braunschweig (2011) and Stuttgart (2012).

The editors and the whole team of organizers have the honor of dedicating IPW11 to Prof. Břetislav Teplý on the occasion of his 80th birthday. We – his former students and present co-workers – are very grateful for the many years we have benefited from his supervision, stimulating discussion and cooperation in the area of structural safety and reliability. He began promoting this field in the Czech Republic a long time ago when it was regarded as being quite a new and pioneering avenue of research. Happy birthday Bret, and keep your energy up for your next research!

Finally, we wish all participants a successful conference in Brno!

This workshop is supported by:

- The South Moravian Region
- Dynardo GmbH
- Cervenka Consulting Ltd.

The organizers appreciate the support of these organizations.

Drahomír Novák and Miroslav Vořechovský
Chairmen of IPW11

Organization Committee

Organized by

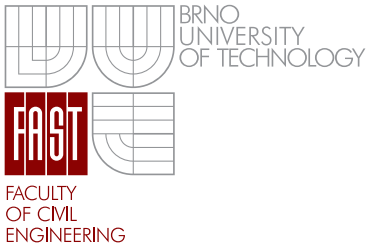

Chair

Drahomír Novák, *Brno University of Technology (BUT), Faculty of Civil Engineering (FCE), Institute of Structural Mechanics, Brno Czech Republic*

Miroslav Vořechovský, *Institute of Structural Mechanics FCE BUT Brno, Czech Republic*

General Chair

Dirk Proske, *University of Natural Resources and Life Sciences (BOKU), Vienna, Austria*

Local Organizing Committee

David Lehký, *Institute of Structural Mechanics FCE BUT Brno*

Václav Sadílek, *Institute of Structural Mechanics FCE BUT Brno*

Stanislav Seitl, *Institute of Physics of Materials, Academy of Sciences of the Czech Republic, v. v. i., Brno, Czech Republic*

Václav Veselý, *Institute of Structural Mechanics FCE BUT Brno*

IPW11 Secretariat

David Lehký, *Institute of Structural Mechanics FCE BUT Brno*

Stanislav Seitl, *Institute of Physics of Materials, Academy of Sciences of the Czech Republic, v. v. i., Brno, Czech Republic*

Technical Support Team

Dana Halíková, *Institute of Structural Mechanics FCE BUT Brno*

Martina Kolaciová, *Institute of Structural Mechanics FCE BUT Brno*

International Scientific Committee

Ivan S.K. Au, *Zürich, Switzerland*
Michael Beer, *Liverpool, United Kingdom*
Konrad Bergmeister, *Vienna, Austria*
Zdeněk Bittnar, *Prague, Czech Republic*
Christian Bucher, *Vienna, Austria*
Josep R. Casas, *Barcelona, Spain*
Marcello Ciampoli, *Roma, Italy*
Bruce R. Ellingwood, *Atlanta, USA*
Dan M. Frangopol, *Lehigh, USA*
Hitoshi Furuta, *Osaka, Japan*
Milan Holický, *Prague, Czech Republic*
Giuseppe Mancini, *Torino, Italy*
Drahomír Novák, *Brno, Czech Republic*
Dirk Proske, *Vienna, Austria*
Radomír Pukl, *Prague, Czech Republic*
Jiří Šejnoha, *Prague, Czech Republic*
Daniel Straub, *Munich, Germany*
Alfred Strauss, *Vienna, Austria*
Mark Stewart, *Newcastle, Australia*
Bruno Sudret, *Zürich, Switzerland*
Luc Taerwe, *Gent, Belgium*
Břetislav Teplý, *Brno, Czech Republic*
Erik Vanmarcke, *Princeton, USA*
Miroslav Vořechovský, *Brno, Czech Rep.*
Hao Zhang, *Sydney, Australia*

Contents

Reliability of damaged structures

Dan M. Frangopol, Duygu Saydam
Department of Civil and Environmental Engineering, Engineering Research Center for Advanced Technology for Large Structural Systems (ATLSS Center),
Lehigh University, Bethlehem, PA 18015-4729, USA
dan.frangopol@lehigh.edu, dus207@lehigh.edu

Abstract: Safety evaluation of damaged structures is crucial for informed-decision making after sudden local damage. Prediction of structural performance involves uncertainties due to the randomness in the loads, material properties, the deterioration processes, and the imperfections in our engineering models. This paper presents a general probabilistic methodology to evaluate performance of damaged structures. A scenario-based approach to evaluate the residual performance of structures suffering sudden local damage is implemented with emphasis on bridges and ships. Time effects due to deterioration are accounted for. The methodology uses finite element method, Latin Hypercube Sampling, and first-order reliability method. Computational procedures for residual capacity and reliability evaluation of damaged bridges and ships are provided. Several performance indicators for damaged bridges and ships are qualitatively illustrated.

Keywords: probabilistic performance assessment, uncertainties, structural damage, bridges, ships.

1 Introduction

Structural systems are subjected to deterioration in strength and performance due to the mechanical and environmental stressors (e.g. corrosion, fatigue). The reliability of these systems is highly affected by their deteriorations. The resistance of a structure to an extreme event reduces in time due to the deterioration process. The tolerance to sudden local damage should be considered together with the effect of progressive deterioration in the lifetime management of structures and infrastructures. Several researchers focused on the field of damage tolerant structures and they referred damage tolerance with various related measures. These measures include collapse resistance [7], vulnerability and damage tolerance [18], robustness [3],[5],[12],[19], and redundancy [8],[10],[11].

The evaluation of performance of damaged structural systems is an important research field not only for civil infrastructure but also marine infrastructure. WANG ET AL. [25] pro-

posed an analytical expression for assessing the residual strength of hull girders with damage and provided simple equations correlating residual strength with damage extent. HUSSEIN AND GUEDES SOARES [15] studied the residual strength and reliability of double hull tankers for different damage scenarios. SAYDAM AND FRANGOPOL [24] provided a probabilistic framework for performance assessment of ship hulls under sudden damage accounting for different operational conditions. The information on the residual strength of a damaged hull structure can be very helpful for making decisions on how to proceed with the damaged ships after accidents. The decision making process could be enhanced greatly when the information regarding the reliability of damaged ship hulls after grounding and collision is available. It is necessary to establish methods for reliability assessment of damaged ships for different operational conditions. For instance, the reliability information for different ship speeds, heading angles and sea states could provide guidance to avoid the ultimate failure of the damaged hull structures. In addition, the aging effects should be integrated in this approach.

The aim of this paper is to present a general probabilistic methodology to evaluate the performance of damaged structures. Time effects due to deterioration are accounted for. A scenario-based approach to evaluate the residual performance of structures suffering sudden local damage is implemented with emphasis on bridges and ships. The methodology uses finite element (FE) method, Latin Hypercube Sampling, and first-order reliability method. Computational procedures for residual capacity and reliability evaluation of damaged bridges and ships are provided. Definitions of several performance indicators for damaged structures are presented. These indicators are qualitatively illustrated for bridges and ships.

2 General methodology

The methodology for assessing the performance of damaged structures considering aging effects is illustrated in Fig. 1. The first step of the methodology is identifying the failure mode to investigate. The next steps can be basically categorized in two parts. These are the computations for the resistance and the load effects. The random variables associated with the resistance must be identified. The load capacity of the structure associated with the failure mode under consideration should be computed accounting for uncertainties. For bridges, the variation of the live load over time is required in order to perform time-dependent reliability analysis. A live load model based on the variation of the number of trucks passing the bridge over time and interpretation of this data by using extreme value statistics can be used. For ships, one component of the load effects is due to the still water. Still water load effects can be evaluated based on expressions given in codes or hydrostatic analysis. Another component of the load effects is due to waves. Wave-induced load effects depend on the operational conditions (e.g., ship speed, heading, sea state). In order to compute the loads for different operational conditions, hydrodynamic analyses of the ship should be performed. The limit state equation including the resistance and the load effects can be established at this stage. First order reliability method (FORM) or second order reliability method (SORM) can be used to obtain the instantaneous probability of failure and/or reliability index associated with a sudden damage scenario (and an operational condition for ships). In order to obtain the variation of the reliability in time the procedure

should be repeated at different time steps with time-variant values of resistance and load effects. For ships, the procedure should be repeated for different operational conditions to obtain the reliability index with respect to speed, heading and sea state.

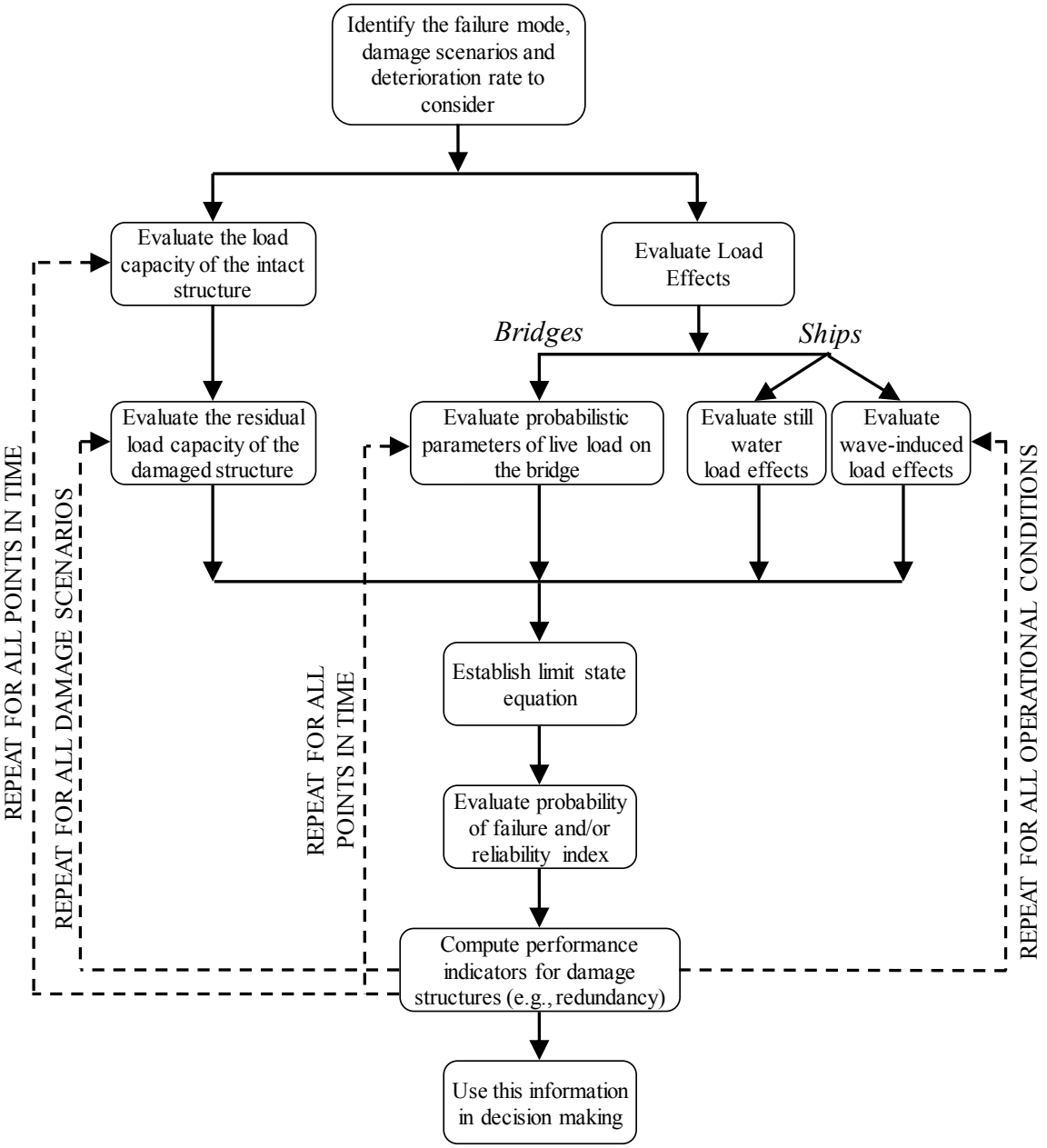

Fig. 1: The general methodology for performance assessment of damaged structures

3 Probabilistic evaluation of structural performance

3.1 Probabilistic evaluation of bridge performance

The bridge system reliability can be evaluated based on appropriate assumptions regarding the interaction of individual components, such as series, parallel and combined system as-

sumptions [6],[13]. In this method, the reliability of a bridge structural system is evaluated by considering the system failure as series-parallel combination of the component failures. First, the random variables and their statistical parameters for component reliability analysis should be determined. The limit states for different possible failure modes of the components can be included in the system model. The derivation of a limit state equation for a bridge girder varies considerably de-pending on whether the girder is simply supported or continuous [2]. Flexural or shear capacity for girders and the slab can be calculated using the formulas given in AASHTO LRFD Bridge Design Specification [1]. One major assumption in this model is that the system failure is considered to occur when either slab fails or any two adjacent girders fail.

Another approach for reliability assessment of bridges makes use of FE method. An appropriate statistical distribution for the desired output of FE analysis (e.g., stress, displacement, bending moment) can be obtained by repeating the analysis for a large number of samples of the random variables associated with the structure. However, for complex structures, the time required to repeat FE analysis many times may be too large. In such cases, Response Surface Method can be used to approximate the relation between the desired output of FE analysis and random variables by performing analyses for only a significantly less number of samples.

Load carrying capacity of a bridge superstructure can be expressed in terms of a load factor, *LF*, when the structure reaches its ultimate capacity or very large vertical displacements causing low levels of safety. Load factor, *LF*, indicates the ratio of the maximum load carried by the bridge to the total weight of AASHTO HS-20 vehicle, when the applied load has the pattern of HS-20 vehicle loading. The failure of the bridge superstructure can be defined by the inequality

$$g = LF - LL < 0 \tag{1}$$

with

LL	the live load effect in terms of the multiples of the AASHTO HS-20 vehicle weight,
g	the performance function.

The material and geometric nonlinearities can be included in the FE model for better accuracy in idealizing the reality. The details of such a procedure can be found in [12],[23].

3.2 Probabilistic evaluation of ship performance

The maximum value of the vertical bending moment is the most important load effect in the analysis and design of ship structures [14]. The ultimate flexural capacity of the hull can be evaluated based on FE analysis, incremental curvature method [16] and progressive collapse method [14]. OKASHA AND FRANGOPOL [21] proposed an efficient deterministic method for computation of the ship hull strength based on optimization. The ship hull cross-section is discretized into elements, each composed of a longitudinal stiffener and its attached plate. Stresses in the hull section are determined using the constitutive models of these elements. The constitutive models take into account the various possible failure modes of stiffened panels. Initial imperfections are also taken into account. For a given curvature, the bending moment of the section is determined in a way similar to that of the

incremental curvature method. However, instead of finding the ultimate strength by incrementing the curvature, the ultimate strength is found by an optimization search algorithm. The curvature is treated as a design variable and the objective is to find the curvature that maximizes the bending moment. In order to find the moment capacity of the hull in a probabilistic manner, the sample space associated with the random variables should be created using a sampling method. Latin Hypercube Sampling is a technique allowing the reduction of the number of necessary samples to reach a certain level of confidence [20]. By combining these two steps, a probability distribution for the maximum moment capacity of the ship hull section can be obtained.

Reliability assessment of ships under different operational conditions requires probabilistic characterization of the loads. The hull is subjected to still water bending moment and wave-induced bending moment. The minimum still water ending moment to be considered in sagging and hogging for seagoing operations can be computed according to IACS common rules [16], in terms of the ship block coefficient, the ship length, the ship breadth, and a wave coefficient. The internal forces within a hull structure due to sea waves can be evaluated based on linear response theory. In this theory, the wave spectrum for a wide range of wave configurations can be obtained through the linear superposition of single waves. Wave-induced vertical bending moments vary for different ship operation conditions. The operational conditions are represented by a set of parameters including ship speed, heading, and sea state. The response of ship structures due to natural sea waves depends on hydrodynamics. In general, hydrodynamic analysis is highly complex and time consuming. Hydrodynamic analysis of ship structures can be performed using strip method [17]. Strip method introduces some simplifications such that the ship hull is divided into prismatic segments. The interaction between the adjacent segments is ignored and the hydrodynamic forces due to harmonic waves are evaluated within the individual segments. The hydrodynamic forces within the segments are integrated to obtain the global load effects. The time-variant limit state equation associated with the flexural failure of amidship for different operational conditions in sagging and hogging, respectively, is expressed as

$$g_{SS,U,H}(t) = x_R \cdot MC(t) - x_{sw} \cdot M_{sw} - x_w \cdot M_{w,SS,U,H} = 0 \tag{2}$$

with

$MC(t)$	time-variant vertical bending moment capacity of the mid-section of the ship in sagging or hogging,
M_{sw}	still water bending moments amidship in sagging or hogging,
$M_{w,SS,U,H}$	wave-induced bending moment amidship reflecting the effects of different operational conditions,
x_R, x_{sw}, x_w	the random model uncertainties associated with the resistance, still water bending moment, and wave-induced bending moment, respectively.

4 Performance indicators for damaged structures

4.1 Redundancy

A measure of redundancy, in the context of availability of warning before system failure, was proposed by FRANGOPOL AND CURLEY [8] as

$$RI_1 = \frac{P_{f(dmg)} - P_{f(sys)}}{P_{f(sys)}} \tag{3}$$

with

$P_{f(dmg)}$ probability of damage occurrence to the system,
$P_{f(sys)}$ probability of system failure.

A measure of redundancy, as the availability of alternative load path after sudden local damage, was proposed by FRANGOPOL & CURLEY [8] as

$$RI_2 = \frac{\beta_{\text{intact}}}{\beta_{\text{intact}} - \beta_{\text{damaged}}} \tag{4}$$

with

β_{intact} reliability index of the intact system,
$\beta_{damaged}$ reliability index of the damaged system.

Redundancy is a system performance measure. The load modifiers that accounts for bridge system redundancy in AASHTO LRFD BRIDGE DESIGN SPECIFICATIONS [1] are based on the redundancy definition in FRANGOPOL AND NAKIB [9]. Application of redundancy concept to deteriorating bridge structures can be found in OKASHA AND FRANGOPOL [22], GHOSN ET AL. [12], and SAYDAM AND FRANGOPOL [23]. In Fig. 2, the effect of a sudden damage is illustrated on the lifetime reliability index profile qualitatively.

4.2 Vulnerability

A probabilistic measure of vulnerability was proposed by LIND [18], defined as the ratio of the failure probability of the damaged system to the failure probability of the undamaged system

$$V = \frac{P(r_d, Q)}{P(r_0, Q)} \tag{5}$$

with

r_d, r_0 particular damaged state and pristine system state, respectively,
Q prospective loading,
$P(r_d, Q)$ probability of failure of the system in the damaged state,
$P(r_0, Q)$ probability of failure of the system in the pristine state,
V vulnerability of the system in state r_d for prospective loading Q.

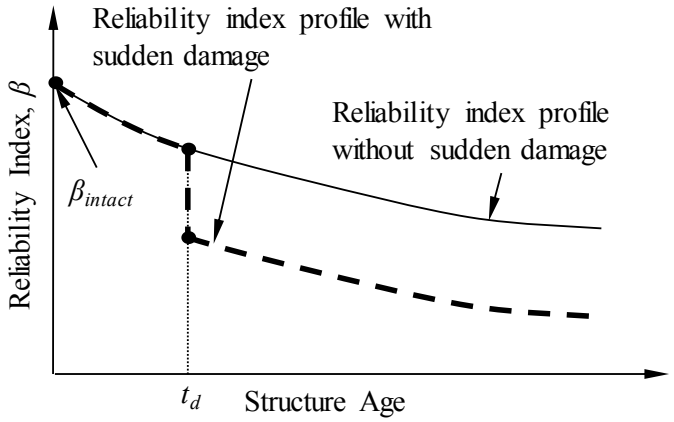

Fig. 2: Qualitative lifetime reliability profile

4.3 Risk

A common formulation of risk in engineering involves the multiplication of probability of occurrence of an event by the consequences of this event. Direct risk is associated with the damage occurrence itself while indirect risk is associated with the system failure as a result of the damage. Direct and indirect risks can be formulated as [3]

$$R_{Dir} = \int_x \int_y C_{Dir} f_{D|E}(y \mid x) f_E(x) \mathrm{d}y \mathrm{d}x \tag{6}$$

$$R_{Indir} = \int_x \int_y C_{Indir} P(F \mid D = y) f_{D|E}(y \mid x) f_E(x) \mathrm{d}y \mathrm{d}x \tag{7}$$

with

C_{Dir} and C_{Indir}	direct and indirect consequences, respectively,
x and y	random variables in the event tree, respectively,
$f_X(x)$ and $f_Y(y)$	probability density functions of random variables x and y, respectively,
E, D and F	hazard occurrence, damage occurrence, and system failure, respectively.

4.4 Robustness

A reliability-based measure of robustness associated with a certain damage scenario is formulated as [24]

$$ROI_1 = \frac{\beta_i}{\beta_0} \tag{8}$$

with

β_i	reliability index associated with the damaged hull for scenario i,
β_0	reliability indices associated with the intact hull.

The reliability and robustness indices for a ship considering different operational conditions are illustrated qualitatively in polar plots in Fig. 3(a) and (b), respectively.

BAKER ET AL. [3] stated that a robust system the one where the indirect risks do not contribute significantly to the total system risk, and proposed a robustness index defined as follows:

$$ROI_2 = \frac{R_{Dir}}{R_{Dir} + R_{Indir}} \tag{9}$$

with

R_{Dir} direct risk,
R_{Indir} indirect risk.

This index varies between 0 and 1.0 with larger values representing a larger robustness. Robustness is a system performance indicator. Additional robustness indicators and applications to bridge structures are indicated in GHOSN ET AL. [12], BIONDINI AND FRANGOPOL [4], and SAYDAM AND FRANGOPOL [23].

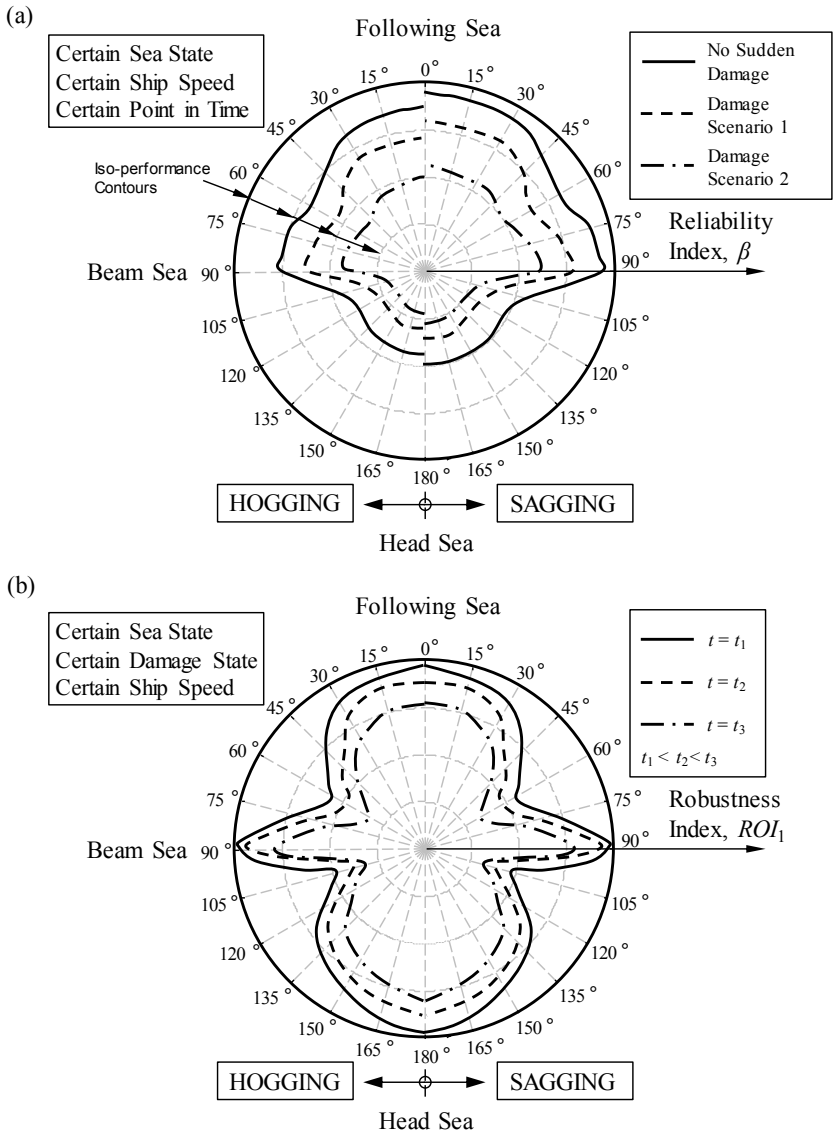

Fig. 3: Qualitative polar representation of ship performance for: (a) reliability index, and (b) robustness index

5 Conclusions

In this paper, a probabilistic methodology to evaluate performance of damaged structures considering time effects is presented. Emphasis is given on bridges and ships. The residual performance of structures suffering sudden local damage is evaluated based on damage scenarios. The methodology uses FE method, Latin Hypercube Sampling, and first-order reliability method depending on the application type. Computational procedures for residual capacity and reliability evaluation of damaged bridges and ships are provided. Several performance indicators for damaged structures are presented and illustrated qualitatively for lifetime of bridges and ships.

The presented framework can be used in optimization of the design and maintenance of structural systems. Further research on this topic should include a methodology for combining the effects of different scenarios in a risk-based approach.

Acknowledgements

The support from (a) the National Science Foundation through grant CMS-0639428, (b) the Commonwealth of Pennsylvania, Department of Community and Economic Development, through the Pennsylvania Infrastructure Technology Alliance (PITA), (c) the U.S. Federal Highway Administration Cooperative Agreement Award DTFH61-07-H-00040, and (d) the U.S. Office of Naval Research through contracts N 00014-08-1-0188 and N 00014-12-1-0023 is gratefully acknowledged. The opinions and conclusions presented in this paper are those of the authors and do not necessarily reflect the views of the sponsoring organizations.

Literature

[1] AASHTO. LRFD Bridge Design Specifications, AASHTO 5th Ed., American Association of State Highway and Transportation Officials, Washington, D.C., 2010

[2] Akgül, F., Frangopol, D. M. Computational Platform for Predicting Lifetime System Reliability Profiles for Different Structure Types in a Network. *Journal of Computing in Civil Engineering* 18(2) (2004), p. 92−104

[3] Baker, J. W., Schubert, M., Faber, M. H. On the Assessment of Robustness. *Structural Safety* 30 (2008), p. 253−267

[4] Biondini, F., Frangopol, D. M. Structural Robustness and Redundancy of Deteriorating Concrete Bridges. *Bridge Maintenance, Safety, Management, Health Monitoring and Optimization*, D.M. Frangopol, R. Sause, and C.S. Kusko, eds., CRC Press/Balkema, Taylor & Francis Group plc, London, full paper on CD-ROM, Taylor & Francis Group plc, London, 2010, p. 2473−2480

[5] Blockley, D. I., Agarwal, J., Pinto, J. T., Woodman, N. J. Structural Vulnerability, Reliability and Risk. *Progress in Structural Engineering and Materials* 4(2) (2002), p. 203−212

[6] Ditlevsen, O., Bjerager, P. Methods of Structural Systems Reliability. *Structural Safety* 3(3−4) (1986), p. 195−229

[7] Ellingwood, B. R., Dusenberry, O. D. Building Design for Abnormal Loads and Progressive Collapse. *Computer-Aided Civil and Infrastructure Engineering* 20 (2005), p. 194−205

[8] Frangopol, D. M., Curley, J. P. Effects of Damage and Redundancy on Structural Reliability. *Journal of Structural Engineering* 113(7) (1987), p. 1533−1549

[9] Frangopol, D. M., Nakib, R. Redundancy in Highway Bridges. *Engineering Journal* 28(1) (1991), p. 45−50

[10] Frangopol, D. M., Klisinski, M., Iizuka M. Optimization of Damage-Tolerant Structural Systems. *Computers and Structures* 40(5) (1991), p. 1085−1095

[11] Fu, G., Frangopol D.M. Balancing Weight, System Reliability and Redundancy in a Multi-Objective Optimization Framework. *Structural Safety* 7(2–4) (1990), p. 165–175

[12] Ghosn, M., Moses, F., Frangopol, D. M. Redundancy and Robustness of Highway Bridge Superstructures and Substructures. *Structure and Infrastructure Engineering* 6(1−2) (2010), p. 257−278

[13] Hendawi. S., Frangopol, D. M. System Reliability and Redundancy in Structural Design and Evaluation. *Structural Safety* 16 (1−2) (1994), p. 47−71

[14] Hughes, O. F. *Ship Structural Design: A Rationally-Based, Computer-Aided, Optimization Approach*. Wiley and Sons, New York, 1983

[15] Hussein, A. W., Guedes Soares, C. Reliability and Residual Strength of Double Hull Tankers Designed According to the new IACS Common Structural Rules. *Ocean Engineering* 36(17−18) (2009), p. 1446−1459

[16] IACS. Common Structural Rules for Double Hull Oil Tankers. International Association of Classification Societies, London, U.K., 2008, website: http://www.iacs.org.uk

[17] Korvin-Kroukowski, B. V., Jacobs, W. R. Pitching and Heaving Motions of a Ship in Regular Waves. *Transactions* 65 (1957), p. 590−632

[18] Lind, N. C. A Measure of Vulnerability and Damage Tolerance, *Reliability Engineering and System Safety*, 43(1) (1995), p. 1−6

[19] Maes, M. A. Fritzson, K. E., Glowienka, S. Structural Robustness in the Light of Risk and Consequence Analysis. *Structural Engineering International* 16(2) (2006), p. 101−107

[20] McKay, M. D., Beckman, R. J., Conover, W. J. A Comparison of Three Methods for Selecting Values of Input Variables in the Analysis of Output from a Computer Code. *Technometrics* 21(2) (1979), p. 239−245

[21] Okasha, N. M., Frangopol, D. M. Efficient Method Based on Optimization and Simulation for the Probabilistic Strength Computation of the Ship Hull. *Journal of Ship Research* 54(4) (2010), p. 1−13

[22] Okasha, N. M., Frangopol, D. M. Lifetime-Oriented Multi-Objective Optimization of Structural Maintenance Considering System Reliability, Redundancy and Life-Cycle Cost Using GA. *Structural Safety* 31(6) (2009), p. 460−474

[23] Saydam, D., Frangopol, D.M. Time-dependent Performance Indicators of Damaged Bridge Superstructures. *Engineering Structures* 33(9) (2009), p. 2458−2471

[24] Saydam, D., Frangopol, D.M. Performance Assessment of Damaged Ship Hulls. *Ocean Engineering* 68 (2013), p. 65−76

[25] Wang, G., Spencer, J., Chen, Y.J. Assessment of Ship's Performance in Accidents. *Marine Structures* 15 (2002), p. 313–333

Are antifragile structures reliable?

Konrad Bergmeister, Hirud Grossberger, Alfred Strauss
University of Natural Resources and Applied Life Sciences, Vienna
konrad.bergmeister@bbt-se.com, hirud.grossberger@ac.at, alfred.strauss@boku.ac.at

Abstract: Fragility and Antifragility are terms recently discussed in economical science. A novel approach is discussed for the application in the technical science. The scope is to reduce fragility of technical systems and structures. In the past, some practical measure of redundancy and robustness has been proposed and robustness or performance indexes have been defined. The different level evaluating an existing bridge system is discussed and the response in form of the load-deflection curve diagram has been evaluated with the various procedures.

Keywords: Antifragility, robustness, performance index

1 What is antifragility

NASSIM NICHOLAS TALEB (2012), the New York times bestselling author of the „Black Swan“ stated, that „antifragility is beyond resilience or robustness“. „A resilient system resists shocks and unforeseen events. This specific property is behind everything that has changed with time, with evolution, with culture, technological innovation, political systems.“

The scope in the technical science must be to strengthen the system in order to move from the fragile toward the antifragile, through reduction of fragility.

„Fragility can be measured“ says Taleb; I am trying to develop a concept for evaluation the „System-Antifragility“. System-Antifragility should be a system evaluation process based on the capability to resist unforeseen events.

Before developing the concept for System-Antifragility, a summary is given about the various parameters and concepts carried out in order to describe the robustness.

2 Robustness and performance indicators

Robustness can be considered as the capability of performing without failure under unexpected conditions. Practical measure of redundancy and robustness which was proposed by FRANGOPOL ET AL. (1987) is defined as the Robustness Index:

$$RI = \frac{P_{f\ damaged} - P_{f\ intact}}{P_{f\ intact}} \tag{1}$$

Where $P_{f,dam}$ damaged is the probability of failure of a damaged structure and $P_{f,int}$ intact is the probability of failure of the intact structure. Obviously, the *RI* would be equal to 0 for a robust structure and may approach infinity for a non-robust structure (TAFERNER ET AL. 2009).

According to GHOSN & MOSES (1998), redundancy is defined as the capability of the system to redistribute and continue to carry load after the failure of one main member. As a provision of capacity, redundant structure has additional structural capacity and reserve strength allowing it to carry a higher load than anticipated when considering the capacity of individual members. The measures of redundancy (acc. to GHOSN & MOSES (1998)) are:

$$R_u = \frac{LF_u}{LF_1}\ , \tag{2}$$

$$R_f = \frac{LF_f}{LF_1}\ , \tag{3}$$

$$R_d = \frac{LF_d}{LF_1}\ , \tag{4}$$

where LF_1 is the load that causes the failure of the first member; LF_u is the load that causes collapse of the system; LF_f is the load that causes the functionality limit state of the initially intact structure to be exceeded; LF_d is the load factor that causes the collapse of a damaged structure which has lost one main member.

An alternative definition was also given in terms of the reliability index using a "redundancy factor" β_R given as (FRANGOPOL 1987):

$$\beta_R = \frac{\beta_{int.}}{\beta_{int.} - \beta_{dam.}}, \tag{5}$$

where $\beta_{int.}$ is the reliability index of the intact structural system and $\beta_{dam.}$ is the reliability index of the damaged structural system. Note that this type of analysis can only be implemented in cases when appropriate data regarding the potential hazards are available and require advanced reliability analysis tools. The software package ATENA-SARA-FREET (PUKL ET AL. 2003) serves well for such type of assessment, an application example is presented in the following section.

The definitions for redundancy and robustness provided above are both related to system effect and the ability of the system to continue to carry load after the capacity of individual members are exceeded or after the removal of individual members from the system. For this reason, redundancy is the umbrella term for both. Implementable measures of redundancy and robustness have been advanced by the offshore industry in the ISO 19902 standards. Several measures of redundancy and robustness are proposed for the offshore structures, including the Reserve Strength Ratio (RSR) defined as:

$$RSR = \frac{L_{ultimate}}{L_{design}}, \tag{6}$$

where $L_{ultimate}$ is the load capacity of the structure and L_{design} is the unfactored design load. Another measure is the Damaged Strength Ratio (DSR) defined as:

$$DSR = \frac{L_{damaged}}{L_{design}}, \tag{7}$$

where $L_{damaged}$ is the load capacity of a structure that is damaged due to corrosion or a fatigue failure.

In the following an example taken from the paper of PODROUŽEK ET AL. (2014) will be given to explain the conceptional sensitivity. The response of a typical bridge system is conceptually depicted in Fig. 1 in form of a load-deflection diagram. Different levels should be considered when evaluating member or system safety as well as redundancy.

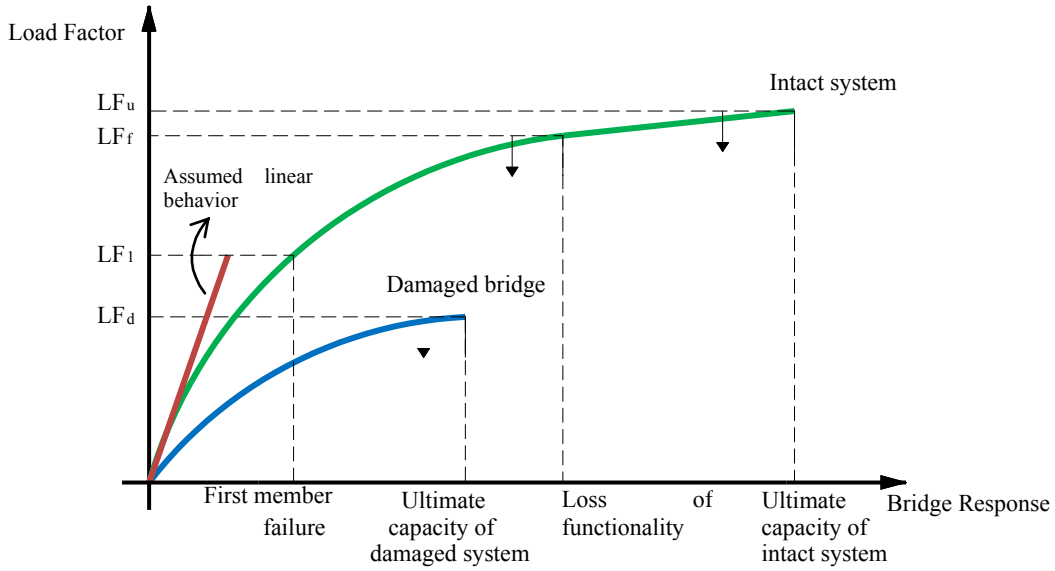

Fig. 1: Representation of typical bridge system (according to GHOSN ET AL. 1998)

The evaluation of the load capacity of the bridge system can be expressed in terms of the traffic load models multiplications, e.g. the number of truck loads it can carry. In this paper it is assumed that the vertical load used as the basis for the evaluation has the configuration of the Eurocode Load model LM1.

The structural system considered in this study is a concrete pre-stressed box-girder Viaduct. Fig. 2 shows the organization of the spans and the topology of the main girder.

The Gossensass Viaduct is part of the Brenner highway in the north of Italy (where the first author has been responsible as a Technical Director for almost a decade). The bridge with a total length of 1028.80 meters consists of 13 spans and was built in 1969. The deck of the post-tensioned box-girder bridge is represented by two box-girder superstructures with a total width of 22.10 m which are linked by the same piers. The bridge was designed fully isostatic. The box-girders consist of cast-in-place balanced cantilever beams with varying

girder depth. The height of the box girder varies from 10.80 m over the middle support to 2.85 m in the mid-span.

The assessment of the Colle Isarco Viaduct consists of a detailed non-linear 3D finite element analysis performed within the ATENA software environment (see Fig. 3), utilizing the state-of-the-art fracture mechanics and constitutive laws. The virtual model includes 496 individual prestressing tendons, i.e. the longitudinal parabolic bottom slab tendons, vertical tendons and top slab tendons; all arranged according to the bridge documentation drawings. Reinforcement is modelled using the smeared reinforcement concept by assigning the reinforcement ratios in given directions. In total, the FEM model consists of ca 2.10^4 brick elements.

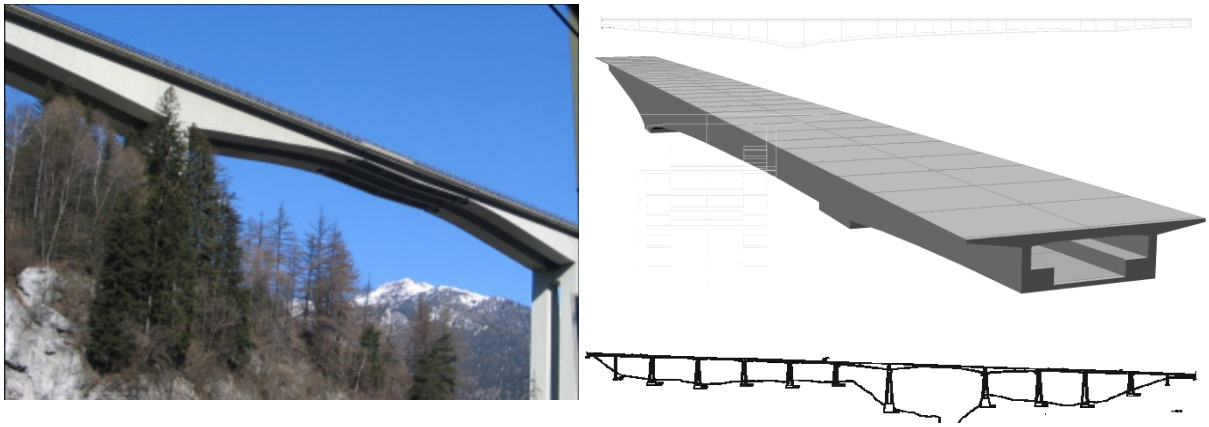

Fig. 2: The main 163 m span, full box girder model and the organization of the spans

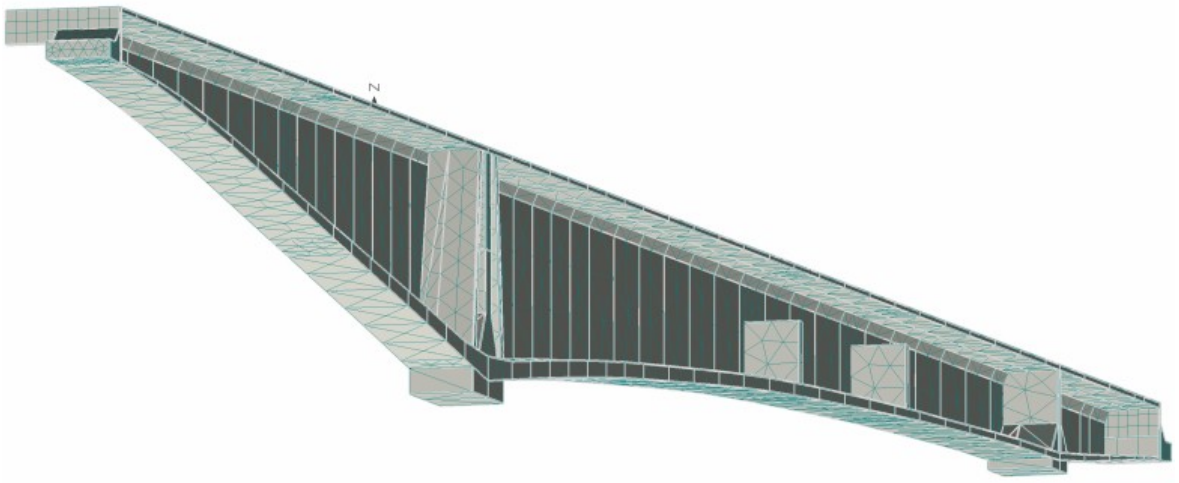

Fig. 3: FEM model (symmetrical half of the superstructure) reproduced according to original documentation from 1970s

The aim is to reproduce the behaviour of the virgin structure and several relevant damage scenarios, reflecting the actual condition and further deterioration due to environmental, mainly chloride, ingress, i.e. reduction of concrete cover, reinforcement corrosion, loss of

pre-stressing cables and to model creep and shrinkage resulting in reduction of prestressing force (NOVÁK ET AL. 2007).

Presented simulated behaviour of various damage scenarios exhibits a trend that is persistent in every realization of the virtual experiment. In terms of mean ultimate capacity, the virgin structure has smaller load carrying capacity when compared to some damage levels. Therefore the non-probability-based performance indicators, such as Eqs. (1), (2), (3), (6) and (7) would yield inverse results due to the fact that the calculated capacities using mean (50% quantile) input are larger for the mild damage instances.

However, the probability-based performance indicators such as Eqs. (4) and (5), i.e. the Robustness index *RI*, will provide opposite effect due to the following fact. The conventional probability density distribution function (PDF) for structural response is assumed to be Lognormal (LN) due to its multiplicative nature. This asymmetric distribution is, however, very sensitive to the coefficient of variation (COV). Therefore, the effect of COV is dominant in this case and the resulting probabilistic characteristics are not in accordance with the mean values of ultimate capacity. In terms of load carrying capacity, the structure under examination has sufficient capacity under all relevant damage scenarios reflecting current and future conditions far beyond the planned life span, having the overloading factor between 2.93 and 5.31.

By considering the worst and best performing scenario in terms of mean ultimate capacity, one may quantify all of the presented redundancy and robustness indicators. The reliability based indicators require the execution of stochastic simulation in order to obtain the statistical characteristics of the response quantities, e.g. in terms of probability density (PDF) distribution parameters, see Tab. 2. In order to obtain the probabilities of failure or safety indexes, the limit state function is formulated using action (*S*) and resistance models (*R*):

$$P_f = P(R - S > 0)\,. \tag{8}$$

The form of Eq. (8) is that of a typical ultimate limit state function (ULS), the action model, *E*, is represented by a deterministic value of 1, i.e. the design load (100% of LM1). The resulting probabilities are presented together with safety indexes in Tab. 2.

Special care has to be taken for small failure probabilities (see TAMPAROPOULOS ET AL. (2011)).

The selected damage-based performance indicators are presented at Tab. 3 for the most extreme scenarios of ultimate capacity, designated in the text as R_{min} and R_{max}. The reliability-based indicators differ from the deterministic indicators in a significant way. The latter are based on comparing various damage scenarios using results from deterministic structural analysis with mean input. The former compare probabilities or safety indexes where the scatter property can and usually has larger effect than the mean value itself. This is evident from Tab. 1 and 2. The lower load capacity of 2.91 (multiples of LM1 load model) has actually higher safety index due to smaller COV than the load capacity of 5.31. Note that the mean response obtained from the deterministic analysis is different from the mean parameter of the statistical distribution as a result of the stochastic analysis.

Tab. 1: Statistical char. of load capacity

	Mean	Cov	Distribution
R_{min} = ds1,45%	2.93	0.09	LN
R_{max} = ds1,30%	5.31	0.13	LN

Tab. 2: Probabilistic characteristics of Eq. (8)

	mean	COV	β	P_f
ULS (R_{min},E)	1.92	0.13	7.32	1.2e−13
ULS (R_{max},E)	4.31	0.16	6.24	2.1e−10

Tab. 3: Relevant performance indicators

Name	Abr.	value
Redundancy factor	β_R	6.77
Robustness index	RI	1749
Reserve Strength Ratio	RSR	5.31
Damaged Strength Ratio	DSR	2.93

3 Antifragility-Evaluation

Since the analytical scenario by calculating the relevant performance indicators is complex and the evaluation is for experts difficult and for nonexpert and decision makers not very helpful an new approach for System-Antifragility is proposed (VLEK 2013).

Topic	Verification	Comment
System response at life time	$AFS = \frac{P_{f\ serv,red} - P_{f\ ult,t=lf}}{P_{f\ ult,t=lf}}$	Defines the structural behavior after 50 (100) years
	$P_{f,ext}\ (ULS) = P(R–S(extreme\ event) > 0) < 10^{-n}$ (e.g. $n = 2$)	Phenomenological scenario; definition of an extreme load
Unforeseen impact (Black Swan scenario)	$AFE = \frac{P_{f\ serv,red} - P_{f,ext}}{P_{f,ext}}$	Defines the system behavior after an extreme, unforeseen impact
	Holistic evaluation with experts in a delphi-round	Evaluate the extreme scenarios and the acceptable risk levels

On the basis of the proposal by FRANGOPOL ET AL. (1987), the Antifragility-System-Index AFS is defined with the probability of failure of the still usable structure in order to allow people to excape $P_{f,\ serv,red}$ ($\beta > 1.5$) and the probability of failure of the intact structure at the ultimate limit state level at the end of the technical life time.

The Antifragility-Extrem-Index AFE indicates the capability to resist after a very extreme impact (MEYER 2012). The probability of failure $P_{f,ext}$ can be calculated with the impact of an extreme load derived from a phenomenological scenario.

The two parameters, the Antifragility-System Index and the Antifragility-Extrem-Index help to evaluate the Resistency of a system after a certain life time and after an extreme event.

The decision about the sensitivity of the calculated Indexes (AFS, AFE) and the evaluation of the measures in order to ensure a certain antifragility should be taken with experts in a delphiround (AKTAN ET AL. 2013, ALE 2013).

Literature:

[1] Aktan, A.E., Brownhohn, J. Structural Identification: Opportunities and Challenges. In: *Journal of Structural Engineering ASCE*, 10 (2013), p. 1639−1647

[2] Ale, B. Better science does not make decisions easier. In: *Safety, Reliability and Risk Management*. Steenbergen & van Gelder (eds). London, Taylor, 2013, p. 3−11

[3] Frangopol, D. M., Curley, J.P. Effects of Damage and Redundancy on Structural Reliability. *Journal of Structural Engineering* 113, no. 7 (1987), p. 1533−49

[4] Glitsch, W. Richtlinie „Integrale Bauwerke“ – Sachstandsbericht. *Stahlbau* 82, Ernst & Sohn Verlag, (2013) S. 708−714

[5] Ghosn, M.; Moses.F. Nchrp Report 406, Redundancy in Highway Bridge Superstructures. Washington. DC: Transportation Research Board, National Academy Press, 1998

[6] Meyer, R., Broad, K., Orlove, B., Petrovic, N. Dynamic Simulation as an Approach to Understanding Hurricane Risk Response: Insights from the Stormview Lab. *Risk Analysis*, Vol. 33, No. 8 (2012), p. 1532−1552

[7] Novák, D., M.; Vořechovský, D.; Lehký,D., Bergmeister, K., Pukl, R., Červenka, V. Stochastic Nonlinear Analysis of Concrete Structures − Part I: From Simulation of Experiment and Parameter Identification to Reliability Assessment, 2007.

[8] Pukl, R., Červenka, V., Strauss, A., Bergmeister, K., Novák, D. An advanced engineering software for probabilistic-based assessment of concrete structures using nonlinear fracture mechanics. In: *9th International Conference on Applications of Statistics and Probability in Civil Engineering*, Berkeley, San Francisco, California, USA, July 6−9, 2003

[9] Taferner, J., Keuser, M., Bergmeister, K. Integrale Konstruktionen aus Beton. In: Bergmeister, K.; Wörner, J.-D.: *BetonKalender* 2009 2, p. 231, Ernst & Sohn Verlag, Berlin; ISBN 978-3-433-01854-5

[10] Taleb, N.N. Antifragile. Things that gain from the disorder. Random House New York, 2012

[11] Tamparopoulos, E.A., Spyridis, P., Bergmeister, K. Small failure probabilities and copula functions: preliminary studies on structural reliability analysis. In: Bérenguer, C.; Grall A.; Soares, C. (Eds.) *Advances in Safety, Reliability and Risk Management*, (2011). ISBN: 978-0-415-68379-1

[12] Podroužek, J., Strauss, A., Bergmeister, K. Robustness based performance assessment of a presstressed concrete bridge. In: *fib-Journal* (accepted for publication) (2014)

[13] Vlek, C. What can national risk assessors learn from decision theorists and psychologists? *Risk Analysis*, Vol. 33, No.8 (2013), p. 1389−1393

Solving the first passage problem using Asymptotic Sampling

Christian Bucher [a]

[a]Center of Mechanics and Structural Dynamics, Vienna University of Technology
christian.bucher@tuwien.ac.at

Abstract: Advanced Monte Carlo methods developed over the past years allow the computation of very small exceedance probabilities such as those required for structural reliability analysis with high precision. Typically these method focus on a particular fixed threshold value for which the exceedance probability is computed. It may, however, sometimes be more convenient to have information about the entire tail of the distribution rather than only one specific quantile. This is particularly useful in the context of reliability-based structural optimization. This paper presents an extension of the asymptotic sampling method to compute the exceedance probability using a small number of samples with artificially increased standard deviations. Numerical examples demonstrate the applicability and efficacy of the suggested approach.

Keywords: random vibration, first passage problem, asymptotic sampling, Monte Carlo simulation.

1 Introduction

Generally, the probability of failure P_F in an n-dimensional space of random variables $X_1, \ldots X_n$ can be computed as

$$P_F = \int_{D_F} \cdots \int f_{X_1,\ldots X_n}(x_1, \ldots x_n) \mathrm{d}x_1 \ldots \mathrm{d}x_n \tag{1}$$

In this equation, $f_{X_1,\ldots X_n}(x_1, \ldots x_n)$ denotes the joint probability function of the random variables $X_1, \ldots X_n$ and D_F denotes the failure domain, i.e. the region of the n-dimensional random variable space in which failure occurs. Typically, this is denoted in terms of a scalar

limit state function $g(.)$ attaining negative values, i.e. $D_F = \{(X_1, \ldots X_n) \mid g(X_1, \ldots X_n) \leq 0\}$. For applications in time-dependent problems as those arising structural dynamics, the appropriate formulation leads to the the first-passage problem. Here the failure domain is typically written as

$$D_F = \{(X_1, \ldots X_n) \mid \max_{1 \leq k \leq N} h_k(X_1, \ldots X_n) \geq \xi\} \tag{2}$$

In this equation, $h(.)$ denotes a response quantity of interest, and ξ is a critical threshold value of this response. The random variables X_i usually denote the random excitation (e.g. earthquake or wind) which is discretized in time. A schematic sketch is shown in Fig. 1. Note

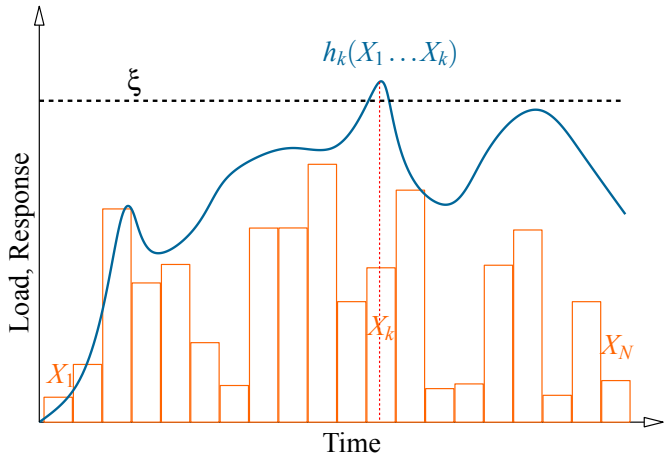

Fig. 1: Schematic sketch of first passage problem

that due to the principle of causality, the values of h at point k in time can only depend on the basic variables $X_1 \ldots X_k$ (i.e. on those in the past put to the present as expressed by the index k), and not on those in the future.

The generalized safety index (or reliability index) β is defined by

$$\beta = \Phi^{-1}(1 - P_F) = \Phi^{-1}[F_H(h)] \tag{3}$$

Here $\Phi^{-1}(.)$ is the inverse standardized Gaussian distribution function. Without loss of generality, it is assumed that the random variables X_i are Gaussian and that they are independent and identically distributed (i.i.d.) with zero mean and unit standard deviation. Shifting and scaling as well as Non-Gaussian properties and possible correlation among them can easily be introduced using marginal transformations and joint probability density function models such as the widely used Nataf-model [10, 6]. Detailed discussions of these topics related to structural reliability theory can be found in several textbooks, e.g. in [3].

Since the failure probabilities to be computed are usually very small (e.g. $P_F = 10^{-5}$) it is not feasible to evaluate the integral in Eq. 1 using standard numerical integration procedures. This is due to the fact that the number of integration points required to perform e.g. Gaussian integration in dimension n grows exponentially with n. Monte Carlo methods do not have this dependence on the dimension, however, crude or plain Monte Carlo simulation requires a number of samples roughly larger than $\frac{10}{P_F}$. This, again, may lead to prohibitively large computational effort.

Recently developed advanced Monte Carlo methods allow the computation of very small exceedance probabilities such as those required for structural reliability analysis with high precision. These method focus on a particular threshold for which the exceedance probability is computed. A representative class of these methods are importance sampling procedures for which frequently the so-called Girsanov-transformation approach has been utilized [7]. These methods bear close relation to the First-Order Reliability Method which locates the most relevant failure region in a high-dimensional random variable space. However, this location depends on the failure criterion and therefore on the chosen threshold value of the response quantity under investigation. This is inconvenient if one is interested to obtain information about the entire tail of the distribution rather than only one specific quantile, particularly for application in probabilistic structural design.

The asymptotic sampling method as described in [2, 3] provides a purely Monte-Carlo-based approach to compute the exceedance probability using samples generated with artificially increased standard deviations. A further developed procedure to obtain the complete CDF (at least in the relevant tail region) based on asymptotic sampling has been presented in [13]. A very simple and straightforward modification of this procedure allows the application of a regression technique covering both the range of the threshold values ξ considered as well as the influence of the magnification factor f of the standard deviations.

It should be mentioned that the asymptotic sampling method is a representative of a very recent family of methods exploiting the dependency of the failure probability on a scaling parameter of the standard deviation of the input variables. Another, independent approach to this is given by [8, 9]. For a comparative review and synthesis of these two approaches it is referred to [11].

2 Method of Analysis

Asymptotic sampling exploits the asymptotic behavior of the failure probability expressed in terms of the reliability index β when changing the standard deviation of the basic random variables. If the original standard Gaussian random variables are replaced by variables with non-unit standard deviations $\sigma = \frac{1}{f}$, then the computed reliability index will depend on the choice of f. As a first simple case, consider a linear function of the basic random variables X_k, say

$$g(\mathbf{X}) = \sum_{k=1}^{N} a_k X_k \tag{4}$$

with arbitrary real-valued coefficients a_k. The random variable $Y = g(\mathbf{X})$ will then be Gaussian with a zero mean and a variance

$$\sigma_Y^2 = \sum_{k=1}^{N} a_k^2 \tag{5}$$

The distribution function $F_Y(y)$ of this variable will therefore be given by

$$F_Y(\xi) = \Phi\left(\frac{\xi}{\sigma_Y}\right) = \Phi\left(\xi/\sqrt{\sum_{k=1}^{N} a_k^2}\right) \tag{6}$$

Upon changing the standard deviation of all basic variables from unity to a value of $1/f$, the standard deviation of Y changes by the same amount. Thus, the distribution function changes to

$$F_Y(\xi) = \Phi\left(\xi f/\sqrt{\sum_{k=1}^{N} a_k^2}\right) \tag{7}$$

from which the generalized reliability index according to Eq. 3 is immediately found as

$$\beta = \frac{\xi f}{\sqrt{\sum_{k=1}^{N} a_k^2}} \quad \rightarrow \quad \frac{\beta}{f} = \frac{\xi}{\sqrt{\sum_{k=1}^{N} a_k^2}} \tag{8}$$

This means that for a linear function of Gaussian variables, the scaled reliability index β/f is invariant with respect to the choice of f.

For the general case, this is not true. There is, however, an asymptotic property which ensures similar behavior for many nonlinear cases. As stated by [1, 5], the reliability index asymptotically depends linearly on f or, in scaled notation

$$\lim_{f\to\infty} \frac{\beta(f)}{f} = \text{const.} \tag{9}$$

In order to exploit this asymptotic relation, [2] suggested to utilize the formulation

$$\frac{\beta}{f} = A + \frac{B}{f^2} \tag{10}$$

in which the coefficients A and B are determined from a regression analysis using the values of β as estimated from several Monte Carlo runs with different values of f. In the previous studies as given in [2, 13], this regression was carried out for fixed values of the threshold ξ. In order to stabilize the regression also at a low number of Monte Carlo samples, it is proposed to include the threshold level ξ into the regression analysis. This means that a regression is carried out in which the reliability index β is assumed to be a function of both the threshold ξ and the sampling factor f. The reliability index itself is computable from the first passage probability through $\beta = -\Phi^{-1}[P_F(\xi)]$ is assumed to be represented by the function

$$\frac{\beta(\xi, f)}{f} = a_0 + a_1 x + a_2 \log x + \frac{a_3}{f^2} + \frac{a_4 x}{f^2} + \frac{a_5 \log x}{f^2} \tag{11}$$

which satisfies the previously mentioned asymptotic requirement that the influence of f should disappear as $f \to \infty$ [3]. The coefficients $a_0 \ldots a_5$ are obtained by a least-squares regression. The desired first passage probability for any threshold level ξ is then obtained by letting $f = 1$ in this equation. The specific choice of the regression function (11) is motivated by its ability to represent both normal and log-normal distribution functions. However, as the sample size increases, the actual choice of this function becomes immaterial since then there will be no extrapolation required. In this way, the method inherently guarantees asymptotic unbiasedness.

3 Numerical Examples

3.1 Linear SDOF system

As a simple first-passage problem, consider the transient response of a SDOF oscillator governed by the differential equation

$$m\ddot{x} + c\dot{x} + kx = w(t) \tag{12}$$

in which $w(t)$ is a stationary white noise with intensity D_0. For the numerical treatment, the white noise is replaced by a sequence of i.i.d. normal variables F_k spaced uniformly at time interval δt. The variables have zero mean and a variance $\sigma_F^2 = \frac{D_0}{\Delta t}$. Numerical values are k = 1 N/m, m = 1 kg, c = 0.1 kg/s, $D_0 = \frac{\pi}{50}$ m^2/s^3, Δt = 0.15 s. The total time considered is T = 40 s. For reference, the stationary limit of the variance of the displacement response is σ_X = 0.5605 m. The failure criterion considered is that the maximum absolute value of the response $x(t)$ exceeds a threshold value ξ anywhere in the entire time duration $[0, T]$. Threshold values considered are ranging from 1 to 5 m (i.e. up to about 9 times the stationary standard deviations).

The asymptotic sampling procedure is carried out using 5 runs of 1000 simulations each. The runs have different scaling factors f for the excitation (ranging from 1 to 1/3) thus covering different regions of the first passage probability. Note that these 5000 simulations cover the entire range of threshold values ξ considered simultaneously, i.e. the analysis does not have to be repeated for different threshold values.

Fig. 2 shows the distribution function of the peak response expressed in terms of the scaled reliability index β/f for different values of the scaling factor f. It can clearly be seen that significantly larger values of the response (and therefore larger range of the distribution function) can be reached by reducing the value of f. For f = 1, the reachable threshold value ξ is approximately 2 with a sample size of 1000. For f = 0.5, the reachable threshold is about 4.

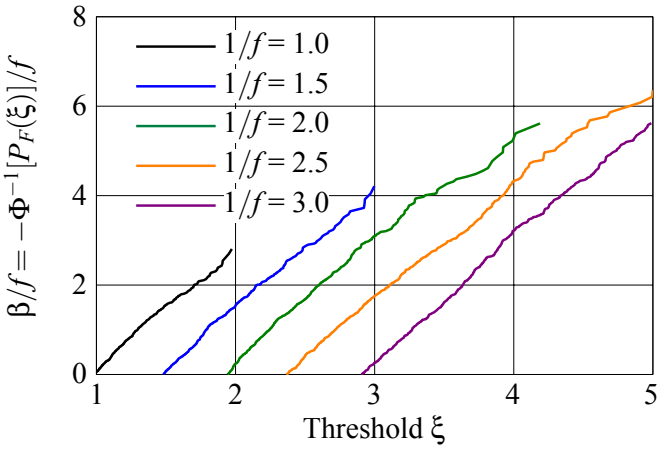

Fig. 2: Distribution function of peak absolute response of SDOF system for different sampling magnifications f

The results of the regression based on Eq. 11 are shown in Fig. 3. For reference, the results

of the Monte Carlo run with $f = 1$ are shown in this figure as well. As mentioned above, his curve barely reaches a threshold level of $\xi = 2$. Furthermore, the results for levels $\xi = 2.5$ and $\xi = 3$ are confirmed by Monte Carlo runs with sample sizes of 10.000 and 5.000.000, respectively. In this range the results match perfectly. Higher threshold levels could not be confirmed with reasonable computational effort.

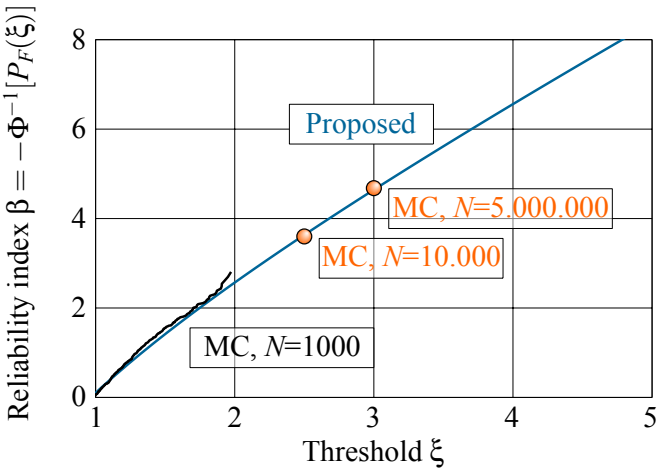

Fig. 3: Exceedance probability of SDOF systems under white noise

3.2 SDOF system with friction pendulum seismic isolation

The structural model considered here is represented by a single-degree-of-freedom oscillator. The structure is supported by a seismic protection device (a friction pendulum system, see e.g. [12]). The mechanical model of the device together with the structure to be protected is shown in Fig. 4. This model contains a friction element with a maximum transmissible

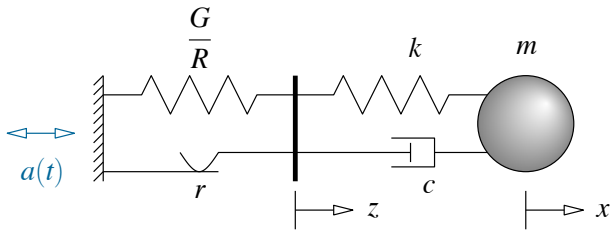

Fig. 4: Mechanical model for structure and seismic protection device

force r which is computed from the weight G of the structure acting on the friction device and the friction coefficient μ. A re-centering spring due to the pendulum effect is included. Its spring constant can be computed from the weight of the structure and the effective radius of curvature R of the pendulum system.

The spring k represents the structural stiffness, the structural mass is given by m. The displacement of the structural mass is given by the variable x, the offset of the friction device by the variable z. In order to represent structural damping, a vicious damper c is added in

parallel to the spring k. In the following computations, the structural damping is represented by a damping ratio $\zeta = 0.02$.

The earthquake excitation is introduced in terms of the ground acceleration $a(t)$ which is modeled as an amplitude-modulated white noise:

$$a(t) = w(t)e(t) \tag{13}$$

in which $w(t)$ is stationary white noise with spectral density $S_0 = 0.01$ m^2/s^3 and $e(t)$ is given as

$$e(t) = 4\left[\exp(-0.25t) - \exp(0.5t)\right] \tag{14}$$

The total time duration is $T = 25$ s.

For this system, the force F_r in the friction element can be computed from the equilibrium condition

$$F_r + \frac{G}{R}z = k(x-z) \rightarrow F_r = Kx - \left(k + \frac{G}{R}\right)z \tag{15}$$

If there is no slip, then the rate of change of this force due to the rates $\dot{x}$ and $\dot{z}$ is therefore

$$\dot{F}_r = K\dot{x} - \left(k + \frac{G}{R}\right)\dot{z} \tag{16}$$

Slip in the friction element occurs under one of the the following two conditions:

$$(F_r \geq r \wedge \dot{x} > 0) \vee (F_r \leq -r \wedge \dot{x} < 0) \tag{17}$$

If one of these conditions is met, then there is no increment in the force F_r, i.e. $\dot{F}_r = 0$ and therefore

$$\dot{z} = \frac{k}{k + \frac{G}{R}}\dot{x} \tag{18}$$

Otherwise we have $\dot{z} = 0$. Together with the state vector form of the equation of motion

$$\begin{aligned} \dot{x} &= y \\ \dot{y} &= -k(x-z) - c(y-\dot{z}) + a(t) \end{aligned} \tag{19}$$

this results in a system of three first-order differential equations which can be solved by the Runge-Kutta method. In the following numerical analysis the values for the structural parameters are $m = 1$ kg, $k = 100$ N/m, $c = 0.1$ Ns/m. The acceleration of gravity $g = 9.81$ m/s^2, and the friction coefficient $\mu = 0.04$.

The primary purpose of the seismic isolation lies in reducing the forces transmitted from the ground into the structure. This effect is easily quantified in terms of the maximum acceleration of the structural mass m. Fig. 5 compares the CDF of the peak acceleration for different values of the radius of curvature R of the friction pendulum system.

It can be seen that the probability of exceeding large acceleration values is dramatically reduced by the FPS. Since the compete tail of the first-passage distribution is obtained, reliability-based optimization of friction pendulum systems as presented e.g. in [4] can be further improved.

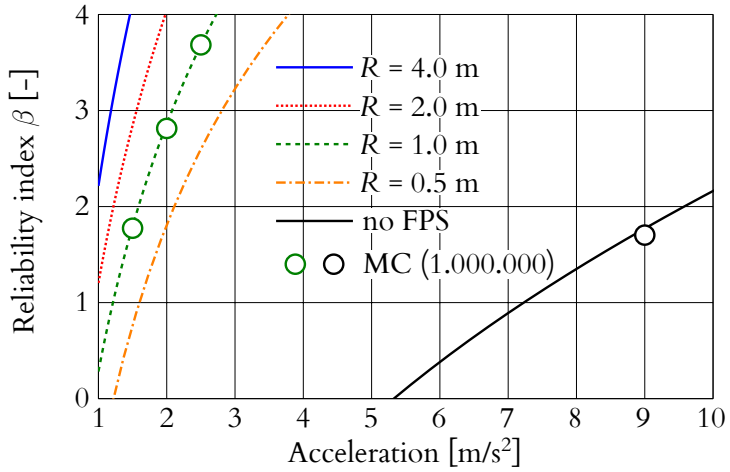

Fig. 5: Tail of peak acceleration of structure depending on radius of curvature R for FPS

4 Conclusions

In view of the results as obtained it may be concluded that the suggested Monte Carlo based method using Asymptotic Sampling to compute the tail probabilities of stochastic dynamic response quantities performs remarkably well. The method provides asymptotically unbiased estimated for the tails of the distribution function. At small sample sizes, there may be a substantial bias if the failure domain is not simply connected, particularly if it consists of separated islands in which failure occurs.

The examples as analyzed here also show that the treatment several thousands of random variable does not pose any difficulties. This very useful property is due to the sole use of Monte Carlo sampling without any specific assumptions such as location of the design point or similar. Therefore the method as presented is particularly suitable for the analysis of first-passage problems in random vibrations. For this class of problems it can be seen that:

- The results agree very well with accurate results in the probability range which is verifiable by Monte Carlo simulation.
- The proposed method can readily predict extremely small failure probabilities with substantially reduced computational effort as compared to conventional MC-based approaches.

Due to its efficacy, the method is especially well-suited for computationally demanding problems such as reliability-based structural optimization.

Acknowledgment

The author would like to acknowledge financial support from the Austrian Science Funds (FWF) as part of the Vienna Doctoral Programme on Water Resource Systems (DK-plus W1219-N22). This research has also been supported by *Stiftung Maurer Söhne*

(Forschungsförderung Technische Dynamik) which is gratefully acknowledged by the author.

Literature

[1] K. W. Breitung. "Asympotic approximations for multinormal integrals". In: *Journal of Engineering Mechanics*, 110, 1984, pp. 357–366.

[2] C. Bucher. "Asymptotic sampling for high-dimensional reliability analysis". In: *Probabilistic Engineering Mechanics*, 24, 2009, pp. 504–510.

[3] C. Bucher. *Computational analysis of randomness in structural mechanics*. Ed. by D. M. Frangopol. Structures and Infrastructures Book Series, Vol. 3. London: Taylor & Francis, 2009.

[4] C. Bucher. "Probability-based optimization of friction damping devices". In: *Structural Safety*, 31, 2009, pp. 500–507.

[5] R. Gollwitzer and R. Rackwitz. "An efficient numerical solution to the multinormal integral". In: *Probabilistic Engineering Mechanics*, 3, 1988, pp. 98–101.

[6] P.-L. Liu and A. DerKiureghian. "Multivariate distribution models with prescribed marginals and covariances". In: *Probabilistic Engineering Mechanics*, 1(2), 1986, pp. 105–112.

[7] M. Macke and C. Bucher. "Importance sampling for randomly excited dynamical systems". In: *Journal of Sound and Vibration*, 268, 2003, pp. 269–290.

[8] A. Naess and O. Gaidai. "Monte Carlo Methods for Estimating the Extreme Response of Dynamical Systems". In: *Journal of Engineering Mechanics*, 134, 2008, pp. 628–636.

[9] A. Naess, O. Gaidai, and O. Batsevych. "Prediction of Extreme Response Statistics of Narrow-Band Random Vibrations". In: *Journal of Engineering Mechanics*, 136, 2010, pp. 290–298.

[10] A. Nataf. "Détermination des distributions de probabilités dont les marges sont données". In: *Comptes rendus de l'Académie des sciences*, 225, 1962, pp. 42–43.

[11] J. Qin, K. Nishijima, and M. H. Faber. "Extrapolation Method for System Reliability Assessment: A New Scheme". In: *Advances in Structural Engineering*, 15, 2012, pp. 1893–1909.

[12] P. C. Roussis and M. C. Constantinou. "Uplift-restraining Friction Pendulum seismic isolation system". In: *Earthquake Engineering & Structural Dynamics*, 35, 2006, pp. 577–593.

[13] M. Sichani, S. Nielsen, and C. Bucher. "Efficient estimation of first passage probability of high-dimensional nonlinear systems". In: *Probabilistic Engineering Mechanics*, 26, 2011, pp. 539–549.

Global safety formats in *fib* Model Code 2010 for design of concrete structures

Vladimir Cervenka
Cervenka Consulting, Prague, Czech Republic
vladimir.cervenka@cervenka.cz

Abstract: Model Code 2010 introduces non-linear analysis in design of concrete structures requires an alternative approach to safety verification and related global safety format. Several methods for verification of limit states using non-linear analysis are presented: full probabilistic method, method ECOV based on the estimate of resistance variation, global safety factor according to EN1992-2 and partial safety factors. The methods are compared on several examples of reinforced concrete structures ranging from ductile to brittle modes of failure.

Keywords: non-linear analysis, safety formats, fracture mechanics.

1 Introduction

The new *fib* MODEL CODE 2010 [1] developed within the international scientific community represents the state-of-the art for design of concrete structures. It reveals trends and ideas for future code development while it is an operational code, useful for practical design. One of the new features is the introduction of a global safety format proposed for verification of resistance assisted by non-linear analysis. This opens possibilities for numerical simulation based on nonlinear analysis to be used as tool in design process. Such innovations observed in other industrial branches are now spreading also to concrete industry.

In a standard design process the load actions are determined for chosen critical cross sections by elastic structural analysis. They represent a possible distribution of internal forces satisfying equilibrium condition, but do not reflect a force redistribution due to nonlinear effects. The safety verification is made in local points whereas a global safety of the whole structure is not evaluated. This deficiency can be removed by applying non-linear analysis.

A non-linear structural analysis based on realistic constitutive relations makes possible a simulation of a real structural behavior. It reflects an integral response, where all local points (sections) interact and therefore it requires an adequate approach for safety verification. The non-linear analysis offers a verification of global resistance and requires a safety format for global resistance.

Several methods for verification of limit states using non-linear analysis are presented: full probabilistic method, method ECOV proposed by the author, global safety factor according to EN1992-2 and partial safety factors. These methods are based on a common probabilistic safety concept for verification of limit states. They differ in the level of implementation of the probability methods. The methods are compared on several examples of reinforced concrete structures ranging from ductile to brittle modes of failure.

2 Global safety formats

2.1 Global design condition

For the verification of resistance the design condition can be approximated by the inequality where the extreme values of actions and resistance are decoupled as follows:

$$F_d < R_d \tag{1}$$

It this F_d is design action and R_d is design resistance and both these entities cover safety margins. The safety of loading and resistance are treated separately, which is a certain approximation as compared to a general probabilistic approach. In design practise based on the partial safety factors this simplification is accepted. $F_d = F(S, \gamma_G, \gamma_Q, \gamma_P, ..)$, where the representative load *S* is factorized by partial safety factors $\gamma_G, \gamma_Q, \gamma_P, ..$ for permanent load, live load, pre-stressing, etc.

In nonlinear analysis, R_d represents the global resistance in terms of forces corresponding to actions (live load, horizontal load, etc.). Note, that in partial safety factor method we assume a failure probabilities of separate materials, but do not evaluate the failure probability on the structural level. Unlike in sectional design, the global resistance reflects an integral response of the whole structure, in which all material points (or cross sections) interact. The safety margin can be expressed by the safety factor:

$$R_d = \frac{R_m}{\gamma_R} \tag{2}$$

where R_m is the mean resistance (This is sometimes referred to as *nominal* resistance.) The global safety factor γ_R covers all uncertainties and can be related to the coefficient of variation of resistance V_R (assuming a log-normal distribution, according to Eurocode 2) as

$$\gamma_R = \exp(\alpha_R \beta V_R) \tag{3}$$

where α_R is the sensitivity factor for resistance and β is the reliability index. It is recognized that variability included in V_R depends on uncertainties due to various sources: material properties, geometry and resistance model. They can be treated as random effects and analyzed by probabilistic methods. Due to available statistical data the probabilistic treatment of materials and geometry can be done in a rational way. However, a random treatment of model uncertainties is more difficult, because of limited data. A simplified formulation was proposed in MC2010, where in denominator of the right hand side in

Eq.(2) is a product of two factors $\gamma_R = \gamma_m \gamma_{Rd}$. (It follows from determination of partial safety factors in MC2010, Sect.4.5.2.2.3) . The first factor γ_m is related to material uncertainty and can be established by a probabilistic analysis. The second factor γ_{Rd} is related to model and geometrical uncertainties and recommended values are in the range 1.05-1.1. (as suggested by Eurocode 2-2.)

Recent investigation by SCHLUNE ET.AL. [7] found such values unsafe and proposed a more general method in which the overall coefficient of resistance variation can be determined as

$$V_R = \sqrt{V_G^{\,2} + V_m^{\,2} + V_{Rd}^{\,2}} \tag{4}$$

where variability due to specific sources are identified: V_G − geometry, V_m − material strength, V_{Rd} − model. This approach allows to include all uncertainties in more rational way. Based on a survey of various blind bench mark studies Schlune concluded that model uncertainties of nonlinear analysis are much higher than in standard design based on engineering formulas and are strongly dependent on modes of failure. Reported coefficients of variation due to model uncertainty for bending failure in range 5 ~ 30%, for shear 15 ~ 64%. Schlune concluded that due to the lack of data, the choice of the model uncertainty often depends on engineering judgment and can be subjective. However, these conclusions do not recognize the effect of model validation, which can decrease model uncertainties. Further research is needed to recommend appropriate values of the model uncertainty for numerical simulations.

The assessment of the safety according to Eq. (1) can be done by various methods, ranging from a full probabilistic analysis to the partial factor method, which differ in the level of approximations involved. They will be briefly described in the next sections.

2.2 Full probabilistic analysis

The probabilistic analysis is the most rational tool for the safety assessment of structures. It can be further refined by introducing non-linear structural analysis as a limit state function. The numerical simulation resembles a real testing of structures by considering a representattive group of samples, which can be statistically analyzed for assessment of safety. We shall only briefly outline an approach implemented in the software tool SARA [3]. More about the probabilistic analysis can be found in [6].

In numerical simulations the probabilistic analysis of resistance can be performed by LHS method, in which the material input parameters are varied in a systematic way. The resulting array of resistance values is approximated by a distribution function of global resistance and describes the random variation of resistance. Finally, for a required reliability index β, or probability of failure P_f, the value of design resistance R_d shall be calculated.

The probabilistic analysis based on numerical simulation with random sampling can be briefly described as follows:

Formulation of a numerical model based on non-linear finite element method. Such a model describes the resistance function and can perform deterministic analysis of resistance for a given set of input variables.

Randomization of input variables (material properties, dimensions, boundary conditions, etc.). This can also include some effects, which are not in the action function (for example pre-stressing, dead load etc.). Random material properties are defined by a random distribution type and its parameters (mean, standard deviation, etc.). They describe the uncertainties due to variation of resistance properties. The randomization can be done by two methods: (1) Random variables, where the parameter is constant within a sample (structure), but changes between samples. (2) Random fields, where the parameter is randomly variable within a sample. A correlation of random variables should be considered appropriately.

Probabilistic analysis of resistance. This can be performed by the numerical method of Monte Carlo-type of sampling, such as the LHS sampling method. Results of this analysis provide random parameters of resistance, such as mean, standard deviation, etc. and the type of distribution function for resistance (PDF).

Evaluation of design resistance based on the reliability index β or probability of failure. In this a design point is found by extrapolation of point around central region based on PDF.

The advantage of a full probabilistic analysis is that it is independent of a failure mode. A potentially higher safety margins of some failure modes, such as for example shear failure, is automatically included in higher sensitivity of numerical resistance to a brittle failure. A disadvantage of this approach is in the fact that the target value of design resistance is located in the tail of probability distribution function (PDF), which is determined by the best fit from the sampling. The design value is obtained by extrapolation and strongly depends on the choice of PDF. On the other hand the approach is numerically robust, computationally efficient and feasible for practical application.

However, due to its computational demands a full probabilistic analysis is justified in special cases, where consequences of failure justify the effort.

2.3 ECOV method – estimate of coefficient of variation

A simplified probabilistic analysis was proposed by the author [4] in which the random variation of resistance is estimated using only two samples. It is based on the idea, that the random distribution of resistance, which is described by the coefficient of variation V_R, can be estimated from mean R_m and characteristic values R_k of resistance. The underlying assumption is that random distribution of resistance is according to a lognormal distribution, which is typical for structural resistance. In this case, it is possible to express the coefficient of variation as:

$$V_R = \frac{1}{1.65} \ln\left(\frac{R_m}{R_k}\right) \tag{5}$$

The global safety factor γ_R of resistance is then estimated by Eq. (3) using the typical values $\beta = 3.8$ (50 years) and $\alpha_R = 0.8$ (which corresponds to the failure probability

$P_f = 0.001$). The global resistance factor can be directly related to the estimated coefficient of variation V_R as $\gamma_R \cong \exp(3.04\, V_R)$ and the design resistance is obtained from Eq. (2).

The keystone in this method is the determination of the mean and characteristic values of the resistance: R_m, R_k. It is proposed to estimate them by two separate nonlinear analyses using mean and characteristic values of input material parameters, respectively.

The method is general and the safety described by the reliability index β can be changed if required. Also the distribution function PDF can be changed if justified. It reflects all types of failure. The sensitivity to random variation of all material parameters is automatically included. Thus, there is no need of special modifications of concrete properties in order to compensate for greater random variation of certain properties as in the next method EN 1992-2.

A similar and refined method with more samples was proposed by SCHLUNE ET AL. [7].

2.4 Method based on EN1992-2

Eurocode 2 for bridges introduced a concept for global safety verification based on nonlinear analysis. Design resistance is calculated from

$$R_d = \frac{R_f}{\gamma_R}, \quad R_f = R(f_{ym}, f_{cf} \ldots) \tag{6}$$

Where f_{ym}, f_{cf} are mean values of material parameters of steel reinforcement and concrete, $f_{ym} = 1.1 f_{yk}$ and $f_{cf} = 0.85 f_{ck}$. The global factor of resistance shall be $\gamma_R = 1.27$. Resistance value R_f is not a mean value if the concrete fails. The concrete strength f_{cf} is reduced to account for higher variability of concrete property.

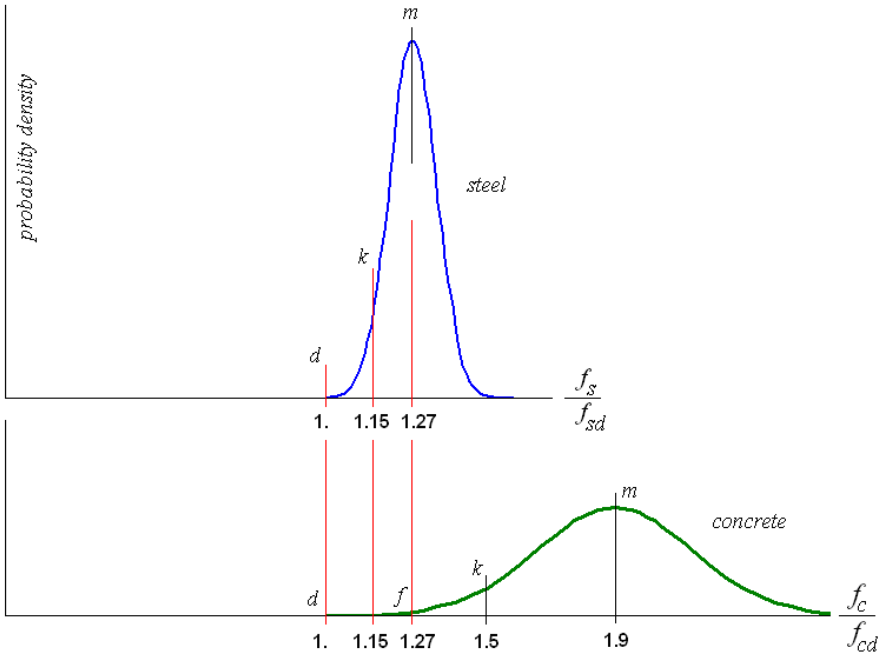

Fig. 1: Probabilistic definition of mean-*m*, characteristic-*k* and design-*d* values for steel and concrete failure, *f*-reduced concrete strength

A justification for the introduction of concrete strength parameter f_{cf} is based on the idea of reflecting the safety of partial safety factors in the newly introduced global safety factor. The concept illustrated in Fig. 1, where probability density functions for both materials are compared. The strength parameters on horizontal axis are nominal with respect to design values. It is assumed that design values for concrete and steel correspond to the same probability. They are located at point 1. on the horizontal axis.

In steel the design value $f_{yd} = f_{yk} / \gamma_s$ is derived from the characteristic strength f_{yk} with the use of partial safety factor $\gamma_s = 1.15$, the mean value is assumed to be $f_{ym} = 1.1 f_{yk}$, which leads to a safety factor 1.27 with respect to mean.

In concrete the design value $f_{cd} = f_{ck} / \gamma_c$, is derived from the characteristic strength f_{ck} with the use of partial safety factor $\gamma_c = 1.5$. We introduce a new parameter for concrete f_{cf}, which correspond to the safety factor of steel for men, and is located at the value 1.27 on the horizontal axis in Fig. 1.

$$f_{cf} = \gamma_R f_{cd} = \gamma_s 1.1 \frac{f_{ck}}{\gamma_c} \cong 0.85 f_{ck} \tag{7}$$

It should be noted that the value of strength f_{cf} does not represent a mean value. Instead, it is a value corresponding to a lower probability than characteristic value and includes the additional safety required for concrete as compared to steel. The subject is also treated by BERTAGNOLI ET AL. [8].

The advantage of the above method is, that it covers both models of failure, due to steel and concrete, without necessity of a prior knowledge of failure mode. For concrete the Eurocode 2 allows only compressive type of failure and excludes failure types relying of tension. This, of course, prevents a wide range of applications, such as shear, or pull-out of fastenings. The study presented in [2] extends its applications also to brittle modes of failure.

2.5 Partial safety factors (PSF)

The method of partial safety factors, which is used in most design codes can be directly applied to global analysis in order to obtain the design resistance $R_d = R(f_d)$. In this, the design values of material parameters $f_d = f_k / \gamma_M$ are used for analysis input (f_k are characteristic values and γ_M partial safety factors of materials).

It can be argued, that design values represent extremely low material properties, which do not represent a real material behavior and thus can lead to distorted failure modes. On the other hand, this method addresses directly the target design value and thus no extrapolation is involved. However, the probability of global resistance is not evaluated and therefore not known.

2.6 Comparison of concepts

The methods outlined above offer an estimation of design resistance with various levels of approximations. The full probabilistic analysis is regarded here as the most rational as suggested by the Joint Committee for Structural safety. The other methods are approximations based on simplifying assumptions, which allow estimation of resistance design values. Brief summary of the methods is show in Tab 1. and the probabilistic concept of these formats is illustrated in Fig. 2.

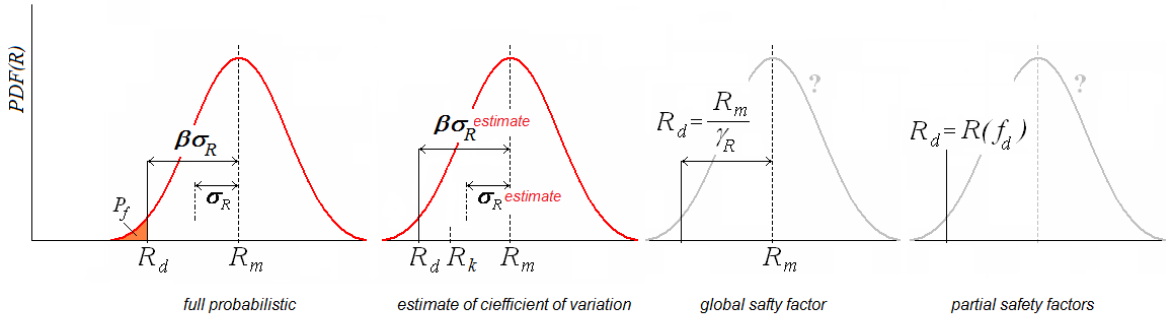

Fig. 2: Probabilistic concept of global safety formats

Tab 1: Summary of methods for verification of global safety

Method	Material parameters required	Required number of resistance calculations	Approximation target
(1) Probabilistic (LHS sampling)	Probability distribution	Depends on number of samples (8 ~ 30)	exact
(2) ECOV	characteristic, mean	2	variability of resistance
(3) EN1992-2	characteristic	1	mean
(4) PSF	design	1	design

It has been observed that the safety of resistance depends not only the variation of basic material parameters, but also to the mode of failure. In other words, for the same concrete material, structures with different type of failure can have different variability of resistance. In this respect the most rational approach is by the full probabilistic format (1), in which the random distribution of resistance is determined and the design value of resistance is chosen for a required probability of failure (and reliability index β).

The other three methods (2, 3, 4 in Tab. 1) can be regarded as approximate from the probabilistic point of view. The concept of the Method (2) is very close to a probabilistic format, since it works with the variance of resistance and calculations with mean and characteristic parameters are relatively robust. Method (3) is using a unique global safety factor. Assessment of resistance near mean is relatively robust and an effect of concrete variability is included in the reduced concrete strength. Method (4) by partial safety factors, offers a direct estimate of design value without a need of estimating global safety margin. In conclusion each method has its merit and, as will be shown later none seems to be superior to the others.

The author has initiated investigations with the aim to compare the various safety formats [2],[4]. The study comprised of a wide range of structures including: simple beam, laboratory test of shear wall, laboratory test of a deep beam, in-situ test of a real structure bridge and a design case of a bridge pier, SFRC concrete. A variety of failure modes covered ductile bending mode, brittle shear modes and a concrete compression mode. Details of this investigation can be found in [2]. A summary of results is shown in Tab. 2. Three approximate methods, namely the partial safety factors (PSF), method based on estimate of coefficient or variation of resistance (ECOV) and method according to EN 1992-2 are evaluated. The table shows the ratio of resistances R_d found by approximate methods to the full probabilistic analysis (which is considered as most exact for this purpose). It is noted that the study does not reflect the model uncertainty in a consistent way. The methods PSF and EN1992-2 include the model uncertainty as given by Eurocode, while the ECOV and full probabilistic analysis it is not considered in order to simplify the comparison. This can explain the average results of ECOV method being slightly higher than the other two methods.

Tab. 2: Summary of methods for verification of global safety

	$R_d / R_d^{prob.}$		
	PSF	ECOV	EN 1992-2
Example 1 bending	1.04	1.04	0.99
Example 2 deep beam	1.02	1.04	1.0
Example 3 bridge pier	0.98	1.04	0.96
Example 4 bridge frame	0.99	0.96	0.92
Example 5 shear beam Y0	1.03	0.98	1.02
Example 6 shear beam Y4	0.81	1.04	0.82
average	0.98	1.01	0.95

The study confirmed feasibility of the approximate methods for the safety assessment. The method ECOV is preferred since it relates the safety to the resistance random variation and is considered more rational as compared to EN1992-2 method.

Multiple failure modes, which are typical features of reinforced concrete structures are inherently included in the numerical models and thus they are reflected in results of analysis and resistance variability. Therefore, the approximate methods of safety verification are generally applicable in design. In significant cases, if justified by failure consequences, a full probabilistic analysis should be applied.

3 Application

For illustration an application of design verification by nonlinear analysis will be shown. The example is a large beam tested in laboratory by YOSHIDA AND COLLINS [9]. The size of the beam is large and exceeds usual beam dimensions (span = 12 m, depth = 2 m) and has no vertical reinforcement. The shear failure is apparently influenced by its large size and is very brittle. The failure mode was well captured by the numerical simulation as illustrated in Fig. 3. Comparison of resistances obtained by various safety formats is shown in Fig. 4. Furthermore, it shows the values of design resistance by codes EN1992-1 and ACI 318.

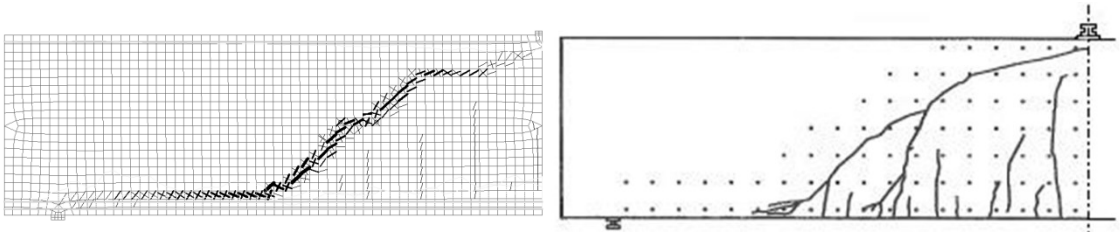

Fig. 3: Numerical and experimental crack pattern

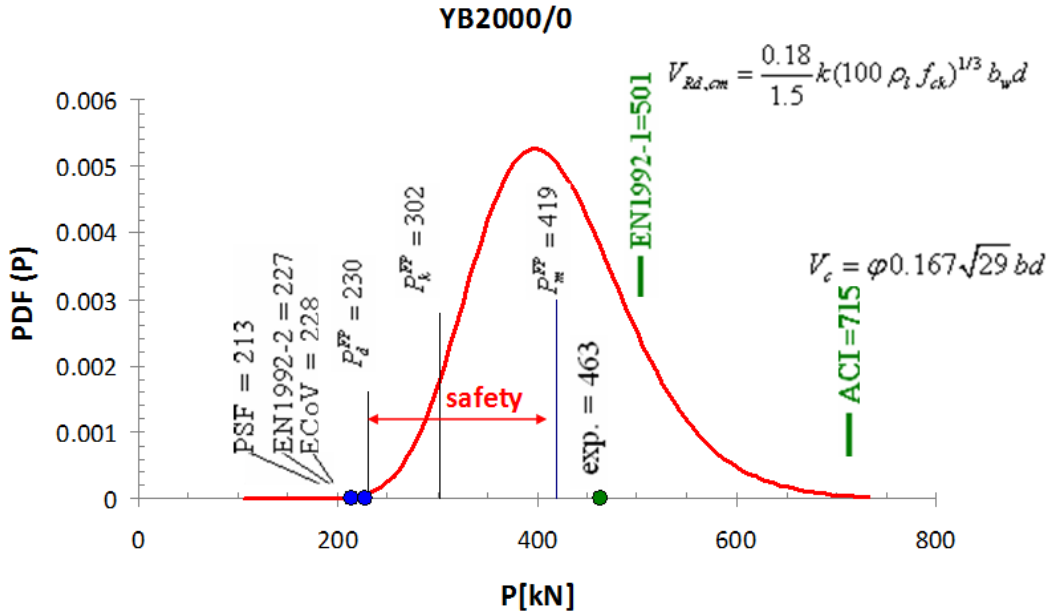

Fig. 4: Design resistance of large beam by YOSHIDA [9] according to various safety formats and codes

This case had shown two remarkable features of numerical simulation. First, a refined constitutive modeling based on fracture mechanics can capture the size effect of brittle shear failure and provides a more safe model of resistance. Second, the global safety formats offer consistent safety margins for the design verification.

4 Closing remarks

Model Code 2010 introduced a verification assisted by numerical simulation as one of the design methods and a global safety format. The of application is extended beyond the

scope of engineering methods based on elastic distribution of internal forces in cross sections into nonlinear analysis. Due to its general approach it overcomes the limits of standard design based on beams and columns. On the other hand it introduces potentially higher model uncertainties. Therefore the model validation becomes an important requirement for its application in engineering practice.

The *fib* Model Code 2010 outlines the framework of limit state verification by numerical simulations and introduces the global safety formats suggested for this purpose.

Further research is needed in order to improve the guide for validation of numerical models and for the classification of model uncertainties.

Acknowledgement

The paper is based in part on the research project by the Czech Science Foundation no. P105/12/2051. The financial support is greatly appreciated.

Literature

[1] Walraven, J., (editor) "fib Model Code for Concrete Structures 2010" September 2013. ISBN: 978-3-433-03061-5. (See also *fib* Bulletin 65 and 66.)

[2] Cervenka, V. Reliability-based non-linear analysis according to fib Model Code 2010, *Structural Concrete*, Journal of the fib, Vol. 14, March 2013, ISSN 1464-4177, pp. 19−28, DOI: 10.1002/suco.201200022.

[3] Cervenka V. (editor) *SARA – Structural Analysis and Reliability Assessment*. User's manual. Cervenka Consulting, Prague 2003.

[4] Cervenka V. Global Safety Format for Nonlinear Calculation of Reinforced Concrete. *Beton- und Stahlbetonbau* 103 (2008), Special Edition, Ernst&Sohn. pp. 37−42.

[5] Cervenka, V., Dolezel, J., Novak, D. Shear Failure of Large Lightly Reinforced Concrete Beams: PART II – Assessment of Global Safety of Resistance. *Proc. of the 3rd fib International Congress – 2010*, May 29-June 2, 2010, Washington DC, USA.

[6] Vrouvenwelder, A.C.W.M. Conclusions of the JCSS Workshop on Semi-probabilistic FEM calculations, Delft, 1−2 December 2009.

[7] Schlune, H., Plos, M., Gylltoft, K. Safety Formats for Nonlinear Analysis of Concrete Structures. *Engineering Structures*, Elsewier, Vol.33, No.8, August 2011.

[8] Bertagnoli, G., Giordano L., Mancini, G. Safety formatfor the nonlinear analysis of concrete structures. *STUDIES AND RESEARCHES – V.25*, Politechnico di Milano, Italy, 2004.

[9] Yoshida Y. *Shear Reinforcement for Large Lightly Reinforced Concrete Members*, MS Thesis under supervision of Prof. Collins, 2000, Univ. of Toronto, Canada.

An integrated probabilistic approach for prediction of remaining life of buried pipes

Chun Qing Li[1], Yanling Ni[2]
[1] School of Civil, Environmental and Chemical Engineering, RMIT University, Australia
[2] Office of Teaching, Hubei University of Economics, P R China
chunqing.li@rmit.edu.au, yanling.ni@hbue.edu.cn

Abstract: This paper proposes an integrated probabilistic approach for the accurate prediction of the safe life of buried infrastructure, using metal water pipes as an example. It will integrate material deterioration, soil mechanics, fracture mechanics and time-dependent reliability theory into a methodology to analyse the behaviour and failure mechanisms of buried metal pipes subjected to simultaneous internal deterioration and external loads, including environmental loads. The research presented in the paper would advance the knowledge in deterioration science and failure theory and provide a sustainable solution to the intelligent management of the vast asset of buried pipelines in the world. It would bring about economical, environmental and social benefits both nationally and internationally.

Keywords: Buried pipes, corrosion, soil-pipe interaction, fracture, time-dependent reliability

1 Introduction

The life expectancy of buried metal pipelines, such as cast iron pipes, can exceed 100 years [1] but the average age of failed pipes is much shorter than the estimated life expectancy. For example, the average age of failed water pipes is only 47 years in the US and Canada [2]. It is noted that buried metal pipes are more prone to failure, than ever before. Long service, coupled with aging, deterioration and damage of buried pipes, exacerbates the situation. For example, it is reported in the UK and Canada that the failure rate of buried pipes is 39 breaks per 100 km per annum [3,4]. The Australian National Water Commission [5] also reported that water mains suffer from 20 breaks per 100 km per annum on average and the cost on replacement of failed pipes has increased by 10% annually since 2006.

Examples of the most recent pipe bursts that can be classified as catastrophic to the public are: (i) the sudden burst of a 200 mm ductile iron water main in the CBD of Adelaide, resulting in chaos and heavy traffic disruption during peak hours on 23 July 2012, and substantial financial consequences (reported in the newspaper Adelaide Now); (ii) the sudden

collapse of a 760 mm cast iron main in Cleveland, US in March 2008, which had been operating without problems since its installation in 1880 and after cement lining in 1996 [6]; and (iii) the sudden bursting of a 686 mm steel water main on 3 December, 2012 in Landsborough Road, Leicester, UK, which damaged about 50 properties, closed roads for a day and resulted in the loss of water supply of 5,000 houses for several hours (reported on BBC News).

One lesson from these sudden failures of buried pipes is that the first principles of pipe behaviour in its lifespan and the mechanisms of pipe failure under multiple influencing factors need to be understood at a fundamental level, and that the time-variant uncertain nature of both the pipe behaviour and influencing factors needs to be accounted for more accurately. It also highlights the urgent need to develop a new theory, based on a new approach with clear understanding of pipe behaviour, interaction with soil, all possible failure modes and advanced predictive methods. Without such a new approach, it is impossible to effectively prevent future unexpected failures. This is a serious scientific challenge that demands considerable intellectual capability. The purpose of this paper is to develop a new framework with such a new approach.

Various attempts have been made to develop a theory for service life prediction of buried pipes [7−16], as have been critically reviewed by the authors. For example, RAJANI AND MAKER [8] developed an empirical model that relates tensile strength of cast iron pipes with defect size and geometry through a stress intensity factor. SADIQ ET AL. [9] used Monte Carlo simulation for risk assessment of cast iron water mains. RAJANI AND ABDEL-AKHER [10] used mechanistic models and finite element method to estimate the safety factor of old cast iron pipes. CHIODO AND RUGGIERI [11] developed a procedure to determine the fracture toughness of pipes with circumferential surface cracks. MOORE ET AL. [12] investigated the soil–pipe interaction of buried cement pipes. MOGLIA ET AL. [13] used an empirical model to predict the failure rates of cast iron pipes. DEGHAN ET AL. [14] developed a new nonparametric technique for failure prediction of different classes of pipes. GOULD ET AL. [15] undertook an exploratory statistical analysis to investigate the effect of climate on the failure rate of water pipes. MELCHERS [16] proposed a bi-modal model to simulate the multi-phase corrosion of grey cast iron with underlying uniform corrosion and the subsequent pitting corrosion in marine and atmospheric environments.

This paper will first discuss current challenges facing researchers and pipeline industry. It will then propose a new methodology for the accurate prediction of the remaining safe life of buried pipelines, using cast iron water pipes as an example. The methodology will integrate material deterioration, soil mechanics, fracture mechanics and time-dependent reliability theory into an algorithm to analyse the behaviour and failure mechanisms of buried metal pipes subjected to simultaneous internal deterioration and external loads, including environmental loads. An example will be provided to illustrate the application of the proposed methodology.

2 Research challenges

Most stakeholders of pipe infrastructure, in particular, the industry and public, have recognised the severe consequences of pipe failures and there is on-going application-focused research funded by industry, e.g., Water Service Association of Australia and Water Re-

search Foundation (US). However, due to the lack of innovation in the theory used for predicting the failure of buried pipes, reoccurrence of these disasters has not been prevented. This advancement is scientifically challenging and intellectually demanding. The scientific challenge is to advance the knowledge of deterioration science of materials (metal) and the failure theory of infrastructure (buried pipeline), integrating metal corrosion, soil mechanics, fracture mechanics, and time-dependent reliability methods as briefly demonstrated below.

Stress is a fundamental measure of the behaviour of built infrastructure. For the example of fracture mechanics, a stress intensity factor K is used as the measure of pipe behaviour [20]:

$$K(t) = \sigma\sqrt{2\pi r} \cdot f\left(\theta, t\right) \tag{1}$$

where σ is stress field, r and θ are geometric parameters and t is time. In determining K, the scientific challenge is accurate modelling of local pitting corrosion since it causes damage (cracking) and hence affects the correction function $f(\theta, t)$. Although corrosion of metal has been widely researched, little has been done in the complex yet real environment of soil. Furthermore, one of the important mechanisms of corrosion that is most relevant to buried pipes, microbial corrosion, has not been considered due to the complexity of the underground environment. Another challenge is the effect of soil movement, in particular climate change-induced fluctuation of saturation of soil since it cause stress re-distribution and cyclic changes with time, and hence affects the stress field σ. The widely projected climate change is also expected to create extreme storm events and changes to the underground water table by altering rainfall patterns and sea level [21], which will lead to soil movement and resultant changes to the stress-fields exerted on buried pipes.

The very nature of the randomness and time variance of all related factors should be taken into account in accurately predicting failures of buried pipes. As such it is more appropriate to use a time-dependent reliability method. With this method, the probability of pipe failure by fracture (for example) as a function of time can be expressed as follows,

$$p_f\left(t\right) = P\left[K\left(t\right) \geq K_c\right] \tag{2}$$

where K_c is the fracture toughness. The scientific challenge here is to derive a solution to Eq. (2) so that the time-dependent reliability method can be used. However, this is extremely intellectually demanding since Eq. (2) represents a typical outcrossing problem in reliability theory. Since Rice developed a general formula for outcrossing problems in the 1940s [22] (known as the Rice formula) very few solutions have been derived. No analytical solution to Eq. (2) exists when its terms and variables (e.g., K, σ) are non-stationary and non-Gaussian as could be the case for buried pipes.

Also in Eq. (2), the fracture toughness K_c is widely treated as constant but it has been suggested [23] that corrosion and other chemical agents in soil can affect the fracture toughness of metal, which would make K_c time-dependent and affect the failure mode of the pipe. Scientific evidence for, and subsequent modelling of, the effect of corrosion and other chemical agents on fracture toughness K_c is another innovative feature of the pro-

posed methodology which will advance the knowledge in deterioration science and failure theory.

3 Proposed methodology

Service life of a pipe or structure in general is a time period at the end of which the pipe stops performing the functions it is designed and built for. To determine the service life for pipes, a performance-based assessment criterion should be established. In reliability theory, this criterion is expressed in the form of a limit state function as follows

$$G(L,S,t) = L(t) - S(t) \tag{3}$$

where $S(t)$ is the action (load) or its effect at time t and $L(t)$ is the acceptable limit (resistance) for the action or its effect. With the limit state function of Eq. (3), the probability of pipe (structural) failure, p_f, can be determined by

$$p_f(t) = P[G(L,S,t) \le 0) = P[S(t) \ge L(t)] \tag{4}$$

At a time that $p_f(t)$ is greater than a maximum acceptable risk in terms of the probability of pipe failure, p_a, it is the time the pipe becomes unsafe or unserviceable and requires the replacement or repairs. This can be determined from the following:

$$p_f(T_L) \ge p_a \tag{5}$$

where T_L is the service life for the pipe for the given assessment criterion and acceptable risk. In principle, the acceptable risk p_a can be determined from a risk-cost optimization of the pipeline system during its whole service life. This is beyond the scope of the paper and will not be discussed herein but can be referred to, e.g., THOFT-CHRISTENSEN AND SORENSEN [24].

Eq. (4) represents a typical upcrossing problem in mathematics and can be dealt with using time-dependent reliability methods. In this method, the structural failure depends on the time that is expected to elapse before the first occurrence of the action process $S(t)$ upcrossing an acceptable limit (the threshold) $L(t)$ sometime during the service life of the structure [0, T_L]. Equivalently, the probability of the first occurrence of such an excursion is the probability of failure $p_f(t)$ during that time period. This is known as "first passage probability" and can be determined by [25]

$$p_f(t) = 1 - [1 - p_f(0)]e^{-\int_0^t \upsilon \, d\tau} \tag{6}$$

where $p_f(0)$ is the probability of structural failure at time $t = 0$ and υ is the mean rate for the action process $S(t)$ to upcross the threshold $L(t)$.

The upcrossing rate in Eq. (6) can be determined from the Rice formula

$$\upsilon = \upsilon_L^+ = \int_{\dot{L}}^{\infty} (\dot{S} - \dot{L})\, f_{S\dot{S}}(L, \dot{S}) \mathrm{d}\dot{S} \tag{7}$$

where υ_L^+ is the upcrossing rate of the action process $S(t)$ relative to the threshold L, $\dot{L}$ is the slope of L with respect to time, $\dot{S}(t)$ is the time derivative process of $S(t)$ and $f_{S\dot{S}}()$ is the joint probability density function for S and $\dot{S}$. An analytical solution to Eq. (7) has been derived for a deterministic threshold L in LI AND MELCHERS [26] as follows

$$\upsilon = \upsilon_{L=det}^+ = \frac{\sigma_{\dot{S}|S}}{\sigma_S} \phi\left(\frac{L-\mu_S}{\sigma_S}\right)\left\{\phi\left(\frac{\dot{L}-\mu_{\dot{S}|S}}{\sigma_{\dot{S}|S}}\right) - \frac{\dot{L}-\mu_{\dot{S}|S}}{\sigma_{\dot{S}|S}} \Phi\left(-\frac{\dot{L}-\mu_{\dot{S}|S}}{\sigma_{\dot{S}|S}}\right)\right\} \tag{8}$$

where $\upsilon_{L=\mathrm{det}}^+$ denotes the upcrossing rate relative to deterministic threshold L, $\phi()$ and $\Phi()$ are standard normal density and distribution functions respectively, μ and σ denote the mean and standard deviation of S and $\dot{S}$, represented by subscripts and " | " denotes the condition. For a given Gaussian stochastic process with mean function $\mu_S(t)$, and auto-covariance function $C_{SS}(t_i, t_j)$, all terms in Eq. (8) can be determined, based on the theory of stochastic processes, e.g. PAPOULIS [27].

4 Model development

To apply the proposed methodology to practical infrastructure models for corrosion, soil-pipe interaction and fracture toughness need to be developed first. It may be appreciated that these fractures are either site or material or climate dependent. Therefore there is no "one size fits all". Further research needs to be undertaken to develop these models as briefly outline below.

Whilst there have been many studies on corrosion of metals, one important factor often missed is microbial induced corrosion. Furthermore, the relationship between the corrosion depth/rate and pipe failure by fracture or strength has not been well understood. Previous work undertaken by LI [18] and his colleagues has shown that localised or pitting corrosion is the dominant mechanism in corrosion of cast iron pipes. It has also been observed that the microstructure of cast iron has a significant influence on corrosion depth. Experiments need to be undertaken to produce necessary dates for developing corrosion model.

4.1 Corrosion model

It is rational to model the corrosion effect as a stochastic process, due to a large degree of uncertainty of both the corrosion process and its contributing factors, and to be consistent with the advanced time-dependent reliability methods, as follows:

$$c(\mathbf{E}, t) = c_m(\mathbf{E}, t) \cdot \xi_c(\mathbf{E}) \tag{9}$$

where $c(\mathbf{E}, t)$ is the corrosion depth on the pipe wall; the vector $\mathbf{E}$ is the contributing factor as identified in WP1 and t is time. In Eq. (9), $c_m(\mathbf{E},t)$ is the mean value function of corrosion depth and $\xi_c(\mathbf{E})$ is the variation function accounting for all random characteristics of

the corrosion process. Mathematical regression will be readily employed to derive the mean function $c_m(\mathbf{E},t)$ with the data produced in the experiment. The variation function $\xi_c(\mathbf{E})$ will be derived from the classic theory of statistics and Monte Carlo simulation techniques.

4.2 Effects of soil movement

In addition to service loads, environmental loads can also lead to soil movement which significantly affects pipe behaviour and can result in its failure. For example, long droughts result in a decrease of soil saturation and an increase of soil suction and cause contractive deformation of soils. On the other hand, rainfall causes an increase of soil saturation and a decrease of soil suction, which may lead to either swelling or wetting collapse of soils. Widely expected climate change will alter the existing rainfall/evaporation pattern, temperature cycle, and the current underground water level, and change environmental loads further in the long term. Buried pipes will deform as a consequence of soil movement, leading to a re-distribution of the stress field in the pipes.

Several climate parameters influencing water table and soil moisture were established in a recently completed project [26]. These climate parameters can be integrated into a recently developed hydro-mechanical interactive constitutive model [27] for soils to predict soil movement in different climate scenarios. The predicted soil movement can then be inputted as known displacement boundary conditions into a commercial finite element program, e.g., ABAQUS, to simulate the stress field in the pipe under both environmental and service loads. The resultant stress will be modelled as a stochastic process in the same form as Eq. (9) because soil parameters and environmental loads are treated as time variant random variables.

4.3 Corrosion effect on fracture toughness

Corrosion and other chemical agents can lead to a reduction in the fracture toughness of metals. For example, corrosion reactions can generate hydrogen leading to embrittlement of metals. This has not been explored by other researchers. Experiments are needed to address these gaps in knowledge.

The same specimens as those of section 4.1 can be used in the experiment. After different degrees of corrosion, as measured by corrosion depth, tests can be conducted on their fracture toughness according to ASTM-E1820-01. A microscopic investigation to determine changes in the microstructure of the metals during the corrosion process and at different degrees of corrosion can also be conducted. The investigation will provide an understanding of how corrosion changes the properties of the material.

Once the change of fracture toughness of the selected metals as a function of corrosion depth is established, a stochastic model in the same form as Eq. (9) can be developed.

5 Preliminary example

Underground cast iron pipes in a typical urban city of the UK are considered here for illustration of the proposed methodology. The pipes selected have a diameter ranging from 254 to 406 mm and the wall thickness ranging from 16 to 20.3 mm correspondently. The

pipes are made of cast iron with the fracture toughness in a range of K_{Ic} = 7.66 to 9.25 MPa/m$^{0.5}$ [19]. Since the purpose of the example is to demonstrate the application of the proposed methodology, the corrosion model is taken from LI AND MAHMOODIAN [29]:

$$\mu_a(t) = 2.54t^{0.32} \tag{10a}$$

$$C_{aa}(t_i, t_j) = \lambda_a^2 \rho_a \mu_a(t_i) \mu_a(t_j) \tag{10b}$$

where λ_a is the coefficient of variation of the pit depth which is determined based on Monte Carlo simulations and ρ_a is (auto-) correlation coefficient for the pit depth $a(t)$ between two points in time.

The formula to determine the stress intensity factor is also taken from LI AND MAHMOODIAN [29] as follows,

$$K(t) = \sigma\sqrt{2\pi r}\, f(\phi, t) \tag{11}$$

where r and ϕ are the polar coordinates of the pit (crack) tip and $f(\phi,t)$ is the correction factor allowing for various geometries of the pit and structural element which also changes with time due to pit growth. Exact expressions for the stress intensity factor $K(t)$ vary and depend on the mode of fracture and geometry of the pit and element which cannot be discussed here in detail due to space limit.

The loads that are applied to the pipes over the service life are taken from design codes, i.e., BS EN 1295 (1997). Due to limited space other information used for calculation is in LI AND MAHMOODIAN [29].

With this preparation, the time-dependent probability of pipe collapse can be calculated using Eq. (2), (6) and (8) with K replacing S and K_c replacing L respectively. Typical results for each case are shown in Fig. 1 to 4. From Fig. 1 it can be seen that the probability of pipe collapse increases with the increase of the diameter of the pipe. Fig. 2 shows the same trend for internal corrosion as well, i.e., that risk of collapse increases with the increase of diameter of the pipes for internal corrosion. Fig. 3 compares the risk of collapse for pipes with external corrosion to those with internal ones. It is very clear that the likelihood of collapse for pipes with external corrosion is much higher than that for pipes with internal corrosion, in particular at initial stage. There are possibly two reasons for this. One is that the external corrosion grows faster than internal one. The other more important reason is that mechanically the corrosion defect on external surface would make it easier for the wall of the pressurised pipe to crack inwardly than that with internal corrosion defect to crack outwardly. From Fig. 4 it can be seen that the tougher the pipe is, i.e., the greater the fracture toughness, the smaller the risk of collapse.

6 Conclusion

A new methodology has been proposed in the paper for the accurate prediction of the safe life of buried pipelines, using metal water pipes as an example. The approach is to integrate material deterioration, soil mechanics, fracture mechanics and time-dependent reliability theory in analysing the behaviour and failure mechanisms of buried metal pipes subjected to simultaneous internal deterioration and external loads. From the results of an

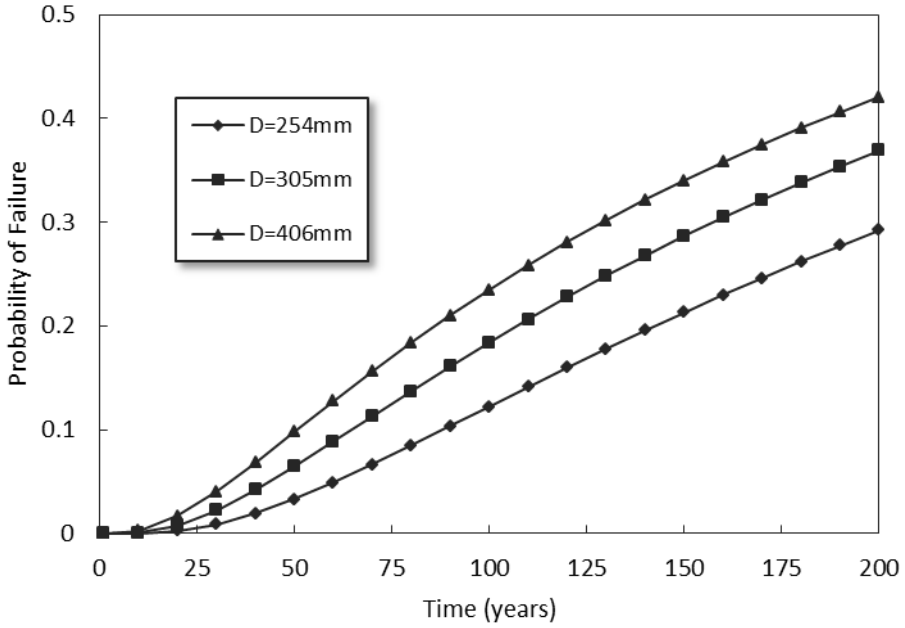

Fig. 1: Probability of pipe collapse for Case 1 with different diameters

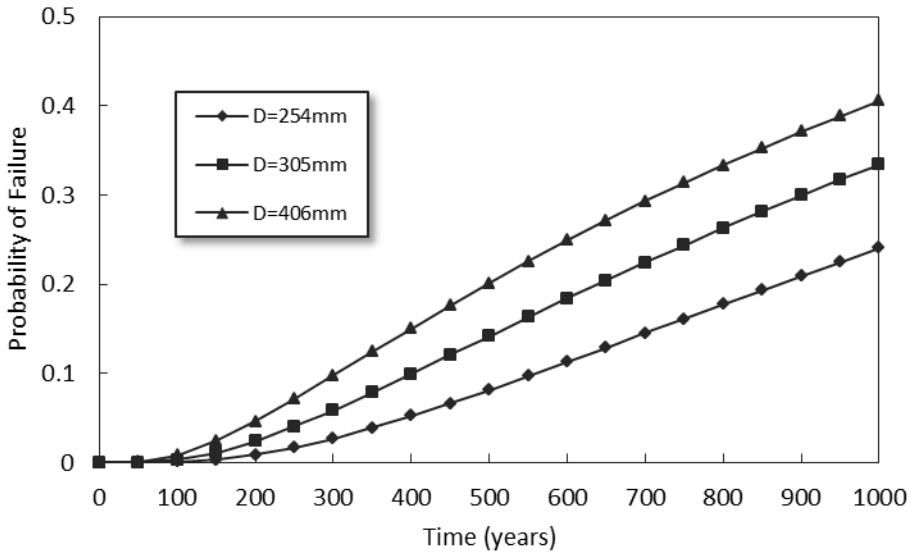

Fig. 2: Probability of pipe collapse for Case 2 with different diameters

example it has been found that the risk of pipe collapse increases with the increase of the diameter of the pipes. It has also been found that the tougher the pipe is, the smaller the risk of its collapse. It can be concluded that an integrated probabilistic approach is a very useful tool to predicting the risk of pipe collapse and its remaining service life.

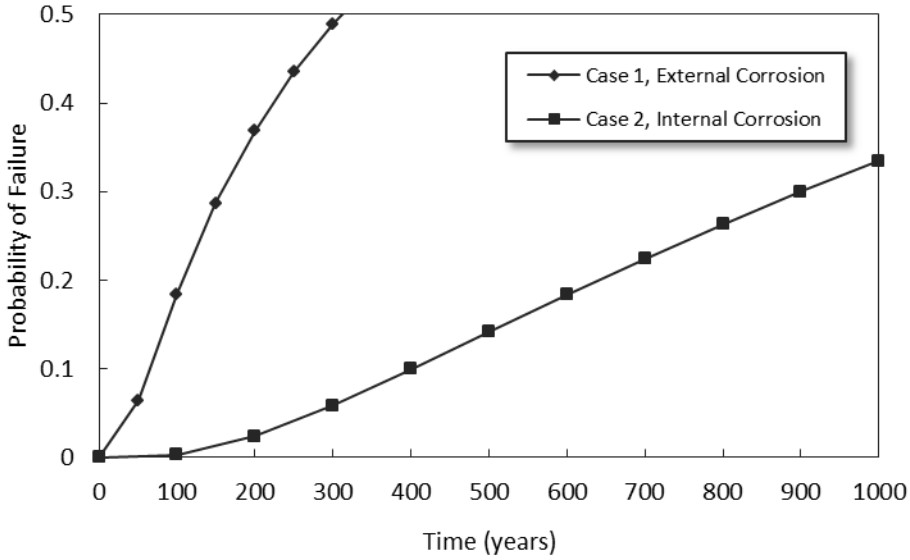

Fig. 3: Probability of pipe collapse for different cases

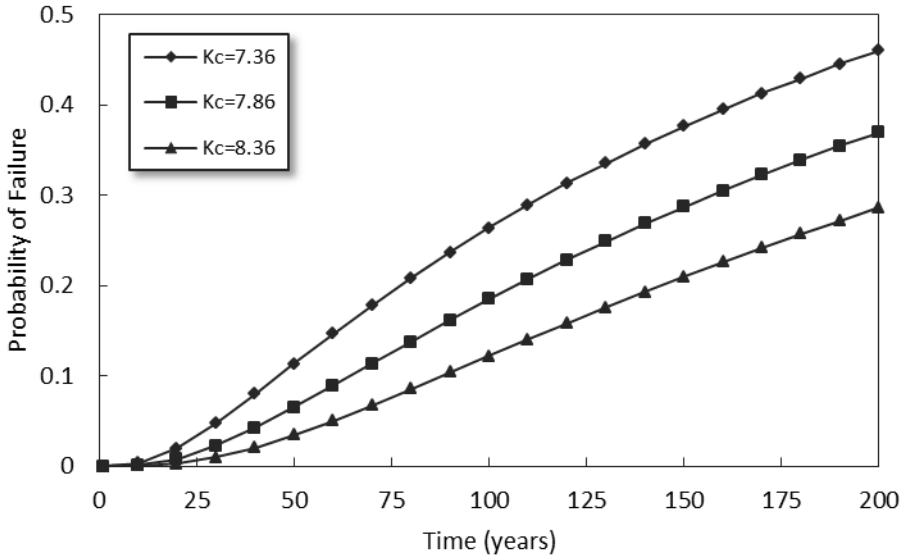

Fig. 4: Probability of pipe collapse for different K_c for external corrosion

Literature

[1] Belmonte, H.M.S., Mulheron, M., Smith, P.A., Ham, A., Wescombe, K. and Whiter, J. Weibull-based methodology for condition assessment of cast iron water mains and its application. *Fatigue and Fracture of Engineering Materials and Structures* 31(5) (2008), p. 370–385

[2] Folkman, S. (2012) *Water Main Break Rates in the USA and Canada: A Comprehensive Study*. Report (April, 2012). the Utah State University, Buried Structures Laboratory

[3] Li, C.Q. and Yang, S.T. Stress intensity factors for high aspect ratio semi-elliptical internal surface cracks in pipes. *International Journal of Pressure Vessels and Piping* 96-97 (2012), p. 13–23

[4] Makar, J.M. A preliminary analysis of failures in grey cast iron water pipes. *Engineering Failure Analysis* 7(1)(2000), p. 43–53

[5] National Water Comission Australia National Performance Report 2009-10 – Urban Water Utilities. 2010. http://archive.nwc.gov.au/library/topic/npr/npr-2009-10-urban

[6] Rajani, B., Lewandowski, J. and Margevicius, A. Failure analysis of cast iron trunk main in Cleveland, Ohio. *Journal of Failure Analysis and Prevention* 12(3) (2012), p. 217–236

[7] Ayatollahi, M.R. and Khoramishad, H. Stress intensity factors for an axially oriented internal crack embedded in a buried pipe. *International Journal of Pressure Vessels and Piping* 87(4)(2010), p. 165–169

[8] Rajani, B. and Makar, J. A methodology to estimate remaining service life of grey cast iron water mains. *Canadian Journal of Civil Engineering* 27(6) (2000), p. 1259–1272

[9] Sadiq, R., Rajani, B. and Kleiner, Y. Probabilistic risk analysis of corrosion associated failures in cast iron water mains. *Reliability Engineering and System Safety* 86(1) (2004), p. 1–10

[10] Rajani, B. and Abdel-Akher, A. Re-assessment of resistance of cast iron pipes subjected to vertical loads and internal pressure. *Engineering Structures* 45 (2012), p. 192–212

[11] Chiodo, M.S.G. and Ruggieri, C. J and CTOD estimation procedure for circumferential surface cracks in pipes under bending. *Engineering Fracture Mechanics* 77(3) (2010), p. 415–436

[12] Moore, I.D., Lapos, B. and Mills, C. Biaxial Testing to Investigate Soil–Pipe Interaction of Buried Fiber-Reinforced Cement Pipe. *Transportation Research Record: Journal of the Transportation Research Board* 1868 (2004), p. 169–176

[13] Moglia, M., Davis, P., and Burn, S. Strong exploration of a cast iron pipe failure model. *Reliability Engineering and System Safety* 93(6) (2008), p. 885–896

[14] Dehghan, A., McManus, K. and Gad, E. Probabilistic Failure Prediction for Deteriorating Pipelines: Nonparametric Approach. *Journal of Performance of Constructed Facilities* 22(1) (2008), p. 45–53

[15] Gould, S.J.F., Boulaire, F.A., Burn, S., Zhao, X.L. and Kodikara, J.K. Seasonal factors influencing the failure of buried water reticulation pipes. *Water Science and Technology* 63(11) (2011), p. 2692–2699

[16] Melchers, R.E. Long-term corrosion of cast irons and steel in marine and atmospheric environments. *Corrosion Science* 68 (2013), p. 186–194

[17] Mohebbi, H. and Li, C.Q. Experimental Investigation on Corrosion of Cast Iron Pipes. *International Journal of Corrosion* 2011 (2011), 17 p

[18] Mohebbi, H. and Li, C.Q. Application of Fracture Mechanics in Reliability Analysis of Corrosion Affected Cast Iron Water Mains. *Proc. 12th Int. Conf. on Durability of Building Materials and Components.* 12-15 April. Porto. (on CD), 2011

[19] Marshall, P. *The Residual Structural Properties of Cast Iron Pipes – Structural and Design Criteria for Linings for Water Mains*. UK Water Industry Research. 2001

[20] Hertzberg, R.W. *Deformation and Fracture Mechanics of Engineering Materials*. Chichester, Wiley, 1996

[21] CSIRO and the Bureau of Meteorology. *Climate change in Australia: technical report 2007*. 2007

[22] Rice, S.O. Mathematical analysis of random noise. *Bell System Technical Journal* 24 (1945), p. 46–156

[23] Mahmoodian, M. and Li, C.Q. Structural System Reliability Analysis of Cast Iron Water Mains. *Proceeding 2nd Iranian Conference on Reliability Engineering.* 24–26, October 2011. Tehran, Iran, 2011

[24] Hasan, M.S., Setunge, S.T., Molyneaux, T.C.K. and Law, D.W. Determination of life expectancy of concrete septic tanks under biogenic sulphuric acid corrosion. *Futures in Mechanics of Structures and Materials – Proceedings of the 20th Australasian Conference on the Mechanics of Structures and Materials, ACMSM20.* Toowoomba, Queensland, Australia, 2008, p. 519–526

[25] Dignan, M. and Li, C.Q. Experimental Investigation into the Effect of Fly Ash on the Fresh Properties of Self-Compacting Concrete. *Proc. 2nd International Conference on Structural and Construction Engineering,* . 23–26, September. Rome, 2003

[26] Kong, D., Setunge, S., Molyneaux, T., Zhang, G. and Law, D. Australian seaport infrastructure resilience to climate change. *Advanced Materials Research* 238 (2012), p. 350–357

[27] Zhou, A.N., Sheng, D., Scott, S.W. and Gens, A. Interpretation of unsaturated soil behaviour in the stress-saturation space, I: Volume change and water retention behaviours. *Computers and Geotechnics* 43 (2012), p. 178–187

[28] Melchers, R.E. *Structural Reliability Analysis and Prediction*. John Wiley & Sons, 1999

[29] Li, C.Q. and Mahmoodian, M. Risk Based Service Life Prediction of Underground Cast Iron Pipes Subjected to Corrosion. *International Journal of Reliability Engineering and System Safety* (2013) (to appear)

An efficient solution of space-variant reliability problems

Diego Lorenzo Allaix, Vincenzo Ilario Carbone, Giuseppe Mancini
Department of Structural, Geotechnical and Building Engineering,
Politecnico di Torino, Torino
diego.allaix@polito.it, vincenzo.carbone@polito.it, giuseppe.mancini@polito.it

Abstract: The topic of this paper is the solution of reliability problems where failure is influenced by the spatial random fluctuations of loads or material properties. A new and efficient approach is proposed in this paper. The Karhunen-Loève series expansion is combined with the FEM for the discretization of continuous random fields. Then, an efficient approach based on the FORM is proposed for the estimation of the effect of random spatial variability of structural properties or loads on the structural reliability. The procedure is applied to the assessment of a deteriorated structure.

Keywords: homogenous random fields, Karhunen-Loeve series expansion, FORM, space-variant reliability problems.

1 Introduction

Often the reliability problems concern structures where the potential locations of failure are known in advance. The reliability assessment of beams of buildings with respect to the ULS is an example. Given the relevant load cases, the critical regions of the structure can be easily identified. Under these circumstances, the reliability problem is called *point-in-space reliability problem*.

However, in many reliability problems, failure can happen everywhere in the structure. As an example, in case of reinforced concrete beam subject to chloride ingress, each section could be a potential location where deterioration takes place. If all input parameters are described by random variables, the probability of deterioration of the whole beam is equal to the one of a single section. However, durability problems are significantly affected by the random spatial variability of the input parameters. When one or more parameters are modelled by random fields, the problem is termed *space-variant reliability problem*. It should be observed that durability problems are time-dependent, at least because the resistance of the structure decreases over time. However, these time-variant and space-variant reliability problems can be reduced to point-in-time and space-variant problems. Space-variant reliability problems were first formulated and solved by Der Kiureghian et al. [1], on the analogy of time-variant reliability problems. An upper-bound to the probability of failure can be obtained using the out-crossing approach and the first-order reliability method (FORM).

The point-to-point variation of structural properties is described by means of the random field theory [2]. The so-called random field discretization of continuous random fields is necessary to perform a reliability investigation. The random field discretization is an approximation of the random field by means of a finite set of random variables. The computational reliability methods, in fact, operate on a finite set of random variables. Thus, the random field discretization takes the probabilistic model as input and it reduces the random fields to a set of random variables which are contained in vector **X**.

The novelty of the paper consists of an efficient combination of the Karhunen-Loève series expansion, for the discretization of random fields, and the FORM for the solution of point-in-time and space-variant problems. The approach is presented in the case of Gaussian random fields. The proposed reliability formulation allows one to estimate the reliability for high truncation orders of the Karhunen-Loève series expansion from the results of a single reliability analysis performed with a low truncation order.

2 Karhunen-Loeve series expansion of random fields

A structural property or an action applied to a structure is considered to vary randomly at different points of the structure. It can be modelled by a random field $w(z)$ with mean value $\mu_w(z)$ and finite variance $\sigma_w^2(z)$, where z denotes the coordinates of a point of the structure. The truncated Karhunen-Loève series expansion is chosen within the discretization methods to approximate the random field [3]. The truncated Karhunen-Loève expansion of the random field is written as [4]:

$$\hat{w}(z) = \mu_w(z) + \sum_{i=1}^{M} \sqrt{\lambda_i}\, f_i(z)\, \xi_i \tag{1}$$

where $\{\lambda_i\}_{i=1}^{M}$ and $\{f_i(z)\}_{i=1}^{M}$ are the eigenvalues and eigenfunctions of the covariance function $C_{ww}(z_1,z_2)$ of the random field, respectively, and $\{\xi_i\}_{i=1}^{M}$ are uncorrelated zero mean random variables. These variables are independent Gaussian random variables in the case of Gaussian random fields. The eigenvalues $\{\lambda_i\}_{i=1}^{M}$ and eigenfunctions $\{f_i(z)\}_{i=1}^{M}$ are the solution of the following Fredholm integral eigenvalue problem [4]:

$$\int_D C_{ww}(z_1, z_2) f_i(z_2)\, dz_2 = \lambda_i\, f_i(z_1) \tag{2}$$

where D is the domain of the structure and z_1 and z_2 represent the coordinates of two points of the structure. The variance and the covariance functions of the truncated series are:

$$\mathrm{Var}[\hat{w}(z)] = \hat{C}_{ww}(z,z) = \sum_{i=1}^{M} \lambda_i\, f_i{}^2 z \tag{3}$$

$$\mathrm{Cov}[\hat{w}(z_1), \hat{w}(z_2)] = \hat{C}_{ww}(z_1,z_2) = \sum_{i=1}^{M} \lambda_i\, f_i(z_1)\, f_i(z_2) \tag{4}$$

As discussed in [5], the accuracy of the discretization of homogeneous random fields is assessed by means of the global discretization error estimator $\bar{\varepsilon}_{M,\sigma_w^2}$, which represents the mean difference between the variance $\sigma_w^2(z)$ and the approximate variance $\mathrm{Var}[\hat{w}(z)]$ over the geometrical domain *D* of the structure. In case of 1D domains, the error estimator is:

$$\bar{\varepsilon}_{M,\sigma_w^2} = 1 - \frac{\sum_{i=1}^{M} \lambda_i}{L_D\, \sigma_w^2} \tag{5}$$

where L_D is the length of the domain *D* of the structure. The truncation order is selected in order to keep the discretization error $\bar{\varepsilon}_{M,\sigma_w^2}$ lower than a prescribed value. The accuracy of the random field approximation and the number of limit state function evaluations increase as the truncation order M grows [6].

In the present paper, the eigenvalues $\{\lambda_i\}_{i=1}^{M}$ and eigenfunctions $\{f_i(\mathbf{z})\}_{i=1}^{M}$ are computed with a robust and efficient numerical procedure based on the finite element method, as discussed in [5, 7−8] for 1D and 2D application examples.

3 Space-variant reliability problems

Let consider a 1D point-in-time and space-variant reliability problem defined in terms of a random vector **X** (describing the input random parameters) and a limit state function *g*. Through a probabilistic transformation, the random vector **X** is transformed into a vector **U** of standard normal random variables. The probability of failure is defined as the probability that failure takes place at any point of the domain *D*:

$$P_f = P[g(\mathbf{u}, z) \le 0] \quad \forall z \in D \tag{6}$$

Due to computational issues, the out-crossing approach [1, 9, 10] is usually resorted. The probability of failure can be bounded as follows [9]:

$$\max_{z \in D} P_f(z) \le P_f \le P_f(z_0) + \int_D \nu(z)\,\mathrm{d}z \tag{7}$$

where $P_f(z)$ is the point-in-space failure probability. The point z_0, where the probability $P_f(z_0)$ is computed, is chosen in order to keep the upper bound to the probability of failure P_f as narrow as possible. Hence z_0 is chosen by minimizing the point-in-space probability of failure $P_f(z)$ with respect to *z*.

The term $\nu(z)$ is the out-crossing rate [1]. Each crossing is associated with a point *z* such that $g(\boldsymbol{u},z) > 0$ and with a point $z + \Delta z$ close to *z* such that $g(\boldsymbol{u},z + \Delta z) \le 0$. The out-crossing rate is defined as the following limit:

$$\nu(z) = \lim_{\Delta z \to 0} \frac{P[(g(\mathbf{u}, z) > 0) \cap (g(\mathbf{u}, z + \Delta z) \le 0)]}{\Delta z} \tag{8}$$

The numerator of the out-crossing rate is computed as the solution of a parallel system reliability problem with two components. This kind of problem is solved using the FORM.

Two separate point-in-space reliability analyses are performed at z and $z + \Delta z$, leading to the reliability indices $-\beta(z)$ and $\beta(z + \Delta z)$ and the sensitivity vectors $\boldsymbol{\alpha}(z)$ and $\boldsymbol{\alpha}(z + \Delta z)$. The reliability index associated with the event $g(\boldsymbol{u},z) > 0$ is $-\beta(z)$, while $\beta(z + \Delta z)$ concerns the event $g(\boldsymbol{u},z + \Delta z) \le 0$. The numerator of Eq. (8) is then estimated as [1, 10]:

$$P\left[\left(g(\mathbf{u},z)>0\right)\cap\left(g(\mathbf{u},z+\Delta z)\le 0\right)\right]=\Phi_2\left(\beta(z),-\beta(z+\Delta z),\boldsymbol{\rho}(z,z+\Delta z)\right) \tag{9}$$

where Φ_2 is the bi-normal cumulative distribution function and $\boldsymbol{\rho}(z,z+\Delta z)$ is the correlation matrix between the two events $g(\boldsymbol{u},z) > 0$ and $g(\boldsymbol{u},z + \Delta z) \le 0$. This matrix is computed as:

$$\boldsymbol{\rho}(z,z+\Delta z)=-\boldsymbol{\alpha}(z)\boldsymbol{\alpha}(z+\Delta z)^T \tag{10}$$

In practice, domain D is discretized by a set of points and a reliability analysis is performed for each one. The results are used to evaluate Eq. (9) and then the out-crossing rate is integrated over domain D.

By means of FORM, Eq. (7) is rewritten in terms of the reliability index β and the cumulative distribution function Φ of standard normal random variables:

$$\max_{z\in D}\Phi^{-1}\left(-\beta(z)\right)\le P_f\le\Phi^{-1}\left(-\beta(z_0)\right)+\int_D\lim_{\Delta z\to 0}\frac{\Phi_2\left(\beta(z),-\beta(z+\Delta z),\boldsymbol{\rho}(z,z+\Delta z)\right)}{\Delta z}\,\mathrm{dz} \tag{11}$$

It is well known that the probability of failure estimated by the FORM may differ from the exact one due to the non-linearity of the LSF. Once the design points corresponding to $\beta(z)$ and $\beta(z + \Delta z)$ have been located, the probability of failure can be accurately estimated by means of more advanced reliability methods [11].

4 Efficient reliability assessment in case of random spatial variability

As already mentioned, the truncation order M of the Karhunen-Loeve series expansion has an effect on the computational effort of the reliability analysis. The number of limit state function evaluations is an increasing function of the number of random variables in the case of the FORM [6, 12]. Therefore, as the discretization accuracy is improved, also the effort of the probabilistic investigation increases. It might be very useful to choose the optimal truncation order of the Karhunen-Loève series expansion on the basis of two criteria: the discretization accuracy and the effect of the truncation order on the reliability index.

4.1 Analytical derivation

For the sake of simplicity, let us consider a reliability problem involving only a homogeneous Gaussian random field. The variation of the reliability index due to the truncation order of the Karhunen-Loève series expansion can be efficiently estimated as follows. Let us suppose that the reliability analysis has been solved for a given truncation order M_1, which leads to the reliability index β_{M1}:

$$\beta_{M1} = -\frac{\nabla_{\mathbf{u}}^{M1} g^T \mathbf{u}_{M1}^*}{\left(\nabla_{\mathbf{u}}^{M1} g^T \nabla_{\mathbf{u}}^{M1} g\right)^{1/2}} \tag{12}$$

where $\nabla_{\mathbf{u}}^{M1} g$ is the gradient vector of the limit state function with M_1 entries. The vector $\mathbf{u}_{M1}^*$ contains the design values of the variables $\{\xi_i\}_{i=1}^{M1}$ of the Karhunen-Loève series expansion.

It is now interesting to estimate of the reliability index β_{M2} for a higher truncation order M_2 ($M_2 > M_1$). A new reliability analysis has to be solved entirely. The reliability index β_{M2} is computed as:

$$\beta_{M2} = -\frac{\nabla_{\mathbf{u}}^{M2} g^T \mathbf{u}_{M2}^*}{\left(\nabla_{\mathbf{u}}^{M2} g^T \nabla_{\mathbf{u}}^{M2} g\right)^{1/2}} \tag{13}$$

where $\nabla_{\mathbf{u}}^{M2} g$ is the gradient vector of the limit state function at $\mathbf{u}_{M2}^*$ with M_2 entries. An approximation of β_{M2} can be obtained by linearization of the limit state function at the point $\widetilde{\mathbf{u}}_{M2}^*$ which is defined as follows:

$$\widetilde{\mathbf{u}}_{M2}^* = \left[\mathbf{u}_{M1}^*, 0, 0..., 0\right]^T \tag{14}$$

The first M_1 components of this vector are the elements of the vector $\mathbf{u}_{M1}^*$, while the remaining $M_2 - M_1$ entries are equal to zero. The point $\widetilde{\mathbf{u}}_{M2}^*$ belongs to the limit state function, since it is coincident with the $\mathbf{u}_{M1}^*$. The limit state function is replaced by the tangent hyper-plane at the point $\widetilde{\mathbf{u}}_{M2}^*$ and the approximate reliability index $\widetilde{\beta}_{M2}$ is the minimum distance to the origin of the **U** space:

$$\widetilde{\beta}_{M2} = -\frac{\widetilde{\nabla}_{\mathbf{u}}^{M2} g^T \widetilde{\mathbf{u}}_{M2}^*}{\left(\widetilde{\nabla}_{\mathbf{u}}^{M2} g^T \widetilde{\nabla}_{\mathbf{u}}^{M2} g\right)^{1/2}} \tag{15}$$

The numerators of Eqs. (12–15) are equivalent. Thus, it is possible to derive $\widetilde{\beta}_{M2}$ from β_{M1} using Eq. (16):

$$\widetilde{\beta}_{M2} = \beta_{M1} \frac{\left(\nabla_{\mathbf{u}}^{M1} g^T \nabla_{\mathbf{u}}^{M1} g^T\right)^{1/2}}{\left(\widetilde{\nabla}_{\mathbf{u}}^{M2} g^T \widetilde{\nabla}_{\mathbf{u}}^{M2} g^T\right)^{1/2}} \tag{16}$$

The practical application of Eq. (16) is explained as follows. A reliability analysis is performed by selecting the truncation order M_1 (the unit value is assumed in the application examples). The reliability index β_{M1}, the gradient vector $\nabla_{\mathbf{u}}^{M1} g$ and the design point $\mathbf{u}_{M1}^*$ are obtained from the reliability analysis. At this point an approximation of the reliability index is computed by means of Eq. (16) for increasing values of the truncation order. It is necessary to compute only the $M_2 - M_1$ additional entries of the gradient vector $\widetilde{\nabla}_{\mathbf{u}}^{M2} g$.

The variation of the reliability index can be explained in terms of the improvement in the approximation of the random field. The limit state function is evaluated after discretizing

the structure in N elements. The values of the random structural property can be assigned to each element by means of Eq. (1). For example, the midpoint of each finite element of the structural mesh is often considered as the point where the realization $\hat{w}(\mathbf{z})$ of the random field is evaluated. Therefore, N random variables $\mathbf{Y}$ can be obtained from the random vector $\mathbf{U}$. It can be shown that Eq. (16) can be rewritten as:

$$\widetilde{\beta}_{M2} = \beta_{M1} \frac{\left(\nabla_{\mathbf{y}} g^T \mathbf{C}_{M1} \nabla_{\mathbf{y}} g\right)^{1/2}}{\left(\nabla_{\mathbf{y}} g^T \mathbf{C}_{M2} \nabla_{\mathbf{y}} g\right)^{1/2}} \tag{17}$$

where $\mathbf{C}_{M1}$ and $\mathbf{C}_{M2}$ are the covariance matrices of the $\mathbf{Y}$ variables obtained with M_1 and M_2 random terms of the Karhunen-Loeve series expansion. This simple formula shows that an increment in the truncation order may lead to a change in the reliability index, due to the improvement in the approximated covariance of the random field. However, the relative variation of the reliability index can also depend to a great extent on the gradient of the limit state function.

4.2 Example

As an example, let us consider a 6 m long cantilever beam with a rectangular cross section subjected to uniformly distributed loads [13]. The serviceability limit state function with respect to the deflection of the free end is formulated as follows:

$$g(\mathbf{X}) = \frac{L}{325} - v_{free\,end} \tag{18}$$

where L is the length of the beam and $v_{free\ end}$ is the deflection of the free end. The elastic modulus and the load are deterministically assumed equal to 26000 N/mm^2 and 1 kN/m, respectively. The depth of the cross-section is modelled by a Gaussian random field with mean equal to 0.25 m and standard deviation of 0.0375 m. The following covariance function is considered:

$$C_{ww}(z_1, z_2) = \sigma_w^2 \exp\left[-\left(\frac{|z_1 - z_2|}{0.5L}\right)\right] \tag{19}$$

Let consider M_1 equal to one. The limit state function Eq. (18) is plotted in Fig. 1. It can be observed that it is equal to zero only for one value of ξ_1, that corresponds to the design point $\mathbf{u}^*_{M1} = [-3.39]$. At this point M_2 equal to two is considered. Fig. 3 shows the limit state function in terms of ξ_1 and ξ_2. At this point, the gradient vector $\nabla^{M2}_{\mathbf{u}} g$ is computed at point $\widetilde{\mathbf{u}}^*_{M2}$, which is coincident with $\mathbf{u}^*_{M1}$. Then, the limit state function is linearized at point $\widetilde{\mathbf{u}}^*_{M2}$. The minimum distance $\widetilde{\beta}_{M2}$ from the origin is equal to 2.92.

If reliability problem is entirely solved considering two random variables, the design point $\mathbf{u}^*_{M2} = [-2.39, 1.62]^T$ is obtained. The reliability index β_{M2} equal to 2.89 follows from Eq. (13). The approximation $\widetilde{\beta}_{M2}$ of β_{M2} is very good in this case. Clearly, the accuracy of Eq. (17) depends on the type of limit state function, since a linearization is involved in the evaluation of $\widetilde{\beta}_{M2}$.

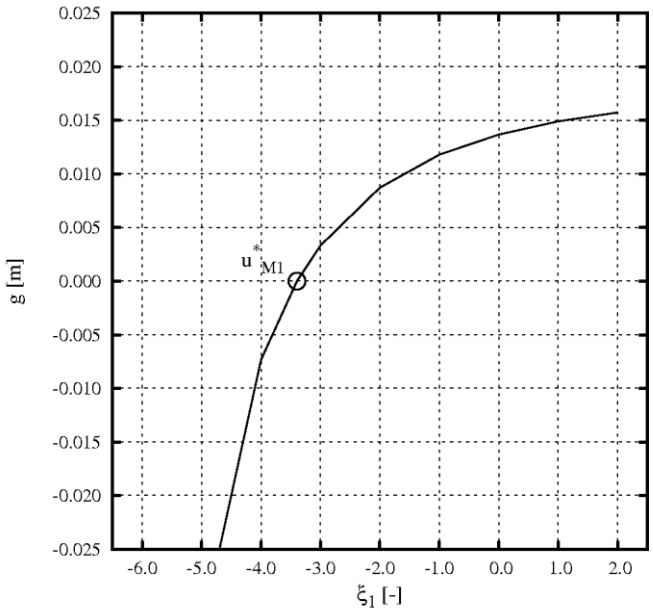

Fig. 1: Limit state function – 1 random variable

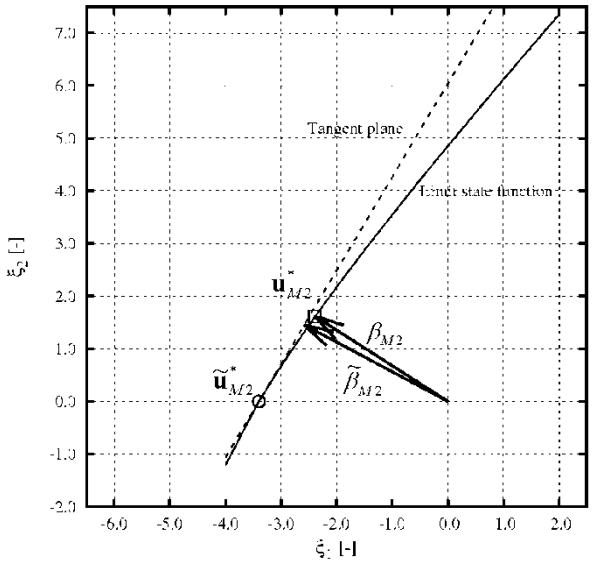

Fig. 2: Limit state function – 2 random variables

4.3 Procedure for space-variant reliability problems

The variation of the lower and upper bounds to the probability of failure P_f due to the truncation order of the Karhunen-Loeve series expansion are now investigated. The objective is to assess these bounds with a reduced computational effort. Three steps are necessary.

First, a set of reliability analyses is performed at each selected point of the domain D. A low value of the truncation order of the Karhunen-Loeve series expansion is assumed (i.e. $M_1 = 1$). The outcomes **y** of the structural property described by the random field are computed at the design point **u*** by means of Eq. (1) for each point of the structure. The gradi-

ent vector $\nabla_y g$ of the limit state function at each point is estimated by means of the finite difference method and the covariance matrix $\mathbf{C}_{M1}$ is computed by means of Eq. (4).

Second, the truncation order is increased ($M_2 > M_1$ is considered). The covariance matrix $\mathbf{C}_{M2}$ is computed by means of Eq. (4). The knowledge of the reliability index β_{M1}, the gradient vector $\nabla_y g$ and the covariance matrices $\mathbf{C}_{M1}$ and $\mathbf{C}_{M2}$ allows us to estimate the reliability index β_{M2} through Eq. (17). At this point, the lower bound to P_f in Eq. (11) can be easily updated with respect to the truncation order of the Karhunen-Loeve series expansion.

Third, the sensitivity vectors $\boldsymbol{\alpha}(z)$ and $\boldsymbol{\alpha}(z+\Delta z)$ are updated in order to apply Eq. (10). Therefore, the update of the reliability indices $\beta(z)$, $\beta(z+\Delta z)$ and the correlation matrix $\boldsymbol{\rho}(z, z+\Delta z)$ do not require to solve again a set of reliability analyses. Finally, the updated out-crossing rate is integrated over the domain D and the updated upper bound to the probability of failure is obtained.

5 Application example

This example concerns the reliability assessment of a deteriorated reinforced concrete beam [14] at 50 years after construction. The objective of the investigation is the upper bound to the probability that, anywhere within the beam, the resisting bending moment is lower than the bending moment due to the applied loads. The structural scheme is shown in Fig. 3.

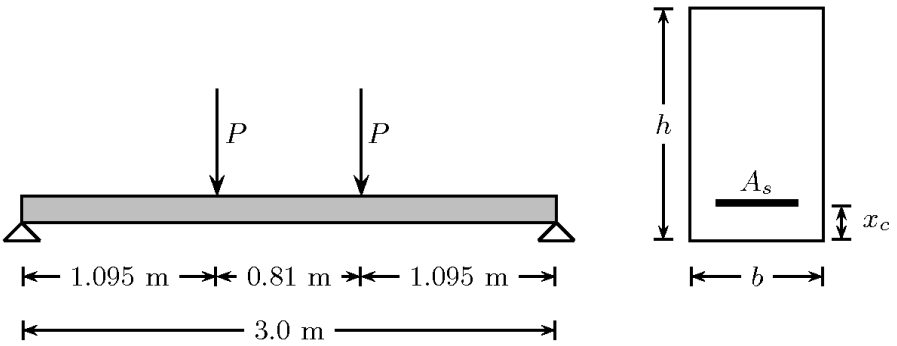

Fig. 3: Beam and loading condition

The beam is 3 m long and it is loaded by a symmetric loading condition consisting of two forces P. A rectangular cross-section with base b equal to 0.25 m and width of 0.40 m is considered. A reinforcement steel area A_s equal to 1185 mm^2 is provided.

The chloride-induced corrosion of the reinforcement bars leads to decrement in the load carrying capacity of the beam. The deterioration of the reinforced concrete beam is described by means of two physical models: the chloride penetration and the steel corrosion models.

The chloride penetration model is based on the assumption that diffusion of chlorides is the main transport mechanism of chlorides into the concrete cover [15−16]. The chloride con-

tent $c(x,t)$ at depth x from the concrete surface and after a period of t years of exposure is derived from the well-known Fick's 2nd law of diffusion [14]:

$$c(x,t) = c_s \left[1 - erf \left(\frac{x}{2\sqrt{\theta\, D \left(\frac{t_r}{t} \right)^n t}} \right) \right] \tag{20}$$

where:

c_s is the chloride content on the concrete surface;

erf is the error function;

θ is the model uncertainty;

D is the diffusion coefficient;

t_r is a reference period;

n takes into account the time dependency of the diffusion process.

It is assumed that corrosion of reinforcement begins when the chloride content at the level of the reinforcement exceeds the so-called critical value c_{cr}.

The model of steel corrosion describes the deterioration of reinforcing steel. The reduction of the reinforcement area and the yield stress are considered hereafter. The reinforcement area after a period of time t is written as [14]:

$$A_s(t) = A_{s0}(1 - \alpha(t)) \tag{21}$$

where A_{s0} is the initial area and the parameter $\alpha(t)$ is defined as:

$$\alpha(t) = \begin{cases} 0 & \text{if } t < t_{init} \\ \dfrac{t - t_{init}}{t_{corr}} \left(2 - \dfrac{t - t_{init}}{t_{corr}} \right) & \text{if } t_{init} \le t < t_{corr} \\ 1 & \text{if } t \ge t_{corr} \end{cases} \tag{22}$$

where t_{init} and t_{corr} are, respectively, the time of corrosion initiation and the period from initiation to total deterioration.

It is recognized that other models different from these could be applied. The reader can refer to [17] for more detailed models. However, it should be kept in mind that the exact way of modelling is not the key-point of the paper. The limit state function is defined as follows:

$$g(\mathbf{X},t) = M_{res}(\mathbf{X},t) - M_{load}(\mathbf{X},t) \tag{23}$$

where M_{res} and M_{load} are the resisting and the soliciting bending moments, respectively. A probabilistic model [14] concerning the chloride surface content c_s, the critical chloride content c_{cr}, the diffusion coefficient D, the concrete cover x_c, the load P, the time to total deterioration t_{corr}, the concrete compressive strength of concrete f_c and the yield stress of

steel f_y is formulated. This model is listed in Table 1. The diffusion reference period t_r is assumed as a deterministic parameter, equal to 0.10 years.

Tab. 1: Probabilistic model

Variable	Description	Distribution	Mean value	Std. dev.
c_s [-]	Chloride surface content	Lognormal	0.0095	0.0019
c_{cr} [-]	Critical chloride content	Normal	0.0016	0.00016
D [mm^2/yr]	Diffusion coefficient	Lognormal	30.0	10.5
θ [-]	Model uncertainty	Lognormal	1.0	0.2
n [-]	Exponent	Lognormal	0.10	0.025
x_c [mm]	Concrete cover	Normal	30.0	4.5
P [kN]	Load	Gumbel	104.4	8.0
t_{corr} [yr]	Time of total deterioration	Lognormal	500.0	175.0
f_c [MPa]	Concrete compr. strength	Lognormal	43.0	5.2
f_y [MPa]	Steel yield stress	Lognormal	573.0	45.8

The concrete cover is modelled by a homogenous Gaussian random field with a square exponential covariance function:

$$C_{ww}(z_1, z_2) = \sigma_w^2 \exp\left(-\frac{|z_1 - z_2|^2}{L_c^2}\right) \tag{24}$$

where the correlation length L_c is assumed equal to 0.75 m [18]. The global discretization error $\bar{\varepsilon}_{M,\sigma_w^2}$ (Eq. (6)) is plotted in Fig. 4 as a function of the truncation order M. Moreover, it can be observed that the first four eigenvalues represent about 95% of the variance of the random field.

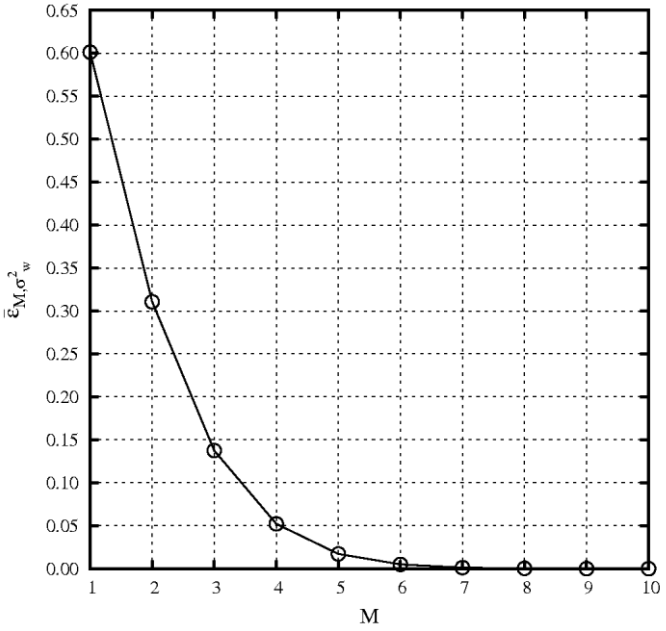

Fig. 4. Global discretization error $\bar{\varepsilon}_{M,\sigma_w^2}$

The point-wise variance (Eq. (4)) normalized to the variance of the random field is plotted in Fig. 5 for M equal to 1, 4, 6 and 10. It can be noticed that the variance tends to be uni-

formly distributed as the truncation order *M* increases. Furthermore, it can be observed that the approximation of the variance is very accurate when the truncation order is equal or larger than 6.

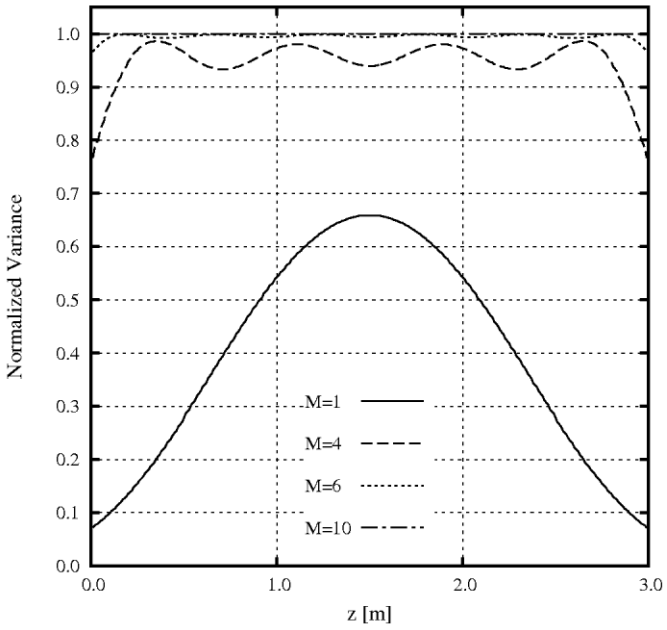

Fig. 5. Point-wise normalized variance

The upper and lower bounds to the probability of failure are computed according to Eq. (16). Their variation with the increase of the truncation order of the Karhunen-Loeve series expansion of the random field is plotted in Fig. 6 for the first ten terms of the series expansion. The so-called "exact" result is obtained through a complete reliability analysis which considers M random variables for the random field discretization. These two approaches are compared in order to assess the accuracy of the approximation.

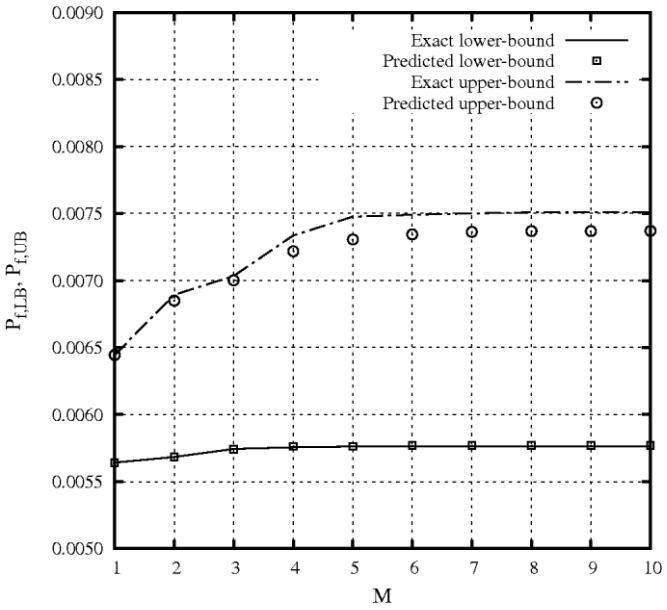

Fig. 6. Lower and upper bounds to the probability of failure

Fig. 6 shows that the estimated upper bound to the probability of failure is almost constant when the truncation order is equal or larger than 6. This result is directly related to the approximation of the variance of the random field. It can also be observed that the lower bound is less affected by the truncation order of the Karhunen-Loeve series expansion than the upper-bound, because the largest point-in-space probability of failure takes place at the midspan of the beam. The difference between the lower and the upper bound means that the probability of failure of the space-variant problem is larger with respect to the point-in-space problem. In terms of accuracy, it can be observed that the proposed approach is able to approximate correctly both the lower and the upper bounds to the probability of failure. The maximum error is less than 2% with respect to the so-called exact upper bound.

6 Conclusions

A procedure for the solution of space-variant reliability problems is present in the paper. The input parameters are modelled by random variables and fields. An upper-bound to the probability of failure is obtained using the out-crossing approach. The out-crossing rate is formulated as a parallel-system reliability problem, which is solved by means of the FORM. The solution of such reliability problem depends on the truncation order of the Karhunen-Loeve series expansion of the random fields. A simple formula, which allows one to extrapolate the reliability index is presented in the paper. Its application to the assessment of a corroded concrete beam leads to an error less than 2% with respect to the upper-bound to the probability of failure.

Literature

[1] Der Kiureghian, A., Zhang, Y. Space-variant finite element reliability analysis. *Computer Methods in Applied Mechanics and Engineering* 168 (1999), p. 173–183

[2] Vanmarcke, E. *Random fields, analysis and synthesis*. Cambridge: The MIT Press, 1983

[3] Stefanou, G. The stochastic finite element method: Past, present and future. *Computer Methods in Applied Mechanics and Engineering* 198 (2009), p. 1031–1051

[4] Ghanem, R.G., Spanos, P.D. *Stochastic finite elements: a spectral approach*. New York: Springer-Verlag, 1991

[5] Allaix, D.L., Carbone, V.I. Numerical discretization of stationary random processes. *Probabilistic Engineering Mechanics* 25 (2010), p. 332–347

[6] Sudret, B., Der Kiureghian, A. Comparison of finite element reliability methods. *Probabilistic Engineering Mechanics* 17 (2002), p. 337–348

[7] Allaix, D.L., Carbone, V.I. Adaptive discretization of 1D homogeneous random fields. In: *Proceedings of the Joint ESREL and SRA-Europe Conference*, 2008

[8] Allaix, D.L., Carbone, V.I. Development of a numerical tool for random field discretization. *Advances in Engineering Software* 51 (2012), p. 10–19

[9] Rackwitz,R. Reliability analysis − a review and some perspectives. *Structural Safety* 23 (2001), p. 365–395

[10] Andrieu-Renaud, C., Sudret, B., Lemaire, M. The PHI2 method: a way to compute time-variant reliability. *Reliability Engineering and System Safety* 84 (2004), p. 75–86

[11] Allaix, D.L., Carbone, V.I., Mancini G. Advanced Response Surface Method for Structural Reliability. *Proceedings of the Thirteenth International Conference on Civil, Structural and Environmental Engineering Computing*. Civil-Comp Press, 2011

[12] Waarts, P.H., Vrouwenvelder, A.C.W.M. Stochastic finite analysis of steel structures *Journal of Construction Steel Research*, 52 (1999), p. 21–32

[13] Rajashekhar, M.R., Ellingwood, B.R. A new look at the response surface approach for reliability analysis. *Structural Safety* 12 (1993), p. 205–220

[14] Vrouwenvelder, T., Schieβl, P. Durability aspects of probabilistic ultimate limit state design. *Heron* 44 (1999), p. 19–99

[15] Engelund, S., Sørensen, J.D. A probabilistic model for chloride-ingress and initiation of corrosion in reinforced concrete structures. *Structural Safety* 20 (1998), p. 69–89

[16] Bertolini, L. Steel corrosion and service life of reinforced concrete structures. *Structure and Infrastructure Engineering* 4 (2008), p. 123–137

[17] Duracrete. *Probabilistic performance based durability design of concrete structures*. The European Union – Brite Euram, 2000

[18] Joint Committee on Structural Safety. Probabilistic Model Code. Internet publication, 2001, www.jcss.ethz.ch

Life cycle costs of selected concrete repair methods demonstrated on chloride contaminated columns

Fritz Binder[a]

[a]Institute of Structural Engineering
University of Natural Resources and Applied Life Sciences, Vienna
[a]ASFiNAG Service GmbH, Vienna
fritz.binder@asfinag.at

Abstract: Among the approximately 5,000 bridges which are maintained by the infrastructure operator ASFiNAG a total number of 1,500 objects are overpasses. Particularly their substructures are subject to increased chloride contamination. Sooner or later this results in damage to the infrastructure and, hence, in a reduced service life. To ensure that the existing budgetary resources are best used to preserve the optimal structural condition, the costs and future effects of repair methods must be known. Based on preliminary surveys, the condition of the investigated structural component is assessed. Following this, a preselection of adequate and sustainable repair methods according to EN 1504 can be made. Based on an example, repair strategies are examined for their economical relevance (Life Cycle Costs (LCC)). Only this permits a comparison of different (repair) strategies, thereby optimizing the available financial resources. The procedure presented in this paper shows that it is possible to find an objective basis for choosing the optimal repair method and its time of application.

Keywords: maintenance, repair principles, repair methods, condition assessment, existing concrete structures

1 Chloride induced corrosion

1.1 General Aspects

Especially near bridges the danger of corrosion induced by clorides due to deicing salt is very high. In general, the reinforcement in reinforced concrete structures is sufficiently protected from corrosion by a passive layer on the steel bar surface due to the highly alkaline solution in the concrete pores (pH values from 12 to 14) [20]. Due to environmental influences this passive layer on the steel is destroyed over time. Foundations are typically affected by corrosion by the chloride containing spray-water originating from deicing salts [2], [7]. When the chlorides reach the reinforcement depth, the steel bars locally loose the passive layer. This areas now offers points of attack for corrosion. The metal dissolution by electrochemical corrosion is increased by a high electrolytic conductivity of the concrete covering the reinforcement. A characteristic feature of this process is the flow of galvanic currents. The corrosion process of steel in concrete can be summarised by the following electrochemical reaction [1] which is composed by four partial processes:

1. The oxidation of iron (anodic process), that discharges electrons in the metallic phase and gives rise to the formation of iron ions ($Fe \longrightarrow Fe^{2+} + 2\,e^{-}$). The consecutive hydrolysis produces acidity ($Fe^{2+} + 2\,H_2O \longrightarrow Fe(OH)_2 + 2\,H^{+}$).
2. The reduction of oxygen (cathodic process) that consumes electrons and produces alkalinity ($O_2 + 2\,H_2O + 4\,e^{-} \longrightarrow 4\,OH^{-}$)
3. The transport of electrons within the metal from the anodic regions where they become available, to the cathodic regions where they are consumed
4. Finally, in order to complete the electrochemical circuit, an electrolytic current is flowing inside the concrete pore solution from the anodic to the cathodic regions.

1.2 Initiation and Propagation of Corrosion

The damaging process due to the chloride-induced reinforcement corrosion can be divided into two phases, namely the phase of corrosion initiation where the reinforcement is in passive state and the phase of corrosion propagation (see Fig. 1).

1.2.1 Initiation Phase

During the initiation phase, aggressive substances such as carbon dioxide and chlorides, which can depassivate the steel, penetrate from the surface into the concrete cover. The duration of this phase depends on the cover depth and the penetration rate of the aggressive agents, as well as on the concentration necessary to depassivate the steel. Obviously, the concrete cover has a major influence on the durability of reinforced concrete structures and is therefore defined in design codes according to the expected environmental class [1].

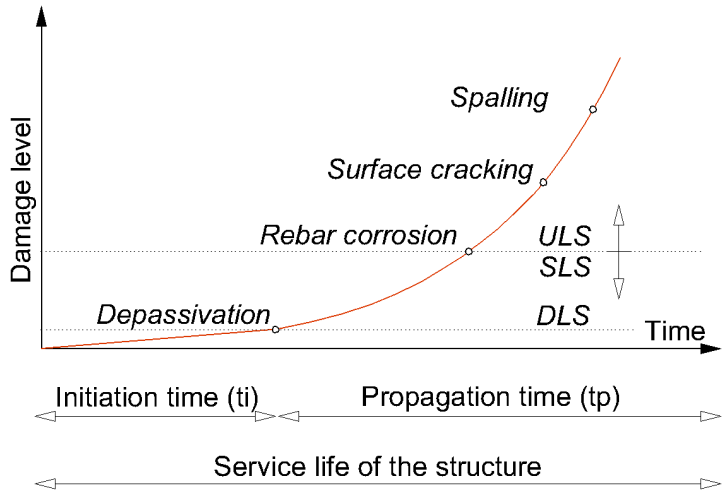

Figure 1: Time depending process of the cumulative deterioration of a concrete structure due to chloride induced corrosion according to [24]

.

1.2.2 Propagation Phase

A necessary prerequisite for the initiation of corrosion of steel in concrete is depassivation. Once the passive layer is destroyed, corrosion will occur only if water and oxygen are available on the reinforcement surface. The corrosion rate determines the time it takes to reach the minimum acceptable state of the structure, but it should be kept in mind that this rate can vary considerably depending on temperature and humidity. The chloride-induced corrosion is caused by locally destroying the passive layer due to chloride attack [1]. This local corrosion, with penetrating attacks of limited area (pits) surrounded by non-corroded areas, is also called pitting corrosion. The anode is the very limited local depassivated area of the steel surface. It is surrounded by large passive areas, which act as cathodes. This areal discrepancy between anode and cathode results in the formation of a macroelement with high potential difference. The progress of corrosion depends significantly on the amount of free chlorides [1]. With the increased supply of chlorides the depassivated anodic areas increase and the individual corrosion pits grow together, so that an extensive corrosion area is formed. The formation of cracks is due to the increase in volume of the corrosion products compared to the original steel volume.

1.2.3 Durability Limit State with respect to the damage process

In civil engineering, reaching a limit state is generally classified as a state of ”failure”. When designing a concrete structure, the Serviceability Limit State (SLS) and the Ultimate Limit State (ULS) are used [4], [8]. Regarding design for durability a new category of limit state has been introduced, namely the Durability Limit State (DLS). Durability is the conservation of the serviceability and loadbearing capacity of a structure over its design life [16]. This kind of limit state precedes the occurrence of both the SLS and the ULS and repre-

sents a simplified limit state intended to prevent the onset of deterioration [21]. Regarding durability considerations, it is not the genuine failure of the construction itself, but rather the exceedance of a defined extent of damage (see Fig. 1). A suggested limit state concerning the DLS is the corrosion of the reinforcement and the degradation of the concrete structure by chemical or mechanical action. A closer look at the chloride-induced reinforcement corrosion reveals that, an adequate limit state is achieved, when the passivating protection of the reinforcing steel is destroyed, or when the chlorides have reached the rebar, and the rebar starts to corrode as well. This moment marks the end of the Initiation phase [22].

2 Condition Assessment

2.1 Condition Survey

Prerequisite for a successful and durable rehabilitation of reinforced concrete structures, is the knowledge of the mechanisms of damage and a reliable detection of all influences of the defects. The first step should always be the determination of the state of condition through a detailed visual inspection of the components and the results of non-destructive material testings. Currently, inspections are mainly conducted visually at regular intervals. On visual inspection, the eye perceives damage which is marked in appropriate plans for damage assessment. Thus, further areas can be determined on which the building inspection is to be complemented by appropriate additional measuring points. Nowadays common concrete research technologies can be listed as follows [15], [25], [13]:

- Determination of the carbonation depth of the concrete
- Measurement of the concrete cover of the reinforcement
- Determination of the compressive strength of concrete
- Determination of the chloride penetration depth of the concrete
- Potential field mapping
- Concrete resistivity mapping
- Crack recording including the measurement of crack widths

On this basis, a concept with possible repair strategies should be worked out. In addition, reports of any risks in repair work can be given and the emerging costs of recommended measures can be determined.

2.2 Condition assessment based on indices

The evolution of the safety level over time will act as a baseline for the determination of the necessity for strengthening or repair methods. For this reason, the need for adequate and objective tools for assessing structures has become a subject of crucial economic interest. Recently, several efforts for quantifying these effects have been undertaken [11], [3]. However, the outcome of a structural assessment has to contain at least the following points:

- Identification of the damage mechanism
- Extent of damage
- Dynamic of the degradation progress

In [11], two procedures, a simplified and a detailed one, are described to establish these three aspects of the assessment in case of concrete structures affected by corrosion. In the context of this paper the simplified procedure is described in detail in the upcoming Chapter.

2.2.1 Simplified corrosion index

The simplified corrosion index (SCI) is calculated from the results of a detailed visual inspection of the components, the nondestructive in-situ material tests, as well as the exposure of the components. The simplified corrosion index shall be a measure of the direct damage to rebars due to corrosion. The corrosion process can be divided into 4 levels, namely no corrosion, low-, moderate-, and high corrosion. To obtain this classification, the SCI index is based on two main corrosion factors, namely the environmental aggressivity (EA) and the actual status of corrosion damage in the structure (corrosion damage index (CDI)). It is calculated as follows:

$$SCI = \frac{EA + CDI}{2} \tag{1}$$

The CDI is obtained from the corrosion indicators as shown in Tab. 1 and calculated as given in Eq. 2 whereas n denotes the number of detected corrosin indicators. The limits for the corrosion indicators are extracted from [11] and [17].

$$CDI = \frac{\sum_{i=1}^{n} \text{Corrosion Indicator level}_i}{n} \tag{2}$$

The CDI is calculated as the average of the determined indicators for corrosion. For the

			Damage levels			
Corrosion indicators			1	2	3	4
Carbonation depth	X_{CO_2}	[mm]	0% C	$\leq$ 75% C	$>$ 75% C	$\geq$ C
Chloride content	X_{Cl^-}	[% c.w.]	$\leq$ 0,2	$>$ 0,2 $\leq$ 0,6	$>$0,6 $\leq$ 1,0	$>$ 1,0
Crackwidth due to corr.	w	[mm]	No cracks	$<$ 0,3 mm	$>$ 0,3 mm	Spalling
Concrete resistivity	R	[Ω m]	$>$ 1000	500 - 1000	100 - 500	$<$ 100
Cross section reduction	ρ	[%]	$<$ 1	1 - 5	5 - 10	$>$ 10
Corrosion current rebar	i_{Corr}	[$\mu A/cm^2$]	$<$ 0,1	0,1 - 0,5	0,5 - 1	$>$ 1,0

C is the depth of the concrete cover

Table 1: Corrosion indicators with respect to the damage levels 1-4 derived from [11] and [17]

EN 206-1 [5] exposure classes, Tab. 2 shows the weighting factors for exposure classification. The higher the environmental aggressiveness is affecting the structure, the higher is the weight assigned to the exposure class. For example, in case of class X0, there is no risk of corrosion or attack. It corresponds to concrete inside buildings with very low air humidity.

For this reason, the weight 0 has been assigned to this class. In case of class XD3, there is an extremely high risk of corrosion due to the presence of chlorides in connection with dry/wet cycles. For this reason, the highest weight has been assigned to these environmental classes. The final calculation of the SCI is carried out by averaging the weighting of the exposure and the actual CDI.

Class	X0	XC1	XC2	XC3	XC4	XD1	XD2	XD3	XF1	XF2	XF3	XF4
Weight	0	1	1	2	3	2	3	4	1	2	3	4

Table 2: Environmental aggressivity (EA) values proposed as weighting factors dependig on different enviroments according to [5]

2.3 Example

The comparison of the repair methods presented in this paper is done by means of an exemplarily real structure. The structure for this case study was built in 1980 and designed as an overpass over a motorway. The overpass has a length of about 100 m and shows a tunnel-like characteristic. The beams are supported by the abutment and the columns are situated between the direction lanes of the motorway. In 1994, concrete spalling was noticed for the first time. A patch repair of the substructure with surface protection up to a height of 2.00 m was executed. The abutment walls, but mainly the columns show massive damage of the concrete structure. Spalling and cracks greater than 0.3 mm width and traces of rust in the day/night and splash zone are visible. Carbonation depth has reached a mean value of 9.3 mm, whereas the maximum values are 22 mm. The mean values of the cover thickness are about 20 mm on two sides of the colums and about 49 mm on the other two sides. The chloride content of the concrete cover is very high in the day/night zone and decreases according to altitude. This is also confirmed by the potential field measurements. The concrete resistivity was determined by surface resistivity meter based on the wenner principle. The measurement results are in the range from 7 to 2000 Ω m. The average value is 454 Ω m. The reduction of the reinforcement cross section is by an average of 7 %. According to [5] an exposure classification of XD3 can be assigned to the columns. So the weighting factor 4 can be set for the enviromental aggressivity . The CDI and SCI can now be determined as follows:

$$CDI = \frac{\mathrm{X_{CO_2}} + \mathrm{X_{Cl^-}} + \mathrm{w} + \mathrm{R} + \rho}{n} = \frac{2+4+4+3+3}{5} = \frac{16}{5} = 3.2 \tag{3}$$

$$SCI = \frac{EA + CDI}{2} = \frac{4+3.2}{2} = 3.6 \tag{4}$$

3 Comparison of different repair methods

When a structure reaches such a level of deterioration that an intervention and repair decision must be made, it is first necessary to analyze several possible repair methods. Furthermore,

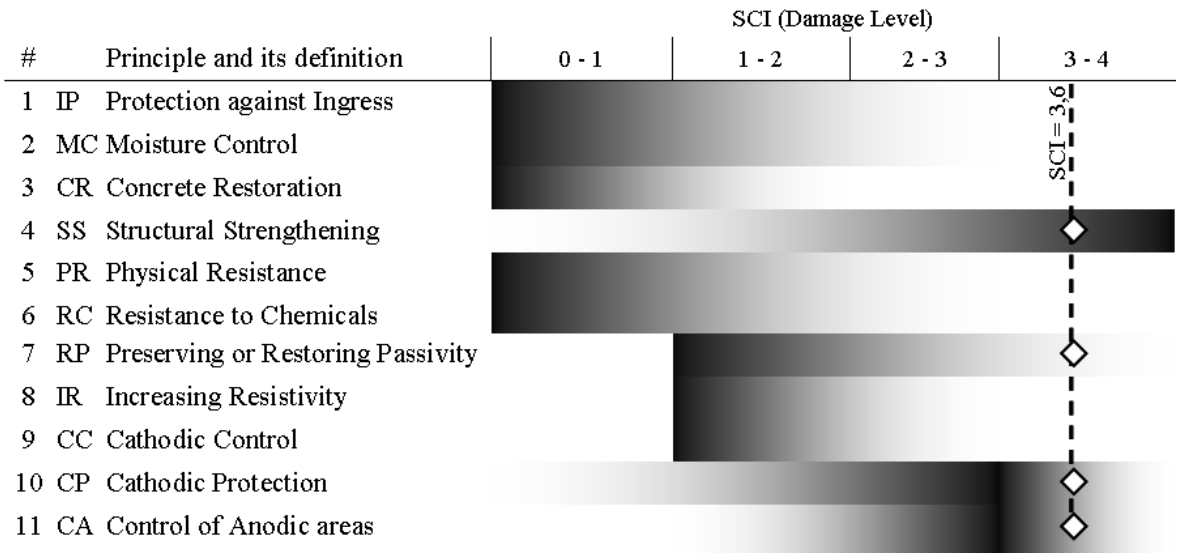

Figure 2: Scheme of the chlorid induced damage process associated with the effectiveness of repair principles (The colour intensity (0-100 %) is indicating the effectiveness of the repair principle (0-100 %))

the most suitable method shall be chosen for the investigated structure. The decision shall be based on minimum economical as well as technical aspects and shall be made by an expert (owner, consultant, ect.) who has an experience in the field of maintainance. The presented approach uses the SCI as well as the repair principles to derive an objective client's decicion. Therefore preselection of various principles is made in the first place. Thereafter, a comparison of different repair methods is done by means of life-cycle costs. Based on the examination of the structural assessment together with Fig. 2, a preselection of the most effective repair method can be made. Thereby, the SCI serves as an input parameter in the aforementioned Figure. First, a classification of different repair methods has to be carried out based on the implementation of the conservation status of the component. Figure 2 shows how this classification can be made. For example, the repair principles 1 and 2 are used as a repair technique in order to prevent concrete damage. Those principles are therefore ineffective for damage levels greater than class 3. The repair principle 4 (SS), however, is increasingly suitable with increasing degradation due to reinforcement corrosion. Basically, principle 4 is suitable for all damage levels. The main reason for this application is, that the principle is also used in case of a change in functional requirement such as an insufficient load carrying capacity. The cathodic protection (IP 10) is getting more effective the worse the SCI gets. Prerequisite for the application of Principle 10 is, however, that the rebar section loss of the reinforcement has not progressed too far, so that one may dispense with extensive concrete removal and additional reinforcement [10].

3.1 Service life of repair methods

The assumed service lives of the various repair methods are taken from the literature [6], [18], [19], [14], [23]. 229 case histories on repaired concrete structures were anal-

ysed in [23]. The cases were located in different countries across Europe whereas about 70 % were located in North Europe. The Investigation confirmed that 50 % of the repaired structures failed and 25 % deteriorated in the first 5 years. Moreover, 75 % of the structures deteriorated within 10 years and 95 % within 25 years. Further empirical data, gained from field investigations done by the author, were also used. Based on these practical and objective determinations of the conservation status, different repair methods are compared with each other now. For the selected repair methods, the life cycle costs are calculated. According to Fig. 2 the suitable repair principles are given in Tab. 3. Further repair methods in principle

#	Acronym	Principle and its definition	Selected Repair method
4	SS	Structural strengthening	Increasing concrete overlay
7	RP	Preserving or restoring passivity	Replacing contaminated or carbonated concrete
10	CP	Cathodic protection	Applying electrical potential

Table 3: Selected repair methods based on Fig 2

11 such as barrier coating of the reinforcement and applying corrosion inhibitors in or to the concrete are surely also possible as an repair strategy. In fact, the three principles chosen above are common practice and can be seen as standard repair methods also in case of the structures maintained by the ASFiNAG. Therefore, other repair methods were not taken into account in this article yet.

Increasing concrete overlay by adding mortar or concrete (IP 4) By applying this repair method (concrete facing) the entire chloride containing concrete has to be removed in accordance to the stability. Moreover reinforcement has to be added or replaced if necessary. Thereafter, the cross section is covered with concrete. In this example an additional thickness of +10 cm was assumed. The service life of this measure is assumed in this example to be 35 years.

Replacing contaminated or carbonated concrete (IP 7) The aim of this repair principle (patch repair) is the permanent replacement of the lost, unsound and contaminated concrete by new concrete or mortar. The service life of this measure in this exposure determined by experience is very short. This predefinition is confirmed with European observations [23]. After restoring a flat concrete surface, a protection against ingress of adverse agents such as hydrophobic impregnation or surface coating can be applied for instance. In this case study, a periodic application of hydrophobic impregnation is carried out every 5 years. This increases the service life of the repaired areas up to 10 years. This means, that after 20 years, the repaired surfaces must be replaced again.

Cathodic protection (IP 10) Cathodic protection (CP-Mesh + CP-Coating) is applied on structures which are already affected by corrosion, mainly induced by chlorides. The general set-up which is valid for all electrochemical methods is that by means of an external conductor, called the anode, a direct current flows through the concrete to the reinforcement, which

thereby is made to act as the cathode in an electrochemical cell. The final outcome of the current flow is to reduce or stop the corrosion rate by repassivation of the reinforcement due to polarisation to an even more negative potential. Titanum activated oxides of different metals are used in the form of meshs, wires or strips, because it is the most reliable and widely used type of anode. Usually, the anode material is embedded in a layer of sprayed concrete. But there are also other methods existing, such as conductive coatings (with graphite as conductor) or carbon fibres [18]. In the case study of this paper, two different anode systems are considered. First, a mortar embedded titanium mesh and second, a conductive coating based on graphite. For the electronic parts a service life of 8 years is assumed. The cathodic protection with titanium mesh has an assumed service life of 30 years. For the conductive coating a service life of 15 years was assumed.

3.2 Life cycle costs of the repair methods

Calculations or estimations of costs can be carried out in different ways by considering various types of costs. This is often referred to as the so-called whole life cycle costing. Life cycle costs may be used as a valuable tool for the assessment of the cost effectiveness of various technical solutions for condition assessment, maintenance and repair strategies during operation of the structure [12]. As a basis for the life cycle costs of a concrete structure up to the time t_N, the following net present value expression may be used:

$$LCC(t_N) = C_I + \sum_{i=1}^{t_N} \frac{C_{t_i}}{(1+r)^{t_i}} \tag{5}$$

where C_I denotes the initial construction costs, C_{t_i} the costs over a service life period $\mathrm{t_i}$ (years), and r the discount rate.

Initial construction costs (C_I), are generated from design, planning, surveying, through to manufacturing and final inspection and listed in Tab. 4. Follow-up costs refer to costs for inspection, maintenance and rehabilitation. The present value of diposal is considered to be negligible since it is discounted over such a long period of time (70-100 years). The functional unit of the life cycle costs is € per m^2 of repaired concrete surface. In this paper, the calculated life cycle costs are taken into account which arise when a component is subjected to a repair. It affects only the costs that occur from the repair measure itself. After expiring the service life of the repair methods they have to be renewed frequently until reaching the theoretical life span of the investigated structure. The mean value of the renewal frequency is given in Tab. 4. It is assumed that the costs associated with a renewal does not change over time and is equal to the initial costs. In this study the average discount rate is primarily estimated at 4 %. The observation period is thereby often given in the literature as 50 years or the theoretical residual service life. According to [9], a theoretical life span of structures of 110 years are accepted. A structure currently 33 years old, results in a remaining useful life span of 77 more years. This is the observation period in this study.The costs of repair work are very individual, depending on the particular installation conditions. Therefore, the calculated results are not fully comparable with other repair situations. However, the difference between the LCC of various repair methods can be compared very well.

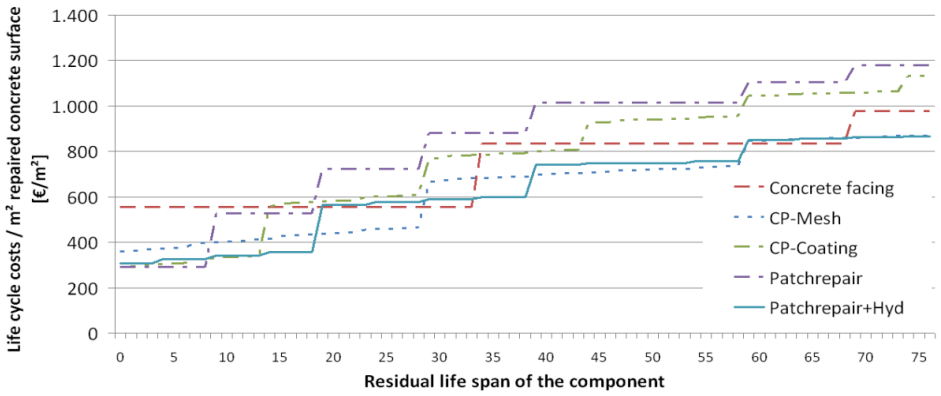

Figure 3: Life cycle costs of selected concrete repair methods developing over time

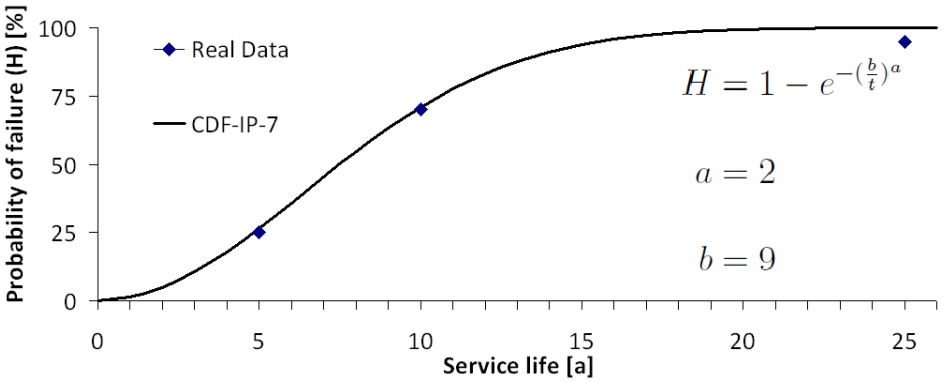

Figure 4: Cumulative density function (CDF) shown by the example patch repair

3.2.1 Results

Figure 3 shows a comparison of the life cycle costs of concrete repair methods over the residual life span of the surveyed component. From the LCC analysis, it turns out that repair methods with low initial costs at the end of the theoretical service life turn out to have higher life cycle costs. In the comparison, the patch repair method (IP 7) with applied hydrophobic surface treatment is, considering the entire life cycle, the most cost effective choice as well as the cathodic protection with titanium mesh. The cathodic protection (IP 10) in form of conductive coating seems to be cost intensive, despite low initial costs. The results also show that a protection against ingress by using a hydrophobic surface treatment has a significant influence on the life cycle costs considering the residual life span of the component.

3.3 Parameter study

The parameter study regarding the investigated repair methods is done by variation of the different service life and examination of the impact of such changes on the results. The study helps testing the robustness of the results in the presence of uncertainty. In general, little knowledge is still available regarding the service life of various repair methods. Only information about the patch repair method is documented [23]. Figure 4 shows the available service life data only for IP 7 highlighted by three data points after 5, 10, and 25 years. This

lack of information leads to high variations in the results of life cycle cost analysis since the service life is a dominant parameter for the cost calculation. A Weibull-distribution, denotated as CDF-IP-7 in Fig. 4, has been fitted into the real service life data according to [23] for showing the complete service life development over time. The Weibull distribution was chosen because it allows also modeling the increase of the failure rate for aging structures. The choice for the Weibull distribution for modelling the uncertainty in service life of aging structures has been verified with the Weibull probability plot. The corresponding shape parameter a and the scale parameter b of the Weibull distribution are $\mathrm{a} = 2$ and $\mathrm{b} = 9$. In a first approach, since no detail data about the service life of the repair method is available, the same service life distribution was assumed for all investigated repair methods. Based on the Weibull-distribution for all repair methods the following service lives with their 10 % fractiles are shown in Tab. 4. The Figure shows a great deviation from the mean value of

#	Repair method	C_I [€/m^2]	$\mathrm{t}_{0.1}$ [a]	$\mathrm{t}_{\mathrm{mean}}$ [a]	$\mathrm{t}_{0.9}$ [a]	f_{R} [-]
IP 4	Concrete facing	553	18	35	58	2
IP 7	Patchrepair	288	5	10	13	7
IP 7	Patchrepair + Hydr.	308	11	20	33	3
	Hydrophobizing	20	3	5	8	15
IP 10	CP-Mesh	354	16	30	50	2
IP 10	CP-Coating	284	8	15	25	5
	Electrical installation	15	4	8	13	9

Table 4: Initial costs, Service lives of repair methods with their 10 % fractiles, and their mean values of the renewal frequency

the LCC for each of the repair method due to the variation of its service life. It is notable that the life cycle costs are increasing by factor two for decreasing service lives, whereas for increasing service lives the LCC are on average decreasing by approximately 70 %.

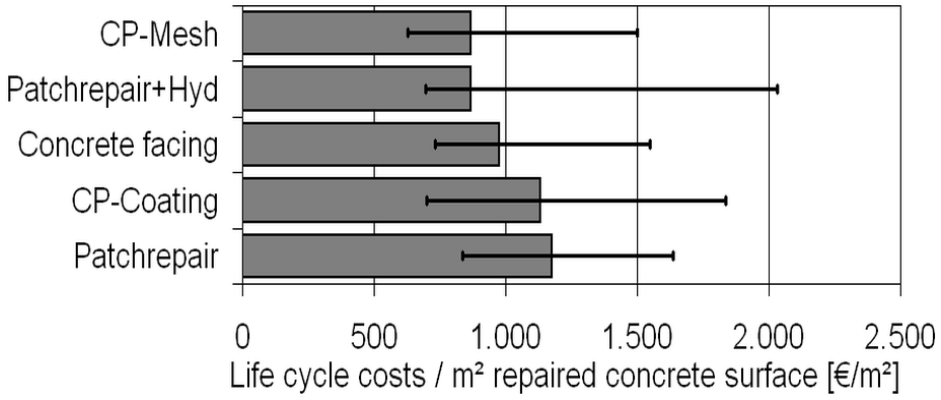

Figure 5: LCC by variation of the service life of selected concrete repair methods

4 Summary and Conclusion

The increasing demands to the transport infrastructure, increasing maintenance costs, high energy consumption and increasing awareness of environmental and human influences generate increasing monetary expenses. For an infrastructure operator such as the ASFiNAG, knowledge about the costs and the moments of maintance measurements is of particular interest but often not available. The approach presented in this paper shall contribute to closing this lack of information. It provides essential information for deciding the most cost-effective repair method in relation to its service life. The decision process is based on the SCI for which an existing example has been chosen for the calculation in this paper. In order to perform such an analysis in-depth knowledge about the state of preservation is of high priority. Based on the preliminary condition survey and the determination of the simplified corrosion index the approach allows a preselection of the most effective repair principles. By means of these fundamental principles, repair methods were selected. As a result of the investigated example the two repair methods, namely the patch repair with hydrophobic impregnation and cathodic protection with titanium mesh, turned out to be the most cost effective repair strategy taking into account the full service life of the structural component. To limit deterioration of existing infrastucture, the selected repair methods are common practice. The LCC results allow a basic ranking of the repair methods. But it does not provide any information about the effectiveness of the chosen repair method. The high LCC for the patch repairing is mainly due to its low service life. The LCC of the cathodic protection principle (CP-Mesh) could be further reduced by the optimization of the service life of the electronic components. The procedure presented in this paper shows clearly that it is possible to find an objective basis for choosing the optimal repair method and its time of application.

5 Outlook

For a complete and objective decision of the repair strategy, both ecological and economical aspects have to be taken into account. Emphasis must be put on a complete data collection regarding the service life of a repair method and the behavior of failure over time. Attention should furthermore be put on a more realistic modelling of environmental impacts. Future research should focus on the interaction between the limit states and the damage levels. This would allow for a probabilistic modeling of the degradation due to reinforcement corrosion. Certainly, there is the possibility of choosing different repair methods on the different degraded zones, which will be established in dividing into spray and splash area. This allows further optimization of the LCC of the considered components.

Acknowledgements

The author would like to express his appreciation to Prof. Dr. Alfred Strauss, University of Natural Ressources and Life Sciences, Institute of Structural Engineering for his valuable

and constructive suggestions during the development of this paper. For the allocation of the data used in the example of the condition assessment in the paper, the author would also like to thank the ASFiNAG.

Literature

[1] L. Bertolini, B. Elsener, P. Pedeferri, and R.B. Polder. *Corrosion of Steel in Concrete*. Wiley-VCH Verlag GmbH & Co. KGaA, 2004.

[2] Wolfgang Breit, Christoph Dauberschmidt, Christoph Gehlen, Christian Sodeikat, Alexander Taffe, and Udo Wiens. Zum Ansatz eines kritischen Chloridgehaltes bei Stahlbetonbauwerken. *Beton- und Stahlbetonbau*, 106(5):290–298, 2011.

[3] C.Andrade and I.Martinez. Use of indices to assess the performance of existing and repaired concrete structures. *Construction and Building Materials*, 23:3012–3019, 2009.

[4] CEN. EN 1992-1 Eurocode 2: Design of concrete structures, 12 2011.

[5] CEN. EN 206 Concrete - Part 1: Specification, performance, production and conformity, 04 2012.

[6] C. Dauberschmidt. Grundlagen des kathodischen Korrosionsschutzes von Stahl in Beton. In *TAE-Symposium 'KKS von Stahlbetonbauwerken'*, Ostfildern, 2009.

[7] Eva-Maria Eichinger-Vill, Johann Kollegger, Francesco Aigner, and Günter Ramberger. Überwachung, Prüfung, Bewertung und Beurteilung von Brücken. In Gerhard Mehlhorn, editor, *Handbuch Brücken*, pages 1009–1068. Springer Berlin Heidelberg, 2010.

[8] fib Special Activity Group 5. Model Code 2010, Final draft, Volume 1 + 2, fib Bulletin, No. 65 + 66, March 2012.

[9] fsv. RVS 15.02.13 Dauerhaftigkeit von Brücken - Grundlagen für die Berechnung von Lebenszykluskosten, 04 2012.

[10] Christoph Gehlen and Christian Sodeikat. Alternative Schutz- und Instandsetzungsmethoden für Stahlbetonbauteile. *Beton- und Stahlbetonbau*, 100(S1):15–23, 2005.

[11] GEOCISA and Torroja Institute. *CONTECVET A validated Users Manual for assessing the residual service life of concrete structures - Manual for assessing corrosion-affected concrete structures*. EC Innovation Program, report number in30902i edition, 2008.

[12] Odd E. Gjørv. *Durability design of concrete structures in serve enviroments*. Taylor & Francis, 2009.

[13] Bernd Hillemeier and Alexander Taffe. *Aktuelle Regelwerke der Bauwerksdiagnostik*, chapter A.3, pages 57–101. Wiley-VCH Verlag GmbH & Co. KGaA, 2012.

[14] CEN/TC219 ISO12696. Kathodischer Korrosionsschutz von Stahl in Beton, 2012.

[15] Michael Küchler. *Instandsetzung von Betontragwerken*, chapter V, pages 345–468. Wiley-VCH Verlag GmbH & Co. KGaA, 2012.

[16] Harald S. Müller and Michael Vogel. Lebensdauerprognose für Betonbrücken - Wo stehen wir heute? In *19. Dresdner Brückenbausymposium, Technische Universität Dresden*, 2009.

[17] OeN. B4706: Repair, reconstruction and strengthening of concrete structures - General rules and national implementation of ÖNORM EN 1504, 06 2009.

[18] OeVBB. Richtlinie kathodischer Korrosionsschutz von Stahlbetonbauteilen, 2003.

[19] OeVBB. Einführung in die neue Richtlinie Kathodischer Korrosionsschutz, 2004.

[20] Luc Schueremans, Dionys Van Gemert, and Sabine Giessler. Chloride penetration in RC-structures in marine environment a long term assessment of a preventive hydrophobic treatment. *Construction and Building Materials*, 21(6):1238 –1249, 2007.

[21] Břetislav Teplý. Durability, reliability, sustainability and client's decision. In *CESB 07 Prague Conference*, 2007.

[22] Břetislav Teplý and Dita Vořechovskà. Reinforcement corrosion: Limit states, reliability and modelling. *Journal of Advanced Concrete Technology*, 10(11):353–362, 2012.

[23] Graham Tilly. Network Newsletter No.4. Technical Report 4, CON REP NET - Thematic Network on Performance-Based Rehabilitation of Reinforced Concrete Structures, 2004.

[24] K. Tuutti. *Corrosion of steel in concrete*. PhD thesis, Swedish Cement and Concrete Research Institut, Stockholm, 1982.

[25] Gerald Schickert; Martin Krause; Herbert Wiggenhauser. ZfPBau - Kompendium - Verfahren der Zerstörungsfreien Prüfung im Bauwesen. http://www.bam.de/microsites/zfp_kompendium/welcome.html, 2007.

A histogram-based approach for evaluation of the Hasofer-Lind reliability index without isoprobabilistic mapping of limit state equations

Markus Derry, Jari Puttonen
Department of Civil and Structural Engineering, School of Engineering,
Aalto University, Espoo, Finland
markus.derry@aalto.fi, jari.puttonen@aalto.fi

Abstract: As reliability analysis of building structures can occasionally involve challenging calculations, this conference publication describes a histogram-based approach for the calculation of the reliability index. A major advantage of the method is the possibility to enrich the distribution of the variable with a case-specific measured data in a straightforward manner. Another advantage is simplified computation as the definition of the limit state function is needed only in the physical space. Uncertainty related to the reliability index itself may also be quantified as the calculation result is a histogram of values of the reliability index. The method consists of three steps. Firstly Monte Carlo simulation (MCS) is applied for distributions described as histograms obtaining random samples of the basic variables. The random samples located in the failure domain are then transformed to the standardized space. In the third step, the reliability index is defined as the minimum value of the distances from the origin to the points transformed to the standardized space.

Keywords: reliability analysis, reliability index, Hasofer-Lind index, structural reliability, histogram

1 Introduction

Structural reliability theory provides the necessary background for conducting reliability analyses of building structures. For example, the Hasofer-Lind reliability index [5] (also referred to as simply ‘reliability index’ from hereafter) can be used as a measure of reliability. Definition of the limit state surface in the standardized space is required in order to calculate the Hasofer-Lind index. However, it may turn out to be challenging to transform distributions of basic variables to the standardized space for the definition of multi variable limit state functions when analysing real structures.

This paper presents a method based on the use of histograms, for evaluating reliability indices of structural members by formulating the limit state equation in the physical space. Advantages of the developed approach are that it is straightforward and reduces computa-

tional difficulties related to calculation of the reliability index. First a description of the developed method is given, following a calculation example to illustrate its use.

2 Description of the histogram-based approach

2.1 Theoretical background

Theoretical background of the histogram-based approach rests on the definition of the Hasofer-Lind index. In structural reliability theory, the Hasofer-Lind reliability index (β_{HL}) is defined as the shortest distance from the limit state surface to the origin in the standardized (or normalized) space [5],[6]. LEMAIRE [5] defines β_{HL} analytically as

$$\beta_{HL} = \min_{G(\{x_i(u_j)\})\leq 0} \sqrt{\{u\}^T\{u\}} \tag{1}$$

with

$G(\{x_i(u_j)\})$	limit state function as a function of the reduced variables,
$\{x_i(u_j)\}$	vector of basic variables, with basic variables expressed as functions of the reduced variables,
$\{u\}$	(column) vector of a point in the standardized space.

Basic variables are transformed from the real (or physical) space to the standardized space using an isoprobabilistic transformation in order to calculate the reliability index [5].

Calculating the reliability index using histograms is essentially based on the precondition given in Eq. (1). The point nearest to the origin used to calculate the reliability index should be located either on the limit state surface or in the failure domain. This point is called the design point [5],[6]. A random sample of points located in the failure domain or on the limit state surface in the standardized space may be used for estimating the reliability index. Distribution of reliability indices is obtained in the form of a histogram by calculating the distance from the origin to each of these points in the standardized space. The minimum value of the histogram is the approximate reliability index (noted as β^*).

Depending on the amount of statistical data available, some assumptions about the statistical properties of the basic variables may be required. Probability distributions can be known, i.e. based on measurement data. However, probability distributions are often assumed based on literature due to lack of data. In this study, probability distributions and distribution parameters of basic variables have been selected according to JCSS PROBABILISTIC MODEL CODE [4]. Basic variables are also assumed to be independent.

2.2 Formulation and calculation steps

The histogram method is divided into three distinct calculation steps: random sampling of basic variables, isoprobabilistic transformation of points located in the failure domain or on the limit state surface of the physical space, and calculating the reliability index related to each point. Random samples, i.e. histograms, of basic variables may be obtained in various ways, for example by using Monte Carlo simulation with Latin hypercube sampling (LHS), which has been used in this study.

Expression of the limit state function is used for locating points in the failure domain of the physical space. From the analytical definition of the limit state function, the selection criterion can be formulated as [5]

$$G(\{x\}) = R(\{x\}) - S(\{x\}) \leq 0 \tag{2}$$

with

$G(\{x\})$	limit state function as a function of the basic variables
$R(\{x\})$	the resistance variable as a function of the basic variables,
$S(\{x\})$	the stress variable as a function of the basic variables,
$\{x\}$	(column) vector of the basic variables in the physical space

Value of $G(\{x\})$ is calculated for each point in the sample. Points that fulfil the condition in Eq. (2) are selected to be transformed to the normalized space.

In the third step, the selected points are transformed to the standardized space by using isoprobabilistic transformation. Cumulative distribution functions (CDF) of the basic variables are needed for this. Analytical definition of the isoprobabilistic transformation is presented in Eq. (3) [5]. The transformation is done only for the selected points, which leads to a shorter calculation time compared to the situation where Eq. (2) is defined in the standardized space.

$$\Phi(u) = F_X(x) \Longrightarrow u = \Phi^{-1}\big(F_X(x)\big) \tag{3}$$

with

$\Phi(\dots)$	CDF of the standard normal distribution,
$\Phi^{-1}(\dots)$	inverse function of the above,
$F_X(x)$	cumulative distribution function of random variable X,
u	(realized) value of a reduced variable.

A histogram of reliability indices related to each point in the standardized space is obtained by calculating the distance from the origin for each point. Uncertainty related to the reliability index can be seen from the shape of the histogram of β. In the case of a smooth and continuous histogram or distribution, the coefficient of variation (CV) gives a numerical estimate of the uncertainty. The approximate reliability index β^* is obtained as the minimum of the histogram of β. Accuracy of the histogram method was tested with the elementary case of two Gaussian variables. Fig. 1 shows a comparison between β^* and the Cornell index β_c, [5],[6] for various sample sizes. Reliability indices presented in Fig. 1 are average values of three separate Monte Carlo simulations. The histogram method gives 2.87% higher values on average than the exact Cornell index; range in this comparison is from 0.54% to 11.77% for all simulation cycles.

The exact minimum distance from the origin to the limit state surface, i.e. the Hasofer-Lind index, can be obtained with a large enough sample size of points on the limit state surface. However, this may require using very large sample sizes in order to obtain a sufficient quantity of points on the limit state surface.

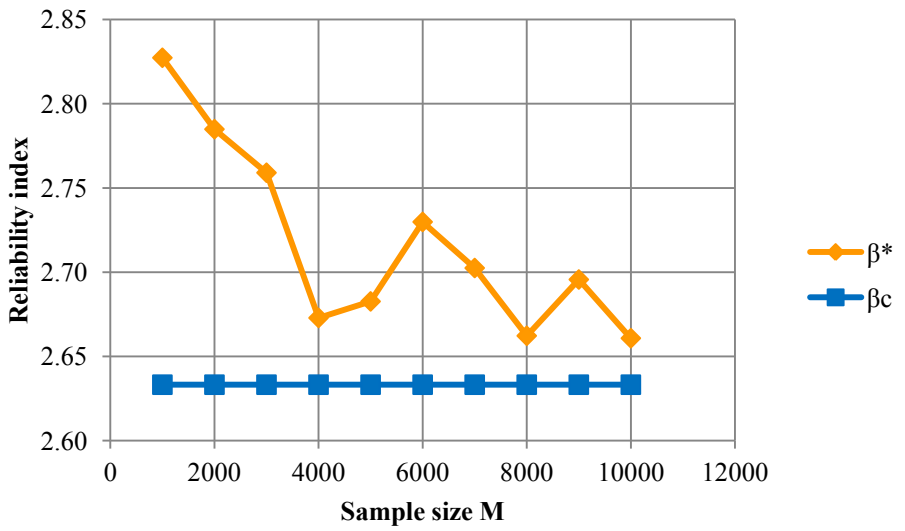

Fig. 1: Graph of the approximate reliability index β^* and the Cornell index β_c

2.3 Advantages and disadvantages

Advantages of the histogram approach include computational simplicity and possibility to use test data in a straight forward manner. Depending on the number of variables and the mathematical formulation of the limit state function in the normalized space, analytical calculation of β_{HL} may require iterative and time consuming calculations; and may in fact in some cases be close to impossible. The histogram method solves this problem: definition of the limit state function in the standardized space is not required, only samples of variables are needed to calculate the reliability index. Another important aspect is that the MCS samples are used directly without any conversions, e.g. without fitting PDFs to the simulation results.

Measurement data may also be easily utilized with the histogram approach. Distribution of a variable can be enriched with case-specific measurement data. This way the reliability analysis is linked with the actual structure. If there is enough measured data, it can be used without assuming any specific distribution, i.e., using the test data simply in a histogram form.

Although the histogram approach has its advantages, there are also some disadvantages. For example, the actual design point is not easily obtained. Selecting the minimum value from the distribution of the reliability index gives only an approximation of the design point. Another disadvantage is related to the minimum observable failure probability. The minimum observable failure probability is dependent on the Monte Carlo simulation sample size and can be formulated as

$$P_f = \frac{M \in [G(\{x\}) \leq 0]}{M}$$
$$\min(P_f) \geq \frac{1}{M} \tag{4}$$

with

P_f	probability of failure,
$M \in [G(\{x\}) \leq 0]$	number of points in the failure domain,
M	sample size of the Monte Carlo simulation.

This equation defines the minimum of the probability of failure as a function of sample size. Typically, this value is non-zero as in reality, and the challenge lies in the determination of very small values due to large sample size required in those cases.

3 Calculation example

3.1 Beam of reinforced concrete

A calculation example of a reinforced concrete (RC) beam is shown to illustrate the histogram approach. Euler-Bernoulli beam theory is applied to the simply supported beam with a span length (L) of 8.5 meters. Structural model of the RC beam is represented in Fig. 2. All loads are given as line loads (kN/m) along the centre line of the beam. Bending failure at mid-span, i.e. location of the maximum bending moment, is used as the failure criterion.

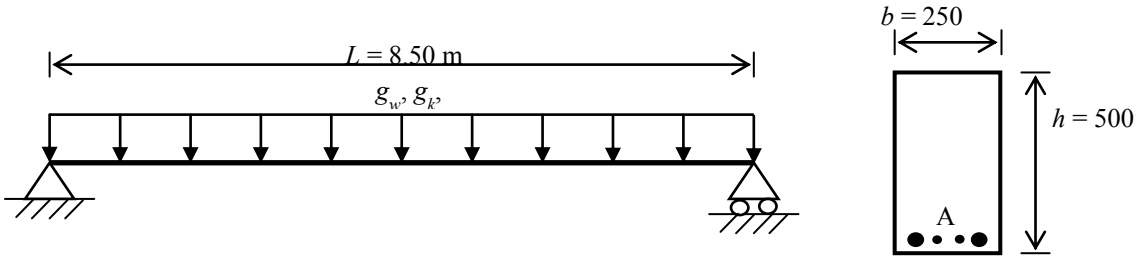

Fig. 2: Structural model and cross section

The RC beam has a 500 mm high (h) and 250 mm wide (b) rectangular cross section and is reinforced with steel bars. The main reinforcement consists of two 20 mm diameter bars and two 10 mm diameter bars, i.e. four bars in total, and is located near the bottom surface of the beam with a total reinforcement area (A_s) of 785.4 mm^2. Stirrups were not included in the analysis. Tab. 1 summarizes deterministic input variables.

3.2 Basic variables

Reliability analysis of the RC beam is performed using six (random) basic variables. Stress and resistance variables, S and R respectively, are expressed as functions of the basic variables, as shown in Eq. (2). Three of the basic variables are related to the stress variable (S); referred to as 'stress variables'. The rest of the basic variables are used in the formulation of the resistance variable (R); referred to as 'resistance variables'. These six basic variables define a 6-dimension normalized space.

The basic variables related to the stress variable include self weight (W), permanent load (G) and variable load (Q). Self weight of the beam is calculated using nominal densities given in informative annex A of standard EN 1991-1-1 [2]. Characteristic values of permanent (g_k) and variable loads (q_k) are initially assumed to be 2.5 kN/m and 4.0 kN/m,

Tab. 1: Input variables of the calculation example

Input variable	Value
Span length, L	8.50 m
Height of cross section, h	500 mm
Width of cross section, b	250 mm
Cross sectional area, $A_c = h \times b$	125 000 mm^2
Unit weight of concrete, γ_c	24 kN/m^3

respectively. Probability distributions and statistical properties of stress variables are selected based on literature [3],[4].

The resistance variable is a function of the following basic variables: compression strength of concrete (f_c), yield strength of reinforcement (f_y), and concrete cover (c). Probability distributions functions (PDF) of resistance variables are based on literature [3],[4]. Distribution parameters of the resistance variables are estimated with the method of moments from test data. Test samples of the basic variables were obtained from intermediate floor beams of an office building [1]. Probability distributions and statistical properties of the basic variables are presented in Tab. 2.

Tab. 2: Statistical properties of the basic variables

Basic variable	Mean value m_X	Coefficient of variation c_X	Distribution type	Distribution parameters
Self weight, W	3.00 kN/m	0.04	Gaussian	$\mu_W = 3$ $\sigma_W = 0.12$
Permanent load, G	2.50 kN/m	0.10	Gaussian	$\mu_G = 2.5$ $\sigma_G = 0.25$
Variable load, Q	2.40 kN/m $(0.6 \times q_k)$	0.35	lognormal	$\lambda_Q = 0.818$ $\xi_Q = 0.34$
Compression strength of concrete, f_c	27.80 MPa	0.169	lognormal	$\lambda_{fc} = 3.311$ $\xi_{fc} = 0.168$
Yield strength of reinforcement, f_y	286.80 MPa	0.019	lognormal	$\lambda_{fy} = 5.659$ $\xi_{fy} = 0.019$
Concrete cover, c	29 mm	0.517	beta	$a = 10$ $b = 69$ $r = 0.508$ $t = 1.069$

3.3 Results and evaluation

The reliability analysis was done using Monte Carlo simulation with LHS and a sample size (M) of 10 000. Bending of the RC beam at mid-span ($L/2$) was studied. Eq. (2) was

formulated with bending resistance of the beam as the resistance variable ($R(f_c, f_y, c)$) and bending moment as the stress variable ($S(w, g, q)$). The results are divided into three groups or cases (Tab. 3). In each case a distribution parameter of a specific basic variable was increased step by step to study the sensitivity of output variables. Range and step values given in Tab. 3 have been selected in relation to values given in Tab. 2. The aim has been to select a wide enough range and a short enough step in order to draw graphs of the output variables and to determine the shape of these graphs, e.g. increasing or decreasing. Moreover, the minimum observable failure probability of 10^{-4}, defined by Eq. (4), has been a selection criterion for range of a variable. All basic variables are, nevertheless, treated as random variables in the analysis, with probability distributions given in Tab. 2. The distribution parameters themselves are treated as deterministic. All results are given as average values of three simulation cycles in order to obtain consistent and representative results; i.e. three cycles per step in each case.

Tab. 3: Result groups of the reliability analysis

Case	Info	Variable	Unit	Range	Step
1	Mean compression strength of concrete	f_{cm} / m_{fc}	MPa	13.90 – 50.04	2.78
2	Mean yield strength of reinforcement	f_{ym} / m_{fy}	MPa	229.44 – 329.82	14.34
3	Characteristic value of variable load	q_k	kN/m	3.20 – 6.40	0.40

Histograms of stress and resistance for cases 1, 2 and 3 are shown in Fig. 3, Fig. 4 and Fig. 5, respectively; all with a bin size of 0.50. The following short notation is used in the figures: e.g. notation ‘c1/s1’ means step 1 of case 1. Tab. 4 presents analysis results of stress and resistance in a tabular form. Strength of concrete seems to have little effect on the mean value of resistance. Increasing f_{cm} from 13.90 MPa to 50.04 MPa, increases m_R by only 7.7 %. This is also seen from histograms of R in Fig. 3. Moreover, the CV of R decreases from 0.041 (step 1) to 0.019 (step 14).

Tab. 4: Results of the reliability analysis: stress and resistance

Case	Step	q_k	f_{cm}	f_{ym}	m_S	σ_S	m_R	σ_R
1	1	4.00	13.90	286.80	71.34	8.07	93.94	3.86
1	14	4.00	50.04	286.80	71.34	8.07	101.16	1.94
2	1	4.00	27.80	229.44	71.34	8.17	80.07	1.58
2	8	4.00	27.80	329.82	71.34	8.19	113.32	2.34
3	1	3.20	27.80	286.80	67.01	6.72	99.20	1.98
3	9	6.40	27.80	286.80	84.35	12.40	99.20	1.97

The two distinct failure mechanisms of a RC beam in bending can be seen from the ‘double peak’ histogram in Fig. 3 (R c1/s1): 1) tension failure of reinforcement (ductile, higher peak in Fig. 3); and 2) compression failure of concrete before the yielding of rebars (brittle, lower peak in Fig. 3). Failure mechanism 2 becomes dominant for some samples in step 1 of case 1 due to the low strength of concrete; hence, the lower peak in the histogram of R. High yield strength or large amount of reinforcement can also make compression failure of concrete more likely, i.e. leads to a more brittle failure mechanism.

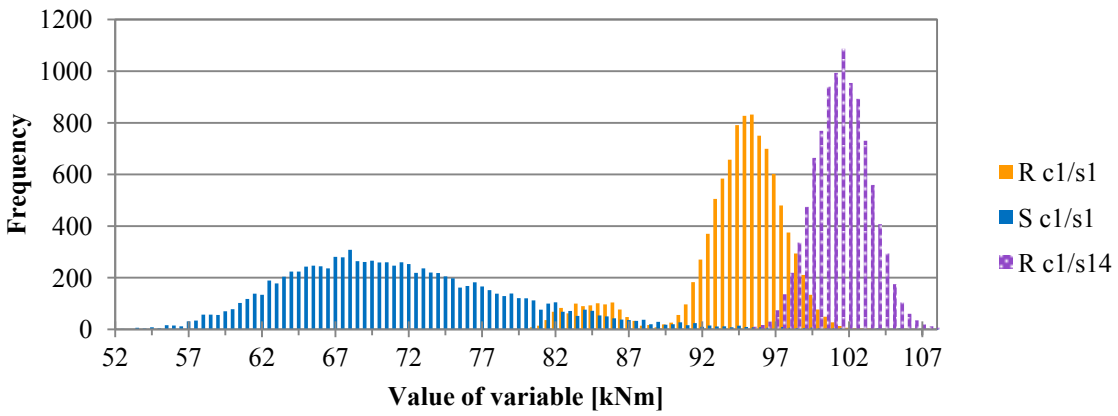

Fig. 3: Histograms of case 1: stress of step 1, resistance of steps 1 and 14

The yield strength of reinforcement has greater effect on the bending resistance (Fig. 4, Tab. 4). A 43.8 % increase in f_{ym} relates to a 41.5 % increase in the mean value of resistance. Histograms of stress are basically identical, apart from small differences due to MCS, in cases 1 and 2 since f_{cm} and f_{ym} have no effect on the stress variable.

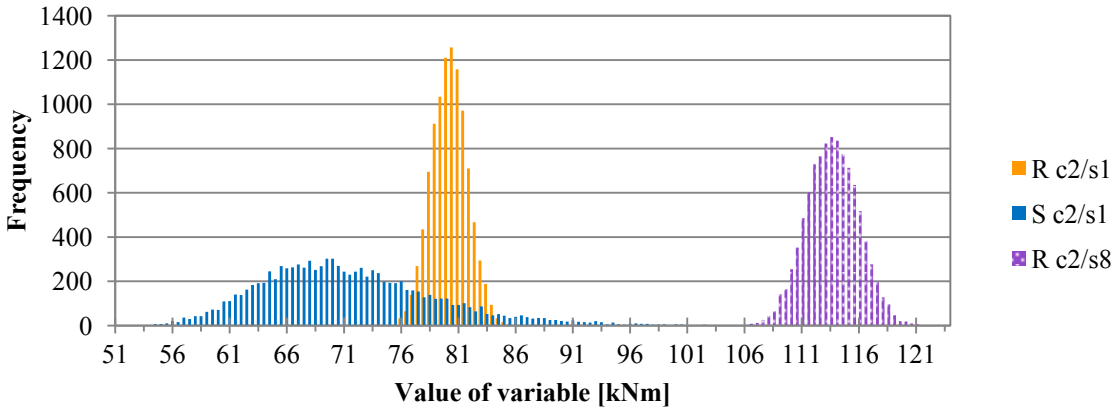

Fig. 4: Histograms of case 2: stress of step 1, resistance of steps 1 and 8

The characteristic value of variable load has a significant influence on the shape of the histogram of stress (Fig. 5). The CV of stress increases from 0.100 (step 1) to 0.147 (step 9) as q_k increases from 3.20 kN/m to 6.40 kN/m. In addition, a 25.9 % higher mean value of stress is obtained in step 9 compared to step 1. The probability of failure is clearly higher in step 9 than in step 1, as seen from the overlapping histograms. Note, the histogram of R for step 9 is basically identical to that of step 1, since stress variables have no effect on the resistance.

Histogram of the reliability index for case 1 is presented in Fig. 6, as an example. Sample sizes for steps 1 and 9 in Fig. 6 are 177 and 42, respectively. The probability of failure decreases as the sample size of β decreases: from 1.75×10^{-2} in step 1 to 3.53×10^{-3} in step 14 (Tab. 5). The CV of the reliability index increased slightly from 0.192 in step 1 to 0.244 in step 4, being 0.221 on average.

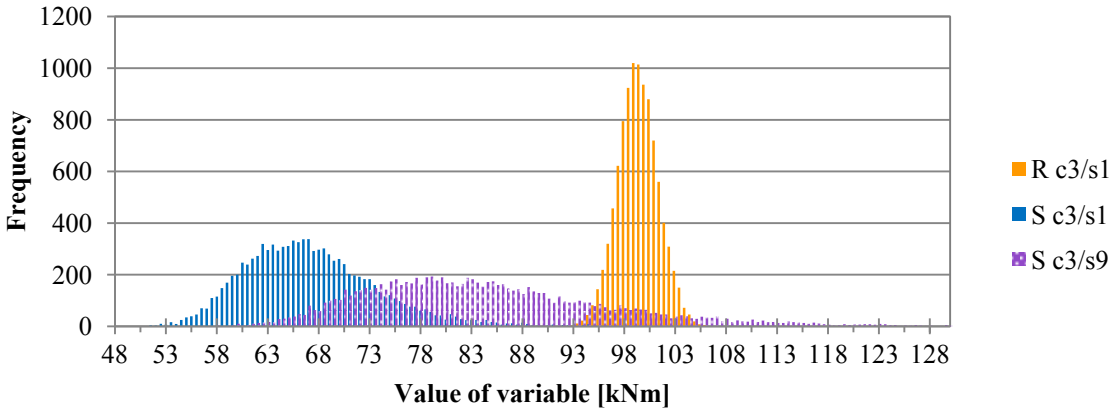

Fig. 5: Histograms of case 3: stress of steps 1 and 9, resistance of step 1

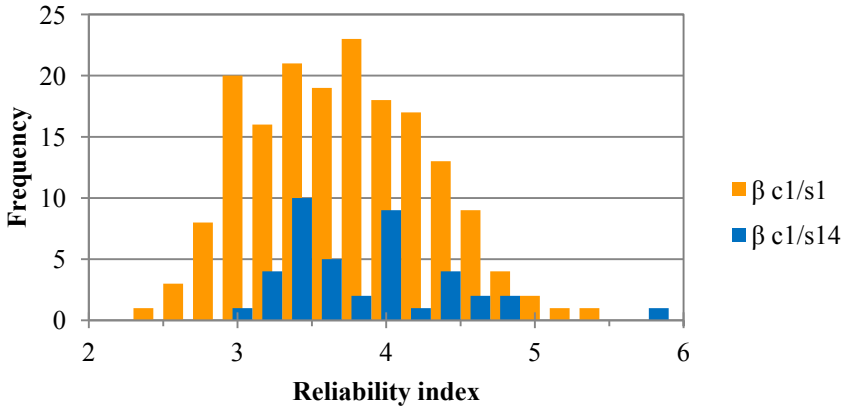

Fig. 6: Histograms of case 1: reliability index of steps 1 and 14

Reliability indices and failure probabilities of cases 1, 2 and 3 are shown in Tab. 5 and as graphs in Fig. 7, Fig. 8 and Fig. 9. Relation of the approximate reliability index (β^*) and the probability of failure (P_f) is logical in all three cases: high reliability indices are associated with low failure probabilities, and vice versa. The bending resistance also changes logically in relation to β^* (Tab. 4 and Tab. 5). The minimum reliability index of 1.275 is found in step 1 of case 2, which is associated with the highest failure probability of 1.369×10^{-1}. The maximum value of β^* is 3.841 and is also observed in case 2, which is likewise associated with the lowest P_f of 4.333×10^{-4}.

Tab. 5: Results of the reliability analysis: reliability index and probability of failure

Case	Step	q_k	f_{cm}	f_{ym}	β^*	P_f
1	1	4.00	13.90	286.80	2.319	1.750E-02
1	14	4.00	50.04	286.80	3.086	3.533E-03
2	1	4.00	27.80	229.44	1.275	1.369E-01
2	8	4.00	27.80	329.82	3.841	4.333E-04
3	1	3.20	27.80	286.80	3.566	5.333E-04
3	9	6.40	27.80	286.80	1.357	1.159E-01

Regression curves are also shown in graphs of the approximate reliability index and the probability of failure (Fig. 7, Fig. 8 and Fig. 9). Logarithmic regression is used for β^* in case 1. This is well in line with the theory of calculating the bending resistance of a RC beam: if bending resistance is plotted as a function of concrete strength, shape of the graph is approximately logarithmic. Power regression is used for the probability of failure in case 1. A high coefficient of determination (R^2) is observed for both regression curves. Using an exponential regression for the probability of failure yields a R^2-value of 0.7666.

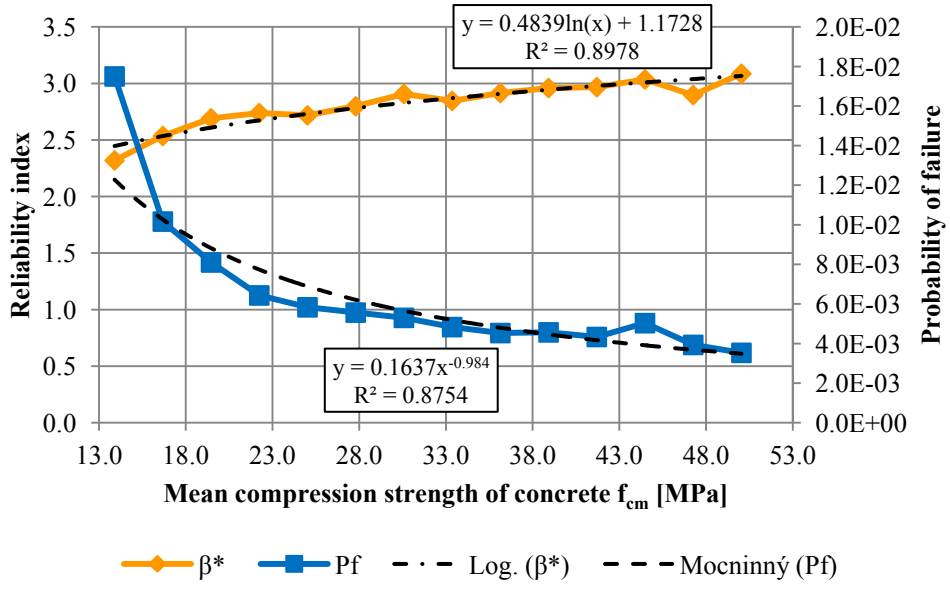

Fig. 7: Reliability index and probability of failure for case 1 (steps 1 to 14)

Curve of β^* is approximated with a linear regression for case 2 in Fig. 8. Linear regression is in conformity with the theory of structural mechanics. When expressed as a function of yield strength of reinforcement, the bending resistance is linear. Exponential regression is selected for the failure probability in case 2. Regression function of P_f approaches asymptotically the value of zero as one could expect. Exceptionally high coefficients of determination are seen for regression curves of case 2.

Linear and exponential regressions are also used in case 3 (Fig. 9). Remembering the definition of the limit state function in Eq. (2) and that the characteristic variable load is a stress variable, the linear regression of β^* seems logical. If the regression function of P_f was correct, which is unlikely; a characteristic variable load of 7.458 kN/m would result in certain failure, i.e. a failure probability of 1.0. High R^2-values are also observed in case 3.

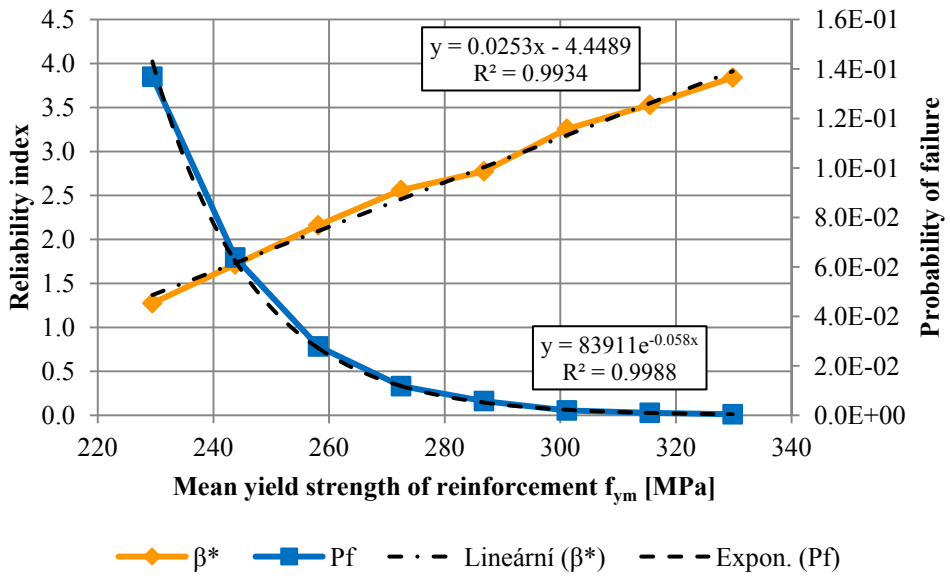

Fig. 8: Reliability index and probability of failure for case 2 (steps 1 to 8)

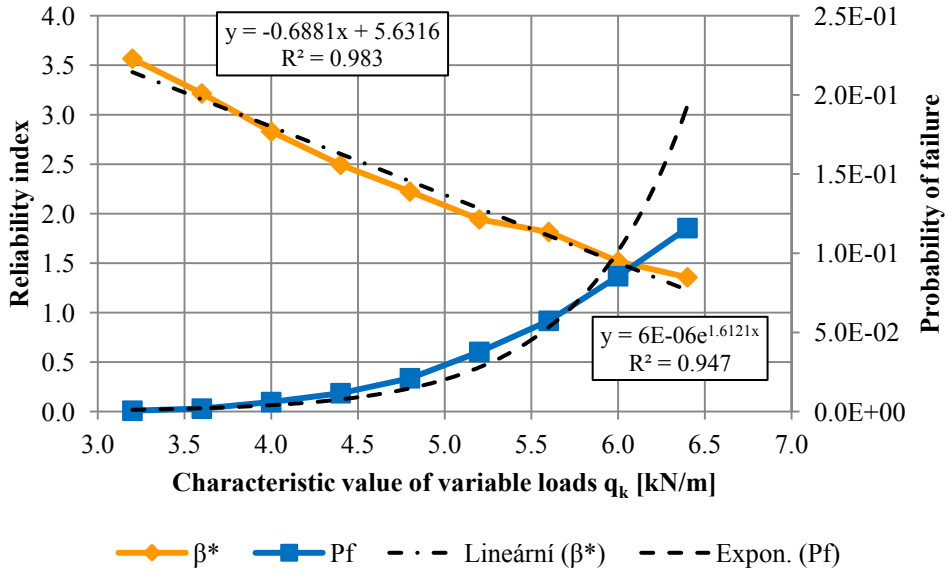

Fig. 9: Reliability index and probability of failure for case 3 (steps 1 to 9)

4 Conclusions

A histogram-based method for evaluation of the Hasofer-Lind index has been developed. The method enables evaluation of the reliability index without definition of the limit state function in the standardized space, hence removing this often challenging step from the reliability analysis. Bending of a reinforced concrete beam was studied as an example, and logical correlation between the bending resistance, the probability of failure and the reliability index was found. Based on simulations done with an elementary case of two Gaussian variables, the histogram approach led to a sufficient accuracy with sample sizes of

8000 and above. A major advantage of the developed approach is the possibility of using test data to enrich a histogram, even without any distribution assumptions.

Literature

[1] Derry, M. *Epistemic uncertainty of an existing concrete structure*. Master's Thesis, Espoo, Finland, 2011

[2] Eurocode 1: *Actions on structures*. Part 1-1: *General actions. Densities, self-weight, imposed loads for buildings*. (SFS-EN 1991-1-1, Finnish Standards Association SFS 2002)

[3] Holicky, M. & Sykora, M. Stochastic Models in Analysis of Structural Reliability. *SMRLO'10 − The International Symposium on Stochastic Models in Reliability Engineering, Life Sciences and Operations Management Proceedings*. Israel, 2010

[4] Joint Committee on Structural Safety (JCSS). Probabilistic Model Code, 2001: Available: http://www.jcss.ethz.ch/publications/publications_pmc.html

[5] Lemaire, M. *Structural Reliability*. London: ISTE Ltd and Hoboken: John Wiley & Sons, Inc., 2009

[6] Thoft-Christensen, P. & Baker, M. J. *Structural Reliability Theory and Its Applications*. Heidelberg, Germany: Springer-Verlag Berlin, 1982

Probabilistic assessment of shear capacity of precast prestressed hollow-core slab ELEMATIC using parameters identification and statistical simulation

Jiří Doležel, Drahomír Novák, David Lehký
Institute of Structural Mechanics, Faculty of Civil Engineering,
Brno University of Technology, Brno
dolezel.j@fce.vutbr.cz, novak.d@fce.vutbr.cz, lehky.d@fce.vutbr.cz

Abstract: A complex approach for statistical and reliability analyses of concrete structures is presented. It describes the virtual simulation used on the way from assessment of experimental results to reliability analysis. The whole approach is based on randomization of nonlinear fracture mechanics finite element analysis of concrete structures. Efficient techniques of both nonlinear numerical analysis of concrete structures and stochastic simulation methods of Monte Carlo type have been combined in order to offer an advanced tool for assessment of realistic behaviour of concrete structures. The stochastic response requires repeated analyses of the structure with stochastic input parameters, which reflects randomness and uncertainties in the input values. The procedure utilizes statistical simulation of Monte Carlo type also for preparation of training set of artificial neural network used for fracture mechanical parameters identification. The application of approach to virtual statistical simulation of shear capacity of prestressed hollow-core slab ELEMATIC is presented. Design shear capacities calculated according to design codes and alternative procedures are compared with simulation of reality representing virtual reliability control of elements production.

Keywords: prestressed hollow-core slab, identification, nonlinear FEM analysis, probabilistic analysis, design value

1 Introduction

Precast prestressed hollow-core slabs are currently designed to day using the method of partial safety factors according to valid European codes for the design of building structures, EC2 PART 1-1 [1]. EC2 PART 2 [2] makes it possible to apply nonlinear calculation in the design, assuming that the values of mechanical parameters of basic material have been modified and the global safety factor value has been defined. The design value of capacity can be estimated by way of method PSF (Partial Safety Factor) or ECoV (Estimation of

Coefficient of Variation) [3]. These approaches can be classified as "classical deterministic methods". The most advanced method of verifying the capacity of a structure or its part is full probabilistic calculation which is the valid method referred to in current codes or standards [4]. The probabilistic analysis used to verify the capacity of structure is based on the Monte Carlo type of numerical simulation (Latin Hypercube Sampling) and on the solution of nonlinear response of construction using the finite element method. The parameters of the nonlinear computational model are considered in stochastic model as random variables including statistical correlation.

This paper is focused on the verification of shear capacity of the ELEMATIC type panel using probabilistic calculation and comparison of the design value of shear capacity based on calculation according to EUROCODE and Fib Model Code 2010 with actual experiments with panels in the conditions of single line loading.

2 Concrete Fracture-Mechanical Parameters Identification

Concrete is classified among quasibrittle materials and can be defined by the values of fracture-mechanical parameters, e.g. work of fracture and specific fracture energy. The fracture energy represents a fundamental parameter for models of cohesive cracks which are frequently used for numerical simulation of specimen/structures made of quasibrittle materials. Sudden catastrophic loss of stability should be considered for correct assessment of fracture energy loading specimen by constant deflection. Selected parameters of concrete can be obtained by two alternative approaches: 1) assessment of load–deflection diagrams obtained from fracture tests of concrete elements; 2) parameters identification based on artificial neural networks. The reason for utilization of identification is the possibility of assessment of tensile strength of concrete. It is very difficult in the event of fracture tests.

2.1 Fracture mechanics of quasibrittle materials

Fracture-mechanical parameters of concrete are usually determined on the basis of evaluation of fracture tests on specimen with a defined concentrator of tension, within a suitable testing configuration. In the case of identification of the parameters of concrete in the ELEMATIC panel four test specimens (beams of nominal sizes 40 × 70 × 500 mm) were available. These were cut from the middle sections of the unit. Three-point bending of notched specimen was used and loading was applied continuously by deformation increment of 0.1 mm per minute in the midspan of beam, Fig. 1. A load–deflection diagram was recorded – see e.g. [5]. Based on the model of equivalent elastic crack, the critical length of effective crack and effective fracture toughness can be determined. Work of fracture and specific fracture energy can be obtained from the load–deflection diagram [6].

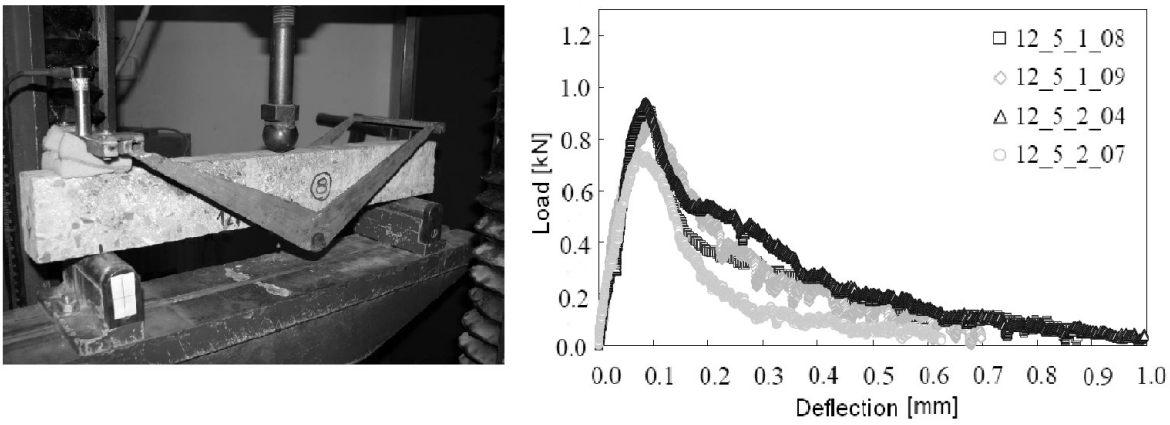

Fig. 1: Test configuration, load−deflection diagram

2.2 Identification of parameters from inverse analysis

The second method utilized to obtain selected parameters of concrete of the ELEMATIC panel was inverse analysis using identification method based on artificial neural network in combination with stochastic analysis. The method is based on numerical simulation of a standardized fracture test. The cornerstone of the method is an artificial neural network which transfers the input data obtained from the fracture test to the desired material parameters. For theoretical details on the ANN-based inverse analysis, as these go beyond the present scope, we refer the interested reader to [7]. Subject to identification selected on the basis of sensitivity analysis were following parameters: modulus of elasticity, tensile strength and fracture energy. An artificial neural network utilized in inverse analysis is of a feed-forward multilayer type. The network consisted of 3 inputs, one hidden layer having 5 neurons with a non-linear transfer function (hyperbolic tangent) and an output layer having 3 neurons with a linear transfer function, see Fig. 2. Each of the output neurons corresponds to one of the identified parameter. The inputs of neural network are 3 parameters taken from *l–d* diagram: Peak load, load at deflection of 0.01 mm and area under *l–d* diagram corresponding to fracture work. The size of training set was set to 100 samples generated using the Latin Hypercube Sampling method. Once ANN was trained the experimental response was used to obtain identified parameters. With this set of parameters a numerical analysis was carried out and the resulting response was compared with the experimental one, see example in Fig. 2. The numerical FEM model was created in ATENA software [8], a 3D Nonlinear cementitious 2 material model for concrete was utilized. Identification was performed using the software for artificial neural networks DLNNET [9] and the probabilistic software FReET [10],[11].

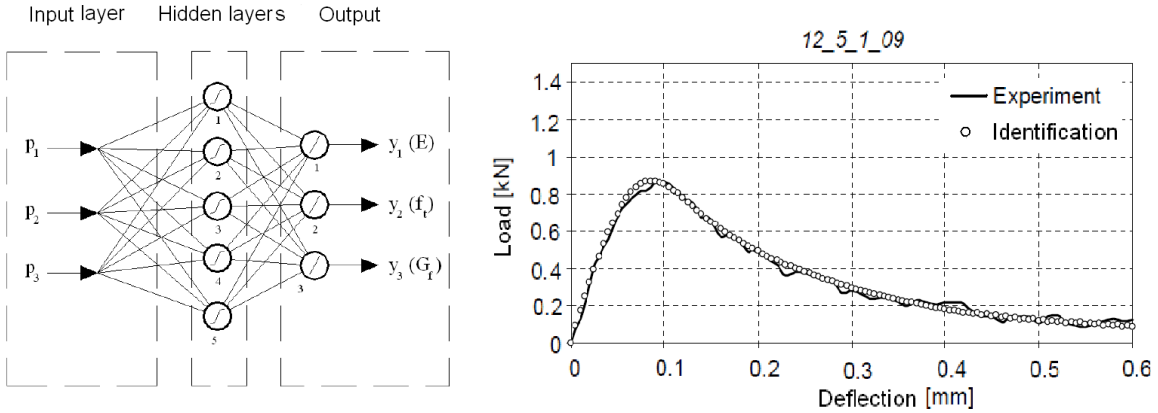

Fig. 2: Scheme of artificial neural network, comparison of *l*–*d* diagrams (experiment vs. identification)

The values of the selected parameters of four analyzed elements taken from the ELEMATIC panel and evaluated from the fracture tests are presented in Tab. 1 together with results obtained from identification. For the modulus of elasticity and fracture energy, the ratios between mean values obtained from the identification and from the experiments are presented for comparison. A good agreement between results obtained using both approaches was achieved. This applies to both mean values and coefficients of variations.

Tab. 1: Selected parameters of concrete obtained on the basis of experimental testing and identification

Variables		*i*	Experiment			Identification			Iden./Exp.
			X_i	Mean	CoV_i	X_i	Mean	CoV_i	
f_{ct}	[MPa]	1	-	-	-	5.0	4.4	0.128	-
		2	-			3.8			
		3	-			4.8			
		4	-			4.1			
E_c	[GPa]	1	20.8	21.9	0.139	22.9	24.1	0.147	1.10
		2	26.4			29.3			
		3	20.5			21.4			
		4	19.8			22.8			
G_f	[Nm^{-1}]	1	112.7	107.3	0.248	112.4	113.5	0.268	1.06
		2	109.3			124.6			
		3	135.7			144.5			
		4	71.4			72.4			

f_{ct} – tensile strength of concrete; E_c – modulus of elasticity; G_f – specific fracture energy

3 Probabilistic nonlinear analysis

The aim of stochastic analyses is the assessment of the capacity function (PDF) of the ELEMATIC panel in case of shear failure for a single line loading (Fig. 3). Numerical simulation was performed with the use of the stochastic modulus FReET and SARA software [12],[13], which mediates data communication with the ATENA 2D programme. Concrete was modelled by 3D Nonlinear cementitious material model, which is defined basically by effective compression and tensile strength, fracture energy and modulus of elasticity. Prestressing strands were modelled by bilinear stress–strain diagram with hardening.

3.1 Basic random variables

Material parameters of concrete and prestressing strands were considered as basic random variables. Statistical parameters of concrete were estimated from fracture-mechanical tests and from artificial neural network based on the identification described above. Eight uniaxial tests were performed for prestressing strands; the parameters of stress–strain diagram of prestressing strand could be estimated from these tests. The probabilistic models of basic random variables were considered according to JCSS guidelines [14]. The statistical parameters of basic random variables are summarized in Tab. 2. Additionally, statistical correlations were considered in sampling scheme, details can be found in [15].

Tab. 2: Probabilistic models of basic random variables

i	Variables		Distribution type	Mean	CoV
1	f_c	[MPa]	Lognormal (2 par.)	−55.0	0.020
2	f_{ct}	[MPa]	Lognormal (2 par.)	4.4	0.128
3	E_c	[GPa]	Lognormal (2 par.)	24.1	0.147
4	G_f	[Nm^{-1}]	Lognormal (2 par.)	113.5	0.268
5	γ_c	[kgm^{-3}]	Normal	2392	0.009
6	$f_{p0.1}$	[MPa]	Lognormal (2 par.)	1738.0	0.010
7	f_{pu}	[MPa]	Lognormal (2 par.)	1951.0	0.003
8	$\varepsilon_{0.1}$	[-]	Lognormal (2 par.)	0.0101	0.005
9	P_t	[kN]	Deterministic	695.0	-

f_c – compressive strength of concrete; γ_c – specific weight of concrete; $f_{p,0,1}$ – 0.1% proof stress of prestressing strand; f_{pu} – tensile strength of prestressing strand; $\varepsilon_{0.1}$ – strain at the proof stress $f_{p,0.1}$; P_t – value of prestressing force in time t

3.2 Results

Monte Carlo type simulation of shear failure of panels PPE 200 was performed (sample size 50). A bundle of random load–deflection curves is a key result of virtual statistical simulation (Fig. 3). Then probability distribution function of shear capacity was estimated. For each nonlinear calculation a realization of random vector for basic random variables was prepared first using stratified sampling LHS and then nonlinear calculation was done simulating the process of crack formation. Statistical parameters of shear capacity in form critical load P_u could be assessed from peaks of *l–d* diagrams. Estimation the design value of the shear capacity is performed as recommended by the EC [18] Appendix C assuming lognormal distribution of critical load P_u in equation (1),

$$P_{u,d} = \mu_{Pu} \exp(-\alpha.\beta.V_{Pu}) \text{ for } V_{Pu} \le 0.2 \tag{1}$$

where

$P_{u,d}$ is design value of critical load,

μ_{Pu}, V_{Pu} are average values and coefficient of variation of critical load,

α, β is sensitivity factor, reliability index.

The average value of critical load is μ_{Pu} = 216.5 kN, coefficient of variation is V_{Pu} = 0.140 and skewness is $Skew_{Pu}$ = − 0.188. Value of probability index and sensitivity factor is on estimate design value of shear capacity is β = 3.8 and α = 0.8.

Histogram with selected probabilistic model in the form of lognormal PDF of shear capacity in form critical load P_u and estimate the design value of the critical load are plotted on Fig 3.

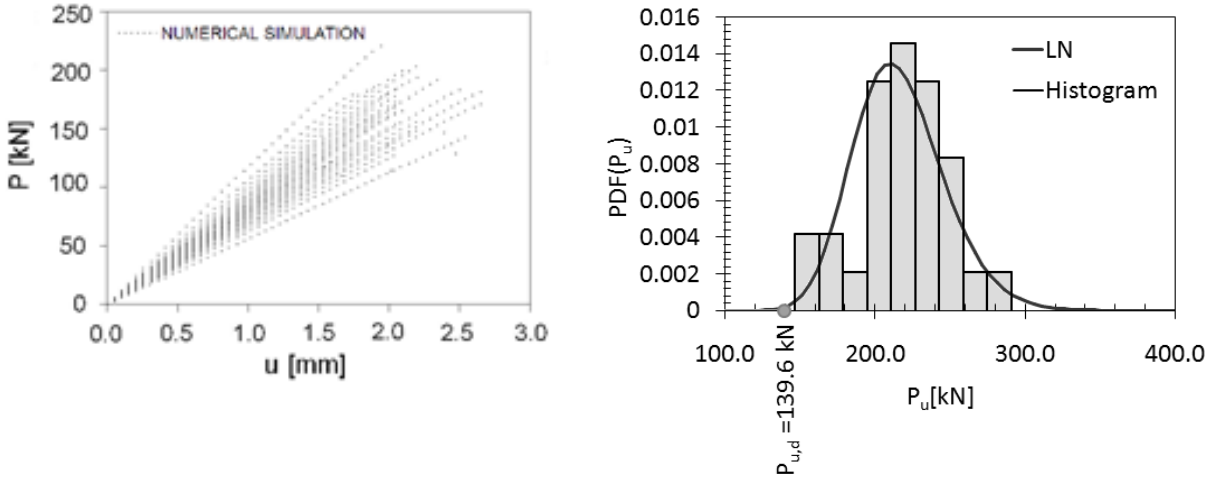

Fig. 3: Load–deflection diagrams from simulations, histogram and probability distribution function of critical load

4 Conclusions

A real experiment was performed for three panels type PPE 200 to verify shear capacity (Fig. 4). The resulting values of critical load P were compared with virtual probabilistic simulation and with value of design shear capacity according by EC2 and different design techniques Fib Model Code 2010.

Fig. 4. Test configuration, shear failure of panel

The result of virtual reliability simulation of shear capacity representing in certain way the reality is shown in Fig. 5 together with three experiments and individual deterministic design techniques in the left tail of PDF. It can be seen that design codes are very conservative. Also confidence intervals are depicted for probabilities 0.05 (0.95) and 0.001 (0.999). The picture gives us an overall view where we are when using different design techniques

(EC2 part 1-1, EC2 part 2, ECoV, PSF) and provide us with a virtual reliability verification to support decisions on design value of shear capacity of particular concrete elements in concrete prefabrication. The main impact of simulation consists in an increase in the design value of shear capacity for elements. The approach presented here goes beyond design codes and represents an alternative individual method taking material uncertainties directly into account to control virtual reliability. It can be routinely applied for other precast concrete elements or concrete structures.

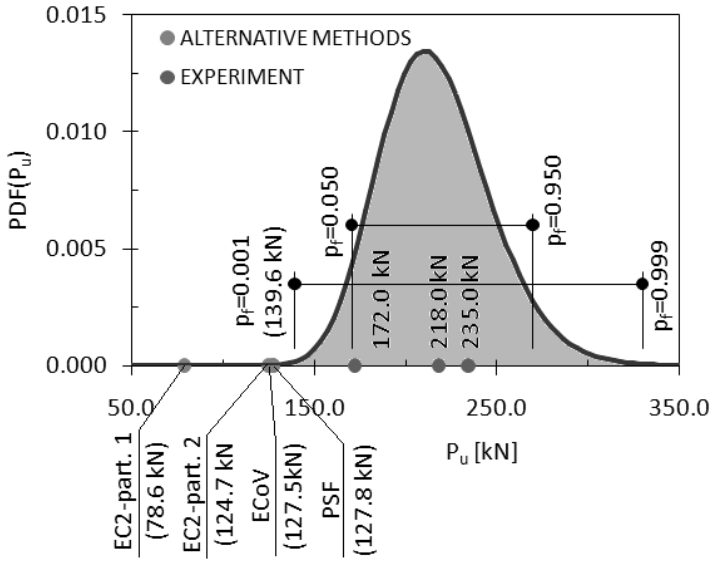

Methods	$P_{u,d}$
EC2–part.1	78.9
EC2– part.2	124.7
ECoV	127.5
PSF	127.8
FP	139.6

Experiment	P_u
Unit A	235
Unit B	218
Unit C	172

Fig. 5. Comparison of shear capacities obtained from experiments, probabilistic approach and different design techniques.

5 Acknowledgement

The authors give thanks for the financial support of the Czech Scientific Foundation, project No. P104-13-03662S, and the project of the specific university research at Brno University of Technology, registered under the number FAST-S-13-2017.

Literature

[1] ČSN EN 1992-1-1, *Eurocode 2: Design of concrete structures - Part 1-1: General reles and rules for buildings.*, Czech Republic: 2006

[2] ČSN EN 1992-2, *Eurocode 2 - Design of concrete structures - Part 2: Concrete bridges - Design and detailing rules*. Czech Republic: 2006

[3] *Fib Model Code 2010.* Fédération internationale du béton, Lausanne, 2010

[4] ČSN EN 1990, *Eurocode: Basis of structural design.*, Czech Republic: 2003

[5] Karihaloo, B.L. *Fracture mechanics of concrete*. Longman Scientific & Technical. New York: 1995

[6] Keršner, Z., Frantík, P. and Veselý, V. Accepting of influence of stability loss during displacement-controlled loading in fracture test. *Proc. of 11th International Conference on Ecology and new building materials and products*, Telč, Czech Republic, p. 324–327

[7] Novák, D. and Lehký, D. ANN Inverse Analysis Based on Stochastic Small-Sample Training Set Simulation. *Engineering Application of Artificial Intelligence*. 19, 2006, pp. 731–740

[8] Červenka, V., Jendele, L. and Červenka, J. *ATENA Program Document. – Part 1: Theory*., Cervenka Consulting, Prague: 2007

[9] Lehký, D. *DLNNET – program documentation. Theory and user's manual*., Brno: 2013 (in preparation)

[10] Novák, D., Vořechovský, M. and Rusina, R. *FReET v. 1.5 – program documentation. User's and Theory Guides*., Brno/Červenka Consulting, http://www.freet.cz, 2013

[11] Novák, D., Vořechovský, M. and Rusina, R. Small-sample probabilistic assessment – software FREET. *Proc. of 9th Int. Conf. on Applications of Statistics and Probability in Civil Engineering – ICASP 9*, San Francisco, USA, Rotterdam Millpress: 2003, p. 91−96

[12] Bergmeister, K., Novák, D. and Pukl, R. An advanced engineering tool for reliability assessment of concrete structures. *Proc. of the 2nd Int. Conf. Progress in Structural Engineering, Mechanics and Computation*, A. Zingoni (ed.), Cape Town, South Africa, Taylor&Francis Group, London: 2004, p. 899−904

[13] Pukl, R., Novák, D. and Bergmeister, K. Reliability assessment of concrete structures. *Proc. of Computational modelling of concrete structures (Euro-C2003)*, N. Bicanic et al. (eds), St. Johann, Austria, Lisse: Balkema. 2003, p. 793−803

[14] JCSS, *JCSS working material.,* Available: http://www.jcss.ethz.ch

[15] Doležel, J. *Probabilistic analysis of precast prestressed units of SPIROLL type*. Diploma Thesis, Institute of Structural Mechanics, Faculty of Civil Engineering, Brno University of Technology, Czech Republic, Brno, 2008 (in Czech)

A practical bridge maintenance scheduling using genetic algorithm considering uncertainty

Hitoshi Furuta*, Ken Ishibashi**, Noriaki Miyoshi**, Mami Aira** and Masato Usui**
* Department of Informatics, Kansai University, Takatsuki, Japan
** Graduate School of Informatics, Kansai University, Takatsuki, Japan
furuta@res.kutc.kansai-u.ac.jp

Abstract: The sustainable management for bridges is necessary to maintain the economic activity and the safety of daily life. In order to achieve a practical long-term maintenance plan established by Genetic Algorithm (GA), it is necessary to consider the uncertainties of deterioration prediction and budget for maintenance. In the past researches, it was demonstrated that the preventive plan includes the period that an executing year of maintenance work can be changed without the increase of cost and the loss of safety. However, it is difficult for GA applied in the previous researches to obtain the robust period which can treat various changes of schedule because the optimization does not consider the influence of uncertainty. In this study, an attempt is made to formulate a reasonable maintenance plan that involves the robust period by using the improved GA considering uncertainty. Numerical examples are presented to demonstrate the effectiveness of the proposed method.

Keywords: bridge management, maintenance plan, optimization, genetic algorithm, uncertainty

1 Introduction

In order to establish the sustainable bridge management, it is important to reduce the life-cycle cost (LCC) of bridges (FURUTA ET AL. [2]). A long-term planning for the bridge maintenance is expected to be effective for ensuring the safety of bridges reasonably. Thus, the optimization of maintenance plan has been studied (FURUTA ET AL. [1], [4], [5]). However, a long-term plan needs to improve the effectiveness for a practical maintenance activity. In the actual bridge management, the change of the schedule of maintenance works is required for keeping the safety level and reducing the annual cost less than the budget constraint. This is because the deterioration prediction and the evaluated state of bridge have possibilities to involve the error. Furthermore, the economic circumstances and the traffic quantity are more likely to change during the service term. Therefore, to improve the prac-

tical applicability of long-term planning for the bridge maintenance, it is necessary to formulate a robust plan against these uncertainties.

In this paper, an attempt is made to propose a method formulating a robust plan by using the improved Genetic Algorithm (GA). In the previous research by NAKATSU ET AL. [4], it was shown that the preventive maintenance plan involves a period in which an executing year of work can be changed without the loss of safety level and the increase of maintenance cost. The preventive maintenance with the flexible period is expected to enhance the robustness of plan against uncertainties. Therefore, the proposed method formulates a robust and useful plan in consideration of uncertainties. In the proposed method, a maintenance plan is obtained by using the improved GA considering uncertainty. In this GA, an individual is evaluated by applying the periods which have the effect of preventive maintenance. This effect of preventive maintenance is estimated by the deterioration prediction based on a genetic array. In addition, all individuals are re-evaluated with considering the change due to the uncertainty of deterioration prediction in every generation. In this way, the proposed method can obtain a robust and reasonable solution efficiently. Several numerical experiments are presented to demonstrate the effectiveness of an obtained plan in the actual bridge management.

2 Optimization for bridge maintenance

The purpose of bridge management is to prolong the life of bridges by repair and reinforcement against the degradation. In order to sustain the safety of bridge, it is common to keep the intact state by regular detailed inspection, high-quality repair, reinforcement and renovation. However, it is actually difficult to perform the above maintenance. This is because these require a lot of cost and manpower. Therefore, it is important to establish a long term bridge management plan. A long term plan is useful to reduce the maintenance cost with sustaining the safety based on the deterioration prediction. In addition, this plan is useful to estimate for long term budget; it is possible to improve the accountability to citizens by visualizing the purpose of budget.

2.1 Application model

A group of ten concrete highway bridges are considered in this paper. Maintenance management planning for ten consecutive piers and floor slabs (composite structure of steel girders and reinforced concrete (RC) slabs) is considered. Each bridge has the same structure and is composed of six main structural components: upper part of pier, lower part of pier, shoe, girder, bearing section of floor slab, and central section of floor slab. This paper uses the bridge model applied in NAKATSU ET AL. [4]. In addition, the maintenance plan is formulated for 10 bridges in the network shown in Fig. 1 (FURUTA ET AL. [2]).

2.2 Life-cycle cost

In this paper, LCC is defined as the summation of the construction cost and user cost. The breakdown of construction cost is shown in Fig. 2 and the user cost represents the social loss of residents caused by the road traffic regulation (Furuta et al. [2]). The performance deterioration of each component can be recovered or prevented by repair and reinforce-

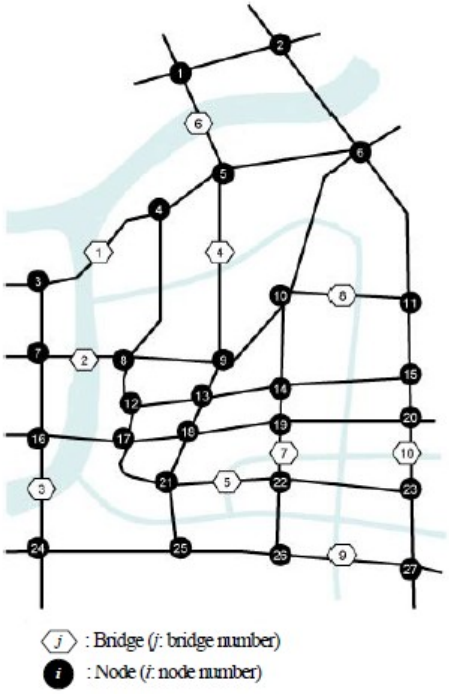

Fig. 1: Road of network

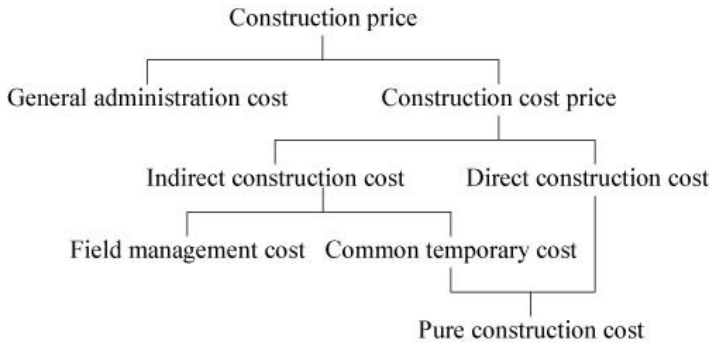

Fig. 2: Breakdown of construction cost

ment. Here, replacement of bearing, steel girder paint and exchange slab is applied to shoe, girder and slab, respectively as the update method. The cost of repair is estimated by adding construction cost which is determined by the area of component and repair method to scaffold cost. The scaffold can be shared among multiple components when they are repaired in the same year. Basically, the scaffold which is required to certain component can be shared with others which are located lower than it.

2.3 Problem setting

In maintenance planning, it is required to sustain the safety of all components during their service period. In this paper, the service period is set to be 100 years. Therefore, the purpose of planning is to minimize the maintenance cost under the circumstances. The performance of component to sustain the safety is more than 0.8 as well as the previous research (FURUTA ET AL. [1]). This is because the purpose of this paper is to verify the applicability of planning method through numerical examples. This value should be determined on the basis of safety required in the maintenance management in the real-world problem.

2.4 Necessity of optimal maintenance planning

The LCC for bridge maintenance can be reduced with deciding the appropriate execution period of works among bridges, as described in 2.2. To maintain lots of bridges, it is necessary to consider every bridge's importance including cost reduction efficiency, sustainable safety and user cost. However, the influence of uncertainties is unable to be removed completely from a long-term plan because the perfect predictions of bridge's deterioration and economic change are quite difficult even if new methods were developed. Thus, it is important to be able to change the schedule partially with minimizing the increase of cost and keeping the safety of bridges.

This study attempts to establish a long-term plan with robust execution terms of works against uncertainties. Past researches (FURUTA ET AL. [2], [4]) have demonstrated that the preventive maintenance is effective for the error of deterioration prediction. Furthermore, to equalize the annual cost in a long-term plan overcomes the difficulty of budget allocation. However, it is difficult to make a long-term plan with the robustness. For example, the simulation based on Monte Carlo method requires a lot of computations per solution to evaluate the robustness. Therefore, this study proposes the method considering the computation efficiency of optimization to establish a robust plan.

3 Robust planning method against uncertainty

3.1 Treatment against uncertainty

The purpose of the long-term maintenance planning for bridges is not only to minimize LCC and ensure their safety but also to estimate the budget during the service period. The previous researches (NAKATSU ET AL. [4], [5]) proposed the method to establish a preventive maintenance plan with the period when the execution of work can be postponed without the huge increase of cost and the loss of safety, using GA. It has been implied that this flexible period improves the plan's robustness against uncertainties. However, the existing planning has possibilities to be difficult to adapt the schedule to the changing situations by using the obtained terms of maintenance works (NAKATSU ET AL. [5]). This is because the length of period which can be changed, involved in the formulated plan, became short due to the minimization of LCC in the constant scenario.

By considering uncertainties during the optimization, this paper attempts to propose a method that formulates the maintenance plan with the adaptable period to a variety of situations. In the previous study, the period that can postpone the work is calculated based on the plan obtained by GA for the preventive maintenance. However, it is considered that the preventive maintenance performed by moving up the established schedule is effective to improve the robustness against uncertainties influencing the safety of bridges as shown in Fig. 3. Therefore, the proposed method aims to develop a robust and economic plan for the bridge management, taking into account the effect of preventive maintenance that accelerates the schedule.

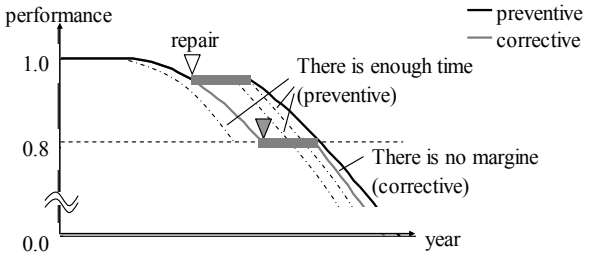

Fig. 3: Deteriorations of preventive and corrective maintenance

3.2 Optimal planning by genetic algorithm

GA Genetic Algorithm Considering Uncertainty (GACU) was proposed to search for robust solutions against uncertainties (TANOOKA ET AL. [6]). However, in the study of the authors (NAKATSU ET AL. [3]), it was difficult to obtain a solution with both robustness and optimality by the original GACU; it is implied that this method requires the improvement in response to the application problem.

The proposed planning by this paper optimizes solutions, based on GACU. In order to adapt the population to the uncertain environment, the proposed method introduces the sorting rule for the setting of fitness and the revaluation involves the change of situations, by using the evaluation criteria to the robustness. Here, the applied coding rule for the maintenance planning is the same as the previous method (NAKATSU ET AL. [5]). In addition, the evaluation of individual is performed by taking into account the period when the execution of work can be accelerated, based on the deterioration prediction for bridge. Through these approaches, the proposed method attempts to formulate a plan with the cost reduction by the flexible period and the robustness improved by the preventive maintenance.

3.2.1 Cording rule

In this paper, the coding of gene is defined as shown in Fig. 4 (FURUTA ET AL. [1]). In this coding, a gene of individual is separated to the repair method and the interval part. The genetic array of each part has the same length. And, the length is determined so as to deal with the service period by using the number of years calculated from the interval part. In this paper, the length of gene is set 50 years in order to establish the 100 years maintenance plan as described in Section 2.3. It is not realistic that 50 times of repairs or reinforcements are performed to a component of bridge in 100 years. Thus the length described above is enough to deal with this problem. Here, unnecessary genes to establish a 100 years plan are not used to optimize.

The information of gene in the repair method part represents the identification number of repair method. In this paper, the identification number of each repair method is set as follows; the surface painting is 1, the surface covering is 2, the section restoring is 3, the desalting and re-alkalization is 4, the cathodic protection is 5, the section restoring with surface covering is 6 and the reconstruction is 7. The genotype described above is converted to the phenotype shown in Fig. 4 in order to use as an annual plan. Here, a part containing 0 in the phenotype represents a year when a repair and reinforcement are not

performed. In the crossover section, the two parts of gene is performed respectively. The uniform crossover is adopted as the crossover method in this paper. In the mutation section, the two parts of gene are performed respectively as well as the crossover section. A value of gene is replaced to a randomly generated number in the repair method part. On the other hand, the operation of mutation in the interval part is performed as shown in Fig. 5. Through this operation, the schedule following to a mutated gene does not change; the mutation is performed without changing the property of solution candidate.

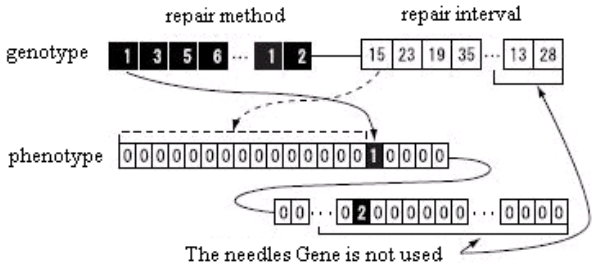

Fig. 4: Coding rule

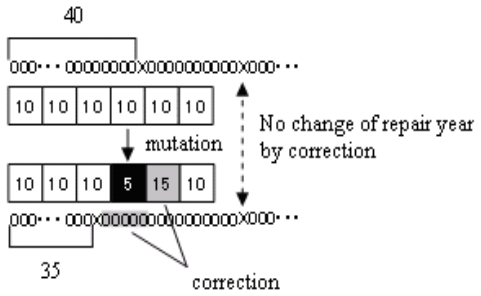

Fig. 5: Mutation of interval part

3.2.2 Evaluation of robustness against uncertainty

The expected value evaluated under various situations is one of evaluation criterion for the robustness of solution against uncertainties. This index can improve its estimation accuracy by increasing the number of evaluations. However, this improvement involves the increase of computation time simultaneously. By introducing the age structure and the inheritance of search information between similar individuals to the conventional GA, GACU is a technique to aim to overcome the computation problem described above. These operations enable this method to search for robust solutions efficiently, but the computation accuracy becomes low in a complicated problem because they are based on the pseudo-estimation. In addition, the evaluation with the expected value does not guarantee the optimality of solution in the situation without the influence of uncertainties; in the maintenance planning for bridge, an obtained solution requires enormous LCC due to more frequent works for the safety.

In the proposed method, individuals are evaluated by using the effective sorting rule to improve their optimality and robustness, focusing on the search process of GACU. In GACU, an individual has higher evaluation under certain situation is more likely to survive during early generations because the fitness is the expectation of evaluation observed per generation. Then, as the search progresses, robust solutions are set to high fitness but others' become lower. Finally, the population converges to the domain where the expectation is highest. On the other hand, the proposed method that sets higher fitness to an individual has the optimality and the robustness enough to use practically. In order to realize this search, individuals that are robust more than the configured border are set the fitness based on not the expectation but the evaluation without the influence of uncertainties. Therefore, the proposed method evaluates all individuals based on the following sorting rules per generation, considering uncertainties.

- Group 1: Robust individuals: Individuals are sorted in ascending order of LCC calculated by Eq. (1). In addition, among individuals with the same cost, they are sorted in

descending order of the expectation of total of performance, shown in Eq. (3), in the service period. In this paper, an individual which has met the safety standard at least once since generated, evaluated with changes due to uncertainties, is treated as this group.

- Group 2: Individuals satisfying constraints: Individuals that satisfy the constraints of the annual cost and safety when evaluated without taking into account uncertainties is treated as Group 2. They are sorted in descending order of the expectation, calculated by Eq. (3) with the performance, as the index of robustness.
- Group 3: Individuals violating constraints: Individuals with the violation of the safety level as shown in Eq. (2) are sorted in ascending order of the total of lack of performance during the service period. In addition, those which were beyond the annual budget in the service period are sorted in ascending order of the sum of exceeded cost.

In this paper, LCC used as the evaluation criterion is defined as in Eq. (1). In Eq. (1), $MC_{b,p}$ represents the maintenance cost required for component p of bridge b and $UC_{b,p}$ is the user cost generated by the repair work of corresponding part. The performance of component during the service is defined as in Eq. (2). In Eq. (2), $PI_{b,p,y}$ represents the performance of component p of bridge b in year y. In the service period, the performance is required to ensure the safety level. This paper sets its border to 0.8 as described in Section 2.3. Eqs. (1) and (2) are determined by the repair method for each year. The expectation of the performance is defined as in Eq. (3), based on the formula of fitness applied by GACU. In Eq. (3), $g(y_i)$ represents expectation of the performance of the individual, and d_i represents the number of survival generations. The term $(d_i - 1)g(p_i)$ is the expected value until the last time, and $h\left(f\left(\hat{w}, x_i\right)\right)$ represents the performance which evaluated in consideration of uncertainty in the present generation.

$$\sum_b \sum_p MC_{b,p} + UC_{b,p} \tag{1}$$

$$PI_{b,p,y} \geq 0.8 \tag{2}$$

$$g\left(y_i\right) = \frac{\left(d_i - 1\right)g\left(p_i\right) + h\left(f\left(\hat{w}, x_i\right)\right)}{d_i} \tag{3}$$

In addition, the sorting between groups of individual in the setting of fitness described above is carried out as shown in Fig. 6. Due to the use of this sorting, the degree of health guaranteed by an obtained plan is inferior to GACU. In contrast, it becomes able to have the flexibility against the change of situations by using the period when the schedule of maintenance works can be moved up, based on the preventive maintenance described later. Furthermore, the proposed method searches for a plan that minimizes LCC in areas where there are robust solutions. Therefore, this method can establish a schedule to reduce LCC than GACU.

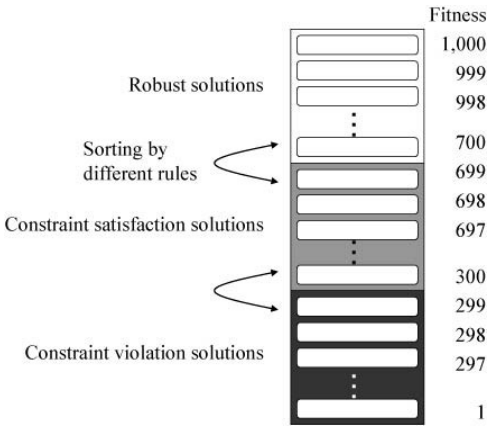

Fig. 6: Determination of fitness

3.3 Maximization of flexible term

In the proposed method, by evaluating individuals in 2 stages, an attempt is made to formulate a plan with maximized periods that are not subject to influence from the change of schedule. At first, an individual generated newly is evaluated under the environment without the influence of uncertainties. This stage aims to determine the maintenance works and their spans to minimize LCC and ensure the safety level in the service period. Next, in order to search for more robust solutions, an individual satisfying constraints is evaluated in consideration of the change of deterioration rate. Here, the period when the work can be front-loaded to improve the safety is estimated by the simulation of deterioration prediction based on the preventive maintenance. In this paper, based on the predicted deterioration curve of corresponding component, that simulation moves up the execution of work from the decided year as far as the performance does not decrease. Thus, this evaluation, based on the front-loaded plan, is effective to inspect the robustness against uncertainties.

When the evaluation involves uncertainties, it is difficult to satisfy the constraint of safety in the optimization. However, since a formulated plan can be changed within the flexible period, it is not necessary to adapt to every situation in the practical problem. In fact, the worst circumstance due to uncertainties hardly occurs. Furthermore, the length of period when the schedule can be changed, calculated by the preventive maintenance described above, is considered as the robustness of plan. Therefore, the proposed method can efficiently search for an optimal plan that involves the flexible period enough to use practically.

4 Numerical experiments

4.1 Configuration parameters

By applying to maintenance planning for a bridge group described in Section 2.1, the usefulness of the proposed method is verified. In this method, a formulated plan involves the schedule which can be changed within the period based on the preventive maintenance. Hence, in order to optimize a plan with this period, the proposed method is applied to single bridge respectively. Then, the plan, obtained by combining the result of each, handles

the influence of uncertainties such as the error of deterioration prediction and the economic change. In this way, the optimal planning for a group of bridges can improve the computational efficiency (NAKATSU ET AL. [5]). On the other hand, by optimizing the 10 bridges at the same time, the previous method (NAKATSU ET AL. [4]) develops a plan that takes into account the cost reduction resulting from large works for a group of bridges.

As the parameters of the proposed method, this paper sets 1,000 to population size, 60% to crossover rate, 0.5% to mutation rate and 1,000 to the number of generations run. On the other hand, in the previous method, the number of executing generations is set 10,000 since a number of bridges are optimized at the same time. In the setting of the degradation curve, the proposed method takes into account the error of the deterioration prediction as the uncertainty. Thus, the deterioration rate becomes higher than the standard randomly. In this paper, the influence of uncertainty is represented as the change of the turnout point of degradation progress. The turnout point T2 in Tab. 2 and 3 is decreased at random and the maximum decrease is about 20% of original T2. Then, the degradation curve is modified based on changed T2. In the previous method, the 2 patterns of constant deterioration, set standard and early speed, are adopted. The numerical experiments with the previous method are performed without considering uncertainties. In addition, in order to verify the robustness of plan, the simulation of 1,000 times evaluations under uncertain environments is applied to the solution obtained by each method.

4.2 Robustness against influence on safety

Tab. 1 shows the results obtained by numerical experiments and the variation of LCC and soundness obtained through the reduction of LCC in the flexible period in which the schedule can be changed is shown in Fig. 3. In Tab. 1, the average and standard deviation of each value are calculated from the result of each method executed 5 times respectively. “Performance” and “Durable performance” are the expectation value calculated by applying the 1,000 times simulations with the uncertainty to an obtained plan. Here, “Performance” represents the degree of soundness of the component based on the degradation model and the degree of soundness of component based on the service life model is represented as “Durable performance”. In Fig.3, the LCC represents the summation of the work cost and user cost and the degree of soundness is the total of the performance and durable performance. The range of the degree of soundness was determined by the maximum and minimum value observed in the 1,000 times simulations to the lowest solution among 5 trials of each method.

Firstly, from Tab. 1, it was found that the proposed method obtained more robust plans than the previous method based on the standard degradation rate but obtained plans increased LCC. This is because the proposed method improved the degree of soundness by increasing the frequency of maintenance works. However, the plan obtained by this method can reduce the LCC by changing the schedule in the flexible period as shown in Fig. 3. The proposed method could reduce the average scaffold cost, work cost and user cost to 403, 4224 and 12747 million yen respectively.

Secondly, the proposed method reduced more LCC than the previous method based on the early degradation speed as shown in Tab. 1. A schedule in the plan obtained by the proposed method is decided by moving up the executing year of works. Thus, by extending

the length of period in which the schedule can be changed, the preventive maintenance was performed without increasing the frequency of work excessively. In this way, the proposed method can reasonably improve the robustness of plan against uncertainties that influence the safety. From Fig. 3, it was found that a plan formulated by the proposed method could save costs with keeping the degree of soundness in the comparison with the previous method based on the prediction of early degradation rate. Therefore, it is expected that the proposed method is effective to formulate a robust and reasonable plan against the uncertainties related to the safety of bridges.

Tab. 1: Application results (each cost is represented in millions of yens)

Method (deterioration rate)	Previous (standard) Av.	Previous (standard) S. d.	Previous (early) Av.	Previous (early) S. d.	Proposed (uncertain) Av.	Proposed (uncertain) S. d.
Maintenance cost	1916	36.072	2585	58.851	2341	26.991
Scaffold cost	331	7.184	507	11.514	430	13.271
Work cost	3447	56.782	4789	108.950	4352	269.912
User cost	10528	375.433	16772	985.206	14280	1321.344
Performance	2820	25.404	2949	17.101	2992	0.468
Durable performance	2879	5.261	3000	0.000	2915	15.119
Average length of flexible periods	6.595	0.475	10.342	0.496	14.317	0.672

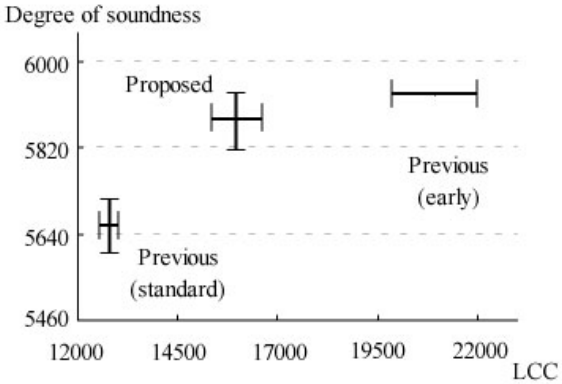

Fig. 7: Variation ranges of LCC

4.3 Robustness against change of schedule

In the long-term bridge management, it is necessary to modify a schedule in response to the change of circumstances such as the economic situation and traffic quantity. This is because the annual budget for maintenance is decided based on these circumstances and the demand of work. If the annual cost exceeds the annual budget, the LCC is more likely to be increased and the safety level may be lost. Thus, a long-term plan has to adapt to the change of annual budget constraint.

A plan formulated by the proposed method involves a flexible period when the schedule can be changed with keeping the safety of bridge. By paying attention to this feature, the proposed method attempted to satisfy the annual budget constraint. The satisfaction result is shown in Fig. 8. In this satisfaction, the annual budget constraint during the service period was set to 70 million yen. The previous method could not reduce the annual mainte-

nance cost to the budget constraint. On the other hand, the plan of the proposed method could satisfy the annual budget constraint. This is because the proposed method extended the flexible period by considering uncertainties in the optimization. In addition, the proposed method is effective for the cost reduction with satisfying the budget constraint. The previous method can satisfy the annual budget constraint by treating it as the constraint condition. Through the optimizations, the average LCC of obtained plans was 18,447 million yen. On the other hand, the LCC of the proposed method was 19,311 million yen. The results of two methods were equivalent because the optimization of the previous method became complicated due to the annual budget limitation. Therefore, it is expected that the proposed method can establish a plan robust against the uncertainties that influence the progress of schedule.

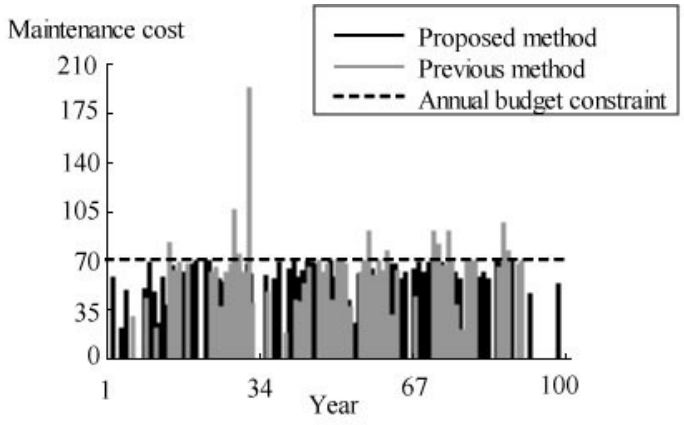

Fig. 8: Satisfaction of budget constraint

5 Conclusion

In order to realize the sustainable bridge management, this paper attempted to propose a method that is able to obtain a robust solution against uncertainties by using the improved GA in the long-term maintenance planning. By searching solutions taking into account error of deterioration prediction, the proposed method develops a plan that has the extended period when its schedule can be changed without increasing large cost, based on the preventive maintenance. Numerical experiments demonstrated that the plan optimized by the proposed method is robust against uncertainties involved in the degradation prediction and the allocated budget. In addition, the effectiveness of this plan for the cost reduction was shown in the application to the change of annual budget.

In real-world problems, it is necessary to manage the safety of bridges in consideration of the impact of various uncertainties such as the budget, institution, deterioration prediction, natural disasters and environmental issues. Due to the optimization under uncertain environments, it was difficult for the previous method to formulate a robust plan that reduces the cost of repair simultaneously. On the other hand, the plan obtained by the proposed method provides the cost reduction effect compared with the previous method. However, the proposed method is able to develop a rational plan with the robustness against uncertainties. In the numerical experiments, by modifying the schedule to the change of circum-

stances within the obtained period, the proposed method demonstrated that its plan could maintain the safety without changing the cost significantly. In the practical problems, the importance of each bridge is not equivalent; it is important to apply the appropriate planning method such as the previous method or the proposed method to each bridge respectively. It is considered that a plan formulated by the proposed method is effective for more important bridges. Furthermore, the flexible period involved in its plan is useful for the determination of appropriate schedules in consideration of a group of bridges.

In the local government, it is necessary to establish a maintenance plan for a large number of bridges such as 800 bridges. The optimization method proposed in the previous study (NAKATSU ET AL. [5]) can formulate a large-scale plan efficiently by using a period when the schedule can be changed, taking into account a group of bridges. By extending that period, the proposed method could be adapted to a variety of situations such as the cost levelling. Therefore, it is expected that a plan obtained by the proposed method is applicable for the planning of large-scale bridge group.

Literature

[1] Furuta, H., Kameda, T. and Nakahara, K. Practical use of bridge management system by improved genetic algorithm, *Journal of Japan Society of Civil Engineers*, Vol.62, No.3, 2006, p. 656−668, (in Japanese)

[2] Furuta, H., Yasuda, K., Kawatani. M. and Takebayashi, M. *Infrastructure Asset Management*, Morikita Publishing, 2010 (in Japanese)

[3] Nakatsu, K., Furuta, H., Nomura, Y., Takahashi, K. and Ishibashi, K. Flexible restoration scheduling of damaged networks under uncertain environments, *Journal of Structural Engineering. A*, Vol.57A, 2011, p.183−194, (in Japanese)

[4] Nakatsu, K., Furuta, H., Nomura, Y., Takahashi, K., Ishibashi, K. and Miyoshi, N. Practical application of long-term bridge management system using Genetic Algorithm. *Journal of Japan Society for Fuzzy Theory and Intelligent Informatic*s, 23(4), 2011, p. 469−479, (in Japanese)

[5] Nakatsu, K., Furuta, H., Takahashi, K., Ishibashi, K. and Umekage, T. Bridge management system of a large number of bridges using genetic algorithm, *Reliability and Optimization of Structural System, IFIP WG 7.5 Working Conference*, 2012

[6] Tanooka, K., Tamaki, H., Abe S. and Kitamura, S. A Continuous Age Model of Genetic Algorithms Applicable to Optimization Problems with Uncertainties, *Proc. of 1999 IEEE Int. Conf. on Systems, Man and Cybernetics (SMC'99)*, Vol.I, 1999, p. 637−642

Contribution to the quantification of model quality in geotechnical engineering

Maximilian Huber [a], Henning Stutz [a]

[a]Research Training Group 1462 "Evaluation of Coupled Numerical and Experimental Partial Models in Structural Engineering", Bauhaus-Universität Weimar, Germany
maximilian.huber@uni-weimar.de, henning.stutz@uni-weimar.de

Abstract: The quantification of model quality in geotechnical is an important issue, but often not recognize by the practical engineers during the design. Important model properties as model sensitivity, complexity, uncertainty and robustness seldom investigated. This publication will contribute to the estimation of the overall model quality using the different model properties measures. For this reason the theoretical background is explained. Following these explanations the different measures for the model quality are computed using typical geotechnical engineering example. This is a bearing capacity problem of a strip footing capacity using limit state equations. As conclusion of these case study some major model properties are identify and some less important measures are identified.

Keywords: model quality, model uncertainty, model sensitivity, model robustness, strip footing bearing capacity

1 Introduction

Uncertainties in geotechnical engineering design are unavoidable. These uncertainties and associated risks can be quantified to improve design in geotechnical engineering. This is recognized in the recent National Research Council (2006) report on *Geological and Geotechnical Engineering in the New Millennium: Opportunities for Research and Technological Innovation*. This report remarked that "paradigms for dealing with ... uncertainty are poorly understood and even more poorly practiced" and advocated a need for "improved methods for assessing the potential impacts of these uncertainties on engineering decisions ...". In

order to understand the consequences of uncertainty in geotechnical engineering, efficient methods to quantify the impact of soil-structure interaction are needed.

Within this contribution, model quality is investigated and different measures are employed to describe model quality: Model complexity, model uncertainty, model sensitivity and model robustness are used within the framework of probabilistic methods. In addition to the theoretical background, these different measures of model quality are applied within a parametric study of the bearing capacity of a vertically loaded strip footing. This parametric study focuses on the effects of model uncertainty and model complexity of the constitutive soil model by comparing different constitutive failure criteria namely Mohr-Coulomb, Matsuoka-Nakai and the Lade-Duncan criteria. These constitutive failure criteria are used to derive semi-analytical equations describing the ultimate limit state. The influences of the uncertain soil properties are investigated by means of local and global sensitivity measures. Moreover, these study is completed by robustness analyses of the bearing capacity of a strip footing.

2 Models in engineering

The core competences of civil engineers are designing, building and maintaining structures and buildings to enable life and business for society. This includes the prevention against natural hazards such as climatological, hydrological, meteorological and geophysical disasters. Such complex hazards asks for sophisticated techniques to ensure appropriate safety standards for society. Too low safety standards can result in many casualties and much economic damage, whereas too high standards results in overly expansive systems. Therefore, these phenomena ask for sophisticated methods to consider their impacts on structures. Especially geotechnical engineers are asked for integrated concepts to design structures withstanding the above mentioned hazards.

Traditionally, engineers have been using safety concepts, which are considering uncertainties in global or partial safety factors, [9]. These methods offer a robust estimate in the design of structures. However, they lake in a precise, mathematical description of uncertainties and their impact on the system response. This can be overcome by using probabilistic methods, which offer a mathematical and statistical framework for the consideration of uncertainties, as shown by PHOON [14] amongst others. By using these statistical models, one has to be aware of the model quality.

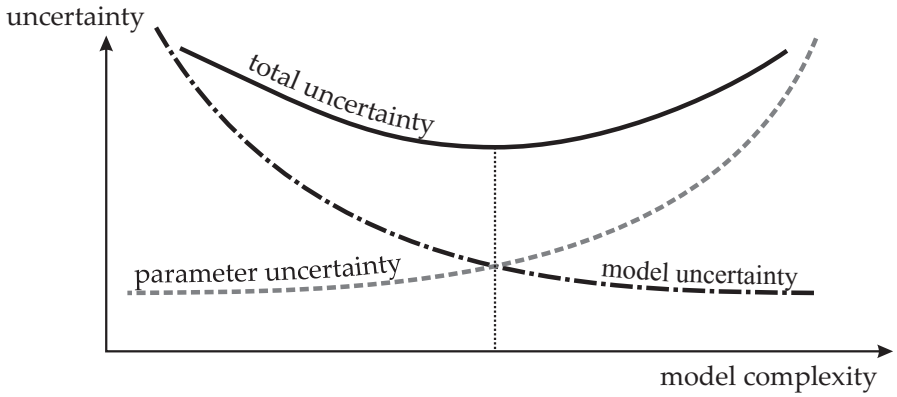

Fig. 1: Schematic parameter and model uncertainty depending on complexity from KEITEL [10]

3 Model quality

Important decisions were made based on model predictions. In the field of civil engineering, these decisions are related to the choice of the construction and its design. In other areas the model outcome is used as decision support for political and economical arrangements. The quality of the model prognosis is of main importance for all of these fields, whereat different criteria for the evaluation of quality can be taken into account.

Model quality can be described by means of model uncertainty, model complexity, model sensitivity and model robustness.

3.1 Model uncertainty

In structural design, the prediction of the structural response is estimated often by using numerical and/or analytical models. Every prediction underlies a certain uncertainty, which could be interpreted as a measure of the quality of the prediction, [13]. Uncertainty is the term to describe incomplete knowledge about models, parameters, constants and data. There are many sources of uncertainty, including the science underlying a model, uncertainty in model parameters and input data, observation error, and code uncertainty. Generally, uncertainties that affect model quality are categorised as prosed by MOST [13]:

- *Model framework uncertainty* comprises the uncertainty in the underlying science and algorithms of a model. Model framework uncertainty is the result of incomplete scientific data or lack of knowledge about the factors that control the behaviour of the system being modelled. Model framework uncertainty can also be the result of simplifications necessary to translate the conceptual model into mathematical terms.

- *Model niche uncertainty* results from the use of a model outside the system, for which it was originally developed and/or developing a larger model from several existing models with different spatial or temporal scales.

- *Model input uncertainty* follows from data measurement errors, inconsistencies between measured values and those used by the model (e.g. in their level of aggregation/averaging), and parameter value uncertainty. We can distinguish between data uncertainty caused by measurement errors, analytical imprecision, and limited sample sizes during the collection and treatment of data, and stochasticity, which are fluctuations in ecological processes that are due to natural variability and inherent randomness.

While there can be many sources of uncertainty, it is convenient to categorize the character of uncertainties as either aleatoric or epistemic in the context of modelling. *Aleatoric uncertainty* is presumed to be due to the intrinsic randomness of a phenomenon, e.g. in the rolling of dice. *Epistemic uncertainty* is related to the lack of knowledge (or data). It is convenient to have this distinction of uncertainties within an engineering analysis model: the ”lack of knowledge” part of the uncertainty can be represented in the model by introducing auxiliary non-physical variables [5]. Thus, additional studies and collection of more information allows errors stemming from epistemic uncertainty to be reduced. However, aleatoric uncertainty is irreducible, but it can be characterized or represented better with further studies.

3.2 Model complexity

The model complexity can be utilised as an additional indicator of model quality. Model complexity is the degree of complexity desired for the model. Models become more complex to treat more physical processes. Their performance tends to degrade because they require more input variables, leading to greater parametric uncertainty. Models tend to uncertainty as they become increasingly simple or increasingly complex. Thus, complexity is an important properties to consider when choosing among competing model frameworks or determining the suitability of the existing model framework to the problem of concern. The optimal choice generally is a model that is no more complicated than necessary to inform the regulatory decision. The types of model uncertainty have a reciprocal relationship, with one increasing as the other decreases. Thus, an optimal level of complexity exists for every model, which is represented by the point of minimum total uncertainty as shown in Fig. 1.

3.3 Model sensitivity

Sensitivity analysis is the study of how uncertainty in the output of a model can be apportioned, qualitatively or quantitatively, to different sources of variation in the input of a model [16]. Within this contribution, the local and global measures of sensitivity analyses are investigated.

3.3.1 Local sensitivity

Local sensitivity analysis investigates the local impact of input parameters on the model. It is based on the computation of the gradient of the response with respect to its parameters

around a nominal value.

Within the calculation of the probability of failure by using the First-Order-Reliability-Method, the linearised limit state function g my be cast as:

$$g_{\text{FORM}}(\boldsymbol{\xi}) = \beta - \boldsymbol{\alpha} \cdot \boldsymbol{\xi} \tag{1}$$

Herein, β is the reliability index and $\boldsymbol{\alpha}$ is the unit vector to the design point. SUDRET [19] considers this linearised limit state function to be a margin function, which quantifies the distance between a realization of the transformed input random vector and the failure surface. Its variance straightforwardly reads:

$$\text{Var}\left[g_{\text{FORM}}(\boldsymbol{\xi})\right] = \sum_{i=1}^{M} \alpha_i^2 = 1 \tag{2}$$

Thus, the coefficients $\{\alpha_i^2, i = 1\ldots, M\}$, which are also called *FORM importance factors*, correspond to the portion of the variance of the linearised margin, which is due to each ξ_i. When the input random variables $\mathbf{X}$ are independent, there is a one-to-one mapping between X_i and ξ_i , $i = 1 \cdots M$. Thus, α_i^2 is interpreted as the importance of the ith input parameter in the failure event, [19].

3.3.2 Global sensitivity

Global sensitivity analysis aims for the quantification of the output uncertainty due to the uncertainty in the input parameters, which are taken singly or in combination with others, [19]. SALTELLI [16] group the different techniques in SA into regression-based and variance-based methods. Within this contribution, only the variance-based method is employed for the calucaltion of the global sensitivities.

The variance-based method aims at decomposing the variance of the output as a sum of the contributions of each input variables or combinations thereof. The computation of global sensitivity indices is traditionally carried out by Monte Carlo simulation as reported by [16], which may be computationally unaffordable in the case of time consuming models. SUDRET [19] has shown that Sobol' indices can be derived analytically from the coefficients of the polynomial chaos expansion Ψ_α of the response S, once the lattes have been compute by the projection or regression approach. The first order sensitivity indices quantify what fraction of the response variance is due to each input variable:

$$\delta_i = \frac{\text{Var}_{X_i}\left[\,\text{E}\left[S|X_i\right]\,\right]}{\text{Var}\left[S\right]} \tag{3}$$

SUDRET [19] derives δ_i^{PC} by employing polynomial chaos expansion Ψ_α as follows:

$$\delta_i^{PC} = \sum_{\alpha \in \boldsymbol{I}_i} S_\alpha^2 \,\text{E}\left[\boldsymbol{\Psi}_\alpha\right] / \sigma_S^2 \tag{4}$$

Herein, σ_S^2 is the variance of the model response computed form the polynomial chaos coefficients and the summation set:

$$\boldsymbol{I}_i = \{\alpha \;:\; \alpha_i > 0 \;,\; \alpha_{j\neq i} = 0\} \tag{5}$$

Higher order sensitivity indices, which correspond to interactions of the input parameters, can also be computed using this approach as described in SUDRET [19] in detail.

By virtue of the knowledge of SA, engineers can rank the input variables by the amount of their contributions to the output, and thus take measures accordingly to improve the performance of the model, which is a core task in engineering.

3.4 Model robustness

Robustness is the ability of a model to perform equally well across the full range of boundary conditions, for which it was designed [15]. In contrast to the sensitivity, where the relative contribution of the input parameters to the model response variation is identified, the robustness quantifies the variation of a model response, which is assumed to be the random variable Y. The robustness compares the random variable Y to the variation of the model input parameters:

$$T = 10 \cdot \log\left(\sigma_Y^{-2}\right) \tag{6}$$

Model robustness only considers the variation of one or more model responses are considered. Further information about mean value or distribution type have no influence on their value of robustness.

4 Parametric study of a vertically loaded strip footing

The aim of this parametric study is to show the steps for the quantification of model quality, which includes model uncertainty, model complexity, models sensitivity and model robustness.

One of the core competences in foundation engineering is the design of footings. FENTON & GRIFFITHS [8] state that the design of a foundation involves the consideration of several limit states, which can be separated into two groups: serviceability, which generally translate into a maximum settlement or differential settlement, and ultimate limit states. The latter are concerned with the maximum load, which can be placed on the footing just prior to a bearing capacity failure. The effects of uncertain soil strength properties has been and is a topic of various publications e.g. BAECHER & CHRISTIAN [1] or BREYSSE [4] amongst others.

Within this case study, the model quality of simulating the bearing capacity of a vertically loaded strip footing is investigated. Within this, different formulas, which are based on different constitutive failure criteria, are compared to each other with respect to their model quality by means of uncertainty, sensitivity, complexity and robustness analyses.

For this reason, the framework of uncertainty quantification (UQ) is adopted to investigate model quality. UQ comprises of four basic steps: At first, the mechanical model is defined thorough a limit state equation in step A. After this, the random variables are employed to represent the uncertainty of the variables of the limit state equation. The probability of failure is calculated in step C. Finally, sensitivity and robustness analyses are performed

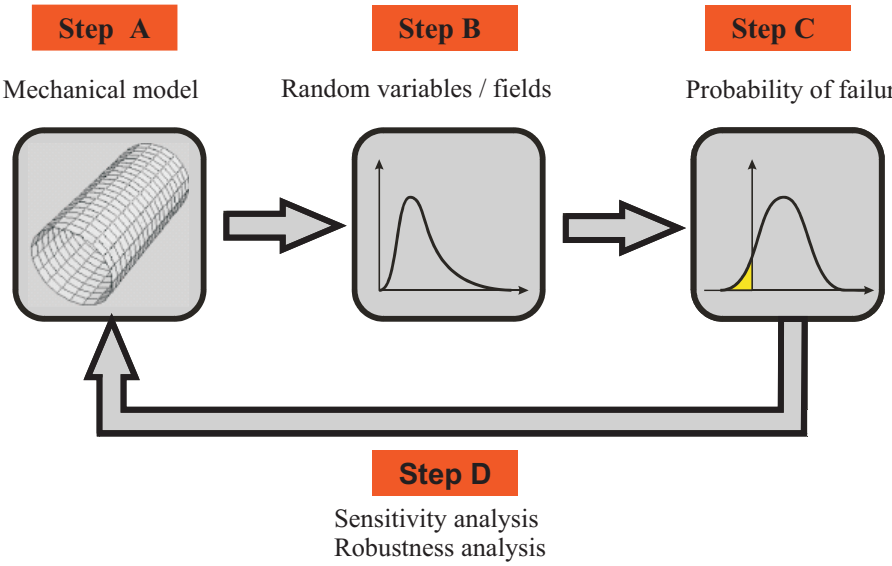

Fig. 2: Framework of uncertainty quantification in engineering from HUBER [9]

to investigate the contribution of the random variables and of the system to the probability of failure. The model complexity is investigated in addition to the UQ analysis in order to provide a more complete picture of the model quality.

4.1 Mechanical model

The German standard [6] is formulating the state-of-the-art and provides Eq. 7 for the calculation of the bearing capacity of a vertically loaded strip footing.

$$q_f = N_c c' + q_0 N_q + \gamma_{soil} b N_b \tag{7}$$

$$N_c = \begin{cases} 2+\pi & \text{for} \quad \varphi' = 0 \\ (N_q - 1)/\tan\varphi' & \text{for} \quad \varphi' \neq 0 \end{cases} \tag{8}$$

$$N_q = e^{\pi \tan\varphi'} \left(\frac{1+\sin\varphi'}{1-\sin\varphi'} \right) \qquad N_b = 2\,(N_q - 1)\tan\varphi' \tag{9}$$

Herein, N_c is the cohesion stability number, c' the cohesion, N_q the depth stability number, q_0 the surface load, φ' is the effective friction angle, N_b the width stability number and γ_{soil} the soil unit weight.

As described by HUBER [9], the Eqs. 7, 8 and 9 are derived from theoretical, experimental and numerical investigations. On basis of this, parametric 2D-FEM studies are carried out to evaluate the stability numbers N_b and N_c for different constitutive failure criteria namely Mohr-Coulomb (MC) [12], Matsuoka-Nakai (MN) [12] and Lade-Duncan (LD) [11]. Herein, the contact between the rigid footing and the contact with the soil is assumed as rough with full bounding. These three constitutive failure criteria are shown in Fig. 3. It can be seen that the MC, MN and LD criteria are identical for triaxial compression, whereas MC and MN are identical for triaxial extension.

Mohr-Coulomb criterion: It is experimentally verified in triaxial compression and extension and is of striking simplicity. However, the Mohr-Coulomb criterion is very conservative for intermediate principal stress states between triaxial compression and extension. The Mohr-Coulomb failure criterion in principal stress space is defined by using the friction angle φ' and the cohesion c':

$$\begin{aligned} f_1 &= |\sigma_1 - \sigma_2| - (\sigma_1 + \sigma_2)\sin\varphi - 2\,c'\cos\varphi' \\ f_2 &= |\sigma_2 - \sigma_3| - (\sigma_2 + \sigma_3)\sin\varphi - 2\,c'\cos\varphi' \\ f_3 &= |\sigma_3 - \sigma_1| - (\sigma_3 + \sigma_1)\sin\varphi - 2\,c'\cos\varphi' \end{aligned} \tag{10}$$

Matsuoka-Nakai and Lade-Duncan criteria: MATSUOKA & NAKAI [12] proposed a failure criterion that is in better agreement with the experimental data, which is shown in Fig. 3 together with the MC and the LD criterion [11].

The likewise well-known failure criterion by LADE & DUNCAN [11] appears compared to the MC and the MN criteria rather optimistic in plane strain conditions and triaxial extension. BENZ [2] points out that using bifurcation analysis, progressive failures would most likely "correct" for the LD criterion's overly optimistic, ultimate material strength estimate.

Both failure criteria, MN and LD, are functions of the first, second, and third stress invariants, I_1, I_2, and I_3 respectively:

$$f_{\text{MN}} = \frac{I_1\, I_2}{I_3} - c_1 = 0 \quad \text{with} \quad c_1 = \frac{9 - \sin^2\varphi}{-1 + \sin^2\varphi} \tag{11}$$

$$f_{\text{LD}} = \frac{I_1^3}{I_3} - c_2 = 0 \quad \text{with} \quad c_2 = \frac{(-3 + \sin\varphi)^3}{(-1 + \sin\varphi)\ (-1 + \sin\varphi)^2} \tag{12}$$

where the stress invariants can be written for principal stresses:

$$\begin{aligned} I_1 &= \sigma_1 + \sigma_2 + \sigma_3 \\ I_2 &= -\sigma_1\,\sigma_2 - \sigma_2\,\sigma_3 - \sigma_3\,\sigma_1 \\ I_3 &= \sigma_1\,\sigma_2\,\sigma_3 \end{aligned} \tag{13}$$

The constants c_1 and c_2 in Eqs. 12 and 12 are defined so that both failure criteria are identical to the MC criterion in triaxial compression.

The results in Fig. 4 (a) show that the width stability number N_b is slightly influenced by the different constitutive failure criteria; the influence of the MC, MN and LD criteria on the cohesion stability number N_c can be clearly seen in Fig. 4 (b). It can be concluded that the MC-criteria is a conservative lower bound for the estimation of the ultimate shear strength of soil, as reported by others e.g. SCHAD [17]. Moreover, it has to be pointed out that the advanced MN and LD criteria have a larger friction angle under plane strain conditions in comparison to the MC criterion.

The bearing capacity problem can be described with the limit state Eq. 14. This limit state equation compares the actual footing pressure q with the bearing capacity q_f.

$$g\,(c, \varphi') = q_f - q \tag{14}$$

Tab. 1: Stochastic variables of the silty sand in two parametric studies

	μ	COV
c'	10 kN/m^2	10 – 160 %
φ'	25°	5 – 80 %
ψ	0°	deterministic
γ_{soil}	20 kN/m^3	deterministic
b	5 m	deterministic
d	0.8 m	deterministic
q	50 – 10,000 kN/m^2	deterministic

4.2 Stochastic variables and uncertainty analysis

The effects of three different levels of soil variability on the probability of failure are investigated in this parametric study. The variability of the friction angle and of the cohesion are summed up in Tab. 1. The reliability of the strip footing is evaluated using the limit state Eq. 14 and the combination of the First-Order-Reliability-Method (FORM) and Importance sampling (IS) within the FERUM [3] libraries. The description of the well known FORM and IS methodology can be found in standard literature e.g. [3, 19].

Fragility curves are used to study the effects of increasing the variability as shown in Fig. 5. Amongst others, SCHULTZ ET AL. [18] describe that fragility curves show how the reliability of a structure changes over the range of loading conditions to which that structure might be exposed. This offers a more general approach for the probabilistic description of a system by incorporating deterministic input parameters into a probabilistic framework. The deterministic input in this parametric study is the footing pressure. Furthermore, it is shown in literature [9, 18] that the fragility curves of buildings follow a lognormal cumulative distribution function in general. This is a benefit because the fragility curve represented by a lognormal distribution function is continuously defined over the entire range of loads instead of discrete points, [7]. Therefore, lognormal cumulative distribution functions are fitted to the calculated failure probabilities as shown in Fig. 5. Furthermore, it can be clearly seen that the larger COV values of the cohesion and the friction angle cause a higher probability

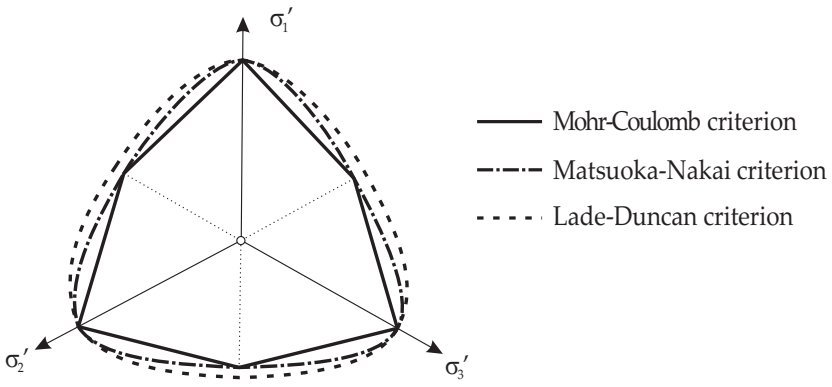

Fig. 3: Different failure criteria of Mohr-Coulomb, Matsuoka-Nakai and Lade-Duncan

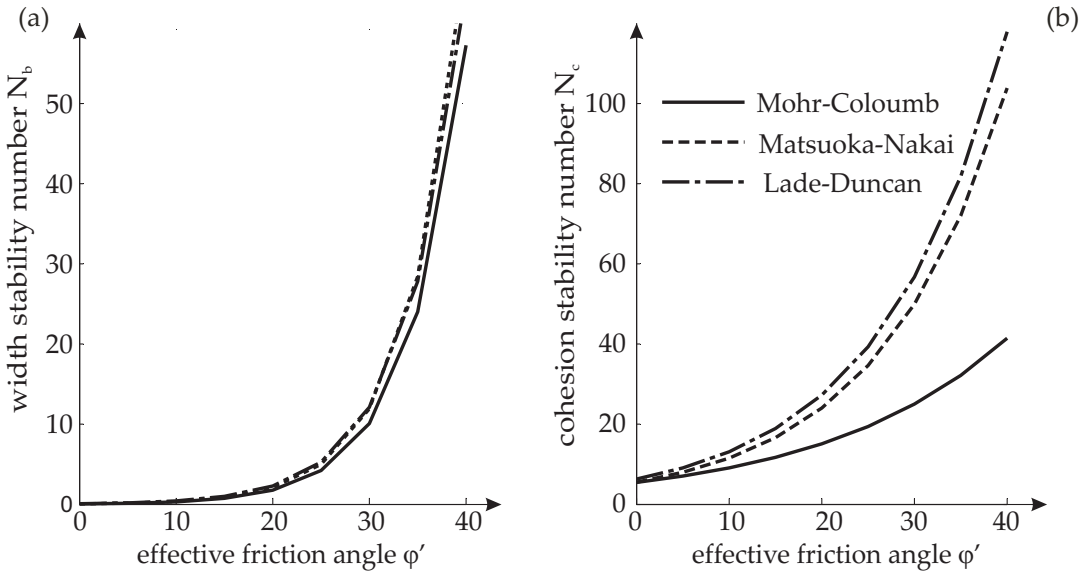

Fig. 4: Stability numbers N_b (a) and N_c (b) for different constitutive failure criteria, [9]

of failure.

In addition to this, the effects of different constitutive failure criteria are shown in Fig. 5. The MC, MN and LD criteria have a significant influence on the probability of failure. For all investigated levels of soil variability, the MC criterion offers a higher probability of failure in comparison to the MN and LD criteria. From these fragility curves it can be concluded that the MC criterion is the most conservative one in this context.

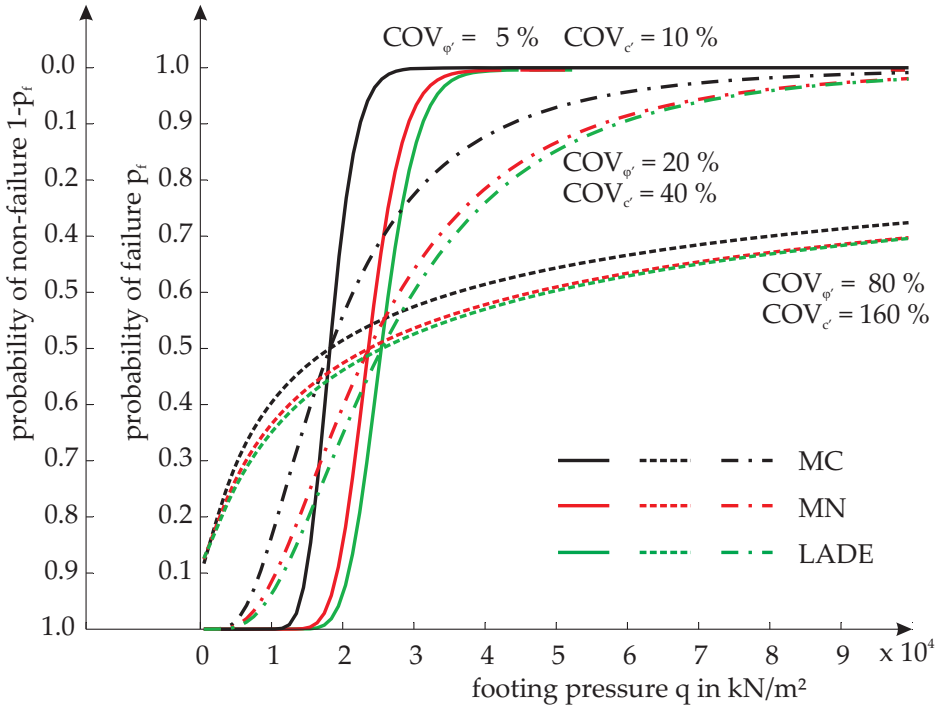

Fig. 5: Fragility curves for different constitutive failure criteria and different COVs of the cohesion c' and of the friction angle φ'

4.3 Complexity analysis

By comparing Eqs. 10, 12 and 12, one can clearly see that these three constitutive failure criteria have the same number of variables. Each constitutive failure criterion is defined by the cohesion c' and the friction angle φ'. Thus, all three approaches have the same number of complexity.

4.4 Sensitivity analysis

Local sensitivity analysis: The local sensitivities are evaluated for the range of the footing pressure from $q = 500$ kN/m^2 to $q = 3{,}500$ kN/m^2 in Fig. 6. Within this, the coefficient of variation for the cohesion and the friction angle is kept constant (COV$_{\varphi'} = 20\,\%$, COV$_{c'} = 40\,\%$).

The local sensitivity measures of the cohesion are decreasing with increasing footing pressure and vice versa in the case of friction angle. Moreover, it is interesting to see that the local sensitivity measures of MC, MN and LD are the same relative to each other. This can be related to the stress state.

Global sensitivity analyses: The global sensitivity measures of the cohesion and the friction angle are constant for the investigated range of footing pressures as shown in Fig. 6. By comparing the three constitutive failure criteria, one can see that the differences between the MC, MN and LD criteria are minor. However, the computed global sensitivity measures of the MC criterion for the cohesion and friction angle are higher in comparison to the MN and LD criteria.

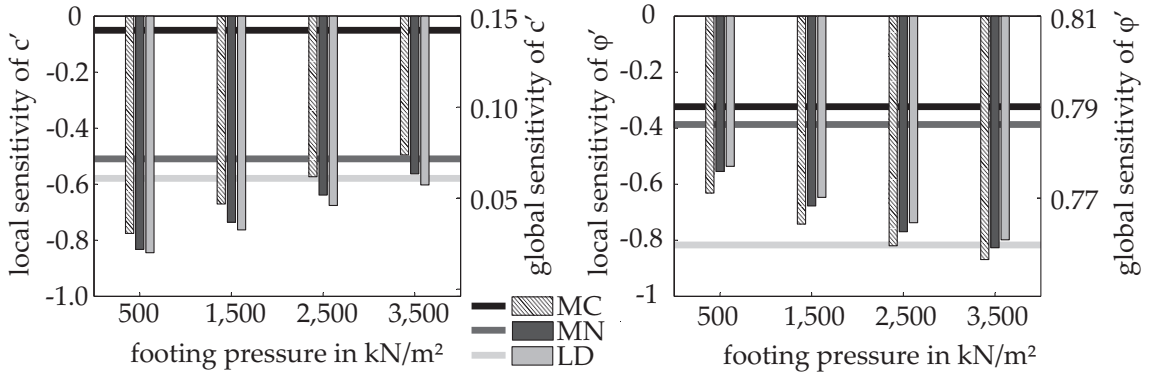

Fig. 6: Local and global sensitivities of the cohesion c' and the friction angle φ' with respect to the deterministic footing pressure

4.5 Robustness analysis

The results of the robustness analysis are shown in Fig. 7. Fig. 7 (a) shows the robustness for the different criteria in comparison to the fragility curves. One can see that the system behaviour with respect to the robustness can be divided into two load levels. By using the MC criterion, the system shows a more robust behaviour in comparison to the MN and LD criterion in case for high loads ($q > 2 \cdot 10^4$ kN/m^2). Fig. 7(a) and (b) clearly indicate the opposite for relatively low load levels ($q \ll 2 \cdot 10^4$ kN/m^2). Here, the MC criterion offers a lower robustness than the other criteria.

4.6 Synopsis

This case study comprises different means of describing model quality of the bearing capacity problem. The analysis of uncertainty, complexity, sensitivity and robustness offers additional insight into the model quality of the calculation of the bearing capacity of a vertically loaded strip footing.

The results clearly indicate that the choice of the constitutive failure criterion within a linear elastic, perfectly plastic constitutive model has a significant impact on the deterministic bearing capacity as well as on the failure probability of strip footings. This can also be concluded from the results of the sensitivity and robustness analyses. Therefore, this source of model uncertainty has to be considered with in the analysis of model quality. From a deterministic as well as from a probabilistic point of view, the Mohr-Coulomb criterion is the most conservative choice in comparison to the Matsuoka-Nakai and the Lade-Duncan criteria.

5 Summary and conclusion

This contribution offers tools to quantify model quality in terms of uncertainty, complexity, sensitivity and robustness. These tools are applied in an illustrative parametric study on the bearing capacity of a vertically loaded strip footing. This study helps to understand the con-

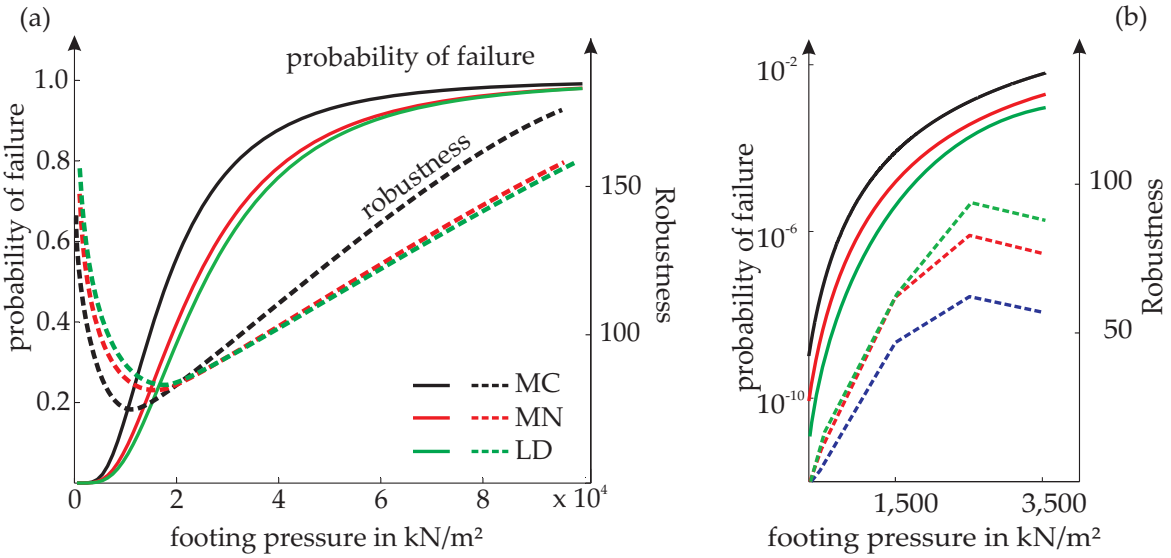

Fig. 7: Robustness in comparison to the fragility curves for the MC, MN and LD criteria in (a) and robustness measures for a footing pressure $q = 500 - 3{,}500$ kN/m^2 (b)

cepts of quantifying model uncertainty in geotechnical engineering. One can deduce from the results of this parametric study that the analyses of uncertainty, complexity and sensitivity provide useful quantities for assessing model quality. In contrast to this, the model robustness is offering less additional insight into the model quality compared to the other measures.

Acknowledgements

This research has been supported by the German Research Council (DFG) through Research Training Group 1462, which is gratefully acknowledged by the authors.

Literature

[1] Baecher, G.B. and Christian, J.T. *Reliability and statistics in geotechnical engineering*. John Wiley & Sons Inc., 2003

[2] Benz, T. *Small-strain stiffness of soils and its numerical consequences*. PhD thesis, University of Stuttgart, Institute of Geotechnical Engineering, 2007

[3] Bourinet, J.-M., Mattrand, C., and Dubourg, V. A review of recent features and improvements added to FERUM software. In *Proceedings of 10th International Conference on Structural Safety and Reliability (ICOSSAR'09)*, Osaka, Japan, 2009

[4] Breysse, D., Niandou, H., Elachachi, S., and Houy, L. A generic approach to soil-structure interaction considering the effects of soil heterogeneity. *Geotechnique*, 55(2) (2005), p. 143–150

[5] Der Kiureghian, A. Analysis of structural reliability under parameter uncertainties. *Probabilistic Engineering Mechanics*, 23 (2008), p. 351–358

[6] DIN 4017. Baugrund-Berechnung des Grundbruchwiderstands von Flachgründungen, 2006

[7] Ellingwood, B.R., Celik, O.C., and Kinali, K. Fragility assessment of building structural systems in mid-america. *Earthquake Engineering & Structural Dynamics*, 36(13) (2007), p. 1935–1952

[8] Fenton, G.A. and Griffiths, D.V. *Risk assessment in geotechnical engineering*. John Wiley & Sons, 2008

[9] Huber, M. *Soil variability and its consequences in geotechnical engineering*. PhD thesis, Institute of Geotechnical Engineering, University of Stuttgart, 2013

[10] Keitel, H. *Evaluation Methods for Prediction Quality of Concrete Creep Models*. PhD thesis, Bauhaus-Universität Weimar, 2011

[11] Lade, P.V. and Duncan, J.M. Elastoplastic stress-strain theory for cohesionless soil. *Journal of the Geotechnical Engineering Division*, 101(10) (1975), p. 1037–1053

[12] Matsuoka, H. and Nakai, T. Relationship among Tresca, Mises, Mohr-Coulomb and Matsuoka-Nakai failure criteria. *Soils and Foundations*, 25(4) (1985), p. 123–128

[13] Most, T. Assessment of structural simulation models by estimating uncertainties due to model selection and model simplification. *Computers & Structures*, 89(17) (2011), p. 1664–1672

[14] Phoon, K.K. *Reliability-Based Design in Geotechnical Engineering – Computations and Applications*. Taylor & Francis, 2008

[15] Reckhow, K.H. Water quality simulation modeling and uncertainty analysis for risk assessment and decision making. *Ecological Modeling*, 72 (1994), p. 1–20

[16] Saltelli, A., Chan, K., and Scott, M. *Handbook of sensitivity analysis* John Wiley & Sons, 2000.

[17] Schad, H. *Zeit-und geschwindigkeitsabhängiges Materialverhalten in der Geotechnik: Experimentelle Erfassung und numerische Analyse*. PhD thesis, Institute of Geotechnical Engineering, University of Stuttgart, 1992

[18] Schultz, M.T., Gouldby, B.P., Simm, J.D., and Wibowo, J.L. Beyond the factor of safety: developing fragility curves to characterize system reliability. Technical report, DTIC Document, 2010

[19] Sudret, B. *Uncertainty propagation and sensitivity analysis in mechanical models– Contributions to structural reliability and stochastic spectral methods*. Habilitation a diriger des recherches, Université Blaise Pascal, Clermont-Ferrand, France, 2007

The risk assessment of the sewage pipeline system in the urban area of Chongqing

Zhaohui Chen, Jinghua Huang
School of Civil Engineering, Chongqing University; Key Laboratory of New Technology for Construction of Cities in Mountain Area, Ministry of Education, Chongqing, China
zhaohuic@cqu.edu.cn, hjh.524@163.com

Abstract: The sewage pipeline system is an important infrastructure for the urban sewage collection and transmission. The pipeline system is friable to various natural hazards in mountain city, such as the rain fall induced flood, internal over pressure and landslide, and the deterioration of the pipeline materials affected by the corrosion of sewage water. In the present paper, the risk assessment methodology of the linear sewage pipeline in Chongqing, a typical mountain city in three gorges reservoir region, is proposed. This proposed risk assessment system is a synthetic system with multiple factors for the linear sewage pipeline in mountain city, based on the consideration of the geological conditions, the amount of the rainfall, the pipeline structural mechanical properties, the supporting and loading situations, and the deterioration of pipeline materials subjected by the sewage corrosion. By application of the synthetic risk assessment system to the primary sewage pipeline in the urban area of Chongqing, the effectiveness of the proposed system is verified.

Keywords: risk assessment, sewage pipeline system, mountain city, landslide, flood, corrosion

1 Introduction

The sewage pipeline system is an important infrastructure for the urban sewage collection and transmission, and also an efficient measure for the releasing of flood water [1]. In recent decades, the pipeline safety inspection, assessment and maintenance are drawn a worldwide attention [2, 3]. The developments on the issues are including the digitalization of the pipeline system map, the safety or risk assessment of the pipeline system, the real-time inspection, the measures to mitigate the damage risk of the pipeline system and the modified design specification with higher safeguard.

The research on the safety or risk assessment and management of long-linear pipeline system in the urban area of China is still in the initial stage. The readily and effective risk as-

sessment approach is the basis of the inspection and management system for the pipeline system. In the present paper, the risk analysis system for the sewage pipeline system in mountain city is proposed. In the present risk assessment method, multiple factors such as landslide, sewage water corrosion, internal and external overload, flood load and the third-party interference are taken into account. In the end, a case study of the primary urban sewage pipeline in Chonqging is undertaken to verify the effectiveness of the proposed system.

2 The Risk Assessment System of the Sewage Pipeline System in Mountain City

According to the terrain and geologic conditions, there are three forms of sewage pipe in mountain area, such as elevated culverts, buried culverts and tunnels. When the level of the landform is higher than the design elevation of the culvert bottom, the buried culvert is used. On condition that the load capacity of the foundation is not less than 320 MPa, the culvert is directly placed on the foundation. Otherwise, the column pier is applied to support the buried culvert to form the elevated buried culvert. When the culvert needs to cross the gulch, or culvert design elevation is 2.5 m high above the original ground line, the elevated culvert supported by column pier is used. Buried culvert and elevated culvert are all reinforced concrete rectangular box girders. The span of each culvert is 16m. The adjacent girders are connected with rubber seals. In other cases, the tunnel is used. The tunnel section is semicircle that the diameter is the same as the width of the box girder. In the present sewage pipeline safety assessment system, the damage risk of the box culvert is focused on.

In the present risk assessment system, the failure modes of the sewage pipeline in mountain area are divided into 3 categories, such as the durability damage mode, the load capacity failure mode and the pipe overturning mode. The pipeline durability damage is caused by the corrosion of sewage water to the concrete cover and the erosion of the steel [4, 5]. The load capacity failure is due to the heavy rainfall caused internal hydrostatic overpressure, landslides and external flood pressure to the gulch-crossed elevated culvert, and also the external over pressure, gas explosions and the so called third-party damage. In addition, the culvert may be overturned under the impact of the heavy rainfall-caused flooding, landslides and other construction activities [6, 7].

Considering the differences in pipeline structure, supporting conditions, geological situations, and the geographical locations, the failure risk of each pipe section is not the same. For the elevated culvert, the internal hydrostatic overpressure in rain storm is the most disadvantage case because of the lack of the external soil pressure to counteract the internal hydrostatic pressure. The gulch-crossed culvert is mainly affected by the lateral pressure and the impact effects of flood. The failure risks of the buried culvert are mainly due to the thrust of landslide and the overpressure of soil caused by the municipal transformation and the third-party damage factors. The slope of the sewage pipeline system is small (i.e. 0.5 ‰), so that the internal dynamic pressure is ignored. Besides, the reinforced concrete pipes are subjected to the corrosion of sewage water.

In the present paper, we propose the hierarchical analysis model for the risk assessment of the mountain city sewage pipeline system (RAM-SAMCSPS) as shown in Fig. 1. In this model, the pipeline system are sub-divided into several sections according to their support and working conditions, such as landslide-prone section of buried culverts, the flood impact prone section of gulch-crossed culverts, over internal pressure section of elevated culverts, over external pressure section of buried culverts, the sewage water corrosion prone section and the third-party damage section [8]. The risk states of the sewage pipeline are classified into 4 grades from the safety Grade 1 to the most severe state Grade 4.

As shown in Fig. 1, the bottom level of the RAM-SAMCSPS is the variety of failure factors. Although the failure of the culverts may be caused by the interaction of several failure factors, the natural and man-made hazards occur simultaneously in the same section is less likely. Therefore, the risk assessment process is simplified to evaluate the safety grade of each section to single factor first, then combine them to get the synthesize Safety grade for the pipeline section and the global pipeline system. By the static loading test and finite element analysis [9, 10], the risk assessment criteria of the culvert of the durability damage mode, the load capacity failure mode and the overturning mode are set as shown in Tab. 1 to 3 respectively. In Tab. 2, Grade 1 correspond to that the pipeline is in good operating condition and no obvious crack, Grade 2 is to the state that small load cracks at the concrete cover may occur and the reinforcement of the culvert will not yield, Grade 3 is to the state the stirrups will be yield and the longitudinal reinforcement will not, and load cracks will be obvious in the tension area of the culvert, and Grade 4 correspond to the state that the longitudinal reinforcement will be yield and the load capacity and stiffness of the culvert is deduced severely.

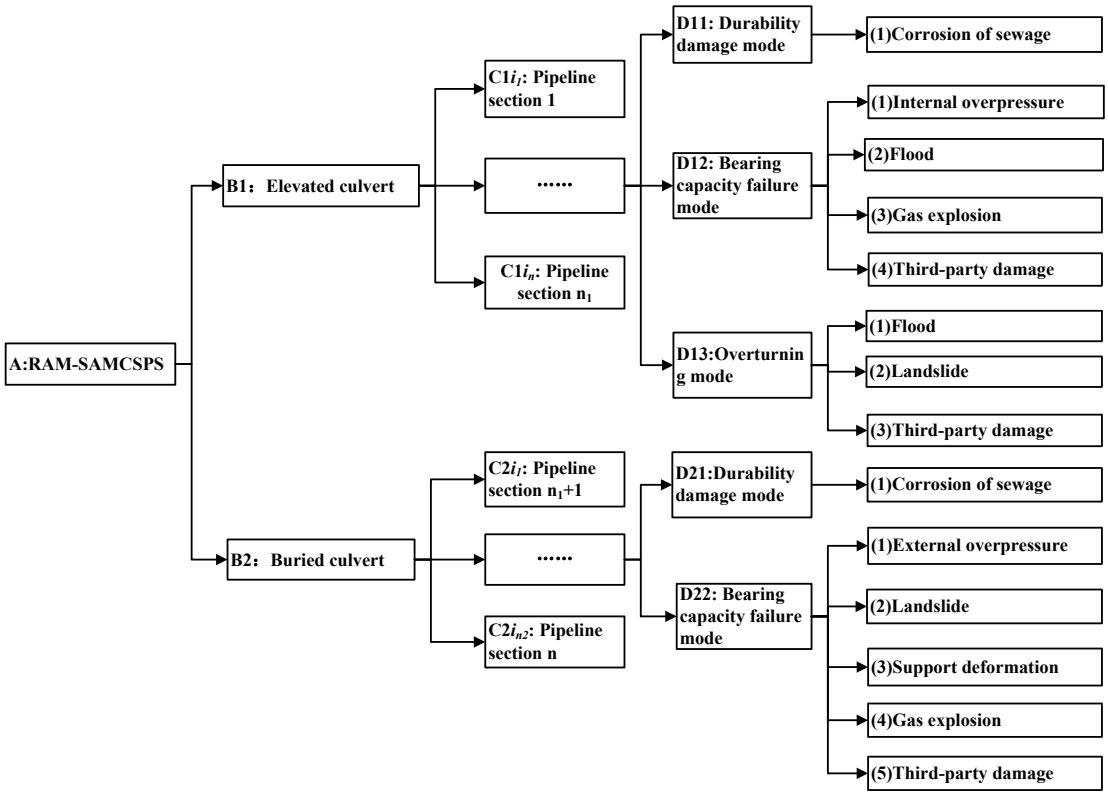

Fig. 1: The hierarchical analysis model for the safety assessment of the mountain city sewage pipeline system

Tab. 1: The durability evaluation criteria of culvert

Safety Grade	Surface Damage Phenomena
1	No peel off or damage at the concrete surface
2	The thickness of the peel off or damage at the surface ≤ 5 mm
3	The thickness of the peel off or damage at the surface is 5 ~ 10 mm, reinforcement or aggregates is exposed
4	The thickness of the peel off or damage at the surface ≥ 10 mm, reinforcement is erosion

Tab. 2: The load capacity evaluation criteria of culvert

Safety Grade	1	2	3	4
Buried culvert	Soil cover ≤ 8 m, Concrete Crack ≤ 0.2 mm, No landslide	Soil cover 8 ~ 15m, Concrete Crack 0.2 ~ 0.5mm, Landslide crush ≤ 200 kPa	Soil cover 15 ~ 19 m, Concrete Crack 0.5~1.0 mm, Landslide crush ≤ 300kPa	Soil cover > 19 m, Concrete Crack > 1.0 mm, Landslide crush > 300 kPa
Elevated culvert	Water head of internal pressure ≤ 15m	Water head of internal pressure 15m ~ 30 m	Water head of internal pressure 30m ~ 37m	Water head of internal pressure > 37m
Gulch-crossed Culvert	Flood level < level of culvert top board, Speed of the flood flow ≤ 4 m/s	Flood level = level of culvert top board, Speed of the flood flow 4 m/s ~ 6 m/s	Flood level > level of culvert top board, Speed of the flood flow 6 m/s ~ 8 m/s	Flood level > level of culvert top board, Speed of the flood flow > 8 m/s

Tab. 3: The overturning evaluation criteria of culvert

Safety Grade	1	2	3	4
Buried Culvert	Sway < 20% of the sway limitation	Sway 20% ~ 40% of the sway limitation	Sway 40% ~ 70% of the sway limitation	Sway > 70% of the sway limitation

The risk evaluation method of a pipe section to several load cases in one failure mode is as follows.

$$\alpha_{i,j} = \max_k \left\{ \alpha_{k,i,j} \right\} + \begin{cases} 1, & \alpha_{k,i,j} \geq \max_k \left\{ \alpha_{k,i,j} \right\} - 1 > 1 \\ 0, & \text{otherwise} \end{cases} \tag{1}$$

in which, $\alpha_{i,j}$ is the safety grade of the failure mode i for pipe section j, $\alpha_{k,i,j}$ is the safety grade of the failure mode i subjected to load case k for pipe section j.

The method described in Eq. (1) shows that the safety grade of the viewed pipe section subjected to a variety of load cases and failed in one mode is obtained by adding the maximum safety grade of this section subjected to specific load. For example, if the maxi-

mum grade to a specific load case is greater than 2, and the difference of the grades of the viewed pipe section to other loads to the maximum value is less than one, the adding parameter is 1, otherwise is 0. It is reasonable to see that this synthesis risk evaluation method for the viewed pipeline to several load cases takes into both the critical load case and the coupled effects of several load cases.

The pipeline may be subject to a variety of damage and failures. The consequences of the various failure modes, such as the load capacity failure mode, the overturning failure mode and the durability damage mode, are quite different. During the hierarchical analysis process [11], failure modes at the hierarchy are compared with each other in pairs to judge the relative importance and simply sorted. Then the judgment matrix is constructed. For example, Durability damage affects the serviceability of the pipe, and affects the load capacity indirectly. Compared to the consequence of the failure mode of load capacity, the durability damage has less impact on the strength of the pipe. During the three failure modes, the overturning failure will result in the most serious consequences. However, it is necessary to take into account the difference of the importance of different failure mechanisms in the risk assessment of the pipeline system. The judgment matrix for elevated culvert is given as follows.

Tab. 4: The judgment matrix for elevated culvert

	Durability mode	Bearing capacity mode	Overturning mode
Durability mode	1	½	1/3
bearing capacity mode	2	1	½
overturning mode	3	2	1

The software MATLAB is used to determine the eigenvector corresponding to the largest eigenvalue of this judgment matrix. The eigenvector is (0.2565, 0.466, 0.8468). After normalization the eigenvector can be approximated to the weighted parameters vector. So the weighted parameters of different failure modes for elevated culvert are (0.163, 0.297, 0.540).

Similar to the elevated culvert, the judgment matrix for buried culvert is given as follows.

Tab. 5: The judgment matrix for buried culvert

	Durability mode	Bearing capacity mode
Durability mode	1	2
bearing capacity mode	½	1

So the weighted parameters of different failure modes for buried culvert are (0.333, 0.667).

Based on the safety grade evaluation of different failure modes, the synthetic risk grade of the viewed pipeline section is obtained by using the weighted average method as follows.

$$\alpha_j = \left[\frac{\sum_i \omega_i \alpha_{i,j}}{\sum_i \omega_i} \right] \tag{2}$$

In the Eq.(2), α_j is the safety grade of pipe section j, ω_i is the weighted parameter of failure mode i which is given as fore-described, and [ ] is the integer operator.

The sewage pipeline system represents a linear risk source that can create unique challenges when assessing risks. At the system level, the risk grade of the whole pipeline system can be evaluated as a deduction of the risk grade of the most severe pipeline section. For example, if the risk grade of the most severe pipeline section is Grade 2 and more than [p] of sections' risk grade is Grade 2, see [p] is 50%, the deduction factor is 1, and otherwise is 0.

$$\alpha_{i,j} = \max_k \left\{ \alpha_{k,i,j} \right\} + \begin{cases} 1, & \dfrac{Num\left[\alpha_{k,i,j} \geq \max\limits_k \left\{ \alpha_{k,i,j} \right\} - 1 \right]}{n} > [p] \\ 0, & \text{otherwise} \end{cases} \tag{3}$$

In which, $Num[\cdot]$ is the counting function, n is the total number of pipeline section.

3 Case Study

In 1998, the primary sewage pipeline project for the urban of Chongqing was built funded by the World Bank Loan. This project includes the two primary sewage systems such as Tangjiatuo and Jiguanshi with 4 interception sewage pipeline labelled as A, B, C and D. The primary sewage pipeline system is design as sewage shunt system. Among them, Line A (see Fig. 2), with length of 22.7 km, is set along the North Shore of Jialing River and collects the sewage water of Jiangbei District of Chongqing, and let the sewage water flow from west to east in it. Line A has 4 typical forms of pipe, such as buried box culvert, elevated box culvert, gulch-crossed box culvert and tunnels. The geological conditions along Line A are complex, and the pipeline is at the risk of landslide, corrosion, rainfall induced flood, and the third-party damage such as inadequate construction.

First, based on the statistic of the rainfall in Chongqing, the risk of rain-caused landslide along Line A is evaluated, as shown in Fig. 3. In Fig. 3, the pipe sections in green indicate the low risk of landslide, in orange means the modesty risk, and in red represents high-risk of landslide. In Fig. 3, it is indicated that the section of Line A with high-risk of landslide are in the region between Yu-Ao Bridge to the Yellow Garden Bridge of Jialing River, and the modesty risk of landslide are at the back part of the pipeline.

Based on the risk assessment of the rain-caused landslide of Line A, and combined with the rainfall statistics, the risk assessment of Line A of the Urban Sewage Pipeline System in Chongqing is present in Fig. 4. During the assessment process, the failure due to the risk of rain-caused landslide, flood impact, the internal over-pressure and the corrosion effects of the sewage water are taken into account. In Fig. 4, it is shown that, most of the pipeline sections are in good working condition with Grade 1 coloured in green. The pipeline section of 120#−124# is the gulch-cross culvert which is at the risk of rain-caused flood, so

the risk grade of this section is 2 coloured in yellow. The pipeline sections of 38#−43# and 70#−80# are located at the region of high-risk of landslide, so the risk grade is 3 coloured in orange.

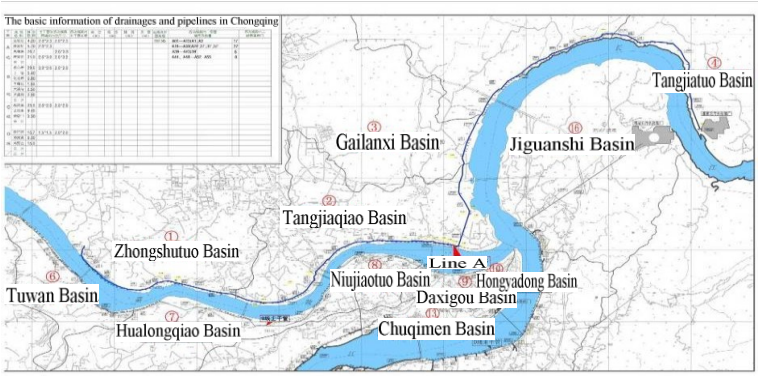

Fig. 2: Line A of the urban primary sewage pipeline system in Chongqing

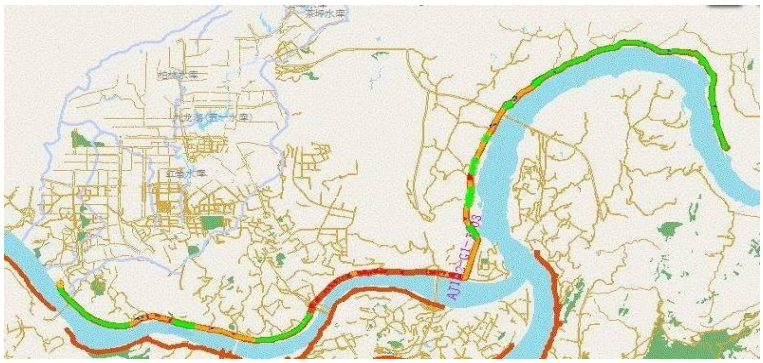

Fig. 3: The risk assessment of the rain-caused landslide along Line A

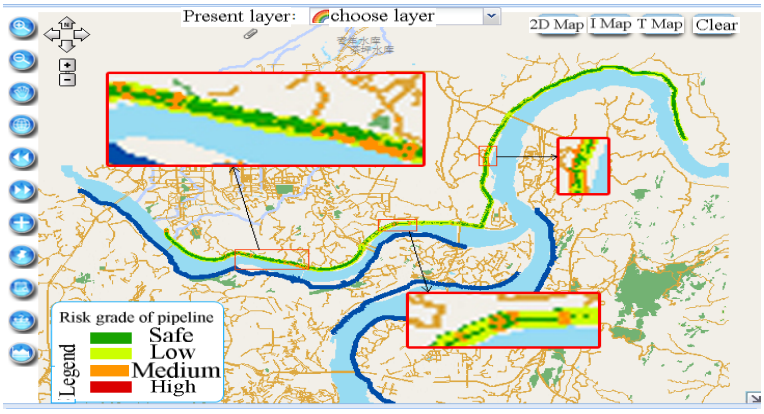

Fig. 4: The risk assessment of Line A of the urban primary sewage pipeline system in Chongqing

4 Conclusions

Because of the particularity of geological and terrain features in mountain cities, such as the fluctuate of the terrain, the great variation of the height of the landform, and the complexity and multivariate conditions of the geology, the sewage pipeline is at the risk of

landslide and flood other than the risk of external and internal over pressure, corrosion and third-party damage. In this paper, we present the hierarchical analysis model for the safety assessment of the mountain city sewage pipeline system which taken into account of the multi-damage factors and failure mode of the pipe. The analysis of A Line of the primary sewage pipeline system in Chongqing had shown that landslide and flood impact are the most severe nature hazard to the pipeline in mountain area. Furthermore, the explosion due to the gas accumulation inside the pipe, the load-corrosion couple action and the third-party damage are also severe damage factors to the sewage pipeline, and are needed to pay more attention in future.

Acknowledgements

This project is supported by the National High Technology Research and Development Program of China (Grant no. 2008ZX07315-001-1).

Literature

[1] Eguchi, R.T. and Honegger D. G. Lifelines: Ensuring the Reliability of Water Supply Systems during Natural Disasters. *Standardization News*, 30(8), 2000, 24−27

[2] Wiese, J. et al. Pipeline safety research and development at the office of pipeline safety, *Proc. of the 5th Biennial Int*. *Pipeline Conf., IPC*, Vol.3, 2004, 2695−2699

[3] Dey, P. K. Analytic Hierarchy Process Analyzes Risk of Operating Cross-Country Petroleum Pipelines in India. *J. Natural Hazards Review*, 4(4), 2003, 213−221

[4] Chen, Z.H., He, Q. and Yan, W.T. Research on the Corrosion of Sewer System Pipelines from Domestic Wastewater. *Proceedings of the ASCE International Conference on Pipeline Engineering and Construction: New Pipeline Technologies, Security, and Safety*, n1, 2003, 524−529

[5] Chen, Z.H. and Huang, H. Constitutive Model of Corroded Concrete under Uni-axial Compression. *J. Journal of Huazhong University of Science and Technology (Nature Science Edition)*, 36(3), 2008, 38−41

[6] Chen, Z. H. et al. The Mechanical Analysis of Corroded Concrete Sewage Pipeline Subjected to Flood Load. Advances in concrete structural durability, *Proceedings of the 2nd international conference on durability of concrete structures ICDCS2010*, 2010, 457−464

[7] Chen, Z. H. et al. Analysis of Sewage Pipeline of Typical Mountain City in Three Gorges Reservoir Region. *J. China Water & Wastewater*, 27(8), 2011, 22−26

[8] Preuth, T., Glade, T. and Demoulin, A. Stability Analysis of a Human-influenced Landslide in Eastern Belgium. *J. Geomorphology*, 120(2), 2010, 38–47

[9] Chen, Z. H. et al. Experimental Analysis on Static Behaviors of Simple-supported Reinforced Concrete Box Girder with Small Depth-to-span Ratio. *J. Journal of Civil, Architectural & Environmental Engineering*, 33(4), 2011, 13−19

[10] Huang, J. H. et al. Experimental Study on Static Behaviors of Simple-supported Deep Rectangular Box Girder. *J. Engineering Mechanics*, 29(Suppl Ⅰ), 2012, 46−52

Behaviour of reinforced concrete slabs strengthened by concrete overlays

Wael Ibrahim, Mohamed El-Adawy and Gouda Ghanen
RWTH Aachen university, Aachen, Germany
and Helwan University, Cairo, Egypt
Wael.ibrahim@rwth-aachen.de

Abstract: This paper discusses the influence of three factors, the distribution of shear connectors, the concrete compressive strength, addition of new concrete thickness on the behaviour of one way composite pre-slabs. The experimental program involves nine tests to study flexure and cracking behaviour of reinforced concrete slabs strengthened with cast in- place new concrete layer. Three of them are reference monolithic slabs and the remaining six slabs are composite pre-slabs composed of two layers with different distributions of shear connectors according to shear force distribution. All slabs are tested under two line loads. The strengthening with cast in- place new concrete layer significantly increases the strength of reinforced concrete (RC) slabs.

Keywords: shear connectors, slabs, compressive strength, strengthening

1 Introduction

RC structures are designed and built to perform adequately with respect to strength, serviceability and durability. During their service life, however, they might, due to several reasons, behave unsatisfactorily with respect to these criteria. Rehabilitation and strengthening interventions are then necessary [3], [8]. The objective of this paper is to present the results of an experimental investigation on the behaviour of one-way reinforced concrete slabs strengthened in flexure with a 4.0 cm concrete overlay. Shear transfer at the concrete interface is provided in one way: bond between the overlay and concrete substrate by dowel action only through shear connectors. Nine slabs are tested; all slabs are loaded up to failure except slabs S no. (2) and S no. (3). For slabs S no. (2) and S no. (3), a two-stage loading procedure is employed. Initially, these slabs are subjected to loads 25% and 75% of their service load level, respectively. This load is then removed and the slabs are strengthened. The rehabilitated slabs are tested twenty-eight days after casting the concrete overlays. During the experiments, displacements, interlayer slips and strains are measured. A design procedure for evaluating the behaviour of the slabs after the different interventions, both in service and at failure, is also presented.

2 Experimental Program

2.1 Test Specimens

The experimental program consists of nine one-way slabs. All slabs had the same flexural reinforcement. The details of the one-way slabs tested in the laboratory are shown in (Tab. 1 and Fig. 1). The major variables of the specimen are shear connectors spacing, concrete overlay and compressive strength of concrete. Each specimen has the same concrete strength and different shear connectors spacing. Specimen no 1 is the original slab without strengthening. Slab no. (2) and slab no. (3) are first loaded to 25% and 75% of their service load level respectively, and then strengthened with a 40 mm concrete overlay. One repair method is used: the concrete overlay is bonded to the original slab; where the shear transfer at the concrete interface is provided by shear connectors with a bond breaker between the two concrete layers. The shear connectors are positioned as shown in Fig. 1.

Tab. 1: Test matrix of the experimental program

Specimen ID	Concrete overlay [mm]	Shear connectors Spacing [mm]			Concrete compressive strength [MPa]	
		L/3	*L*/3	*L*/3	First Layer	Second Layer
S1	-	-	-	-	-	-
S2	40	250	250	250	33	34
S3	40	250	250	250	33	34
S4	40	150	150	150	33	34
S5	40	250	250	250	33	34
S6	40	200	-	200	33	34
S7	40	200	250	200	33	34
S8	80	250	250	250	33	34
S9	40	250	250	250	33	38

2.2 Materials

Concretes with compressive strengths of f_c = 30 MPa are used. Steel reinforcing bars with yield strength and ultimate strength 400, 600 MPa and an elasticity modulus of 200 GPa respectively, are used. Steel reinforcing bars, with a nominal diameter of 12 mm and a length of 80 mm are used as shear connectors. Total of 14 to 33 connectors/specimen would be necessary in each shear span for the composite slab to reach its ultimate bending capacity. This number of connectors is reasonable when compared to the maximum values commonly used in CALIXTO ET AL. [3] practice (25 to 30 connectors/m^2). With this number of connectors, partial composite action should be expected at service load levels during the tests.

2.3 Strengthening Procedures

The strengthening procedure consisted of initially machine grinding the top surface of the slab. Holes are then drilled for the shear connectors, which penetrated 6 cm into the original slab. The slab, immediately before casting the concrete overlay, is shown in Fig. 2. The concrete overlay is cast manually and an internal vibrator is used for consolidation. The

concrete slump averaged about 180 mm. The overlays are covered with wet burlap for 7 days.

2.4 Testing Set-up

The slabs are tested in a simply supported condition with a two-point load equidistant from the two supports, as shown in Fig. 3. As a result, each slab had a region of constant bending moment (between the applied loads) and a region of constant shear force along the shear span. Throughout the loading tests, mid-span deflections and strains in the concrete as well as in the longitudinal reinforcement are measured. In the repaired slabs, the interlayer slip at the supports is also evaluated.

3 Test results and analysis

3.1 Effect of strengthened by concrete overlays

Generally, the overall behaviour of the strengthened slabs S no. (2) to S no. (9) with respect to the original slab S no. (1) and strengthened slabs can be compared through the load versus mid-span deflection relationship shown in Figs. 4 to 9. The repaired slabs exhibited a much larger stiffness and strength, which in turn led to the increases of load carrying capacity both in service and at failure. The new service load is around 66 % to 260 % higher than the original one. Thus, this rehabilitation procedure produced significant improvements in the performance of the slabs. This result emphasizes that the number of connectors at the interface between the overlay and substrate is enough to transfer the shear stresses.

3.2 Effect of number of shear connectors

As expected, strengthened slabs S no. (4), S no. (6) and S no. (7) with respect to the strengthened slab S no. (5) exhibited a much larger stiffness and strength, which in turn led to increases in load carrying capacity both in service and at failure. This result emphasizes that the number of connectors at the interface between the overlay and substrate is important to transfer the shear stresses.

During these tests, no slip is observed over the supports of the slabs. This indicates that the bond strength at the interface between the different concretes is sufficient to withstand the shear stresses being transferred. Consequently, full composite action occurred up to failure. These strain measurements indicated yielding of the tensile reinforcement. Both slabs failed due to bending with crushing of the concrete in the overlay directly below the loading pads.

3.3 Effect of number of shear connectors

The behaviour of the strengthened slab S no. (8) with respect to strengthened slab of the same number of connectors S no. (5) is also compared. Fig. 5 presents the load versus mid-span deflection relationship for the slabs S no. (8) and S no (5). The load versus mid-pan deflection relationship for the original slab S no. (1) is also presented in the plot. These results show that the slab S no. (8) is stiffer with respect to the original slab S no. (1) and strengthened slab S no. (5) for all loads. This larger stiffness resulted in smaller mid-span

deflections up to failure. The partial composite action behaviour associated with the existence of the initial mid-span deflection and the fact that this strengthened slab S no. (8) is already cracked are the reasons for the differences in the load mid-span deflection relationship.

3.4 Effect of concrete overlay compressive strength

The test results indicates expressively the overall better performance, for both service and failure load, when the slabs are repaired with high concrete overlay compressive strength. Fig. 6 presents the load versus mid-span deflection relationship for the slabs S no. (9) and S no. (5). Thus the values of the deflections and the cracking stage of the slab at the time of the repair are very important aspects to consider when assessing the behaviour of repaired slabs under service loads; more research is necessary optimizing the concrete overlay compressive strength.

4 Conclusion

The major conclusions deduced from this research are given below as follows:

1. Experimental study, as presented in this paper, emphasizes the influence of shear connectors on the structural behavior of strengthened slabs and on the debonding mechanism.
2. The overall analysis of the test results indicates expressively the better performance of slabs that are repaired with a larger number of shear connectors. These slabs exhibited increased stiffness and similar load carrying capacity compared to slabs with lower number of shear connectors of the same geometry.
3. Strengthening slabs by adding high concrete overlay compressive strength indicates expressively the overall better performance, for both service and failure load.
4. The design procedures for evaluating the behavior of the strengthened slabs, at service and failure loads is still needed especially when shear connectors are used.
5. Deflection is significantly reduced in the strengthened slabs.
6. Finally, strengthening slabs by adding concrete overlays will only enhance their load carrying capacity as long as the existing tensile reinforcement is sufficient to accommodate the increased load.

S1: Control slab

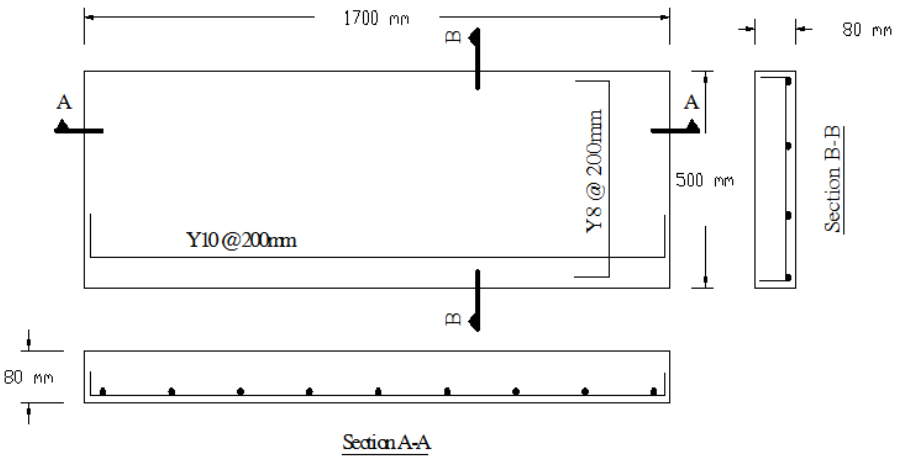

S2: Control slab
F_y = 25%

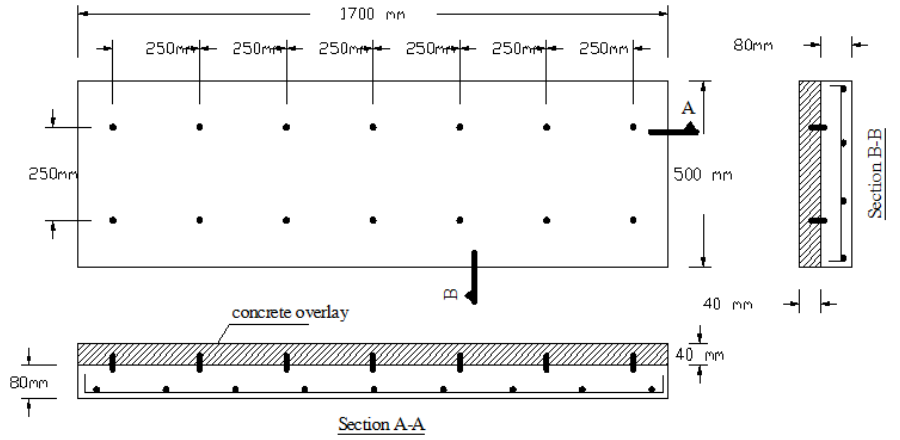

S3: Control slab
F_y = 75%

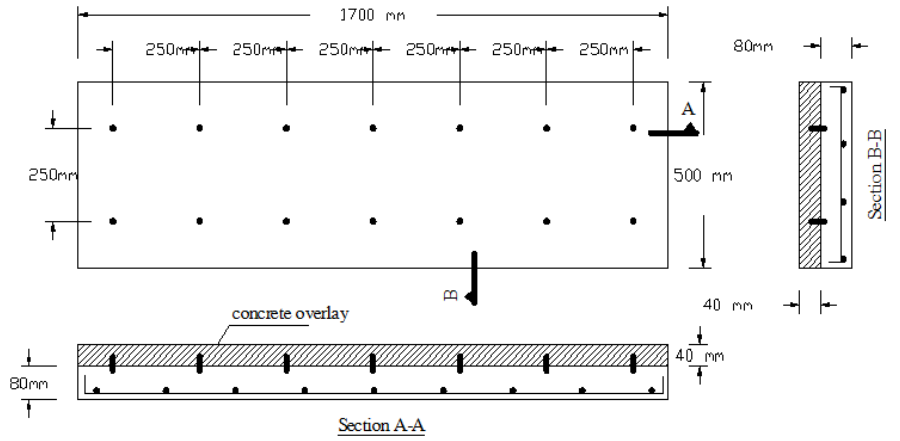

Fig. 1 (part 1): Test specimen details

S4: Strengthened slab with shear connectors (spacing 150 mm) and smooth interface

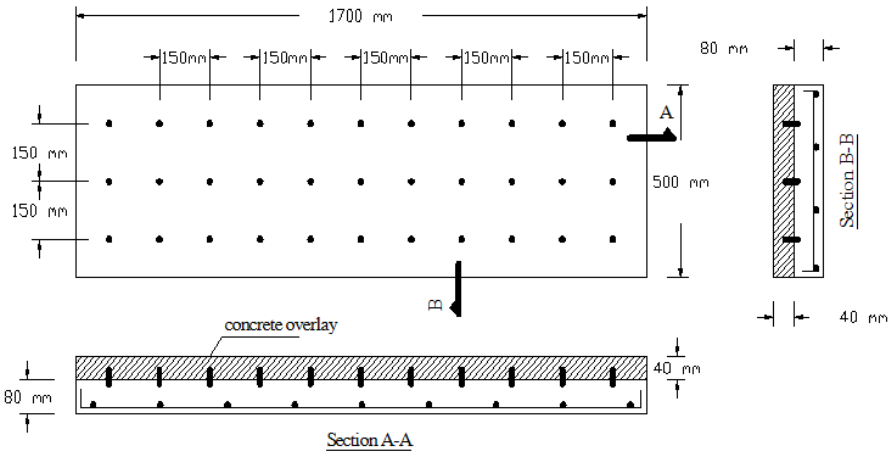

S5: Strengthened slab with uniform shear connectors (spacing 250 mm) and smooth interface

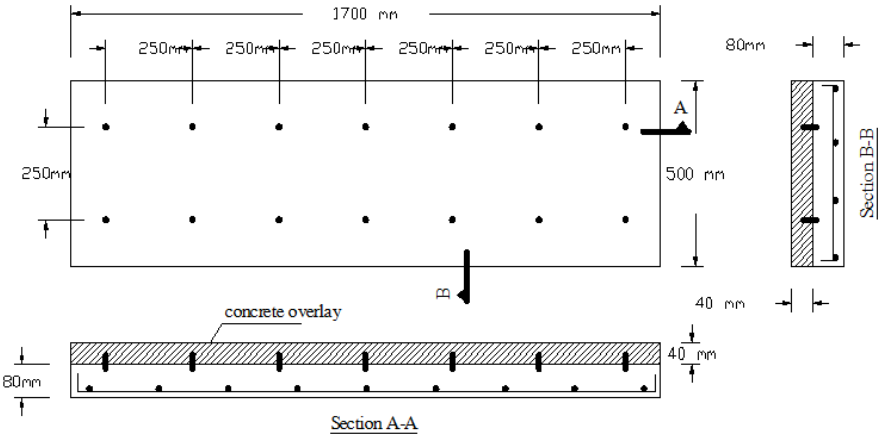

S6: Strengthened slab with concentrated shear connectors at quarter, without Min shear connectors at mid span and smooth interface

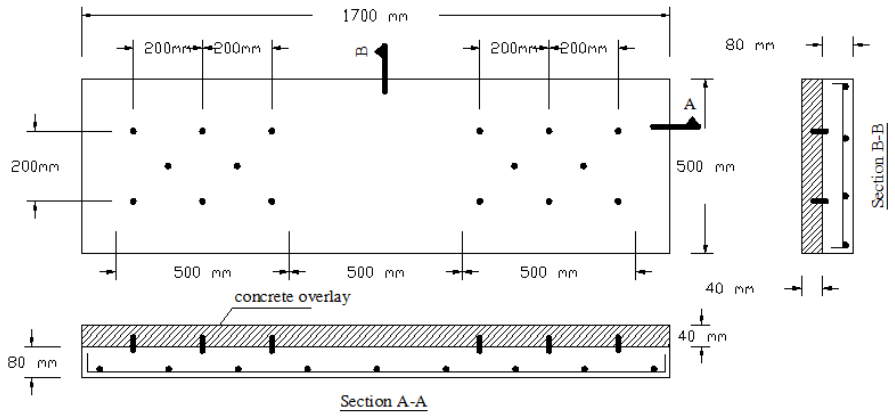

Fig. 1 (part 2): Test specimen details

S7: Strengthened slab with concentrated shear connectors at quarter, Min shear connectors at mid span and smooth interface

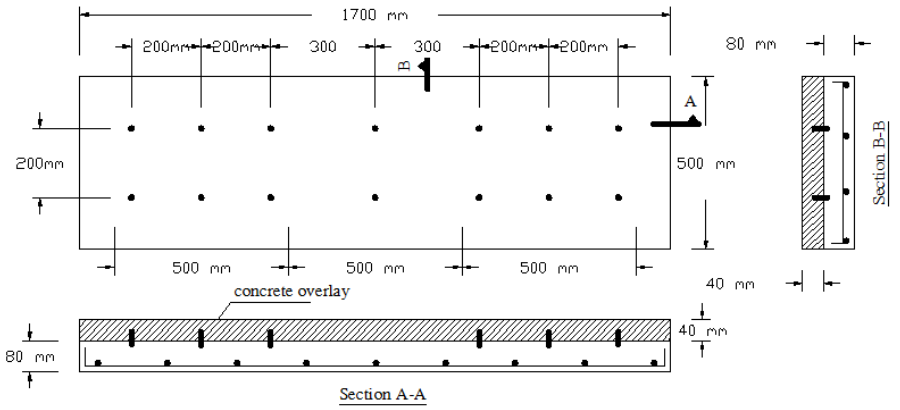

S8: Strengthened slab with shear connectors (spacing 250 mm) and smooth interface (add new concrete 80 mm)

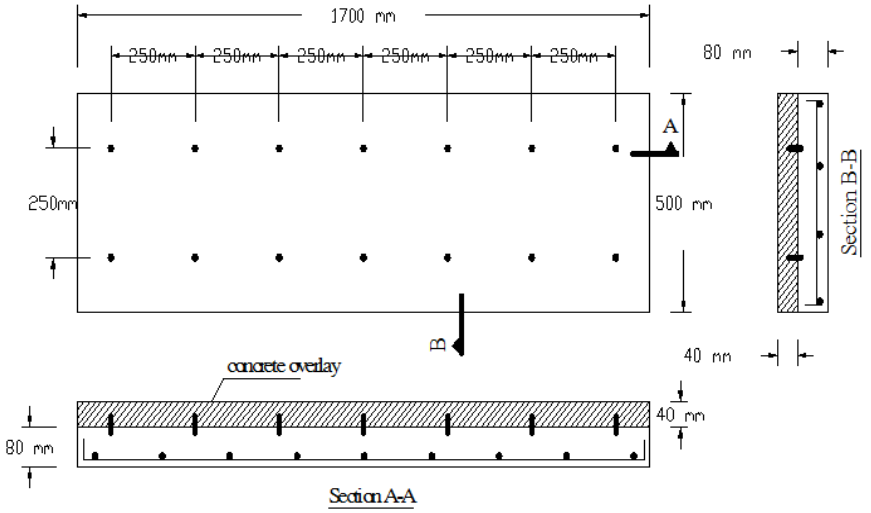

S9: Strengthened slab with shear connectors (spacing 250 mm) and smooth interface (add new concrete 40 mm with different compressive strength)

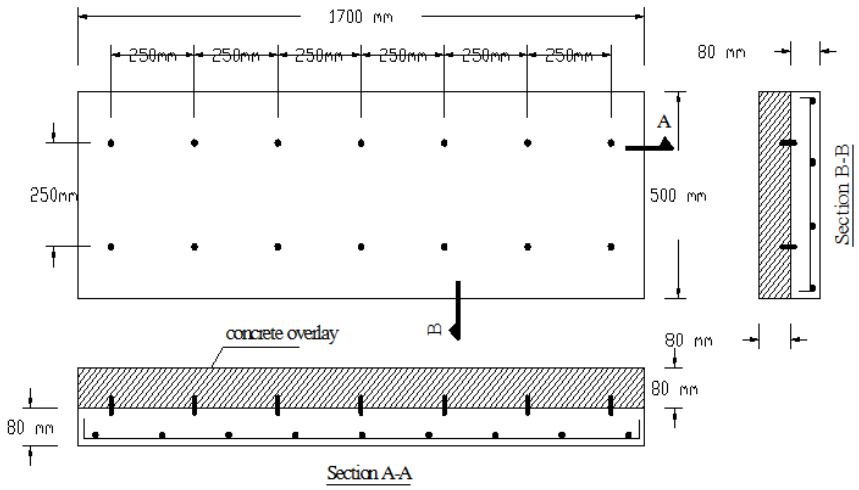

Fig. 1 (part 3): Test specimen details

Fig. 2: Technique for the strengthening of reinforced concrete slabs

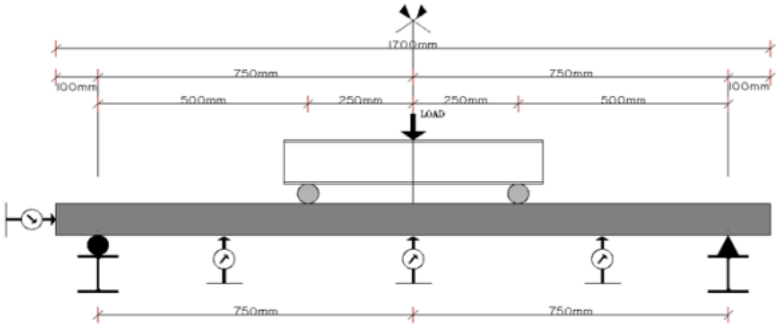

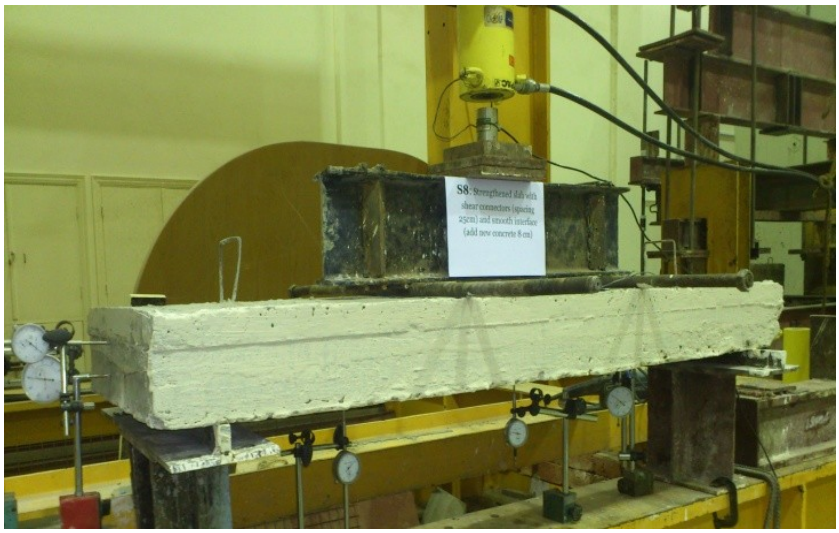

Fig. 3. Test set-up

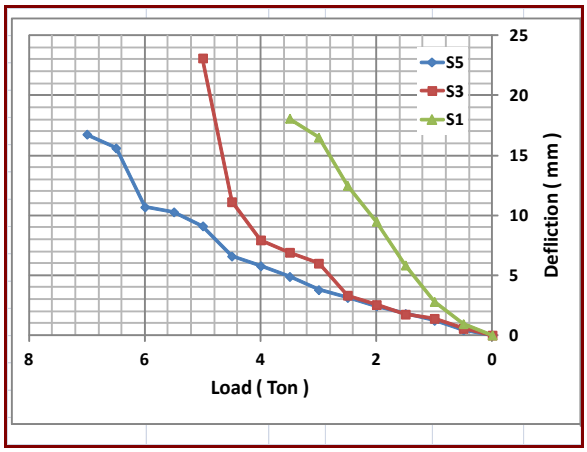

Fig. 4: Load−deflection curves [S1, S3, S5]

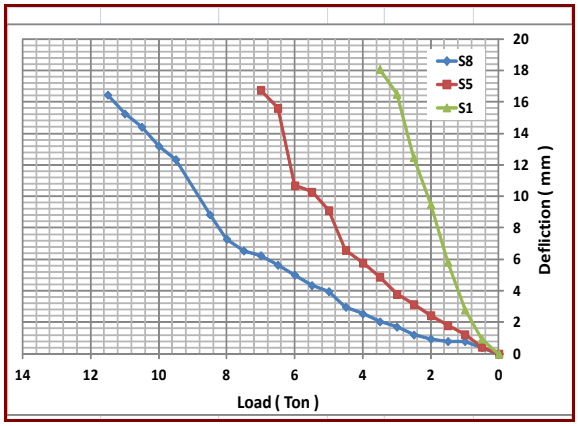

Fig. 5: Load−deflection curves [S1, S5, S8]

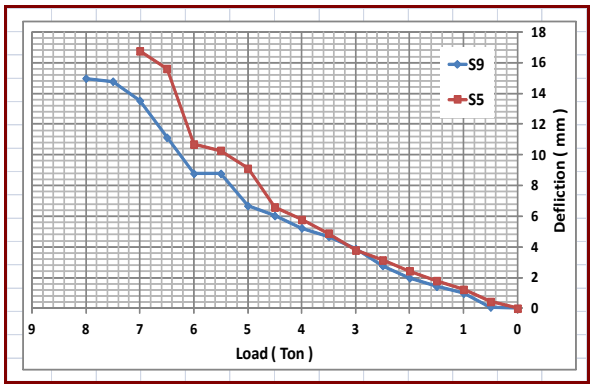

Fig. 6: Load−deflection curves [S5, S9]

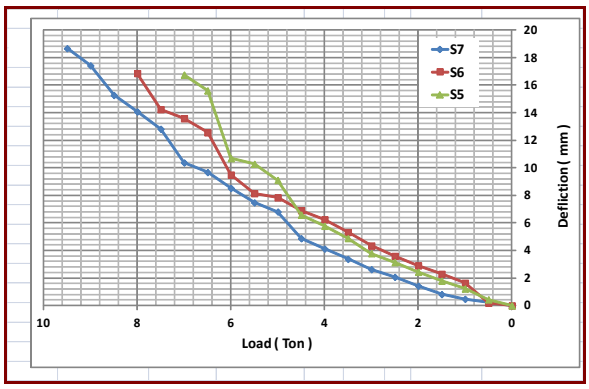

Fig. 7: Load−deflection curves [S5, S6, S7]

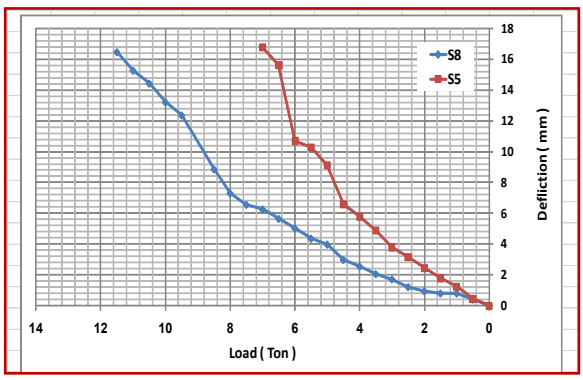

Fig. 8: Load−deflection curves [S5, S8]

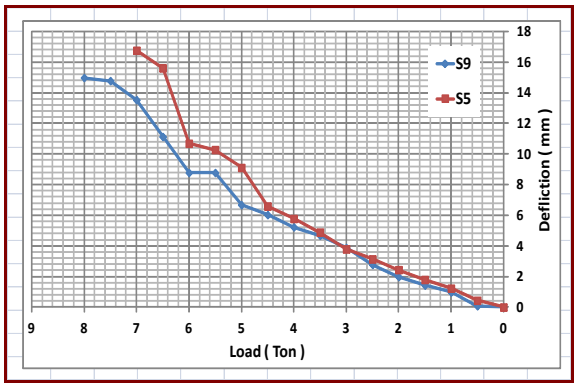

Fig. 9: Load−deflection curves [S5, S9]

Literature

[1] Bijen, J., Salet, T. Adherence of young concrete to old concrete development of tools for engineering, Wittman F.W. (ed) *Proceeding of 2nd Bolomey workshop on adherence of young on old concrete*, 1994, p. 1−24

[2] *Building Code Requirements for structural concrete (ACI 318-05) and Commentary (ACI 318E-05)*, ACI Committee 318, 2005, Farmington Hills, MI.

[3] Calixto, J. M., Pires, E. F., Lima, S. A., Piancastelli, E. M. Behavior of reinforced concrete slabs strengthened in flexure by concrete overlays, *ACI Structural Journal*, Vol. 229, 2003, p. 389−406

[4] Mellinger, F. M. Structural design of concrete overlays, *ACI Journal*, 60(2), 1963, p. 225−237

[5] Perez, F., Bissonnette, B., Gagné, R. Parameters affecting the debonding risk of bonded overlays used on reinforces concrete slab subjected to flexural loading, *Materials and Structures*, Vol. 42, Issue 5, 2009, p. 645−662

[6] Saiidi, M., Vrontinos, S., Douglas, B. Model for the response of reinforces concrete beams strengthened by concrete overlay, *ACI Structural Journal*, 87(6), 1990, p. 687−695

[7] Silfwerbrand, J. Improving concrete bond in repaired bridge decks, *Concrete International Journal,* Vol. 12, Issue 6, 1990, p. 61−66

[8] Thanoon, W. A., Jaafar, M. S., Razali, M., Kadir, A., Noorzaei, J. Repair and structural performance of initially cracked reinforced concrete slabs, *Construction and Building Materials,* Vol. 19, Issue 8, 2005, p. 595−603

Polynomial chaos-based evaluation of failure probability: A numerical study

Eliška Janouchová [a], Anna Kučerová [a], Jan Sýkora [a],

[a]Department of Mechanics, Faculty of Civil Engineering, Czech Technical University in Prague, Czech Republic
eliska.janouchova@fsv.cvut.cz, anicka@cml.fsv.cvut.cz, jan.sykora.1@fsv.cvut.cz

Abstract: An extensive development of efficient methods for stochastic modelling enabled uncertainty propagation through complex models. In this contribution, we present a review and comparison of several approaches such as stochastic Galerkin method, stochastic collocation method or regression based on Latin Hypercube Sampling for construction of a polynomial chaos-based approximation of model response. The approximation is then employed for evaluation of structural failure probability using Monte Carlo method.

Keywords: uncertainty propagation, stochastic modelling, polynomial regression, stochastic collocation, stochastic Galerkin method, Monte Carlo method

1 Introduction

The service life of buildings is dependent on many important factors such as the environmental conditions as well as structural properties. Uncertainties in these factors have to be taken account in an appropriate reliability analysis. Thanks to the growth of powerful computing resources and technology, recently developed procedures in the field of stochastic mechanics have become applicable to realistic engineering systems.

Methods quantifying uncertainties can be classified into two groups: (i) reliability analysis methods, such as the first- and second-order reliability method (FORM/SORM [4]) computing the probability of failure related to limit states; (ii) the higher moment analysis focused on estimation of the higher-order statistical moments of structural response as stochastic finite element methods (SFEM), see [10, 11] for a review. SFEM is a powerful

tool in computational stochastic mechanics extending the classical deterministic finite element method (FEM) to the stochastic framework involving finite elements whose properties are random [5].

In this contribution we concentrate on the SFEM based on polynomial chaos expansion (PCE) used for approximation of the model response in the stochastic space. Uncertainty in the model output can be then quantified using Monte Carlo method employed for sampling model parameters and evaluating the PCE instead of full numerical model. The efficiency of SFEM thus depends on computational requirements of the PCE construction and its consequent accuracy.

There are several methods for construction of PCE-based approximation of a model response: linear regression [3], stochastic collocation methods [2, 13] and stochastic Galerkin method [1, 9]. The principal differences among these methods are follows. The linear regression is a stochastic method based on a set of model simulations performed for a stochastic design of experiments, usually obtained by Latin Hypercube Sampling. The PCE coefficients are then obtained by regression of a model results at the design points, which leads to a solution of a system of equations. On the other side stochastic collocation method is a deterministic method, which uses a set of model simulations on a sparse grid constructed for a chosen level of accuracy. The computation of PCE coefficients is based on explicit formula. Stochastic Galerkin method is also deterministic, but leads to solution of large system of equation and needs an intrusive modification of the numerical model itself. The aim of this paper is to compare these methods in terms of computational requirements and resulting accuracy on a simple illustrative example of a frame structure.

2 Motivation

In order to demonstrate a performance of the methods on an engineering structure, we have chosen a simple frame presented in [8].The geometry, load distribution and supports of the frame are shown in Fig. 1.

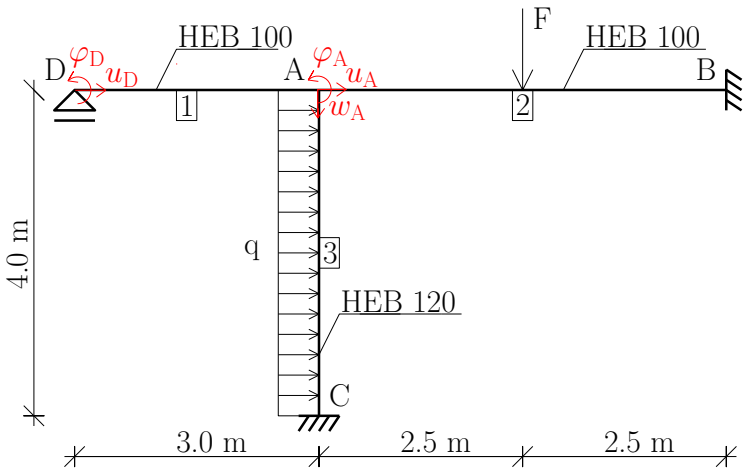

Fig. 1: Scheme of a frame structure

Tab. 1: Material and geometrical data and variations

Data	Nominal value	Variable	Histogram
Yield stress	$f_{y,\mu} = 235\text{GPa}$	$f_{y,\sigma}$	Fy235A
Moment of inertia	$I_1 = 449.5\ \text{cm}^4$	$I_{\sigma 1}$	N1-05
Cross-sectional area	$A_1 = 26.04\ \text{cm}^2$		
Moment of inertia	$I_2 = 449.5\ \text{cm}^4$	$I_{\sigma 2}$	N1-05
Cross-sectional area	$A_1 = 26.04\ \text{cm}^2$		
Moment of inertia	$I_3 = 864.4\ \text{cm}^4$		
Cross-sectional area	$A_3 = 34.01\ \text{cm}^2$	$I_{\sigma 3}$	N1-05
Elastic section modulus	$W_3 = 144.1\ \text{cm}^3$		
Length	$l_1 = 3$ m		
Length	$l_2 = 5$ m	l_σ	N1-01
Length	$l_3 = 4$ m		

Material of the frame is steel with Young's modulus $E = 210$ GPa and uncertain yield stress f_y obtained by the product of the nominal value $f_{y,\mu}$ and uncertain variation $f_{y,\sigma}$ defined by a prescribed histogram Fy235A (see Fig. 2). Also the geometrical parameters of particular beams are considered as uncertain and defined as products of the corresponding nominal values and variations given in [8] and listed in Tab. 1. Particular histograms are also depicted in Fig. 2.

The prescribed loading are linear combinations of dead, long-lasting and short-lasting load given as: $q = D_1 D_{\sigma 1} + S_1 S_{\sigma 1} + L_1 L_{\sigma 1}$ [kN/m] and $F = D_2 D_{\sigma 2} + S_2 S_{\sigma 2} + L_2 L_{\sigma 2}$ [kN], where particular loads are statistically independent and described by random variables with extreme values and variations defined by histograms given in Tab. 2 and depicted in Fig. 2.

Tab. 2: Loading and variations

Load	Extreme Value	Variable	Histogram
Dead load	$D_1 = 11$ kN/m	$D_{\sigma 1}$	DEAD2
Short-lasting load	$S_1 = 9$ kN/m	$S_{\sigma 1}$	SHORT1
Long-lasting load	$L_1 = 5.5$ kN/m	$L_{\sigma 1}$	LONG1
Dead load	$D_2 = 3.5$ kN	$D_{\sigma 2}$	DEAD2
Short-lasting load	$S_2 = 2.2$ kN	$S_{\sigma 2}$	SHORT1
Long-lasting load	$L_2 = 1.7$ kN	$L_{\sigma 2}$	LONG1

Since the axial force in the column does not achieve critical intensity, the instability does not play any role and thus the column has only one failure mode given by the material yield stress. The maximal internal forces will appear in the column at support C and can be computed from the displacement and rotation of the joint A. The unknown displacements $\boldsymbol{r}$ can be – in case of geometrical and material linearity considered here – computed by the finite element method or displacement method, which are very well-known. Hence, we start

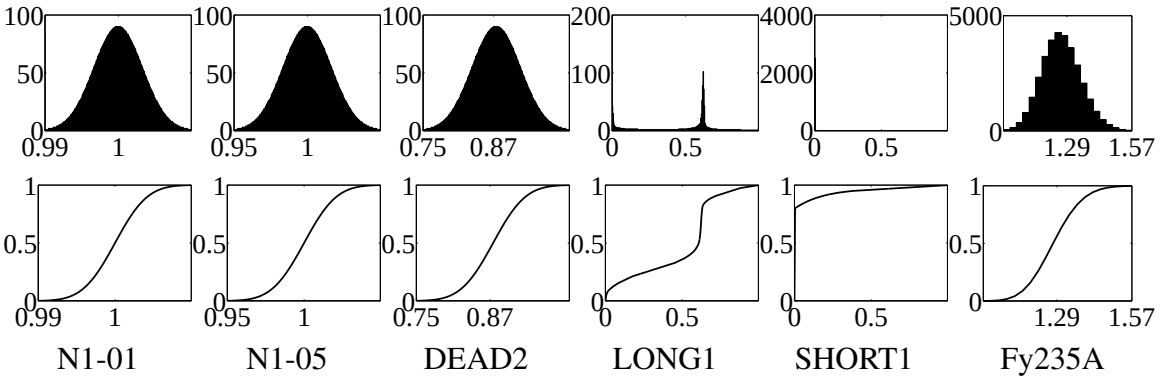

Fig. 2: Histograms of uncertain parameters and corresponding cumulative density functions

directly with the latter one from discretised form of equilibrium equations:

$$\mathbf{K}\boldsymbol{r} = \boldsymbol{f}\,, \tag{1}$$

which – after applying the boundary conditions – is a system of 5 linear equations for unknown $\boldsymbol{r} = (u_{\mathrm{D}}, \varphi_{\mathrm{D}}, u_{\mathrm{A}}, w_{\mathrm{A}}, \varphi_{\mathrm{A}})$.

Safety margin M of the column is the difference between the yield stress f_y and stress produced by external load σ. Failure F occurs when σ exceeds f_y. Probability of failure $\Pr(F)$ is then estimated as the number of failures divided by the total number of executed simulations n:

$$\Pr(F) = \frac{1}{n}\sum_{i=1}^{n} I[f_y - \sigma \leq 0], \tag{2}$$

where $I[f_y - \sigma \leq 0]$ is the indicator function, which takes value one if $f_y - \sigma \leq 0$ and zero otherwise.

3 Polynomial chaos expansion

In order to accelerate the sampling procedure in uncertainty propagation process, the evaluations of a numerical model including solutions of Eq. 1 can be replaced by evaluations of a model surrogate. In particular, we search for an approximation of the response $\boldsymbol{r}$ by polynomial chaos expansion (PCE) [10, 11]. PCE can be used to approximate the response with respect to probability distribution of the random variables. The approximation of the response is then weighted according to the probability distribution of variables i.e. the approximation is more precise in regions with higher probability. The convergence of the approximation error with the increasing number of polynomial terms is optimal in case of orthogonal polynomials of a special type corresponding to the probability distribution of the underlying variables [12]. For example, Hermite polynomials are associated with the Gaussian distribution, Legendre polynomials with the uniform distribution and so on.

In the example described in the previous section, all the random variables are listed in Tab. 1 and 2. Let us simplify the notation and denote them as m_i, $\boldsymbol{m} = (\ldots, m_i, \ldots)^{\mathrm{T}} =$

$(I_{\sigma 1}, I_{\sigma 2}, I_{\sigma 3}, l_\sigma, D_{\sigma 1}, S_{\sigma 1}, L_{\sigma 1}, D_{\sigma 2}, S_{\sigma 2}, L_{\sigma 2})^{\mathrm{T}}$. Since none of these variables has a continuous probability density function (PDF), but their distribution is described by discrete histograms, we introduce new standard random variables $\boldsymbol{\xi} = (\dots, \xi_i, \dots)^{\mathrm{T}}$ with a continuous PDF. The variables m_i can be then expressed by transformation functions t_{jk} of variables ξ_i according to the given histogram j and type k of the ξ_i distribution, i.e.

$$m_i = t_{jk}(\xi_i)\,. \tag{3}$$

For case of discrete histograms, the transformation functions are non-smooth. Particular examples of transformation functions will be discussed in Section 4.

Once we have expressed the model variables $\boldsymbol{m}$ as functions of standard variables $\boldsymbol{\xi}$, also the model response becomes a function of these variables. This function can be thus approximated by the PCE of a type corresponding to the type of $\boldsymbol{\xi}$ distribution, i.e.

$$\tilde{\boldsymbol{r}}(\boldsymbol{\xi}) = \sum_{\alpha} \boldsymbol{\beta}_\alpha \psi_\alpha(\boldsymbol{\xi}), \tag{4}$$

where $\boldsymbol{\beta}_\alpha$ is a vector of PC coefficients $\beta_{\alpha,i}$ corresponding to a particular component of system response r_i. $\psi_\alpha(\boldsymbol{\xi})$ are multivariate polynomials. The expansion (4) is usually truncated to the limited number of terms n_β, which is very often related to the number of random variables n_ξ and to the maximal degree of polynomials n_{p} according to the relation $n_\beta = \frac{(n_{\mathrm{p}}+n_\xi)!}{n_{\mathrm{p}}! n_\xi!}$.

3.1 Linear regression

A very general method of computing PC coefficients in Eq. (4) is a well-known linear regression [3]. The underlying assumption of linear regression is that the surrogate $\tilde{\boldsymbol{r}}$ is a linear combination of the parameters $\boldsymbol{\beta}$, but does not have to be linear in the independent variables $\boldsymbol{\xi}$. The application is based on the three following steps: (i) preparation of data $\boldsymbol{\Xi} \in \mathbb{R}^{n_\xi \times n_{\mathrm{d}}}$ which are obtained as n_{d} samples of parameter vector $\boldsymbol{\xi}_i$ (ii) evaluation of the model for samples $\boldsymbol{\xi}_i$ resulting in response samples $\boldsymbol{r}_i$ organised into the matrix $\mathbf{R} \in \mathbb{R}^{n_{\mathrm{r}} \times n_{\mathrm{d}}}$, where n_{r} is a number of response components and (iii) computation of PC coefficients $\boldsymbol{\beta}_\alpha$ organised into the matrix $\mathbf{B} \in \mathbb{R}^{n_{\mathrm{r}} \times n_\beta}$ using e.g. the ordinary least square method.

Since the most time-consuming part of this method consists in evaluations of the model for samples of random variables, the choice of these samples represents a crucial task with the highest impact on the computational time requirements. The simplest way is to choose the samples by Monte Carlo method, i.e. to draw them randomly from the prescribed probability distribution. However, the accuracy of the resulting surrogate depends on a quality, how the samples cover the defined domain. The same quality can be achieved by smaller number of samples when drawn according to some stratified procedure called design of experiments (DoE). Latin Hypercube Sampling (LHS) is a well-known DoE able to respect the prescribed probability distributions. There exist also more enhanced way of optimising the LHS (see e.g. [7]), but these are not subject of the present work and the simplest version of unoptimised LHS is employed. Each computation of a response sample $\boldsymbol{r}_i$ then includes the evaluation of the transformations (3) and the evaluation of the model (1).

The computation of the PC coefficients $\mathbf{B}$ starts by evaluation of all the polynomial terms ψ_α for all the samples $\boldsymbol{\xi}_i$ and saving them in the matrix $\mathbf{Z} \in \mathbb{R}^{n_\mathrm{d} \times n_\beta}$. The ordinary least square method then leads to $\mathbf{Z}^\mathrm{T}\mathbf{Z}\mathbf{B}^\mathrm{T} = \mathbf{Z}^\mathrm{T}\mathbf{R}^\mathrm{T}$ which is a linear system of n_β equations.

3.2 Stochastic collocation

Stochastic collocation method is based on an explicit expression of the PC coefficients:

$$\beta_{\alpha,i} = \int r_i(\boldsymbol{\xi})\psi_\alpha(\boldsymbol{\xi}) \, \mathrm{d}\mathbb{P}(\boldsymbol{\xi}) \,, \tag{5}$$

which can be solved numerically using an appropriate integration rule (quadrature) on $\mathbb{R}^{n_\xi}$. Eq. (6) then becomes

$$\beta_{\alpha,i} = \sum_{j=1}^{n_\mathrm{d}} r_i(\boldsymbol{\xi}_j)\psi_\alpha(\boldsymbol{\xi}_j)w_j \,, \tag{6}$$

where $\boldsymbol{\xi}_j$ stands for an integration node and w_j is a corresponding weight. Here we employ versions of the Smolyak quadrature rule, in particular quadratures with the Gaussian rules (GQN) and nested Kronrod-Patterson quadrature rules (KPN) as basis for normal distribution, see [6].

It is clear that the stochastic collocation method is similar to linear regression, because in both cases the most computational effort is needed for evaluation of a set of model simulations. The principal difference can be seen in sample generation, where stochastic collocation method uses a preoptimised sparse grids while the linear regression is based on stochastic LHS.

3.3 Stochastic Galerkin

Stochastic Galerkin method is principally different to the previous ones, which are based on a set of independent model simulations. Stochastic Galerkin method is an intrusive method, i.e. it requires reformulation of the governing equations of the model (1). To this purpose, we rewrite Eq. (4) using matrix notation

$$\tilde{\boldsymbol{r}}(\xi) = (\mathbf{I} \otimes \boldsymbol{\psi}(\boldsymbol{\xi}))\boldsymbol{\beta}, \tag{7}$$

where $\mathbf{I} \in \mathbb{R}^{n_\mathrm{r} \times n_\mathrm{r}}$ is the unity matrix, $\otimes$ is the Kronecker product, $\boldsymbol{\psi}(\boldsymbol{\xi})$ is a n_β-dimensional vector of polynomials and $\boldsymbol{\beta}$ is a $(n_\beta \cdot n_\mathrm{r})$-dimensional vector of PC coefficients organised here as $\boldsymbol{\beta} = (\dots, \boldsymbol{\beta}_i, \dots)^\mathrm{T}$, where $\boldsymbol{\beta}_i$ consists of PC coefficients corresponding to ith response component.

Substituting the model response $\boldsymbol{r}$ in Eq. (1) by its PC approximation $\tilde{\boldsymbol{r}}$ given in Eq. (7) and applying Galerkin conditions, we obtain

$$\int \boldsymbol{\psi}(\boldsymbol{\xi}) \otimes \mathbf{K}(\boldsymbol{\xi}) \otimes \boldsymbol{\psi}^\mathrm{T}(\boldsymbol{\xi}) \, \mathrm{d}\mathbb{P}(\boldsymbol{\xi}) \cdot \boldsymbol{\beta} = \int \boldsymbol{\psi}(\boldsymbol{\xi}) \otimes \boldsymbol{f}(\boldsymbol{\xi}) \, \mathrm{d}\mathbb{P}(\boldsymbol{\xi}) \,, \tag{8}$$

which is a linear system of $(n_\beta \cdot n_\mathrm{r})$ equations. The integration can be done numerically or analytically. The analytical solution is available e.g. when all terms in the stiffness matrix

and in the loading vector are polynomials with respect to $\boldsymbol{\xi}$. In such a case, the method is called *fully intrusive*. In our particular example, we can multiply the governing Eq. (1) by l_σ^3 so as to obtain polynomials in terms of model parameters $\boldsymbol{m}$. However, we will not obtain polynomials in terms of $\boldsymbol{\xi}$ due to non-smooth transformations (3) produced by discrete nature of histograms prescribed to $\boldsymbol{m}$. Hence, in such a case, a numerical integration leading to *semi-intrusive* Galerkin method is inevitable. Here we use again Smolyak integration rule, in particular GQN [6].

4 Results

The goal of the presented work is to compare the described methods for approximating the model response and accelerating the Monte Carlo (MC) sampling performed for estimation of probability distribution of safety margin M and probability of structural failure. In this numerical study two variants of model response are considered, the first one is directly safety margin, in the second case the model response is displacement vector $\boldsymbol{r}$ and safety margin is calculated from its approximation.

Tab. 3: Time requirements and errors in predicting safety margin in the case of *prescribed histograms* for model parameters $\boldsymbol{m}$

Model response:		**Safety margin**				**Displacement vector**			
Method	p	n_{d}	Time [s]	$\Pr(F)$	ε_M [%]	n_{d}	Time [s]	$\Pr(F)$	ε_M [%]
MC	–	10^7	23825	$735 \cdot 10^{-7}$	–	10^7	22352	$735 \cdot 10^{-7}$	–
LHS	1	23	32	$7 \cdot 10^{-7}$	4.2024	19	217	$282 \cdot 10^{-7}$	1.3289
	2	243	164	$1580 \cdot 10^{-7}$	2.6572	163	896	$617 \cdot 10^{-7}$	0.6323
	3	1607	757	$15678 \cdot 10^{-7}$	2.1177	871	2746	$1795 \cdot 10^{-7}$	0.4434
	4	7789	2702	$13842 \cdot 10^{-7}$	1.7934	3481	11021	$1830 \cdot 10^{-7}$	0.3740
KPN	1	23	31	$10 \cdot 10^{-7}$	4.3112	19	250	$172 \cdot 10^{-7}$	0.8836
	2	243	164	$4910 \cdot 10^{-7}$	3.1118	163	896	$947 \cdot 10^{-7}$	0.6350
	3	1607	760	$11272 \cdot 10^{-7}$	2.9822	871	2776	$1327 \cdot 10^{-7}$	0.5904
	4	7789	2701	$8352 \cdot 10^{-7}$	3.4264	3481	8770	$1114 \cdot 10^{-7}$	0.6519
GQN	1	23	31	$0 \cdot 10^{-7}$	3.5143	19	214	$42 \cdot 10^{-7}$	0.7086
	2	265	164	$505 \cdot 10^{-7}$	9.7539	181	703	$382 \cdot 10^{-7}$	1.7807
	3	2069	764	$71942 \cdot 10^{-7}$	6.9817	1177	2795	$6179 \cdot 10^{-7}$	1.2896
	4	12453	2713	$322860 \cdot 10^{-7}$	15.7367	5965	11143	$9332 \cdot 10^{-7}$	2.7486
GM	1					–	194	$42 \cdot 10^{-7}$	0.6911
	2					–	868	$395 \cdot 10^{-7}$	1.7709
	3					–	2766	$6201 \cdot 10^{-7}$	1.2705
	4					–	12539	$9167 \cdot 10^{-7}$	2.7066

We assume $\boldsymbol{\xi}$ as standard Gaussian variables and thus we employ Hermite polynomials for model surrogate. The reference estimation of probability distribution of safety margin M is obtained by MC sampling with 10^7 samples. Tab. 3 shows the required computational

time and relative errors in predictions for linear regression, stochastic collocation method and semi-intrusive Galerkin method for four polynomial degrees p. The relative errors in the prediction of safety margin are obtained as $\varepsilon_M = \frac{1}{n}\sum_{i=1}^{n} \frac{|M_{\mathrm{PCE}} - M_{\mathrm{MC}}|}{\max(M_{\mathrm{MC}}) - \min(M_{\mathrm{MC}})} \cdot 100$, where M_{MC} stands for the safety margin estimated by the MC method and M_{PCE} stands for the safety margin obtained using a chosen surrogate.

The results show relatively good predictions of M, but the prediction of failure probability is unsatisfactory for all the examined methods. Moreover, the errors in both predictions do not decrease with the increasing polynomial order and do not promise any significant reduction to be achieved in a realistic computational time, which increases exponentially. Significant difference in prediction of M for particular variants of model response is caused by the different number of random variables involved in the approximated response. While the displacement vector depends only on ten random variables, safety margin is influenced also by the uncertain yield stress f_y. The whole probability density functions of M for both variants of model response are depicted in Fig. 3.

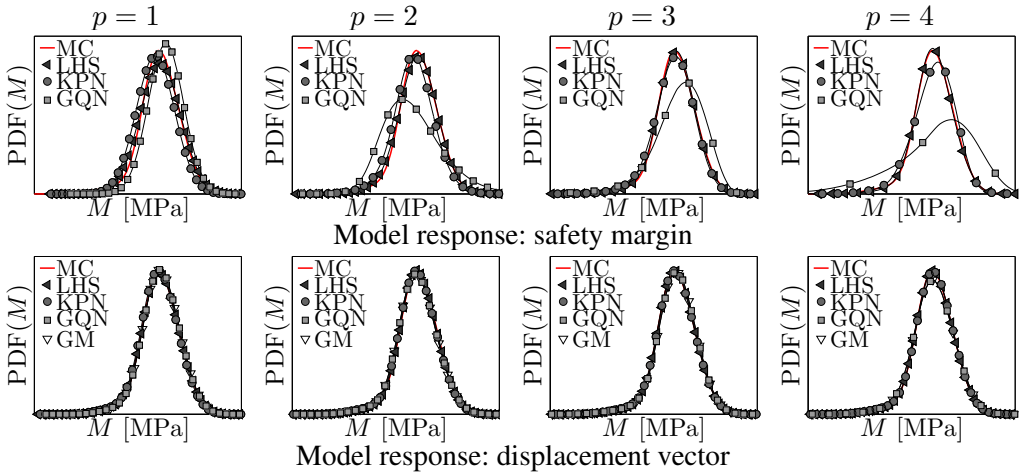

Fig. 3: Probability density functions of safety margin M in case of *prescribed histograms* for model parameters $\boldsymbol{m}$

The reason for these unsatisfactory results is probably highly nonlinear transformation (3) for parameters with prescribed histograms LONG1 and SHORT1, as shown in Fig. 4.

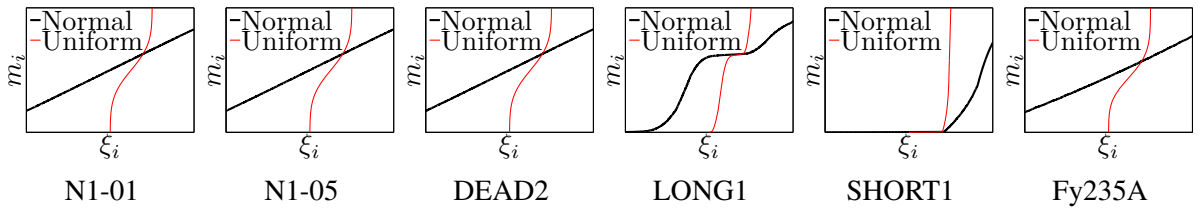

Fig. 4: Transformation relations for prescribed histograms

In order to test this assumption, we have replaced these two prescribed histograms by the new ones more close to normal distribution, see Fig. 5. New errors in predicting safety margin are listed in Tab. 4.

One can see that the replacement of the two histograms led to a significant improvement of the results achieved by all the methods. We can also notice that the GQN-based collocation

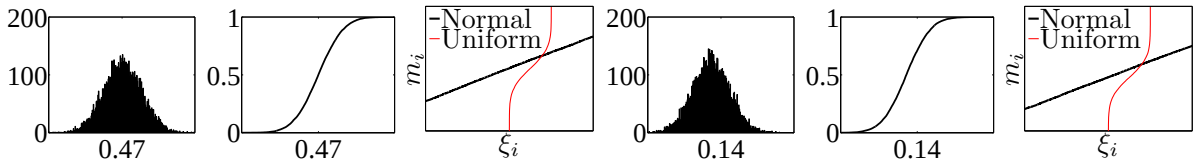

Fig. 5: New histograms of model parameters with corresponding cumulative density functions and transformation relations

Tab. 4: Time requirements and errors in predicting safety margin in case of *new histograms* for model parameters $\boldsymbol{m}$

Model response:		**Safety margin**				**Displacement vector**			
Method	p	n_d	Time [s]	$\Pr(F)$	ε_M [%]	n_d	Time [s]	$\Pr(F)$	ε_M [%]
MC	–	10^7	23833	$5 \cdot 10^{-7}$	–	10^7	22027	$5 \cdot 10^{-7}$	–
LHS	1	23	32	$9 \cdot 10^{-7}$	0.2855	19	216	$5 \cdot 10^{-7}$	0.0320
	2	243	165	$6 \cdot 10^{-7}$	0.0798	163	743	$5 \cdot 10^{-7}$	0.0142
	3	1607	753	$3 \cdot 10^{-7}$	0.0826	871	2787	$5 \cdot 10^{-7}$	0.0143
	4	7789	2701	$15 \cdot 10^{-7}$	0.2003	3481	8762	$5 \cdot 10^{-7}$	0.0275
KPN	1	23	31	$10 \cdot 10^{-7}$	0.2592	19	216	$5 \cdot 10^{-7}$	0.0202
	2	243	164	$6 \cdot 10^{-7}$	0.0821	163	719	$5 \cdot 10^{-7}$	0.0132
	3	1607	758	$1 \cdot 10^{-7}$	0.1663	871	2876	$5 \cdot 10^{-7}$	0.0241
	4	7789	2786	$8 \cdot 10^{-7}$	0.1299	3481	9561	$5 \cdot 10^{-7}$	0.0220
GQN	1	23	31	$10 \cdot 10^{-7}$	0.2407	19	237	$5 \cdot 10^{-7}$	0.0212
	2	265	164	$6 \cdot 10^{-7}$	0.1466	181	895	$5 \cdot 10^{-7}$	0.0235
	3	2069	763	$1 \cdot 10^{-7}$	0.1981	1177	2865	$5 \cdot 10^{-7}$	0.0339
	4	12453	2714	$2 \cdot 10^{-7}$	0.2944	5965	9332	$5 \cdot 10^{-7}$	0.0348
GM	1					–	194	$5 \cdot 10^{-7}$	0.0502
	2					–	871	$5 \cdot 10^{-7}$	0.0392
	3					–	2780	$5 \cdot 10^{-7}$	0.0537
	4					–	12448	$5 \cdot 10^{-7}$	0.0543

provides the worst results in the case of response equal to M, in the second case Galerkin method gives the worst prediction. Behaviour of these two methods is very similar due to numeric integration in Galerkin method based on GQN rule. The same improvement can be seen also in prediction of the whole probability density function depicted in Fig. 6.

In both previous examples, the discrete nature of prescribed histograms led to necessity of numerical integration in stochastic Galerkin method resulting to its semi-intrusive variant. In order to investigate the performance of fully intrusive stochastic Galerkin method avoiding all the numerical approximations, we have changed the prescribed distributions for model parameters once more. This time, we assume all the parameters to be normally distributed with the original values of mean and standard deviation. In such a case, the transformation (3) becomes the 1st order polynomial and hence, analytical integration is available. Fig. 7 shows the functional dependence of safety margin M for described types of probability distribution prescribed to model parameters. Fig. 7a shows that the relation between M and

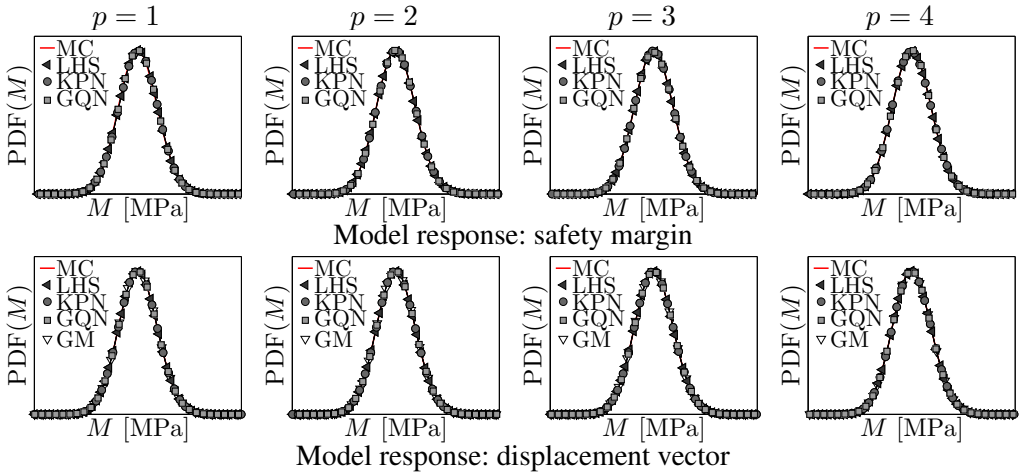

Fig. 6: Probability density functions of safety margin M in case of *new histograms* for model parameters $\boldsymbol{m}$

model parameters $\boldsymbol{m}$ is linear, while the high nonlinearity appears in the relation to standard variables $\boldsymbol{\xi}$ in case of prescribed histograms, see Fig. 7b. Replacement of the two histograms LONG1 and SHORT1 by the new ones more similar to normal distributions leads to almost linear M–$\boldsymbol{\xi}$ relation namely in the high probability region, see Fig. 7c. Finally, prescription of the normal distribution to model parameters provides the linear M–$\boldsymbol{\xi}$ relation as shown in Fig. 7d. The errors in prediction of safety margin are shown in Tab. 5 and Fig. 8.

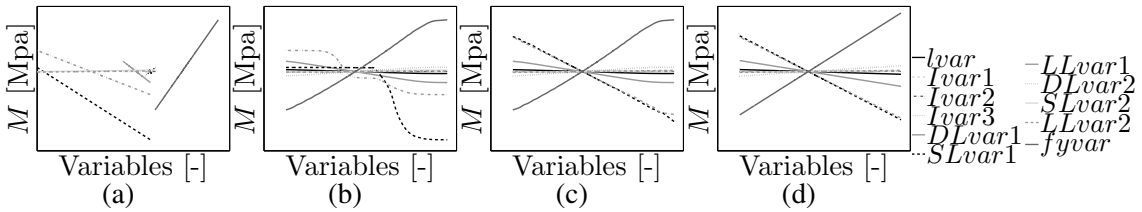

Fig. 7: Functional dependence of safety margin M on model parameters $\boldsymbol{m}$ (a), on standard variables $\boldsymbol{\xi}$ in case of prescribed histograms (b), in case of new histograms (c) and in case of normal distribution (d)

The results proof that the M–$\boldsymbol{\xi}$ relation is now linear and thus the 1^{st} order polynomials are sufficient for an excellent surrogate and the differences among the particular methods are here negligible in terms of accuracy as well as the time requirements.

5 Conclusion

The presented paper presents a review and comparison of three methods for construction of a polynomial chaos-based surrogate of a numerical model under the assumption of random model parameters. In particular, the investigated methods are polynomial regression based on Latin Hypercube Sampling, stochastic collocation method and stochastic Galerkin method. Particular features of these methods are discussed throughout the paper. The quality of obtained surrogates in terms of accuracy as well as the time requirements are demonstrated

Tab. 5: Time requirements and errors in predicting safety margin in case of *normal distribution* for model parameters $\boldsymbol{m}$

Model response:		**Safety margin**				**Displacement vector**			
Method	p	n_d	Time [s]	$\Pr(F)$	ε_M [%]	n_d	Time [s]	$\Pr(F)$	ε_M [%]
MC	–	10^7	3819	$12 \cdot 10^{-7}$	–	10^7	3773	$12 \cdot 10^{-7}$	–
LHS	1	23	32	$12 \cdot 10^{-7}$	0.1139	19	181	$12 \cdot 10^{-7}$	0.0249
	2	243	179	$12 \cdot 10^{-7}$	0.0021	163	704	$12 \cdot 10^{-7}$	$2.50 \cdot 10^{-4}$
	3	1607	802	$12 \cdot 10^{-7}$	$4.17 \cdot 10^{-5}$	871	2823	$12 \cdot 10^{-7}$	$3.05 \cdot 10^{-6}$
	4	7789	2987	$12 \cdot 10^{-7}$	$1.35 \cdot 10^{-6}$	3481	9139	$12 \cdot 10^{-7}$	$4.88 \cdot 10^{-8}$
KPN	1	23	38	$12 \cdot 10^{-7}$	0.0742	19	181	$12 \cdot 10^{-7}$	0.0134
	2	243	214	$12 \cdot 10^{-7}$	0.0013	163	746	$12 \cdot 10^{-7}$	$1.49 \cdot 10^{-4}$
	3	1607	875	$12 \cdot 10^{-7}$	$3.32 \cdot 10^{-5}$	871	2851	$12 \cdot 10^{-7}$	$2.21 \cdot 10^{-6}$
	4	7789	2997	$12 \cdot 10^{-7}$	$1.00 \cdot 10^{-6}$	3481	9401	$12 \cdot 10^{-7}$	$4.08 \cdot 10^{-8}$
GQN	1	23	31	$12 \cdot 10^{-7}$	0.0742	19	182	$12 \cdot 10^{-7}$	0.0134
	2	265	212	$12 \cdot 10^{-7}$	0.0013	181	697	$12 \cdot 10^{-7}$	$1.49 \cdot 10^{-4}$
	3	2069	848	$12 \cdot 10^{-7}$	$3.32 \cdot 10^{-5}$	1177	2836	$12 \cdot 10^{-7}$	$2.21 \cdot 10^{-6}$
	4	12453	2796	$12 \cdot 10^{-7}$	$9.98 \cdot 10^{-6}$	5965	9233	$12 \cdot 10^{-7}$	$4.08 \cdot 10^{-8}$
GM	1					–	157	$12 \cdot 10^{-7}$	0.0135
	2					–	644	$12 \cdot 10^{-7}$	0.0014
	3					–	2698	$12 \cdot 10^{-7}$	0.0013
	4					–	8729	$12 \cdot 10^{-7}$	0.0013

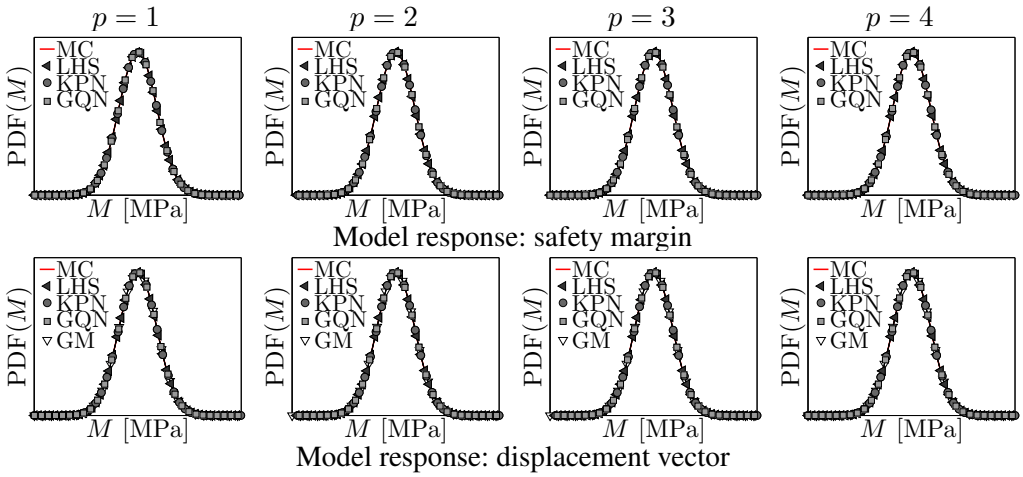

Fig. 8: Probability density functions of safety margin M in case of *normal distribution* for model parameters $\boldsymbol{m}$

within the comparison with the traditional Monte Carlo method on a simple illustrative example of a frame structure.

Acknowledgements

This outcome has been achieved with the financial support of the Czech Science Foundation, projects No. 105/11/0411 and 105/12/1146, and Grant Agency of the Czech Technical University in Prague, grant No. SGS OHK1-042/13.

Literature

[1] Babuska, I., Tempone, R. & Zouraris, G. E. Galerkin Finite Element Approximations of Stochastic Elliptic Partial Differential Equations. *SIAM Journal on Numerical Analysis* 42(2), 2004, 800–825

[2] Babuska, I., Nobile F. & Tempone, R. A Stochastic Collocation Method for Elliptic Partial Differential Equations with Random Input Data. *SIAM Journal on Numerical Analysis* 45(3), 2007, 1005–1034

[3] Blatman, G. & Sudret, B. An adaptive algorithm to build up sparse polynomial chaos expansions for stochastic finite element analysis. *Probabilistic Engineering Mechanics* 25(2), 2010, 183–197

[4] Ditlevsen, O. & Madsen, H. O. *Structural Reliability Methods*, John Wiley & Sons Ltd, Chichester, England, 1996

[5] Ghanem, R. G. & Spanos, P. D. *Stochastic finite elements: A spectral approach*, Springer-Verlag New York, Inc., 1991

[6] Heiss, F. & Winschel, V. Likelihood approximation by numerical integration on sparse grids. *Journal of Econometrics* 144(1), 2008, 62–80

[7] Janouchová, E. & Kučerová, A. Competitive Comparison of Optimal Designs of Experiments for Sampling-based Sensitivity Analysis. *Computers & Structures*, 124, 2013, 47–60

[8] Marek, P., Brozzetti, J., Guštar, M. & Tikalsky, P. editors. *Probabilistic assessment of structures using Monte Carlo simulation*, Institute of Theoretical and Applied Mechanics, Academy of Sciences of the Czech Republic, Prague, second edition, 2003

[9] Matthies, H. G. & Keese, A. Galerkin methods for linear and nonlinear elliptic stochastic partial differential equations. *Computer Methods in Applied Mechanics and Engineering* 194(12–16), 2005, 1295–1331

[10] Matthies, H. G. Uncertainty quantification with stochastic finite elements. In Erwin Stein, René de Borst, and Thomas J. R. Hughes, editors, *Encyclopaedia of Computational Mechanics*. John Wiley & Sons, Chichester, 2007

[11] Stefanou, G. The stochastic finite element method: Past, present and future. *Computer Methods in Applied Mechanics and Engineering* 198(9–12), 2009, 1031–1051

[12] Xiu, D. & Karniadakis, G. E. The Wiener–Askey Polynomial Chaos for Stochastic Differential Equations. *SIAM Journal on Scientific Computing* 24(2), 2002, 619–644

[13] Xiu, D. Fast Numerical Methods for Stochastic Computations: A Review. *Communications in Computational Physics* 5(2–4), 2009, 242–272

Reliability-based management of underground pipeline network using genetic algorithm

Lutfor Rahman Khan, Kong Fah Tee, Amir M. Alani
Department of Civil Engineering, University of Greenwich, United Kingdom
L.R.Khan@gre.ac.uk, K.F.Tee@gre.ac.uk, M.Alani@gre.ac.uk

Abstract: When the residual ultimate strength of buried pipeline has exceeded the limit due to external loadings, failure becomes imminent and overall reliability is reduced. Therefore, the concerned industry has to plan how to operate and maintain the system within budget constraints. This paper is concerned with estimating reliability and deciding when and how interventions are needed to prevent unexpected failures of flexible buried metal pipelines subject to externally applied loadings and corrosion at minimal cost. The probability of failure due to corrosion induced excessive deflection with respect to varying time has been estimated in this study. Then intervention year for maintenance is determined and the most appropriate renewal solution is identified by minimising failure risk and whole life cycle cost using genetic algorithm. An example is presented to validate the proposed method with a view to prevent unexpected failure by prioritising maintenance based on failure severity and pipeline reliability.

Keywords: probability of failure, reliability, optimisation, pipeline network, genetic algorithm, life cycle cost, condition index, renewal priority.

1 Introduction

The world is moving towards adopting more proactive and optimised approaches to manage underground pipeline systems in a more sustainable way. Different management approaches exhibit different capabilities, limitations, costs and benefits. The particular characteristics of the buried pipes (e.g., material, diameter, etc.) and site conditions (e.g., soil, water table, traffic etc.), along with other operational, social and environmental factors determine the applicability of method of management strategy in a particular situation [1]. For example, in some cases, the maintenance costs on a system can exceed the initial costs. Therefore, asset managers need to be able to develop the optimal strategy regarding inspection as well as maintenance works or rehabilitation works [2]. In any given scenario, some renewal methods are more applicable and cost effective than others and therefore, a systematic procedure for selecting feasible methods is needed. Different research show that

the vast majority of existing underground pipeline systems focus primarily on managing day-to-day operational activities, e.g., issuing and tracking work orders, mapping and data management, logging service requests, cost estimating, etc., and optimum long-term management planning for the pipeline network is limited [3]. This scarcity is mainly attributed to the lack of systematised, standardised and quantitative models, e.g., deterioration, risk, prioritisation and optimisation models and the lack of adequate reliable data to support the application of such models. However, finding the optimal strategy is not easy and the wrong maintenance strategy may result in excessive risks, costs and losses. Optimisation models for pipeline maintenance methodologies are still in their infancy condition when compared to those in bridges, buildings and other civil engineering structures, although optimum design approaches for pipe structural systems are continuously evolving and improving [4]. To address these problems, several countries have developed or initiated the development of pipe management systems to optimise the inspection and maintenance of deteriorated pipe structures. Different optimisation approaches have been implemented in the different buried pipe management systems ranging from simplified economic models to advanced Markovian decision processes [5].

Due to uncertainty associated with the rate of failure and behaviour of buried pipeline system, the probabilistic pipe reliability methodology has been applied in optimisation process in this study. According to SARMA AND HOJJAT [6], a few researchers have presented probabilistic reliability models for life cycle cost optimisation of pipe structures. Numerous potential failure modes are found in a buried pipe structure system. Therefore, it is important to have a method by which the most critical failure modes can be identified. The critical failure modes are those contributing significantly to the reliability of the system at the chosen level. The failure criterion adopted in this paper is due to loss of structural strength of pipelines which is influenced by corrosion through reduction of the pipe wall thickness. The chosen dominating failure mode in flexible buried metal pipeline system is time-dependent corrosion induced excessive deflection. Then, an optimisation algorithm, genetic algorithm (GA) has been developed to optimise the management strategy. Life cycle cost (LCC) of pipeline network has been used as an objective function in this process. LCC consists of initial cost or installation cost, maintenance cost and failure risk cost of the system. The propose management option has yield a performance according to the risk involved and cost of the activities throughout the service life. The proposed maintenance strategy will enable the decision makers to select appropriate renewal methods based on the identified optimal time to renew i.e. repair or replace.

2 Problem formulation

In this study, the LCC is used as an optimisation objective with effects of pipe failure according to Eq. (1). The total life cycle cost can be presented as follows:

$$\mathrm{C}_{\mathrm{LCC}}(T) = C_A + \sum_{i=1}^{T} C_O(i) \tag{1}$$

where C_A = the capital cost; $C_O(i)$ = operation cost; and i = 1,2,3,…..,T years. The operation cost C_O (i) can be calculated by Eq. (2) as below:

$$C_O(i) = C_M(i) + C_R(i) \tag{2}$$

where $C_M(i)$ is the maintenance cost and $C_R(i)$ is the failure risk cost. The failure risk cost, $C_R(i)$ is influenced by the failure cost, $C_f(i)$ and the failure probability, P_f. The faillure risk cost can be estimated as below:

$$C_R(i) = C_f(i) \cdot P_f \tag{3}$$

Based on Eqs. (2) and (3), Eq. (1) can be rewritten as follows:

$$C_{LCC}(T) = C_A + \sum_{i=1}^{T} C_M(i) + \sum_{i=1}^{T} C_f(i) * P_f \tag{4}$$

The cost terms in the right-hand side of Eq. (4) are the costs in the year they actually occur. The $(1 + r)^T$ factor is used to convert the cost into its present value discounted by the discount rate of r, for the T years period. The discount rate depends on the prevailing interest rate and the depreciation of the currency or inflation rate which is not a constant term and may vary over time. From an economical point of view, the ideal goal of risk and cost management of pipe network should be minimising the total LCC of the network. In this study, the problem of identifying the optimal intervention year is transformed into minimisation of total LCC (Eq. (4)).

The time-dependent corrosion depth (D_T), moment of inertia (I) and cross-sectional area (A_s) of thin walled buried pipe can be estimated as below [7], [8]:

$$D_T = kT^n,\ I = \left(t - D_T\right)^3/12 \text{ and } A_s = t - D_T \tag{5}$$

where k = multiplying constant, n = exponential constant and t = thickness of pipe wall.

Actual deflection (Δ_y) and allowable deflection (Δ_a) can be predicted as below [9], [10]:

$$\Delta_y = \frac{K(D_L W_c + P_s)D}{\left(\frac{8EI}{D^3} + 0.061E'\right)} \text{ and } \Delta_a = 5\% \text{ of diameter of pipe} \tag{6}$$

where D = mean diameter of pipe, D_L = deflection lag factor, E = modulus of elasticity of pipe material, E' = Soil modulus of reaction, K = Bedding constant and P_s = live load and W_c = soil load.

For this failure mode, limit state, $Z(X)$ ($\Delta_a - \Delta_y$) < 0 represents failure state, $Z(X) > 0$ indicates a safe state and the limit state boundary at $Z(X) = 0$. The probability of failure for excessive deflection can be predicted as Eq. (7) [11]:

$$p_f = P[Z(X) < 0] = \Phi\left[\frac{0 - \overline{Z}}{\sigma(Z)}\right] = \Phi(-\beta) \tag{7}$$

where Φ = the cumulative standard normal distribution function (zero mean and unit variance) and $\beta = \overline{Z}/\sigma(Z)$ is known as the safety index or reliability index.

3 Renewal methods and condition index

The buried pipelines renewal methods can be grouped into four main categories: replacement, structural, semi structural and non-structural lining methods [2]. Structural liners are defined to be capable of carrying hydrostatic, soil and live loads on their own. Structural liners are expected to be independent i.e., bonding with original underground pipeline is not required. Semi structural liners are designed to withstand hydrostatic pressure or perform as a composite with the existing pipelines. Semi structural liners could be designed as interactive or independent. Semi structural liners typically are used for non-gravity pipeline system. Non-structural liners are used mainly to improve flow, resist corrosion, or to seal minor cracks in gravity pipelines [12]. The maintenance strategy can be implemented by identifying applicable renewal categories based on the underground pipeline condition which is called condition index or mean structural pipe grade. The purpose of the condition index is to objectively rate or scale the current condition of buried pipes based on several physical, environmental, and operational factors, which provide the basic terminology and framework [13].

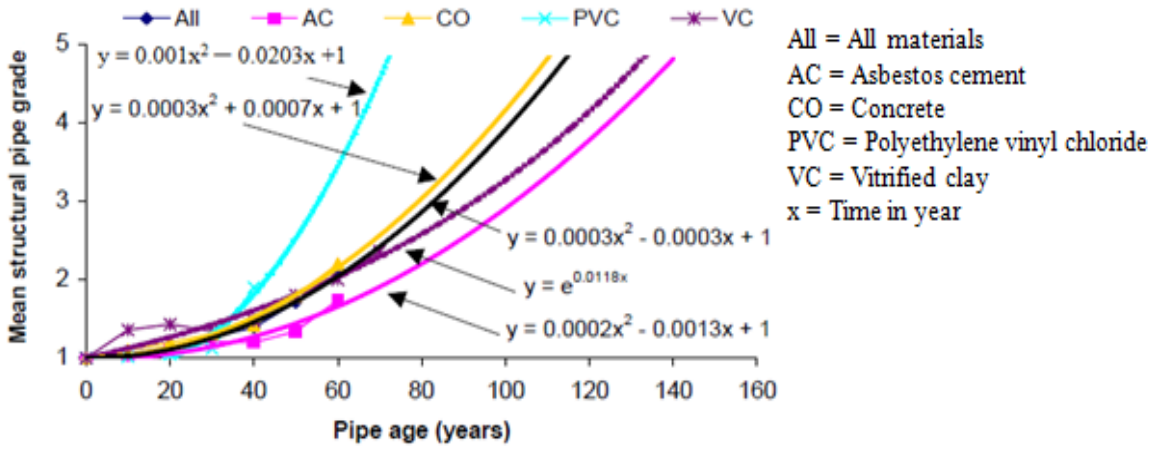

Fig. 1: Underground pipeline deterioration models using MIIP [12] dataset

The mean structural pipe grade or structural condition index (*CI*) for underground pipeline can be calculated from the regression model in Fig. 1 as follows [13].

$$CI = 0.0003T^2 - 0.0003T + 1 \tag{8}$$

where T = age of the underground pipeline (in year) which corresponds to the intervention year obtained from the risk-cost optimisation. The renewal methods are selected based on detailed analysis of possible defects, as indicated by the condition index and the possible scenarios of soil loss (Tab. 2 and 3) [13]. For example, an underground pipeline with condition index 3 and high possibility of soil loss will need replacement or the use of a structural liner to carry loads and stabilize deformation. At a minimum, a semi structural liner that can withstand hydrostatic pressure is required.

4 Impact assessment and prioritisation

The criterion used to renewal of pipes is the degree of impact of an underground pipeline failure. The impact assessment ranks the pipe segments in unit length in terms of six major factors: location, embedment soil, burial depth, pipe size, functionality and seismic zone. The assessment generates a ranking of impact for the underground pipeline system. Each of the six factors is assigned a degree of impact defined by low, medium or high [4]. A weighted impact rating (I_w) formula is used to combine the influence of each of the six factors for each pipe segment within the system as below.

$$I_w = 0.2 f_l + 0.16(f_s + f_z + f_d + f_f + f_q) \tag{9}$$

where f_l = location factor, f_s = embedment soil factor, f_z = size factor, f_d = burial depth factor, f_f = underground pipeline function factor and f_q = seismic factor. Although these factors do not change dramatically from year to year, periodic updating may be necessary. The failure impact rating can be assessed based on Tab. 1 with respect to I_w values [4].

Tab. 1: Failure impact rating

Weighted impact factor, I_w	Failure impact rating, R_{imp}
1.00	1
1.01 – 1.60	2
1.61 – 2.20	3
2.21 – 2.80	4
> 2.81	5

For all of the factors listed above, the low value is 1 and high value is 3. Medium degree of impact falls between the high and low extremes and is assigned a value of 1.5. Once the weighted impact rating is determined for individual pipe segments, the impact assessment can then be used in a number of ways in the decision-making process. The impact ratings can be used in combination with the physical condition index of a pipe to prioritise rehabilitation or replacement work and the future inspection frequencies. For the pipe segments with the same physical condition index/rating, those with higher impact ratings would be considered first for rehabilitation and lowest impact ratings would be considered no renewal required, as shown in Tab. 4.

Tab. 2: Possibility of soil loss based on soil type and groundwater level

Soil Type	Groundwater level		
	Below sewer	Same line with sewer	Above sewer
Clay	Low	Medium	High
Gravels and low plasticity clay	Low	Medium	High
Silt and sand	High	High	High

Tab. 3: Selection of renewal categories based on condition index and soil loss possibility

Cond. Index	Possibility of soil loss		
	Low	Medium	High
2	Non-structural or semi-structural	Non-structural or semi-structural	Semi- structural, structural or replacement
3	Non-structural or semi-structural	Semi- structural or structural	Semi- structural, structural or replacement
4 and 5	Structural or replacement	Structural or replacement	Structural or replacement

Tab. 4: Renewal priority

Structural condition index	Implication	Failure impact rating (R_{imp})	Renewal priority
5	Failed or failure imminent	1 to 5	Immediate
4	Very poor condition	5	Immediate
	High structural risk	1 to 4	High
3	Poor condition	4 to 5	Medium
	Moderate structural risk	1 to 3	Low
2	Fair condition/ Minimal structural risk	1 to 5	Low
1 or 0	Good or excellent condition	1 to 5	Not required

The possibility of surrounding soil loss, a very important parameter to assess the renewal process is determined on a high, medium, or low scale according to the soil type, groundwater level and condition index, as shown in Tabs. 2 and 3 [13]. Finally, the renewal priorities are predicted based on CI, I_w and R_{imp} values as metioned in Tab. 4.

5 Numerical example

An underground pipeline network under a heavy roadway subjected to hypothetical operating conditions where some sections of the networks has passed under commercial/business areas and some parts has crossed residential areas, are taken as a numerical example to validate the proposed risk-cost optimisation management strategy. The underground pipeline network consists of approximately total 775 km of sanitary underground pipelines, made from steel and ductile iron, constructed in 1940. The underground pipelines and soil parameters are listed in Tabs. 5 and 6. The pipes are circular and buried in a mean trench width of 2 m. The backfill material has a mean unit weight of 18 kN/m^3 and mean soil modulus of 2 MPa. There are 9 random variables with the mean and coefficients of variations are listed in Tab. 6.

The underground pipelines consist of six types of pipeline sections as A – F, as mentioned in Tab. 5. The whole network constructed above ground water table. It is presumed that the whole underground pipeline network located in a high seismic vulnerable zone area. The cost data are presented in Tab. 7 for the whole pipeline sections (A – F). Note that in Tab. 7, the capital cost, maintenance cost and failure consequence cost are presumed based

on MELBOURNE WATER report [14], typical 12.5% of capital cost and DAVIS ET AL. [15], respectively. The typical discount rate (UK) = 5% is considered in this example. The pipes in the network are consisted of medium size steel and ductile iron pipes. The network is subjected to corrosion and its corrosion is presumed as uniform over the pipe sections.

Tab. 5: Pipe materials and location properties

Pipe section	Material	Location	Embed-ment soil	Length (km)	Mean diameter (mm)	Thick-ness (mm)	Soil height above pipe invert (m)	Traffic load, kPa
A	Steel	Commercial	Clay	150	500	8	2.0	100
B	Ductile iron	Commercial	Clay	100	600	8	2.0	100
C	Steel	Residential	Sand	110	600	9	2.1	100
D	Steel	Residential	Sand	225	480	7.5	2.5	90
E	Ductile iron	Residential	Sandy Gravel	85	350	7	2.2	100
F	Ductile iron	Commercial	Sandy Gravel	115	500	8	1.8	100

Tab. 6: Statistical properties

Symbol description	Mean value	Coefficient of variation (%)	Distribution
Elastic modulus of steel pipe	210 GPa	1.0	Normal
Elastic modulus of ductile iron pipe	170 GPa	1.0	
Soil modulus, E_s	2 MPa	5	Normal
Unit weight of soil, γ	18.0 kN/m^3	2.5	Normal
Traffic load (Live load), P_s	See Tab. 5	3.0	Normal
Deflection coefficient, K_b	0.11	1.0	Lognormal
Multiplying constant, k	0.3	10.0	Normal
Exponential constant, n	0.6	5.0	Normal
Thickness of pipe, t	See Tab. 5	1.0	Normal

Tab. 7: Cost data for pipe network

Pipe section	Operation cost	Maintenance cost	Failure cost
A	£100000	£20000	£100m
B	£50000	£10000	£80m
C	£70000	£8000	£90m
D	£100000	£15000	£140m
E	£30000	£8000	£70m
F	£55000	£7000	£85m

5.1 Pipeline reliability

The probabilities of buried pipe failure due to corrosion induced excessive deflection, with respect to time are estimated based on the parameters and basic variables given in Tabs. 5 and 6. The failure probabilities are predicted using First Order Reliability method and results are shown in Figs. 2 – 7. When the thickness of the pipe is reduced due to corrosion, the moment of inertia and the cross-sectional area of pipe wall are decreased with a resulting reduction in pipe strength. All the random variables are considered as uniformly distributed, except deflection coefficient which is log-normally distributed. Thus Rackwitz-Fiessler algorithm has been applied to transform its distribution from log-normal to normal in this study.

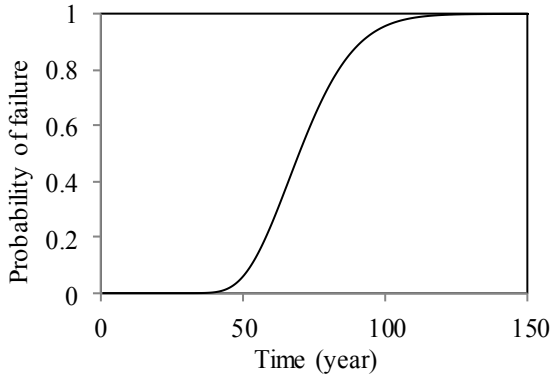

Fig. 2: P_f for pipeline section A

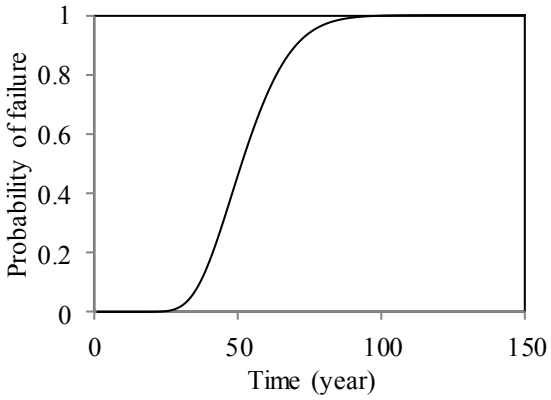

Fig. 3: P_f for pipeline section B

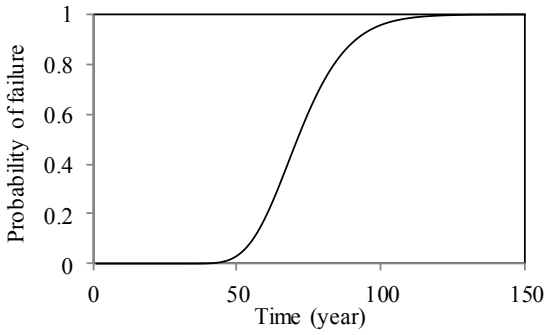

Fig. 4: P_f for pipeline section C

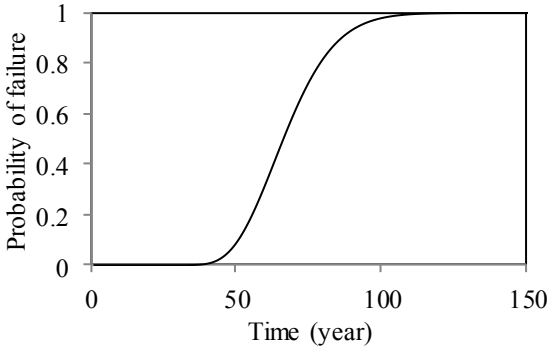

Fig. 5: P_f for pipeline section D

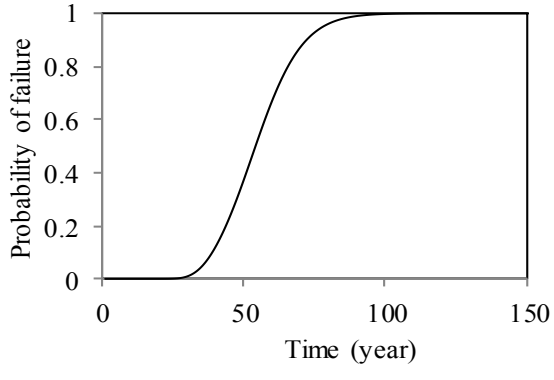

Fig. 6: P_f for pipeline section E

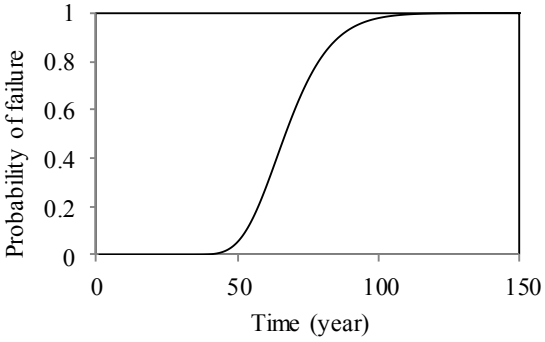

Fig. 7: P_f for pipeline section F

The study shows that on average the probability of pipe failure at the beginning is close to zero and it remains unchanged until about 40 years of service life, then it gradually changes as time increases and after 50 years, the probability of failure rises drastically. Failure probability as shown in Fig. 2 – 7 has been used for the subsequent risk-cost optimisation for cases A – F.

5.2 Optimum renewal cost, time and priority

As shown in Eq. (4), the failure risk cost is calculated by multiplying failure cost with the probability of system failure. Once the probability of system failure has been calculated, the optimal time to repair or replace and the associated life cycle cost can be obtained from the risk-cost optimisation using GA. Figs. 8 – 13 show the best and mean convergence values of total LCC obtained from risk-cost optimisation by applying 150 generations in GA. The best value for each pipeline section is considered as the optimal LCC as shown in Tab. 8. The optimal LCC cost is associated with the first maintenance of the pipeline.

Next, the proposed maintenance strategy is extended to determine an applicable and feasible renewal method using Tabs. 2 – 4 [13]. The recorded database shows that the sanitary steel and ductile iron underground pipelines are built on clay and sand or sandy gravel. Based on this information and according to Tab. 3, the possibility of soil loss for sanitary underground pipelines is low for sections A and B whereas, for sections C – F, the possibility of surrounding soil loss is high. The *CI* for the underground pipeline network is estimated as shown in Tab. 8, using Eq. (8) by substituting the identified optimal time to renew from the risk-cost optimisation. Applicable renewal categories are then selected from Tab. 3 based on the *CI* and the possible scenario of soil loss.

It is obtained from the proposed risk-cost optimisation that the pipeline sections A, B and C are required to renew using non-structural or semi-structural lining method based on the estimated *CI* and low possibility of soil loss. On the contrary, due to high possibility of soil loss and $CI > 2$, the sections D and E are needed to renew using semi-structural or structural liners. Finally section F should be renewed with structural liners or replacement. Alternatively, replacement is recommended when the repair cost is greater than the cost of replacing the pipes.

Based on the underground pipeline's inventory information and alignment, the renewal assessment has been carried out considering all six major impact factors and results of the renewal priority based on the structural condition index and failure impact index as shown in Tab. 8. According to Tab. 8, the pipes which are in fair or minimal structural risk condition needs low renewal priority and on the other hand, pipe with highly structural risk condition requires immediate rehabilitation or replacement for safety of the network.

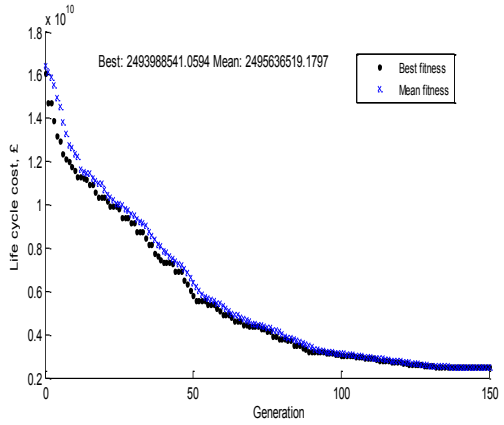

Fig. 8: LCC for pipeline section A from GA

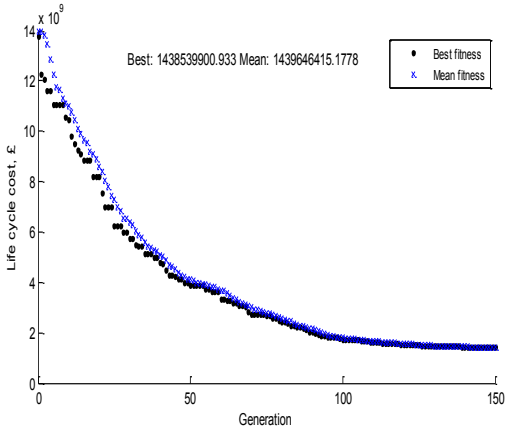

Fig. 9: LCC for pipeline section B from GA

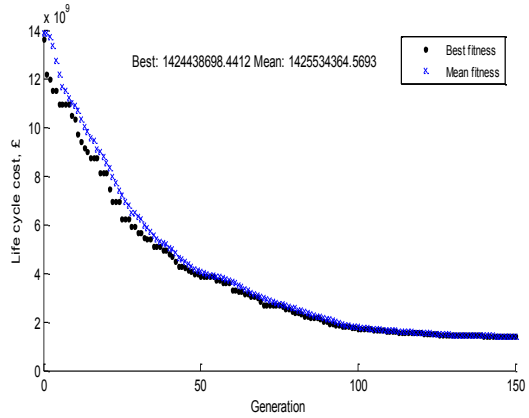

Fig. 10: LCC for pipeline section C from GA

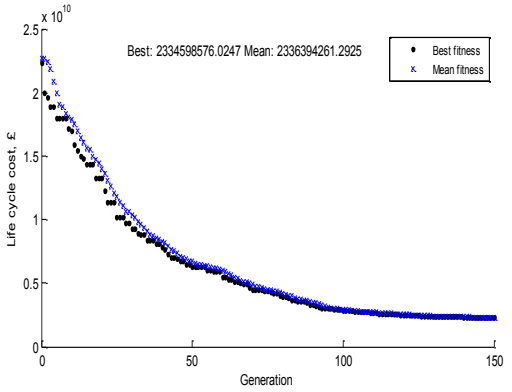

Fig. 11: LCC for pipeline section D from GA

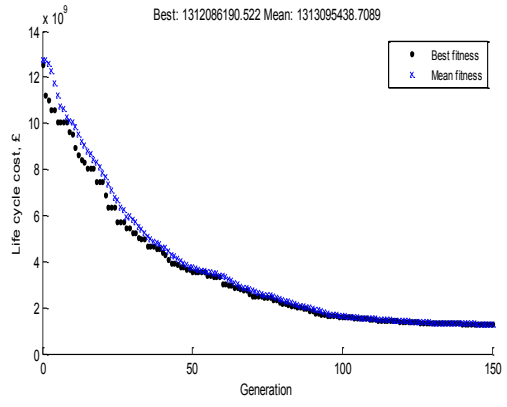

Fig. 12: LCC for pipeline section E from GA

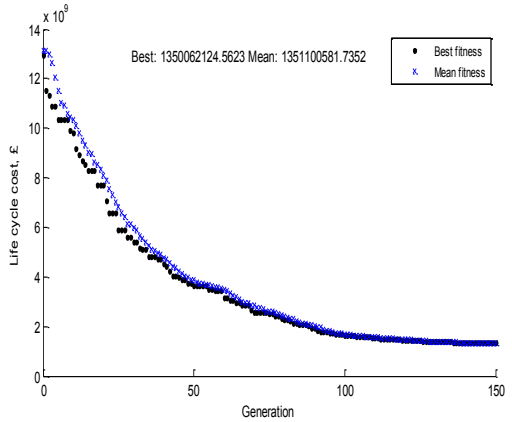

Fig. 13: LCC for pipeline section F from GA

Tab. 8: Results of pipeline network optimisation

Pipe section	Optimum Life cycle cost (£b)	Renewal time (year)	Structural Condition index (CI)	Renewal priority	Renewal methodology
A	2.4	62	2.2	Low, minimal structural risk	Semi-structural, structural
B	1.43	63	2.3	Low, minimal structural risk	Semi-structural, structural
C	1.4	66	2.25	Low, minimal structural risk	Semi-structural, structural
D	2.33	62	2.2	Medium, poor condition	Semi-structural, structural or replacement
E	1.3	72	2.5	Medium, poor condition	Semi-structural, structural or replacement
F	1.35	88	3.5	Immediate, high structural risk	Structural or replacement

6 Conclusion

This paper presents a novel approach for managing underground pipeline network. The proposed approach is integrated with two main criteria in the planning process: pipe reliability and life cycle cost. It follows that a rigorous decision process should find a balance between the risk of failure and the cost to mitigate it. The proposed management strategy also enables decision maker to select appropriate renewal methods based on the identified optimal time to renew, pipe condition index and the possibility of surrounding soil loss. Note that if historical data and current pipe thickness are available, then the real data can be used instead of corrosion model in the proposed approach to estimate pipe reliability and to determine the optimum management strategy. The proposed technique can help in making the appropriate decisions concerning the intervention to ensure the reliable and serviceable operation of the underground pipelines.

References

[1] Tee, K.F. and Khan, L.R. Risk-Cost Optimization and Reliability Analysis of Underground Pipelines. *Proc. of the 6th International ASRANet Conference*. London, UK, July 2–4, 2012

[2] Tee, K.F. and Li, C.Q. A Numerical Study of Maintenance Strategy for Concrete Structures in Marine Environment. *Proc. of the 11th International Conference on Applications of Statistics and Probability in Civil Engineering*. Zurich, Switzerland, August 1–4, 2011, p. 618–625

[3] Halfawy, M.R., Dridi, L. and Baker, S. Integrated decision support system for optimal renewal planning of sewer networks. *Journal of Computing in Civil Engineering* ASCE 22(6) (2008), p. 360–372

[4] McDonald, S. and Zhao, J. Condition assessment and rehabilitation of large sewers. *Proc. International Conference on Underground Infrastructure Research.* University of Waterloo, Canada, 2001, p. 361–369

[5] Lounis, Z. Risk-based maintenance optimisation of aging highway bridge decks. *Proc. of International Conference on Advances in Engineering Structures, Mechanics and Construction*. Ontario, Canada, 2006, p. 723–734

[6] Sarma, K.C. and Hojjat, A. Life-cycle cost optimisation of steel structures. *International Journal for Numerical Methods in Engineering* 55 (2002), p. 1451–1462

[7] Sadiq, R., Rajani, B. and Kleiner, Y. Probabilistic risk analysis of corrosion associated failures in cast iron water mains. *Reliability Engineering and System Safety* 86(1) (2004), p. 1–10

[8] Watkins, R.K. and Anderson, L.R. *Structural Mechanics of Buried Pipes*. Washington, USA: CRC Press, 2000

[9] Gabriel, L.H. *Corrugated polyethylene pipe design manual and installation guide*. Plastic Pipe Institute, USA, 2011

[10] AWWA (American Water Works Association). *Fiberglass Pipe Design*, AWWA Manual M45, USA, 1999, p. 35–53

[11] Tee, K.F., Li, C.Q. and Mahmoodian, M. Prediction of time-variant probability of failure for concrete sewer pipes. *Proc. of the 12th International Conference on Durability of Building Materials and Components*, Porto, Portugal, April 12–15, 2011

[12] Newton, L.A. and Vanier, D.J. *MIIP Report: The State of Canadian sewer – Analysis of asset inventory and condition*. Ottawa, Canada: National Research Council, Institution for Research in Construction, 2006

[13] WRc (Water Research Centre). *Sewerage Rehabilitation Manual*. Vol. I, II, 4th edition, Wiltshire, United Kingdom, 2001

[14] Melbourne Water (Melbourne Water, owned by Victorian Government). *Melbourne Main Sewer Replacement*. Australia, 2012

[15] Davies, J.P., Clarke, B.A., Whiter, J.T. and Cunningham, R.J. Factors influencing the structural deterioration and collapse of rigid sewer pipes. *Urban Water* 3(1), 2001, p. 73–89

Design optimization of segmental tunnel linings based on probabilistic finite elements analyses

Spyridon Konstantis[1], Panagiotis Spyridis[2]
[1] Marsh, London, [2] Dr. Sauer & Partners, London
spyridon.konstantis@marsh.com, pspyridis@dr-sauer.com

Abstract: In conceptual and preliminary design stages of tunnel projects a critical decision to be made concerns the method of excavation and the lining support to be installed. The selection of the structural dimensions and reinforcement of the lining depends primarily on factors associated with the desired structural robustness and durability of the lining as well as the geotechnical, hydrological and environmental regime. It is generally anticipated that the inherent uncertainties of the geotechnical parameters pose greater influence to the structural safety and robustness of the lining. The contribution discusses the value of using quantitative risk analysis techniques and probabilistic finite element analysis to define the optimum characteristics of the lining in terms of structural performance and durability. A typical case of a shallow urban tunnel excavated in soft ground with a Tunnel Boring Machine (TBM) is considered and the segmental lining, reinforced either with steel fibres or bar reinforcement, is analysed. The results are presented in the form of structural interaction diagrams and on the basis of a proposed, geometrically defined, utilisation factor.

Keywords: tunnel lining, risk, uncertainty, interaction diagram, utilisation factor, probabilistic analysis, optimisation

1 Introduction

During the various design stages of a tunnel project, a decision has to be made upon the method of excavation and the type and structural characteristics of the lining. This decision is rarely straightforward but rather the outcome of a comprehensive and thorough comparative study as well as a weighted evaluation of hydrogeological, structural and financial considerations.

The structural performance of the tunnel lining depends on one hand on the concrete characteristics and reinforcement and on the other hand on the loading that results from the ground response and the different load cases, static or dynamic. Due to the inherent uncertainties associated with the underground space and its geomechanical properties, the

strength and deformability characteristics of the surrounding ground display a much larger variation in comparison to the structural concrete. Therefore and in order to develop a reliable and robust design approach, the designer must make use of stochastic methods to deal with the uncertainties and variability of the predominant geotechnical parameters affecting the lining design [16].

In the case of tunnels excavated with a closed face Tunnel Boring Machine (TBM), the precast concrete (PCC) segments of the lining can be reinforced with steel bars in the form of pre-fabricated cages, with steel fibres or a combination of both. The choice of the type and quantity of reinforcement depends, among others, on the corrosion potential, tensile strength post-cracking, durability, toughness, resistance against impact and cost [17], [18].

As a result of the continuous evolution of computer science, the use of numerical methods has become very popular and is now standard practice for the design of tunnels and the analysis of the ground/tunnel lining interaction. Additionally, the rapid increase in the offered computational capacity has allowed the introduction and integration of stochastic methods in numerical methods and analysis. One of the probabilistic methods that can easily be applied to the analysis of underground works is the Point Estimate Method [22] as it has been shown by NASEKHIAN ET AL. [21].

The present work discusses the value of using probability-based techniques within an overall quantitative risk management and decision making process to define the optimum characteristics of tunnel linings in terms of structural performance and reliability. A typical case of a shallow urban TBM tunnel excavated in soft ground and supported with PCC segmental lining is considered. Three different lining configurations in terms of number of segments are stochastically analysed taking into account geotechnical uncertainties. The results are presented in the form of structural interaction diagrams and on the basis of a proposed, geometrically defined, utilisation factor. This newly introduced factor, namely the *Index for the Capacity Utilisation of Linings in Tunnels* (CULT-I), can serve as a measure of reliability or robustness of the discussed structural components and quantify the sensitivity of the tunnel structure's response to variation of the design parameters, as for example the surrounding ground properties in conjunction with a probabilistic analysis, or the structural layout (i.e. number of lining segments).

2 Analysis of PCC segmental tunnel linings

2.1 General

A PCC segmental tunnel lining is a sequence of distinct rings, although adjacent rings may be structurally connected, and each ring comprises of distinct, inter-connected PCC segments that are transported and assembled inside the shield of an advancing TBM.

In general, the PCC segments are subject to three main loading categories, i.e. load cases arising from the segment production to the segment placement in the ring prior to full ring assembly; load cases after the full ring assembly inside the TBM shield and; short and long term loads resulting from the interaction of the tunnel lining with the surrounding ground and environment [1]. This paper focuses on the latter loading category.

In design practice, PCC segment rings are assumed to behave as beams which are subject to their own weight and the external loads from the interaction with the surrounding environment. This ground/tunnel lining interaction results in sectional loads (axial load, shear load and bending moment) that have to be sustained by the PCC segments.

2.2 Analysis methods

The analysis of PCC segmental linings, depending primarily on the ratio between tunnel radius and overburden height, can be carried out with closed-form continuum models e.g. [11], bedded-beam spring models, numerical analyses and/or a combination of the above. Numerical analysis offers the ability to explicitly simulate complex structures (including adjacent structures), different geological strata, complex constitutive behaviour and construction sequences.

2.3 Effective ring stiffness

In order to realistically simulate the PCC segmental tunnel linings, the non-linear rotational behaviour and stiffness of the longitudinal joints between the segments in the ring has to be taken into account.

Alternatively, an empirical formula developed by Muir-Wood [20] can be used to estimate the effects of the longitudinal joints of uncoupled rings considering a monolithic, rigid ring with effective (reduced) second moment of area of the lining through equation (1) below.

$$I_{ring} = I_{joint} + I_{full} \cdot (4/m)^2 \tag{1}$$

with

I_{ring}	effective (reduced) second moment of area of ring
I_{joint}	second moment of area of the force transmission zone between segments.
I_{full}	second moment of area of segment's full cross section.
m	number of segments (small key segment not counted).

The maximum bending moments calculated with this approach are quite close to the maximum bending moment calculated for a hinged uncoupled ring. In the present work, the effective ring stiffness 'approach' was used in the numerical analyses.

3 Cross section structural design

Despite the extensive use of segmental tunnel linings around the world, there are still no recognised design codes and standards specifically developed for PCC segments. This gap is partially covered by design guides and recommendations, such as those published by AFTES [1], BTS [3] and ITA [15], however none of these guides contain definitive recommendations on the most relevant and economic method for PCC tunnel lining design.

The current engineering and design practice for PCC segmental tunnel linings adopts general structural design codes and assumes that the linings behave as beams. In this framework, the design loads resulting from the different load cases and scenarios of the analyses

are compared against the structural capacity of the lining which is represented in the form of interaction diagrams (hoop thrust against bending moment), also called Capacity Limit Curves (CLC) [24]. CLC for Reinforced Concrete (RC) segments can be produced in accordance with national and international codes and standards, such as EUROCODE 2 [4], while various existing guidelines can be used to account for the fibre reinforcement effect, most recent and perhaps notable of which being the FIB MODEL CODE 2010 [12] .

CLC can present all design combinations of axial forces and bending moments (potentially shear forces too) juxtaposed to the envelope of the cross-section's design capacity, providing a transparent and comprehensive graphical and numerical structural verification, as well as the design's safety factor [14].

4 CULT-I: Tunnel Lining Capacity Utilisation Index

In order to realise a comparative assessment of the structure's performance and reliability, this paper introduces an engineered *Index for the Capacity Utilisation of Linings in Tunnels* (CULT-I). This index measures the proximity of a design point to the lining capacity envelope (in this case the Moment-Axial forces CLC) and compares it to the 'maximum' distance of a design point, i.e. when the design point lies in the 'centre' of the CLC (axial force corresponding to maximum bending moment). This index ranges in the [0,1] interval, where 0 represents the limit condition load = resistance and thus the failure point or minimum reliability, and 1 represents the optimum utilisation of the lining capacity and thus the maximum robustness of the lining. Based on this unit-less index, a comparison of the performance and reliability for various tunnel lining designs is accommodated, which leads to a consistent design optimisation. The CULT-I can be calculated as shown in Eq. (2) and Fig. 1 below.

$$CULT-I=\sqrt{\frac{N_{rel,i}^2+M_{rel,i}^2}{N_{rel,\max}^2+M_{rel,\max}^2}}\in[0,1] \tag{2}$$

It has to be noted that typically a tunnel lining design concept utilises the compression induced by the soil structure interaction to exhibit flexural resistance (an alternative of active pre-stressing). Therefore the maximum reliability (or robustness) in a lining exists for a centrically compressed section well above zero-stress, or in other wording well beyond the threshold of the section to tension. Consequently, structural reliability and robustness in the context of this study are identified as the load situations which are less prone to failure (which counter-intuitively is not the unloaded tunnel structure).

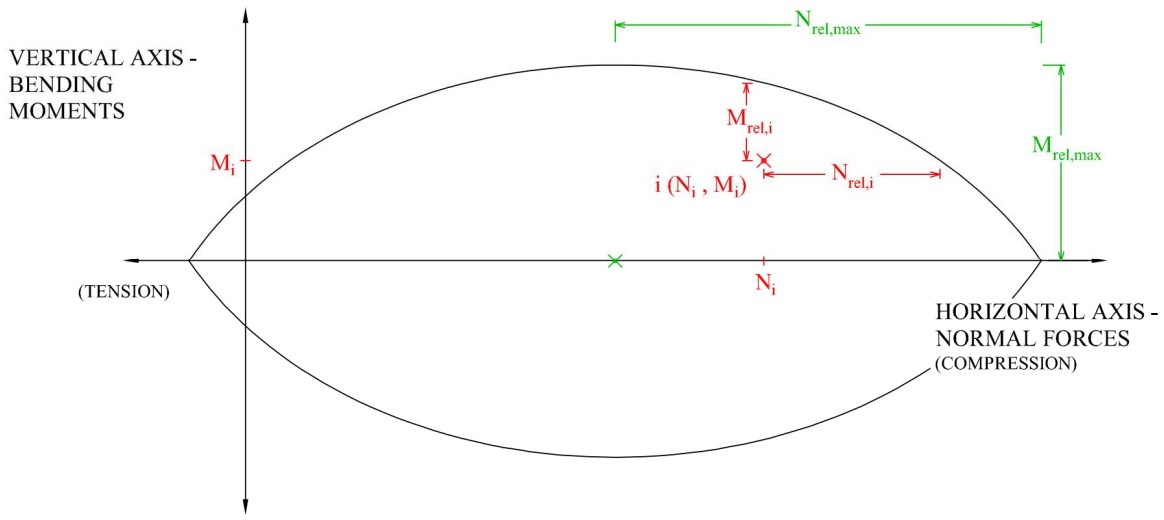

Fig. 1: Elements for the calculation of the Index for the Capacity Utilisation of Linings in Tunnels (CULT-I), in a Capacity Limit Curve

5 Case study

5.1 Overview of the studied system

The aspects discussed above are used below for the design optimisation of a PCC segmental lining for a typical rail tunnelling scheme in central London. The analyses were based on 2D plane strain non-linear finite element modelling by use of the geotechnical software Phase2 (www.rocscience.com), which also facilitates a basic probabilistic analysis by use of the Point Estimate Method (PEM, further discussion are provided in [25]). The PEM relatively is a simple sampling method that constructs a two-value sample for each input stochastic variable by the definition of its mean value and standard deviation: $\mu_{\underline{X}} \pm \sigma_{\underline{X}}$, which is the minimum needed to construct a normal probability distribution. In the present analysis, all values are then combined, i.e. the output statistics are derived by 2^n sets of results, where n is the population of random variables. Fig. 2 illustrates the geology, the geometry, and the meshing of the models used herein. Three different lining designs have been implemented with the same thickness (275 mm), width (1250 mm), and concrete properties (C35/45 − steel fibre reinforced see also CLC's below), but a different number of precast segments, i.e. five, six, and seven respectively (excluding the final key segment). Internal diameter of the tunnel is 6.2 m and tunnel axis depth at 35 m.

The numerical models implemented non-linear Mohr-Coulomb plasticity with a graded mesh of 6-noded triangular solid material elements and Timoshenko-beam elements to model the ground and the liners respectively. Drained analyses were carried out, accounting for a soil material with the parameters shown in Tab. 1. Uncertainty effects were considered for the Young's modulus, the friction angle, the cohesion, and the in-situ stress coefficient (K_0) of London Clay where the tunnel is excavated (Tab. 2). A softening factor is accounted for to simulate the three-dimentional stress relief and arching effects of the TBM excavation based on past experiences in similar conditions, which technically means

that the excavation area is left to deform to an interim equilibrium before the lining installation. This modelling technique allows for simulation of the soil's arching effects, theoretically validated in the framework of the convergence-confinement method [22].

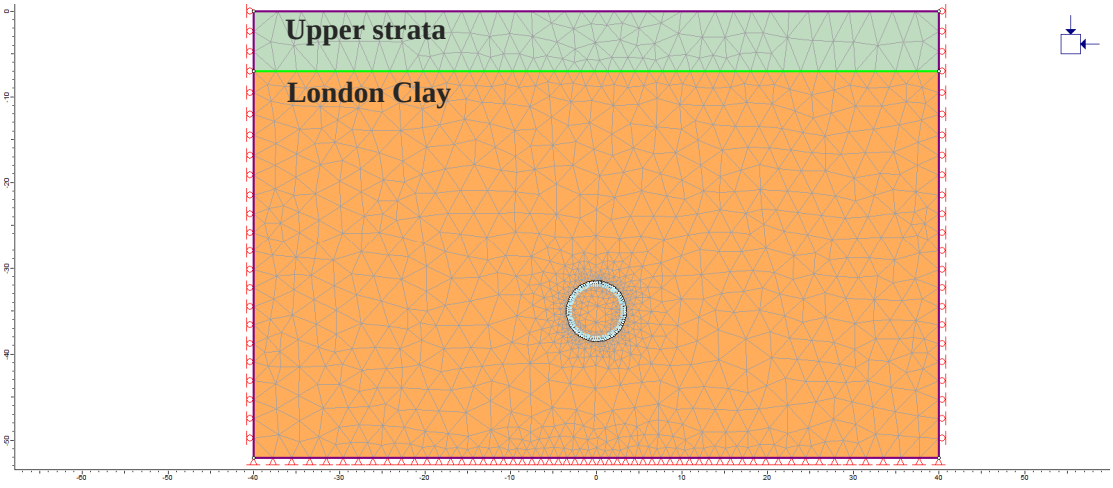

Fig. 2: Geometry, soil stratification and mesh of the discussed FE models

Tab. 1: Input for FE models

SOIL PROPERTIES		Upper strata[1]	London clay[2]
Stratification (thickness)	[m]	7	28
Drained Young's modulus	[MPa]	10	38[3]
Drained Poisson's ratio	[-]	0.3	0.20
Drained Friction Angle	[°]	-	22 − 28
Cohesion	[kPa]	-	10

1 modelled elastic
2 mean values at tunnel axis
3 depth dependent

Tab. 2: Input for the probabilistic FE models; variation parameters for London Clay (taken at tunnel axis)

Property	Units	Mean (μ)	Std. Dev. (σ)
Young's Modulus	[Mpa]	38	5.7
Friction Angle	[°]	33	1.65
Cohesion	[kPa]	10	1.5
Stress Coeffcient	[-]	0.45	0.045

5.2 Results

As disclosed from the results presented in Tab. 3, and the CLC's in Fig. 6−8, ground variability may prove to be critical for the design of the segmental lining, while in all cases, a requirement for reinforcement appears in order to cover some worse-case soil conditions. The results presented herein are extracted from the base case (run for average soil parameters, see Fig. 3−5) and the probabilistic analyses for each lining type. A comparative presentation of the lining forces involves the minima and maxima of bending moments and axial forces and their statistical moments, which intuitively discloses the scatter of results in each case. This correlates well with the associated CULT-I introduced herein. It is evident, both from the CLC plots and the selective results of Tab. 3 that an increase in segments for the tunnel lining reduces the flexural stiffness of the system (as discussed above) and consequently the marked bending moments in the lining. On the other side, axial forces remain approximately equal for all lining types, as the axial stiffness of the systems remains unchanged for each lining type.

The reduction of sectional forces (bending moments) as the number of segments in the ring increases, is reflected in the CULT-I. In the base case of 5 + 1 segments the minimum CULT-I along the lining (the lining's design point) approaches zero, meaning that the lining capacity tends to be exhausted, i.e. the lining's structural robustness/reliability is diminished (it is reminded though that the presented results for both the sectional forces and the CLC are un-factored). The safety reserves in the lining's design points for the 6 + 1 and 7 + 1 cases are identified by the higher CULT-I, meaning that a more 'safe' design is carried out in these cases. The same conclusion is drawn when a comparison of the average CULT-I's is performed, as a higher number of segments used, and thus a less stiff lining, leads to a higher CULT-I. Juxtaposing these CULT-I results to the logistics of each lining system can provide a cost-efficiency measure and facilitate a rationalised design solution.

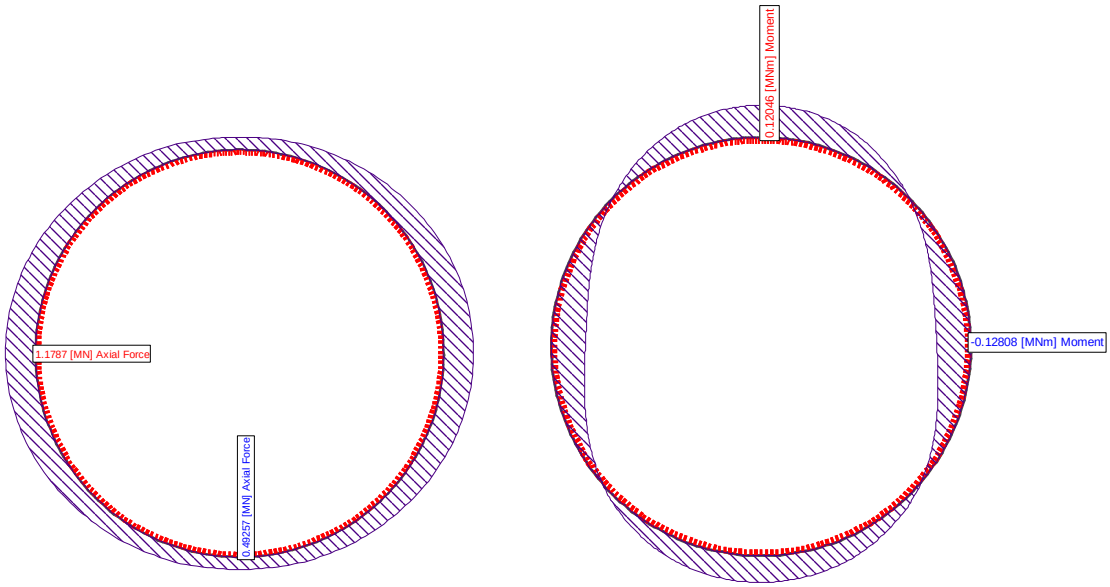

Fig. 3: Section force diagrams for the base case (average soil parameters) of a lining with 5 + 1 segments

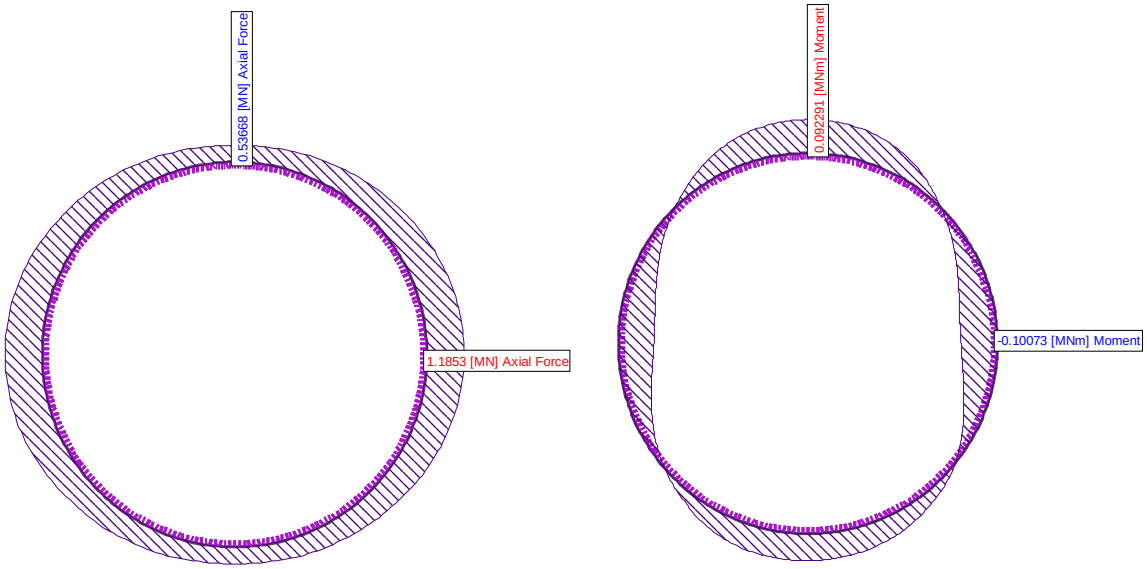

Fig. 4: Section force diagrams for the base case (average soil parameters) of a lining with 6 + 1 segments

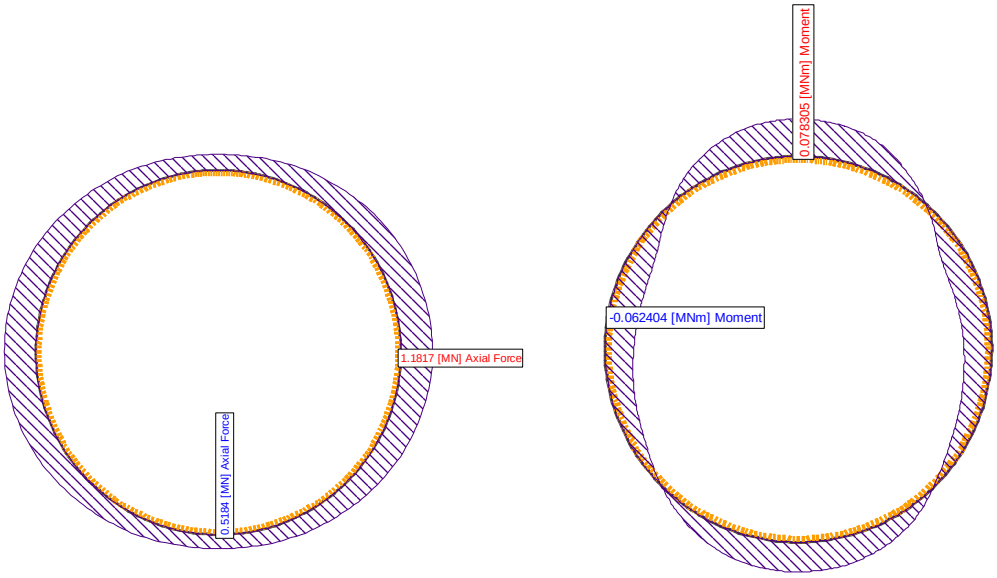

Fig. 5: Section force diagrams for the base case (average soil parameters) of a lining with 7 + 1 segments

Tab. 3: Indicative results of lining forces un-factored (see Figs. 3−5 for the base case). The factored values for the entire lining and the various sample sets are presented in the CLC's of Figs. 6−8.

	Value		5 + 1 segments	6 + 1 segments	7 + 1 segments
Base case	N_{max}	[kN]	1178	1185	1182
	M_{max}	[kNm]	121	92	78
	N_{min}	[kN]	493	537	518
	M_{min}	[kNm]	−128	−101	−62
	$CULT\text{-}I_{min}$	[-]	0.001	0.037	0.080
	$CULT\text{-}I_{average}$	[-]	0.124	0.157	0.161
Probabilistic analyses	$\mu(N_{max})$	[kN]	1206	1201	1190
	$\sigma(N_{max})$	[kN]	97	94	82
	$\mu(M_{max})$	[kNm]	132	100	82
	$\sigma(M_{max})$	[kNm]	32	30	24
	$\mu(N_{min})$	[kN]	524	557	551
	$\sigma(N_{min})$	[kN]	45	47	54
	$\mu(M_{min})$	[kNm]	−144	−109	−68
	$\sigma(M_{min})$	[kNm]	42	35	20
	$CULT\text{-}I_{min}$	[-]	0	0	0
	$CULT\text{-}I_{average}$	[-]	0.115	0.152	0.180

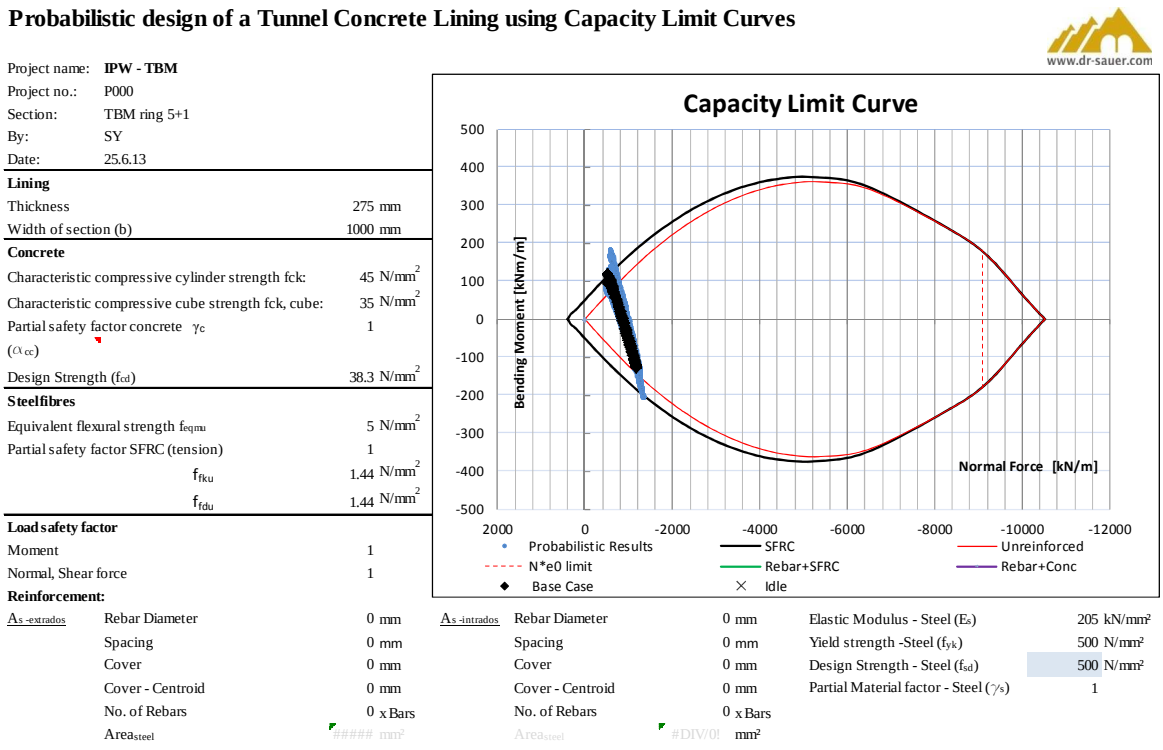

Fig. 6: Results for the studied lining with 5 + 1 segments (CLC un-factored), see also Fig. 3 for section forces

Probabilistic design of a Tunnel Concrete Lining using Capacity Limit Curves

www.dr-sauer.com

Project name:	**IPW - TBM**	
Project no.:	P000	
Section:	TBM ring 6+1	
By:	SY	
Date:	25.6.13	
Lining		
Thickness	275	mm
Width of section (b)	1000	mm
Concrete		
Characteristic compressive cylinder strength fck:	45	N/mm²
Characteristic compressive cube strength fck, cube:	35	N/mm²
Partial safety factor concrete γ_c (α_{cc})	1	
Design Strength (f_{cd})	38.3	N/mm²
Steelfibres		
Equivalent flexural strength f_{eqmu}	5	N/mm²
Partial safety factor SFRC (tension)	1	
f_{fku}	1.44	N/mm²
f_{fdu}	1.44	N/mm²
Load safety factor		
Moment	1	
Normal, Shear force	1	
Reinforcement:		
$A_{s\,-extrados}$ Rebar Diameter	0	mm
Spacing	0	mm
Cover	0	mm
Cover - Centroid	0	mm
No. of Rebars	0	x Bars
$Area_{steel}$	#####	mm²

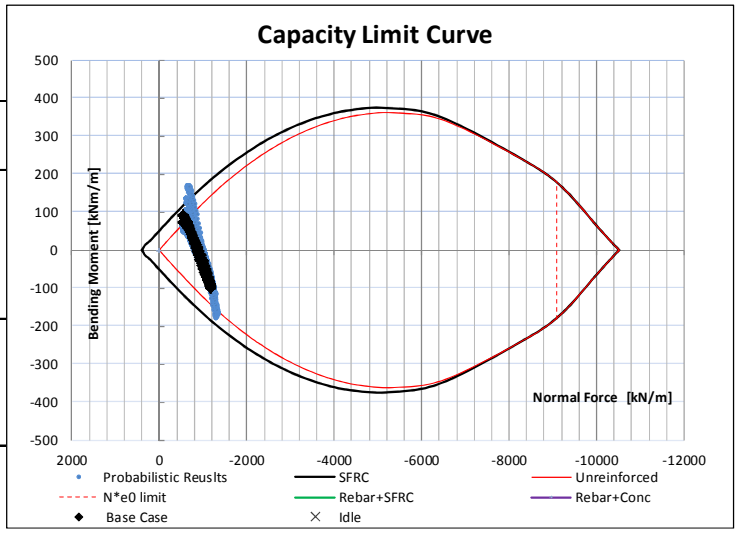

$A_{s\,-intrados}$ Rebar Diameter	0	mm	Elastic Modulus - Steel (E_s)	205 kN/mm²
Spacing	0	mm	Yield strength -Steel (f_{yk})	500 N/mm²
Cover	0	mm	Design Strength - Steel (f_{sd})	500 N/mm²
Cover - Centroid	0	mm	Partial Material factor - Steel (γ_s)	1
No. of Rebars	0	x Bars		
$Area_{steel}$	#DIV/0!	mm²		

Fig. 7: Results for the studied lining with 6 + 1 segments (CLC un-factored), see also Fig. 4 for section forces

Probabilistic design of a Tunnel Concrete Lining using Capacity Limit Curves

www.dr-sauer.com

Project name:	**IPW - TBM**	
Project no.:	P000	
Section:	TBM ring	
By:	SY	
Date:	25.6.13	
Lining		
Thickness	275	mm
Width of section (b)	1000	mm
Concrete		
Characteristic compressive cylinder strength fck:	45	N/mm²
Characteristic compressive cube strength fck, cube:	35	N/mm²
Partial safety factor concrete γ_c (α_{cc})	1	
Design Strength (f_{cd})	38.3	N/mm²
Steelfibres		
Equivalent flexural strength f_{eqmu}	5	N/mm²
Partial safety factor SFRC (tension)	1	
f_{fku}	1.44	N/mm²
f_{fdu}	1.44	N/mm²
Load safety factor		
Moment	1	
Normal, Shear force	1	
Reinforcement:		
$A_{s\,-extrados}$ Rebar Diameter	0	mm
Spacing	0	mm
Cover	0	mm
Cover - Centroid	0	mm
No. of Rebars	0	x Bars
$Area_{steel}$	#####	mm²

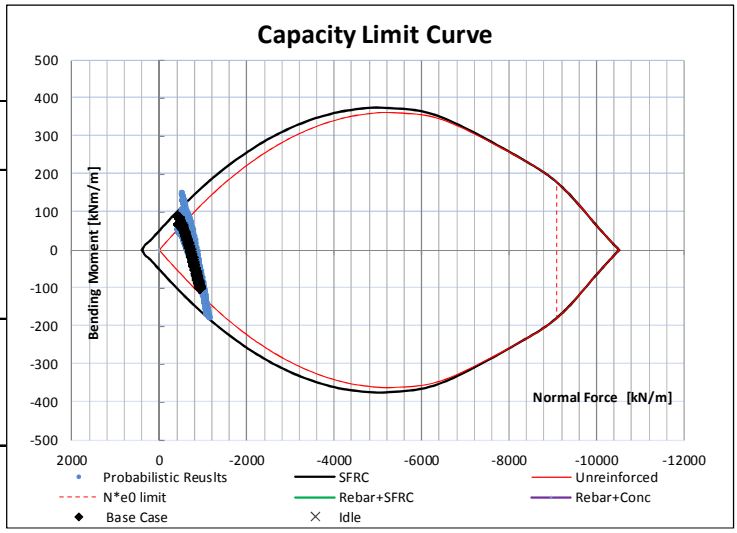

$A_{s\,-intrados}$ Rebar Diameter	0	mm	Elastic Modulus - Steel (E_s)	205 kN/mm²
Spacing	0	mm	Yield strength -Steel (f_{yk})	500 N/mm²
Cover	0	mm	Design Strength - Steel (f_{sd})	500 N/mm²
Cover - Centroid	0	mm	Partial Material factor - Steel (γ_s)	1
No. of Rebars	0	x Bars		
$Area_{steel}$	#DIV/0!	mm²		

Fig. 8: Results for the studied lining with 7 + 1 segments (CLC un-factored), see also Fig. 5 for section forces

6 Discussion

The design of tunnel linings is in principle an iterative (trial and error) process and the result of a comprehensive and thorough comparative study as well as a weighted evaluation of, among others, hydrogeological, structural, financial and logistical considerations. Other factors that can influence the design are related to the contractor's experience and preferences, social acceptance and perspective, political motivations, environmental constraints, etc.

In any case, the engineer must provide a design which is robust, durable, reliable, sustainable and economic. These objectives are unavoidably contradictive and therefore 'optimum' design is a subjective term and based on the client's or owner's demands, requirements and specifications.

However, the natural and inherent variability and uncertainty associated with the underground conditions and its geomechanical properties can introduce loading situations and scenarios that can compromise the structural integrity, performance and durability of a tunnel lining.

The present contribution has introduced an engineered, geometrically defined *Index for the Capacity Utilisation of Linings in Tunnels* (CULT-I). Based on this unit-less index, a comparison of the structural performance and reliability for various tunnel lining designs can be accommodated, which can lead to a consistent design optimisation. Moreover, the proposed methodology is consistent with modern project and tunnel risk management principles and approaches.

Literature

[1] AFTES. The design, sizing and construction of precast segments installed at the rear of a Tunnel Boring Machine (TBM). Association Francaise des Travaux en Souterrain, Paris. TR265, 1998

[2] Bond, A., Harris, A. *Decoding Eurocode 7*. London: Taylor & Francis, 2008

[3] BTS, ICE (British Tunnelling Society, Institution of Civil Engineers). Tunnel Lining Design Guide. London: Thomas Telford, 2004

[4] CEN (European Committee for Standardization). EN 1992-1-1: Eurocode 2, "Geotechnical design – Part 1: General rules." Brussels: CEN, 2002

[5] CEN (European Committee for Standardization). EN 1997-1-1: Eurocode 7, "Design of concrete structures – Part 1: General rules and rules for buildings." Brussels: CEN, 2004

[6] Crossrail C121 Non Linear Numerical Modelling Parameters – Rev 2. London, 2011

[7] DfT (Department for Transport) – Highways Agency. Interim Advice Note 95/07. DfT, 2007 (www.dft.gov.uk/ha/standards/ians/ accessed on 04.02.2013)

[8] Ditlevsen, O., Madsen, H.O. *Structural Reliability Methods*. Lyngby: Technical University of Denmark, 2007

[9] Dr. Sauer and Partners Ltd. Crossrail C121 – Independent Check Work Plan – Whitechapel Station. London, 2011

[10] Dr. Sauer and Partners Ltd. Crossrail C121 – Independent Check Work Plan – Fisher Street Shaft. London, 2012

[11] Duddeck, H., Erdmann, J. On structural design models for tunnels in soft soil. USA: Pergamon Journals Ltd, *Underground Space* 9 (1985), p. 246–259. TR306.

[12] fib (The International Federation for Structural Concrete). fib – Bulletin N° 65: Model Code 2010 – Final draft, Volume 1. Lausanne: fib, 2012

[13] Hight, D.W., Gasparre, A., Nishimura, S., Minh, N.A., Jardine, R.J., Coop, M.R. Characteristics of the London Clay from the Terminal 5 site at Heathrow Airport. *Géotechnique* 57 (1) (2007), p. 3–18

[14] Hoek, E., Carranza-Torres, C., Diederichs, M., Corkum, B. The 2008 Kersten Lecture Integration of geotechnical and structural design in tunneling, In *56th Annual Geotechnical Engineering Conference.* 2008, p. 1–53

[15] ITA. Working Group No. 2: Guidelines for the design of shield tunnel lining. Oxford: Elsevier Science, *Tunnelling and Underground Space Technology* 15(3) (2000), p. 303–331. TR329.

[16] ITA. Working Group No. 2: Guidelines for tunnelling risk management. *Tunnelling and Underground Space Technology* 19 (2004), p. 217–237

[17] King, M.R., Adler, A.J. The practical specification of steel fibre rein-forced concrete (SFRC) for tunnel linings. *Underground Construction Conference*. London, 2001

[18] King M. The Design and use of Steel Fiber Reinforced Concrete Segments. *Proc. of Rapid Excavation and Tunneling Conference*. 2005

[19] London Underground. Tottenham Court Road Station Upgrade, Geotechnical interpretative report. London, 2007

[20] Muir Wood, A.M. The circular tunnel in elastic ground. *Géotechnique* 25(1) (1975)

[21] Nasekhian, A., Schweiger, H., Marcher, T. Point Estimate Method vs. Random Set – A case study in Tunnelling. In Huber, Moormann & Proske (eds.) *Proceedings 10th International Probabilistic Workshop*. 2012, p. 243–256

[22] Potts, D.M., Zdravkovic, L. F*inite element analysis in geotechnical engineering: theory & application* (Vol. 2). London: Thomas Telford, 2001

[23] Rosenblueth, E. Point estimates for probability moments. *Proc. Nat. Acad. Sci. USA* 72(10) (1975), p. 3812–3814

[24] Sauer, G., Gall, V., Bauer, E., Dietmaier, P. Design of tunnel concrete linings using limit capacity curves. In: Siriwardane & Zaman (eds) *Computer Methods and Advances in Geomechanics*. Rotterdam, 1994. p. 2621–2626

[25] Spyridis, P., Tamparopoulos, A. Adjustment of tunnel lining design life based on nominal safety in LRFD. In Novák and Vořechovský (eds.) *Proceedings of the 11th International Probabilistic Workshop*, Brno, 2013

[26] Tubes Lines Ltd. Green Park Station step-free access. Geotechnical interpretative report. London, 2009

Coherent risk measures assessment based on the coupled analysis of multivariate distributions of multisource observation data

Yuriy V. Kostyuchenko[1,2], Yulia Bilous[1], Ivan Kopachevsky[1], Dmytro Solovyov[3]
[1] Scientific Centre for Aerospace Research of the Earth of NationalAcademy of Sciences of Ukraine, yvk@casre.kiev.ua
[2] Shevchenko Kiev National University, Faculty of Geography, Geomorphology and Soil Sciences Department, yuriy_kostyuchenko@ukr.net
[3] Marine Hydro-physical Institute of National Academy of Sciences of Ukraine, solmit@gmail.com

Abstract: Long-term regional statistics of meteorological measurements and disasters distributions have been analyzed. The spatially and temporally normalized and regularized distributions of the parameters investigated have been obtained. Further analysis of regional climatic parameters distribution allows to estimate the probability of extremes (both on seasonal and annual scales) toward mean climatic values change. Therefore the most probable distributions of extreme values of climate parameters toward the mean values change have been calculated on regional scale. Using the method of assessment of complex risk measures on the base of coupled analysis of multidimensional multivariate distributions of data the regional risk of climatic, meteorological and hydrological disasters were estimated basing on kernel copula semi-parametric algorithm.

Keywords: multisource statistics, regularization, regional climate distribution, kernel copulas, coherent risk measures, disasters

1 Introduction

Main problem of local and regional climate analysis and predictions is the how the climate parameters mean values change is reflected in its extreme values distribution. Is it possible to propose a correct algorithm to calculate the most probable local extreme variations toward the distribution of mean values known from climate models, and based on georeferred long-term observations? What is the real correlation between the mean and extreme distributions? Deterministic approach based on climate models requires huge sets of heterogeneous data about climate system on regional scale. This data usually is unavailable and these types of models usually characterizes by high uncertainties. Our understanding

of climate system and its local features is incomplete, so it is possible to calculate adequate only the mean values distributions with low spatial resolution [13].

Long and mid-term variations of mean values of climatic parameters (first of all, the mean air temperature) we able to calculate with sufficient confidence using multi-scale climate models and multidimensional sets of the observation data (meteorological measurements, satellite observations) [13, 10]. At the same time regional disaster risk depends of extreme values distribution. Therefore the analysis of stable correlations between well calculated mean values distributions and extreme values is necessary for regional disaster risk analysis. So, regional and local analysis of behavior of extreme climatic values distributions is one of core elements of climate-related disaster risk analysis.

Multivariate character of multidimensional distributions of climate parameters generates high uncertainties, which makes impossible to use deterministic models. The system is not ergodic in rigorous sense. So the using of parametric methods is also limited.

To estimate a regional risk measure we need an approach to understand the complex systemic interrelations between distributions of mean and extreme values of climatic parameters and disasters frequency and intensity. Therefore development of alternative ways of analysis of multivariate distributions is the next core element of regional climate-related disaster risk analysis.

In this paper we propose to calculate the most probable distributions of extreme values of climate parameters toward the mean values change on regional scale using modified kernel-based nonlinear principal component analysis (KPCA) algorithm [15, 11]. Further, using the method of assessment of complex risk measures on the base of coupled analysis of multidimensional multivariate distributions of data, we try to estimate the regional risk of climatic, meteorological and hydrological disasters basing on kernel copula semi-parametric algorithm.

2 Extreme distribution assessment based on analysis of meteorological measurements

Existing climate models, including reanalysis, have a spatial resolution 300–500 km [13, 10]. However for regional and local risk analysis we need resolution less than 100 km: about 40–70 km [14]. Downscaling algorithms allow obtaining correct mean values distribution with necessary spatial grid, but not extreme values distributions. At the same time the density of meteorological stations and measurement points is about 30–50 km in developed regions and populated areas. So we have enough data for correct analysis. The problem is to construct a correct approach directed not to global but to regional and local analysis of data.

So this consideration directed to determination of explicit form of corresponding between known mean and studied extreme values of climatic parameters. In this case we should analyze probability distribution of set of data of meteorological measurements. So for every interval $[a, b]$ should be assessed probability $\Pr[a \le X \le b]$ of random value X will be belong to $[a, b]$. Let use the non-descending probability function $F(x)$ of simple event $p(x_i)$:

$$F(x) = \Pr[X \le x] = \sum_{x_i \le x} p(x_i), \tag{1}$$

$$\lim_{x \to -\infty} F(x) = 0, \ \lim_{x \to \infty} F(x) = 1. \tag{2}$$

The task in this case may be formulated as determination of probability distribution:

$$P(x) = \Pr(X > x), \tag{3}$$

and the corresponding probability distribution function $F(x)$, with $x \to \infty$.

For this purpose the distributions of meteorological measurements have been analyzed using the KPCA algorithm [11]. Analysis was directed to determination of relationships between mean and extreme values distributions.

The area studied includes 15 meteorological stations in the site 250 × 250 km with center on 50.5N, 26E (Northern-West part of Ukraine, Ukrainian Polissya: Prypiat River basin), for the period 1979–2010. Mean max and min detected values of daily air temperature have been analyzed, as well as the monthly distributions of precipitation.

As the analysis demonstrates, over the whole 30-year period average annual distribution of extremes toward mean temperatures is close to normal. This is obvious result, which is interesting for strategic planning of adaptation, but is not useful for local disaster risk analysis. Climate-related disaster drivers have a seasonal nature, so extremes should be analyzed on the seasonal scale. The results obtained (Fig. 1−4) demonstrate significant deviation of seasonal distributions from the normal low.

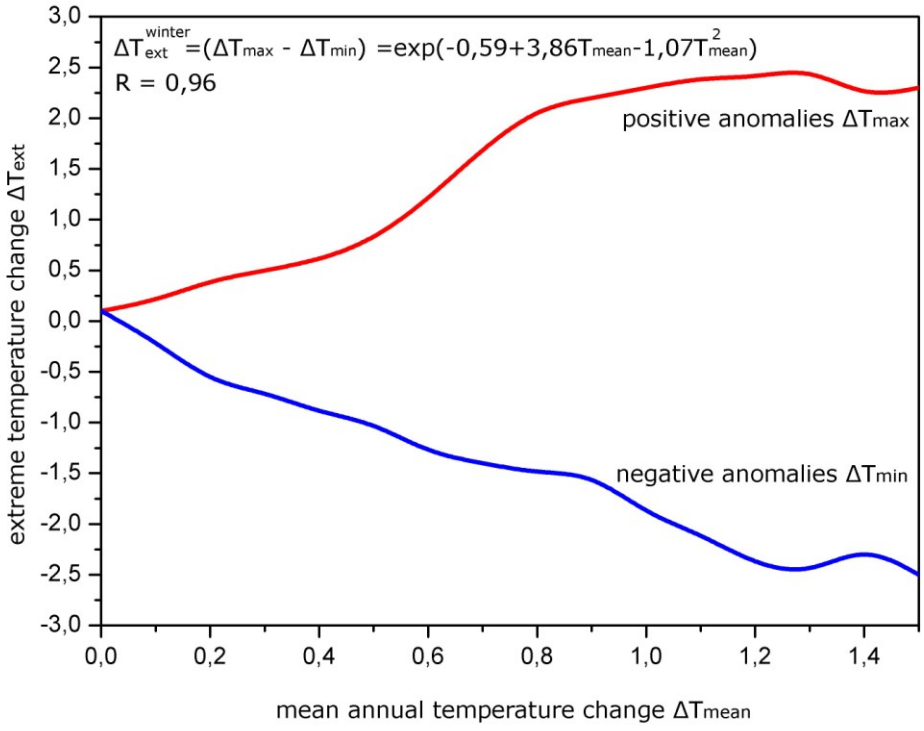

Fig. 1: Distribution of changes of max and min winter (December–February) air temperatures toward the change of mean air temperature in the study area 1990–2010

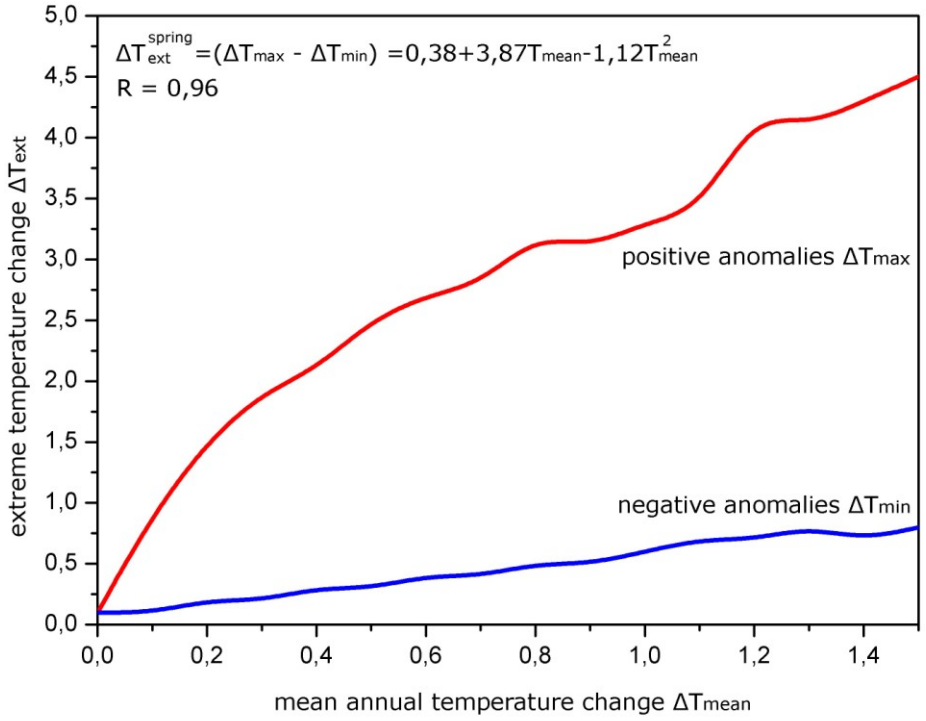

Fig. 2: Distribution of changes of max and min spring (March–May) air temperatures toward the change of mean air temperature in the study area 1990–2010

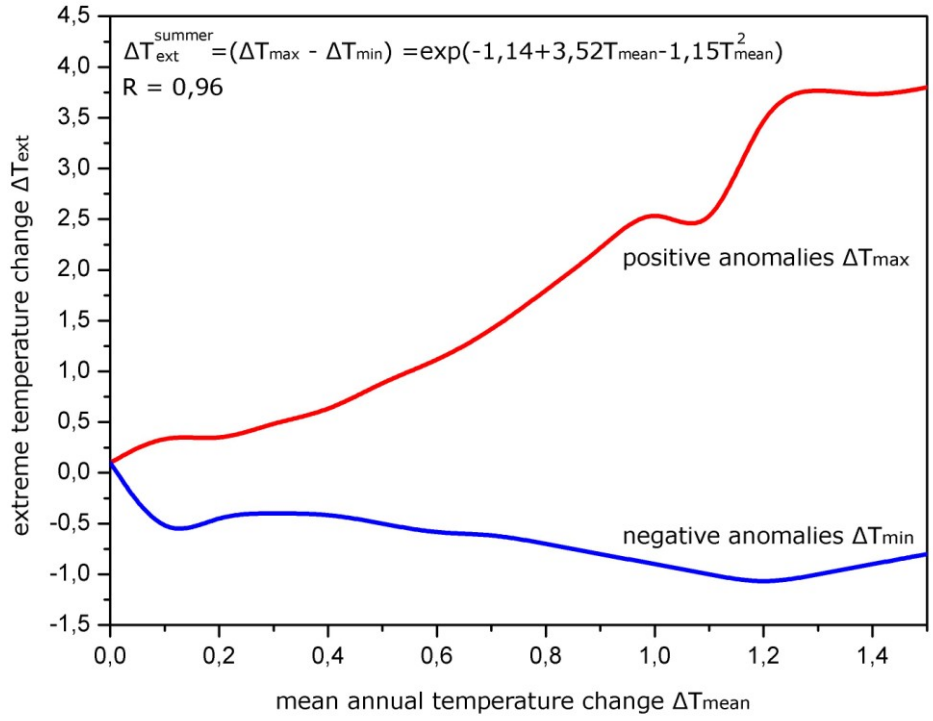

Fig. 3: Distribution of changes of max and min summer (June–August) air temperatures toward the change of mean air temperature in the study area 1990–2010

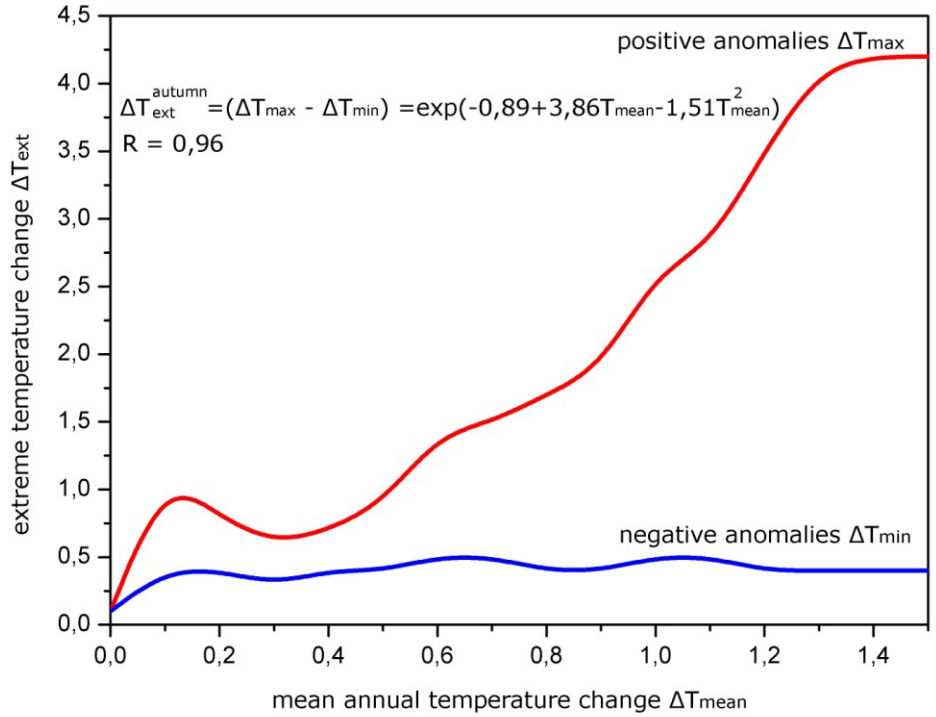

Fig. 4: Distribution of changes of max and min autumn (September–November) air temperatures toward the change of mean air temperature in the study area 1990–2010

Therefore we obtain a relation for determination of distribution of most probable values of temperature extremes toward known mean values. So it makes possible to estimate corresponding risks more correctly.

3 Way to coherent risk measures assessment based on coupled analysis of multidimensional multivariate distributions

For assessment of regional climate-related disaster risk measures we propose to use the analysis of statistics of climate mean and extreme variations and multisource disasters records.

The main issue of such type of analysis is the quantitative estimation of risk measure in multidimensional multivariate case. It requires the correct assessment of every components of loss function distribution [18]. But risks in complex multi-component systems could not be described by linear superposition of scalar functions on the quite long time intervals [5]. The complex temporal-spatial heterogeneities and significant uncertainties should be analyzed [5].

For analysis of the studied phenomena on intervals, in which its behavior is differs essentially from normal, we propose to use a following copula [6]:

$$C(u_1,u_2)=\exp\left(-V\left(-\frac{1}{\log u_1},-\frac{1}{\log u_2}\right)\right), \tag{4}$$

$$V(x,y)=\int_0^1 \max\left(\frac{\omega}{x},\frac{1-\omega}{y}\right)\mathrm{d}H(\omega), \quad \text{where} \tag{5}$$

$$H(\omega)=\begin{cases}0, & \omega<0;\\ 1/2(\omega(1-\omega))^{-1-\alpha}(\omega^{-\alpha}(1-\omega)^{-\alpha})^{\frac{1}{\alpha-2}}d\omega, & 0\le\omega<1;\\ 1, & \omega\ge 1\end{cases} \tag{6}$$

For analysis of interdependent (or weak dependent) phenomenon, for example hydrological disasters, we can use form $0 \le \omega < 1$.

This formalization allows better understand interdependencies between climatic parameters and disaster distribution on regional scale, and additionally allows to integrate regularization algorithms for uncertainty reducing [9].

For further analysis of behavior of risk measure dependent of number of climatic, ecological etc., independent heterogeneous parameters we propose other algorithm. This method based on approach to coupled nonparametric analysis of multidimensional multivariate distributions by kernel copulas [3]. Using this approach it is possible to reduce uncertainties and errors connected with differences of measurement intervals, and to smooth gaps in data distributions [4].

If $K_{u,h}(x)$ is kernel-vector for $u \in [0;1]$ on interval $h > 0$ we can propose according [3]:

$$K_{u,h}(x)=\frac{K(x)(a_2(u,h)-a_1(u,h)x)}{a_0(u,h)a_2(u,h)-a_1^2(u,h)}, \tag{7}$$

$$a_l(u,h)=\int_{\frac{u-1}{h}}^{\frac{u}{h}} t^l K(t)\,\mathrm{d}t,\ l=0,1,2\ . \tag{8}$$

Also in this case can be defined functions $G_{u,h}(t)$ and $T_{u,h}$:

$$G_{u,h}(t)=\int_{-\infty}^{t} K_{u,h}(x)\,\mathrm{d}x, \tag{9}$$

$$T_{u,h}=G_{u,h}\left(\frac{u-1}{h}\right). \tag{10}$$

Distribution function of the complex parameter will be determined by distribution functions of studied parameters $X_1, X_2, \ldots, X_n$ using copula C:

$$F(x_1,x_2,...,x_n)=C(F_1(X_1),F_2(X_2),...,F_n(X_n)). \tag{11}$$

Distribution of extremes of studied parameters will be described by distribution functions $F_i(x)$ corresponding to threshold $x_i > u_i$ as:

$$\hat{F}_i(x) = 1 - \frac{N_{u_i}}{n}\left(1 + \hat{\xi}_i \frac{x - u_i}{\hat{\beta}_i}\right)^{-\frac{1}{\hat{\xi}_i}}, \; i = 1,2\,, \tag{12}$$

where

ξ smoothing parameter,

β interdependence parameter ($\beta \in [0,1]$; $\beta = 0$ for independent distributions, and $\beta = 1$ for absolutely dependent distributions).

In this case the optimal kernel copula estimator may be presented as [10]:

$$\hat{C}(u,v) = n^{-1}\sum_{i=1}^{n} G_{u,h}\left(\frac{u - \hat{F}_1(X_{i1})}{h}\right) G_{u,h}\left(\frac{v - \hat{F}_2(X_{i2})}{h}\right) - (uT_{u,h} + vT_{u,h} + T_{u,h}T_{v,h})\,. \tag{13}$$

For the area studied on the base of multi-year statistics it was determined for the of "optimal correlator" between air temperature and disaster frequency: "reduced max temperature":

$$T_{red} = \left(1 - \frac{\frac{1}{N}\sum_{n=1}^{N} T_n}{T^{\max}}\right)\left(1 - \frac{1}{T^{\max} - \frac{1}{N}\sum_{n=1}^{N} T^{\max}}\right). \tag{14}$$

Here

N number of meteorological measurements,

T_n measured air temperature

T_{max} max registered air temperature.

Average correlation coefficients of T_{red} with quantity of disasters lie in interval 0.95–0.98, and is higher than correlation with mean temperature (0.69–0.73), and max temperature (0.85–0.9) for the period 1960–2010. Correlation coefficients are presented in Tab. 1.

Tab. 1: Correlation between number of disasters N_d and climatic parameters: mean air temperature T_{mean}, max detected air temperature T_{max} and the "reduced max temperature" T_{red} on different time intervals

Climate parameters:	T_{mean}	T_{max}	T_{red}
Observation periods			
1960–1990	0.7	0.88	0.95
1990–2010	0.73	0.9	0.98
1960–2010	0.69	0.85	0.95

Therefore the approach proposed is more correct relative to analysis with traditional values. Depending on time interval the multi-component correlation obtained allows increase

accuracy of assessment of disasters frequency up to 22% (11–34%). This is essential value for mid- and long-term regional forecasting.

4 Conclusions

The results obtained are demonstrating the possibility of determination of explicit form of extremes distributions (which could be interpreted in terms of probability) on the base of spatial-temporal analysis of meteorological data. Basing on the results of climate modeling and reanalysis, and using the formalizations proposed it is possible to analyze disaster drivers and calculate multi-scale regional risks.

Basing on existing ensemble of observation data it is possible to suppose that extremes distributions could be described by exponential distributions [16]. In separate cases (for example in spring season) this distribution is degenerates [12] to Pareto distribution [1].

Such form of long-term approximations nonetheless not allows concluding that observed processes are ergodic. It amount that capability of parametric methods for disaster analysis and forecasting is essentially limited, and we should focusing on non-parametric and semi-parametric approaches [2, 7].

The studied shifts of extreme values distribution toward mean values change is not linear and non-normal on regional scale. For example, increasing of mean air temperature to 1°C leads to increasing of max temperature to 2.5–4°C correspondingly. This is essential driver for disasters [13]. Besides, this is important factor of environmental and socio-ecological security [17, 8].

It is important to note that in view of current regional temperature change about 0.91 ± 0.27°C, we entering to zone of increasing of risks: we still in period of high risk of spring season, entering into high risks of autumn and winter seasons, and closely to zone of max risk of summer season. It should be considered in policy making.

Literature

[1] Arnold, B.C. *Pareto Distributions*. International Co-operative Publishing House, 1983

[2] Buhlmann, H. *Mathematical Methods in Risk Theory*. Berlin: Springer-Verlag, 1970

[3] Chen, S.X. and Huang, T. Nonparametric Estimation of Copula Functions For Dependence Modeling. *Technical Report*, Department of Statistics, Iowa State University, Ames, IA 50011-2008, USA, 2010, 20 p

[4] Embrechts, P., Lindskog, F. and McNeil, A. Modelling Dependence with Copulas and Applications to Risk Management. *Handbook of Heavy Tailed Distributions in Finance*, ed. S. Rachev, Elsevier, 2003, p. 329–384

[5] Ermoliev, Y. and Hordijk, L. Global Changes: Facets of Robust Decisions. In: K. Marti, Y. Ermoliev, M. Makowski, G. Pflug (eds.). *Coping with Uncertainty, Modeling and Policy Issues*. Berlin: Springer-Verlag, 2006, p. 4–28

[6] Genest, Ch., Ghoudi, K. and Rivest, L.-P. Discussion of ‘‘Understanding Relationships Using Copulas’’ by Edward Frees and Emiliano Valdez. *North American Actuarial Journal* 2(3) (1998), p. 143–149

[7] Goovaerts, M.J., Kaas, R.J. and Tang, Q. A Unified Approach to Generate Risk Measures. Leuven: Leuven Univ. Press. *ASTIN Bulletin* 33 (2) (2003), p. 173–191

[8] Grigorieva, E. and Matzarakis, A. Physiologically equivalent temperature as a factor for tourism in extreme climate regions in the Russian Far East: preliminary results. *European Journal of Tourism, Hospitality and Recreation* 2 (2011), p. 127–142

[9] Juri, A. and Wuthrich, M.V. Copula Convergence Theorems for Tail Events. *Insurance: Mathematics and Economics* 30 (2002), p. 405–420

[10] Kalnay, E., Kanamitsu, M., Kistler, R., Collins, W., Deaven, D., Gandin, L., Iredell, M., Saha, S., White, G., Woollen, J., Zhu, Y., Leetmaa, A., Reynolds, R., Chelliah, M., Ebisuzaki, W., Higgins, W., Janowiak, J., Mo, K.C., Ropelewski, C., Wang, J., Roy, J., Dennis, J. The NCEP/NCAR 40-year reanalysis project. *Bull. Amer. Meteor. Soc*. 77 **(**1996), p. 437–470

[11] Kostyuchenko, Yu.V., Yuschenko, M. and Movchan, D. Regional risk analysis based on multisource data statistics of natural disasters. *Integrated modeling of food, energy and water security management for sustainable social, economic and environmental developments.* ed. by Zagorodny A.G., Yermoliev Yu.M. – Kyiv, 2013, p. 229–238

[12] Lawless, J.F. and Fredette, M. Frequentist predictions intervals and predictive distributions. *Biometrika* 92(3) (2005), p. 529–542

[13] Parry, M.L., Canziani, O.F., Palutikof, J.P., van der Linden, P.J. and Hanson, C.E. *Contribution of Working Group II to the Fourth Assessment Report of the Intergovernmental Panel on Climate Change*. IPCC, Cambridge: Cambridge University Press, 2007, p. 987

[14] Pflug, G. and Roemisch, W. *Modeling, measuring, and managing risk*. Singapore: World Scientific Publishing Co. Pte. Ltd., 2007.

[15] Scheolkopf, B., Smola, A.J. and Muller, K. Nonlinear component analysis as a kernel eigenvalue problem. *Neural Computation* 10(5) (1998), p. 1299–1399

[16] Schmidt, D.F. and Makalic, E. Universal Models for the Exponential Distribution. *IEEE Transactions on Information Theory* 55(7) (2009), p. 3087–3090, doi:10.1109/TIT.2009.2018331

[17] Schneider, A., Panagiotakos, D., Picciotto, S., Katsouyanni, K., Lowel, H., Jacquemin, B., Lanki, T., Stafoggia, M., Bellander, T., Koenig, W., Peters, A. and AIRGENE Study Group. Air temperature and inflammatory responses in myocardial infarction survivors. *Epidemiology* 19 (2008), p. 391–400

[18] Venter, G.G. Tails of Copulas. *Proceedings of the Casualty Actuarial Society* 89 (2002), p. 68–113

System identification by using influence lines based on experimental testing

Alexander Krawtschuk, Oliver Zeman, Thomas Zimmermann & Alfred Strauss
Institute for Structural Engineering, University of Natural Resources
and Life Sciences, Vienna
alexander.krawtschuk@boku.ac.at, oliver.zeman@boku.ac.at
zimmermann.thomas@boku.ac.at, alfred.strauss@boku.ac.at

Abstract: The concept of influence lines is well known from theory. Considering practical approaches as the determination of cracked areas in bridges made from reinforced concrete this concept can be used for being able to define the bearing behaviour of a structure under various loading situations. Considering new and altered loading situations and regulations, this can be quite helpful for an estimation of the bearing capacity of an existing structure. Based on conducted experimental tests on a beam with defined boundary conditions and loads from an arch bridge structure, in this contribution the influence line concept is verified and a few approaches are presented.

Keywords: influence lines, reinforced concrete, experimental testing

1 Introduction

1.1 General

In lots of cases the loading on an existing civil engineering structure is unknown and cannot determined by measurement data directly. By means of the concept of influence lines and assumed static systems it is possible to identify a system's behaviour as result of given measurement data. In this contribution based on conducted experimental tests the structural behaviour of a steel beam under an undefined loading situation is discussed. Influence lines and system stiffness concepts are used for the estimation of the structural behaviour.

1.2 Influence lines

Influence lines serve for the explicit determination of a structure specific mechanical quantity at a defined location, such as an internal moment, shear force or deformation, due to a defined load magnitude and position. Influence lines allow the easy determination of mechanical quantities for individual loads and load combinations without the use of complex equilibrium and compatibility conditions as used in classical mechanics for statically de-

termined and undetermined systems [1]. In particular, the mechanical quantities due to specific loads or load combinations can be obtained from the load associated deflection of the influence lines by the following energy based general approach:

$$\sum W^* = W_a^* + W_i^* = Z_i \cdot \Delta\delta_i + P(x) \cdot w(x) - \int Z \cdot \delta \, dx \tag{1}$$

with $W_{a,i}^*$ = external or internal work, Z_i = actual internal force in the entire system due to the force $P = 1$, $\Delta\delta_i$ = virtual mutual deformation of the inserted degree of freedom of the associated mechanical quantity of interest, $w(x)$ = virtual deflection of the influence lines on the location and in the direction of P due to $\Delta\delta_i = -1$, and δ = virtual deformation of the entire system due to $\Delta\delta_i = -1$. Eq. (2) yields the following form for statically determined systems:

$$Z_i \cdot \Delta\delta_i + P(x) \cdot w(x) = 0 \tag{2}$$

which is the basis for the following statement done by Betti [2] and Maxwell [3]: The relationship between mechanical quantity Z_i and the displacement of the influence line $w(x)$ for a moving load $P = 1$ in $x$is valid as long as the relative displacement in i, $\Delta\delta_i = -1$ is used for the generation of $w(x)$:

$$Z_i = w(x) \tag{3}$$

The generalization of this approach for statically indeterminate systems was formulated by Land [4] as follows: The influence line for an internal force Z_i (e.g. N_i, Q_i, M_i) in i due to a variable load $P = 1$ in space is equal to the bending line $w(x)$ which is caused by the relative displacement in i, $\Delta\delta_i = -1$ (Δu_i, Δw_i, $\Delta\varphi_i$) at the location of the associated internal force Z_i of interest. Influence lines can be generated numerically (e.g. using the finite element method) by the gradual assignment of the mechanical quantity Z_i in i due to the unit load $P = 1$ to the P associated location.

2 Experimental tests

2.1 Introduction

It is well known that the boundary conditions and the supports have a significant influence on the bending moment and the influence lines of a static system. On the results of conducted laboratory tests in the testing laboratory of the Institute for Structural Engineering, Vienna, in the following chapter the behaviour of the measured strains on a double T-beam which is loaded by a masonry arch bridge is studied. This masonry arch was built on two abutments which were positioned on beams. These beams were supported and fixed by a concrete specimen at one abutment and were welded to a steel girder which is part of the testing machine on the other abutment. After an adequate hardening time, the arch was roped into the testing machine of the laboratory by means of threaded bars. While pulling the arch into the testing machine, the strains on the supporting beams were measured by strain gauges on different positions for being able to determine the structural behaviour.

2.2 Theoretical background

For getting a sense for the structural behaviour the bending moment of three different types of supports is evaluated and compared to each other. Therefore a standard beam with the same length as in the laboratory tests was considered for the calculations. The beam has a length of altogether l = 3.5 m. For the determination of the influence of the boundary conditions on the bending moment an unit force of F = 1 kN was applied and moved over the beam with a space of Δx = 0.5 m as it is shown in Fig. 1 (a) for a single-span beam with two bearings, in Fig. 1(b) for a beam with one fixed support and in Fig. 1(c) for abeam with two fixed supports. As it was mentioned above, strain gauges were arranged on defined positions on the beam. For being able to make a comparison to the measured values, the strains at the defined measurement points M1 – M5 were calculated for each loading position with of the unit force. In Fig. 1 (a) this correlation is depicted for the single-span beam, in Fig. 1 (b) for a beam with one fixed support and in Fig. 1 (c) for a beam with two fixed supports

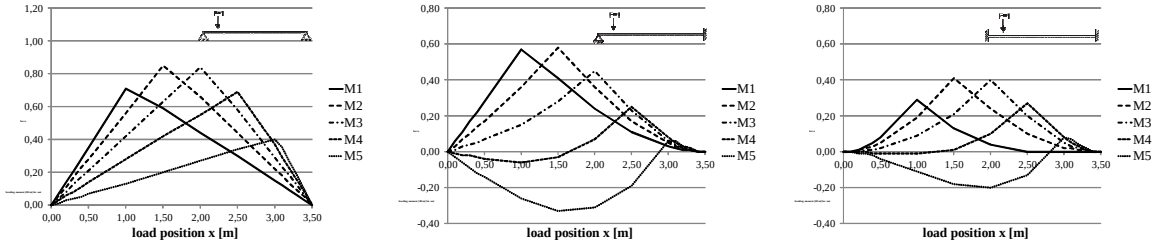

(a) Single-span beam with two bearings (b) Beam with one fixed support (c) Beam with two fixed supports

Fig. 1: Calculated influence line at the defined measurement points M1 – M5 for (a) Single-span beam with two bearings, (b) Beam with one fixed support (c) Beam with two fixed supports

The results which can be obtained from these theoretical considerations show that the type of the bearing hast a high influence on the shape and the value of the distribution of the bending moments and – if a linear material behaviour and a constant cross section is postulated – on the strains. If the shape of the measured values is compared to the theoretical shapes for different boundary conditions shown in Fig. 1, a conclusion of the real structural behaviour including the existing boundary conditions can be made. According to the unit values depicted in Fig. 1, it is evident that a negative value of the measured strains at these points might lead to the assumption of a fixed support as it is shown on the real structure in Fig. 2.

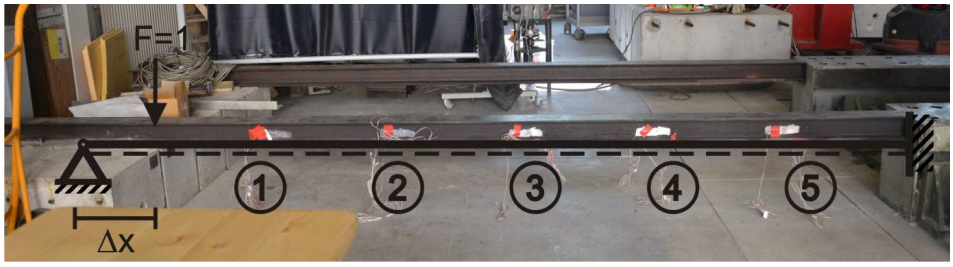

Fig. 2: Real structure of the beam the tests were conducted

2.3 Experimental tests results

The tests were performed in the testing laboratory of the Institute for Structural Engineering, Vienna in May 2013. The tests are part of a larger testing programme which is conducted on a large scale masonry arch bridge made of bricks [5]. The scale to the existing object was defined with 1:2. For conducting these vertical and horizontal tests (statically and dynamically) with the testing machine as depicted in Fig. 3, the arch bridge was built on a false work outside the machine. To ensure an equal level to the steel girder which is part of the testing machine, a concrete specimen and steel beams were arranged. The arch bridge itself was constructed on two abutments made of steel (see Fig. 4), which were positioned on the steel beams symmetrically.

Fig. 3: Laboratory arch bridge with the testing machine

Fig. 4: Steel abutment for the laboratory arch

Considering these symmetrically arrangement, it can be assumed that the half of the altogether dead load of the arch bridge is derived to one single beam of the substructure. On one of the two beams of the substructure altogether 15 strain gauges were arranged at five predefined measurement points. At each measurement point three strain gauges were applied on positions along the cross section as depicted in Fig. 5 (a). By means of this adjustment it should be ensured that both the influences from bending (position U), buckling of the flange (position M) and of normal forces (position O) were taken into account. In Fig. 5 (b) the strain distribution of the performed measurements on position O, M and U are evaluated and as a consequence a linear distribution of the strains caused by the bending moment can be seen as valid.

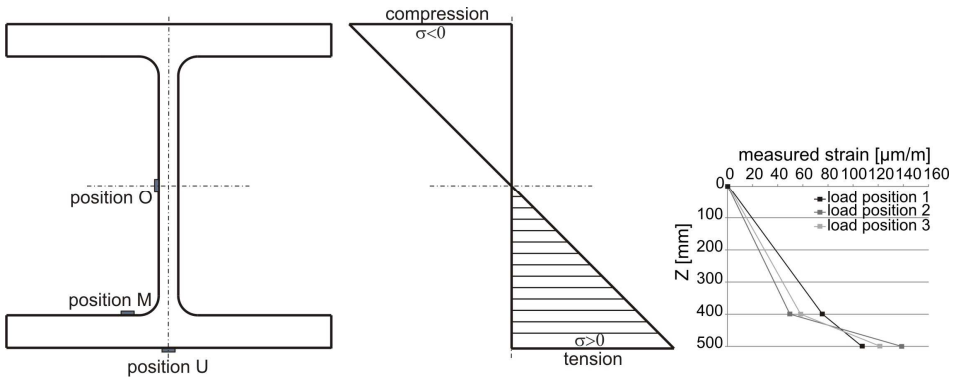

Fig. 5: Position of the strain gages on the steel beam and measured strains for different load positions

Fig. 6 shows an example of the measured strains on the mentioned loading positions during testing.

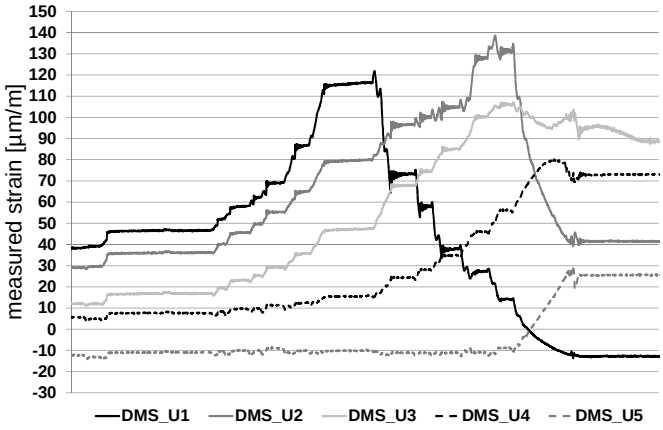

Fig. 6: Measurement data of the strains while testing

As adequate model for simulating the boundary conditions of the real beam at first a system with one fixed support was chosen as it is shown in Fig. 1(b). In the following sections, three different models are presented and evaluated with regards to their accordance to the measurement data. These models consider a point load on a beam with one fixed support (2) with two fixed supports and, (3) a distributed load along the whole beam.

2.3.1 Point load on a beam

Initially a simple load distribution of the dead load of the arch on the steel beam is assumed. Hence the load transfer can be simplified with altogether four reaction forces, two on both side of the arch as it is depicted in Fig. 7 (a) schematically. Two other possibilities for the boundary conditions have been investigated, systems as depicted in Fig. 7 (b) and Fig. 7 (c). The adequate static system can be determined from the moments based on the measurement data for the single loading positions which are shown in Fig. 8.

(a) (b) (c)

Fig. 7: (a) point load on a beam with one fixed support,(b) point load on a beam with two fixed supports, (c) point load on a beam with two supports with varied stiffness

2.3.2 Distributed load along whole beam

This model has also been taken into account, due to the fact that a wooden false work was located as substructure under the arch bridge. A part of the total load may be distributed on the steel beam, but is not discussed further in this contribution. In this model it is assumed that the distributed load is acting along the whole beam where the arch bridge and its superstructure is arranged.

2.4 Evaluation of experimental tests results

From the measurement data provided in Fig. 6 and the corresponding loading situations to each maximal strain value which were determined during testing, the distribution of the bending moments for the steel beam can be determined. The bending moments were calculated with the assumption of a linear material behaviour and a linear strain distribution as it can be derived from the strain distribution given in Fig. 5 and are depicted in Fig. 8. The considered steel beam has a moment of inertia of I = 450 cm^3 and a modulus of elasticity of E = 210 000 MPa.

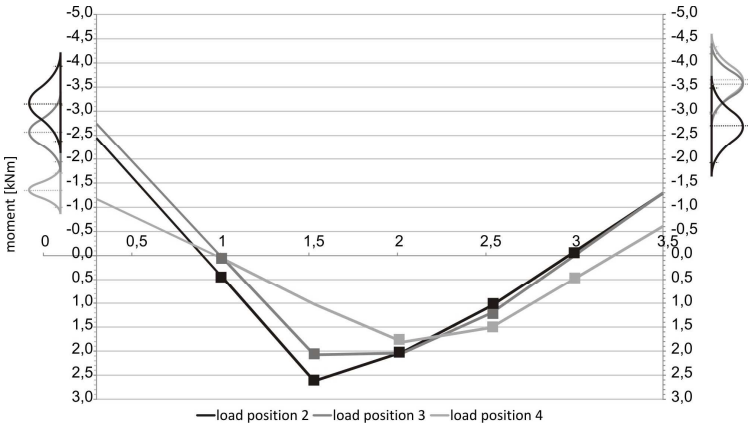

Fig. 8: Distribution of the bending moments [kNm] on the considered beam, extrapolation on the base of measurement data and comparison to the stochastic calculated values

From the bending moments in Fig. 8 it can be derived that the static system of the beam cannot be covered by the model of a single-span beam with two bearings and a beam with one fixed support, either. This conclusion is a result of the fixed-end moments on both sides which occur in all considered loading situations as a result of the linear extrapolation of the bending moment line as it is shown in Fig. 8. For the determination of the acting load, the theoretical model of a beam with two fixed supports is taken for determine the applied load from the measured strains. The following parameters were considered for defining the point load F on the various loading situations: (1) measured strains on the corresponding loading position, (2) moment of inertia, (3) modulus of elasticity, (4) position of the load, and (5) length of the beam. As fixed support the edge of the concrete member which was the substructure for the steel beam was taken into consideration, so that the length of the beam is reduced to l = 3.20 m. The calculated loads from the different loading positions on the beam have an average value of F_m = 7.2 kN and an coefficient of variation of 16.4 %. As first approximation the total weight of the arch can be given with at least 28.5 kN because one point load simulates a quarter of the total load. In addition there are some undetermined which cannot be denominated due to load distribution effects. Assuming a normal distribution for loads according to [6] a stochastic analysis with the programme *Freet* for the fixed-end moments M_i and M_k on the base of the theoretical model was done. The exact probability density functions of the single values are shown detailed in Fig. 9. The results of this analysis are the mean value and the 5%- resp. 95%-fractile value based on a k-value of k = 1.654 as it is shown in Eq. (4) for the fixing moment M_i.

$$M_{\mathrm{i},5\%/95\%} = M_{\mathrm{i,m}} \pm k \cdot s \tag{4}$$

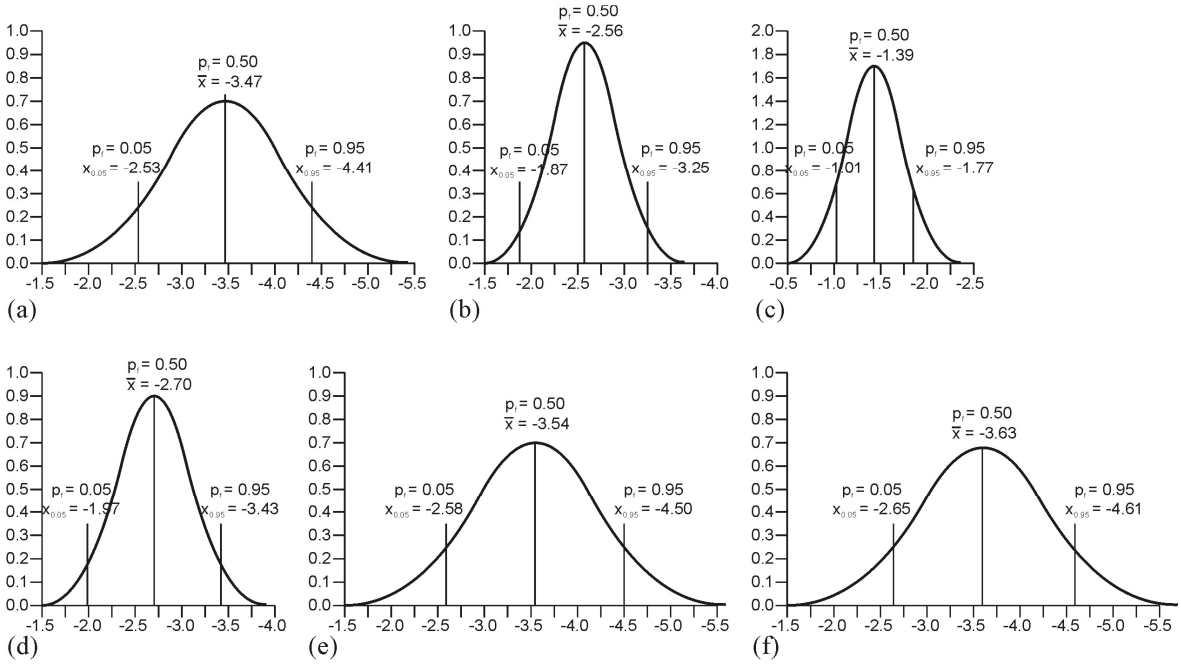

Fig. 9: Probability density functions including the characteristic values for the stochastically determined fixing moments M_i (a, b, c) and M_k (d, e, f)

From the normal distributions for the fixed-end moments which are depicted in Fig. 8 it can be derived if the assumption of a fixed support can be seen as valid. For the left support, all considered extrapolated fixing moments of the various loading situations are between the 5%-fractile and the 95%-fractile value of the normal distributions; hence the presumption of a fixed support could be verified. In case of the right support there is an obvious difference between the extrapolated and the calculated values. This might be a result of the undefined boundary condition as it is shown in Fig. 2. The beam is welded to the steel girder of the testing machine due to the fact that the arch is pulled over there are uncertainties in the load distribution. If the extrapolated values are compared to the calculated ones from theory, the mean value for the degree of fixity can be set with ~0.82 with a coefficient of variation of 12.1 %.

Fig. 10 shows the procedure for determining the load which is applied on a structure by a model updating process. At first based on unknown boundary conditions and available measurement data the grade of fixture of the supports is determined containing the statistical distributions. Based on this information it is possible to determine the structural behaviour from other, different loading situations on the same structure for which measurements are taken, too.

3 Conclusion

As it is known from theory influence lines can be an appropriate way for determining the structural behaviour of a static system, both statically determined and undetermined. In this contribution for a steel beam with two supports various boundary conditions are discussed. For the existing beam the most favourable static system was elected. Further the measured strains on various measurement points are evaluated and compared to the theoretical calculated ones.

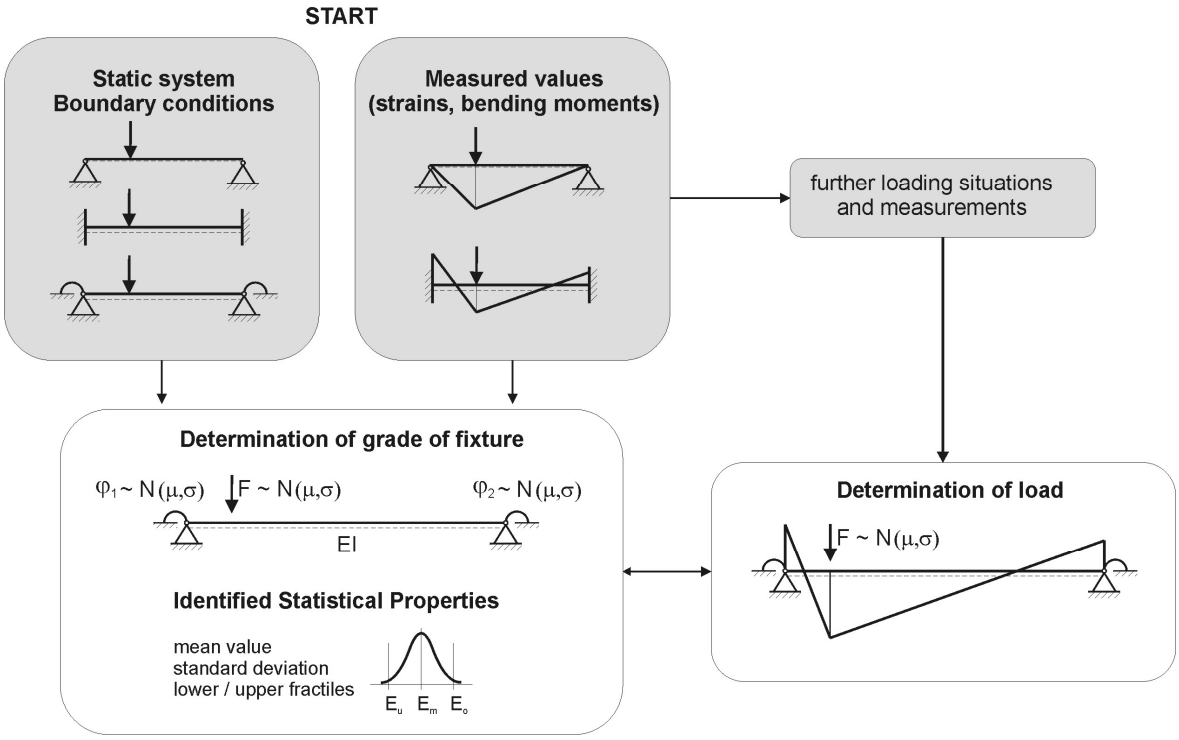

Fig. 10: Procedure for model updating based on the static system, measured values and identified statistical properties

As it can be seen in the final results, the load distribution of the arch bridge on the substructure does not follow a simplified approach. Both a local increase of loading under the load plates which was modelled by point loads, and a distributed load along the whole beam between the abutments has to be taken into account.

Additionally this contribution covers a probabilistic approach of the fixed-end moments which are evaluated with regards to the extrapolated moments taken from the measurement data. As a result of this the sudden result is, that due to load distribution processes the degree of fixity varies for one support, whereas the other support can be seen as fully fixed. Moreover, there are lots of uncertainties in geometry, which can be seen in the position of the strain gauges, the cross section of the beam and the load plates. For a full adequate model these uncertainties with their variability have to be taken into account.

Literature

[1] Rubin, H. and Schneider, K. J. Baustatik Theorie I. und II. Ordnung. Düsseldorf, Werner Verlag, 1996

[2] Betti, E.Teorema generale intorno alle deformatzioni che fanno equilibro a force che agiscono alla superficie. *Il Nuovo Cimento* 2(7–8) (1872), p. 87–97

[3] Maxwell, J. On the calculation of the equilibrium and stiffness of frames. *Philosophical Magazine* 22 (1864), p. 294–299

[4] Land, R. Über die Gegenseitigkeit elastischer Formänderungen als Grundlage einer allgemeinen Darstellung der Einflusslinien aller Trägerarten, sowie einer allgemeinen Theorie der Träger überhaupt. Wochenblatt für Baukunde, Berlin, 1887, p. 14–16, 24–25, 33–35

[5] Krawtschuk, A., Zeman, O., Zimmermann, T., Schellander, J., Strauss, A. Masonry arch bridges under vertical and horizontal loading and numerical modelling. *12th Canadian Masonry Symposium*. Vancouver, 2013

[6] ÖNORM EN 1990. Eurocode-Grundlagen der Tragwerksplanung, 2003

Probabilistic calculation using DOProC method with statistically dependent input variables

Martin Krejsa, Petr Janas, Vlastimil Krejsa
Department of Structural Mechanics, Faculty of Civil Engineering,
VSB−Technical University Ostrava, Czech Republic
martin.krejsa@vsb.cz, petr.janas@vsb.cz, vlast.krejsa@seznam.cz

Abstract: In probabilistic tasks, input random variables are often statistically dependent. This fact should be considered in correct computational procedures. In case of the newly developed Direct Optimized Probabilistic Calculation (DOProC), the statistically dependent variables can be expressed by the so-called multidimensional histograms, which can be used e.g. for probabilistic calculations and reliability assessment in the software system ProbCalc.

Keywords: direct Optimized Probabilistic Calculation, DOProC, random variable, statistical dependence, probability, double histogram, HistAn2D, triple histogram, HistAn3D

1 Introduction

The Direct Optimized Probabilistic Calculation (DOProC) is the probabilistic method which has been developed since 2002. Detailed information about this method is available in several publications, for instance, in JANAS ET AL. [3, 4, 8] and KREJSA ET AL. [11]). Attention to the statistic dependence of the random input quantities has been paid within DOProC, for instance, in RANDÝSKOVÁ & JANAS [17]. Investigations have resulted to the algorithm which can be used for creation of multidimensional histograms of the statistically dependent variables.

Using this technique, DOProC methods can be reliably extended to cover calculations where statistically independent as well as the statistically dependent input variables are used (as in KALA [9], KRÁLIK & KRÁLIK [10], MARDIA [13], OWEN [16], VOŘECHOVSKÝ [19], VOŘECHOVSKÝ & NOVÁK [20]).

The multidimensional histogram of the statistically dependent variables enters the calculation as a whole. For each interval/class, it is possible to generate, with a certain non-zero probability, the values of those dependent variables which identify the interval.

2 Theoretical analysis

In each standard histogram A, one axis includes the a_j class which is limited by $a_{\min}$ and $a_{\max}$, while the other axis shows typically the probability, p_{aj} , of occurrence of that class, a_j. The sum of probabilities for each class a_j in the histogram is $\sum p_{aj} = 1$. In the double histogram of two random variables, Z_1 and Z_2, the quantity z_1 is limited again by $z_{1,\min}$ and $z_{1,\max}$, while z_2 is limited by $z_{2,\min}$ and $z_{2,\max}$.

The values can be divided, using the step Δz_1, into N_1 intervals for random quantities Z_1, or, using the step Δz_2, into N_2 intervals for the random quantities Z_2. The number of intervals is as follows:

$$N_1 = \frac{z_{1,\max} - z_{1,\min}}{\Delta z_1} \tag{1}$$

and

$$N_2 = \frac{z_{2,\max} - z_{2,\min}}{\Delta z_2} . \tag{2}$$

If the input variable z_1 is in the j^{th} class of $z_{1,j}$ in theory, z_2 could acquire following values: $z_{2,1}, z_{2,2}$, … , $z_{2,j}$, … , $z_{2,N2}$. This means, it can acquire N_2 values. The double histogram of the random quantities z_1 and z_2 can contain $N_1 \cdot N_2$ classes. This means, each class is determined by two values, $z_{1,j}$ and $z_{2,j}$, and by the probability of occurrence of that class, $p_{z,1,j,z,2,j}$.

And again: $\sum p_{z,1,j,z,2,j} = 1$. The number of classes with the non-zero histogram can reach the product of $N_1 \cdot N_2$. If the random quantities are dependent, the number of classes in the histogram with the non-zero probability can be considerably lower than the product $N_1 \cdot N_2$. This is not, however, the general case but parametric calculations with statistically dependent input variables have been proving this (see below).

The occurrence of intervals with the non-zero probability plays a major role in DOProC calculations because, in case of double or multidimensional histograms, it is not necessary to enter the non-zero probability classes. The number of classes, T_C, in such a histogram will be same as the number of classes with the non-zero probability of occurrence. For each class T_s, a certain probability exists for occurrence, p_{Ts}, of all random variables in the class. In case of the double histogram, in each class T_s there are random variables $z_{1,Ts}$ and $z_{2,Ts}$, which are characterized by the mean value from the interval.

If M random variables enter the probabilistic calculation, in the multidimensional histogram there will be not more than $T_M = N_1 \cdot N_2 \cdot \ldots \cdot N_m \cdot \ldots \cdot N_{M\text{-}1} \cdot N_M$ classes. Because these are mostly dependent quantities, the number of non-zero classes will be, typically:

$$T_C << T_M . \tag{3}$$

The source for creation of a multidimensional histogram of M independent random quantities is the primary data which can be obtained by measurements or observations. For each random quantity z_n, the number of interval N_n, will be determined. Each random quantity can have a different number of intervals. The total number of classes (incl. zero classes), which can be formed from the chosen number of intervals for each random dependent in-

put quantity, will be T_M. When the zero-probability classes are eliminated, the number of classes will go down to T_C.

The primary data of random quantity should be checked for statistic dependence. This can be done using the Pearson's correlation coefficient, Spearman's rank correlation coefficient or Kendall correlation coefficient (e.g. NELSEN [15]). The correlation coefficient of the primary data should correspond to the correlation coefficient obtained after creation of the histogram.

It follows from the analyses that this depends on the chosen number of classes for each random input quantity. The more classes exist, the more the correlation coefficient converges to the correlation coefficient of the primary data.

Using the same interval for the dependent random quantity, z_n, the step Δz_n will be as follows:

$$\Delta z_n = \frac{z_{\max} - z_{\min}}{N_n}. \tag{4}$$

Each interval is given the mean (average) value of the interval for z_n. That value is $z_{n,p}$. Calculation of the values is very simple because:

$$\begin{gathered} z_{n,p,1} = z_{\min} + \frac{\Delta z_n}{2},\ z_{n,p,2} = z_{n,p,1} + \Delta z_n,\ \ldots \\ \ldots,\ z_{n,p,m} = z_{n,p,m-1} + \Delta z_n,\ \ldots,\ z_{n,p,M} = z_{n,p,M-1} + \Delta z_n \end{gathered} \tag{5}$$

The dependent input variable z_1, which will be divided in the multidimensional histogram into N_1 intervals, will occur in the first interval of the multidimensional histogram in $N_2 \cdot \ldots \cdot N_m \cdot \ldots \cdot N_{M\text{-}1} \cdot N_M = T_M / N_1$ classes. The situation will be similar in all intervals of the dependent input quantity z_i. It is advisable to determine the class sequence for both reduced and unreduced multidimensional histograms. In the unreduced multidimensional histogram, there will be classes with the zero probability, while the reduced multidimensional histogram will comprise only classes with the non-zero probability. In the unreduced histogram, there will be T_M classes, while the reduced histogram will include T_c classes only.

In order to include a group of the random dependent variables into the global unreduced multidimensional histogram, it is necessary to calculate the number (sequence) of the class P in the unreduced histogram. The calculation is simple:

$$\begin{aligned} P = a_1 \cdot N_2 \cdot \ldots \cdot N_m \cdot \ldots \cdot N_{M-1} \cdot N_M + a_2 \cdot N_3 \cdot \ldots \cdot N_m \cdot \ldots \\ \ldots \cdot N_{M-1} \cdot N_M + a_3 \cdot N_4 \cdot \ldots \qquad \ldots \qquad\qquad \ldots \end{aligned} \tag{6}$$

In Eq. (6) the coefficients a_1, a_2, a_3 , … , a_M result from the following equation:

$$a_1 = \text{integer division of } \frac{z_{1,s,k} - z_{1,\min}}{\Delta z_1} \tag{6a}$$

or

$$a_1 = \frac{z_{1,s,k} - z_{1,\min}}{\Delta z_1} - 1 \text{, if } \frac{z_{1,s,k} - z_{1,\min}}{\Delta z_1} \text{ is an integer.} \tag{6b}$$

In analogy:

$$a_2 = \text{integer division of } \frac{z_{2,s,k} - z_{2,\min}}{\Delta z_2} \tag{6c}$$

or

$$a_2 = \frac{z_{2,s,k} - z_{2,\min}}{\Delta z_2} - 1 \text{, if } \frac{z_{12s,k} - z_{2,\min}}{\Delta z_2} \text{ is an integer.} \tag{6d}$$

For a_M :

$$a_M = \text{integer division of } \frac{z_{m,s,k} - z_{m,\min}}{\Delta z_m} + 1 . \tag{6e}$$

The same sequence can exist for several groups of primary data of the random dependent input quantities. Some sequences (a majority of them, in case of the dependent random quantities) will not occur there at all. The probability of occurrence of a class is given by the sum of occurrences of same sequences divided by the sum of total number of groups of the random independent input quantities.

If the coefficients a_1, a_2, a_3 , … , a_M are known for the P sequence of the class in the global histogram (the coefficients can be determined from the P sequence), it is possible to determine the mean values of the dependent input quantities in the class within the corresponding sequence. If the sequence of the class is P in the global unreduced histogram, the following equations are valid for the coefficients and mean values of the class:

$$z_{1,p} = z_{1,\min} + \Delta z_1 \cdot \left(a_1 + \frac{1}{2} \right), \; z_{2,p} = z_{2,\min} + \Delta z_2 \cdot \left(a_2 + \frac{1}{2} \right) , \ldots$$

$$\ldots , \; z_{M-1,p} = z_{M-1,\min} + \Delta z_{M-1} \cdot \left(a_{M-1} + \frac{1}{2} \right), \tag{7}$$

$$z_{M,p} = z_{M,\min} + \Delta z_M \cdot \left(a_M - \frac{1}{2} \right) .$$

Finally, it should be pointed out that the sets of random dependent input quantities for the probabilistic calculations can be depicted in charts in a form of multidimensional histograms, if these are two dependent input quantities. If there are more dependent input quantities, it is impossible to depict them in charts.

It should be also emphasized that even the independent random input quantities can be entered into the calculation in a form of double or multidimensional histograms. This means, it is not necessary to define criteria for dividing the input data clearly into statistically dependent and independent ones. If it is assumed that the input data could be statistically dependent, this fact should be considered during calculations. Computational algorithms in DOProC can be used in calculations using the statistically independent ran-

dom input quantities as well as using the data where statistical dependence could be taken into account (e.g. in the cross-section parameters or strength parameters obtained, for instance, in ČAJKA ET AL. [1], MELCHER ET AL. [14]).

3 Software: HistAn2D and HistAn3D

Having applied the technique described above, primary data have been analyzed for cross-section parameters of rolled sections, IPE 140. These data were published in ROZLÍVKA ET AL. [16]. Special software applications HistAn2D and HistAn3D JANAS ET AL. [6, 7] (see Fig. 1 and 2) were developed for creation of the double and triple histograms which describe the statistical dependence between two or three random variables.

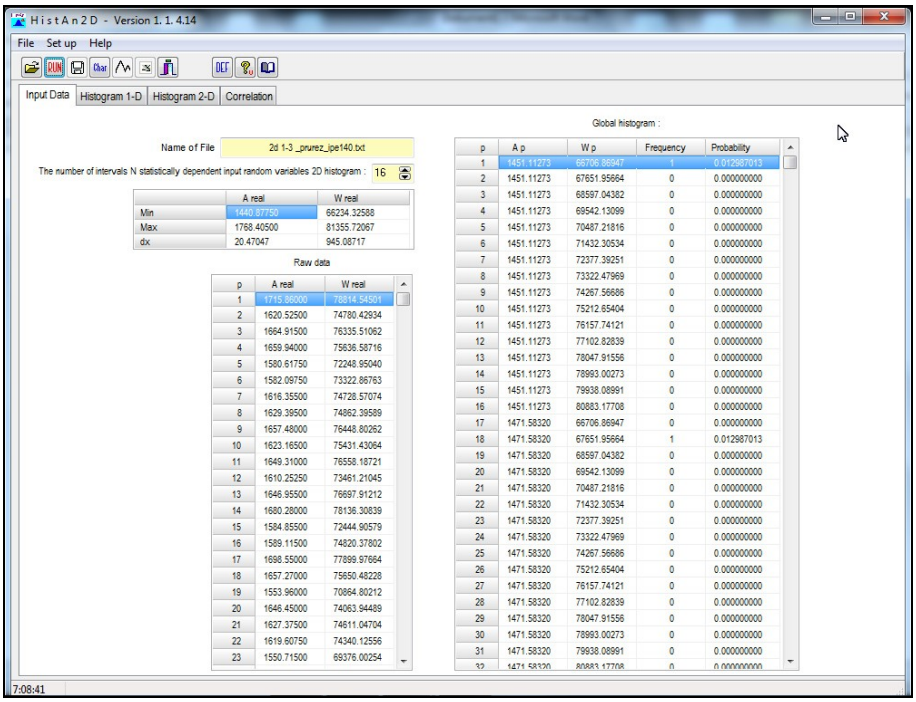

Fig. 1: Desktop in HistAn2D for analysis of statistical dependence of two random quantities and double histograms

Once the text file with the statistically dependent primary data is read, it is necessary to enter only the number of interval/classes of the double or triple histogram which should be created. Using the software, it is possible to view for each random variable a simple histogram with non-parametric (empirical) distribution of probability (Fig. 3 and Fig. 4) as well as a multidimensional histogram which describes the statistical dependence between the quantities. The double histogram can be shown in a chart (see Fig. 6).When creating the histogram, the primary data need to be divided into 16^2 intervals. If the double histogram were created from an histogram for a cross-section area A (Fig. 3) and histogram of a cross-section module W (Fig. 4) (this means, for two statistically independent quantities), the double histogram would correspond to the chart in Fig. 5 which is very different from a double histogram of two dependent quantities (Fig. 6). It is impossible to view a triple histogram (this was mentioned at the end of the previous chapter), but HistAn3D can show this histogram in layers.

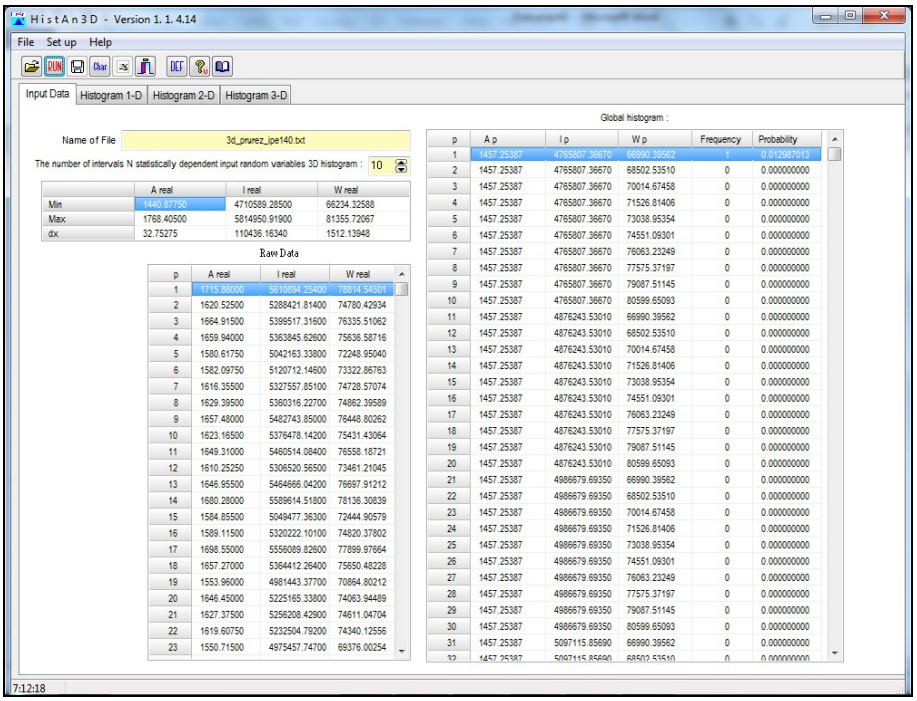

Fig. 2: Desktop in HistAn3D for analysis of statistical dependence of three random quantities and triple histograms

Correlation coefficients suggested by Pearson and Spearman (see Tab. 1) were calculated for the primary data and for double histograms of the dependent input data with different number of intervals. It is clear that the correlation coefficients of the double histograms are different and that they converge towards the correlation coefficients of the primary data with the increasing number of intervals. See Fig. 7 and 8. Using the statistically dependent input quantities (see Sec. 4), 16^2 intervals were chosen for creation of a double histogram. For that number of interval, the calculated correlation coefficients do not differ too much from the correlation coefficients of the primary data (see Fig. 7 and 8).

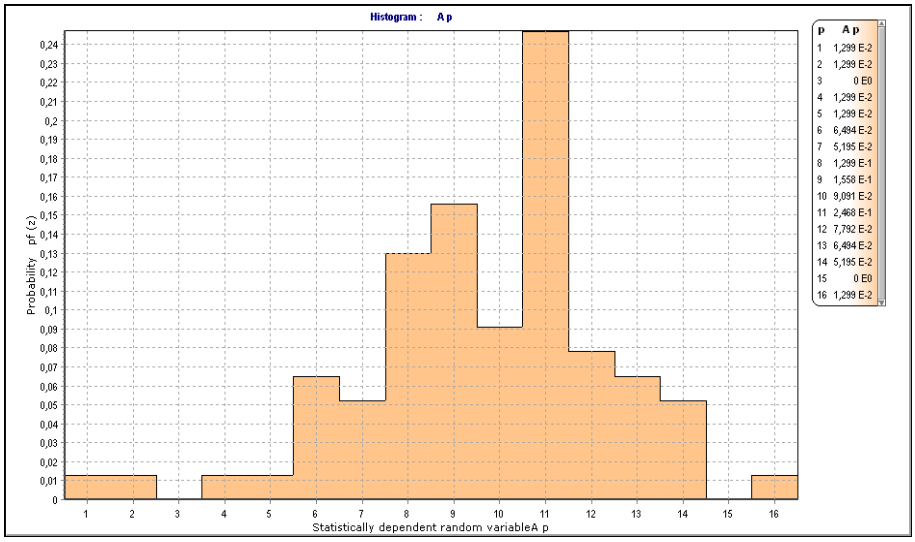

Fig. 3: Histogram of the cross-section area *A*

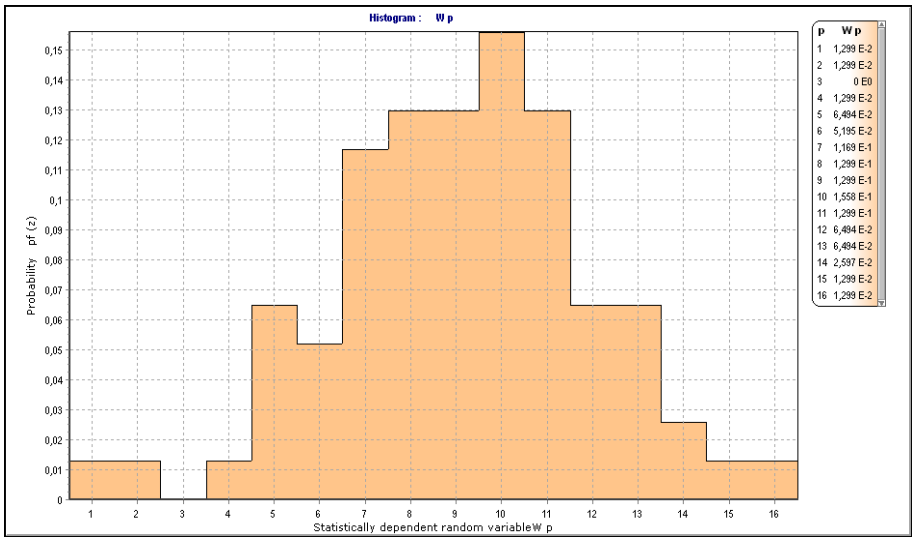

Fig. 4: Histogram of the cross-section modulus W_y

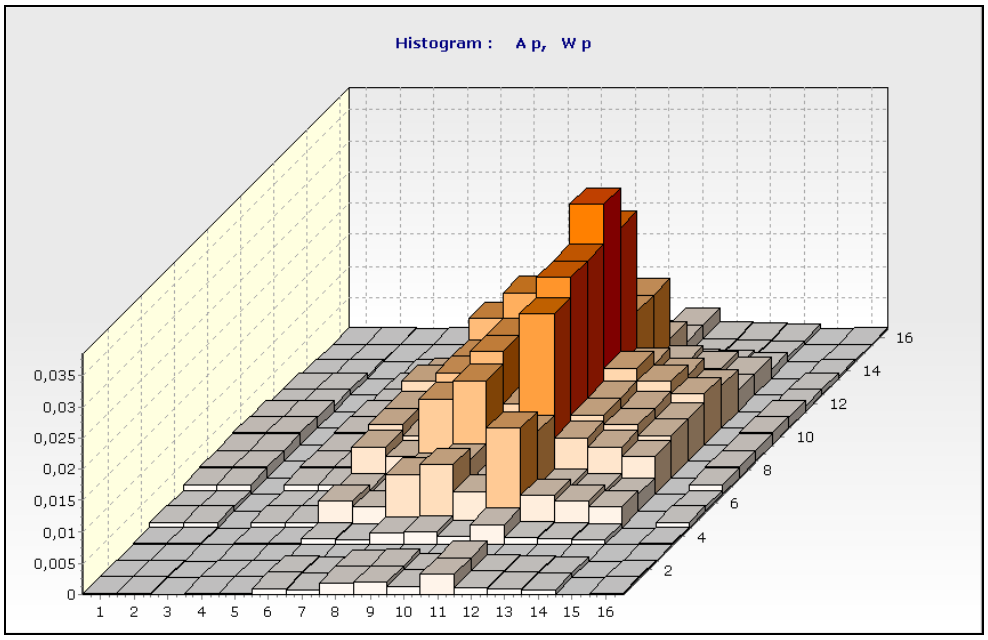

Fig. 5: Behaviour of two statistically independentrandom quantities − cross-section area A and cross-section modulus W_y

The calculations prove that the correlation coefficients in a double histogram of the independent random quantities in Fig. 5 are zero. Tab. 2 lists the numbers of classes of the zero probability double histograms for a total number of intervals. For the double histogram in Fig. 5, the number of zero probability classes is considerably lower than the number of a double histogram based on the same primary data which are, however, regarded as statistically dependent (Fig. 6). This fact is shown also in a chart in Fig. 9. The multidimensional histograms can be used for description of the statistical dependence of the random input variables in those probabilistic calculations which are solved using DOProC techniques. This includes, for instance, ProbCalc JANAS ET AL. [2, 5].

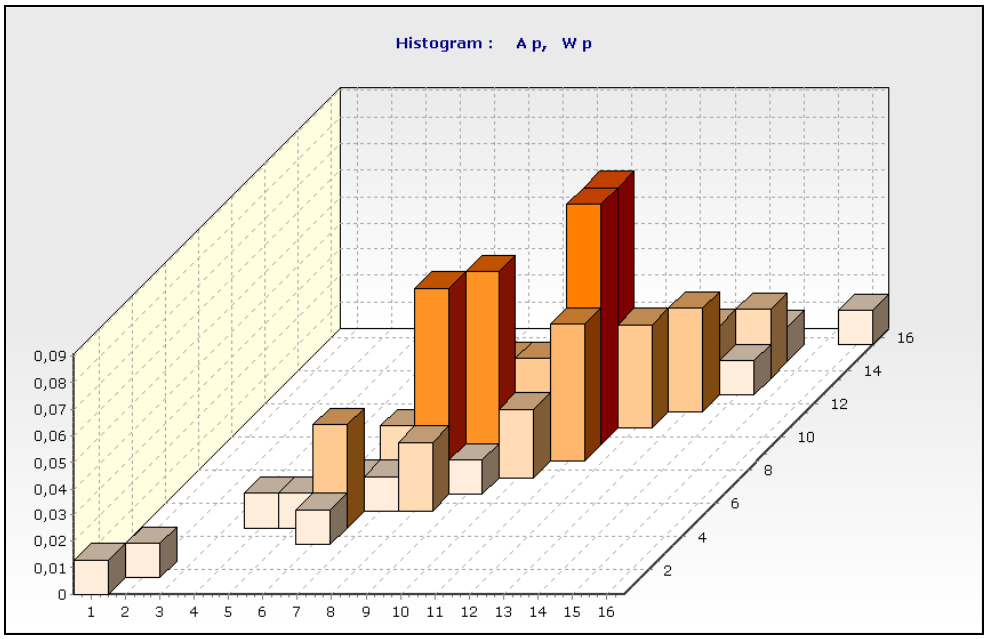

Fig. 6: Double histogram for two statisticallydependent random quantities – cross-section area A and cross-section modulus W_y

Tab. 1: Correlation coefficients of a double histogram of the statistically dependent quantities with different numbers of intervals (Pearson's correlation coefficient for primary data is 0.9645; Spearman's correlation coefficient for primary data is 0.9499)

Number of intervals in a double histogram	*Pearson's correlation coefficient*	*Spearman's rank correlation coefficient*	*Number of intervals in a double histogram*	*Pearson's correlation coefficient*	*Spearman's rank correlation coefficient*
$4^2 = 16$	0.79985097	0.79507798	$18^2 = 324$	0.95267109	0.94023800
$6^2 = 36$	0.86661900	0.86360377	$20^2 = 400$	0.96046634	0.94378886
$8^2 = 64$	0.91530000	0.91194405	$22^2 = 484$	0.95940904	0.94355084
$10^2 = 100$	0.93984931	0.92352904	$24^2 = 576$	0.95903334	0.94989866
$12^2 = 144$	0.94381175	0.93613068	$26^2 = 676$	0.96464064	0.95260826
$14^2 = 196$	0.95443331	0.93939308	$28^2 = 784$	0.96017017	0.94660574
$16^2 = 256$	0.94876401	0.93694950	$30^2 = 900$	0.95938019	0.94245225

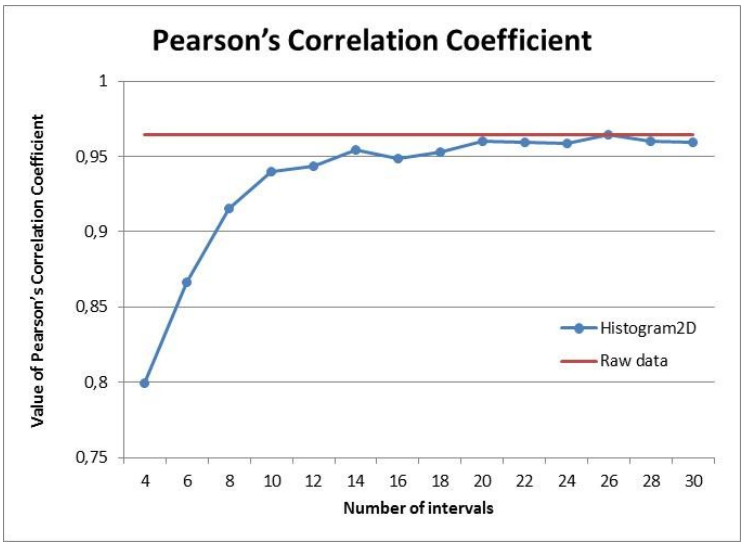

Fig. 7: Pearson's correlation coefficient of a double histogram vs.number of intervals

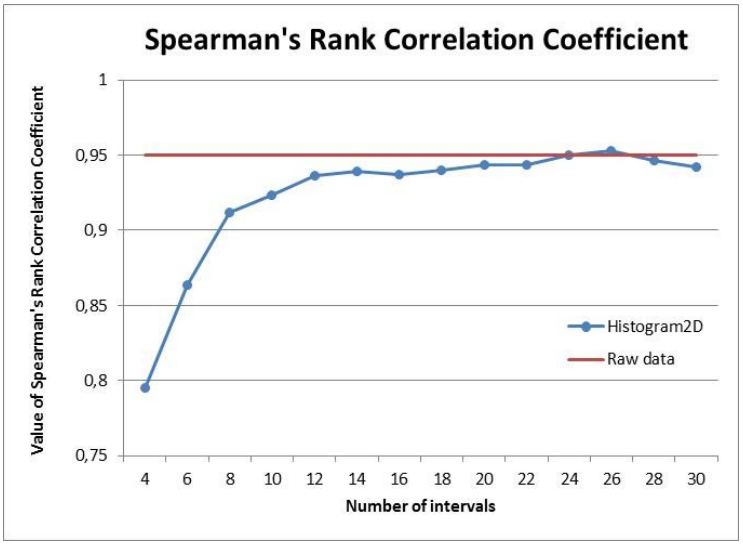

Fig. 8: Spearman's rank correlation coefficient of a double histogram vs. the number of intervals

Tab. 2: The number of classes for double histograms with zero probability vs. the number of intervals chosen during creation of the histograms from the primary data

Number of intervals in a double histogram	*Number of zero-probability intervals*		*Number of intervals in a double histogram*	*Number of zero-probability intervals*	
	Statistically dependent quantities	*Statistically independent quantities*		*Statistically dependent quantities*	*Statistically independent quantities*
$4^2 = 16$	6	0	$18^2 = 324$	288	69
$6^2 = 36$	24	0	$20^2 = 400$	361	112
$8^2 = 64$	48	0	$22^2 = 484$	443	160
$10^2 = 100$	80	0	$24^2 = 576$	531	216
$12^2 = 144$	119	0	$26^2 = 676$	627	258
$14^2 = 196$	166	14	$28^2 = 784$	735	322
$16^2 = 256$	222	46	$30^2 = 900$	847	372

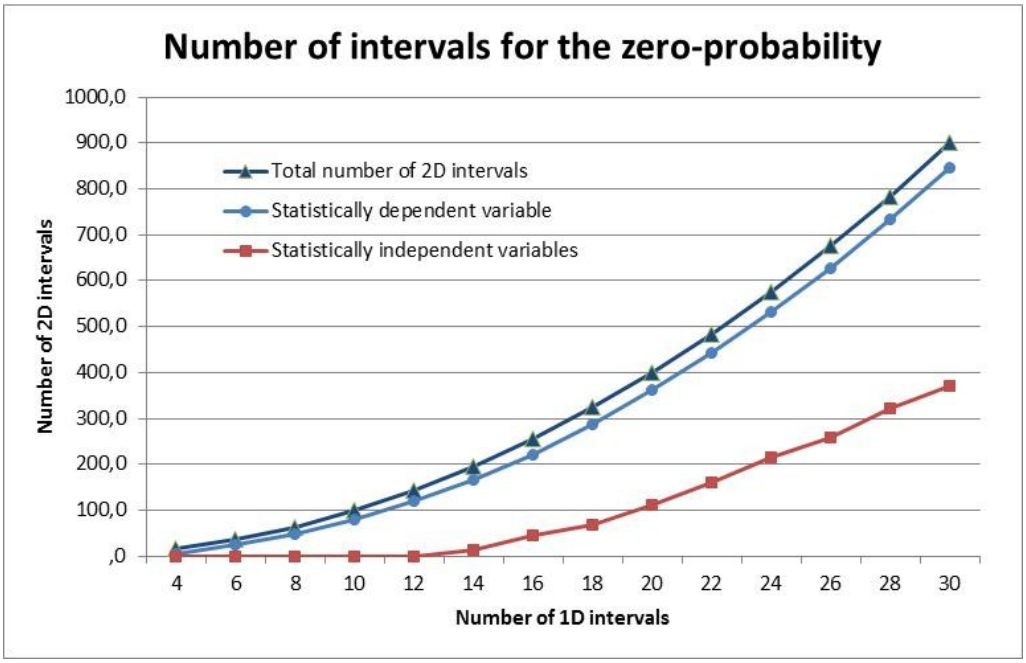

Fig. 9: Number of intervals for the zero-probability in double histogram

4 Applying the computational technique with the statistically dependent input quantities

For the sake of clarity, ProbCalc performed the probabilistic calculation for the reliability assessment of a cross-section in a vertex of an elemental parabolic arch fixed in both ends and loaded in a vertex with a single load. The static scheme is shown in Fig. 10.

The centre line of the parabolic arch in the coordinate system in Fig. 10 is defined by the following curve and equation:

$$y(x) = \frac{4 \cdot f \cdot x}{l^2} \cdot (l - x), \tag{8}$$

where f is the upward deflection and l is the outspan (in this case: f = 4 m and l = 12 m).

The assessment has been made using the interaction formula:

$$\left(\frac{N_{Ed}}{N_{Rd}}\right)^2 + \frac{M_{Ed}}{M_{Rd}} \leq 1, \tag{9}$$

with following variables:

- Normal force in the cross-section:

$$N_{Ed} = -\frac{15 \cdot l \cdot F}{64 \cdot f}; \tag{10}$$

- Bending moment in the cross-section:

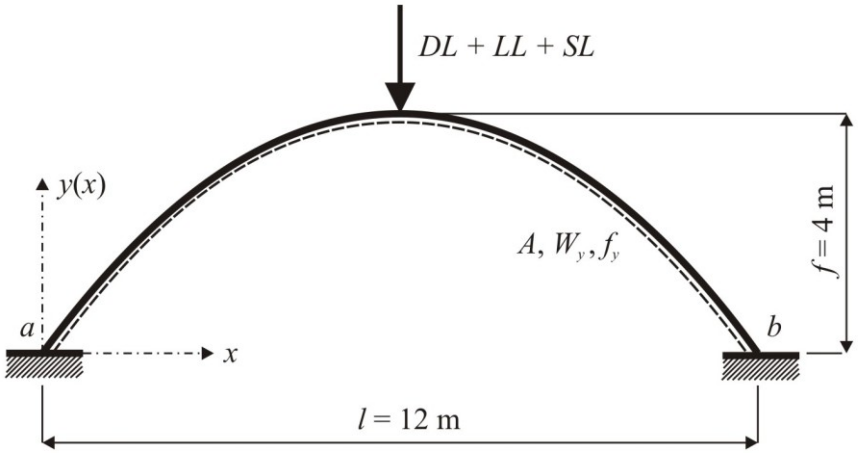

Fig. 10: Static scheme of the elemental structure of a parabolic arch fixed in both ends and loaded with combination of three single loads in a vertex

$$M_{Ed} = \frac{3}{64} \cdot F \cdot l \,; \tag{11}$$

- Load-carrying capacity in simple compression:

$$N_{Rd} = f_y \cdot A \,; \tag{12}$$

- Bending capacity:

$$M_{Rd} = f_y \cdot W_y \,. \tag{13}$$

The cross-section has been assessed in terms of reliability by calculating the failure probability P_f and by comparing it with the designed probability P_d pursuant to ČSN EN 1990. The failure probability P_f was determined using the reliability function RF:

$$P_f = P(RF < 0) = P\left(1 - \left[\left(\frac{N_{Ed}}{N_{Rd}}\right)^2 + \frac{M_{Ed}}{M_{Rd}}\right] < 0\right). \tag{14}$$

For purposes of the reliability assessment of the structure, following parameters were used: the random variable yield point f_y of steel S235 taken from ROZLÍVKA ET AL. [18], permanent load (extreme value: 8 kN, histogram DEAD1.dis), short-term load (extreme value 15 kN, histogram LONG1.dis) and long-lasting random (variable) load (extreme value 10 kN, histogram SHORT1.dis). (The histograms describing the three random variable components of the load were taken from KREJSA ET AL. [12]).

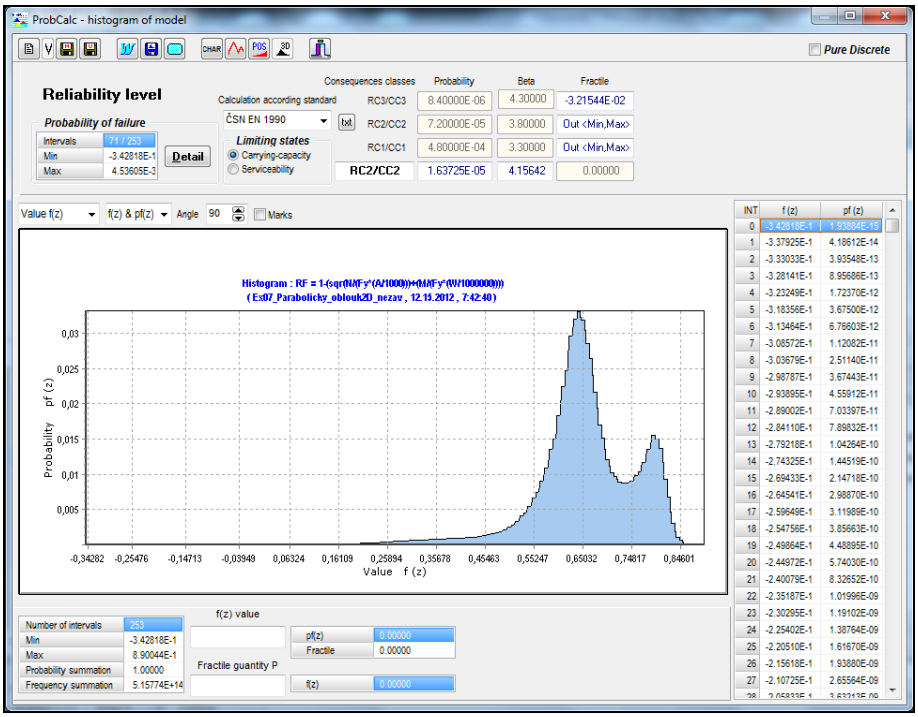

Fig. 11: Histogram − reliability function *RF*, for the probabilistic calculation with statistically independent cross-section parameters of the cross-section area A and cross-section modulus W_y, failure probability $P_f = 1.637 \cdot 10^{-5}$

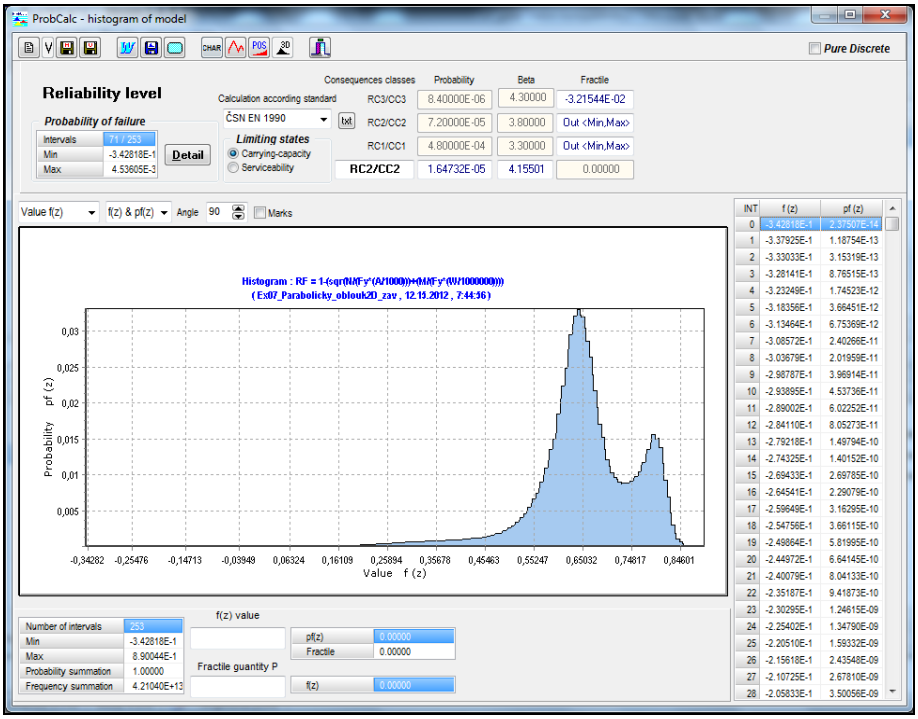

Fig. 12: Histogram − reliability function *RF*, for the probabilistic calculation with statistically dependent cross-section parameters of the cross-section area A and cross-section modulus W_y, failure probability $P_f = 1.647 \cdot 10^{-5}$

The probabilistic assessment of the structure was made in the vertex of the arch. First, the both random quantities − the cross-section area A and cross-section modulus W − were

regarded at statistically independent (see Fig. 11) and then as statistically dependent (see Fig. 12). A double histogram was used. It consisted of the primary data of the cross-section parameters of the rolled sections IPE 140 in line with data published in ROZLÍVKA ET AL. [18] and described using the mentioned method in HistAn2D JANAS ET AL. [6]. Fig. 11 and 12 show the resulting failure probability P_f for both alternatives of the probabilistic calculation.

The designed failure probability P_d (and the reliability index β_d) are differentiated now in ČSN EN 1990 "Eurocode: Basis of structural design" depending on the required reliability, types of ultimate conditions and assumed service life of the structure T_d. Three classes of consequences, CC1 through CC3, and three classes of reliability, RC1 through RC3, are defined in the standard. The standard also lists the designed values of the failure probability P_d and reliability index β_d. In both cases of the probabilistic task, the cross-section of the structure meets requirements of CC2/RR2 with medium consequences in terms of lost lives or with considerable economic/social/environmental consequences. This corresponds to the designed failure probability $P_d = 7.2 \cdot 10^{-5}$ and reliability index $\beta_d = 3.8$.

The final failure probability P_f in the calculation with the statistically independent cross-section parameters is slightly lower than in the calculation where the cross-section area A and cross-section modulus W are statistically dependent on each other. In general, it is less safe to use the probabilistic calculation where the input quantities are statistically independent random quantities, if it is beyond doubt that the input random variables statistically depend on each other. In that case, the difference in the failure probability is not too significant between the statistically-dependent and statistically-independent cross-section parameters. The reason is that the rolled sections are manufactured with relatively high accuracy and have considerably less dispersion of geometry and cross-section parameters than other random variables that enter the calculation.

5 Conclusion

This work describes the algorithm used for creation of multidimensional histograms of statistically dependent variables. This algorithm can be used in calculations based on DOProC techniques – for instance, in ProbCalc. This can describe correlation between the random input variables, e.g. in the cross-section parameters, as explained in this paper, or strength parameters.

There is still space for investigation of the statistically dependence of the random variables in DOProC. The next objective might be determination of the correlation coefficients for triple histograms or use of parametric distribution of probability for creation of multidimensional histograms. It would be also advisable to determine the relation between this method and linear transformation carried out, for instance, by Choleski decomposition of the correlation matrix or between this method and orthogonal transformation which uses eigen vectors and eigen numbers of the correlation matrix.

Final comment

The mentioned DOProC techniques with the statistically dependent input variables have been gradually implemented into ProbCalc. A light version of ProbCalc is available at http://www.fast.vsb.cz/popv. On the same website, it is possible to download light versions of HistAn2D and HistAn3D which describe statistical dependence of two or three random variables.

Acknowledgement

This paper has been prepared within the project which has been co-financed from the financial support provided to VŠB−Technical University of Ostrava by the Czech Ministry of Education, Youth and Sports from the budget for conceptual development of science, research and innovations for the year 2013.

Literature

[1] Čajka, R., Stará, M., Matečková, P., Janulíková, M. Experimental Test of Brick Corner. *Transactions of the VŠB−Technical University of Ostrava*: *Construction Series* 11(2) (2011), p. 1–6 (6 p). Warsaw, Poland: Versita. ISSN 1804-4824 (Online); ISSN 1213-1962 (Print). DOI: 10.2478/v10160-011-0021-z

[2] Janas, P., Krejsa, M., Krejsa, V. *Software ProbCalc [EXE] − Program System for Probabilistic Reliability Assessment using DOProC method*. Authorized software, Lite version 1.1, 12,4 MB. Reg. num. 003/27-01-2009_SW. VŠB-TU Ostrava, 2008

[3] Janas, P., Krejsa, M., Krejsa, V. Assessment Using Direct Determined Probabilistic Calculation. In: *Proceedings of the 12th International Conference on Civil, Structural and Environmental Engineering Computing: CC 2009*, Funchal, Madeira, Portugal. Kippen, Stirlingshire, Scotland: Civil-Comp Press, 2009. ISBN 978-1-905088-31-7. Elsevier B.V., 2012. ISBN 978-190508830-0. DOI: 10.4203/ccp.91.72

[4] Janas, P., Krejsa, M., Krejsa, V. Using the Direct Determined Fully Probabilistic Method (DDFPM) for determination of failure. In: *Proceedings of European Safety and Reliability Conference (ESREL 2009)*: *Reliability, Risk and Safety: Theory and Applications, Vols 1−3, Prague, Czech Republic, 2009*. London: Taylor & Francis Group, 2010, p. 1467–1474 (8 p). ISBN 978-0-415-55509-8. WOS:000281188500203

[5] Janas, P., Krejsa, M., Krejsa, V. Software Package ProbCalc from the Poin of View of a User. *Transactions of the VŠB−Technical University of Ostrava*: *Construction Series* 10(1) (2010), p. 1–11 (11 p). Warsaw, Poland: Versita. ISSN 1804-4824 (Online); ISSN 1213-1962 (Print). DOI: 10.2478/v10160-010-0010-7

[6] Janas, P., Krejsa, M., Krejsa, V. *Software HistAn2D [EXE] – Program for creating and analyzing 2D histograms representing statistical dependence of two random variables*. Authorized software, lite version 1.1, reg. num. 013/03-10-2012_SW. VŠB−TU Ostrava, 2012

[7] Janas, P., Krejsa, M., Krejsa, V. *Software HistAn3D [EXE] – Program for creating and analyzing 3D histograms representing statistical dependence of tree random variables*. Authorized software, lite version 1.1, reg. num. 014/03-10-2012_SW. VŠB−TU Ostrava, 2012

[8] Janas, P., Krejsa, M., Krejsa, V. Statistical Dependence of Input Variables in DOProC Method. *Transactions of the VŠB−Technical University of Ostrava*: *Construction Series* 12(2) (2012), p. 48–58 (11 p). Warsaw, Poland: Versita. ISSN 1804-4824 (Online); ISSN 1213-1962 (Print). DOI: 10.2478/v10160-012-0017-3

[9] Kala, Z. Sensitivity analysis of steel plane frames with initial imperfections. *Engineering Structures* 33(8) (2011), p. 2342–2349 (8 p). ISSN 0141-0296, DOI: 10.1016/j.engstruct.2011.04.007

[10] Králik, J., Králik, J., Jr. Deterministic and Probability Analysis of the Steel Chimney under Wind Loads. *In Proceedings of 17th International Conference on Engineering Mechanics*, Svratka, Czech republic (2011), p. 311–314 (4 p). ISBN 978-80-87012-33-8, WOS:000313492700071

[11] Krejsa, M., Janas, P., Čajka, R. Using DOProC method in structural reliability assessment. Eds: Ching Kuo Wang and Jing Guo. Zurich, Switzerland: Trans Tech Publications. *Applied Mechanics and Materials: Mechatronics and Applied Mechanics II* 300-301 (2013), p. 860–869 (10 p). ISSN 1660-9336, ISBN 978-303785651-2, DOI: 10.4028/www.scientific.net/AMM.300-301.860

[12] Krejsa, M., Marek, P. Transition from deterministic to probabilistic structural steel reliability assessment with special attention to stability problems. *Stability and Ductility of Steel Structures* (1999), p. 19–26 (8 p). ISBN 0-08-043016-3, WOS: 000083313700003, doi: 10.1016/B978-008043016-4/50003-9

[13] Mardia, K. V. Statistics of Directional Data. *Journal of the Royal Statistical Society Series B-Methodological* 37(3) (1975), p. 349–393 (45 p). ISSN 0035-9246

[14] Melcher, J., Kala, Z., Holický, M., Fajkus, M., Rozlívka, L. Design characteristics of structural steels based on statistical analysis of metallurgical products. *Journal of Constructional Steel Research* 60(3-5) (2004), p. 795–808 (14 p). ISSN 0143974X, DOI: 10.1016/S0143-974X(03)00144-5

[15] Nelsen, R. B. Correlation, regression lines, and moments of inertia. *American Statistician* 52(4) (1998), p. 343–345 (3 p). ISSN 0003-1305, DOI: 10.2307/2685438, WOS: 000076853500010

[16] Owen, A. B. Controlling correlations in Latin hypercube samples. *Journal of the American Statistical Association Theory and Methods* 89(428) (1994), p. 1517–1522

[17] Randýsková, L., Janas, P. Pravděpodobnostní výpočty metodou PDPV se závislými náhodnými veličinami. In: *Proceedings of 6th international conferenceNew Trends in Statics and Dynamics of Buildings*. Bratislava: Slovak University of Technology in Bratislava, Slovakia, 2007, 11 p. ISBN 978-80-227-2732-7 (in Czech)

[18] Rozlívka, L., Fajkus, M. Reálné pevnostní hodnoty konstrukčních ocelí a rozměrové úchylky válcovaných materiálů pro pravděpodobnostní posuzování spolehlivosti ocelových nosných prvků a konstrukcí metodou SBRA. In *Proceedings of conference "Structural Reliability"*. Ostrava, 2003. ISBN 80-02-01551-7 (in Czech)

[19] Vořechovský, M. Correlation control in small sample Monte Carlo type simulations II: Analysis of estimation formulas, random correlation and perfect uncorrelatedness.

Probabilistic Engineering Mechanics 29 (2012), p. 105–120 (16 p). ISSN 0266-8920, DOI: 10.1016/j.probengmech.2011.09.004

[20] Vořechovský, M., Novák, D. Statistical correlation in stratified sampling. *Applications of Statistics and Probability in Civil Engineering*, 1 & 2 (2003), p. 119–124 (6 p). ISBN: 90-5966-004-8, WOS: 000189453300017

The foundation slab monitoring of the "National Supercomputing Center − IT4 Innovations" during construction

Martin Krejsa, Radim Čajka
Department of Structural Mechanics & Department of Building Structures,
Faculty of Civil Engineering, VSB−Technical University Ostrava,
Czech Republic
martin.krejsa@vsb.cz, radim.cajka@vsb.cz

Abstract: The paper focuses on the monitoring of basic material and mechanical features of the foundation slab in the "National Supercomputing Center − IT4 Innovations" during construction and on the statistics analysis of measured data. The obtained data have been processed by the ProbCalc software within statistics and sensitivity analyses.

Keywords: monitoring, foundation slab, concrete, National Supercomputing Center − IT4 Innovations, Direct Optimized Probabilistic Calculation, DOProC, random variable, ProbCalc, HistAn, HistAn2D, HistAn3D

1 Introduction

On 3rd December 2012 the construction site in the campus of VSB–Technical University Ostrava was handed over and construction of the "National Supercomputing Center − IT4 Innovations" started. This unique centre, once completed, will make it possible to process various challenging tasks and will rank among supercomputers in the European network. The area of the building will be 2,180 m^2 and the total area of all floors with IT systems will be about 6,500 m^2.

During construction, attention has been paid to the strength and rigidity of concrete. Samples of the concrete were taken during the casting of the foundation slab. The samples were investigated then in the Laboratory of Building Materials at the Faculty of Civil Engineering, VSB-Technical University Ostrava. Dynamic modules of elasticity of concrete were tested in a non-destructive test of measuring the resistivity (resistance of concrete to the passage of electric current). Time records of temperature and stress in the concrete and reinforcement were measured by built-in sensors and strain-meters in the foundation slab CAJKA ET AL. [6].

The obtained data have been processed by the ProbCalc software within statistics and sensitivity analyses. The data resulted in simple or multiple bounded histograms. In the future research and investigation, those data will be used for probabilistic modelling of static behaviour of the foundation slab.

2 Description of the load-carrying structure

The load-carrying structure of the "National Supercomputing Center – IT4 Innovations" (Fig. 1) is a three-dimensional reinforced concrete structure which consists of a foundation slab, load-carrying columns and ceiling slabs for each floor. The foundation slab is 400 mm thick. In the longitudinal and transversal directions it is reinforced with ribs which are located in the upper part of the slab. This means, a sliding joint can be created at the lower part of the slab CAJKA ET AL. [3] The sliding joint eliminates there shear stress caused by changes in concrete's volume.

Fig. 1: View at construction of the load-carrying structure of the Supercomputing Centre

3 Monitoring of the foundation slab

During construction of the load-carrying system, the temperature and state of stress are measured in the foundation slab. The purpose is to check quality of construction works during concrete curing and during construction of other parts of the structure. String strain gauges have been used to measure the temperature in different heights of the foundation slab and subsoil. The string strain gauges have been also monitoring the state of stress in certain heights of the concrete slab. Changes in the state of stress of the reinforcement at the upper and lower edges have been monitored by foil strain gauges. In the structure, optical fibres have been also installed for control checks CAJKA ET AL. [6].

Those sensors are normally used in laboratories, but application in a real structure during construction works appears to be problematic because there is much moisture and the sensor might be easily mechanically damaged. The measuring sensors were installed into the foundation slab structure between the ribs, approximately in the middle of the span onto "measuring pillars" (Fig. 2) which make it possible to install the floating string strain-

meters in the correct height and direction. Data transmission cables were connected then to the reinforcement CAJKA ET AL. [6].

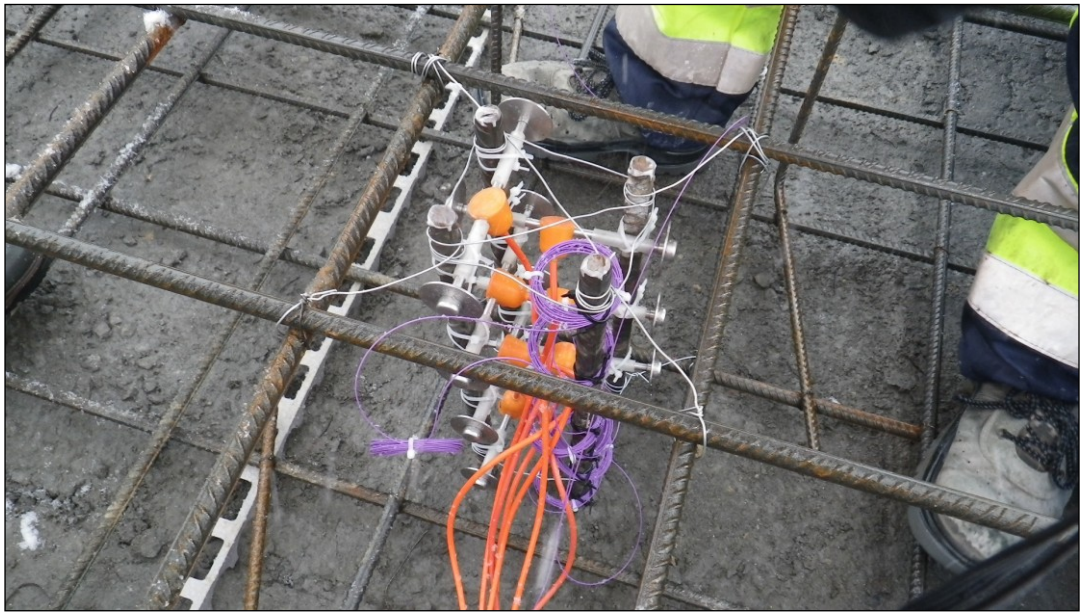

Fig. 2: Installation of a measuring pillar in the structure

4 Time records of the measured data

The monitoring of the foundation slab started immediately after the concrete was cast. During the casting, optical fibres were damaged. Consequently, only the string strain gauges were used to measure the data. A non-contact digital thermometer was used to measure the temperature of the outside surface of the concrete slab and ambient environment CAJKA ET AL. [6].

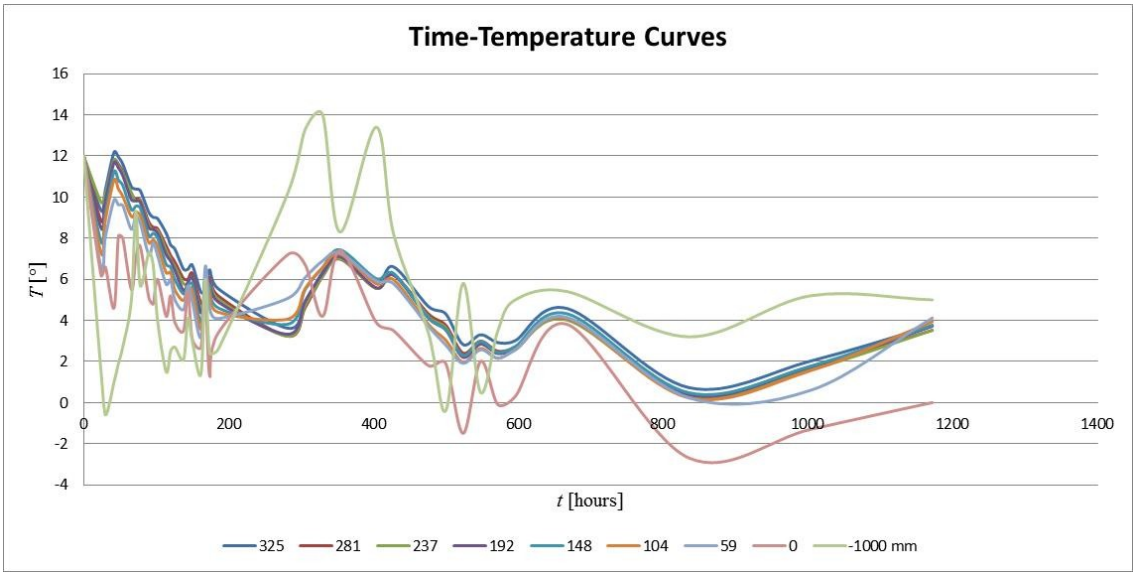

Fig. 3: Time records of the temperature in the concrete foundation slab made for 9 different heights

The temperature data from the string strain gauges were read off three times a day throughout 14 days during the casting of the concrete. Then, the measured data were read

off once a day only. Fig. 3 shows the temperatures in the course of time for nine different heights (+325 mm, +281 mm, +237 mm, +192 mm, +148 mm, +104 mm, +59 mm, 0 mm and −1000 mm). The green curve (−1000 mm) corresponds to the ambient temperature – in the first stage of the concrete curing temperatures reached negative values. In terms of compliance with the technological process of concreting this fact represented adverse factor. Hydration heat which releases from the concrete curing caused this negative factor to influence unfavourably the temperature of the concrete slab. Fig. 3 also proves that the ambient temperature and temperature of the concrete slab became stable once the hydration had been completed. In the same time intervals, changes in relative deformation were read out in the structure. They were transformed into changes of normal stress. The resulting time behaviour (Fig. 4 and Fig. 5) was obtained using the string strain gauges cast at different heights and in both main direction of the structure's ground plan.

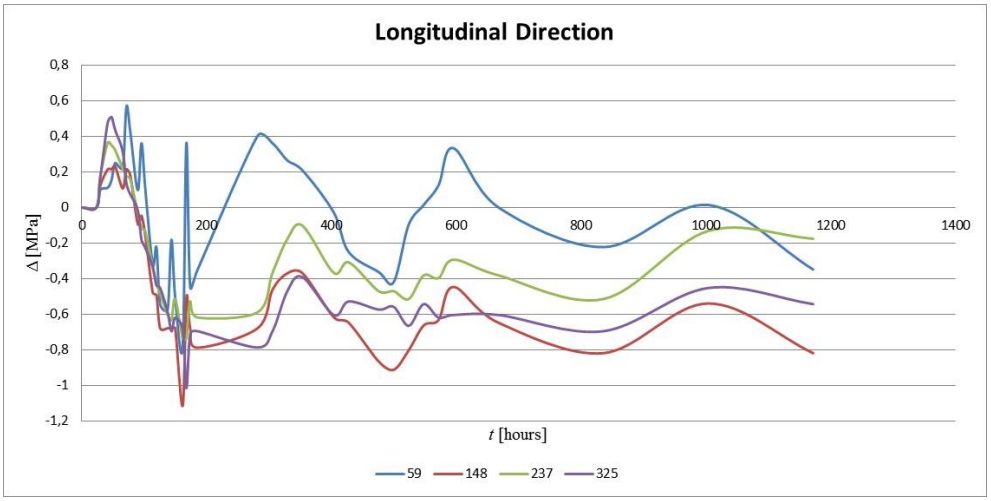

Fig. 4: Changes in time of the normal stress in the concrete slab in a longitudinal direction for 4 different heights

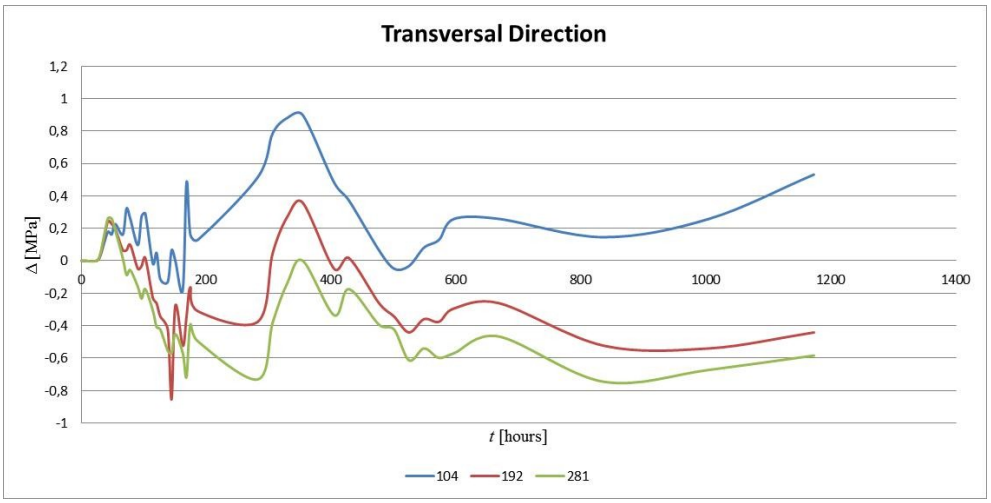

Fig. 5: Changes in time of the normal stress in the concrete slab in a transversal direction for 3 different heights

A similar approach was used to determine the changes in time of the normal stress in the reinforcing steel in the foundation slab – Fig. 6.

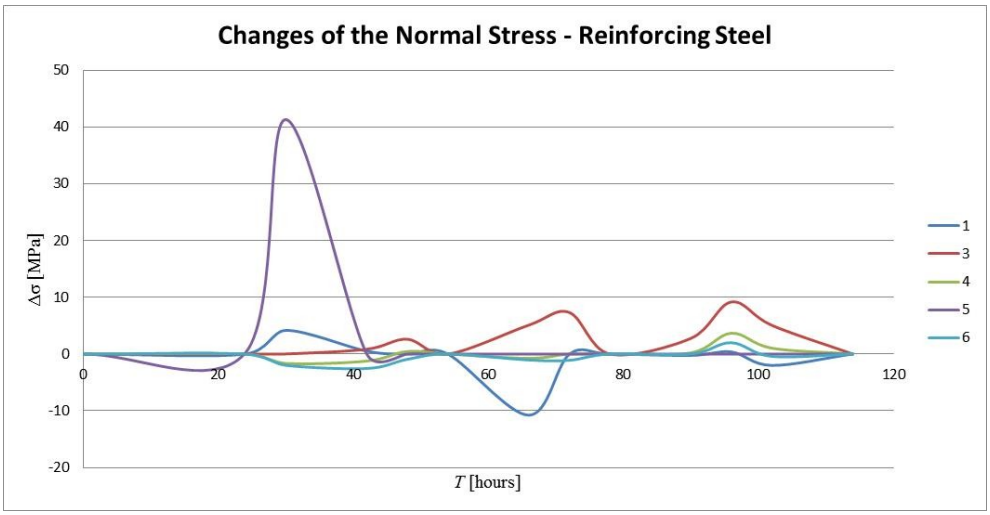

Fig. 6: Changes in time of the normal stress in the reinforcing steel in the foundation slab

In the Laboratory of Building Materials of VSB−TUO destructive tests were carried out, the goal being to check quality of building works. Compressive cube and cylinder strengths were tested for various ages of concrete samples taken during the casting of the foundation slab on the site. Analysis of resistivity measurement was carried out and the dynamic modulus of elasticity was measured in cube bodies. The compressive cube strength of the concrete after 28 days of ageing was determined pursuant to ČSN EN 12390-3 Testing hardened concrete – Part 3: Compressive strength of test specimens [8]. The testing was performed in the Cemex s.r.o. laboratory.

5 Statistics and sensitivity analyses of the measured data

Various calculation methods based on the theory of probability and mathematical statistics are used now in technical and structural assignments (e.g. KRALIK [16], KRIVY ET AL. [20]). Those methods have been becoming very popular recently. The methods which are referred to as probabilistic make it possible to analyse a reliability reserve defined by a calculation model where at least some input quantities are of a random nature. New methods include the Direct Optimized Probabilistic Method ("DOProC"). This method has been under development since 2002. It is a purely numerical method which uses no simulation techniques. Results of the probabilistic tasks are more accurate and, often, more fast to reach. Theoretical background of DOProC has been published in sufficient detail in many publications (for instance, JANAS ET AL. [10, 11] or KREJSA ET AL. [17, 18]) and applied e.g. in KREJSA [19].

DOProC can be used in ProbCalc – this software is still under development (JANAS ET AL. [9]) and consists of several computational modules. HistAn, HistAn2D and HistAn3Dare the utilities which were used for the statistics and sensitive analysis of the values measured in the foundation slab of the "National Supercomputing Center – IT4 Innovations" during the site monitoring (JANAS ET AL. [12, 13]). Those three software applications use the primary data to create and analyse the bounded histograms. If two or three random quantities are statistically dependent, it is possible to use HistAn2D and HistAn3D to determine the degree of dependency and to create double or triple histograms which can be used for probabilistic computations with respect to the statistic dependence JANAS ET AL. [14].

5.1 Statistic dependence of two or more random variables

If there are two random variables, *X* and *Y,* the statistic dependence can be described using the Pearson's correlation coefficient which is defined as follows:

$$r = \frac{\sum_{i=1}^{n}(x_i - \bar{x})(y_i - \bar{y})}{\sqrt{\sum_{i=1}^{n}(x_i - \bar{x})^2 \sum_{i=1}^{n}(y_i - \bar{y})^2}} \tag{1}$$

where x_i and y_i are elements of the both random quantities and $\bar{x}$ and $\bar{y}$ are mean values of those quantities.

The correlation coefficient may range between −1 and +1. The limit values represent the ideal linear relation between the both random quantities. In case of positive correlation, the values of the both variables increase. If the correlation coefficient is negative, the value of one variable increases, while the other one decreases. If there is not any linear dependence, the correlation coefficient is zero and describes the statistic independence of the both random variables which do not correlate at all.

In case of ordinal data or deviation from the expected data distribution (e.g. linear distribution)it is recommended to use, for example, a non-parametric Spearman's coefficient of sequential correlation which can be determined by arranging *n* values x_i and y_i of the both random quantities by their size and by allocating sequence numbers p_i and q_i in Eg. (1). After modification, the equation is as follows:

$$\rho = 1 - \frac{6\sum_{i=1}^{n}(p_i - q_i)^2}{n(n^2 - 1)} \tag{2}$$

If there are more than two random variables, the degree of statistic dependence can be well described using the correlation matrix which is symmetric. On the main diagonal, the elements equal to one. Out of the main diagonal, there are correlation coefficients for respective pairs of the random variables in the matrix column and row.

5.2 Analysing the temperature in the foundation slab

The statistic and sensitivity analyses were performed first for the temperature measured at different heights of the foundation slab and for the ambient temperature. The Pearson's and Spearman's correlation coefficients were used to create pairs of correlation matrixes in Tab. 1 and 2 which describe the statistic dependence of temperatures in all measurement heights. With the increasing value of the correlation coefficient (where the absolute value approaches one), the random variables correlate more and more and become linearly dependent. Fig. 7 shows as an example the chart which describes the statistics dependence of the temperature at +325 mm and in other measuring points. It is evident that the values become non-correlatable with the increasing distance between the temperatures in the both measuring levels.

If the available software employs the DOProC method, the statistic dependence between the pairs/triples of the input random variables can be described using a double or triple

histogram which can be used, in turn, for probabilistic calculations. Fig. 8 shows, for instance, a double histogram which describes the statistic dependence of the random variable temperature at +325 mm and +281 mm.

Tab. 1: The correlation matrix which uses the Pearson's correlation coefficients to describe the statistics dependence of the temperature at different heights of the foundation slab and ambient temperature

[mm]	325	281	237	192	148	104	59	0	−1000
325	**1**	0.999179	0.996923	0.995500	0.983759	0.971624	0.930670	0.785600	−0.034170
281		**1**	0.998172	0.997997	0.988557	0.978113	0.941768	0.793464	−0.129316
237			**1**	0.997222	0.988365	0.978245	0.942759	0.798301	−0.007715
192				**1**	0.995390	0.988138	0.957607	0.809621	0.028066
148					**1**	0.997432	0.978363	0.839512	0.106057
104						**1**	0.988934	0.859433	0.148671
59							**1**	0.899881	0.252198
0		**sym.**						**1**	0.298942
−1000									**1**

Tab. 2: The correlation matrix which uses the Spearman's correlation coefficients to describe the statistics dependence of the temperature at different heights of the foundation slab and ambient temperature

[mm]	325	281	237	192	148	104	59	0	−1000
325	**1**	0.997100	0.994693	0.992175	0.974777	0.955080	0.907967	0.744175	−0.093153
281		**1**	0.998468	0.996990	0.981617	0.963234	0.919626	0.749822	−0.725701
237			**1**	0.998523	0.985556	0.969800	0.928818	0.762627	−0.051773
192				**1**	0.989439	0.975540	0.938054	0.769048	−0.024796
148					**1**	0.993216	0.967774	0.800925	0.068958
104						**1**	0.985939	0.836969	0.115915
59							**1**	0.881010	0.207761
0		**sym.**						**1**	0.244649
−1000									**1**

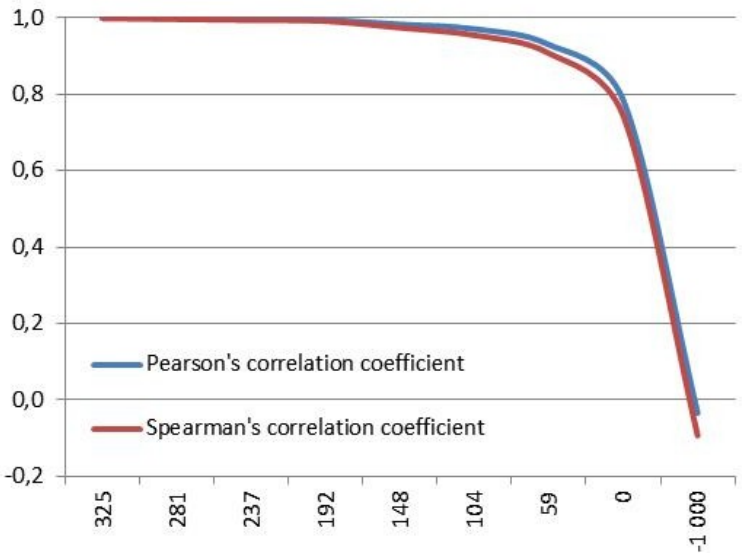

Fig. 7: The Pearson's and Spearman's correlation coefficients between the temperatures measured at +325 mm and temperatures in other measuring points

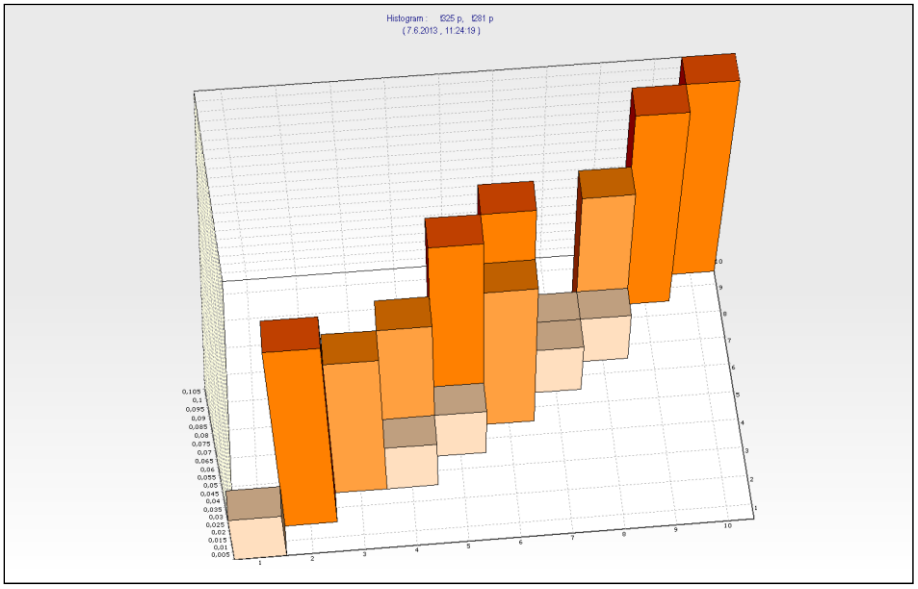

Fig. 8: Desktop of HistAn2D:The double histogram which describes the statistic dependence of the random variable temperature at +325 mm and +281 mm using DOProC method

5.3 Analysing changes in normal stress in a concrete slab

The measured changes in the normal stress in the foundation slab were analysed in a similar way in a longitudinal direction (in 4 heights) and in a transversal direction (in 3 heights). The resulting correlation matrixes are shown in Tab. 3 and 4 and in charts in Fig. 9 and 10. The changes in the normal stress in the foundation slab are random variables with a high degree of statistic dependence.

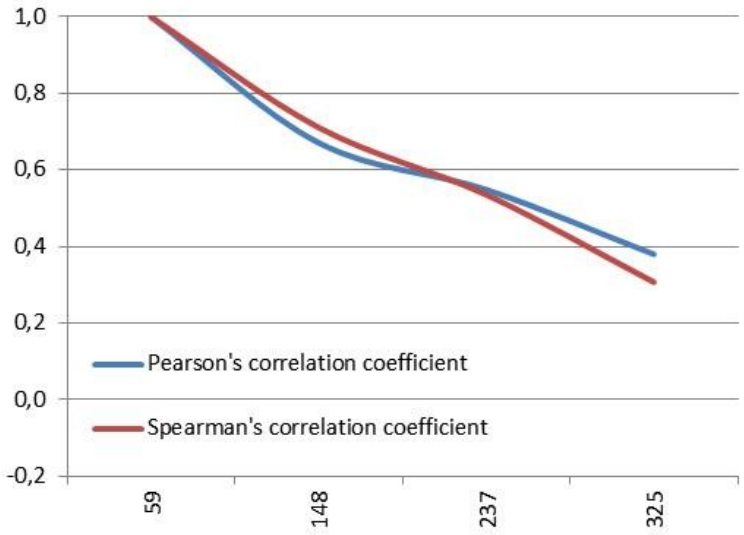

Fig. 9: The Pearson's and Spearman's correlation coefficient for the randomly variable change in the normal stress of the foundation slab in a longitudinal direction measured at +59 mm combined with the values at other heights

Tab. 3: The correlation matrix which describes the statistic dependence of changes in the normal stress in a concrete slab in a longitudinal direction in four heights using the Pearson's (left) and Spearman's (right) correlation coefficient

	59	148	237	325
59	**1**	0.671255	0.548708	0.379817
148		**1**	0.906740	0.894987
237			1	0.906740
325	**sym.**			**1**

	59	148	237	325
59	**1**	0.711119	0.535419	0.307283
148		**1**	0.860507	0.784488
237			**1**	0.860507
325	**sym.**			**1**

Tab. 4: The correlation matrix which describes the statistic dependence of changes in the normal stress in a concrete slab in a transversal direction in three heights using the Pearson's (left) and Spearman's (right) correlation coefficient

	104	192	281
104	**1**	0.443257	0.092120
192		**1**	0.874841
281			**1**

	104	192	281
104	**1**	0.393268	0.094875
192		**1**	0.918306
281			**1**

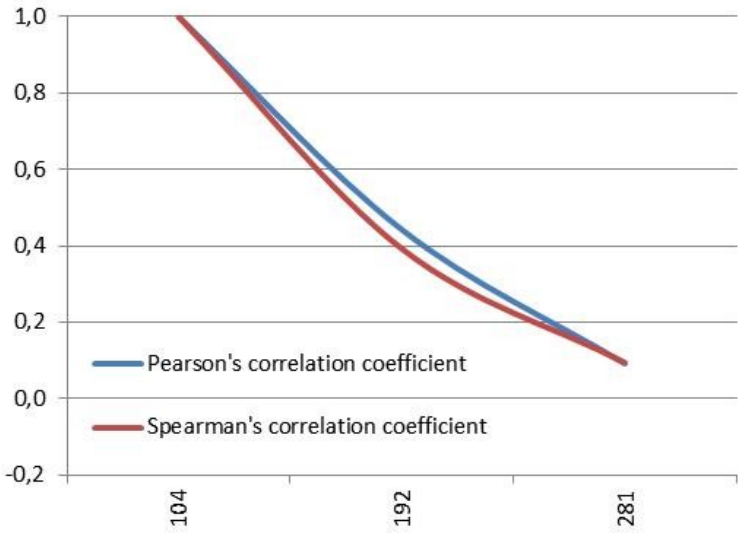

Fig. 10: The Pearson's and Spearman's correlation coefficient for the randomly variable change in the normal stress of the concrete foundation slab in a longitudinal direction measured at +59 mm combined with the values measured at other heights

5.4 Analysing changes in normal stress in reinforcing steel

Five sensors were installed to detect changes in the normal stress in the steel reinforcement of the foundation slab. Results of the statistics and sensitivity analyses are given in Tab. 5 and 6 and in Fig. 11 – it is clear that the measured data are considerably independent in terms of statistics. It would need further investigation to determine whether the reason is the static behaviour of the reinforcing steel during the ageing of concrete in the foundation slab or a too high measurement error which has affected negatively the obtained values.

Tab. 5: The correlation matrix which describes the statistic dependence of changes in the normal stress in reinforcing steel in the concrete slab using five sensors and the Pearson's correlation coefficient

sensor	1	3	4	5	6
1	**1**	−0.326076	0.020921	0.438671	−0.013040
3		**1**	0.659559	−0.267758	0.357575
4			**1**	−0.426226	0.861452
5				**1**	−0.401796
6					**1**

Tab. 6: The correlation matrix which describes the statistic dependence of changes in the normal stress in reinforcing steel in the concrete slab using five sensors and the Spearman's correlation coefficient

sensor	1	3	4	5	6
1	1	−0.340521	−0.244565	0.300965	−0.067029
3		1	0.369197	−0.254437	−0.172053
4			1	−0.541736	0.632246
5				1	−0.290020
6					1

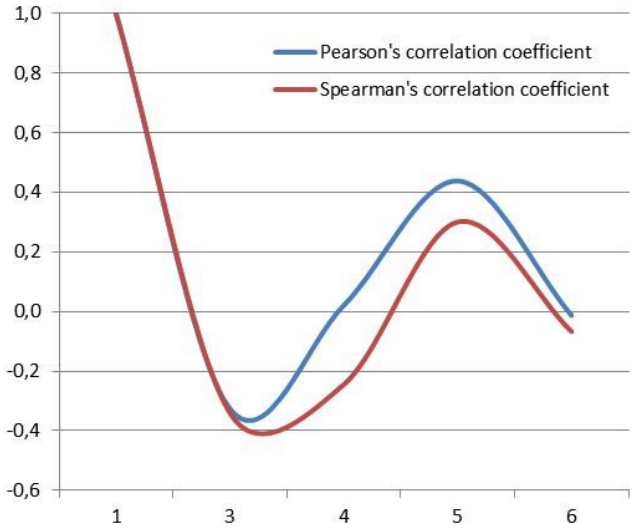

Fig. 11: The Pearson's and Spearman's correlation coefficient for the randomly variable change in the normal stress in reinforcing steel in the foundation slab measured by the sensor #1 combined with the values measured by the sensors #3 through #6

5.5 Analysing the statistic dependence of the dynamic modulus of elasticity of the concrete and compressive cube strength of the concrete

The statistic dependence of the dynamic modulus of elasticity of the concrete and compressive cube strength of the concrete were analysed using the data obtained within non-destructive tests performed by the Laboratory of Building Materials at the Faculty of Civil Engineering, VSB–Technical University Ostrava. The statistic dependence between the two randomly variable quantities can be described again using a pair of correlation

coefficients (the Pearson's and Spearman's correlation coefficient equal to 0.541351 and 0.524191, respective) or using a double histogram, see Fig. 12, which can be used as the input data for DOProC probabilistic calculation.

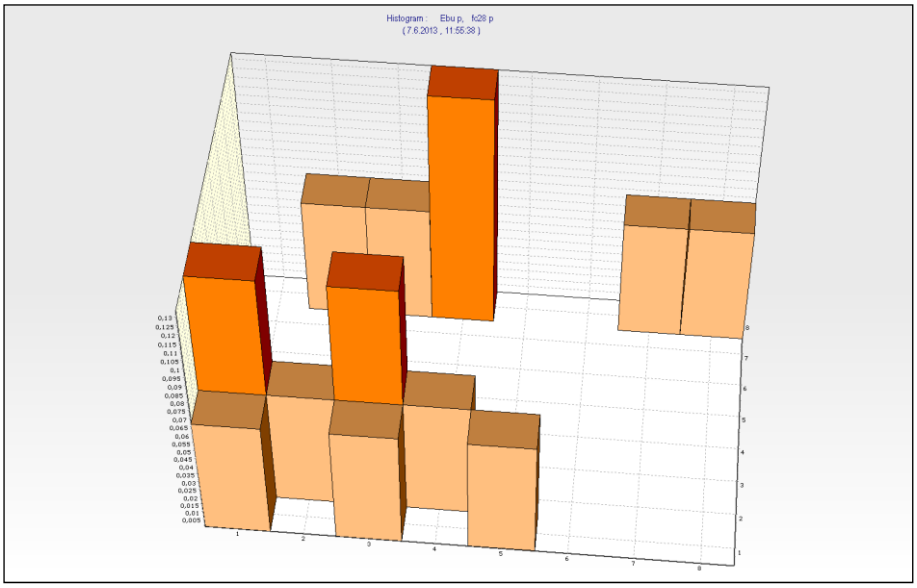

Fig. 12: Desktop of HistAn2D: A double histogram which describes the statistic dependence of the dynamic modulus of elasticity of the concrete and compressive cube strength of the concrete

5.6 Analysing the compressive cube strength

The laboratory, Cemex s.r.o., carried out the destructive tests and determined the compressive cube strength of the concrete samples taken from the foundation slab. The statistical analysis was performed in HistAn software. Results of the analysis included a bounded histogram with empirical distribution of probability (Fig. 13). Considering a limited number of measured points, it is also possible to draw the parametric distribution of probability with the best coefficient of closeness with respect to the obtained data (Fig. 14).

6 Conclusions

The paper dealt with the monitoring of basic material and static features of the foundation slab in the "National Supercomputing Center – IT4 Innovations" during construction works CAJKA ET AL. [6] and with the statistical analysis of the measured data. This has helped considerably to understand behaviour of the load-carrying structure after the concrete was cast. The obtained data have been processed by the ProbCalc software (JANAS ET AL. [9]) within statistics and sensitivity analyses. It has been found out that non-destructive tests of resistivity measurement (resistance of concrete to the passage of electric current) aren't much reliable for measurements of the dynamic modulus of elasticity of the concrete.

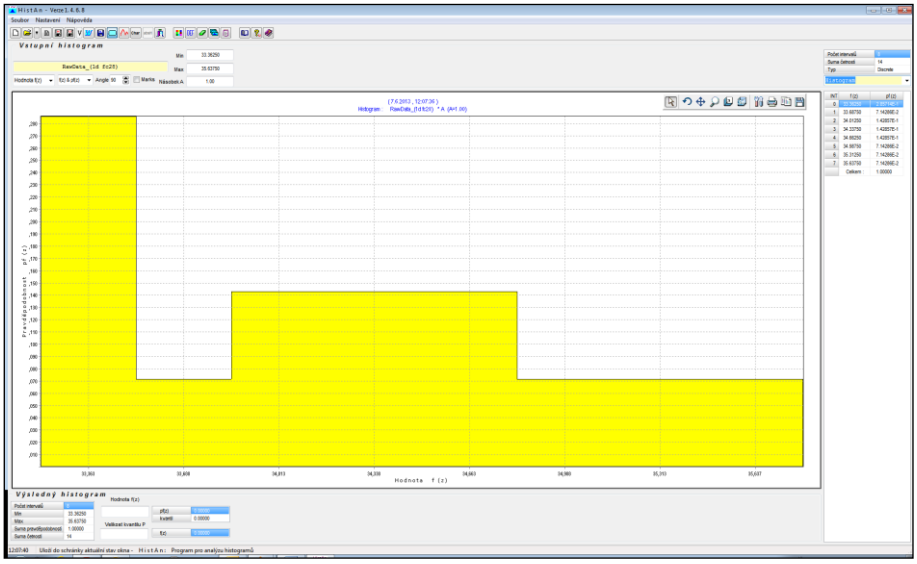

Fig. 13: Desktop of HistAn: The histogram with an empirical (non-parametric) distribution of probability in eight classes which describes the compressive cube strength of the concrete and which was obtained from the values measured in a destructive compression test

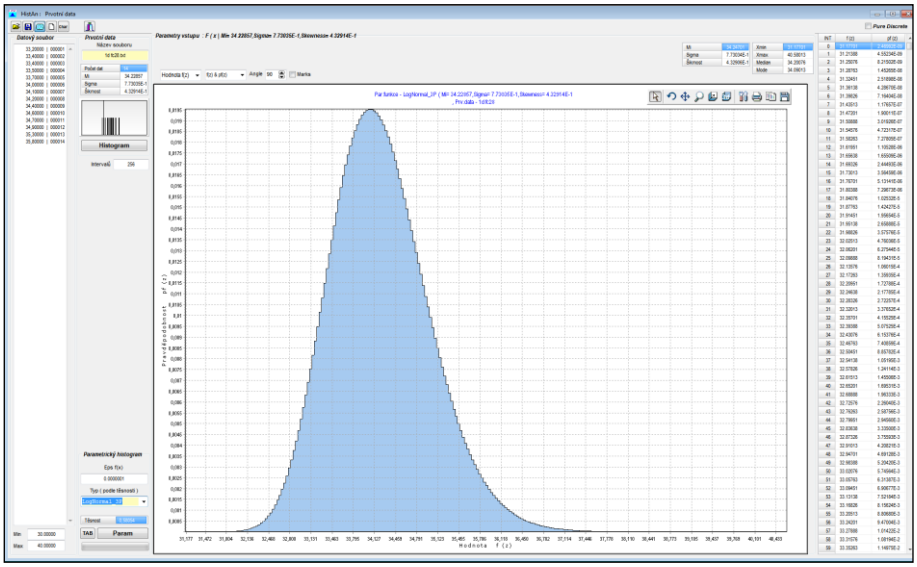

Fig. 14: Desktop of HistAn: The histogram with parametric distribution of probability which describes the compressive cube strength of the concrete obtained by smoothing the measured values with the best parametric distribution curve (three-parameter lognormal distribution)

In the case of other experimental quantities, such as the changes in temperature and stress in the concrete, a rather good correlation has been identified. The bounded histograms were created for the obtained data. They will be used then for the probabilistic modelling of static behaviour of the load-carrying structure. Numerical models will be used there for calculation on non-stationary thermal fields incl. release of hydration heat CAJKA ET AL. [2], CAJKA [5] and influence of a sliding joint CAJKA ET AL.[3], JANULIKOVA ET AL.[15] on the state of stress of the foundation slab which will interact with subsoil CAJKA ET AL.[1], CAJKA [4],[7].

Final comment

The mentioned DOProC techniques with the statistically dependent input variables have been gradually implemented into software HistAn2D, HistAn3D and ProbCalc, which are available to download in light versions at http://www.fast.vsb.cz/popv.

Acknowledgement

This paper has been prepared within the project which has been co-financed from the financial support provided to VSB−Technical University Ostrava by the Czech Ministry of Education, Youth and Sports from the budget for conceptual development of science, research and innovations for the year 2013 and project TIP No. FR-TI2/746.

Literature

[1] Cajka, R., Manasek, P. Building Structures in Danger of Flooding. *IABSE Conference New Delhi, India: Role of Structural Engineers towards Reduction of Poverty*. New Delhi, India, 2005, p. 551–558 (8 p). ISBN 978-3-85748-111-6, WOS: 000245746100072

[2] Cajka, R., Matecková, P. Temperature distribution of slide joint in reinforced concrete foundation structures. In: *Proceedings of 17th International Conference Engineering Mechanics 2011*. 2011, p. 95–98 (4 p). ISBN 978-80-87012-33-8. WOS: 000313492700017

[3] Cajka, R., Mateckova, P., Janulikova, M. Bitumen Sliding Joints for Friction Elimination in Footing Bottom. Switzerland: Trans Tech Publications. *Applied Mechanics and Materials* 188 (2012), p. 247–252 (6 p). ISSN: 1660-9336, ISBN: 978-303785452-5, DOI: 10.4028/www.scientific.net/AMM.188.247

[4] Cajka, R. A Subsoil Model based on Numerical Integration of a Nonlinear Halfspace, in B.H.V. In: *Proceedings of the 8th International Conference on Engineering Computational Technology*. Civil-Comp Press, Stirlingshire, UK, Paper 114, 2012. ISBN 978-1-905088-55-3, DOI: 10.4203/ccp.100.114

[5] Cajka, R. Numerical Solution of Transient Temperature Field of Layered Plane Structures. *In Proceedings of the 3rd International Conference on Mathematical Models for Engineering Science (MMES´12),* WSEAS Press, Paris, France, 2012, p. 29–34 (6 p). ISBN 978-1-61804-141-8

[6] Cajka, R., Fojtik, R. Experimental Measurement of Temperatures and Stresses in the Foundation Slab of National Supercomputer Centre. In: *Proceedings of scientific conference Modelling in mechanics 2013*. VSB−TU Ostrava, Faculty of Civil Engineering, 2013, p. 1–9 (9 p). ISBN 978-80-248-2985-2

[7] Cajka, R. Accuracy of Stress Analysis Using Numerical Integration of Elastic Half-Space. Switzerland: Trans Tech Publications. *Applied Mechanics and Materials* 300-301 (2013), p. 1127–1135 (9 p). ISSN 1660-9336, ISBN 978-303785651-2, DOI: 10.4028/www.scientific.net/AMM.300-301.1127

[8] ČSN EN 12390-3 *Testing hardened concrete* – Part 3: Compressive strength of test specimens, European Committee for Standardization. 2001

[9] Janas, P., Krejsa, M., Krejsa, V. *Software ProbCalc [EXE] − Program System for Probabilistic Reliability Assessment using DOProC method*. Authorized software, Lite version 1.1, 12,4 MB. Reg. num. 003/27-01-2009_SW. VSB−TU Ostrava, 2008

[10] Janas, P., Krejsa, M., Krejsa, V. Assessment Using Direct Determined Probabilistic Calculation. In: *Proceedings of the 12th International Conference on Civil, Structural and Environmental Engineering Computing: CC 2009*. Funchal, Madeira, Portugal. Kippen, Stirlingshire, Scotland: Civil-Comp Press, 2009. ISBN 978-1-905088-31-7. Elsevier B.V., 2012. ISBN 978-190508830-0. DOI: 10.4203/ccp.91.72

[11] Janas, P., Krejsa, M., Krejsa, V. Using the Direct Determined Fully Probabilistic Method (DDFPM) for determination of failure. In: *Proceedings of European Safety and Reliability Conference (ESREL 2009)*: *Reliability, Risk and Safety: Theory and Applications, Vols 1–3, Prague, Czech Republic, 2009*. London: Taylor & Francis Group, 2010, p. 1467–1474 (8 p). ISBN 978-0-415-55509-8. WOS: 000281188500203.

[12] Janas, P., Krejsa, M., Krejsa, V. *Software HistAn2D [EXE] - Program for creating and analyzing2D histograms representing statistical dependence of two random variables*. Authorized software, lite version 1.1, reg. num. 013/03-10-2012_SW. VSB–TU Ostrava, 2012

[13] Janas, P., Krejsa, M., Krejsa, V. *Software HistAn3D [EXE] - Program for creating and analyzing3D histograms representing statistical dependence of tree random variables*. Authorized software, lite version 1.1, reg. num. 014/03-10-2012_SW. VSB–TUOstrava, 2012

[14] Janas, P., Krejsa, M., Krejsa, V. Statistical Dependence of Input Variables in DOProC Method. *Transactions of the VSB - Technical University of Ostrava*: *Construction Series* 12(2) (2012), p. 48–58 (11 p). Warsaw, Poland: Versita. ISSN 1804-4824 (Online); ISSN 1213-1962 (Print). DOI: 10.2478/v10160-012-0017-3

[15] Janulikova, M., Cajka, R., Mateckova, P., Buchta, V. Laboratory Testing of Asphalt Belts Rheological Properties Exposed to Shear Loads. *Transactions of the VSB–Technical University of Ostrava*: *Construction Series* 12(2) (2012), p. 59–66 (8 p). Warsaw, Poland: Versita. ISSN 1804-4824 (Online); ISSN 1213-1962 (Print). DOI: 10.2478/v10160-012-0018-2

[16] Kralik, J. A RSM method for probabilistic nonlinear analysis of reinforced concrete bubbler tower structure integrity. In: *Proceedings of European Safety and Reliability Conference (ESREL 2009): Reliability, Risk and Safety: Theory and Applications, Vols 1–3, Prague, Czech Republic, 2009*. London: Taylor & Francis Group, 2010, p. 1369–1372 (4 p). ISBN 978-0-415-55509-8. WOS: 000281188500188

[17] Krejsa, M., Janas, P., Cajka, R. Using DOProC method in structural reliability assessment. Eds: Ching Kuo Wang and Jing Guo. Zurich, Switzerland: Trans Tech Publications. *Applied Mechanics and Materials: Mechatronics and Applied Mechanics II* 300–301 (2013), p. 860–869 (10 p). ISSN 1660-9336, ISBN 978-303785651-2, DOI: 10.4028/www.scientific.net/AMM.300-301.860

[18] Krejsa, M., Janas, P., Krejsa, V. Direct Optimized Probabilistic Calculation. In: *Recent Advances in Systems Science & Mathematical Modelling: Proceedings of the 3rd International Conference on Mathematical Models for Engineering Science*

(MMES '12). Paris, France: WSEAS Press, North Atlantic University Union, 2012, p. 216–221 (6 p). ISBN 978-1-61804-141-8

[19] Krejsa, M. The Probabilistic Calculating of Fatigue Crack Propagation Using FCProbCalc Program. In: *Proceedings of 18th International Conference Engineering Mechanics 2012*. Prague: The Institute of Theoretical and Applied Mechanics AS CR, 2012, p. 745–754 (10 p). ISBN 978-80-86246-39-0

[20] Krivy, V., Cajka, R. Design and reliability assessment of roof structural elements using the new digital ground snow load map of the Czech Republic. In: *Proceedings of 17th International Conference Engineering Mechanics 2011*. 2011, p. 335–338 (4 p). ISBN 978-80-87012-33-8. WOS: 000313492700077

Assessment of existing reinforced concrete bridges exposed to military loads

Roman Lenner[1], Miroslav Sýkora[2], Manfred Keuser[1]
[1] Institute of Structural Engineering, University of Bundeswehr, Munich
[2] Klokner Institute, Czech Technical University, Prague
roman.lenner@unibw.de, miroslav.sykora@klok.cvut.cz, manfred.keuser@unibw.de

Abstract: This paper aims at establishing methods for assessment of existing reinforced concrete bridges subjected to military traffic by investigating the military loads and at the same time at developing methods for calibratingpartial factor that can be utilized during the assessment. A number of factors regarding the military variable loading must be taken in account − dynamic amplification factor, military load stochastic parameters and model uncertainties. It is shown, that the calculated partial factors are largely dependent on these parameters. Therefore special care is devoted to the proper selection of respective variables and special regard is dedicated to different bridge crossing conditions, which have a significant influence the resulting partial factor.

Keywords: bridge assessment, military load, reinforced concrete, dynamic amplification

1 Introduction

Military vehicles often utilize the bridges built and maintained by civilian authorities. The use of civilian bridges by military vehicles is in the NATO countries regulated and governed by STANAG 2021 [12], however this standard does not fully deliver some of the essential aspects important to safe and reliable crossing of military vehicles over existing bridges. It is a general document that aims at establishing common grounds and language among military engineers within NATO. In the respect of national interests it does not set nor requires any specific procedures or concepts for the classification itself, although in order to ensure a consistent level of safety any used methodology should adhere to the guidelines and minimum outlined criteria. There are no in-depth provisions regarding the safety and more importantly no provided partial factors. It is implicitly assumed that military engineers would utilize the current civilian structural standards published in their respective countries – in most cases utilizing the semi-probabilistic safety concept. However, it is often problematic to use the partial factors originally developed for civilian traffic when performing the analysis with military loads, because, for example, Eurocode [4] and its national versions have never been calibrated for the assessment of existing bridges under military loading.

There are fundamental differences in treatment of bridges under either civilian or under military traffic, identification of these differences is not in the particular scope of this paper, but the most important fact is that military traffic can be much better described in terms of expected load value and its variation. Additionally, civilian traffic load models include dynamic effects, whereas axle loads in STANAG 2021 [12] are listed without any dynamic allowances. It is therefore inconsistent to use partial factors intended for civilian traffic when assessing bridges under military loading.

Considering existing differences between the two models of civilian and military traffic, it is necessary to properly reflect the military traffic on bridges and develop calibrated methods for the bridge assessment under military loading. The aim of this paper is to study the military loading and its aspects such as stochastic parameters, model uncertainty, dynamic load effect and crossing conditions and to develop a suitable concept for existing bridge assessment within the semi-probabilistic safety format.

2 Military traffic

Military traffic is described in terms of defined Military Load Classes (MLC). It is necessary to briefly study the process of military load classification as described in STANAG in order to understand how the partial factors for military use can be developed.

2.1 Military load class

STANAG defines 32 hypothetical Military Load Classes (MLC) − 16 different classes for wheeled vehicles and 16 for tracked vehicles. Each MLC is represented by a hypothetical vehicle with given axle weights and axle spacing for wheeled vehicles, and total weight and length for tracked vehicles (Fig. 1). The mass in "short tons" (907 kg) of each hypothetical tracked vehicle is chosen as the MLC, but the mass of the hypothetical wheeled vehicle is different from its MLC.

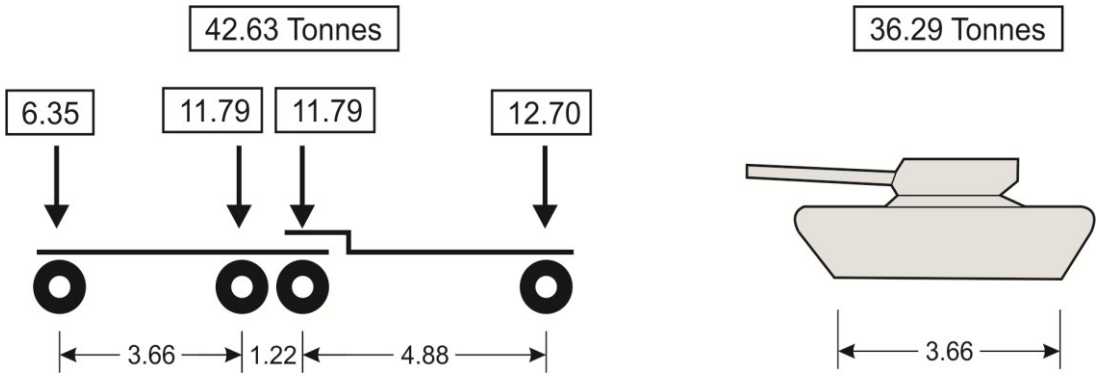

Fig. 1: Example − Wheeled and Tracked MLC 40.

Every single real vehicle used by the military is assigned a certain MLC number. This number then serves as an indicator to which Military Load Class this vehicle belongs. Vehicle MLC number is not assigned on the basis of total weight of the vehicle, but it is rather based on the bending moment produced by the vehicle on a single span. The particular axle loads and axle configuration of each vehicle are therefore key for its MLC classification.

The classification process of any given vehicle begins with measurements of axle loads and spacing and continues with calculation of various bending moments for span lengths between 1 to 100 m. These calculated bending moments are then compared to the tabulated moments resulting from hypothetical MLC vehicles. It is usual that calculated bending moments of real vehicles do not exactly match the numerical values resulting from hypothetical vehicles. It is necessary to interpolate the unit bending moment between the two adjacent classes to obtain a final vehicle MLC number, which is rounded to an integer number.

The specific way of MLC classification process is important, because it provides valuable information about each vehicle used by the military. When compared to a simple classification purely based on weight, the MLC number is much suitable description in terms of expected results. Furthermore, the separation in many different classes allows for much narrower division and more accurate description of loads. More importantly, such defined loads are time-invariant – vehicles might get larger or heavier, but that would only result in assignment of a higher MLC class. This means prediction of possible future traffic loads is in end effect unnecessary.

2.2 Crossing conditions

In addition to defining the MLC the STANAG 2021 [12] also provides regulation regarding different modes of crossing of military vehicles over bridges. This is to ensure potential maximizing of the allowable load by minimizing load effects resulting from load positioning, dynamic impact and dynamic amplification when dictated by certain tactical or emergency situations, where crossing of vehicles with higher MLC is necessary. This is accomplished by either more controlled crossing conditions or relaxed safety criteria.

2.2.1 Normal crossing

The normal crossing condition is the main crossing mode and should be regarded as standard for the assessment if not stated otherwise. The minimum criteria for safety outlined in STANAG are valid for this condition. A normal crossing allows for an unrestricted use of bridge by military traffic and for all vehicles or convoys operating at or below the maximum allowable MLC. Only rating associated with the normal crossing may be permanently assigned to a bridge.

2.2.2 Caution crossing

While maintaining the same safety level as for the normal crossing, the caution crossing allows for a higher allowable MLC by limiting the maximum speed to 5 km/h and restricting the use of braking, accelerating and switching gears. Vehicles must drive along the centreline and are only allowed to cross one at a time across each structurally independent span. Rating associated with the caution crossing may be only regarded as temporary.

2.2.3 Risk crossing

Risk crossing allows for transportation of higher MLC vehicles by adapting the same conditions as the caution crossing (speed up to 5 km/h, single vehicle at the centreline of an independent span, no braking, accelerating and changing gears), but additionally decreasing a minimum required safety. It greatly increases the probability of failure, and even if the bridge does not fail, permanent damage to the bridge may occur.

3 Military bridge assessment

During military bridge assessment each structure receives an MLC number corresponding to a maximum allowable load effect resulting from a defined STANAG class. A bridge MLC number is assigned on the basis of load capacity calculations resulting from the traditional semi-probabilistic concept in the ultimate limit state, where appropriate partial factors are applied to both loads and resistance variables. It is hereafter assumed that loads and resistances can be treated separately (which may not be the case e.g. for geotechnical structures).

The variable action for the calculations is represented by the hypothetical MLC vehicle. No provisions for mixed civilian and military traffic on a bridge are available. In this study it is assumed that civilian traffic is not present when military vehicles are crossing the bridge under consideration. In addition to the case of a single standard vehicle on the bridge, an indefinitely long column of vehicles spaced at a minimum distance of 30.5 m is taken in account. This is particularly important for bending moments in multi-span structures. Shear force is always governed by the maximum number of vehicles that can be present on a single span.

3.1 Partial factor definition

In a semi-probabilistic safety concept a set of partial factors γ resulting from probabilistic analysis serves to achieve certain reliability level for any structure of interest. The design value for variable action Q_d, or the value required for assessment in the ultimate limit state, can be obtained from the characteristic value Q_k as follows:

$$Q_d = \gamma_Q \cdot Q_k , \tag{1}$$

where γ_Q is the partial factor for variable action that can in turn be defined as (CASPEELE ET AL. [2]):

$$\gamma_Q = \gamma_{Ed,q} \cdot \gamma_q , \tag{2}$$

where $\gamma_{Ed,q}$ stands for partial factor accounting for the model uncertainty in estimation of the load effect from the load model; γ_q is reliability-based partial factor accounting for the variability of variable action, statistical uncertainty and uncertainties related to the model of variable action.

As discussed in Introduction, during the military assessment γ_Q is generally taken from the current bridge standards. Problematic is that the factor was developed using substantially different properties and assumptions on effects of traffic loads. Main differences between the civilian and military approach are summarized below:

1. The civilian loading (based on observations on European highways [6]) is described rather generally by loading models developed to represent the complete actual and predicted traffic. The military loading is assigned a defined time-invariant MLC and therefore the expected traffic can be captured more accurately.
2. Civilian codes usually assume design life ranging from 50 to 100 years. For military needs such a time frame is in many cases impractical as it depends on a number of factors, such as location, strategic and tactical significance or purpose of

assessment. These conditions dictate the expected time frame, which is in many cases significantly less than 50 to 100 years.

3. Dynamic effects are included in traffic models in current bridge codes; no dynamic allowances are provided in STANAG.
4. The characteristic value of civilian traffic load corresponds a 1000-year return period (EN 1991-2 [4]) while a nominal (mean) value is considered for military vehicles; considerable reliability margin is thus included already in the characteristic value of civilian traffic load.

It is therefore proposed to assess the design load effect of military traffic Q_d as follows:

$$Q_d = \gamma_Q \cdot Q_{MLC}, \tag{3}$$

where the characteristic load effect Q_{MLC} is defined as bridge $MLC_{\max}$, or as the upper limit of the maximum load effect resulting from a hypothetical STANAG MLC.

During a period considered for the reliability analysis,*n* potentially different MLC vehicles (MLC 32, 36 etc.) can pass bridge. This will lead to a set of *n* load effects *Q* (such as bending moments or shear forces). For sufficiently large *n* the expected load effect Q_{MLC} converges to the limiting value $MLC_{\max}$ for a vehicle still within the maximal allowable MLC. For purposes of this paper Q_{MLC} is conservatively taken as $MLC_{\max}$, which is equal to the load effect value resulting from maximum allowable hypothetical MLC.

It is hereafter assumed that the load effect due to the passage of military vehicle(s) *Q* can be obtained as follows:

$$Q = \theta_E \delta Q_{\mathrm{MLC}}, \tag{4}$$

where θ_E denotes the model uncertainty in estimation of the load effect from the load model, $\delta$is a dynamic amplification factor and Q_{MLC} is a static load effect as defined above (including uncertainties in measurements of weights and spacing).

It is further realistically assumed that mean values of the basic variables included in relationship (4) equal to their characteristic values. Assuming lognormally distributed θ_E and $\delta$and a normal distribution of Q_{MLC}, a lognormal distribution can be considered for the load effect *Q* since greater variability is commonly associated with bothθ_E and δrather than with a well-described Q_{MLC}. Based on these assumptions partial factor γ_Q can be written as:

$$\gamma_Q = \exp(-\alpha_E \cdot \beta \cdot V_Q), \tag{5}$$

where $\alpha_E \approx -0.7$ denotes the FORM sensitivity factor approximated in accordance with EN 1990 [3], β target reliability index and V_Q coefficient of variation of *Q* obtained as follows:

$$V_Q \approx \sqrt{V_\theta^2 + V_\delta^2 + V_{Q\mathrm{MLC}}^2}, \tag{6}$$

where V_θ, V_δ and $V_{Q\mathrm{MLC}}$ are the coefficients of variation of model uncertainty, dynamic amplification and of military static load effect, respectively.

3.2 Load effect

Extensive numerical simulations were performed in order to determine a realistic coefficient of variation $V_{Q\mathrm{MLC}}$ for military vehicles and traffic. Traditionally, for estimation of traffic models, civilian vehicular traffic is measured by using for example Weight-in-Motion technology. Stochastic traffic models can thus be extrapolated. However, this method is deemed difficult to implement for military traffic, because there are virtually no situations where only military vehicles are allowed during the time necessary to collect enough of diverse data. Additionally, military vehicles are divided in many different classes and it is difficult to assign stochastic data to a single class based on a general data sample.

Numerical simulation methods, as presented in LENNER ET AL. [11], were employed in order to simulate the effect of uncertainty related to the measurements of axle load and spacing and of the influence on the resulting bending moment. In other words the purpose of the simulation was to show how well the assigned MLC number actually represents the expected bending moment on a single span.

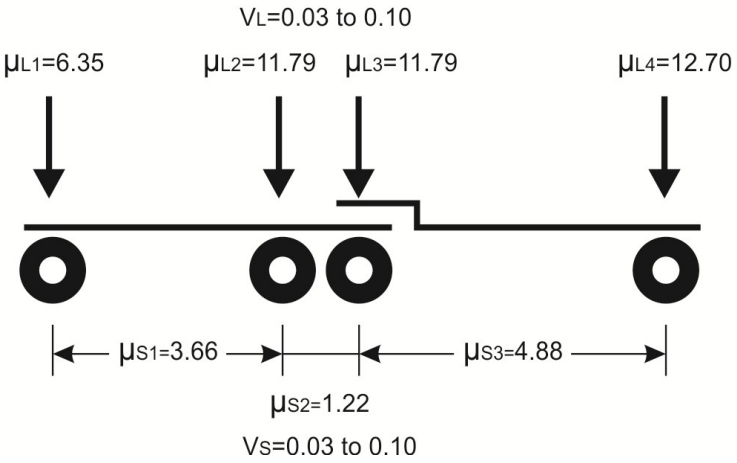

Fig. 2: Model of MLC40 in terms of mean values and coefficients of variation

As an example, load effect of a vehicle MLC 40 (Fig. 2) was analysed. Each axle load L_i and axle spacing S_i ($i = 1..n_{\mathrm{sim}}$) were n_{sim} times generated as identically distributed, independent normal variables with:

- Mean values μ equal to theload due to a hypothetical STANAG vehicle and
- Coefficients of variation V_L for axle load and V_S for axle spacing ranging from 3 % to 10 %; these limits were selected in order to study the sensitivity of results and to introduce realistic values that would represent uncertainty associated with measurements of axle loads and spacing.

The maximum resulting bending moments for each set of L_i and S_i were calculated for different span lengths – 5 to 60 meters for a single vehicle. Mean value Q_{MLC} and coefficient of variation $V_{Q\mathrm{MLC}}$ are then easily obtained from the data sets of each span length.

Exemplarily results for $V_{Q\mathrm{MLC}}$ are plotted in Fig. 3 for different span lengths. In the case of exceptionally short spans (< 5 m) the bending moment is governed by a single axle response and therefore $V_{Q\mathrm{MLC}}$ is directly tied to the value of V_L.

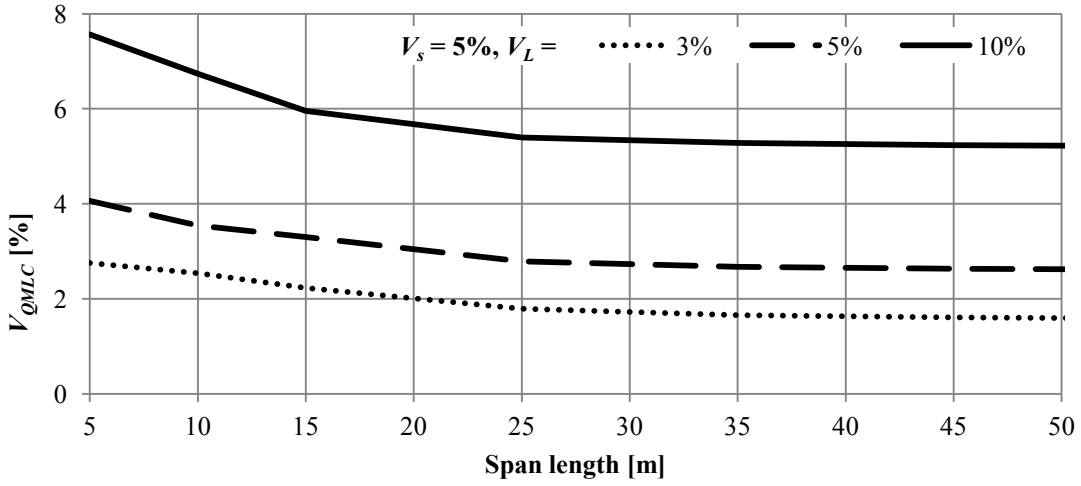

Fig. 3: $V_{Q\mathrm{MLC}}$ for constant V_S and variable V_L

Depending on the actual measurement accuracy of both load and axle spacing, the range of $V_{Q\mathrm{MLC}}$ from 3 % to 5 % is considered in this paper to describe the most of practical situations.

3.3 Dynamic amplification

In general dynamic effect of traffic load is influencedby number of factors, such as maximal bridge span length, bridge natural frequency, vehicle weight, axle loads, axle configuration, position of a vehicle on the bridge, quality of pavement, stiffness of structural members etc. Considerable differences exist between different approaches in capturing the dynamic effects and there is no consensus among the scientific community. However, generally, large contribution may be attributed to vibrations of the vehicle induced by the road profile roughness (PRATT [14]) and surface unevenness between the approach and the bridge deck.

The most accurate way to determine a dynamic amplification factor δ is to use full-scale dynamic bridge testing under controlled or normal traffic conditions. However, this approach is unsuitable for the purposes of military traffic assessment, since it is aimed at a single specific bridge and usually can envelop only limited vehicle dynamic characteristics, thus is difficult to be related to general bridge assessment under military loading. A general approach used in the earlier yearwas to tie the bridge span length to the dynamic amplification value, but PAULTRE [13] notes that it has been recently replaced by therelationship betweenthe dynamic responseand the natural frequency of bridge, if the frequency is known.

A number of recent studies were able to relate the increased static loading to lower value of δ, COUSSY ET AL. [3], HWANG AND NOWAK [8]. At the maximum (critical) loading level the dynamic component of the total load effect is small and well below the levels specified in the design codes. Lightly loaded vehicles may produce comparably higher dynamic amplifications, but at low static load effect and therefore are generally disregarded in determination of δ. Another important fact regarding the static loading is that the increase of this loading produces a reduction in variability of the dynamic amplification as shown in GONZALES [7].

The review of literature does not provide a single value for dynamic amplification that could be used. The dynamic amplification factor varies from country to country due to different assumptions and test outcomes. Within the ARCHES project [1] a number of bridges were tested. For heavy loads and smooth roadway the amplification factors remained typically below 1.1, but unevenness of the bridge approach or damaged roadway surface may lead to higher values.

The partial factor γ_Q, a primary concern of this study, is affected by the ratio of the mean to the nominal (characteristic) value of δ and its coefficient of variation rather than by an absolute magnitude of δ. That is why it may be acceptable to assess δ in a simplified manner on the basis of the ratio between themaximum static loading and total load effect. Furthermore the dynamic amplification factor is assumed to be independent of bridge natural frequencies.

To summarize the considered procedure is assumed unbiased, i.e. the mean value of δ equals to its nominal value. With reference to ARCHES [1] and considering lower variability associated with maximum static loading,the coefficient of variation $V_\delta = 0.05$ is conservatively accepted here for the normal crossing condition.

STANAG 2021 [12] indicates that different amplification factors δ may be utilized for different crossing modes. GONZALES [7] suggests that vehicular speeds between 5−15 km/h are sufficiently low to consider the loading as quasi-static. Therefore,the dynamic amplification factor needs not to be applied. This is relevant for the two controlled crossing conditions – caution and risk. STANAG 2021 [12] also supports this by stating that the "impact factor is not required" for thesetwo types of conditions. The δ values need to be further investigated.

3.4 Model uncertainty

According to the JCSS PROBABILISTIC MODEL CODE [10] model uncertainty is generally a random variable accounting for effects neglected in the models and simplifications in the mathematical relations. Model uncertainty in the load effect θ_E should cover numerous aspects including idealization of supports, composite actions of structural members, computational options, description of input data etc. JCSS further recommends a lognormal distribution of θ_E with a unity mean; the following values of $V_{\theta E}$ are indicated:

- $V_{\theta E} = 0.05$ for axial forces in frames,
- $V_{\theta E} = 0.1$ for moments and shear forces in frames and forces in plates,
- $V_{\theta E} = 0.2$ for moments in plates.

Appropriate model for the model uncertainty should be selected considering bridge-specific conditions. For bridges with apparent static behaviour the model uncertainty θ_E can be even neglected. In further numerical studies $V_{\theta E}$ is considered in the range from 0 to 0.1.

Crossing conditions can certainly influence the model uncertainty with the respect of static response of the superstructure. More controlled crossing along the centreline of theway at a lower speed should provide more predictable response and therefore reduce the model uncertainty.

3.5 Target reliability

In accordance with ISO 13822 [9]the target reliability index β for assessment of existing structures can be adjusted by optimisation of the total cost related to an assumed remaining working life, SÝKORA AND HOLICKÝ [15] and VROUWENVELDER AND SCHOLTEN [17]. More recent study by SÝKORA ET AL. [16] shows the modification of target reliability factor for emergency situation.The obtained values,ranging mostly from 2.0 up to 3.5, are clearly lower then values provided in structural codes for new structures [4].

With regards to the military loading and crossing conditions it is therefore possible to modify the target reliability to reflect:

- Actual conditions of a fixed civilian bridge,
- Reliabilityrequired for each crossing conditions,
- Minimum human safety (regarding users of the bridge as well as safety of people endangered by closure of the bridge).

STANAG 2021 requires that normal and cautious crossing reflect the same degree of safety, or another words − are based on the same reliability level. Risk crossing can be associated with higher probability failure. This suggests that the β should be adjusted − decreased considering case-specific conditions.

In this study β equal to 3.8 (the fundamental value of the target reliability index considered in derivation of the partial factors in Eurocodes [4]) is associated with the normal and caution crossing. For the risk crossing β in the range of 2.0−3.5 as suggested by SÝKORA ET AL. [16] is considered.

4 Partial factor for military loading

Resulting partial factor γ_Q is calculated according to Eq. (5). Particular parameters considered in the analysis are summarized in Tab. 1 according to respective crossing conditions.

Since the specific target reliability values for existing bridges under military loading are out of scope of this paper, Fig. 4 shows the relationship between the partial factor γ_Q and different β values with regard to different crossing conditions and variables from Tab. 1.

Tab. 1: Parameters considered in the analysis of the partial factor γ_Q

	Normal	Caution	Risk
Characteristic Load Effect Q_{MLC}	$MLC_{\max}$	$MLC_{\max}$	$MLC_{\max}$
Coefficient of variation $V_{Q\mathrm{MLC}}$	0.05	0.05	0.05
Model Uncertainty θ_E	1.0	1.0	1.0
Coefficient of variation $V_{\theta E}$	0.1	0.075	0.05
Dynamic amplification factor δ	1.1−1.3	1.0	1.0
Coefficient of variation V_δ	0.05	0	0.0
Coefficient of variation V_Q (6)	0.12	0.09	0.07

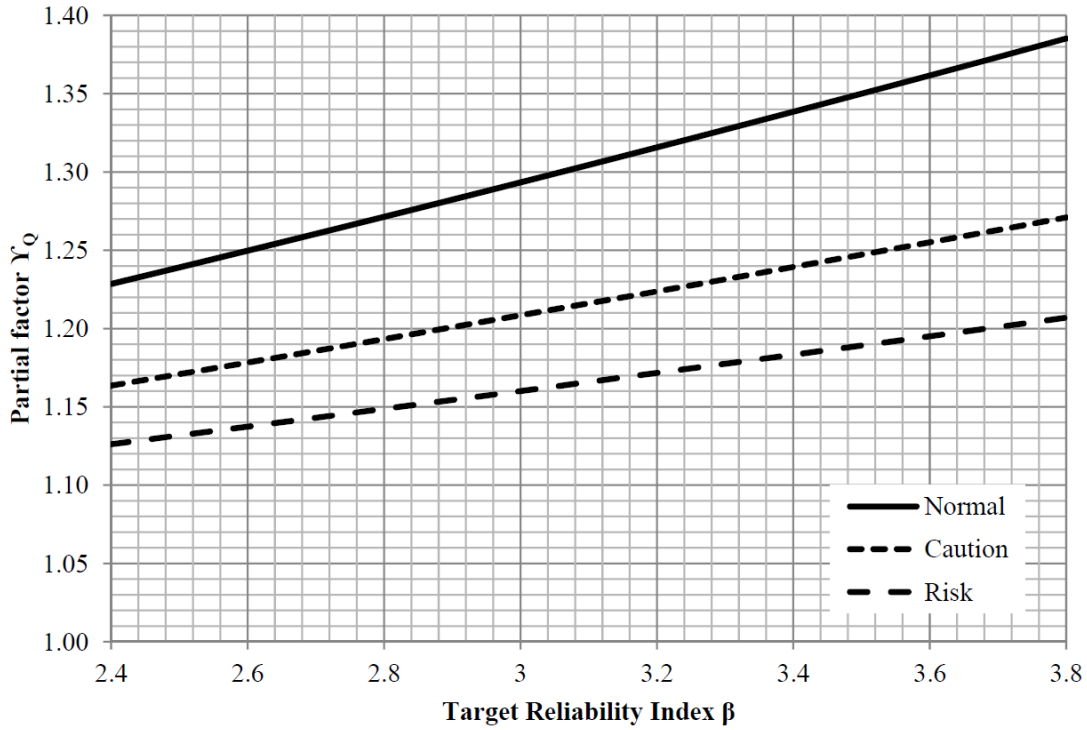

Fig. 4: Partial factor γ_Q for different crossing conditions according to Eq. (5)

The load effect coefficient of variation V_Q influences the particular slope value of the curve describing for each crossing condition the relationship between the partial factor γ_Q and target reliability index β, indicating the influence of the reliability index on the resulting factor. At the same time larger V_Q produces a higher partial factor.

It is apparent that the normal crossing is tied to the higher value of the required partial factor as mandated by the conditions specified in Tab. 1.The relaxed criteria in terms of dynamic amplification and model uncertainty for caution and risk crossing allow for a lower partial factor while maintaining the same reliability level as normal crossing.

The chosen β as 3.8 for study purposes indicates the appropriate values of partial factors for both normal and caution crossing in the range 1.25 to 1.40. The resulting value is however largely influenced by the exact selection of the target reliability level, as can be observed from nature of the curves.

Risk crossing is to be associated with a lower reliability level and therefore the partial factor associated with this crossing mode can be determined in the range of 1.10 to 1.15 as the slope is seemingly constant and a change in target reliability does not significantly influence the resulting partial factor.

5 Conclusion

Current partial factors for load effects in Eurocodes are not optimal for reliability verifications of existing bridges under military loads. Modification for specific military use is deemed necessary and a number of different factors must be taken in account in the calibration process. This paper investigated some of the most important aspects affecting the partial factor for military traffic load. The numerical simulation served to investigate sto-

chastic properties of the military load and along with dynamic amplification and model uncertainty allowed for indication of appropriate values of the partial factor.

It is observed that particularly important variable influencing the partial factor is the model uncertainty in load effect. In addition considerable differences in the definition of characteristic value for civilian and military traffic loads affect the value of the partial factor for traffic load. Characteristic civilian traffic is broadly defined with a large return period while a mean value of well-defined military traffic is taken into account. Numerical part of the study indicates that the partial factor of the military traffic load can range from 1.1 up to 1.4 depending on the chosen stochastic properties and a selected target reliability level dependent on crossing conditions.

Dynamic amplification certainly deserves additional work, there is no consensus regarding the specific values of dynamic amplification factor and most of the work was aimed at civilian traffic. Further investigation should be also aimed at improvements of the model for uncertainties in a traffic load effect and the development of partial factors for mixed military and civilian traffic on the bridge.

Acknowledgements

The study is based on outcomes of the research projects Neue Berechnungsverfahren zur Brückenbelastbarkeit Nr.: E/KR2G/7A026/7F152 supported by the Federal Office of Defense Technology and Procurement in Germany and VG20122015089 supported by the Ministry of the Interior of the Czech Republic.

Literature

[1] ARCHES, Assessment and Rehabilitation of Central European Highway Structures, Deliverable D 15, Final Activity Report, ARCHES-MG-AR04, 2009.

[2] Caspeele, R., Allaix, D.L., Steenbergen, R.D.J.M., Sykora, M. On a partial factor approach for existing concrete structures: the Design Value Approach and Adjusted Partial Factor Method (accepted for publication). *Structural Engineering International* (2013)

[3] Coussy, O., Said, M., Van Hoore, J.P. The influence of random surface irregularities on the dynamic response of bridges under suspended moving load. *Journal of Sound and Vibration* 130(2) (1989), p. 313–320.

[4] EN 1990. Eurocode – Basis of structural design. CEN, 2002

[5] EN 1991-2. *Actions on Structures – Part 2:Traffic loads on bridges.* DIN Deutsches Institut für Normung e. V., 2010

[6] Hintergrundbericht zum Eurocode 1 – Teil 3.2: "Verkehrlasten auf Straßenbrücken". *Forschung Straßenbau und Straßenverkehrstechnik* 711 (1995)

[7] Gonzales, A., Dowling, J., O´Brian, E.J., Znidaric, A. Experimental determination of dynamic allowance for traffic loading in bridges, *Transportation Research Board 89th Annual Meeting Compendium of Papers*. 2010

[8] Hwang, E.S., Nowak, A.S. Simulation of dynamic load for bridges. *ASCE Journal of Structural Engineering* 113(9) (1991), p. 1413–1434

[9] ISO 13822. Bases for design of structures − Assessment of existing structures. ISO, 2010

[10] *JCSS Probabilistic Model Code.* Zurich: Joint Committee on Structural Safety, 2001 <www.jcss.byg.dtu.dk>

[11] Lenner, R., Sykora, M., Keuser, M. Partial factors for military loads on bridges. In: Krivanek, V.; Stefek, A. (eds.): *Proc. ICMT'13,* Brno, 22−23 May 2013. Brno: University of Defence, 2013, p. 409–418

[12] NATO Standardisation Agreement (STANAG) 2021: Military Load Classification of Bridges, Ferries, Rafts and Vehicles. Edition 6

[13] Paultre, P., Chaallal, O., Proulx, J. Bridge dynamics and dynamic amplification factors – a review of analytical and experimental findings. *Canadian Journal of Civil Engineering* 19(2) (1992), p. 260–278

[14] Pratt, M. Traffic load models for bridge design: recent developments and research. *Prog Struct Engng Mater* 3(4) (2001), p. 326–334

[15] Sýkora, M., Holický M. Target reliability levels for the assessment of existing structures – case study. In Strauss, A., Bergmeister, K., Frangopol, D.M. (eds.) *Proceedings of the 3th International Symposium on Life-Cycle Civil Engineering (IALCCE 2012)*. Vienna, Austria, 3−6 October 2012. Leiden: CRC Press/Balkema, 2012, p. 813–820

[16] Sýkora, M., Lenner, R., Maňas, P. Optimum target reliability for bridges considering emergency situations (accepted for publication). In: *Proc. 11th IPW*, Brno, 2013

[17] Vrouwenvelder, A.C.W.M., Scholten, N. Assessment Criteria for Existing Structures. *Structural Engineering International* 20 (2010), p. 62–65

Algorithms for optimal risk-based planning of inspections using influence diagrams

Jesus Luque & Daniel Straub
Engineering Risk Analysis Group, Technische Universität München, Germany
jesus.luque@tum.de, straub@tum.de

Abstract: Risk-based optimization of inspection using influence diagrams is investigated. To this end, a fatigue deterioration model using a Dynamic Bayesian Network (DBN) approach is presented. The DBN incorporates information from previous inspection campaigns. Decision and utility nodes are defined inside the network to represent inspection and repair activities. The optimal inspection strategy (subject to safety or utility constraints) is approximated using the Limited Memory Influence Diagram (LIMID) approach, and is solved using the single policy updating, a local optimization strategy. In a numerical investigation, this method is found to give solutions that are slightly better than those obtained with simple heuristics that were previously applied, such the reliability threshold or periodic inspection heuristic. Finally, the numerical example demonstrates the superiority of adaptive inspection strategies, whereby inspections are planned based on the results of previous inspections.

Keywords: optimal inspections, Bayesian network, decision models, fatigue, influence diagrams.

1 Introduction

Deterioration processes, in particular fatigue and corrosion, lead to a reduction of the reliability of structural systems. Because deterioration processes are commonly associated with significant uncertainty, inspection and monitoring are often an effective means to increase the reliability. Based on the results of inspections, repair and replacement actions can be planned. This is known as condition-based maintenance [11].

The uncertainty in deterioration processes is commonly represented through probabilistic models, comprising of deterministic deterioration models whose parameters are represented by random variables. In order to assess the effect of different inspection and/or monitoring strategies, their expected costs, including the risk associated with potential failures, can be computed and compared. This is commonly known as risk-based planning of inspection and monitoring [9] and is a special case of the pre-posterior analysis of the Bayesian decision theory [3], [6]. The computation of the expected costs for a given inspection strategy requires integration over the entire outcome space of all random variables in the deterioration model as well as over all possible inspection outcomes. This is a com-

putationally demanding problem. In addition, to compute the expected cost it is also necessary to include (and optimize) the maintenance and repair actions into the analysis. Since the number of potential alternative inspection and monitoring strategies is very large, solving the complete optimization problem is thus computationally intractable for realistic applications. For this reason, different heuristics (e.g. [9], [5]) have been developed in order to approximate the optimal solution, including periodic inspections (PI) and reliability threshold (RT). More recently, the use of the limited memory influence diagram (LIMID) was suggested by NIELSEN & SØRENSEN [5].

In this paper, we present and compare different algorithms for the optimal planning of inspections in a structural element subject to fatigue deterioration. The fatigue crack growth process is represented through a dynamic Bayesian network (DBN). The optimization parameters are the times of inspections and times of repair actions. This decision problem is modelled as an influence diagram. Besides the classical PI and RT heuristics, we investigate two alternative formulations of the problem as a LIMID. We find that the LIMID outperforms the classical approaches, but also has increased computational demands. However, the complexity of the LIMID algorithm is shown to be of similar order than PI and RT. It is thus a viable alternative, which is particularly promising for planning inspections in systems, where the number of decision alternatives is much larger and simple heuristics such as PI and RT are not available.

2 Dynamic Bayesian networks and influence diagrams

2.1 Bayesian networks

A Bayesian network (BN) is a probabilistic model. It consists of a set of random variables (nodes) and directed links which form a directed acyclic graph (DAG), i.e. there is no directed path from any variable to itself. A discrete BN furthermore fulfils the following requisites [2]:

- Each variable has a finite domain.
- To each variable X with parents Y_1, Y_2, …, Y_N is attached a conditional probability table $p(x|y_1, y_2, \dots, y_N) = \Pr(X = x|Y_1 = y_1 \cap \dots \cap Y_N = y_N)$. Y_i is called a parent of X if it has a link towards X. If a variable has no parents, the table corresponds to its unconditional probability mass function (PMF).

In Fig. 1, exemplarily a simple BN representing the condition of a structural element before and after applying a load is shown. The condition of the element is represented by a_0 and a_1, the damage size (crack depth) before and after the application of load L_1, respectively. Variable Z_1 represents a possible inspection outcome of the condition a_1 in case an inspection is carried out. Nodes a_0 and L_1 are described by unconditional PMFs. The probability table of a_1 contains the PMFs of the damage size conditional on the previous damage size a_0 and the load L_1. The probability table attached to Z_1 describes the likelihood of the inspection outcome, i.e. the probability of an observation (e.g. detect damage) given the condition a_1.

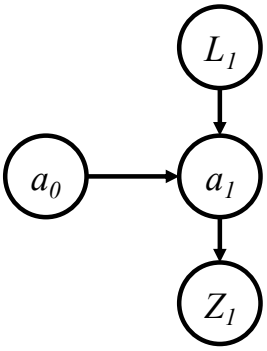

Fig. 1: Example of a Bayesian network

If the states of some variables are known (i.e. instantiated) in the BN, the PMFs of the remaining nodes can be updated to their posterior. For example, in the BN of Fig. 1, an inspection outcome Z_1 can be included by instantiating the corresponding node with the observed state z_1, e.g. no detection of a defect. The PMFs of the remaining nodes a_0, a_1, and L_1 are then updated to their conditional PMF given z_1. This ability to efficiently perform Bayesian updating makes BNs suitable for modeling deterioration processes when partial observations from inspections and monitoring are to be included [8].

2.2 Dynamic Bayesian networks

In some cases, BNs contain a repetitive sequence of nodes which are associated with multiple times or spatial locations. Such a BN is called dynamic Bayesian network (DBN) and is useful for modeling time-dependent processes, including structural deterioration [8]. Extending the BN of Fig. 1 to multiple loads L_t, conditions a_t, and observations Z_t at times $t = 1, \dots, T$ the DBN shown in Fig. 2 is obtained.

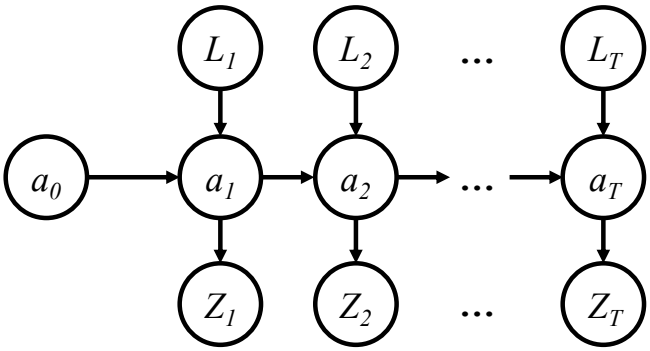

Fig. 2: Example of a dynamic Bayesian network

2.3 Influence diagrams

BNs can be extended to influence diagrams (ID), which additionally include decisions and utility (cost). In the ID, decisions are shown as squared nodes and utilities as diamond-shaped nodes. In the latter, a utility value is assigned to each combination of states of the parents nodes, which can be either random variables or decision nodes, but not utility nodes. In case there are several utility nodes, the total utility is the sum of the individual utilities. In the ID, the optimal decision is the one that maximizes the total expected utility, in agreement with classical decision analysis [6].

The decision nodes describe different decision options, which influence the random variables that are children of the decision node. This influence is quantified through the conditional PMF of these child nodes. Links pointing towards the decision nodes represent the available information at the time of making the decision. All parents of the decision nodes are known when making the decision. However, there exist different versions of IDs, which differ in the way information is handled. Often, the ID is based on the no-forgetting assumption: When making a decision, all previous decisions as well as previous observations are known. This requires that there is a temporal ordering of the decisions. The no-forgetting assumption leads to significant computational demands. For this reason, the limited memory ID (LIMID) was introduced, which makes an explicit link between the nodes that are known before taking the decision and the decision node [4]. In the LIMID, only the direct parents of a decision node are known at the time of making the decision. This reduces (or limits) the number of nodes that will be considered for the decision, decreases the size of the policy domain and facilitates the obtaining of the optimal strategy that gives the maximum expected utility. In this paper, we use LIMIDs to represent the inspection and repair decision processes.

Fig. 3 shows an example ID for the deterioration example presented earlier as a DBN in Fig. 2. Here, the decisions R_t are included on whether or not to repair the structural element at times $t = 1, \dots, T$. These decisions are made based on the result of the inspections Z_t, hence the links $Z_t \rightarrow R_t$. To differentiate the condition of the element before and after the repair, the nodes a_t' are introduced. The conditional PMF of these nodes are identical to that of a_t in case no repair is carried out, and they differ if a repair is carried out. The utilities $U_{R,t}$ are the (negative) cost of repairs and the utilities $U_{F,t}$ are the cost associated with failure at time t. The last slice does not include a repair decision, since such an action would be pointless at the end of the service life.

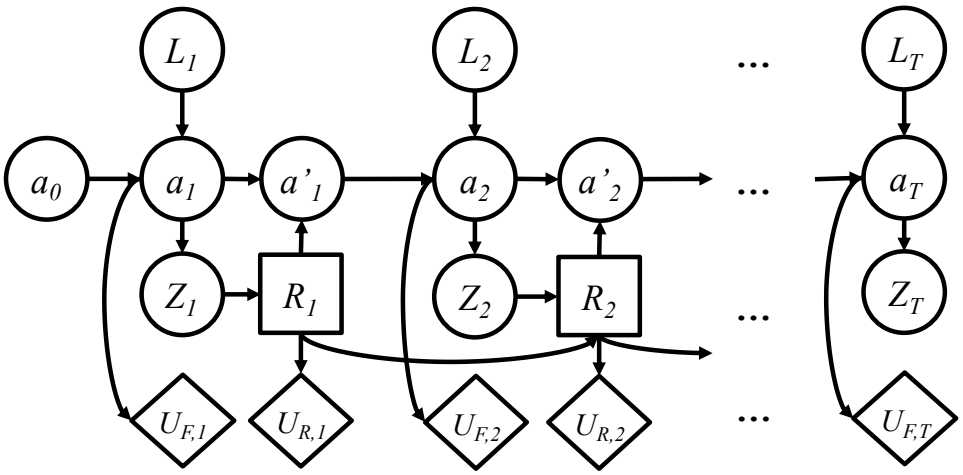

Fig. 3: ID of the multi-decision structure condition example

2.4 Policies and strategies

In the ID, decisions are taken based on information available when making that decision. In the LIMID, these are the nodes with links pointing to the decision node. A policy consists of a set of rules defining which decision to take as a function of the available information. The more information is used for making a decision, the larger the policy domain

and consequently the computational demand. A set of policies of all decision nodes in the ID is called a strategy.

3 Risk-based planning of inspections using influence diagrams for a structural element subject to fatigue

In condition-based maintenance of structures, it has to be decided when, where and how to inspect. Here we restrict ourselves to finding optimal decisions on when to inspect, and we present IDs to solve this problem. The optimal inspection strategy is defined as the one that minimizes the expected cost, defined as the sum of inspection, repair and failure cost. Note that the expected cost of failure is the risk.

For the numerical investigation, a structural element subject to fatigue deterioration is considered. Inspections are possible in each year of the service life, potentially followed by repair actions in case of adverse inspection outcomes.

3.1 Fatigue crack growth model

To model the fatigue crack growth, we consider a simplified case corresponding to crack growth in an infinite plate, described by Paris' law (e.g. [1]):

$$\frac{da(n)}{dn} = C\left[\Delta S\sqrt{\pi a(n)}\right]^m \tag{1}$$

where a is the crack depth; n is the number of stress cycles; ΔS is the stress range per cycle with constant stress amplitudes; and C and m are empirically determined model parameters. Parameters ΔS, C, and m are modeled as time invariant random variables. Using the boundary condition $a(n=0) = a_0$, the previous equation leads to

$$a(n) = \left[\left(1-\frac{m}{2}\right)C\Delta S^m \pi^{m/2} n + {a_0}^{(1-m/2)}\right]^{(1-m/2)^{-1}} \tag{2}$$

In order to use a DBN for the fatigue model, the time is discretized in intervals of 1 year. If $n_t = n(t)$ is the number of cycles at time step t, then the crack depth at the end of each year can be expressed recursively as a function of the crack depth in the previous year as

$$a_t = \left[q\pi^{m/2} + {a_{t-1}}^{(1-m/2)}\right]^{(1-m/2)^{-1}} \tag{3}$$

where $q = \left(1-\frac{m}{2}\right)C\Delta S^m\,\Delta n$. Here, $\Delta n = n_t - n_{t-1}$ is the number of stress cycles per year. Variable q is defined in order to reduce the dimension of the variable space.

The failure event of the component is defined by the limit state function

$$g = a_c - a(n) \tag{4}$$

where a_c represents the critical crack depth. The condition of the component is indicated by the binary variable E_t, which takes value 1 when $g > 0$ (i.e. safe event) and 0 when $g \leq 0$ (i.e. failure event).

In STRAUB [8], a DBN model and algorithm was developed for this simple crack growth law, as presented in Fig. 4a. For the purpose of the present study, the model is simplified

by eliminating the variables q_t and m_t, leading to a simple homogeneous Markovian deterioration model for a_t as shown in Fig. 4b. The resulting discrete Markov process for the crack depth a_t follows the recursive relation

$$\mathbf{p}_a(t) = \mathbf{A}\,\mathbf{p}_a(t-1) \tag{5}$$

where $t = 1,2,\ldots,T$, $\mathbf{A}$ is the transition probability matrix and $\mathbf{p}_a(t)$ is the vector describing the discretized probability distribution of a_t. $\mathbf{p}_a(0)$ is given by the probability distribution of a_0. The Markov model is homogenous if all random variables in the model are time-invariant. Note that the unconditional marginal distribution of the crack depth and the unconditional probability of failure of the two models in Fig. 4 are identical. However, as soon as observations are made, the conditional distributions computed with the two models will differ.

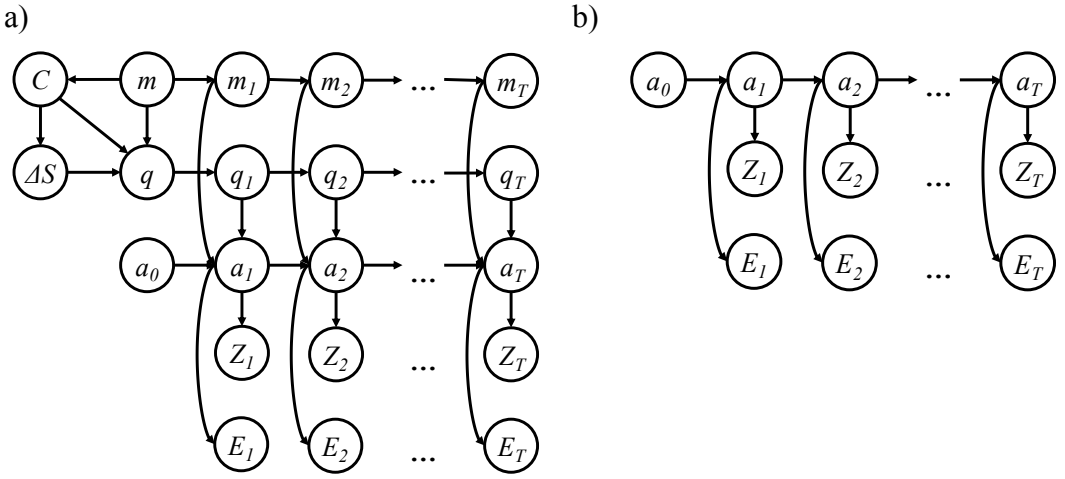

Fig. 4: DBN of the original (a) and simplified (b) fatigue crack growth model

3.2 Influence diagram for modeling inspections

To assess the effect of inspections and to determine optimal inspection times, the fatigue DBN of Fig. 4 is extended to an influence diagram (ID). The ID is presented in Fig. 5. The elements of this ID are introduced in the following.

Inspection decisions. At every time step t, a decision node D_t is included in the BN. Each decision has two possibilities: no inspection ($D_t = 0$) or inspection ($D_t = 1$). In the ID shown in Fig. 5, this decision node has no parents. Because we follow the LIMID convention described above, this implies that the inspection is planned without any previous knowledge. This assumption will later be relaxed.

Observations. In case an inspection is carried out at time t, the random variable Z_t will indicate if a crack was *detected* ($Z_t = 1$) or *not detected* ($Z_t = 2$). If no inspection was carried out (i.e. $D_t = 0$), then the corresponding state of the variable will be *no measurement* ($Z_t = 3$). In case an inspection is performed, the *probability of detection* (PoD) describes the probability of detecting the crack. It is a non-decreasing function of the crack depth (i.e. larger cracks have larger probabilities to be detected) and is here represented by the following relation [8]:

$$\Pr(Z_t = 1|a_t) = PoD(a_t) = 1 - \exp(-a_t/10\,mm) \quad (6)$$

Repairs. Repair actions are included in the model as a function of the observed conditions of the component and the system. Whether or not to repair at time t is in principle also a decision that may be optimized jointly with the inspection decision. However, it has been found that simple decision rules are sufficient for the repair action in the considered case, and no optimization is needed [9]. The rule is that if the system fails or a crack is detected during an inspection, the component will be repaired. This is included in the ID through the variable a_t'. If no repair is carried out, the state of a_t' will be identical to a_t; if a repair is carried out, its conditional distribution is equal to the distribution of the initial crack depth a_0, assuming that the new condition is probabilistically identical to the original one.

Component and system condition. Structural systems are often redundant, so that failure of an element does not necessarily imply a system failure. Here, the redundancy of the system with respect to component failure is defined in a simplifying manner as the probability that the system does not fail when the component does. $E_{S,t}$ and $E_{C,t}$ denote the condition (i.e. failure or safe) of the system and the component, respectively, at time t. We define the redundancy r as:

$$\Pr\left(E_{S,t} = \text{safe}\middle|E_{C,t} = \text{failure}\right) = r \quad (7)$$

In the extreme case with no redundancy $r = 0$, element failure will directly lead to system failure. Similarly, if the system is fully redundant with respect to element failure, $r = 1$, then the system will not fail if only this element fails. This simple model does not account accurately for multiple element failures, which must addressed by an advanced model [7].

Utilities. The variables $E_{S,t}$ (system condition), D_t (inspection decision), and Z_t (observation) are associated with costs. These are modeled by the utility nodes $U_{S,t}$, $U_{I,t}$, and $U_{R,t}$. The utility of an inspection, repair and system failure events are $-C_I$, $-C_R$, and $-C_S$,.

3.3 Memory assumptions in the ID model

In the LIMID, only those nodes with links to the decision nodes are assumed to be known at the time of making the decision. This assumption can strongly reduce the computational effort when optimizing the decisions. With increasing memory, i.e. with increasing number of links to the decision nodes, the policy domains of the decision nodes increases, making the solution of the optimization problem intractable. On the other hand, reducing the number of information links toward the decision node leads to suboptimal solutions, in particular if compared to the no-forgetting assumption.

In the first ID presented in Fig. 5, it is assumed that no information is available when the inspection decision is made. We call this the *no-memory ID*. The advantage of the no-memory ID is that all inspections can be planned a-priori, since no observation during the service life will influence the inspection decisions.

Alternatively, we consider the ID presented in Fig. 6, where information from previous observations and decisions is taken into account when planning the inspections. In this ID, it is assumed that the observation made at the previous inspection is known when deciding upon inspection. Two additional variables, Z_t^* and τ_t, are included in the model and con-

tain the observation from the last inspection and the time when it was performed. We call this ID the *last-inspection ID*.

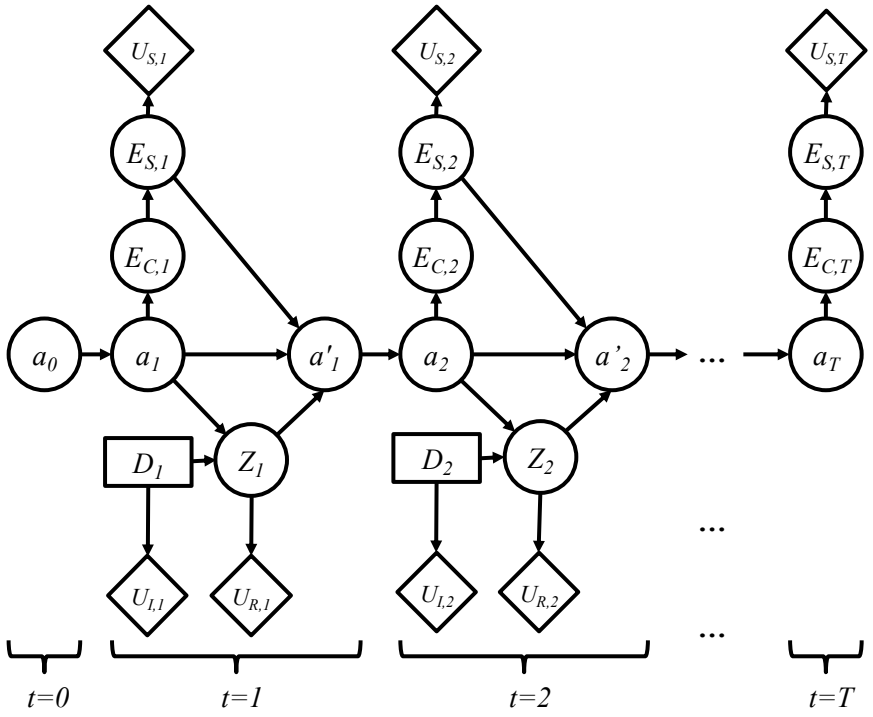

Fig. 5: ID modeling the fatigue inspection planning (no-memory ID)

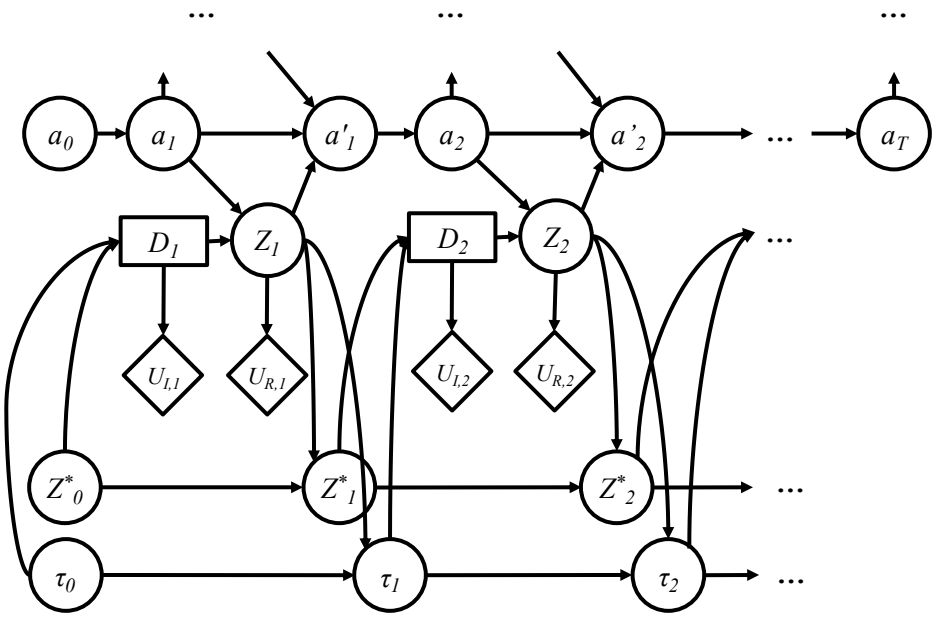

Fig. 6: ID modeling the fatigue inspection planning (last-inspection ID)

3.4 Finding optimal inspection times with the ID

When solving decision problems, the size of the solution domain can quickly become intractable as the number of decision nodes increases. Depending on the type of application, some characteristics (e.g. symmetry) can be used to reduce the computational demands of the decision problem [2]. Alternatively, approximate solutions can be obtained. In particular, s*ingle policy updating* (SPU) is an iterative algorithm for solving LIMIDs that runs over each decision node, obtaining its locally optimum policy that maximizes the expected utility of the decision problem by keeping the remaining policies fixed. An iteration is completed when all decision nodes are locally maximized and the algorithm stops when the next iteration does not further reduce the expected utility. Due to its local nature, the solution obtained with SPU is likely to be suboptimal.

For the inspection planning problem, simple heuristics were defined in the past to reduce the solution space (see e.g. [9]). The two most common heuristics are summarized in the following.

Periodic inspections (PI), also known as equidistant inspections: The number of possible inspection times of the decision problem increases exponentially with the number of time steps T (i.e. 2^T combinations). However, if it is required that the inspection intervals are fixed, then the number of possible combinations is reduced to T. The optimization problem can be formulated in terms of a single variable, the number of inspections n_p. If n_p periodic inspections are performed in T time steps, then the inspection times are

$$\left\lfloor \frac{T}{n_p+1} \right\rfloor, \left\lfloor \frac{2T}{n_p+1} \right\rfloor, \ldots, \left\lfloor \frac{n_p T}{n_p+1} \right\rfloor \tag{8}$$

where $\lfloor \cdot \rfloor$ is the smaller integer function. The goal is to find the optimal number of equally spaced inspections that gives the maximum expected utility.

Reliability threshold (RT). The reliability of the component at time step t is its probability of being in a safe condition $\Pr(\overline{F}_t) = \Pr(a_C - a_t > 0)$. Often, it is expressed through the reliability index $\beta_t = \Phi^{-1}[\Pr(\overline{F}_t)]$, with Φ^{-1} being the standard normal cumulative distribution function. A reliability threshold β_m defines a lower bound of the reliability index. For a given threshold, an inspection is planned at time t if it would hold that $\beta_{t+1} < \beta_m$ without this inspection. In this way, the inspection times follow directly from β_m. Note that the implementation of the RT heuristic with the ID differs slightly from the original version, because the computation of $\Pr(\overline{F}_t)$ and β_t is based on the averaged performance, i.e. it is not computed based on the actual repair history as in STRAUB & FABER [9].

The PI and RT heuristics approximate the solution of the no-memory decision problem. Their possible solutions domains are considerably smaller subsets of the complete solution domain, thus reducing the computational effort. Both PI and RT approaches define a single parameter optimization problem. Their algorithms have a linear complexity order with respect to the number of time steps whereas SPU complexity depends on the maximum size of the variable domains considered in the decision problem.

4 Numerical investigations

To investigate the different algorithms for optimizing the inspection planning with respect to the minimal life cycle cost, the simple DBN crack growth model presented in Sec. 3.1 is implemented. The parameters of the model are summarized in Tab. 1. These parameters as well as the discretization scheme are taken from STRAUB [8]. In Tab. 2, the variables of the IDs are summarized. The cost of repair, C_R, and system failure, C_S, are expressed relative to the cost of inspection, C_I. The transition matrix $\mathbf{A}$ of Eq. (5) is estimated by Monte Carlo simulation with 10^6 samples of parameters C, ΔS and m according to the prior distributions of Tab. 1.

In this analysis, the following parameter values were assumed for the life cycle model: total time period $T = 15$ years; system failure cost $C_S = 5000$; inspection cost $C_I = 1$; repair cost $C_R = 0.1$; and redundancy $r = 0.2$. Discounting was neglected for the purpose of this example.

The inspection planning problem was solved for the no-memory ID (Fig. 5) with the PI and RT heuristics, with the SPU algorithm and – for comparison – with a full search (i.e. covering all 2^{15} possible inspection schedules). Furthermore, it was solved for the last-inspection ID (Fig. 6) with the SPU algorithm.

Tab. 1 Parameters of the decision problem

Variable	Distribution	Mean	Standard deviation and correlation
a_0 [mm]	Exponential	1	1
a_c [mm]	Deterministic	50	–
ΔS [N mm^{-2}]	Normal	60	10
$\ln(C), m$ [a]	Bi-Normal	$(-33; 3.5)$	$(0.47; 0.3)$, $\rho = -0.9$
Δn [yr^{-1}]	Deterministic	10^5	–

[a] Dimensions corresponding to Newton and millimeter

Tab. 2: Domains and variables discretization

Variable	Number of states	Discretization / states	Conditional Probability Distribution
a_t (mm)	80	0,exp{ln(0.01): [ln(50) − ln(0.01)]/78 : ln(50) }, ∞	$Pr(a_t \in I_j \mid a_{t-1} \in I_k) = A_{j,k}$ where I_j is the jth interval of the discretization of a_t or a'_{t-1}.
$E_{C,t}$	2	1: Safe 0: Fail	$\Pr(E_{C,t} = e \mid a_t) = \begin{cases} 0 & if\ e = 1, a_t \geq a_c \\ 1 & if\ e = 0, a_t \geq a_c \\ 1 & if\ e = 1, a_t < a_c \\ 0 & if\ e = 0, a_t < a_c \end{cases}$
$E_{S,t}$	2	1: Safe 0: Fail	$\Pr(E_{S,t} = e \mid E_{C,t}) = \begin{cases} r_i & if\ e = 1, E_{C,t} = 0 \\ 1 - r_i & if\ e = 0, E_{C,t} = 0 \\ 1 & if\ e = 1, E_{C,t} = 1 \\ 0 & if\ e = 0, E_{C,t} = 1 \end{cases}$
$U_{S,t}$	1	–	$U_{S,t} = \begin{cases} 0 & if\ E_t^S = 0 \\ -C_S & if\ E_t^S = 1 \end{cases}$
D_t	2	0: No inspection 1: Inspection	
$U_{I,t}$	1	–	$U_{I,t} = \begin{cases} 0 & if\ D_t = 0 \\ -C_I & if\ D_t = 1 \end{cases}$
Z_t	3	1: Insp. with detection 2: Insp. with no detection 3: No measurement	$\Pr(Z_t = z \mid a_t, D_t) = \begin{cases} 1 & if\ D_t = 0, z = 3 \\ PoD(a_t) & if\ D_t = 1, z = 1 \\ 1 - PoD(a_t) & if\ D_t = 1, z = 2 \\ 0 & \text{otherwise} \end{cases}$
$U_{R,t}$	1	–	$U_{R,t} = \begin{cases} 0 & if\ Z_t = 2,3 \\ -C_R & if\ Z_t = 1 \end{cases}$
a'_t (mm)	80	0,exp{ln(0.01): [ln(50) − ln(0.01)]/78 : ln(50) }, ∞	$\Pr(a'_t \in I_j \mid a_t, Z_t, E_{S,t}) = \begin{cases} \Pr(a_0 \in I_j) & if\ E_{S,t} = 0 \\ \Pr(a_0 \in I_j) & if\ E_{S,t} = 1, Z_t = 1 \\ 1 & if\ E_{S,t} = 1, a_t \in I_j, Z_t = 2,3 \\ 0 & \text{otherwise} \end{cases}$ where I_j is the jth interval of the discretization of a_t or a'_{t-1}.

4.1 Results

The total expected cost of the inspection planning solutions obtained with the PI and the RT heuristics are shown in Fig. 7. For the PI approach, the optimal number of inspections is found to be 6, with the RT approach the optimal reliability threshold is found to be $\beta_m = 3.34$.

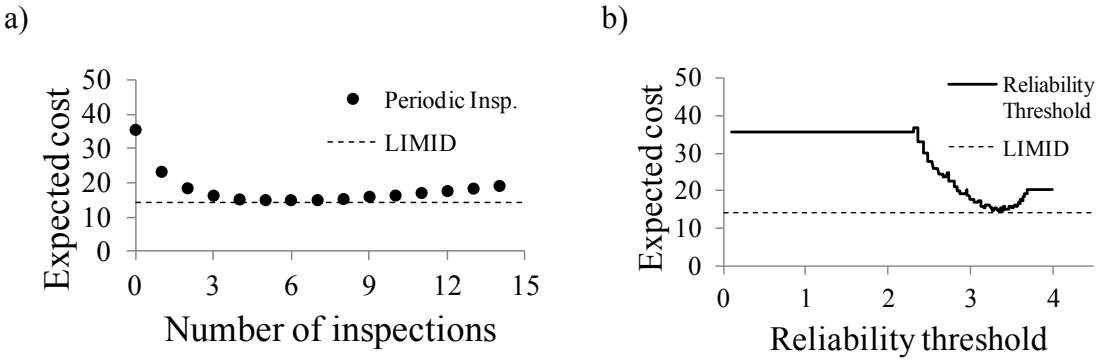

Fig. 7: Expected cost of inspection schedules with (a) periodic inspections and (b) reliability thresholds

The total expected costs for all five solution strategies are summarized in Tab. 3. The difference in the total expected cost among the optimal solutions is relatively small despite the inspection times and disaggregated costs (i.e. failure, inspection and repair costs) being quite different among the solutions. As an example, Fig. 8 shows the disaggregated expected costs for the PI and the SPU (no-memory ID) solution. The reason for the small differences in expected costs is likely the fact that all optimal solutions of the no-memory ID have six inspections, and the minimum reliability obtained with these optimal solutions is also fairly similar, as evident from Fig. 9.

The optimal solution is obtained with the last-inspection ID, solved using the SPU algorithm. This is not surprising, since this is the only strategy that allows adapting the inspection times based on inspection results. The disadvantage of this strategy is that inspections cannot already be planned at the beginning of service life.

Tab. 3 Optimal solutions obtained with different algorithms.

Approach	Expected cost	Inspection times	CPU time (sec)
PI	14.91	2, 4, 6, 9, 11, 13	0.4
RT	14.70	2, 4, 6, 8, 10, 13	4.3
SPU (no-memory ID)	14.05	1, 2, 4, 5, 7, 9	164
Exact solution (no memory)	13.97	1, 2, 3, 5, 7, 10	313
SPU (last-inspection ID)	13.75	Policies for each decision node	165

Comparing the SPU solutions obtained for the two different IDs, it is seen that the minimum expected cost decreases from 14.05 to 13.75 when the observation from the last performed inspection is taken into account for deciding on the next inspection (the last-inspection ID). In this case, the SPU algorithm provides an adaptive policy for each decision node. For example, the resulting policy of the decision node D_{12} indicates that an inspection is to be carried out unless there was an inspection in the previous year (independent of what was observed) or two years ago without crack detection.

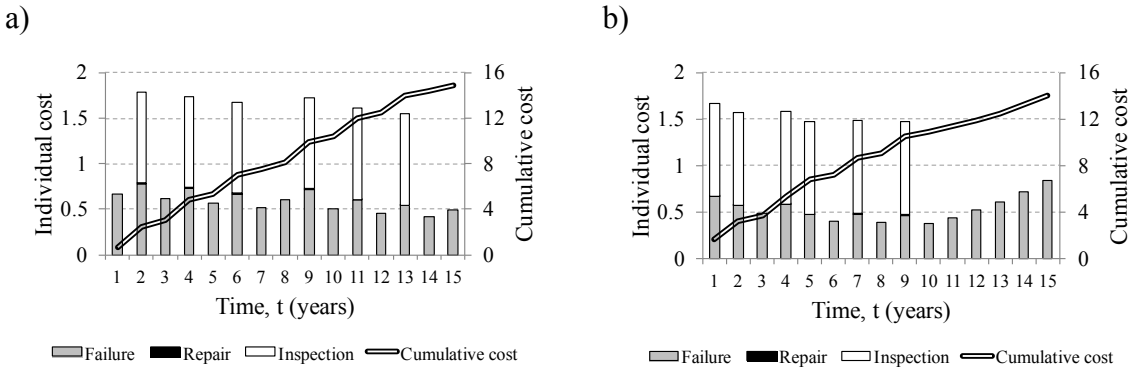

Fig. 8: Expected cost of optimal solution for: a) PI, and b) SPU (no-memory ID)

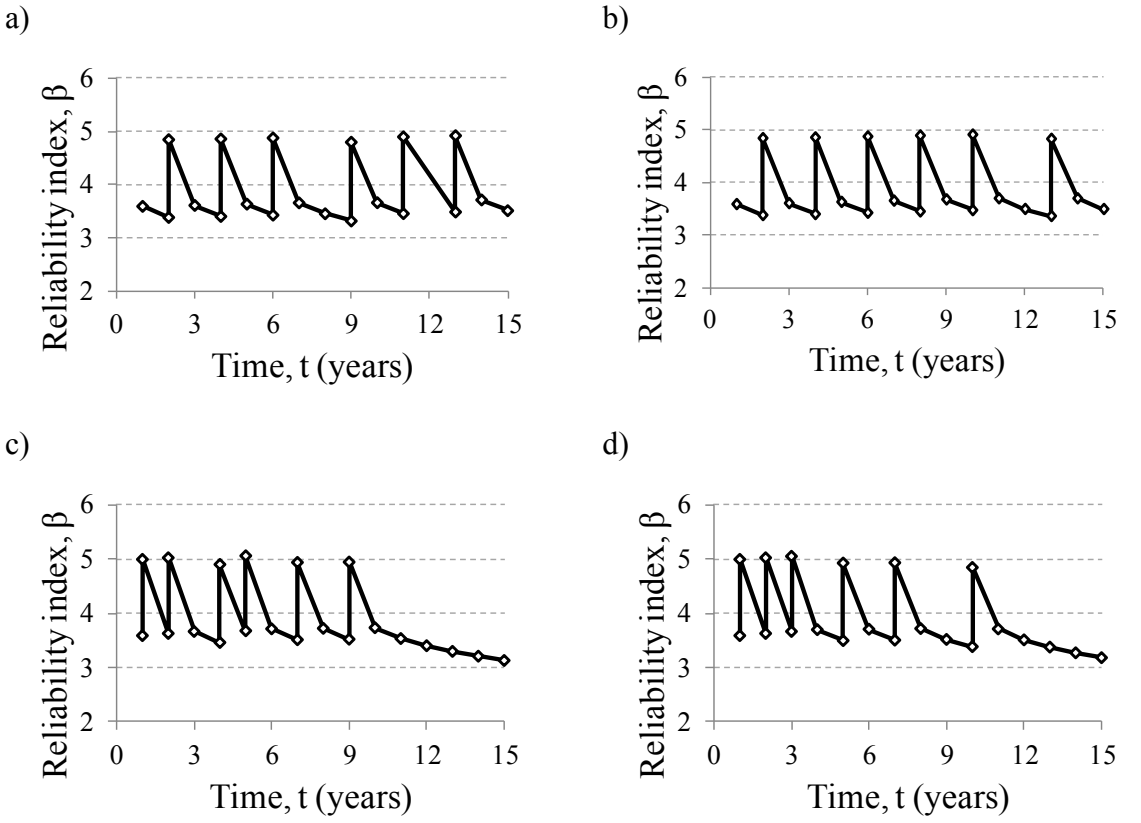

Fig. 9: Reliability index of the optimal solutions for (a) periodic inspections; (b) reliability threshold; (c) SPU (no-memory ID); and (d) the exact solution (no-memory ID)

The computation time for the SPU solution is considerably larger than for PI and RT. The same is observed when increasing the considered service life period T, and hence the number of steps in the DBN (see Fig. 10). However, all these algorithms show a similar complexity order (a linear increase with the number of time steps). In contrast, the exact solution of the no-memory ID was obtained by a complete search among all possible combinations of inspection times. This procedure has an exponential complexity order with respect to the number of time steps. For illustration purpose, the last two points of the exact

solution (no-memory) curve in Fig. 10 ($T = 25$ and $T = 50$) were estimated by extrapolation.

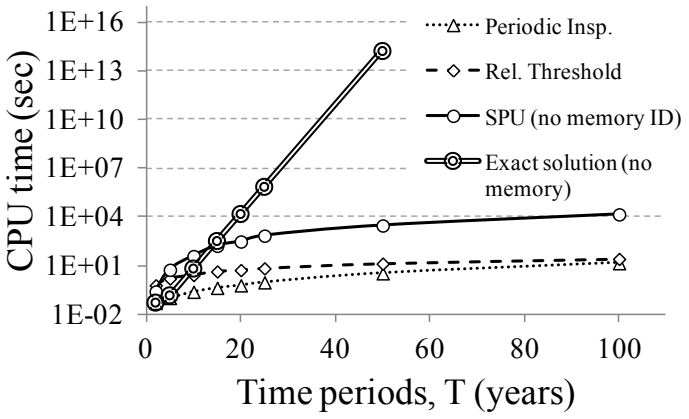

Fig. 10: CPU time for finding the optimal solution

While the SPU algorithm requires significantly more computation time than the PI and RT heuristics, it is more flexible because it allows to adapt the inspections to the results of previous observations, as shown for the case of the last-observation ID. If the observations from the previous inspections are considered before deciding to inspect, an adaptive policy is followed. Since any information can only increase the expected utility of optimal decisions [3], [10], it follows that the maximum expected utility of the last-observation ID (or any other adaptive policy implemented through an ID with memory) must be larger or equal than that of a fixed inspection schedule based on the no-memory ID.

5 Conclusions and outlook

In this paper, the optimal inspection times for a structural element subject to fatigue are identified through a set of algorithms. The optimization problem is formulated through influence diagrams, whereby varying assumptions regarding the adaptivity of the inspection schedule were made. As expected, the adaptive inspection scheduling leads to lower expected costs. Among the algorithms for optimizing a non-adaptive inspection plan, the one obtained with the single policy updating (SPU) algorithm performs the best. However, the examined heuristics, which allow to significantly reduce the computational effort in the optimization, also perform well.

These results of this paper are useful in the investigation of inspection planning problems in systems with multiple elements, whose deterioration characteristics are correlated. The proposed DBN/ID framework can be extended to solve such problems, but the associated computational complexity will increase with increasing system size, and simple heuristics are no longer readily available. Therefore, it is essential to have efficient algorithms for solving these problems, and the SPU algorithm seems promising for this purpose.

Acknowledgements

This work was supported by the Deutsche Forschungsgemeinschaft (DFG) through Grant STR 1140/3-1 and the Consejo Nacional de Ciencia y Tecnología (CONACYT) through Grant No. 311700.

References

[1] Ditlevsen, O., Madsen, H.O. *Structural reliability methods*. New York, Wiley, 1996

[2] Jensen, F., Nielsen, T. *Bayesian networks and decision graphs*. 2nd ed. New York, Springer, 2007

[3] Jordaan, I. J. *Decisions under uncertainty. Probabilistic analysis for engineering decisions*. Cambridge, Cambridge University Press, 2005

[4] Lauritzen, S., Nilsson, D. Representing and solving decision problems with limited information. *Management Science*, 47(9), 2001, 1235−1251

[5] Nielsen, J., Sørensen, J. Risk-based operation and maintenance of offshore wind turbines using bayesian networks. *Proceedings of the 11th International Conference on Applications of Statistics and Probability in Civil Engineering*, CRC Press LLC, 2011, 311−317

[6] Raiffa, H., Schlaifer, R. *Applied Statistical Decision Theory*. Cambridge: Cambridge University Press, 1961

[7] Straub, D., Der Kiureghian, A. Reliability Acceptance Criteria for Deteriorating Elements of Structural Systems. *Journal of Structural Engineering*, *Trans. ASCE*, 137 (12), 2011, 1573–1582.

[8] Straub D. Stochastic modeling of deterioration processes through dynamic bayesian networks. *Journal of Engineering Mechanics, Trans. ASCE*, 135(10), 2009, 1089−99

[9] Straub, D., Faber, M. H. Computational aspects of risk based inspection planning. *Computer-Aided Civil and Infrastructure Engineering*, 21(3), 2006, 179−192

[10] Straub, D. Value of Information Analysis with Structural Reliability Methods. *Structural Safety*, 2014, in print

[11] Swanson, L. Linking maintenance strategies to performance. *International Journal of Production Economics*, 70: 2001, 237–244.

Ingredients for an innovative uncertainty quantification platform in MATLAB

Stefano Marelli & Bruno Sudret

Chair of Risk, Safety and Uncertainty Quantification, Institute of Structural Engineering, ETH Zürich
marelli@ibk.baug.ethz.ch, sudret@ibk.baug.ethz.ch

Abstract: Uncertainty quantification is an emerging field in computer simulation-based scientific applications. Its general formulation covers a vast field of approaches including, e.g., structural reliability, sensitivity analysis, reliability-based design optimization and Bayesian techniques. The UQLAB project aims at developing a MATLAB-based framework that could enable researchers and field engineers to both use and develop new uncertainty quantification algorithms in several types of distributed computing environments. Ease of use, extendibility and handling of non-intrusive stochastic methods are core elements of its development philosophy. The platform comprises a highly optimized core probabilistic modelling engine, a simplified API layer that provides unified access to heterogeneous high performance computing resources and a content management system that allows users to develop additional custom modules to suit their needs. In this contribution we intend to present the global architecture and to demonstrate some of the core capabilities of the UQLAB framework in its early stages of development.

Keywords: Uncertainty Quantification, Global Uncertainty Framework, UQLab, Structural Reliability, Matlab

1 Introduction

Uncertainty quantification through computer simulation is an emerging field at the boundary between computer simulation-based engineering and applied mathematics, statistics and probability theory. Broadly speaking, it aims at identifying sources of uncertainty in each of the components of the simulation of physical quantities and propagating this uncertainty into the model responses. This is a general formulation that covers a vast field of approaches

including, among others, structural reliability, sensitivity analysis, reliability-based design optimization and Bayesian techniques for calibration and validation of computer models.

In terms of research, contributions to this broad topic equally come from the engineering, statistics and applied mathematics communities, sometimes with their own vocabulary. In terms of computational tools, only a few are readily available (*e.g.* free software like FERUM [2] and OpenTURNS [1], or commercial ones like COSSAN and Nessus). A review on structural reliability software is available in [5]. None of them, however, covers the broad scope mentioned above.

Furthermore, to our knowledge none of the existent software is designed to be easily extended by the engineering research community. The use of powerful but complex languages like C++ and Python as well as the widespread adoption of Object-Oriented programming at all levels of development may discourage the scientific developers to make use of the facilities provided by existing software and opt instead for in-house re-development of yet more heterogeneous codes.

In an attempt to overcome such limitations, the Chair of Risk, Safety and Uncertainty Quantification in ETH Zürich has started the UQLAB (**U**ncertainty **Q**uantification in MAT**LAB**) project, aiming at the development of a powerful, modular and simple to extend software framework for uncertainty quantification in Engineering.

The main defining goals of the UQLAB project can be summarized as:

- providing a complete set of tools for uncertainty quantification in engineering applications;
- ensuring ease of use for both academic students, researchers and field engineers;
- designing a modular structure easy to extend by not highly-IT-trained scientists;
- providing high interoperability with existing third party software in a non-intrusive, "black box"-type approach;
- easing the deployment of uncertainty quantification algorithms on a variety of high-performance computing platforms.

In order to achieve all of the mentioned goals, our software architecture eventually converged to a MATLAB based highly modular software framework.

2 A global uncertainty quantification framework

Uncertainty quantification in civil and mechanical engineering is a vast scientific research topic that has seen active development for more than 40 years. Due to the broad spectrum of its possible applications, uncertainty quantification is a highly heterogeneous field. Therefore, in order to build an uncertainty quantification software with a general enough scope, a correspondingly general theoretical framework is required. At the backbone of the architecture of the UQLAB software lies the global uncertainty framework developed by SUDRET (2007) and reviewed, *e.g.* in [7, 3], that is sketched in Fig. 1.

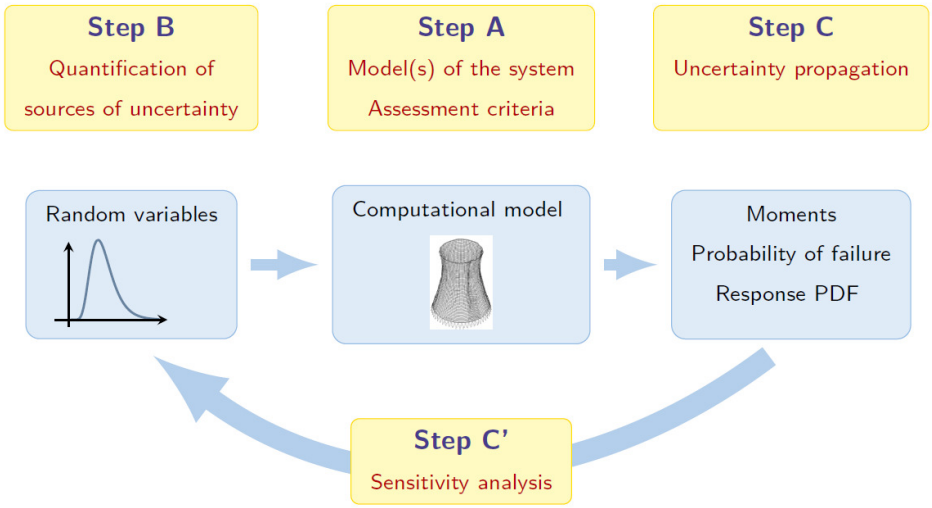

Fig. 1: Visual representation of the global theoretical framework for uncertainty quantification developed by [7] and [3], which gives the theoretical foundation to the UQLAB software

According to this framework, several common steps need to be undertaken in every uncertainty quantification problem:

- **Step A** consists in defining the physical model and the quantities of interest on which the analysis will be performed (*e.g.* a failure criterion). It is a deterministic representation of an arbitrarily complex physical model (*e.g.* a finite element model).

- **Step B** consists in identifying, quantifying and representing the sources of uncertainty in the system. Such quantities will serve as the input for the modelling in Step A, and are usually represented by a vector of random variables whose joint probability density function (PDF) is defined on the basis of the available information and data.

- **Step C** consists in the propagation of the uncertainty in the input random variables defined in Step B through the modelling in Step A, thus evaluating the resulting uncertainty in the model response.

- **Step C'** is an optional step that consists in exploiting by-products of the analysis in Step C in order to rank the sources of uncertainty according to their impact onto the quantities of interest. This step is known as sensitivity analysis.

Each problem of uncertainty quantification can be solved by following this approach, as long it can be decomposed in three main components: physical model, input variables, uncertainty propagation analysis. These three components introduce a semantic distinction between the actors involved in any uncertainty quantification problem. This theoretical framework, therefore, provides the ideal foundation to the development of the information flow model in a multi-purpose uncertainty quantification software.

3 From a theoretical framework to its implementation

3.1 The software architecture

To achieve the same level of generality and flexibility of the theoretical framework presented in Section 2, we decided to opt for the development of a computational framework, rather than a monolithic software package. A computational framework substantially differs from a "packaged software" in several important aspects:

- it focuses on the creation of content, rather than on the content itself;
- its development model plays a relevant role in its own architecture;
- its features can be arbitrarily extended, as long as they can be represented within its structure.

The core architecture of the UQLAB uncertainty quantification framework closely follows the semantics defined in the previous Section by implementing a modular, partially hierarchical structure sketched in Fig. 2. The three steps identified in Fig. 1 directly map to

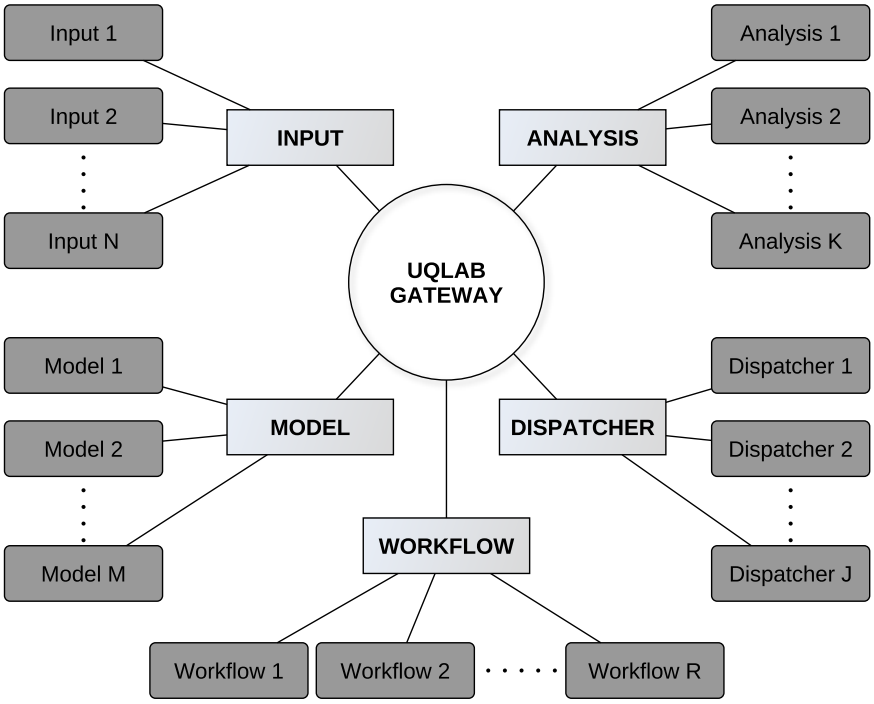

Fig. 2: The modular core at the heart of the UQLAB framework architecture. At any stage of the analysis, an arbitrary number of elements can be connected.

supermodules represented as light shaded boxes in Fig. 2: Step A (physical modelling) is mapped to the **MODEL**, Step B (sources of uncertainty) to the **INPUT** and Step C (uncertainty propagation) to the **ANALYSIS** supermodules, respectively. Auxiliary supermodules (*e.g.* **DISPATCHER** and **WORKFLOW** in Fig. 2) similarly represent additional actions that need to be handled during a calculation (*e.g.* dispatching calculation on HPC resources).

Each supermodule has several connections: a single connection to a central unique **GATEWAY** (the central circle in Fig. 2), and an arbitrary number of connections to children *mod-*

ules (represented by grey boxes in Fig. 2). The **GATEWAY** is a unique entity that can be retrieved at any time and from any location within the framework, with the function of providing a unique access point to every supermodule, thus making the information ubiquitous throughout the framework. Finally, each module connected to a supermodule represents an actual "entity" belonging to it. To give a few examples, a module connected to the **ANALYSIS** supermodule could be the "reliability analysis" module, while modules connected to the **MODEL** supermodule could be, *e.g.* an analytical function or a finite element model.

Implementing an uncertainty quantification analysis within the framework, therefore, would consist in defining the necessary modules and their configuration for each of the supermodules in Fig. 2. To give a practical example (full pseudo-code will be given in Section 5), a Monte-Carlo reliability analysis of a simply supported beam would require the user to define the following modules:

- an **INPUT** module: a set of probability density functions representing the uncertainty in the beam geometry and applied loads. Dependent variables my be defined using the copula formulation [6];
- a **MODEL** module: the midspan deflection of a simply supported beam as a function of the variables defined in **INPUT**;
- an **ANALYSIS** module: a Monte Carlo reliability analysis associated with a failure criterion related to the maximal *admissible* deflection.

Once all the ingredients are defined, the analysis is started and it is executed over the defined modules. It should be noted, however, that an arbitrary number of modules can be connected to each supermodule in Fig 2. Therefore, in analogy with the possibilities offered by the theoretical framework in section 2, it is possible to combine different module types for different uncertainty quantification problems.

The simplest case in which this property may be desirable is that of a validation of a new modelling method. Let us imagine that in the previous example we decided to test a newly developed modelling strategy that makes use of, *e.g.*, a complex FEM scheme to accurately predict the beam midspan deflection, and that we wanted to compare it with results based on the analytical solution of the problem. It would then be sufficient to add a new module to the **MODEL** supermodule based on the new FEM modelling routine and to define a new *workflow* that makes use of the same **INPUT** and **ANALYSIS**, but replaces the old **MODEL** module with the new one.

Handling multiple workflows is exactly the purpose of the **WORKFLOW** supermodule depicted in Fig. 2. In practice, a user can define an arbitrary number of workflows that can be executed sequentially over the course of an uncertainty quantification analysis. The importance of this facility becomes clear when solving highly complex uncertainty quantification problems on shared high-performance-computing platforms: surrogate modelling, higher-order reliability methods and other sophisticated techniques can be streamlined in a set of sequential workflows that can be queued and executed in a single HPC job, minimizing repeat calculations and queue waiting times. Another typical application example of the workflow feature is the case when the impact of different probabilistic **INPUT** should be compared.

Starting from the existing *Input 1*, a new *Input 2* may be built up, and a new workflow accordingly.

The final supermodule in Fig. 2 is the **DISPATCHER**. Once again semantically separated from the other supermodules, the **DISPATCHER** aims at offering a unified interface to a set of heterogeneous High Performance Computing facilities via the use of simple configuration cards. When requesting the execution of an analysis, the dispatcher would appropriately select the actual commands that need to be executed to perform the analysis on the correct infrastructure. As an example, the default **DISPATCHER** is the "local" one, which simply executes the program locally without modifications. A more complex example (but perhaps more useful in a real world scenario), is the "ssh+cluster+queuing system" dispatcher, that first connects to the configured computing resource (cluster) via the specified connection type (ssh), copies the data necessary to the execution to the remote host, creates any job scripts necessary for its execution (queuing system), submits them and finally retrieves and merges the results when the computations are done. As arbitrarily complex as those operations may be, they are semantically completely detached from the the other aspects of the computational problem, therefore they have been included into a separate supermodule.

3.2 The MATLAB implementation

One of the defining goals of our endeavour in developing UQLAB (see Section 1) is making both the use of existing and the development of new uncertainty quantification algorithms easily accessible to not-IT-trained professionals (*e.g.* students and field engineers). Due to its widespread use in the engineering community, its quick learning curve, its portability and the advanced programming interface it offers, we adopted MATLAB as the programming language for our framework.

The core structure of the UQLAB software presented in Fig. 2 is coded in an object-oriented fashion to preserve the semantics defined in Section 2. The **GATEWAY** is a MATLAB implementation of the *singleton* design pattern, guaranteeing its uniqueness and retrievability at any point in the MATLAB session, by means of a single protected global variable (its instance handle). The supermodules are created as soon as an instance of the **GATEWAY** instance is created, and they are linked with it. Each of the supermodules is in turn an object that only contains information about the existent modules, as well as methods to add, retrieve and remove them. Due to their nature, the **GATEWAY** and the supermodules are lightweight entities that introduce negligible overhead. In particular, retrieving the current gateway and the pointers to the existing module handles can be done at the cost of a handful of memory operations within any scope of a MATLAB session. High performance, stability and small overhead are extremely important in the design of these components, as they are ubiquitous throughout the execution of any software in the framework.

Each module created by a supermodule is by itself an object that contains all of the information needed to perform the task it is in charge with. As an example, a module created by the **INPUT** supermodule would contain all the information about the probability distributions that need to be sampled in the analysis, as well as a method that extracts a sample from them. Analogously, a module created by the **MODEL** supermodule would contain any necessary runtime parameter, as well as a method to run the modelling routines on the current

input.

Due to this highly modular structure and its object oriented nature, diagnostic tests can be executed at each module creation, or by means of more advanced infrastructures provided by MATLAB, like event listeners and callbacks. Therefore, a healthy degree of internal coherency in the framework can always be guaranteed at any stage of its execution.

This high-level functionality is exposed to the users by means of a simple command line interface (CLI) and a more advanced programming interface (Application Programming Interface), neither of which requires any knowledge of object-oriented programming. Examples of both interfaces will be presented in Section 5.

The conceptual separation between actors in an uncertainty quantification introduced in Section 2 has an important property: the uncertainty quantification framework is intrinsically *non-intrusive*. Non-intrusiveness guarantees that, should any of the modules be substituted by a "black box" equivalent, all of the remaining modules would remain unaffected. This is a highly desirable property in a framework that aims at unifying existing software tools with different technical requirements and input-output formats.

4 Extendibility and accessibility: a multilevel collaborative development model

The collaborative nature of the UQLAB project, has relevant consequences on the design model of the platform. The audience of the software, intended as both final users and scientific developers/collaborators, has been grouped in three categories, distinguished mainly by their role in the use and/or development of the framework:

- **end users**: users that will not contribute to the extension of the facilities offered by the platform, therefore interested mostly in the deployment of existent techniques. They are not required to possess any particular programming skill, only the basic knowledge of the theoretical framework (see Fig. 1). It is expected that these users learn how to use UQLAB through existing documented analyses, which they can modify and tailor to their needs. This is the profile of most field engineers and university students;
- **scientific developers**: trained scientists with relevant expertise in the field of uncertainty quantification, interested both in taking advantage of the existing features and in testing and adding new algorithms into the platform. They possess scientific programming skills as well as the knowledge of the theoretical framework. It is the typical profile of the academic researcher;
- **core developers**: scientists highly trained in IT and high performance programming, mainly concerned with the development of the core routines that provide access to the platform contents, as well as with the optimisation of contents provided by other scientific developers. They possess advanced programming skills in Object-Oriented MATLAB and other languages, as well as knowledge of system architecture and related fields. This is the profile of a small number of IT-professionals that are concerned with the "software" perspective of the the UQLAB framework development.

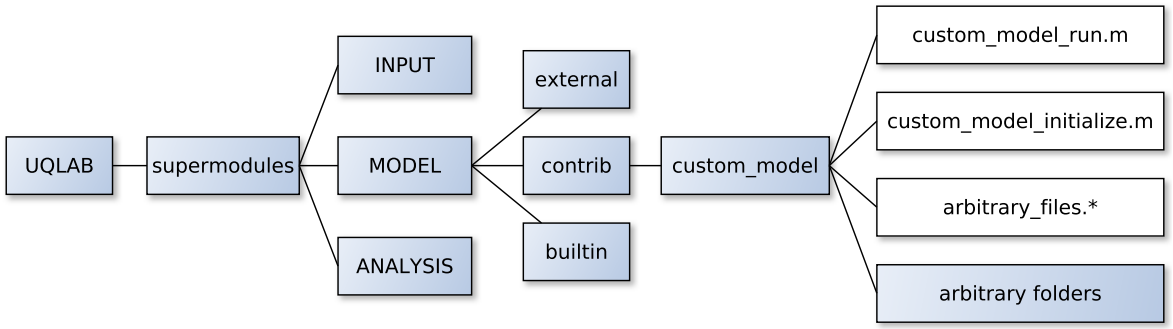

Fig. 3: The folder-based content management system of UQLAB at the *contrib* stage. Note how, provided the *custom_model_run.m* and *custom_model_initialize.m* scripts exist, the sub-folder structure of *new method* is completely arbitrary.

The development model of UQLab is designed following this classification, offering a folder-structure-based, content management system (CMS) for collaboration-driven and user-contributed code (Fig. 3), that makes integration of new features or improvements in the existing code-base simple.

A researcher (scientific developer) willing to include his newly discovered "new method" of modelling in the framework, could simply operate as follows:

- he can copy his own code into the "external" sub-folder of the **MODEL** super-module source tree node, under the name *custom_model*. Extra additional MATLAB scripts can be added in the same folder, with a suitable naming convention (*e.g. custom_model_initialize.m* or *custom_model_run.m*), that perform additional consistency checks/initializations/operations;
- upon restart, the framework recognizes the existence of a new **MODEL** type and makes it available for use;
- the **GATEWAY** and all the supermodules are made available ubiquitously at any point of his code with a very simple set of API functions, allowing for a very fast integration;
- as soon as the "new method" is tested thoroughly, it can be moved to the "contrib" sub-folder of the **MODEL** source tree and committed to the main code repository. This is the stage depicted in Fig 3.
- upon functionality verification from the core developers, the module is now available as an optional module to the end-users, who are free to enable/disable *contrib* codes at will.
- finally, if the end-user feedback is positive enough, the *new method* may undergo a thorough review and optimization from the core developers, and finally be moved into the *builtin* sub-folder of the **MODEL** source tree node, to be shipped into the next public release of the framework.

This simple content management system, together with the highly non-intrusive core structure of UQLAB (see 3.1), make it very simple to add plug-ins to existing software without

the need to change it in any way. This is achieved by writing simple wrapper codes that provide the necessary input to the external software, execute it, and parse its results back into the UQLAB framework.

The UQLAB framework will be released as an open-source project under the terms of the GNU Lesser General Public License (LGPL), therefore promoting its further development from both the academic research community and industrial R&D environments.

5 A simple example

Although UQLAB is still in its early stages of development, its modular core has already reached pre-alpha stage (stable for demonstrative purposes), and a basic set of tools for structural reliability analysis has been implemented within the framework. In this Section we will use a Monte Carlo reliability analysis of a simply supported beam to showcase some of the features of the framework.

5.1 Reliability analysis I: the end-user perspective

The basic "textbook example" of reliability analysis of a simply supported beam under uniform load is sketched in Fig. 4.

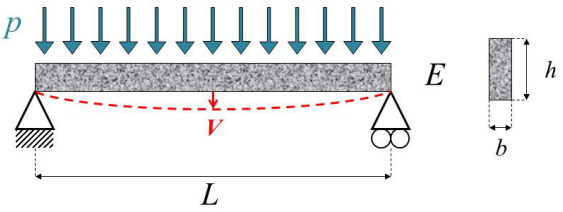

$$V = \frac{5}{32}\frac{pL^4}{Ebh^3}$$

pseudocode:

```
uqlab

Marginals.Type= ...;
Marginals.Moments= ...;
Marginals.Copula='independent';
uq_create_input('myInput',Marginals);

Model.Type='function';
Model.Function_name='SSBeam';
uq_create_model('myBeam', Model);

Analysis.Type='Reliability';
Analysis.Failure=...;
Analysis.Options='MonteCarlo';
uq_create_analysis('myAnalysis',Analysis);

uq_run_analysis;
```

Fig. 4: Reliability analysis of a simply supported beam: problem representation (left) and pseudocode in UQLAB that performs the analysis (right). The results will be stored into a *uq_results* variable in the current MATLAB workspace.

On the left panel the sketch of the beam and its uncertain parameters (the uniform Young's modulus E, the beam length, thickness and height, L, b and h, respectively, and the uniform load p) are given. Each of the input variables is defined by a normal (or lognormal) distribution identified by its first and second order moments. The variables are assumed independent. The failure criterion in this reliability analysis is defined as a threshold on the displacement at midspan V, which has the simple analytical expression given under the beam scheme in Fig. 4. On the right panel the pseudo-code necessary to run the analysis within the framework for an end-user (see Section. 4) is given. The sequence of commands is commented in

the following:

- The framework is initialized with the *uqlab* command.
- A set of input distributions is defined through their moments in the "Marginals" structure. This structure is then passed as an argument to the *uq_create_input* function, which creates the appropriate **INPUT** module with the specified properties. Note that the module is also given a text identifier ("myInput") that will uniquely identify it when defining multiple workflows (cf. Section 3.1).
- In full analogy, a **MODEL** module is created with the *uq_create_model* function by specifying that it is a simple function type, and that the function that needs to be executed is "SSbeam". It is given the text identifier "myBeam".
- An **ANALYSIS** module is finally created by *uq_create_analysis*, and named "myAnalysis". It is a "Reliability"-type analysis, to be performed with the "Monte Carlo" method. A value for the failure threshold is also specified.
- Finally, the analysis is run with the uq_run_analysis command, and the results are stored in an appropriate variable within the MATLAB workspace.

This simple workflow accurately follows the theoretical framework described in Section 2 and sketched in Fig. 1. The results of this analysis for a realistic set of input parameter distributions and 10^9 Monte Carlo iterations are shown on the left panel of Fig. 5.

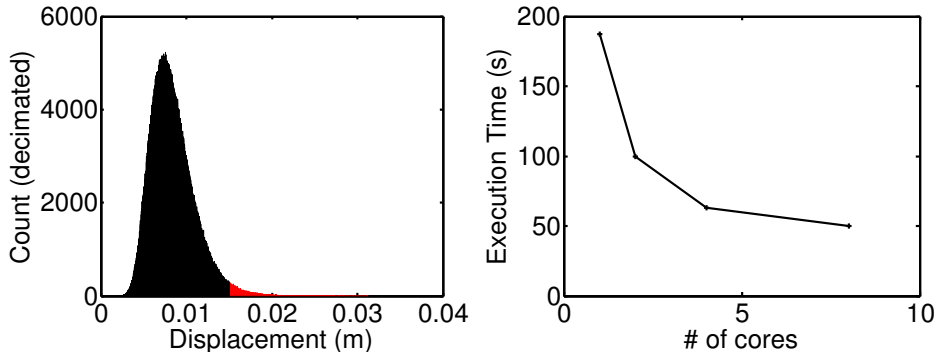

Fig. 5: Left: sample from the 10^9 calculated displacements from the Monte Carlo reliability analysis described in Section 5.1. Right: corresponding scalability plot on a remote cluster.

Distributing the calculation on several cores on a remote machine simply requires the addition of the following lines to the pseudo-code in Fig. 4, before the uq_run_analysis line:

```
HPCOpts.configCard='ssh+torque+cluster';
HPCOpts.nCPU=N;
uq_create_hpc_dispatcher('myDispatcher',HPCOpts);
```

This simple additional configuration allows one to build scalability performance analyses like the one represented on the right panel in Fig. 5. The target computational facility was in this study an 8-core shared-memory remote system with a Torque queuing manager set-up to mimic most of the HPC facilities largely available in both academic and industrial research.

5.2 Reliability analysis II: the scientific developer perspective

The simple interface for the end-users was outlined in the previous section, but an equally important goal in the UQLAB development philosophy is its ease of extendibility. In this Section we illustrate how a scientific developer can create his own analysis routines by taking advantage of the facilities offered by the UQLAB framework.

The pseudo-code that implements the core Monte-Carlo routine in the simply supported example in Fig. 4 is shown in Fig. 6.

```
function results = MonteCarlo
% retrieve the framework: several variables will be created
% in the workspace: UQ_input, UQ_analysis and UQ_model
uq_retrieve_session;

% retrieve the analysis parameters (failure threshold
% and number of samples) from the framework
failure = UQ_analysis.failure;
nsamples = UQ_analysis.nsamples;

% evaluate the model response on a sample from the current input
% of the retrieved sample size
displacements = uq_get_model_response(nsample);
totfailures = length(find(displacements >= failure));

% store the failure probability in the framework's results array
UQ_analysis.results{end}.failure_probability = totfailures/nsamples;
```

Fig. 6: Pseudo-code of the simple Monte-Carlo reliability analysis used in Section 5.1 and Fig 4. Note that *uq_get_model_response* will retrieve which **MODEL** needs to be evaluated and which **INPUT** automatically from the current **WORKFLOW** module (cf. Fig. 3.1)

The crucial interaction point with the underlying framework is provided by the *uq_retrieve_session* helper function. It is a lightweight function that retrieves all the pointers to the core elements in Fig. 2 and to the currently selected modules, and conveniently exposes them to the user in the form of a set of variables *UQ_input, UQ_analysis*, etc. An additional set of helper functions like *uq_get_model_response* (that automatically evaluates the currently selected **MODEL** module on a sample from the currently selected **INPUT** module) are available to the developer as a part of the scientific developers programming interface. A comprehensive reference to such functions is outside the scope of this paper and is currently being rapidly extended.

As it is clear from the pseudocode in Fig. 6, the amount of code rework that is necessary to include a script within the UQLAB framework is minimal, *de-facto* only substituting the standard information-passing practices (e.g., function arguments, global variables) with a single call to *uq_retrieve_session*, and the input-sampling and modelling stages with the proper *uq_** helper functions.

6 Current state of the framework and outlook

At its current stage of development, only the "core structure" of the framework, the content management system and a number of wrappers for existing modelling and meta-modelling software have been implemented to a satisfactory degree and thoroughly tested. A tight

schedule for porting and rewriting a number of other existent uncertainty quantification algorithms has been set in place for the coming months, and will be developed in the short term by the members of the Chair of Risk, Safety and Uncertainty Quantification at ETH Zürich. As soon as a minimalistic set of techniques will be available and well documented, a first public release of the UQLAB software will be published, and an effort to start a collaborative development stage with other research institutions will be initiated.

Foreseen features will include reliability analysis à la FERUM [2], meta-modelling techniques (polynomial chaos expansions [7], Kriging [4], support vector machines), sensitivity analysis (Sobol indices), Markov Chain Monte Carlo methods, etc.

7 Conclusions

We successfully implemented a software framework based on the global uncertainty quantification theoretical framework described in [7, 3]. With its innovative design philosophy and development model, it is well suited to encourage both the academic and the industrial R&D research communities to employ and further develop state-of-the-art uncertainty quantification algorithms. In the coming years, the set of features it offers to end-users will be substantially increased to include most of the latest developments in the rapidly evolving field of uncertainty quantification.

Literature

[1] G. Andrianov, Burriel, S., Cambier, S., Dutfoy, A., Dutka-Malen, I., de Rocquigny, E., Sudret, B., Benjamin, P., Lebrun, R., Mangeant, F. & Pendola, M., Open TURNS, an open source initiative to Treat Uncertainties, Risks'N Statistics in a structured industrial approach. *Proceedings of the ESREL'2007 Safety and Reliability Conference*, Stavenger: Norway, 2007

[2] Bourinet, J.-M., Mattrand, C. and Dubourg, V. A., Review of recent features and improvements added to FERUM software, *Proceedings of the 10th International Conference on Structural Safety and Reliability, ICOSSAR'09*, 2009

[3] De Rocquigny, E., Devictor, N. and Tarantola, S., Uncertainty in industrial practice – A guide to quantitative uncertainty management. *John Wiley & Sons 2008*

[4] Dubourg, V., Sudret, B. and Bourinet, J.-M., Reliability-based design optimization using kriging surrogates and subset simulation. Struct. Multidisc. Optim. 44(5) (2011), p. 673–690

[5] Ellingwood, B. R., Structural safety special issue: General-purpose software for structural reliability analysis. Structural Safety, Structural Reliability Software, 28 (2006), p. 1–2

[6] Nelsen, R. B. *An introduction to copulas*. Springer Verlag, 1999

[7] Sudret, B., *Uncertainty propagation and sensitivity analysis in mechanical models - Contributions to structural reliability and stochastic spectral methods*. Habilitation à diriger des recherches, Université Blaise Pascal, Clermont-Ferrand, France, 2007

Modelling of the probability of merging at an entrance ramp of a highway

J. Mint-Moustapha [a], D. Daucher [a] & B. Jourdain [b]

[a]Laboratoire Exploitation, Perception, Simulateurs et Simulations,
Institut Français des Sciences et Technologies des Transports,
de l'Aménagement et des Réseaux, Champs-sur-Marne, France.
[b]Centre d'Enseignement et de Recherche en Mathématiques et Calcul Scientifique,
École Nationale des Ponts et Chaussées, Champs-sur-Marne, France.
jyida.mint-moustapha@ifsttar.fr, dimitri.daucher@ifsttar.fr, jourdain@cermics.enpc.fr

Abstract: Road safety intends to offer optimal safety conditions and acceptable risk levels to the road users, together with the required mobility. The first objective is to reduce the fatalities and casualties on the roads due to the vehicles. Another objective is to contain the frequency of material accidents, which induce high costs and congestion. The progress of road equipments permits to collect a large amount of data on an instrumented suburban freeway segment (site SAROT in France). Within the general framework of updating the French design guidelines for urban freeways, studies are conducted for building new models for traffic operations at on-ramps. Our research work is aimed at a better understanding of the interactions between vehicles in the merging lane and vehicles in the motorway lane, in order to improve driver behaviour and the intrinsic qualities of the road. We discuss new approaches of merging modelling for motorway traffic. The models aim to gather general knowledge on the merging process, from the analysis of microscopic traffic data collected on the site SAROT.

Keywords: Road safety, behaviour of vehicles in insertion, partner vehicle, modelisation of the probability of insertion, logistic regression, road design

1 Introduction

In this paper, we discuss new approaches of merging modelling for motorway traffic. The models aim to gather general knowledge on the merging process, from the analysis of mi-

croscopic traffic data collected on the French experimental site SAROT. In a first part, we recall usual merging models. Then we present the SAROT site. In section 4, we present a statistical method for estimating the probability of insertion of vehicles in the merging lane between two consecutive points of measure. In section 5, we introduce a behavioural model to reproduce the merging behaviour observed.

2 Literature review

In order to model a merging-giveway in a merging section, [8] proposed an approach based on game theory to reproduce the behaviour of couples of merging and through vehicles as a two-person non-zero-sum non-cooperative game with perfect information. Each driver tries to take the best actions in forecasting the other's driver actions. The merging probability and giveway probability are obtained by solving the Nash equilibrium condition. The model estimates the payoff functions for both vehicles based on their position and relative speed with neighboring cars.

[15] presented a simulation model for merging behaviour on motorway based on acceleration, gap acceptance, cooperation behaviour. The authors suggest that interactions in a merging process are results of cooperative lane changing and courtesy yielding behaviour and that these behaviours have a significant effect on merging events. Sensitivity analysis indicates that the model is sensitive to the length of the acceleration lane and the average flow on the motorway section.

[16] are interested in modelling the speed-flow relationship and the merging behaviour. They developed three models of merging desired location, merging distance and merging probability. The authors observed that the merging probability is positively impacted by the relative speed with the leader vehicle and negatively impacted by the relative speed with the follower.

[9] investigated the contribution of drivers' merging behaviour to the breakdown event at freeway-ramp merges and evaluated the influence of the interactions between the vehicles on the traffic flow. They combined a gap acceptance model and a deceleration (forced and cooperative) model to estimate the probability of merging. To validate their model, Kondyli & al. used data resulting from an experiment of an instrumented vehicle moving along I-95 in Jacksonville in Florida.

Otherwise, another category of simulation models admitting an important position among the merging models, is the so-called lane changing simulation models ([2, 6, 1, 13]). [2] considered four levels in the merge decision process: initiating courtesy merging, initiating forced merging, a normal gap acceptance, and gap acceptance of courtesy and forced merging. The model supposes that a vehicle accepts lead and lag gaps to perform a lane change and it has been extented by integrating deceleration and acceleration actions to facilitate merging maneuvers. [1] added the car-following model and the free-flow acceleration model in the classic lane changing model to better describe merging behaviour. Based on observations, [6] proposed to classify the lane changes into free, cooperative and forced. He included intelligent agent concepts to model interactions between vehicles in microsimulation merg-

ing and weaving. [13] developed an integrated driving behaviour model relevant to freeway traffic. They considered two lane changing situations to allow trade-offs between mandatory (performed when the driver must leave the current lane) and discretionary (performed in order to improve the driving conditions in traffic stream) lane changes. They introduced a model structure to capture interdependencies between various decisions of lane changing and acceleration.

3 Presentation of the site

3.1 Description of collected data

The instrumented SAROT site is an experimental platform containing three traffic flow lanes: an on-ramp merge lane marked by 0 and two freeway lanes marked by 1 and 2. The site is located on the A87 in the east of Angers, in western France.

The measure instruments consist of 10 sensors equidistributed and spaced of 50 meters, numbered from 10 to 1 in the direction of traffic flow. Each sensor line includes a couple of electromagnetic loops on the freeway lanes and one loop on the on-ramp segment. The merging vehicles are detected at sensor line 8 (see Fig. 1) and followed until their merging in the freeway flow before point 3, or, at the latest until the end of merge lane (expand on 250 meters). The freeway through vehicles are detected at the sensor line 10 until their exit of site at sensor line 1.

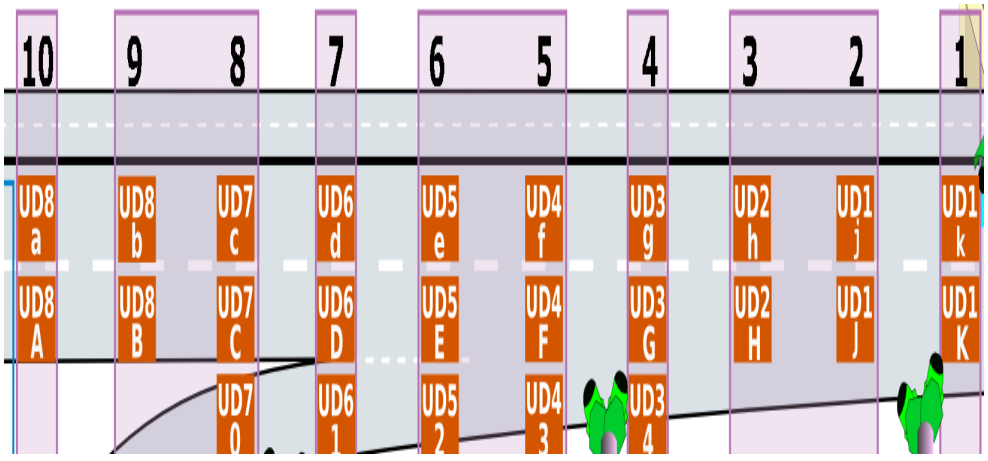

Fig. 1: SAROT site

The data collection system is composed by loops, detections units to ensure the signal processing issue from the loops and control post aggregation of information to reconstruct the vehicles traces and store them in a data basis.

The aim of the installation is to measure in real time the drivers behaviour and the traffic road stream in order to allow research agencies and professionals to analyze and detect the dangerous situations. Further, cameras to record video images and cameras to read number plates are fixed to the roadway edge.

The average flow can reach up 22000 vehicles per day. The speed is limited at 90 km/h and generally, the traffic is free-flow stated and the speeds are homogeneous. 15% of the vehicles are heavy and the merging vehicles represent 18% of traffic.

The gathered data are at a microscopic level. For each vehicle, these are: the timestamp, speed, length and the number of lane on every sensor line.

3.2 Definitions

At a given sensor line, we designate by:

- The "partner leader" (respectively "partner follower") of the merging vehicle, the nearest vehicle which passes just before (behind) it on lane 1 during the previous (following) 5 seconds.
- The lead (lag) time gap as the time headway separating the passing of a partner leader (follower) and a merging vehicle.
- The relative speed (with a leader or a follower) as the difference between the speed of the merging vehicle and its partner (leader or follower).

We consider throughout this document the situation illustrated in Fig. 2 representing a current merging vehicle C with a partner leader L and a partner follower F in a merge area.

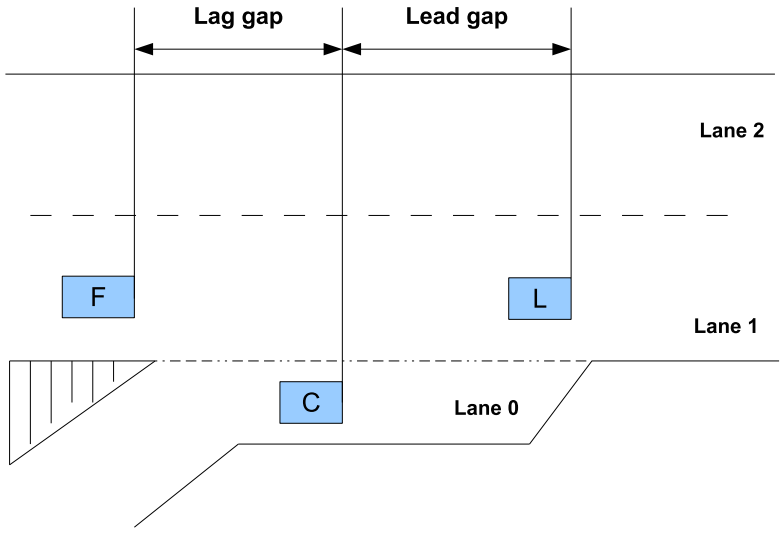

Fig. 2: Merging framework for the merging vehicle C; the traffic direction is left to right

3.3 Empirical analysis

Merging maneuvers may bring about an inconvenience either to the partner follower (it decelerates or changes lane to lane 2) or to the merging vehicle if its partner does not give way and overtakes it.

An analysis of merging locations shows that most (almost 50%) merges occur at[1] sensor line 5 (see Fig. 3). This first peak is situated in the middle of the site independently of the hour in the day. Second and third small peaks are observed in respectively sensor lines 4 and 6. Accordingly, we shall focus this analysis on the area limited by these three points.

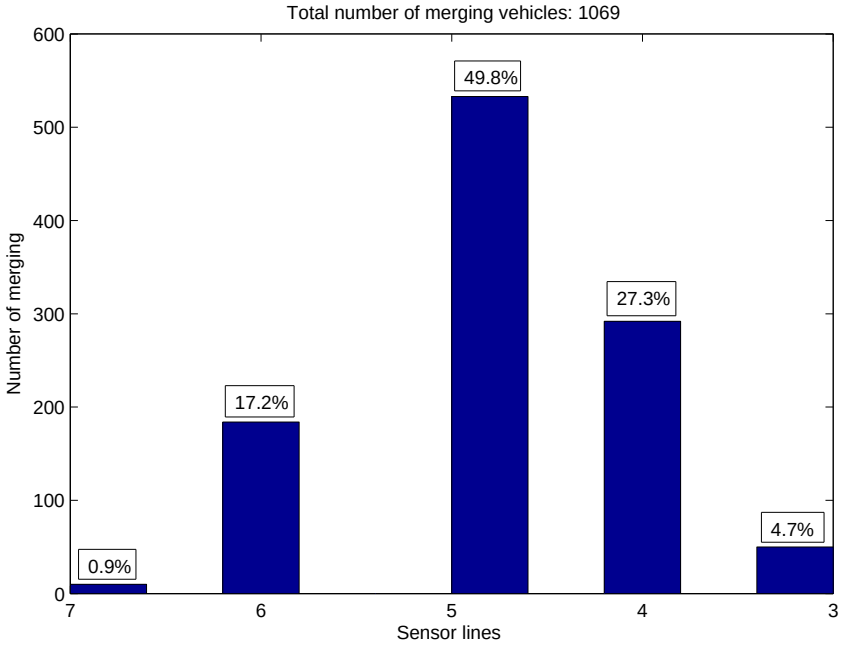

Fig. 3: Histogram of merge location

Analysis of the median values of the lead time gap accepted shows that the median varied from 0.89s at sensor line 3 to 1.3s recorded at point 5, whereas, the median lag time gap accepted are slightly higher and varied from 1.5s at point 5 to 2.1s at point 3. The lead time gap refused are around 1.2s and the lag gap time refused are around of 1.5s at all measuring points.

The drivers often accept small gaps. We observe that nearby line 5, 65% of the merging vehicles merged in a lead gap less than 2 s and 61% with a lag time gap less than 2s. This trend grows at sensor lines 6 and 4, with more than 75% of lead time gaps smaller than 2 s. And respectively 58% and 75% of lag time gaps smaller than 2s at sensor lines 6 and 4. Moreover, gaps less than 0.2 s were recorded.

4 Statistical modelling of merge behaviour

4.1 The *logit* model

The modelling proposed here will be completely at the microscopic level, due to the structure of individual data. We want to predict the merging probability of the merge vehicle at a given

[1]It should be noted that merging occurs a few meters before a merging point.

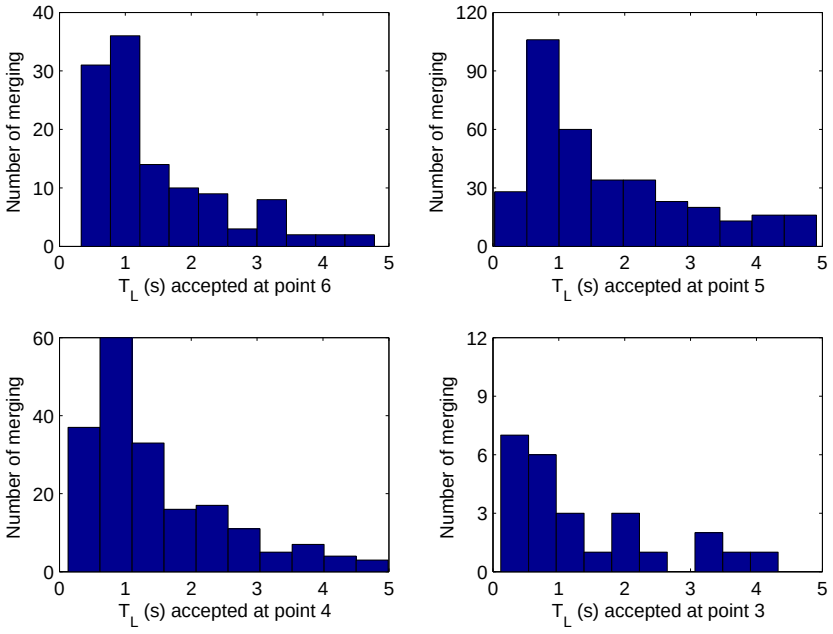

Fig. 4: Lead gaps T_L accepted at sensor lines 6, 5, 4 and 3

point ($Y = 1$ or not $Y = 0$). To do this, we use a logistic regression procedure ([7, 12, 16]) based on the observations of the following explanatory variables which can contribute to the decision of merging: speed of merging vehicle ($X_1 = V_C$), lead time gap ($X_2 = T_L$), relative speed of merging vehicle with respect to its partner leader ($X_3 = Dv_L = V_L - V_C$), lag time gap ($X_4 = T_F$) and relative speed of merging vehicle with respect to its partner follower ($X_5 = Dv_F = V_C - V_F$). The model can be expressed as follows:

$$\eta(x) = \mathbb{P}(Y = 1|X = x) = \frac{\exp\left(\beta_0 + \sum_{j=1}^{p} \beta_j x^j\right)}{1 + \exp\left(\beta_0 + \sum_{j=1}^{p} \beta_j x^j\right)}$$

where, the x^j denote the realizations of the descriptive variables. The p coefficient estimators of β_j are obtained from the likelihood maximization method by solving the system of equations:

$$\begin{cases} \dfrac{\partial \ell(\Theta; y)}{\partial \beta_0} = \displaystyle\sum_{i=1}^{n} (y_i - \eta(x_i)) \\ \dfrac{\partial \ell(\Theta; y)}{\partial \beta_j} = \displaystyle\sum_{i=1}^{n} x_i^j (y_i - \eta(x_i)), \forall j \in \{1, .., p\} \end{cases}$$

where ℓ is the log-likelihood function of the model expressed by:

$$\ell(\Theta; y) = \sum_{i=1}^{n} y_i \ln(\eta_i) + (1 - y_i) \ln(1 - \eta_i) \quad (*)$$

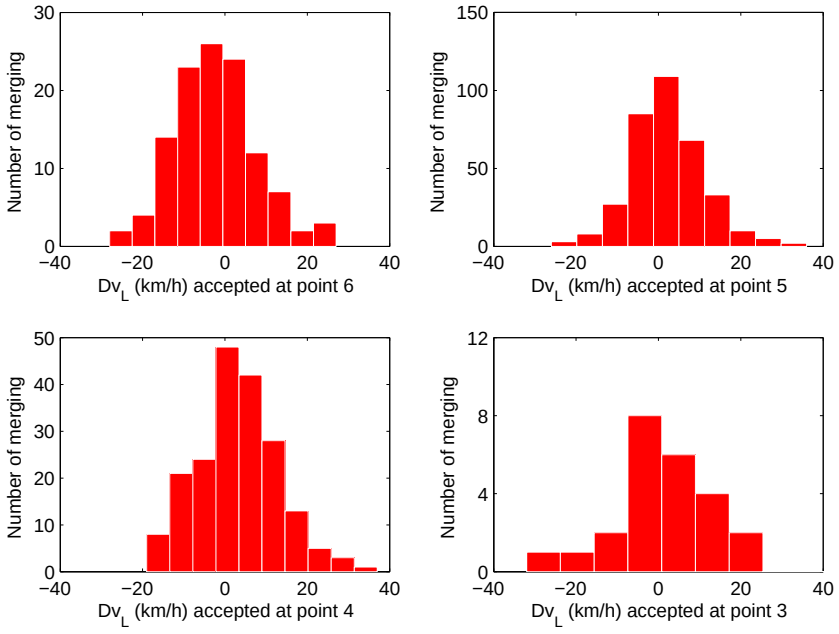

Fig. 5: Relative speed of merge vehicle C with respect to lead vehicle L if "merging" at sensors 6, 5, 4 and 3

and Θ is the set of parameters $(\beta_0, \beta_1, \beta_2, \beta_3, \beta_4, \beta_5)$ associated with the explanatory variables, and β_0 is the intercept. The decision rule to assign a "merge" is taken when $\hat{\eta}(x)$ the estimator of $\eta(x)$ is greater than $\frac{1}{2}$, otherwise we assign "no merge" for the vehicle.

4.2 Application to data

We carry out *logit* procedure using the previously presented data collected between 7a.m. and 10a.m. We select the 3049 merging vehicles which possess both a leader and follower partners at the sensor line before their merging. Other cases where the merge vehicle has only a leader or only a follower will be discussed later. The data sample is separated into two parts: one set to establish a learning base and to estimate the parameters of the model and another set to test the model. In the data used here, no vehicle merged before point 7 and the number of vehicles that merged at point 3 is insignificant.

Tab. 1 lists for every sensor line, the estimated parameters $(\hat{\beta}_0, \hat{\beta}_1, \hat{\beta}_2, \hat{\beta}_3, \hat{\beta}_4, \hat{\beta}_5)$ of the model and the corresponding standard errors, t-statistics and p-values associated to the Student test.

Figs. 6 and 7 present the influence of the variables time gap and relative speed between the merging vehicle and its partners on the a posteriori merging probability at the sensor line 6.

Tab. 2 presents the results of performance of the *logit* model at differents point of merging for n merging vehicles.

The influence of the different variables on the model will be discussed in the Sec. 4.3.

Tab. 1: Estimation of regression parameters for sensors 6, 5, 4

Sen.	Estimated parameters	Standard errors	t-Statistic	p-Value
6	(-2.93,0.02,-0.14,-0.10,0.26,0.04)	(1.99,0.02,0.15,0.02,0.14,0.02)	(-1.47,0.99,-0.89,-5.18,1.81,1.55)	(0.14,0.32,0.37,0.00,0.07,0.12)
5	(-1.67,0.03,0.22,-0.08,0.16,0.001)	(1.68,0.02,0.12,0.02,0.12,0.02)	(-0.99,1.22,1.79,-4.37,1.25,0.33)	(0.32,0.22,0.07,0.00,0.21,0.74)
4	(-0.59,0.03,-0.26,-0.04,0.37,0.06)	(3.76,0.05,0.29,0.03,0.31,0.04)	(-0.16,0.62,-0.92,-1.25,1.19,1.44)	(0.87,0.53,0.36,0.21,0.23,0.15)

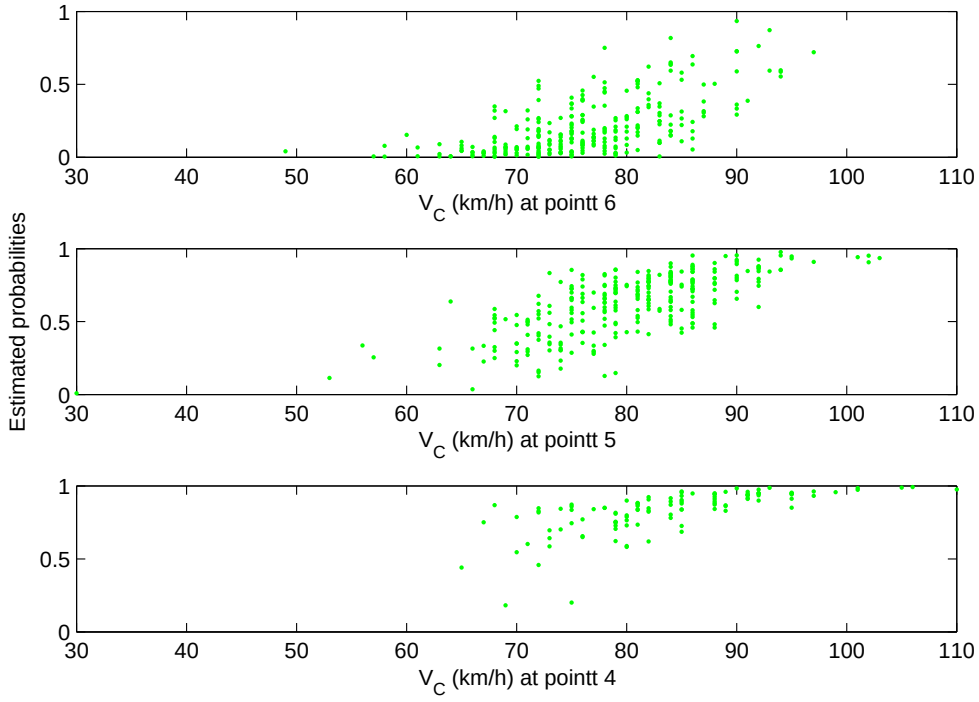

Fig. 6: Probabilities predicted depending on V_C at sensors 6, 5 and 4

4.3 Model selection

We intend to investigate the contribution of every regressor variable in the prediction of the probability of merging. Indeed, some variables do not provide information and complicate the model. We will use many procedures such as model selection criteria and hypothesis tests. To this end, we shall test the significance of parameters β_j of X_j with two statistical tests: the Wald test and the likelihood ratio test (LRT) ([7], [12]) together with the so-called AIC Akaike's and BIC Schwartz's criteria ([7], [12]).

We apply these tests on the $2^p - 1$ models derived from the possible combinations of X_j vectors. Denote $M_g = (V_C, T_L, Dv_L, T_F, Dv_F)$, the general model composed of all explanatory variables.

The Akaike information criterion is grounded in the concept of penalization of log-likelihood by a function of the number p of parameters, when a given model is used. As to the Schwartz

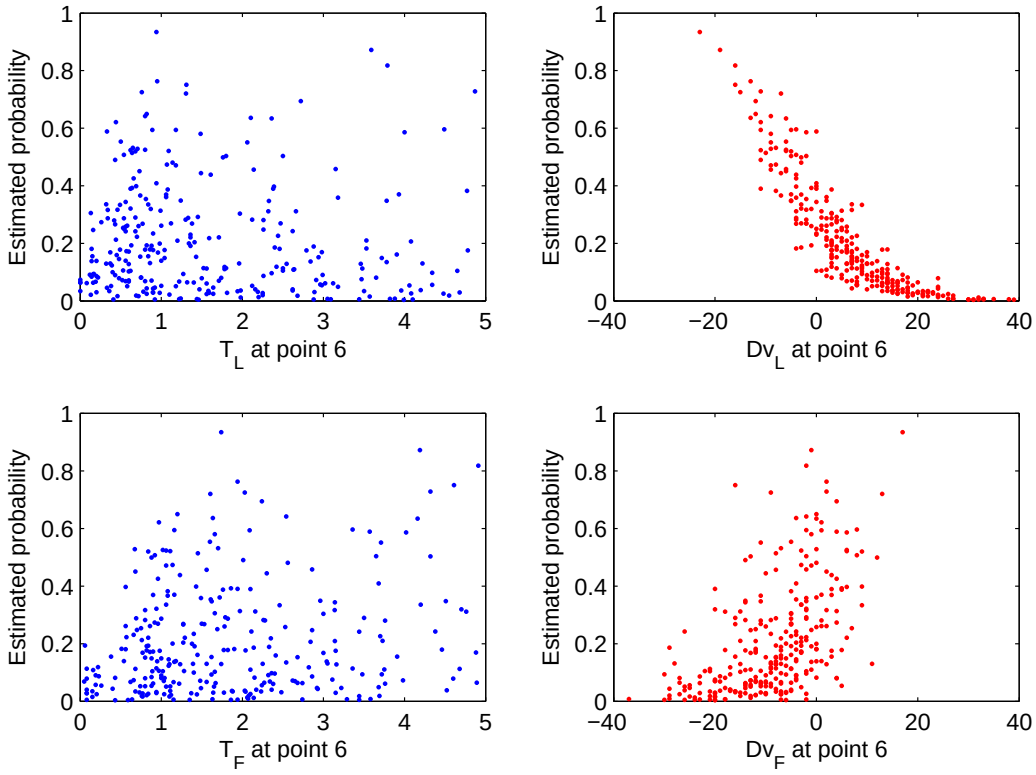

Fig. 7: Probability of merging predicted depending on T_L, Dv_L, T_F and Dv_F at sensor 6

information criterion, it is based on a Bayesian formalism. The value of the penalty function is $2p$ for AIC and $p \ln n$ for BIC. The general expression of these criteria are:

$$AIC = -2 \times \ell + 2p$$

$$BIC = -2 \times \ell + p \times \ln n$$

where ℓ is the log-likelihood given by the equation $(*)$ and n is the sample size. The model selected is the first model to minimize the information AIC, BIC.

The Wald test allows testing the nullity of q $(1 \leq q \leq p)$ parameters of the *logit* model from generalizing the test of significance of a single parameter. The Wald test is performed for

Tab. 2: Results of the *logit* model per sensor line

Sensor	n	Predicted merges	Real merges	Predicted no-merges	Real no-merges	Successfully
6	282	32	54	250	228	81.6%
5	282	203	169	79	113	71.6%
4	113	109	100	4	13	90.3%

submodels. The null hypothesis is:

$$\mathcal{H}_0 :$$

$$\beta_{j_1} = \beta_{j_2} = ... = \beta_{j_q} = 0, \ \ \forall 1 \leq j_1 \leq ... \leq j_q \leq p$$

against

$$\mathcal{H}_1 : \overline{\mathcal{H}_0}\,.$$

The Wald statistic is given by $\Lambda_q = \hat{\Theta}_q' \hat{\Sigma}_q^{-1} \hat{\Theta}_q$, where $\hat{\Theta}_q$ is the vector of estimated parameters to test and $\hat{\Sigma}_q$ is their empirical variance-covariance matrix. The reject area of the Wald test is: $\Lambda_q \geq \chi^2_{1-\alpha}(q)$.

We start to share the set of submodels of M_g into four groups of same number of parameters. Then, we apply the Wald test to all models of each cluster. Later, the model validated by the test is identified and when several models are accepted, the model choosen is the optimal model selected for the AIC criterion. Thereby, we obtain an optimal model on each group. The final selected model is the one with the Wald statistic Λ_q the most discarded from its reject area.

The LRT selects the best model among nested models. The hypotheses to be tested are:

$$\mathcal{H}_0 : M_s \textit{ is more suitable than } M_g$$

against

$$\mathcal{H}_1 : M_s \textit{ is not more suitable than } M_g\,.$$

We first set a benchmark model M_g that we would like to compare to its submodels M_s with p' ($\leq p$) parameters. For each identified submodel, we calculate the associated deviance $D_s = -2\ell$. Where ℓ is the log-likelihood function given by the equation $(*)$. The LRT statistic is $\Delta D = D_s - D_g$. Under the null hypothesis $\mathcal{H}_0$, the variable ΔD is Chi-square distributed with $p - p'$ degrees of freedom. The null hypothesis is rejected if $\Delta D > \chi^2_{1-\alpha}(p - p')$. In case $\mathcal{H}_0$ is favoured for several models with the same number of parameters, the model which has the smallest AIC value is kept.

The LRT is a powerful test and it detects the alternative hypothesis more often than the Wald test.

4.4 Discussions of results of statistic model

The model yields an average success rate of 85.1% on the three sensor lines 6, 5 and 4. The details are presented in Tab. 2.

Thus, we can see that the highest success rate is obtained for the model at point 4, where, the model predicts 99% of the good merging and only 23.1% of the good no-merging, partly due to the low number of no-merging in the learning dataset at this point. Furthermore, the *logit* model M_g predicts 93% of the good no-merging and 31.5% of the good merging at point 6. At point 5, it predicts 86.4% of the good merging and 49.6% of the good no-merging. In the main, this model tends to overestimate the merging into measurement points 4 and 5, and to underestimate the no-merging at these same points. The trend is inverted at point 6.

The performance of model is overall satisfactory. Although the success rate of the model is low at point 5 however, it predicts the no-merging better than at point 4, whereas the merging conditions should be close as only 50m separate the sensor line 5 from each of the two other points.

Only 30.8% among the badly classified of the *logit* model have an estimated probability $\hat{\eta}(x)$ belonging to the uncertainty area $([0.4; 0.6])$.

Comparison of submodels of M_g by different criteria and tests:

Tab. 3 presents the selected model through the various criteria at each measurement point. The last column of Tab. 3 presents the selected model which has the highest success rate among the submodels of M_g and the corresponding percentage value.

Tab. 3: Comparison of models selected by many criteria

Sensor	AIC	BIC	LRT	Wald test	Success rate
6	Dv_L	Dv_L	$T_L + Dv_L + T_F$	$Dv_L + T_F + Dv_F$	$T_L + Dv_L + Dv_F$ 82.6%
5	$V_C + Dv_L$	Dv_L	$V_C + Dv_L$	$V_C + Dv_L$	$V_C + T_L + Dv_L$ 71.6%
4	V_C	V_C	V_C	$V_C + Dv_L$	$V_C + T_L + Dv_L + T_F + Dv_F$ 90.3%

All statistic tests and criteria of selection agree on the importance of the variable V_C in the modelling at sensor 4. At points 6 and 5, the drivers seem to consider also the relative speed Dv_L to take their "merging" or "no-merging" decision. The Wald test reject the hypothesis that all model parameters are simultaneously null at each point. The Wald test accepts the hypothesis of individual nullity of coefficients β_j of model M_g at point 4, this is maybe due to possible collinearity between the explanatory variables themselves. The Wald test rejects the hypothesis that $\beta_3 = 0$ at all points, thus confirming that the associated variable Dv_L is influential. Nevertheless, the conclusions of this test must be used with carefulness because it is not enough powerful and it frequently tends to choose the null hypothesis.

In conclusion, the statistical modelling argued that to take its decision (merge or not merge), merging driver is mainly refered to its own speed V_C, and to its relative speed with respect to its leader Dv_L, and this, at the beginning and middle of lane 0. But at the end of the merging lane, only its own speed adjustment matters because he/she wants to merge even forcing to avoid stopping at the end of merging lane.

The choice of the most influential variables is decisive in the *logit* modelling and will serve in order to construct a behavioural model of gap acceptance.

5 Behavioural modelling

5.1 Building of the model

We propose some variables that can be incorporated in a behavioural model (kind of gap acceptance). We use the values of variables X_j corresponding to a predicted probability equal to $\frac{1}{2}$ from the $logit$ model. The realizations belonging the hyperplane $\mathbb{H} = \{x_j \in \mathbb{R}^p : \hat{\eta}(x_j) = \frac{1}{2}\}$ are used as input of critical gap. Then we vary the threshold value between the minimum and maximum of observations of each variable. The threshold is the first achieving a compromise between the success rates for merging and no-merging. The value must be realistic. The tested gap acceptance model are composed from combinations of conditions on the following variables.

- Speed of merging vehicle V_C.
- Relative speed of merging vehicle with respect to its partner leader vehicle $V_C - V_L$.
- Relative speed of merging vehicle with respect to its partner follower vehicle $V_F - V_C$.
- Lead time gap T_L.
- Lag time gap T_F.
- Ratio of the speed of lead vehicle and the speed of merging vehicle $\frac{V_L}{V_C}$.
- Ratio of the speed of lag vehicle and the speed of merging vehicle $\frac{V_F}{V_C}$.
- Gap distance with the leader vehicle $T_L \times V_C$.
- Gap distance with the follower vehicle $T_F \times V_C$.
- Some estimators of the time to collision such as: $\frac{T_L \times V_C}{V_C - V_L}$, $\frac{T_L \times V_C}{V_L - V_C}$, $\frac{T_F \times V_C}{V_F - V_C}$, and $\frac{T_F \times V_C}{V_C - V_F}$.

5.2 Discussion of the results

The variables used in the behavioural model are those mentioned in section 5.1 regarding to the merging vehicle and the partner leader. When the vehicles have a leader and a follower partners, the selected models are less successful at points 5 and 4 where the rate success do not exceed respectively 70% and 88%. When the vehicles just have a partner leader, the selected model at sensor line 5 is the following, with a success rate equal to 74%:

$$(M): \quad V_C \geq \delta_v \text{ and } V_C \times T_L \geq \delta_x$$

where $\delta_v = 75$ km/h and $\delta_x = 9.6$ m.

At measuring point 4, several models give the same success rate equal to 91.5% with always the shared condition on $V_C \geq \delta_v$. The model (M) with thresholds $\delta_v = 59km\ /h$, $\delta_x = 2.1m$

is one of them. The model (M) gives 82% of success rate at point 6 with the thresholds $\delta_v = 88$ km/h and $\delta_x = 2$ m.

We also note that the values of the thresholds chosen do not depend on the association of the variables in the model. Thus, it is possible to estimate separately the thresholds of critical gap in manner more specific using for example the maximum-likelihood estimation methods [14] or the *probit* method ([11], [5]). This could optimize the computation time because it is very long by our approach and these methods can ensure the uniqueness of the threshold obtained.

6 Conclusion

This study has investigated drivers' merging behaviour in the SAROT site. The observations showed that some merging vehicles accept a short time gap ($< 2s$), which is consistent with an empirical analysis of [4] on the observed data collected at A12 in Netherlands. Furthermore, we observed that over 95% of the merging maneuvers were finished at about 50m before the end of merging lane (point 3). On the other hand, the drivers that merge at point 4 only pay little attention to their partners. Maybe some education could be needed to take advantage of the remaining length of the merging lane to compare the merging conditions and therefore the safety.

A statistical method has been used to predict the merging probabilities and the obtained results like the important influence of the vehicle in front of the merging vehicle have been used in the construction of behavioural models based on gap acceptance. The results of the two kinds of models are satisfactory.

The same modelling approach was carried out to vehicles which merge with only a lead vehicle and without follower. In this case, the *logit* model gives a slight improvement with a success rate of 80.8% at point 6, of 73.8% at point 5 and 91.5% at point 4. The most influential variables remain the speed of the merging vehicle and the relative speed of merging vehicle with respect to its partner leader.

The modelling in presence of only a follower partner was investigated in [10] and [3]. The modelling is performed using kernel density methods and the nearest neighbor methods to estimate the probability of insertion, and the authors abtained a success rate around 84%.

The methodology would be validated and the results would be improved, if we had a finer mesh of data, which would allow a better follow up of vehicles. In fact, on account of the layout of sensors (every 50 meters) there is a loss of information between two measuring points, such as: the exact merging location, changes of partners or speed variation. Unfortunately, to our knowledge, a similar installation in an uncongested state, with a better mesh is not yet available in the world.

The proposed model can be used in order to simulate data at an entrance ramp of a freeway.

Acknowledgements

The authors would like to thank Frédéric Bosc at the LRPC of Angers for producing the SAROT data to us. Thanks also to the ANR project MoCoPo for their financial support.

Literature

[1] Ahmed, K. Modeling drivers acceleration and lane changing behaviors. *Ph.D. thesis*, Department of Civil and Environmental Engineering, MIT, 1999

[2] Choudhury, C., M. Ben-Akiva, T. Toledo, G. Lee, & A. Rao. Modeling cooperative lane changing and forced merging behavior. Transportation Research Board, *Proc. of* 86^{th} *Annual Meeting*, 2007

[3] Conde Céspedes, P. Étude et caractérisation de pelotons sur des routes a forte circulation-applications. *Technical report*, Université Pierre et Marie Curie, 2010

[4] Daamen, W., M. Loot, & S. Hoogendoorn. Empirical analysis of merging behavior at freeway on-ramp. Transportation Research Board, *Proc. of* 89^{th} *annual meeting*, Washington, USA, 2011

[5] Daganzo, C. Estimation of gap acceptance parameters within an across the population from roadside observation. *Transportation Research Part B*, Pergamon Press, 15B, 1981, p. 1–15

[6] Hidas, P. Modelling vehicle interactions in microscopic simulation of merging and weaving. *Transportation Research Part C*, 13, 2005, p. 37–62

[7] Hosmer, D.W. & S. Lemeshow. *Applied Logistic Regression*. Wiley and Sons, 2000

[8] Kita, H. A merging-giveway interaction model of cars in a merging section: a game theoretic analysis. *Transportation Research Part A*, 33, 1999, p. 305–312

[9] Kondyli, A. & L. Elefteriadou. Modeling driver behavior at freeway-ramp merges. *Transportation Research Board*, 2011, p. 29–37

[10] Louah, G. P. Conde-Céspedes, D. Daucher, B. Jourdain, & F. Bosc. Traffic operations at an entrance ramp of a suburban freeway first results. 6^{th} *International Symposium on Highway Capacity and Quality of Service*, 2011

[11] Mahmassani, H. & Y. Sheffi. Using gap sequences to estimate gap acceptance functions. *Transportation Research Part B*, 15, 1981, p. 143–148

[12] Tenenhaus, M. *Statistiques; méthodes pour décrire, expliquer et prévoir*. Dunod, 2nd edition, 2007

[13] Toledo, T., H. N. Koutsopoulos, & M. Ben-Akiva. Integrated driving behavior modeling. *Transportation Research Part C*, 15, 2007, p. 96–112

[14] Troutbeck, R. Capacity of limited-priority merge. *Transportation Research Board* 1678, 2007, p. 269–276.

[15] Wang, J. A Merging Model for Motorway Traffic. *Ph.D. thesis*, Institute for Transport Studies, University of Leeds, 2006

[16] Weng, J. & Q. Meng. Modeling speed-flow relationship and merging behavior in work zone merging areas. *Transportation Research Part C*, 19, 2011, p. 985–996

Probabilistic inversion for estimating the variability of material properties: A Bayesian multilevel approach

Joseph Nagel, Bruno Sudret

Chair of Risk, Safety & Uncertainty Quantification,
Institute of Structural Engineering, ETH Zürich, Switzerland
nagel@ibk.baug.ethz.ch, sudret@ibk.baug.ethz.ch

Abstract: Bayesian inference provides a convenient framework for the solution of inverse problems and the purposes of uncertainty quantification. It allows the estimation of model parameters from noisy data in a large variety of experimental situations. A major asset of the Bayesian paradigm is its unique and consistent treatment of complex models. Within the realms of Bayesian multilevel models aleatory variability and epistemic uncertainty can be naturally accounted for. In this contribution we will present the joys and sorrows of Bayesian multilevel modeling with a focus on probabilistic inversion, i.e. the inference of the variability of model inputs throughout a number of similar experiments. The possibilities it opens up as well as the problems it suffers from will be presented in the context of engineering applications. To that end we devise a simple academic example within the domain of structural engineering. On the basis of this simple problem we will develop the Bayesian multilevel perspective and exemplify its computational machinery. Under consideration is an ensemble of simply supported beams which are subjected to concentrated point loads. Measuring deflections allows for the identification of the variability of Young's moduli across the sample of beams.

Keywords: inverse problems, Bayesian inference, multilevel/hierarchical modeling, probabilistic inversion, Markov chain Monte Carlo, data augmentation, simply supported beams

1 Inverse problems

Broadly speaking solving an *inverse problem* is the inference of model parameters or the identification of system states from noisy measurements. This covers a wide range of problems that arise in nearly all branches of natural science and engineering. Driven by the rise of powerful general-purpose computing facilities and the availability of dedicated software environments the Bayesian approach has become prevalent. It establishes a rigorous probabilistic framework and ships with a vast set of dedicated computational techniques. Scarce data and available expert information can be easily dealt with in Bayesian data analysis. A manifest advantage of the Bayesian frame is that it inherently is a means to *uncertainty quantification*. The result of any full Bayesian parameter estimation is basically a measure of epistemic (un)certainty over a set of admissible values.

1.1 Parameter estimation

The generic *parameter estimation* problem can be stated as follows. A physical forward model $\mathcal{M}$ describes the system or phenomena under consideration and a fixed yet unknown model parameter $\boldsymbol{x}$ is to be identified in an experiment. Such a model may be viewed as a map $\boldsymbol{x} \in \mathcal{D}_{\boldsymbol{x}} \subset \mathbb{R}^p \mapsto \boldsymbol{y} = \mathcal{M}(\boldsymbol{x}) \in \mathbb{R}^q$. In engineering applications it can be a merely analytical expression, the numerical solution of a set of partial differential equations or even a surrogate model [8]. Subjected to known experimental conditions $\boldsymbol{d}_i$ a set of observations $\boldsymbol{y}_i$ is acquired for $i = 1, \dots, n$. Thus for parameter estimation the prototype of a statistical data model is written as

$$\boldsymbol{y}_i = \mathcal{M}(\boldsymbol{x}, \boldsymbol{d}_i) + \boldsymbol{\varepsilon}_i. \tag{1}$$

The residual $\boldsymbol{\varepsilon}_i \sim f_{\boldsymbol{E}}(\boldsymbol{\varepsilon}_i)$ accounts for the discrepancy between data $\boldsymbol{y}_i$ and model predictions $\mathcal{M}(\boldsymbol{x}, \boldsymbol{d}_i)$ due to measurement errors, numerical approximations as well as model inadequacies. The most widespread choice for a residual distribution is Gaussian one $f_{\boldsymbol{E}}(\boldsymbol{\varepsilon}_i) = \mathcal{N}(\boldsymbol{0}, \boldsymbol{\Sigma})$. The likelihood function is given as

$$\mathcal{L}(\boldsymbol{y}_1, \dots, \boldsymbol{y}_n | \boldsymbol{x}) = \prod_{i=1}^{n} f_{\boldsymbol{E}}\big(\boldsymbol{y}_i - \mathcal{M}(\boldsymbol{x}, \boldsymbol{d}_i)\big). \tag{2}$$

The Bayesian approach to parameter estimation consists in updating a prior or expert knowledge $\pi(\boldsymbol{x})$ in the light of the data $\boldsymbol{y}_i$. The elicitation of this prior distribution is a delicate issue in any Bayesian data analysis. By conditioning on the data the result of Bayesian inference is the posterior density

$$\pi(\boldsymbol{x} | \boldsymbol{y}_1, \dots, \boldsymbol{y}_n) \propto \mathcal{L}(\boldsymbol{y}_1, \dots, \boldsymbol{y}_n | \boldsymbol{x})\, \pi(\boldsymbol{x}). \tag{3}$$

This density quantifies an epistemic a posteriori degree of plausibility. Since it is analytically-closed only on rare occasions one commonly relies on Monte Carlo (MC) sampling from it [7]. Markov chain Monte Carlo (MCMC) can provide powerful mechanisms to draw samples from the posterior by constructing a suitable Markov chain over its support. This only requires the evaluation of posterior density at a number of specific points.

1.2 Probabilistic inversion

Beyond Bayesian updating of an unknown model parameter another interesting class of problems is known as *probabilistic inversion*. Instead of attributing the discrepancy in the data $\boldsymbol{y}_i = \mathcal{M}(\boldsymbol{x}_i, \boldsymbol{d}_i) + \boldsymbol{\varepsilon}_i$ solely to a residual $\boldsymbol{\varepsilon}_i$, one assumes an aleatory variability

$$(\boldsymbol{x}_i|\boldsymbol{\theta}) \sim f_{\boldsymbol{X}|\boldsymbol{\Theta}}(\boldsymbol{x}_i|\boldsymbol{\theta}) \tag{4}$$

over the set of experiments for $i = 1, \ldots, n$. The vector of hyperparameters $\boldsymbol{\theta}$ determines the variability of the model inputs $\boldsymbol{x}_i$. Instead of a fixed yet unknown model parameter $\boldsymbol{x}$ inferential interest concentrates on the unknown hyperparameters $\boldsymbol{\theta}$. One therefore constructs a marginalized likelihood

$$\mathcal{L}(\boldsymbol{y}_1, \ldots, \boldsymbol{y}_n|\boldsymbol{\theta}) = \prod_{i=1}^{n} \int_{\mathcal{D}_{\boldsymbol{x}_i}} f_{\boldsymbol{E}}\big(\boldsymbol{y}_i - \mathcal{M}(\boldsymbol{x}_i, \boldsymbol{d}_i)\big)\, f_{\boldsymbol{X}|\boldsymbol{\Theta}}(\boldsymbol{x}_i|\boldsymbol{\theta})\, \mathrm{d}\boldsymbol{x}_i. \tag{5}$$

by integrating out the intermediate variables $\boldsymbol{x}_i$. Depending on the context these quantities are also called latent variables or missing data. Having elicited prior information $\pi(\boldsymbol{\theta})$ the updated posterior follows as

$$\pi(\boldsymbol{\theta}|\boldsymbol{y}_1, \ldots, \boldsymbol{y}_n) \propto \mathcal{L}(\boldsymbol{y}_1, \ldots, \boldsymbol{y}_n|\boldsymbol{\theta})\, \pi(\boldsymbol{\theta}). \tag{6}$$

However, the evaluation of the marginalized likelihood Eq. (5) when sampling from the posterior Eq. (6) remains an issue. Indeed the numerical integration involves a large number of calls to the forward model $\mathcal{M}$ which may be computationally expensive to run.

2 Multilevel modeling

As there seems to be no universal definition, we define here *multilevel* or *hierarchical models* as being "an assembly of submodels at different levels of a hierarchy", where conditional dependencies and deterministic maps between the quantities involved constitute the hierarchy. Indeed the problem outlined as probabilistic inversion is a multilevel problem. Treating it as such provides some conceptional insight and suggests computational enhancements. To summarize the overall model with a three-level hierarchy we write

$$(\boldsymbol{y}_i|\boldsymbol{x}_i) \sim f_{\boldsymbol{E}}\big(\boldsymbol{y}_i - \mathcal{M}(\boldsymbol{x}_i, \boldsymbol{d}_i)\big), \tag{7a}$$

$$(\boldsymbol{x}_i|\boldsymbol{\theta}) \sim f_{\boldsymbol{X}|\boldsymbol{\Theta}}(\boldsymbol{x}_i|\boldsymbol{\theta}), \tag{7b}$$

$$\boldsymbol{\theta} \sim \pi(\boldsymbol{\theta}). \tag{7c}$$

A directed acyclic graph (DAG) as in Fig. 1 provides an intuitive representation of this hierarchical model. Such graphs are widely known as Bayesian networks, too. Bayesian multilevel modeling provides the proper Bayesian framework for formulating complex inverse problems involving parameter variability and uncertainty together with a wealth of well-established computational techniques to solve them. It allows for a unique and consistent way of inference.

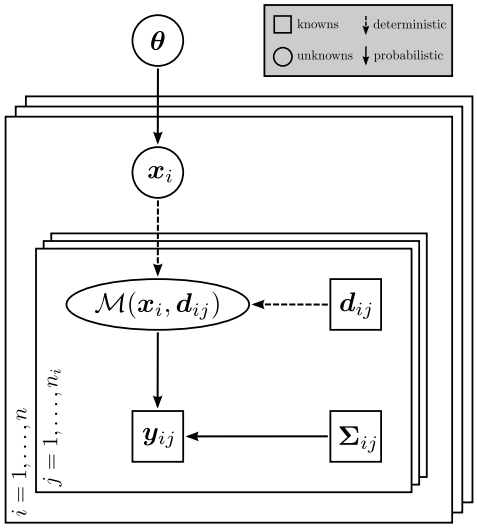

Fig. 1: DAG of the generic framework. The overall multilevel model is assembled from probabilistic (⟶) and deterministic (⇢) relationships between unknown (○) and known (□) variables. The three main levels of variables are shown: the observable data $\boldsymbol{y}_{ij}$, the unobservable parameters $\boldsymbol{x}_i$ and the hyperparameter $\boldsymbol{\theta}$. Moreover there are known forward model inputs $\boldsymbol{d}_{ij}$ as well as known residual covariances $\boldsymbol{\Sigma}_{ij}$. There are $j = 1, \ldots, n_i$ observations for each individual unit $i = 1, \ldots, n$.

2.1 Types of inference

Bayesian inference in hierarchical models is based on constructing the joint posterior $\pi(\boldsymbol{x}_1, \ldots, \boldsymbol{x}_n, \boldsymbol{\theta} | \boldsymbol{y}_1, \ldots, \boldsymbol{y}_n)$ of all unknowns $(\boldsymbol{x}_1, \ldots, \boldsymbol{x}_n, \boldsymbol{\theta})$ conditioned on all knowns $(\boldsymbol{y}_1, \ldots, \boldsymbol{y}_n)$. This posterior is given as

$$\pi(\boldsymbol{x}_1, \ldots, \boldsymbol{x}_n, \boldsymbol{\theta} | \boldsymbol{y}_1, \ldots, \boldsymbol{y}_n) \propto \left(\prod_{i=1}^{n} f_{\boldsymbol{E}}\big(\boldsymbol{y}_i - \mathcal{M}(\boldsymbol{x}_i, \boldsymbol{d}_i)\big) \right) \left(\prod_{i=1}^{n} f_{\boldsymbol{X}|\boldsymbol{\Theta}}(\boldsymbol{x}_i | \boldsymbol{\theta}) \right) \pi(\boldsymbol{\theta}). \quad (8)$$

What is considered *nuisance* is then subsequently integrated out from the posterior. This is the unique Bayesian perspective to inference in multilevel models. Individual parameters $\boldsymbol{x}_i$ and/or the hyperparameter $\boldsymbol{\theta}$ can be of inferential interest.

On the one hand inference of individual $\boldsymbol{x}_i$ becomes possible by treating and estimating them as latent variables instead of integrating them out as nuisance. This allows for a joint learning mechanism that bases the estimation of $\boldsymbol{x}_i$ not only on the inversion of $\boldsymbol{y}_i$ but indirectly also on the information provided by $\boldsymbol{y}_j$ with $j \neq i$. In this context this is generally referred to as the optimal combination of information. The result is the posterior $\pi(\boldsymbol{x}_i | \boldsymbol{y}_1, \ldots, \boldsymbol{y}_n)$ where the hyperparameter and all parameters but $\boldsymbol{x}_i$ have been marginalized out.

On the other hand we will concentrate here on the optimal and efficient estimation of the unknown hyperparameter $\boldsymbol{\theta}$. The correspondingly marginalized posterior density is given as

$$\pi(\boldsymbol{\theta} | \boldsymbol{y}_1, \ldots, \boldsymbol{y}_n) = \int_{\mathcal{D}_{\boldsymbol{x}_1}} \ldots \int_{\mathcal{D}_{\boldsymbol{x}_n}} \pi(\boldsymbol{x}_1, \ldots, \boldsymbol{x}_n, \boldsymbol{\theta} | \boldsymbol{y}_1, \ldots, \boldsymbol{y}_n) \, \mathrm{d}\boldsymbol{x}_1 \ldots \mathrm{d}\boldsymbol{x}_n. \quad (9)$$

It can be seen that constructing the joint posterior Eq. (8) and thereafter integrating out the intermediate parameters Eq. (9) is equivalent to Eq. (6) where they have already been integrated out in the likelihood Eq. (5).

2.2 MCMC sampling

As far as the inference on $\boldsymbol{\theta}$ is concerned there is no conceptional difference between Eq. (6) and Eq. (9). However, the two schemes pose different numerical tasks and differ in their computational efficiency when it comes to MCMC sampling. While the former provides a relatively crude sampling scheme that involves the intricate marginal version of the likelihood, the latter suggests a sampling scheme that is based on the conditional densities $f_{\boldsymbol{E}}\big(\boldsymbol{y}_i - \mathcal{M}(\boldsymbol{x}_i, \boldsymbol{d}_i)\big)$ and $f_{\boldsymbol{X}|\boldsymbol{\Theta}}(\boldsymbol{x}_i|\boldsymbol{\theta})$. Constructing a Markov chain over the joint posterior Eq. (8) and discarding the samples of the intermediate variables $\boldsymbol{x}_i$ directly provides samples from the marginal posterior of $\boldsymbol{\theta}$. This way drawing but neglecting $\boldsymbol{x}_i$ facilitates to draw $\boldsymbol{\theta}$ from the marginal. While when normally stated as the output of a Bayesian analysis, marginals tend to hide dependencies between parameters, in our case this marginalization is indeed the final objective. That technique is sometimes called *data augmentation* [6] and has been trivially derived here for multilevel models. The key challenge posed lies now in the efficient sampling in a possibly high-dimensional parameter space.

2.3 Literature review

The outlined framework represents some kind of an all-embracing superstructure that embeds formerly proposed approaches to handle variability and uncertainty in inverse problems as being particular facets or approximations of it. As a generic framework it allows to interrelate various established ideas and methods and it suggests some fundamentally new ones. Previously established approaches to probabilistic inversion subsume frequentist methods based on the explicit marginalization of the likelihood [4] and the approximate treatment based on linearization [2] or kriging [1] and expectation-maximization-type (EM) algorithms. Moreover there are approximate two-stage approaches that consist in the separate estimation of individual parameters and a subsequent direct statistical estimation of the hyperparameter [5] and Bayesian inference of the hyperparameter by means of MCMC and data augmentation [6]. A nice review of many methodologies for such and associated problems is found in [3].

3 Application example: Simply supported beam

The system under consideration is a set of simply supported beams $i = 1, \ldots, n$ that are subjected to a pinpoint load F_i at midspan. The Young's modulus E_i is constant along the beam span of individual beams i. Individual beams i are assumed to be made out of the same material that exhibits an aleatory variability in E_i. Across the sample Young's moduli E_i are distributed according to a lognormal distribution $\mathcal{LN}(\lambda, \zeta)$ with mean value $\mu_E = \exp(\lambda + \zeta^2/2)$ and standard deviation $\sigma_E = \sqrt{\exp(2\lambda + \zeta^2)(\exp(\zeta^2) - 1)}$. We will assume here that the beam lengths L_i, widths b_i, heights h_i and the applied forces F_i are sufficiently well-known. These model inputs are therefore assigned deterministic values. For each beam the displacement $v_i(s_j)$ at positions $0 \leq s_j \leq L_i/2$ with $j = 1, \ldots, n_i$ along the

beam axis is given as

$$v_i(s_j) = \frac{F_i s_j}{48 E_i I_i} \left(3L_i^2 - 4s_j^2\right) . \tag{10}$$

For $L_i/2 \leq s_j \leq L_i$ a symmetric expression holds. Since the moment of inertia is given by $I_i = b_i h_i^3/12$, the maximal displacement at midspan $s_j = L/2$ is $v_i^{(\max)} = F_i L_i^3/48 E_i I_i$. Eq. (10) will constitute the forward model $v_i(s_j) = \mathcal{M}(E_i, F_i, L_i, I_i, s_j)$ for individual beams i. An individual beam is shown in Fig. 2, a simplified DAG for the full hierarchical problem is shown in Fig. 3. We envisage the experimental identification of how Young's moduli E_i are distributed across a sample of e.g. $n = 100$ timber beams. The procedure will be illustrated by conducting a numerical computer experiment. Therefore we fix and simulate the experimental setup to obtain synthetic pseudo-data and the available prior knowledge as follows.

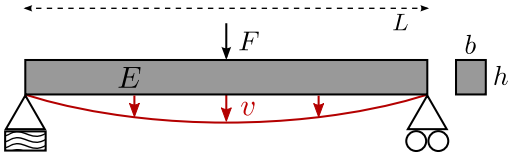

Fig. 2: The simply supported beam

The beam dimensions are set to $L_i = 1\,\mathrm{m}$ and $b_i = h_i = 10\,\mathrm{cm}$ and the applied loads are chosen to be $F_i = 30\,\mathrm{kN}$. For $i = 1, \ldots, 100$ we sample E_i according to a lognormal distribution with $\mu_E = 15\,\mathrm{GPa}$ and $\sigma_E = 3\,\mathrm{GPa}$. This corresponds to a coefficient of variation $c = 20\,\%$. A set of pseudo-measurements for the displacements $v_i(s_j)$ at $n_i = 3$ arbitrarily chosen positions $s_1 = 25\,\mathrm{cm}$, $s_2 = 50\,\mathrm{cm}$ and $s_3 = 75\,\mathrm{cm}$ are generated for every i by perturbing the model predictions Eq. (10) with normally distributed and independent measurement noise $\varepsilon_{ij} \sim \mathcal{N}(0, \sigma_{ij}^2)$ with $\sigma_{ij} = 0.1\,\mathrm{mm}$. Component-wise the hyperprior on the hyperparameters $\boldsymbol{\theta} = (\theta_1, \theta_2)$ with a shape $\theta_1 = \mu_E$ and a scale parameter $\theta_2 = \sigma_E$ is set priorly independent $\pi(\boldsymbol{\theta}) = \pi(\mu_E)\,\pi(\sigma_E)$. The marginals are chosen to be the nearly non-informative uniform and proper prior distributions $\pi(\mu_E) \sim \mathcal{U}(0, 100)$ and $\pi(\sigma_E) \sim \mathcal{U}(0, 100)$.

4 Results

To the extent deemed reasonable we treat the forward model Eq. (10) as a representative black-box. For the sake of universality its role is to represent any other computational forward model, e.g. a FEM model, too. Approaches based on the analytical form of the model or possibly some linearization of it are therefore not considered. Given the described setup we will conduct the Bayesian probabilistic inversion by means of MCMC methods. For a start the probabilistic inversion is based on a simple random walk Metropolis sampling of the posterior Eq. (6). The results will be subsequently compared to a blockwise MCMC sampling scheme of the joint posterior Eq. (8). We rely on Matlab as the platform of our choice. A vectorized function implements the forward model Eq. (10) under consideration.

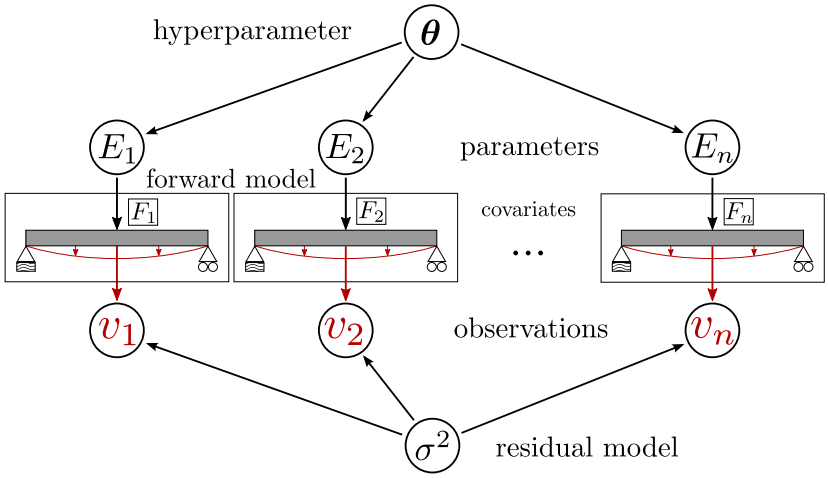

Fig. 3: Simplified DAG of the simply supported beam example. The Young's modulus E_i is varying over a set of simply supported beams $i = 1, \ldots, n$ and a number of similar experiments is carried out to infer individual E_i or their variation $\boldsymbol{\theta} = (\mu_E, \sigma_E)$. The beam dimensions are assumed to be well-known and constant across the sample while the forces F_i act as covariates. A refinement of the residual model σ^2 allows to take more specific models σ_{ij}^2 into account.

4.1 Marginalized likelihood

First of all we show the results of Bayesian probabilistic inversion that is based on the posterior Eq. (6). The integral in Eq. (5) is evaluated by means of simple Monte Carlo techniques, where the number of samples to simulate the likelihood is carefully set to the smallest yet acceptable number. This is accomplished by a systematic comparison to the results of an accurate numerical quadrature and MC sampling with an unreasonably high number of utilized samples. A sample size of $N = 10^5$ per factor in Eq. (5) was employed. The algorithm is tuned by reasonably setting the stepsize and initialized with a two-stage estimate $\hat{\boldsymbol{\theta}}$ of the hyperparameter. With a standard deviation of the Gaussian proposal density of $0.2\,\mathrm{GPa}$ an acceptance rate of ca. $65\,\%$ has been obtained. Traceplots of the resulting MCMC sample of μ_E and σ_E are shown in Fig. 4. The total sample size $N_{ML} = 10^3$ is chosen in such a way that the total execution time $t_{ML} = 1363\,\mathrm{s}$ is of similar magnitude as in the following run. Although being of crucial importance at this place we neither discuss any issues regarding convergence nor its diagnostics.

For the analysis a slightly optimized forward model Eq. (10) has been implemented. We take up the position that when comparing two methods their respective optimum should be compared together. One could also consider the employment of identically implemented forward models for different purposes a fairer comparison. For the sake of completeness we therefore run the same analysis again with the identical implementation of the forward model Eq. (10) which is not optimized for the integration Eq. (5) in particular. In this case the total execution amounted to ca. $t_{ML} = 1797\,\mathrm{s}$.

As the total runtime crucially depends on the number of utilized samples to do the MC integration we shortly state the execution times $t_{10^4} = 206\,\mathrm{s}$ and $t_{10^3} = 41\,\mathrm{s}$ for when $N_{ML} = 10^4$ or $N_{ML} = 10^3$ samples are employed, respectively. As in these cases the evaluation of Eq. (5) turns out to be only insufficiently accurate, these numbers are just intended to provide

a rough measure for if it were sufficient.

4.2 Joint posterior sampling

We carry out the analysis based on the joint posterior Eq. (8) and compare the results to the crude scheme above. A Markov chain over the $n + 2 = 102$-dimensional parameter space is constructed by means of a blockwise random walk Metropolis algorithm. The set of parameters $(\boldsymbol{x}_1, \ldots, \boldsymbol{x}_n)$ and the hyperarameter $\boldsymbol{\theta}$ constitute the different blocks. Tuning of the algorithm takes place by conveniently setting specific stepsizes for the different blocks. We use a Gaussian proposal density with standard deviations $0.02\,\mathrm{GPa}$ for the first block and $0.1\,\mathrm{GPa}$ for the second. This provides an acceptance rate of ca. $65\,\%$. Initialization is done with separate maximum likelihood estimates $\hat{\boldsymbol{x}}_i$ and the two-stage estimate $\hat{\boldsymbol{\theta}}$.

Traceplots of the Markov chain over μ_E and σ_E are given in Fig. 5 while Fig. 6 displays the corresponding simulated marginal posterior densities. This is done by conveniently binning the sample and normalizing the resulting histogram. The sampled two-dimensional posterior of $\boldsymbol{\theta}$ is shown in Fig. 7. For the sake of convenience the binning is the two-dimensional analogue of the one shown in Fig. 6 above. To produce the sample of size $N_{JP} = 10^6$ the execution time adds up to $t_{JP} = 1613\,\mathrm{s}$.

By comparison of Fig. 4 and Fig. 5, the sample sizes of $N_{ML} = 10^3$ and $N_{JP} = 10^6$ and the durations $t_{ML} = 1363\,\mathrm{s}$ and $t_{JP} = 1613\,\mathrm{s}$ the joint approach is shown to be superior to the integrated likelihood one. Having comparable mixing properties the two approaches differ in their computational demand and execution times, though. In our case the difference basically amounts to three orders of magnitude. When involving the integrated likelihood the executions time crucially depends on the exact method and specifications chosen. Nevertheless it seems plausible to generally conclude that these schemes suffer from the numerical burden posed by the integral.

5 Conclusion & Outlook

Bayesian inversion in multilevel models for the treatment of variability and uncertainty has been addressed. Multilevel models provide a convenient framework for probabilistic inversion and other types of inference whereas classical approaches can be considered partial or approximate treatments thereof. Here we have demonstrated the computational benefits of data augmentation for the purpose of probabilistic inversion. The variation of model inputs over a set of similar experiments has been identified in a multilevel analysis. The key challenge was the sampling of the marginal posterior of the hyperparameter that either involves an integrated likelihood or a high-dimensional parameter space. For that purpose the whole range of Bayesian computations as well as dedicated data augmentation sampling schemes are readily available. Future research plans involve the implementation of more efficient dedicated sampling techniques. Moreover the framework will be expanded by stochastic model inputs whose realizations are only imperfectly known but follow a known and prescribed distribution. The influence of these insufficiently well-known inputs on the estimation of

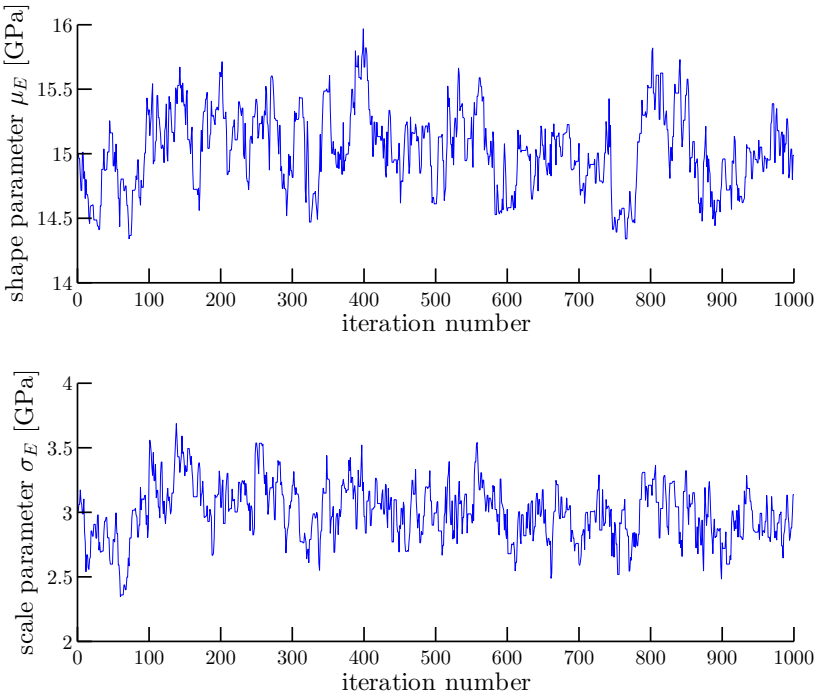

Fig. 4: Traceplots of the Markov chain over μ_E and σ_E are shown for the crude probabilistic inversion. The total algorithm runtime was measured to be ca. $t_{ML} = 1363\,\mathrm{s}$. Mixing properties are comparable to the ones of the joint posterior approach below.

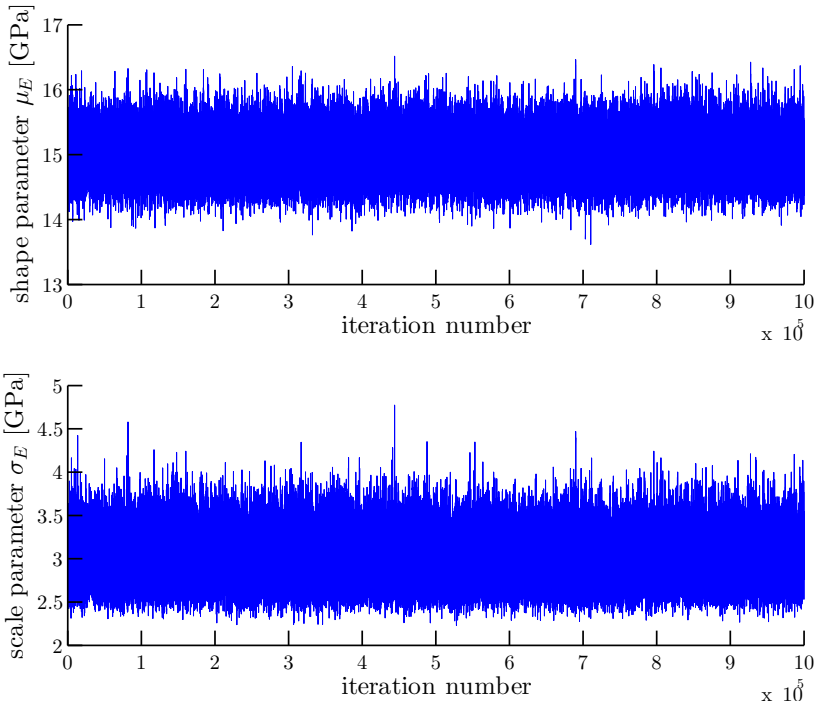

Fig. 5: Traceplots of the Markov chain over the joint parameter space are depicted for μ_E and σ_E. Execution time has amounted to ca. $t_{JP} = 1613\,\mathrm{s}$. Since for comparable runtimes a much higher number of samples $N_{JP} \gg N_{ML}$ is provided the approach is clearly preferable.

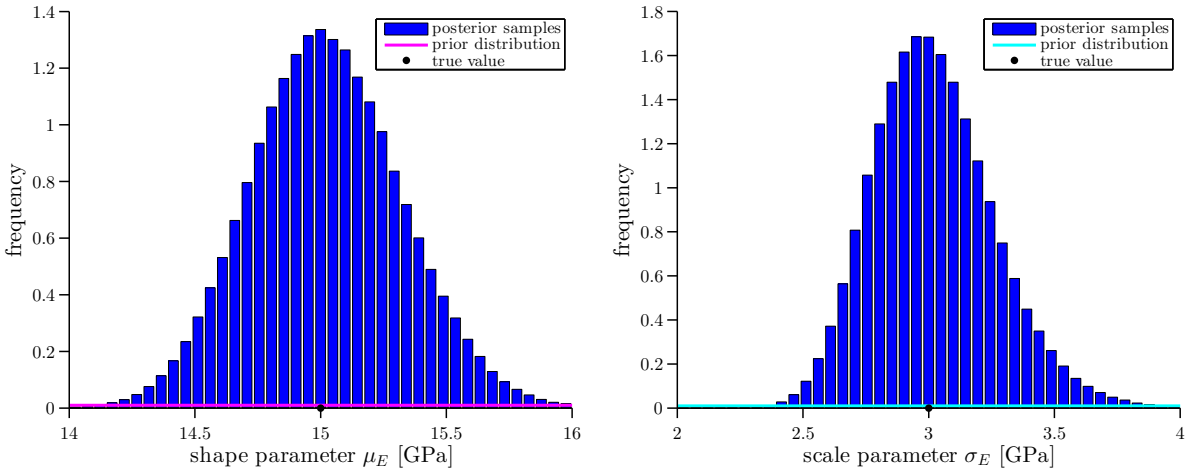

(a) marginal posterior of μ_E (b) marginal posterior of σ_E

Fig. 6: Sampled marginal posterior densities of μ_E and σ_E are shown, respectively. MCMC sampling was based on a blockwise random walk Metropolis algorithm. Here the true values $\mu_E = 15\,\mathrm{GPa}$ and $\sigma_E = 3\,\mathrm{GPa}$ have been recovered quite well.

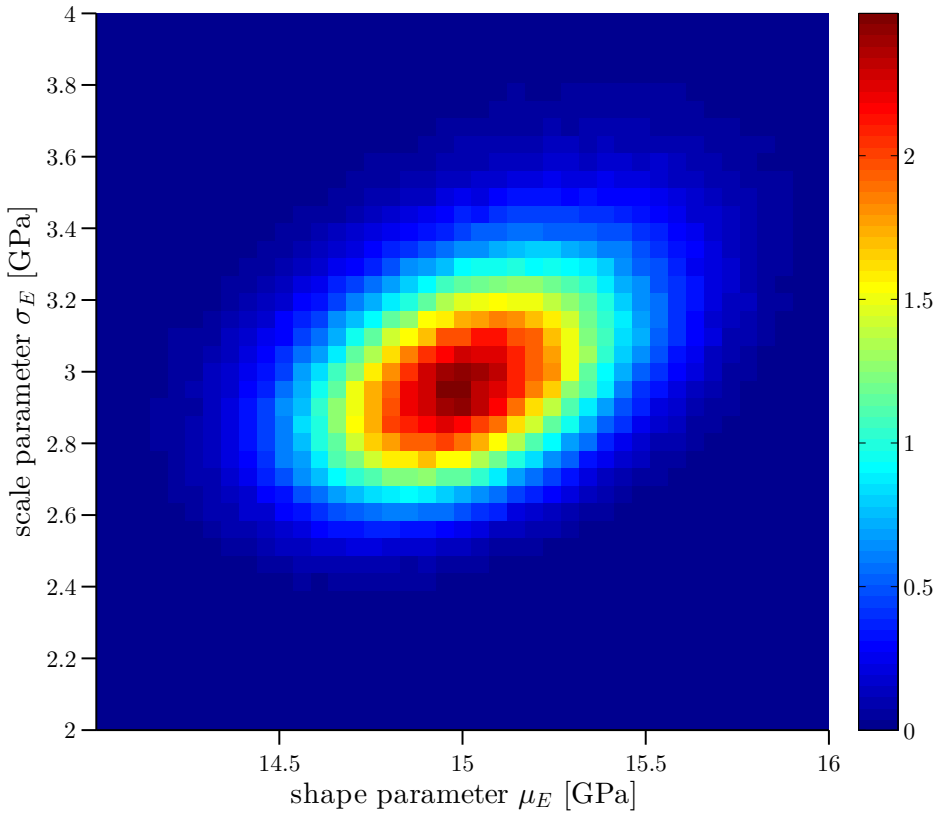

Fig. 7: The sampled two-dimensional marginal posterior of the hyperparameter $\boldsymbol{\theta} = (\mu_E, \sigma_E)$ is shown. A blockwise random walk Metropolis MCMC algorithm was employed. Being priorly independent the components μ_E and σ_E are seen to be correlated a posteriori. The Pearson correlation coefficient amounts to $r_{\mu_E,\sigma_E} \approx 0.4$.

the quantities of interest and the computational expense this requires will be investigated in the future. The introduction of those inputs allows to better resemble realistic situations encountered in applied engineering practice.

Literature

[1] Barbillon, P., Celeux, G., Grimaud, A., Lefèbvre, Y. and de Rocquigny E. Nonlinear methods for inverse statistical problems. *Comput. Stat. Data Anal.*, 55(1), 2011, p. 132–142

[2] Celeux, G., Grimaud, A., Lefèbvre, Y. and de Rocquigny, E. Identifying intrinsic variability in multivariate systems through linearized inverse methods. *Inverse Prob. Sci. Engng.*, 18(3), 2010, p. 401–415

[3] de Rocquigny, E. *Modelling Under Risk and Uncertainty: An Introduction to Statistical, Phenomenological and Computational Methods*. Wiley, 1$^{\text{st}}$ edition, 2012

[4] de Rocquigny E. and Cambier, S. Inverse probabilistic modelling of the sources of uncertainty: a non-parametric simulated-likelihoodmethod with application to an industrial turbine vibration assessment. *Inverse Prob. Sci. Engng.*, 17(7), 2009, p. 937–959

[5] Desceliers, C., Ghanem, R. and Soize, C. Maximum likelihood estimation of stochastic chaos representations from experimental data. *Int. J. Numer. Meth. Engng.*, 66, 2006, p. 978–1001

[6] Fu, S. *Inversion probabiliste bayésienne en analyse d'incertitude*. PhD thesis, Université Paris-Sud, Faculté des Sciences d'Orsay, 2012 (in English)

[7] Robert, C.P. and Casella, G. *Monte Carlo statistical methods* (2$^{\text{nd}}$ Ed.). Springer Series in Statistics. Springer Verlag, 2004

[8] Sudret, B. Meta-models for structural reliability and uncertainty quantification. In K.K. Phoon, M. Beer, S.T. Quek, and S.D. Pang, editors, *Proc. 5th Asian-Pacific Symp. Struct. Reliab. (APSSRA'2012)*, Singapore (Keynote lecture), p. 53–76, 2012

Probabilistic fatigue analysis of a railway bridge

Markus Petschacher [a]

[a]PEC - Petschacher Consulting, ZT-GmbH
Feldkirchen, Austria.
mp@petschacher.at

Abstract: The ageing infrastructure requires sophisticated assessment methods in order to get decision basis for future maintenance actions. It is important to know the actual and past loading history of a bridge and correlate that to investigated hot spots of the structure. Old riveted steel bridges are still common in railway nets and should survive for the next 40 years. Therefore it is important to combine several state-of-the-art approaches like weigh in motion techniques, probabilistic crack growths analysis in combination with modern sampling methods to predict future behaviour.

Keywords: Cross entropy method, BWIM, crack growth analysis, probability

1 Introduction

The paper explains a practical approach of a bridge assessment procedure where shortcomings has been recorded during an inspection and the further actions are not that obvious from an economical point of view. The question about residual lifetime arises and must be answered in an efficient way. The first step is to collect information about the structure. This is normally done by reading existing documents like static analysis, inspection reports and studying drawings. Next the environment situation is analysed, i.e. the realistic loading of the particular bridge must be estimated. The third step will be the lifetime estimation.

The investigated railway bridge consists of two separated single span structures each carrying one track. Each of them have a box cross section made by steel framework girders with a span of $L = 41\,\text{m}$ and lateral bracings at top and bottom. The main system has a lattice of $e = 4.1\,\text{m}$ longitudinal spacing. At top cross girders support a secondary system directly carrying sleepers and rails. This subsystem is made by I-beams connected to main system by

(a) Overview (b) Secondary-primary system

Fig. 1: Railway bridge in Austria with investigated elements (red).

lateral steel plates fixed at the cross girders, see fig. 1(b). The whole structure is riveted and built in 1951. The crucial point therein is that cracks has developed there at stiffening steel plates leading to an weakly connected secondary to primary system.

The presented approach can be described as combination of modern methods not common in practice. The project started with an estimation of the real loading and measuring effects at crucial points in the structure. Therefore the bridge weigh in motion (BWIM) method has been employed probably the first time for a railway bridge in Austria. The actual configuration of measurement is also unique compared to other BWIM railway measurements, see LILJENCRANTZ [12], where sensors have been embedded into concrete or other where the rail has been instrumented. In this particular case laser sensors has been used for axle detection. The results from sensors at hot spots have been used in estimation strain histograms. On basis of that a probabilistic formulation of the fatigue problem has been established. The solution of the numerically very sensitive crack growth formulation has been done by means of the cross-entropy method (CE).

2 Actual loading

2.1 General

In the assessment of bridges often considerably more attention is paid to the modeling of the structure than to the load assumptions. This statement mainly applies on the area of traffic loads. Considering the increasing amount of bridges with a distinct damage pattern, state evaluations will become more important, because also economic considerations depend on them since an immediate intervention is not always possible. The task is to provide realistic traffic load patterns of the bridge that is examined in conjunction with a probabilistic analysis to obtain decision criteria for the further operation of the bridge.

Using load models of standards like Eurocode (EC1) to evaluate existing bridges will often result in a conservative assumption for two reasons. First, the load model targets at a newly built bridge at time $t = 0$ and with a lifetime of 100 years, see EC-0 [6]. Second, the load

model 71 for trains with a classification factor α, see EC1-2 [7] and national regulations like B 45 [1], describe a situation in the future, which does not reflect the actual situation and the particular bridge, on which a specific combination of freight, cargo and passenger trains are running.

Normally, at this point fatigue load models are taken from EC1-2, APPENDIX E [7], and used with a analytical analysis. The simplest but straight forward approach would be to use influence lines and count maxima and minima. The codified combinations of train compositions may not fit reality and lead to conservative results assessing existing bridges. Therefore, monitoring of loading for a particular bridge is recommended. It is economically very attractive compared to computer simulations and provides valuable data.

2.2 Measurement

The single bridges have been instrumented with strain gauges, laser and necessary electronic devices, a patented system named IBWIM [10]. The aim was to record each train during crossing over bridge, weighing the train and measuring strains at the stiffening plates between secondary and primary system. After and loading event happened data are sent to central database where further processing has taken place. A BWIM measurement gives indications about the axle load, train velocity, real lateral distribution of load, dynamic amplification and other statistical parameters.

The advantage of this kind of measurement is the correlation of quantified load event and structural response. Sensors produce differences in voltage while a load passes over the bridge, which is proportional to strain. The crucial part of such a system is the accurate coordination of typically 16 up to 48 sensors each sampled by $500\,\mathrm{Hz}$. The accuracy therefore is about $\pm 3\,\mathrm{ms}$. Analog signals transformed immediately into digital and sent over local area network to a server. The records are analysed by solving an optimization problem.

$$\min \Phi(v, D_1, \ldots, D_{n-1}, W1, \ldots, W_n) \tag{1}$$

The outcome are unknown parameters velocity v, axle spacings $D_1, \ldots, D_{n-1}$ and axle loads $W_1, \ldots, W_n$ of train where n is the number of axles. The number of axles ranges from 4 when locomotive runs over bridge up to 160 and more axles when a freight train is recorded. Other strain records like those at steel plates are bound exactly to the load position of train along the girder and is that way strictly correlated. The measured strains at main girders over time is used to solve eq. 1. The analytical description for the algorithm is given for example in ZHAO ET AL. [18].

It has to be pointed out, that no sensors have been glued onto the rails. The strain gauges at I-beams in combination with laser sensors have been used to detect axles accurately.

In fig. 3(a) strains from I-beams at midspan are shown. It can be seen that noice is very low and only low frequency vibrations from steel structure are given. The high quality of strain records is crucial for further analysis. The stiffening plates between secondary I-beam and cross girder of primary system act together as torsion bearing. After damage observation

(a) Crack (b) Sensor

Fig. 2: The bridge with instrumentation for monitoring.

only outside part of cracked plates could by replaced, inner plates remained as they are. Some of them have short cracks others are completely cracked through. In case only one plate is working i.e. taking over torsonal moments of longitudinal grider it behaves like a cantilever beam. Consequently, the strain amplitudes are doubled which in turn effects the fatigue behaviour.

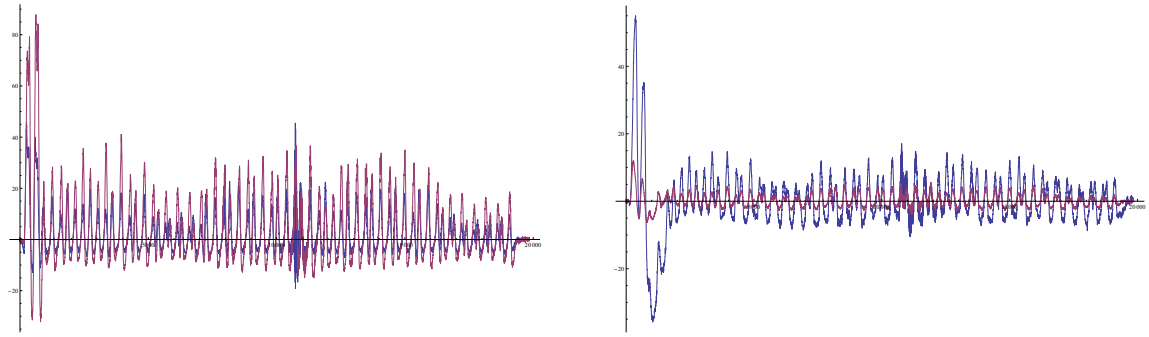

(a) Longitudinal grider (b) Investigated plates

Fig. 3: Records of some sensors from one freight train.

Stress history of stiffening plates is shown in fig. 3(b) for two spots when a light freight train is passing over. One curve shows positive and negative peaks at the beginning of record. That sensor is at a place where the inner plate is cracked. The amplitude becomes roughly double the size compared to the other strain record. This directly effects the fatigue life by higher stress intensities.

For fatigue problem the sequence of loaded and unloaded heavy freight waggons or leight carriages is of interest. This can result in big strain amplitudes depending on the structural element under consideration. The data can be used to re-evaluate the past time using train time tables and combine it with similar recorded train compositions. The load effect for further investigation are defined by stress ranges from strain recordings at mentioned steel plates. The rainflow counting method has been used transforming strain history into load cycles. Within the measurement period of 2 weeks approximately 10000 load cycles for several points has been recorded.

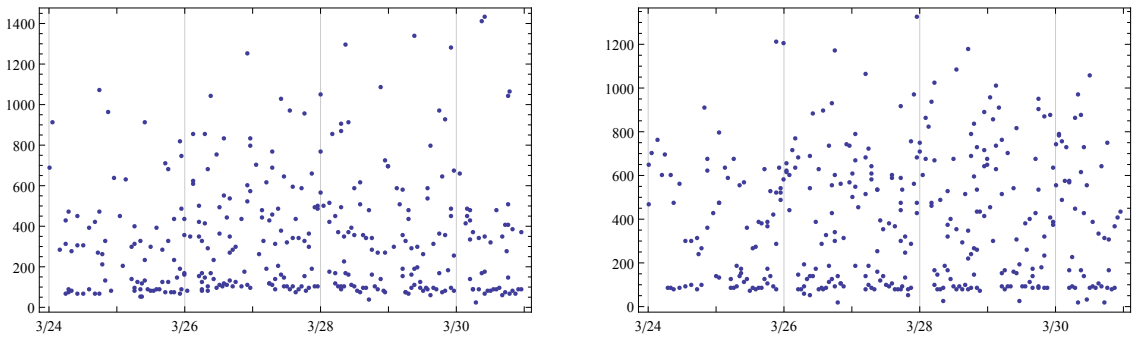

(a) Track 1 (b) Track 2

Fig. 4: Week 13/2013: Total weight of trains in [to].

3 Fatigue Analysis

3.1 Model

There exists a threshold value of ΔK_{th} below which fatigue cracks will not propagate. At the other extreme, $K_{\max}$ will approach the fracture toughness K_C, and the material will fail. Note that ΔK depends on the crack size. For small ΔK, called region I, crack propagation is difficult to predict since it depends on microstructure and flow properties of the material. For larger magnitudes of ΔK, known as region II, the crack growth rate will be governed by a power law, such as the Paris law as the simplest form.

$$\frac{da}{dN} = C_P \, \Delta K^{m_P} \tag{2}$$

with material parameters C and m correlated to each other. The crack growth rate is fairly insensitive to the microstructure. The constants m and C are, of course, different for different materials. If region II includes the dominating part of the fatigue life, the fatigue life can be directly estimated by integrating Paris law. If the stress intensity ratio is increased even further, the region III, the crack growth rate will accelerate and finally fracture will occur. The behavior of this fracture is rather sensitive to the microstructure and flow properties of the material.

A fatigue crack growth analysis uses following probabilistic formulation with limit state function as

$$K_c - K_{\max}(t) = 0 \tag{3}$$

The fracture toughness K_c is compared to time variant and contiounisly increasing stress intensity factor $K_{\max}$. The maximum stress intensity is given by

$$K_{\max}(t) = \sqrt{\pi a(t)} \cdot \sigma_{\max} \cdot Y(a) \tag{4}$$

The crack growth life integration is done by an incremental method. For each increment the stress intensity factor is updated and the number of cycles required to produce a small crack

growth increment is computed. The process is repeated for each step and the accumulated number of cycles is updated.

$$\frac{da}{dN} = \begin{cases} 0 & \Delta K < \Delta K_{th} \\ \frac{C(\Delta K)^m}{(1-R)K_{Ic}-\Delta K_{th}} & \Delta K \geq \Delta K_{th} \end{cases} \tag{5}$$

Crack growth rates computed according to the equivalent constant amplitude stress range approach. This requires that the da/dN versus ΔK curve is linear in a log-log format. The threshold stress intensity ΔK_{th} has been accounted which filters out small cycles in the stress range spectrum, i.e. causing only part of the stress range distribution to be effective. The effect depends on the threshold level, the extent of crack size and the stress range distribution. Computationally the threshold causes $\Delta\sigma_{eq}$ to increase as the crack grows.

Analysis is carried out uses a generic code in VAP 3.1 [17] of an iterative procedure for fatigue crack growth calculation. Thereby, the estimated strain record must be imput as wells as a stress intensity relation $Y(a)$ has to be selected. Due to the limited time of monitoring overload sequences have only be recorded in a small amount which influences the quality of the results of course.

In detail the analysis carries out a numerical integration of crack growth equation. The crack range a_0 to a_c is divided in sufficent small intervals Δa. During each step the crack growth da/dN is evaluated at average crack length of interval. The resulting partial cycles N_t are summed up.

$$N = \sum N_t = \sum \frac{\Delta a_t}{da/dN} \tag{6}$$

The stress intensity factor K is given for a single edge cracked plate under tension taken as simplified model for stiffening plates. The analytical functions for various cases are implemented in VAP 3.1 [17] and can be changed that way easily for a limit state formulation.

4 Analysis

4.1 Motivation

The solution of eq. 2 gives a closed solution when $Y(a)$ is assumed to be constant and no real strain records have to be considered. Then a first order approximation method (FORM) or second order (SORM) approach is possible, see MADSEN ET AL. [13] or GEISSLER [9]. Depending on the distribution of basic variables and used formulation of dependency between material parameters C and m, the analysis can give conservative results. In order to solve a broad range of realistic fatigue problems simulation methods tend to be very promising. Typically adaptive importance simulation schemas are used, like that from MELCHERS [14]. They are useable in most practical problems but need in the particular case a large number of iteration steps and in consequence of simulations. This approach uses one Gassian impor-

tance density. The need of a more elaborate method has found a solution in the rare-event simulation approach, RUBINSTEIN [16].

4.2 Cross Entropy Method

The cross-entropy (CE) method is an adaptive importance sampling procedure that has been successfully applied to a diverse range of complicated simulation problems, RUBINSTEIN AT AL. [15]. Main ideas are reviewed herein briefly. Similar to Bayesian approach, the CE starts with a prior probability density about importance sampling function. Let $\boldsymbol{X} = \{\boldsymbol{X}_1, \ldots, \boldsymbol{X}_n\}$ be the stochastic variables with parameters $\boldsymbol{u}$. Denote the probability density function $f(\cdot; \boldsymbol{u})$.

Let $S(X)$ be the score function, i.e. the limit state formulation describing the boundary between safe and unsafe region. From simulation following result is expected

$$\ell = P(S(\boldsymbol{X}) < 0) = \mathrm{E}[I_{\{S(\boldsymbol{X})<0\}}] \tag{7}$$

that is the probability of failure for a given componential limit state function.

The straight forward way is to estimate ℓ by crude Monte Carlo (CMC) simulation. This is done by drawing a random sample from $X_1, \ldots, X_n$ from distribtion of X and use

$$\frac{1}{N} \sum I_{\{S(\boldsymbol{X}_i)<0\}} \tag{8}$$

as an unbiased estimator of ℓ. The proposed way ist to use an adaptive schema of importance sampling (IS) like described in CHAN ET AL. [3]. Let $g(\boldsymbol{x})$ be another probability density such that $g(\boldsymbol{x}) = 0 \Rightarrow I_{\{S(\boldsymbol{X})<0\}} f(\boldsymbol{x}) = 0$. Using $g(\boldsymbol{x})$ then ℓ is represented as

$$\ell = \int I_{\{S(\boldsymbol{X})<0\}} \frac{f(\boldsymbol{x})}{g(\boldsymbol{x})} g(\boldsymbol{x}) \mathrm{d}\boldsymbol{x} = \mathrm{E}_g[I_{\{S(\boldsymbol{X})<0\}} \frac{f(\boldsymbol{X})}{g(\boldsymbol{X})}] \tag{9}$$

The expectation is taken with respect to function g the importance sampling density. An unbiased estimator of ℓ is

$$\hat{\ell} = \frac{1}{N} \sum I_{\{S(\boldsymbol{X}_i)<0\}} W(\boldsymbol{X}_i; \boldsymbol{u}, \boldsymbol{v}) \tag{10}$$

where $\hat{\ell}$ is called the importance sampling or the likelihood ratio (LR) estimator of $W(\boldsymbol{x}; \boldsymbol{u}, \boldsymbol{v}) = f(\boldsymbol{x}; \boldsymbol{u})/g(\boldsymbol{x}; \boldsymbol{v})$. The random samples $\boldsymbol{X}_1, \ldots, \boldsymbol{X}_n$ are taken from g. In particular case when there is no *change of measure*, i.e. $g = f$, then $W = 1$ and the LR estimator reduces to the CMC estimator.

An adaptation procedure proposed originally by DOUC ET AL. [5], developed further by CAPPE ET AL. [2] formulates the kernel as mixture of densities.

$$g(\boldsymbol{x}) = \sum \pi_i \, q_i(\boldsymbol{X}; \boldsymbol{v}_i) \tag{11}$$

Instead of locating optimal parameters θ_i for a particular problem directly, the cross-entropy (CE) method aims to locate an optimal sampling distribution $g(\boldsymbol{x})$. The sampling distribution is optimal if only optimal solutions can be sampled for it. First the state space $\boldsymbol{X}$ is provided over which the problem is defined, along with an performance measure S. Next the parameterized sampling distribution is defined from which samples are generated. A general form of the procedure is explained next. The paramters N, N_1, ρ, and α has to be defined before starting with sampling.

1. Initialize parameter vector $\boldsymbol{v}_0$. Set $t = 1$
2. Generate $X_1, \ldots, X_N$ from density $g(\cdot; \boldsymbol{v}_{t-1})$
3. Compute the sample $(1-\rho)$-quantile, $\hat{\gamma}_t = S_{(\lceil (1-\rho)N \rceil)}$. Estimate from elite sample new parameter $\widetilde{\boldsymbol{v}}_t$. Set the current estimate for the optimal parameter vector to: $\boldsymbol{v}_t = \alpha \widetilde{\boldsymbol{v}}_t + (1-\alpha)\boldsymbol{v}_{t-1}$
4. If stopping criteria is met, go to step 5. Otherwise set $t = t + 1$ and return to step 2.
5. Run final importance sampling for N_1 samples and estimate eq. 10.

This method is called cross entropy adaptive importance sampling (CEAIS) method and implemented in the stochastic code VAP 3.1 [17]. In particular the kernel $g(\boldsymbol{x})$ has been defined as a mixture of p-dimensional Normal distributions $N(\boldsymbol{X}; \boldsymbol{\mu}_i, \boldsymbol{\Sigma}_i)$. The reason is that both densities $f(\boldsymbol{x})$ and $g(\boldsymbol{x})$ should be of same distribution family. For reliability problem statements this can be easily archived by transforming arbitrary densities $f(\boldsymbol{x})$ into the correlated normal space **Z** employing the Nataf transformation, see DITLEVSEN ET AL. [4].

The kernel $g(\boldsymbol{x})$ is adapted subsequently during pre-sampling steps of size N, by adjusting the weight factor α_i, as well as adjusting parameters for each single distribution $N(\boldsymbol{X}; \boldsymbol{\mu}_i, \boldsymbol{\Sigma}_i)$. The idea of CE is to reduce the cross entropy *distance* between zero-variance pdf $f(\boldsymbol{x})$ and a proposed importance sampling pdf $g(\boldsymbol{x})$. The distribution parameters $\boldsymbol{v}$ are chosen to solve the following stochastic program

$$\boldsymbol{v}_{\mathrm{CE}} = \underset{v}{\operatorname{argmax}} \, \mathrm{E}_f[\log g(\boldsymbol{X}; \boldsymbol{v})] \tag{12}$$

The distribution to fit is a mixture distribution and eq.12 has no closed-form solution. The problem is resolved by splitting the rare event of interest $S(\boldsymbol{X}_i)$ into a series of not necessarily disjoint events. To each one of these events parameters are estimated using only those elements of the sample that correspond to the event occuring. Then normalizing proportions with which each event occurs as estimates for the weights π_i of the distribution, as well as for distribution parameters $\boldsymbol{v}_i$, see also KURTZ ET AL. [11].

4.3 Results

The limit state formulation in eq.3 is analysed by CEAIS method, as presented before. The measured strains cycles are collected in histograms and rainflow matrices as presented fig. 5.

The cycle histograms are put into analysis employing eq. 6. The quality of analysis strongly depends on duration of measurement i.e. having catched a broad range of train compositions. Observation shows that heavy freight trains can give big amplitudes due to some empty waggons between loaded ones.

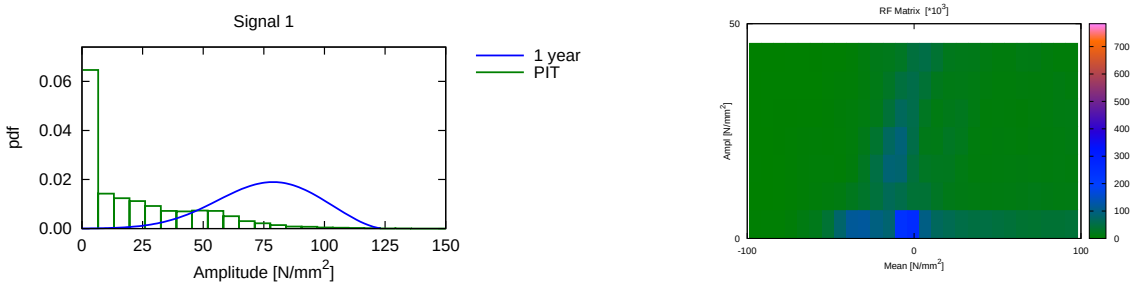

(a) Cycle histogram

(b) Rainflow matrix

Fig. 5: Outcome from BWIM measurement used in analysis.

The basic variables for analysis are defined in tab. 1. The fracture toughness K_{IC} and corresponding material parameters are taken out of GEISSLER [9], where similar old bridges in Berlin has been investigated. The material parameters C and m are correlated by $\rho = 0.6$. Alternatively, the well known Gurney relation can be used to simplify analysis. The material parameters f_y and f_u have minor influence on the result and defined as deterministic herein. Stress due to traffic load σ_Q seems to be crucial in definition and depends on solution strategy. Using FORM method this variable tends to take extreme position resulting in unrealistic physical meaning and tending to give wrong β values. The proposed CEAIS method in turn gives very good reasonable results. As a side product the mean vector of the final importance sampling densitiy equals a point of maximum likelihood.

The assumption, that crack growth follows only tension loading is clearly a simplification. In case I-beam support has only one stiffening plate working, out of the plane bending has to be combined. Due to field measurements both effects have been considered. Inital crack size A_0 and that way probability of detection (PoD) is determined by flang width of L-angle which are used to produce a $90°$ connection with rivets.

Tab. 1: Basic variables used in analysis

BV	EH	Type	E[X]	D[X]	Note
A_0	[]	Rayleigh	2.8	0.3	initial crack length
C	[]	LN	$2.9E-13$	$1.0E-13$	material parameter
ΔK_{th}	[Nmm$^{-3/2}$]	Det	70		threshold
K_{IC}	[Nmm$^{-3/2}$]	LN	3000	1500	fracture toughness for modus I
f_u	[N/mm^2]	Det	330		yield strength
f_y	[N/mm^2]	Det	230		ultimate limit strength
M	[]	LN	3	0.4	material parameter
σ_G	[N/mm^2]	N	10	1	stress due to dead load
σ_{Q_i}	[N/mm^2]	T1L	52.2	12	stress from life load

Results from cross entropy adaptive importance sampling analysis, 50000 samples :
`pf = 1.289e-006 cov = 1.173e-001 beta = 4.7`

BV	x*
A0	3.804
C	$2.247 \cdot 10^{-13}$
M	2.387
DKth	70
Fy	235
Fu	330
Kc	2552
SG	9.533
SQmax	33.09

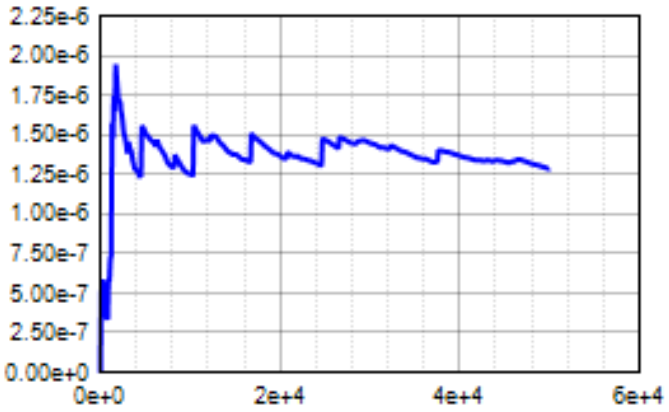

Analysis used $K = 10$ multinormal distribution as indicated in eq. 11, $N = 2000$ for pre-sampling and fractile value $\rho = 0.08$ for quality control. After some pre iteration steps simulation has given results shown above. Depending on the limit state formulation and its non-linearity some trails regarding parameter K, N and ρ has to be done. The resulting coefficient of variation should be below $\mathrm{COV} \leq 0.10$. The crack growth integration points out to be a numerically challenging problem.

5 Conclusion

The presented approach for lifetime evaluation of a railway bridge is a concise methodology taking resistance and loading aspects of a structural problem into account with same accuracy. It is a fact that influence of loading and knowledge about its nature is of same importance as investigation on structure about resistance capabilities. Due to BWIM it is possible to measure primary and secondary stress effects directly not setting up complicated mechanical models. Results from monitoring should in fact be used to calibrate analytical models in case they are necessary. Statistical information about load patterns have been collected which forms the basis for re-evaluation of past loading and prediction of future as well. In case BWIM results are available fatigue loading models from code have not necessarily be used.

The probabilistic analysis is done by a crack growth calculation at the crucial element of the structure. The iterative solution procedure for crack growth integration has caused development of new simulation method for probabilistic analysis. With help of cross entropy method an adaptive importance sampling scheme has been established. The aim of this approach is to find an optimal importance density for a problem using a mixture of multinormal densities. Compared to other simulation approaches the new method performs very well and reduces significantly the computation effort.

Considering the influence of single basic variables in the fatigue problem stress due to traffic as well as fracture toughness guard the solution. This underlines the importance to give same

attention to loading part as it is done for resistance aspects.

Acknowledgements

Investigation and analysis of the railway bridge has taken two months leading to a concrete rehabilitation plan for the Austrian Railway Organization, namely the ÖBB-Infrastruktur AG. The author has to thank Mr. Petraschek and his colleagues Mr. Themessl as well as Mr. Umfahrer for supporting the BWIM measurement and giving the stage to a practitioner to show state-of-the-art methods.

Literature

[1] Austrian Federal Railway, *Technical guidelines for railway bridges and civil engineering structures*, 2011

[2] Cappe, O., Randal, D., Guillin, A., Marin, J.M., Robert, Ch.P. *Adaptive importance sampling in general mixture classes*. Stat Comput 18 (2008), p. 447-459

[3] Chan, C., Kroese, D. *Improved Cross-Entropy Method for Estimation*. Stat Comput 22 (2012), p. 1031-1040

[4] Ditlevsen,O.,Madsen,H.O., *Structural Reliability Methods*,John Wiley & Sons Ltd., 1996

[5] Douc, R., Guillin, A., Marin, J.M., Robert, Ch.P. *Convergence of adaptive mixtures of importance sampling schemes*. Ann. Stat. 35 (2007), p. 420-448

[6] EN 1990, *Eurocode 0: Basis of structural design*, Austrian Standardisation Institute, 2003

[7] EN 1991-2, *Eurocode 1: Actions on structures Part 2: Traffic loads on bridges*, Austrian Standardisation Institute, 2004

[8] EN 1993-9, *Eurocode 3: Design of steel structures Part 1-9: General Fatigue strength*, Austrian Standardisation Institute, 2004

[9] Geissler, K. *Beitrag zur probabilistischen Berechnung der Restnutzungsdauer stählener Brücken*. Schriftenreihe des Instituts für Tragwerk und Baustoffe, TU Dresden, 1995

[10] iBWIM *iBWIM - bridge weigh-in-motion system*. PEC GmbH, www.petschacher.at, 2012

[11] Kurtz, N., Song, J., *Cross-entropy-based adaptive importance sampling using Gaussian mixture*, Structural Safety 42 (2013), p. 35-44

[12] Liljencrantz, A. *Monitoring railway traffic loads using Bridge Weight-in-Motion* Royal Institute of Technology (KTH), Stockholm. Bulletin 90, 2007

[13] Madsen,H. O.,Krenk,S.,Lind,N.C. *Methods of Structural Safety*, Prentice-Hall, Inc., Englewood Cliffs, New Jersey, 1986

[14] Melchers,R. E., *Search-based importance sampling*, Structural Safety 6 (1990), p. 117-128

[15] Rubinstein, R.Y. *The Cross-Entropy Method: A Unified Approach to Combinatorial Optimization Monte-Carlo Simulation, and Machine Learning*. Springer-Verlag, New York, 2004

[16] Rubinstein, R.Y., Kroese, D.P. *Optimization of computer simulation models with rare events*. European Journal of Operational Research 99 (1997) p. 89-112

[17] VaP 3.1 *VaP - Variables Processor*. PEC GmbH, www.petschacher.at, 2013

[18] Zhao,H.,Uddin,N. *Algorithm to identify axle weights for an innovative BWIM system-Part I*. IABSE-JSCE Joint Conference on Advances in Bridge Engineering-II. Amin, Okui, Bhuiyan (eds.), 2010, p. 527-536

Sampling strategy for feasible high dimensional Monte Carlo computations

Jan Podroužek[1], Christian Bucher[2]
[1] Centre for Water Resource Systems (CWRS),
[2] Institute of Building Construction and Technology,
Vienna University of Technology, A-1040 Wien, Karlsplatz 13/222, Austria
podrouzek@waterresources.at, christian.bucher@tuwien.ac.at

Abstract: The proposed sampling strategy enables feasible computation of high dimensional Monte Carlo simulation tasks by minimizing the number of necessary executions. The original aspect of this contribution is a special sampling design that focuses on realizations of stochastic nonstationary processes as input for computationally intensive models in a seismic protection context. Since nonlinear oscillators always respond in a very uncertain manner to random vibrations, the input and output mapping is based on small sample training and image processing. Application example demonstrates the benefits and limitations of the nontraditional approach and implies application analogies from across various disciplines, such as hydrology, water resources, etc.

Keywords: stochastic process, Critical excitation, Reliability analysis, Importance sampling, Identification problem

1 Introduction

The following discussion concerns the application of random sampling technique to the problem of engineering risk analysis with particular focus to structural reliability. In the context of probabilistic Monte Carlo (MC) simulations many engineers and researchers are constrained by excessive computational costs. The minimum required number of repeated trials is constrained according to several limit theorems. The scenarios of interest typically involve a low-probability and high-consequence events. Since typical safety margins in engineering risk analysis range 10^{-4} to 10^{-9}, high number of MC trials is necessary to obtain an outcome with a fixed level of confidence, e.g. in terms of variance or other measures of error.

There are several methods routinely used since the 1950s of reducing the sample size in MC computations. Typically the problem is to estimate, in structural reliability context, from a sample $y_1, y_2, \ldots, y_n$ of n simulated realizations of the structural performance obtained by sampling from the model of the structure, either (a) the moments of the probability distribution of the random variable y, or (b) the probability of the random variable y

exceeding some threshold performance value Y; i.e. $P(y \geq Y)$. Note that by introducing a new random variable $z = 1$ if $y \geq Y$, $z = 0$ if $y < Y$ the problem (b) reduces to problem (a) and $P(y \geq Y) = E(z)$.

In most cases deterministic numerical integration (e.g. **F**inite **E**lement **M**ethod, **M**odel **O**rder **R**eduction and **P**roper **O**rthogonal **D**ecomposition) is used to solve the model of the structure, since no closed-form solution exists.

$$f(\boldsymbol{x_i}) \xrightarrow{NSolve} y_i \tag{1}$$

Where $\boldsymbol{x_i}$ represent a vector of scalar input variables, such as dimensions, strength, loads, etc., and y_i represent a scalar response quantity, e.g. displacement, in a static equilibrium.

For the case outlined above the MC sample size reduction is rather straight-forward and has been treated by many authors, e.g. [1], [2] and [3].

For cases of nonlinear structural dynamics, on the other hand, MC reduction schemes are extremely rare. Either the stochastic excitations patterns are avoided by means of smooth functions [4] or the original MC reliability problem is avoided by closed form analytical approximations [5].

It is worthwhile to emphasize that currently the suggested identification approach is a unique attempt of reducing the MC sample size while maintaining (a) the stochastic non-stationary excitation patterns $\boldsymbol{r}$ and (b) the probabilistic aspects of the original MC simulation task. This enables for realistic high dimensional MC simulations by identifying the critical samples of given stochastic process as a loading for structural model.

The existence of systematic covariation emerges after small number of randomly selected training samples are calculated, transformed into 2-Dimensional graphical array (e.g. evolutionary spectra) and overlaid by ranked minimum and maximum subsets.

2 Identification approach

The proposed identification strategy (originally labelled “STS”) utilizes a transparent image processing paradigm completely independent of state-of-the-art structural dynamics, aiming at delivering simple and wide purpose method. The detailed description of the development, acceleration and structural models can be found in [6]. While there exist many analogical problems to structural dynamics, the basic principles will be formally described on the basis of mathematical rigor.

The task is to obtain probabilistic characteristics from samples of $y(y_1, y_2, \ldots, y_n)$ obtained by sampling from the model f returning and arbitrary scalar response quantity y_i, e.g. peak displacement

$$f(\boldsymbol{r_i}) \xrightarrow{NSolve} y_i \tag{2}$$

where *NSolve* stands for arbitrary deterministic solver (e.g. FEM), possibly further reducing the original physical model by means of MOR [7] or POD [8]. In the following example the structural system is a base isolated frame story building. The respective computational model was adopted from BAMER AND BUCHER [9] as a POD meta-model of the structural system (800 **D**egrees **O**f **F**reedom).

The finite fundamental probability Set $\boldsymbol{S}$ is assumed as 1-Dimensional stochastic process realizations vector

$$\boldsymbol{S} \in \langle \boldsymbol{r_1}, \boldsymbol{r_2}, \dots, \boldsymbol{r_n} \rangle \tag{3}$$

such as

$$\boldsymbol{r_i} \in \langle v_1, v_2, \dots, v_t \rangle \tag{4}$$

where v_i can be and arbitrary scalar value, e.g. acceleration values recorded in t time steps. In the context of the present demonstration $\boldsymbol{S}$ represent amplitude and frequency modulated random process whose objective is to reproduce the general frequency variation characteristics of the acceleration record from the 1964 Niigata earthquake [10].

In the next step, one has to define the Algorithm for 2-D graphical representation $\boldsymbol{G}$ of individual r_i's. In this paper such purpose fulfils the *wd* transform.

$$wd(\boldsymbol{r_i}) \xrightarrow{maps} \boldsymbol{G_i} = \begin{bmatrix} c_{1,1}^{(i)} & \cdots & c_{t,1}^{(i)} \\ \vdots & \ddots & \vdots \\ c_{1,o}^{(i)} & \cdots & c_{t,o}^{(i)} \end{bmatrix} \tag{5}$$

Here the wavelet vector coefficients (1,..,o) are plotted as rows of colorized rectangles $c_{t,o}$, in which large absolute values are shown darker and each subsequent row corresponds to different wavelet index specifications.

Finally, the proposed identification strategy uses 3 parameters with default values m = 100 (training sample size), p = 5(training subset size) and o = 100(number of $\boldsymbol{G}$ octaves).

STS Identification strategy steps:

1) Construct a training subset $\boldsymbol{s}$ randomly sampled from $\boldsymbol{S}$ having the length m.

$$\boldsymbol{s} \in \langle r_1, r_2, \dots, r_m \rangle \tag{6}$$

2) Solve the training subset $\boldsymbol{s}$:

$$\langle f(r_1), f(r_2), \dots, f(r_n) \rangle \xrightarrow{yields} \boldsymbol{s_f} \in \langle y_1, y_2, \dots, y_m \rangle \tag{7}$$

3) Create ranked minimum and maximum sets $\boldsymbol{s_{f,min}}$ and $\boldsymbol{s_{f,max}}$:

$$\boldsymbol{s_{f,min}} = \langle 1, \dots, p \rangle^{th} \text{ smallest elements in } \boldsymbol{s_f} \tag{8}$$

$$\boldsymbol{s_{f,max}} = \langle 1, \dots, p \rangle^{th} \text{ largest elements in } \boldsymbol{s_f} \tag{9}$$

4) Transform $\boldsymbol{r_i}$'s corresponding to $\boldsymbol{s_{f,min}}$ and $\boldsymbol{s_{f,max}}$into graphical representation

$$wd\left(\boldsymbol{r}_{\boldsymbol{S}_{f,min}}\right), wd\left(\boldsymbol{r}_{\boldsymbol{S}_{f,max}}\right) \xrightarrow{yields} \langle \boldsymbol{G_{min,1}}, \dots, \boldsymbol{G_{min,p}} \rangle, \langle \boldsymbol{G_{max,1}}, \dots, \boldsymbol{G_{max,p}} \rangle \tag{10}$$

4) Calculate the 2-Dimensional correlation pattern $\boldsymbol{P}$ using the $\boldsymbol{G_{min}}$ and $\boldsymbol{G_{max}}$:

$$\boldsymbol{P} = \left| \sum_{i=1}^{p} \sum_{x=1}^{t} \sum_{y=1}^{o} \frac{c_{x,y}^{(min,i)}}{p} - \sum_{i=1}^{p} \sum_{x=1}^{t} \sum_{y=1}^{o} \frac{c_{x,y}^{(max,i)}}{p} \right| \tag{11}$$

From the formula above it is clear that $\boldsymbol{P}$ has the same dimension as $\boldsymbol{G}$ and that the higher values $\boldsymbol{P}$ coefficients hold, the more relevant this location becomes for the classification of the original set $\boldsymbol{S}$ (for a sample pattern see Fig. 1). Note that there is a number of useful modifications of $\boldsymbol{P}$ for increasing accuracy that will not be detailed in this paper due to its limited scope. These can be found in [11].

5) Quantification of importance $\boldsymbol{I}$ on the original set $\boldsymbol{S}$ using the scalar product of $wd(\boldsymbol{r_i})$ transform and $\boldsymbol{P}$

$$\boldsymbol{S} \xrightarrow{wd(\boldsymbol{ri})} \boldsymbol{G_S} \tag{12}$$

$$\boldsymbol{I_S} = \langle \boldsymbol{G_{r1}}, \boldsymbol{G_{r2}}, \dots, \boldsymbol{G_{rn}} \rangle \cdot \boldsymbol{P} = \langle I_1, I_2, \dots, I_n, \rangle \tag{13}$$

6) Classification of S according to the highest values of $\boldsymbol{I_S}$ with respect to the response quantity y_i. Both values I_i and y_i are correlated now and the identification results are known. The associated likelihoods can be approached as evidence supporting the hypotheses $y_i \geq y_{max}$.

$$\text{Probability}(y_i \geq y_{max}) = \frac{1}{n} \tag{14}$$

The computational savings and accuracy compared to the Brute force Monte Carlo verification would yield for the presented example ($n = 10^3$) the maximal value of 98.99 [%].

$$\text{savings} = \left(1 - \left(\frac{m+1}{n}\right)\right) \cdot 100 \tag{15}$$

The typical tradeoff between accuracy and efficiency demonstrates the plot at Fig. 2. Here, the $m + 1$ term from the Eq. (14) is replaced by $m + cp$ where the confidence parameter, cp, is gradually increasing from 1 to 400. This means that the total number of solver run equals the training subset length m and $\langle 1, \dots, cp \rangle^{th}$ highest values of $\boldsymbol{I_S}$, i.e. corresponding critical realizations $\boldsymbol{r_i}$.

3 Probabilistic interpretation and Conclusion

It should be pointed out that the STS method does not provide a one-to-one correspondence between the true response and the classification value since only small percentage of all samples were analyzed using the full (and expensive) model. Nevertheless, the STS technique allows with high confidence detecting the subset of the most relevant samples as critical loading for given structural models. The overall behaviour of the probabilistic information generated from the STS method can be seen in Fig. 3. Here the empirical probability density function as obtained from simulation of the full model (10.000 samples) is compared to that obtained by applying the less accurate (much cheaper) STS technique.

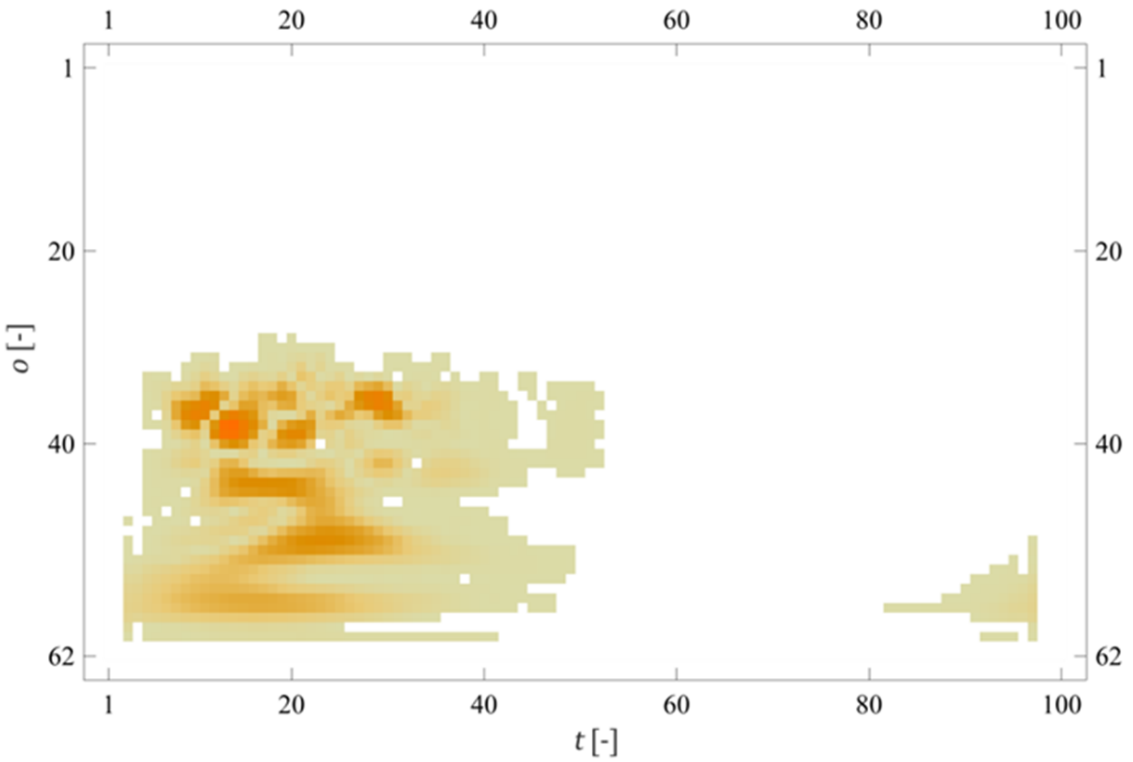

Fig. 1: Sample correlation pattern according to Eq. (11)

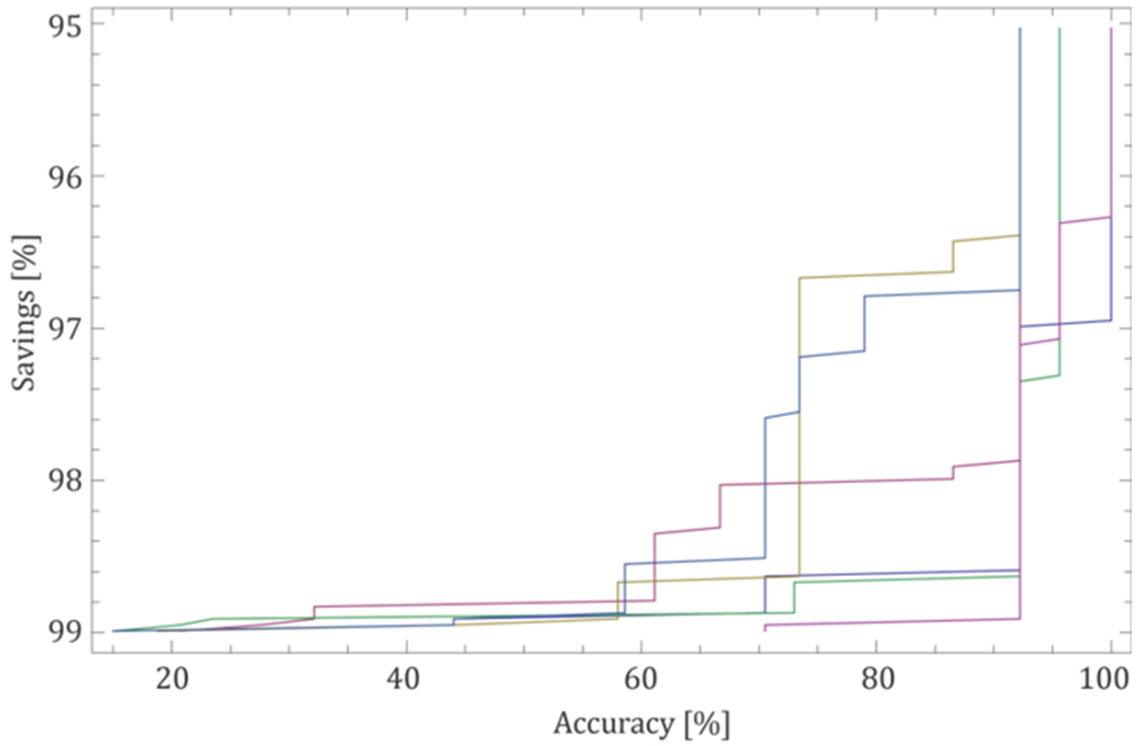

Fig. 2: The cost of quality and base information for optimal *cp* control from several identification runs

For reliability purposes, the comparison in the upper tail region of the maximum response is most relevant. The respective curves at Fig. 3 match very well in the tails while the STS utilized only about 100 training samples for prediction of exceedance probabilities in the range of 10^{-4}. This is efficiency gain of two orders of magnitude. Hence it may be anticipated that for practical reliability analysis a speed-up of about 100 may be achieved. This is sufficient to enable full probability-based design of structures, and furthermore enables the application of optimization strategies to minimize cost either in the construction phase or in the entire structural life-cycle.

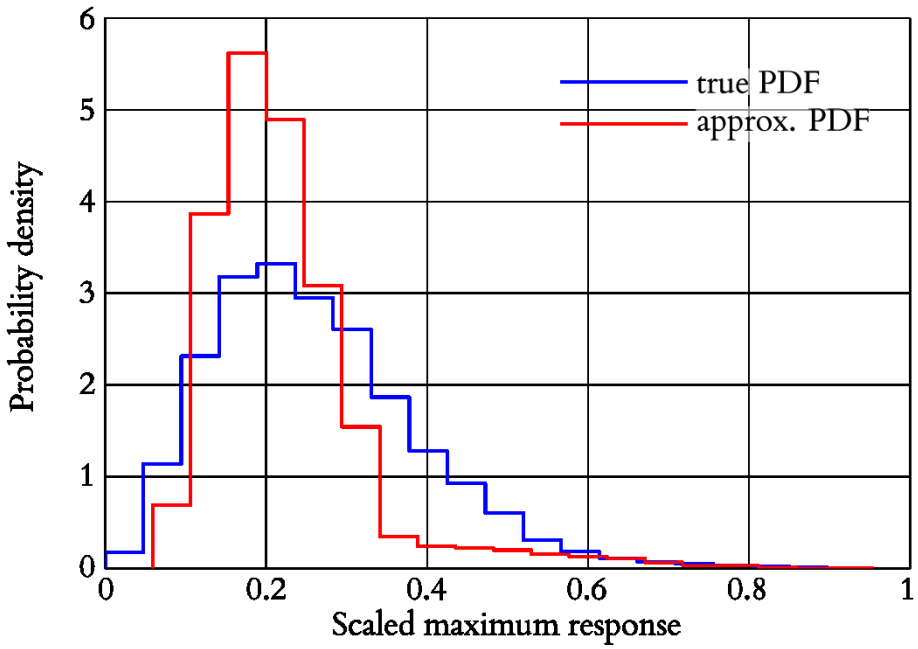

Fig. 3: Comparison of empirical PDF (histogram) of the maximum response based on simulation of the full model (blue curve) and based on STS identification (red curve)

Acknowledgements

Authors would like acknowledge financial support from the Austrian Science Funds (FWF) as part of the Vienna Doctoral Programme on Water Resource Systems (DK-plus W1219-N22).

Literature

[1] Kahn, H., Marshall, A.W. *Methods of Reducing Sample Size in Monte Carlo Computations*. Santa Monica, CA: RAND, 1953

[2] McKay, M.D., Beckman, J., Conover, W.J. A Comparison of Three Methods for Selecting Values of Input Variables in the Analysis of Output from a Computer Code. *Technometrics* 21(2) (1979), p. 239–245

[3] Melchers, R.E. Importance sampling in structural systems. *Structural Safety* 6(1) (1989), p. 3–10. ISSN 0167-4730

[4] Macke, M., Bucher, Ch. Importance sampling for randomly excited dynamical systems. *Journal of Sound and Vibrations* 268 (2003), p. 269–290

[5] Barbato, M., Conte, J.P. Structural Reliability Applications of Nonstationary Spectral Characteristics. *Journal of Engineering Mechanics, ASCE* (2011), p. 371–382

[6] Podrouzek, J. Importance Sampling Strategy for Oscillatory Stochastic Processes. *Journal of Mechanics Engineering and Automation (JMEA)* 2(11) (2012), ISSN 2159-5283

[7] Rega, G., Troger, H. Dimension Reduction of Dynamical Systems: Methods, Models, Applications. *Nonlinear Dynamics* 41 (2005), p. 1–15

[8] Cusumano, J.P., Sharkady, M.T., Kimble, B.W. *Spatial coherence measurements of a chaotic flexible-beam impact oscillator*. American Society of Mechanical Engineers, Aerospace Division AD, 33:13–22, 1993

[9] Bamer, F., Bucher, Ch. Application of the proper orthogonal decomposition for linear and nonlinear structures under transient excitations. *Acta Mechanica* 223 (2012), p. 2549–2563

[10] Shinozuka, M., Deodatis, G. Simulation of Stochastic Processes by Spectral Representation. *Appl. Mech. Rev*. 44(191) (1991). DOI:10.1115/1.3119501

[11] Podrouzek, J. Separating stochastic processes by robust measures. *Proceedings of the European Congress on Computational Methods in Applied Sciences and Engineering*. Vienna, Austria, 2012

Multi-objective adaptive design of experiments for reliability-based design optimization

Adéla Pospíšilová, Eva Myšáková, Matěj Lepš

Faculty of Civil Engineering, Czech Technical University in Prague
adela.pospisilova@fsv.cvut.cz, leps@cml.fsv.cvut.cz

Abstract: Reliability-based design optimization (RBDO) is a research area that tries to optimize structures under assumption of uncertainties. Usually, the objective function is to be minimized with respect to constraints in which the probabilistic approach is included. Our solution utilizes a surrogate-based Monte Carlo approach which is enhanced by an adaptive Design of (Computer) Experiments (DoE). The space-filling properties of the DoE are optimized by maximizing the minimal interpoint distance, i.e. the Maximin approach. The second objective is the distance to the limit state function. Both objectives are optimized by NSGA II algorithm to obtain maximum information out of the model with a minimal number of sampling points. Kriging meta-model with this adaptive updating procedure is also proposed. The studied RBDO problems consist of the minimization of the weight of the structure as the first objective and minimization of the probability of failure as the second objective. The latter is evaluated by selected sampling strategy on the previously updated surrogate model. This RBDO problem is again multiobjective and already presented NSGA II algorithm is used.

Keywords: Reliability-Based Design Optimization, Asymptotic Sampling, adaptive Design of Experiments, multi-objective optimization, meta-modeling.

1 Introduction

Reliability-based design optimization (RBDO) is a research area that tries to account for the stochastic nature of engineering problems. Usually, the objective function (e.g. a structure weight, a maximal displacement etc.) is to be minimized with respect to constraints in which the probabilistic approach is included [6]. It is hard or nearly impossible to create an analytical probabilistic approach on real structures thus some alternative method should be used.

Our solution utilizes a surrogate-based Monte Carlo approach [3] which is enhanced by an adaptive Design of (Computer) Experiments (DoE) [15].

As the model is enumerated many times, it is appropriate to use some meta-model (surrogate) that is easier to solve and give the approximation for the response on the original model. Kriging [12] is an example of a very popular meta-model that can be applied in our work. For generating meta-models, an appropriate number of sampling points is needed [5]. Moreover, to improve the quality of the surrogate, an adaptive updating procedure is proposed. It is based on the miniMax metric as an objective coming from the space-filling domain of the Design of Experiments. Overall, there are two criteria that have to be optimized. The first criterion (i.e. miniMax) is to maximize the nearest distance of the added point from already sampled points. The second criterion is to be as close as possible to the approximate Limit State Function, i.e. we are not concentrated on the whole domain, but only on the border between the failure and safe region. These two criteria lead to multi-objective optimization. In our work, a modified Nondominated Sorting Genetic Algorithm II is used.

A Nondominated Sorting Genetic Algorithm II (NSGA-II) [2] is a method based on evolutionary principles. To create a new generation, only a mutation operator is used to support an exploration part of the algorithm [7]. A selection from several consecutive Pareto fronts is followed by the computation of the crowding distances. Selected individuals with the greatest crowding distance are then used as a new generation. After a predetermined number of generations, only Pareto front is added as an adaptive update.

The final Reliability Based Design Optimization (RBDO) problem consists of the minimization of the weight of the structure as the first objective and minimization of the probability of failure characterized by a reliability index as the second objective. The latter is evaluated by a new method called Asymptotic Sampling [1] that minimizes the need for the sampling of the previously updated surrogate model. And again, the RBDO problem is multi-objective and already presented NSGA-II algorithm is used.

To demonstrate the efficiency of the mentioned approach, the results of a well-known benchmark are compared with the literature. Particularly, the 23-bar planar truss [9] with 10 independent random variables (cross-sectional areas, Young's moduli and the loading) is investigated. The optimization problem is to find two cross-sectional areas such that the structure has the minimum weight ensuring the minimal reliability index.

The remainder of the paper is organized as follows. Next section is devoted to the description of the Asymptotic Sampling method. The short introduction of the second main algorithm, NSGA-II is then followed by the description of the surrogate and the definition of the optimization problem. Sec. 6 is the core of the presented paper describing the shift of the single-objective Reliability Based Design Optimization into its multi-objective counterpart. Consequent section is devoted to a sampling methodology for the Asymptotic Sampling method. The section with obtained results is then closed by discussion and concluding remarks.

2 Asymptotic sampling

A probability of failure in an n-dimensional space of random variables $X_1 \dots X_n$ is defined as

$$p_f = \mathbf{Prob}[g(\mathbf{X}) \leq 0] = \int_{g(\mathbf{X})\leq 0} \cdots \int f_X(\mathbf{x}) \mathrm{d}\mathbf{x} \,, \tag{1}$$

where $f_X(\mathbf{x})$ is the joint probability density function, $g(\mathbf{X})$ is a safety margin and $g(\mathbf{X}) \leq 0$ denotes the failure domain. An exact solution can be computed analytically only in some special cases. Several numerical methods have been proposed to determine approximate value of p_f. For instance, simulation methods such as Crude Monte Carlo or quasi Monte Carlo methods like Latin Hypercube Sampling generate samples as pseudorandom numbers from given distributions. A ratio of samples inside the failure domain to all samples then represents an approximation of the probability of failure. The approximate reliability index β is then an inverse cumulative distribution function of the standard normal distribution

$$\beta = \Phi^{-1}(1 - p_f) \,. \tag{2}$$

Monte Carlo method utilizes a common pseudorandom generator thus the number of samples needed to obtain a precise approximation of p_f is very high. A common rule of thumb recommends $\frac{100}{p_f}$ samples. Latin Hypercube Sampling exploits division of the investigated space to strata so it covers the space more uniformly. But still, the required number of samples is high thus more efficient methods are needed.

An Asymptotic Sampling is a relatively novel methodology that predicts a reliability index from an asymptotic behaviour of the probability of failure in n-dimensional normal space [1]. A principal idea is to scale random variables through the growing standard deviation σ to get more samples inside a failure domain. The reliability index is then assumed to be a function of the scale factor $f = \frac{1}{\sigma}$

$$\beta = Af + \frac{B}{f} \,. \tag{3}$$

Note that it is recommended to use a scaled reliability index as

$$\frac{\beta}{f} = A + \frac{B}{f^2} \,. \tag{4}$$

Coefficients A and B are obtained by a nonlinear regression analysis through several so called *support points* for different values of the factor f, see Fig. 1. The number of samples m for one support point, the minimum number of samples that must fall inside the failure domain N_0 and a decrease coefficient f_d for the factor f are determined in advance. If the number of failures is higher than N_0 the reliability index β_i and a corresponding factor f_i are stored as one support point. In other case the factor f is decreased. After gathering a sufficient number of support points K the procedure is stopped and coefficients A and B are obtained through curve fitting. Summation of A and B then represents estimated reliability index β for unscaled random variables. For more information see e.g. [1] or [14].

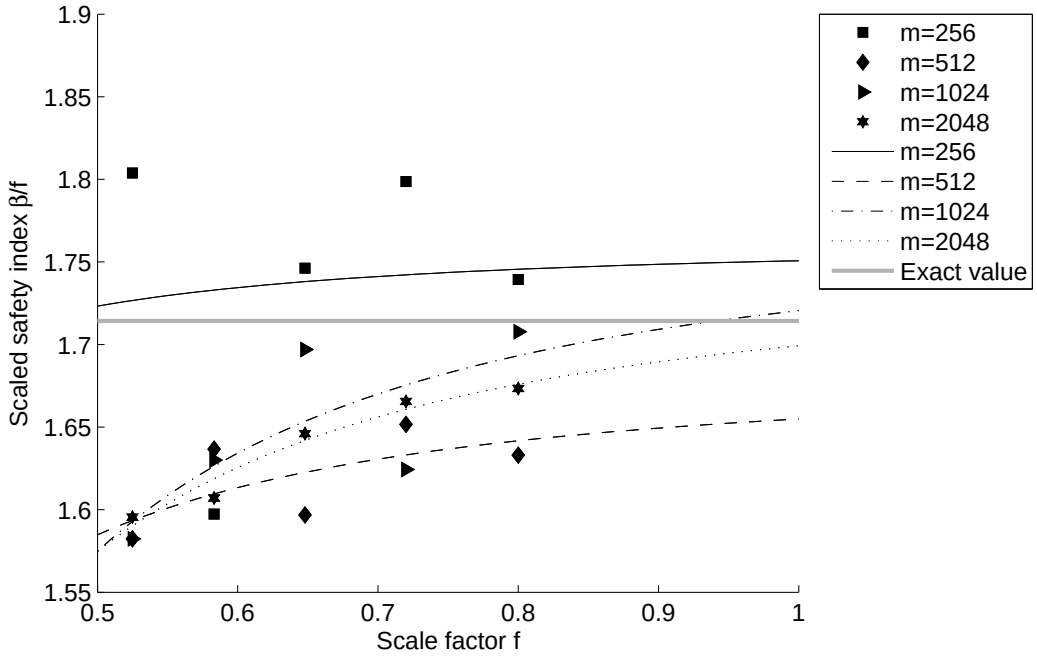

Fig. 1: Example of the Asymptotic Sampling method: Five support points along x-axis for different number of samples followed by nonlinear curve fitting; Reliability index is then predicted for scale factor $f = 1$

3 Nondominated sorting genetic algorithm II

A *non-dominated Sorting Genetic Algorithm II* (NSGA-II), first published in [2], is one of the multi-objective optimization techniques. It works on the basis of replacing parental population with better offsprings. The first parental population is created randomly and all individuals are evaluated by values of several objective functions. Values of the same objective functions are compared for different solutions (see comparison for the particular solution $\mathbf{x}$ in Fig. 2a)) and individuals are rated by ranks (see Fig. 2b)).

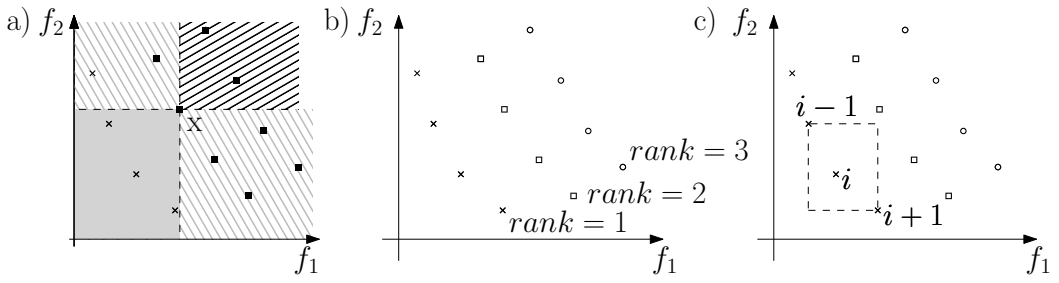

Fig. 2: Calculations for NSGA-II (both objective functions have to be minimized) of a) Dominance, b) Nondominated rank and c) Crowding distance

The rank equal to 1 is assigned to solutions that are better than or incomparable with others. Categorized solutions are taken out of the classification and solutions with a rank equal to 2 are located, etc. After ranking whole population, all solutions are sorted according to ranks

(see Figs. 2b) and 3) and half of them are accepted as the parental population. In case that the amount of the last front exceeds the required size, a crowding distance is used as the second criterion (see Fig. 2c)). The further the solution from the rest of the population is, the higher diversity to the population is brought. Individuals are sorted in descending order according to an enumerated crowding distance and the needed number of individuals is taken to the next parental population. The next offspring population is created by classical operators such as a selection, a crossover and a mutation (for more details see e.g. [13]) and the method is applied anew. An optimization run terminates after a predetermined number of generations.

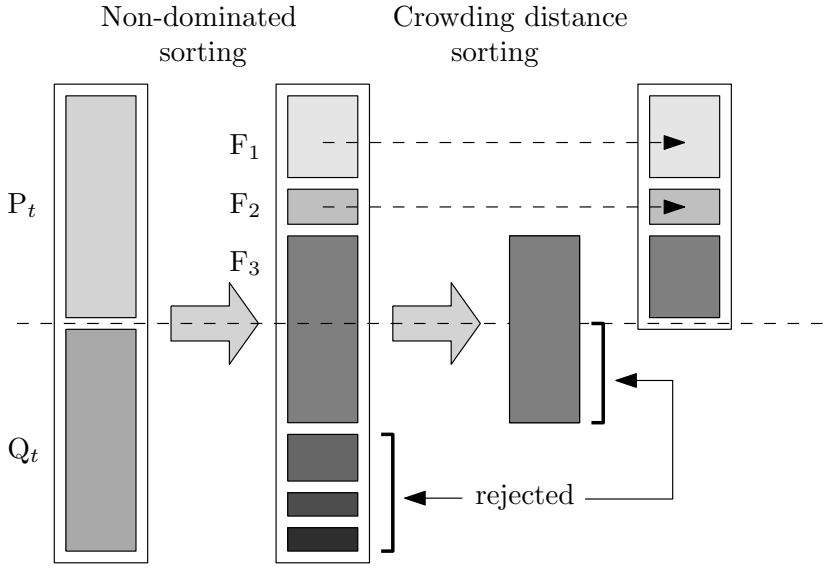

Fig. 3: Schematic of the NSGA-II procedure

4 Surrogate

Kriging is an approximation method frequently used in geostatistics, global optimization and statistics [16]. Kriging was originally developed by the South African mining engineer D.G. KRIGE in the early fifties. In the 1960s the French mathematician G. MATHERON gave theoretical foundations to this method and named the method after Krige. Generally, the Kriging predictor is composed of a regression and interpolation part that constitutes the nonlinear surface among available data [10]:

$$\hat{y} = f(x)^T \beta^* + r(x)^T \gamma^* \,, \tag{5}$$

where $f(x)$ is an *a-priori* selected set of basis functions creating the response surface and $r(x)$ is the correlation term between an unsampled point x and known points s_i, $i = 1, ..., m$: $r(x) = [R(\theta; s_1; x), ..., R(\theta; s_m; x)]^T$, where R is *a-priori* selected correlation function with unknown coefficients θ, see later. The regression part is solved by a generalized least squares solution

$$\beta^* = (\mathbf{F}^T\mathbf{R}^{-1}\mathbf{F})^{-1}\mathbf{F}^T\mathbf{R}^{-1}\mathbf{Y} \ , \tag{6}$$

where $\mathbf{F}$ is a matrix containing $f(x)$ evaluated at known sites s_i, $\mathbf{R}$ stems for correlation among s_i using again the correlation function R and $\mathbf{Y}$ are known values of y_i at s_i. The Kriging part then interpolates the residual leading to the system of linear equations

$$\mathbf{R}\gamma^* = \mathbf{Y} - \mathbf{F}\beta^* \ . \tag{7}$$

The use of such a metamodel for optimization purposes is less demanding on the regression part since an interpolation is dominant and hence, the constant regression part usually suffices. Then, the correlation function is traditionally selected to obtain a positive-definite system of equations, mainly restricted to the form

$$R(\theta, w, x) = \prod_{j=1}^{n} R_j(\theta, w_j - w_i) \ . \tag{8}$$

In our case, a free MATLAB toolbox DACE [10] is utilized where gaussian correlation function has been used. Note that at this point we still do not know the tuning/shape parameters θ. Their functionality is twofold: they express the anisotropy among dimensions and also determine the shape of the metamodel in the vicinity of given samples. Traditionally, these parameters are found *a-posteriori* by minimizing an expected mean squared error (MSE), which leads to the constrained nonlinear optimization problem. See e.g. [4] for discussion on how to efficiently solve this problem without re-calculation of β^* and γ^* for these new θ.

5 Optimization benchmark

Presented benchmark together with a probabilistic description of the problem was firstly published in [8]. Subsequently, an optimization problem was defined in [3]. A topology of the 23-bar planar truss bridge is depicted in Fig. 4. The structure is a simply supported truss with a hinge support on the left side and with a roller support on the right side. 23 truss bars are divided into two groups; upper and lower chords (11 members) are included in one group and 12 diagonals create the second group. The vertical static loading is located in all six upper chord nodes. All truss bars are made from the same material.

The probabilistic description of 10 independent random variables is given in Tab. 1. Young's moduli E_1 and E_2 as well as cross-sectional areas A_1 and A_2 assigned to two groups are lognormally distributed; six gravity loads P_i have the Gumbel distribution. Means of the cross-sectional areas are not defined in the table since they represent design variables to be optimized.

The design rule in this task is that the mid-span displacement should not exceed $w_{\max} = 10$ cm, mathematically expressed

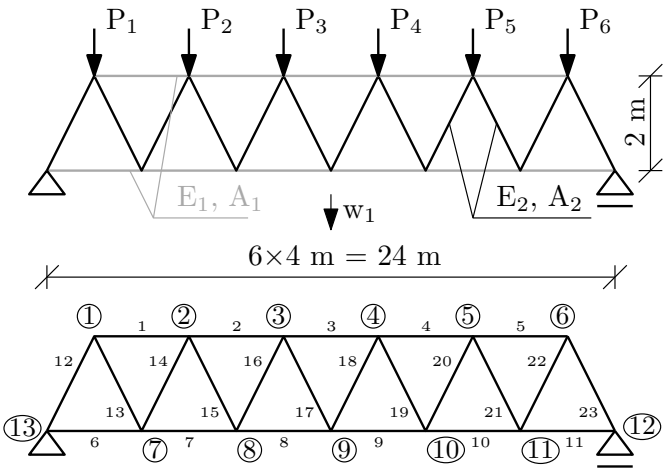

Fig. 4: A 23-bar plane truss bridge

Tab. 1: A probabilistic description of the 23-bar planar truss bridge

Variable		Distribution	Mean	Standard deviation
E_1, E_2	Pa	Lognormal	$2.1 \cdot 10^{11}$	$2.1 \cdot 10^{10}$
A_1	m^2	Lognormal	μ_{A1}	$2 \cdot 10^{-4}$
A_2	m^2	Lognormal	μ_{A2}	$1 \cdot 10^{-4}$
$P_1 \ldots P_6$	N	Gumbel	$5 \cdot 10^4$	$7.5 \cdot 10^3$

$$g(\mathbf{x}) = w_{\max} - |w_1(\mathbf{x})| \,, \tag{9}$$

$g(\mathbf{x})$ greater than or equal to zero denotes safety of the system, $g(\mathbf{x})$ lesser than zero indicates failure[1].

On one hand, the optimal design of the structure should be light-weighted as possible; on other hand as safest as possible. Nevertheless these two criteria are antagonistic. DUBOURG [3] formulated the single-objective optimization problem as

$$\mathbf{d}^* = \arg\min_{\mathbf{d}\in\mathbb{D}} L_1\mu_{A1} + L_2\mu_{A2} : \mathbb{P}[g(\mathbf{x}(\mathbf{d})) \leq 0] \leq \Phi(-\beta_0) \,, \tag{10}$$

in which L_1 and L_2 are cumulative lengths of all bars in each group, β_0 is a prescribed reliability index equal to 3 and $\Phi(\cdot)$ is a Laplace function that represents a cumulative distribution function of the standard normal distribution. A $\mathbb{D}$ space is bounded to $[6 \cdot 10^{-4}, 6 \cdot 10^{-3}] \times [3 \cdot 10^{-4}, 3 \cdot 10^{-3}]$.

6 Multi-objective optimization for RBDO

The single-objective optimization with reliability as a constraint need not be effective since the problem can be multimodal and all of the optima might not be discovered. Thus, the op-

[1]The mid-span displacement need not to be the maximal due to the randomness of variables, however, the mid-span displacement is presumed as the maximum one.

timization task is reformulated in this paper. First of all, the minimization of the probability of failure $\mathbb{P}[g(\mathbf{x}(\mathbf{d})) \leq 0]$ towards the prescribed limit is replaced by maximization of the reliability index β (more or less for the sake of readability and scaling). The bi-objective problem is then composed of the minimization of the weight of the structure and by maximization of the β. To limit the search above the prescribed limit, a penalty function approach is used. To ensure the preference of the feasible solutions over the infeasible ones, i.e. those below $\beta_0 = 3$, the weight of the infeasible solutions is increased by a penalty term p equal to the average weight of feasible solutions among current population. In this way, the solutions close and above the limit are always dominating solutions below the limit. To sum it up, the final multi-objective problem reads

$$\max_{\mathbf{d}\in\mathbb{D}} \quad \beta \,, \tag{11}$$

$$\min_{\mathbf{d}\in\mathbb{D}} \quad L_1\mu_{A1} + L_2\mu_{A2} + p \,, \tag{12}$$

$$p = \begin{cases} 0 & \text{if } \beta \geq 3 \,, \\ \mu_V & \text{if } \beta < 3 \,, \end{cases} \tag{13}$$

where μ_V is a mean value of a structural volume of feasible solutions with reliability index higher than or equal to 3.

The NSGA-II algorithm is designed to uniformly cover the entire Pareto front, which is not needed in our case. Therefore, to force the algorithm to search more often around the $\beta_0 = 3$, the NSGA-II algorithm is modified. Here, the crowding distance is not necessary to be considered as a criterion for choosing individuals from the overlapping front, as described in Sec. 3. This is replaced by the distance to the $\beta_0 = 3$ limit, i.e. solutions with the highest rank are truncated based on their ascent from the given limit.

7 Sampling methodology for Asymptotic Sampling method

First of all, we have tested whether the Asymptotic Sampling is set properly. Therefore, we have started with the direct model by evaluation of the original structural model. Note that the statistics is made out of 100 runs.

We made a comparison for discovering the best suitable sampling method to obtain the most precise reliability index in a tolerable time. The Crude Monte Carlo, Latin Hypercube Sampling method and quasi-random sequences were examined. To get the best results from the LHS we used non-optimized as well as optimized LHS designs, see e.g. [11] for more details. Fig. 5 shows obtained boxplots. Tab. 2 indicates means of the runtime for one simulation to get the approximated reliability index.

The influence of the growing number of samples on the standard deviation of the obtained reliability indices is clear. Note that the Crude Monte Carlo based reliability index with 10^6 samples is $\beta_{CMC} = 1.7142$. Also the computational demands are dramatically growing with the complexity of the used method. Based on these results, we have selected Halton sequences with 2048 samples as the sampling strategy for the Asymptotic Sampling.

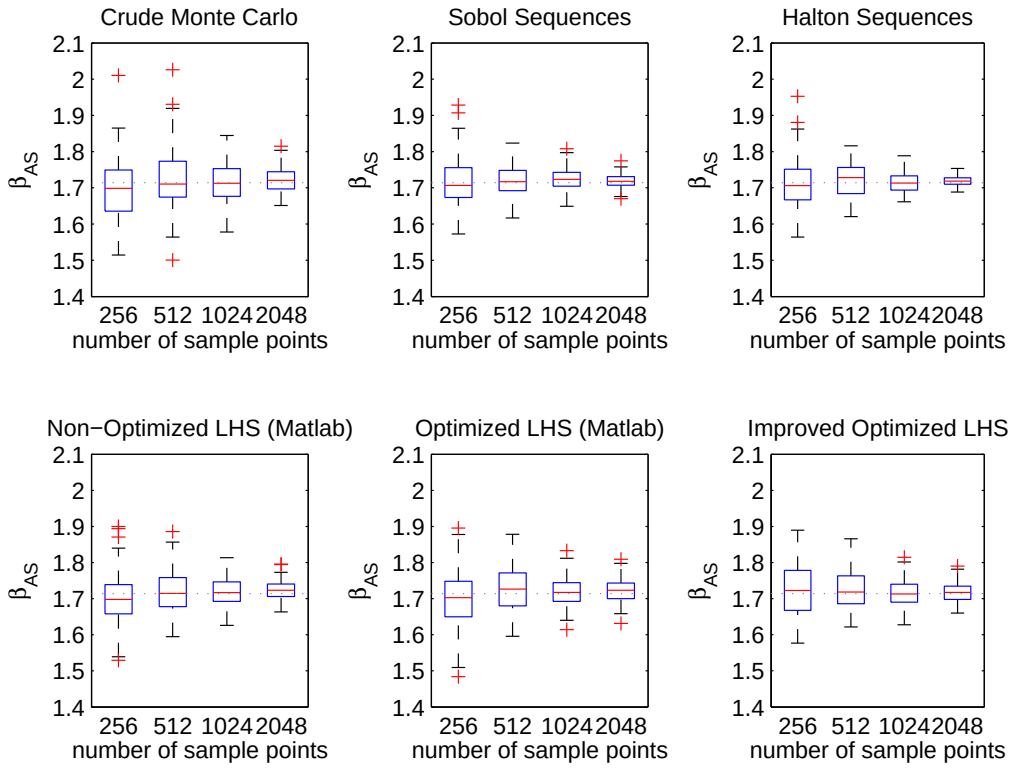

Fig. 5: Boxplots for reliability index obtained by the asymptotic sampling; six methods with different numbers of sampling points were used; dotted line is a "precise value" computed with 10^6 Crude Monte Carlo samples with corresponding $\beta = 1.7142$

Tab. 2: Average times in seconds for different methodologies used to obtain reliability index β for different number of sampling points m. Crude Monte Carlo Sampling (CMC), Latin Hypercube Sampling (LHS) and quasi-random sequences were used. MATLAB provides `lhsdesign()` that offers non-optimized designs (Non-Opt. LHS) as well as optimized designs (Opt. LHS). We chose 1000 optimization steps to obtain better results. We also tested improved LHS methodology [11] with 1000 optimization iterations. At the end, Sobol and Halton sequences from MATLAB are presented.

m	CMC	Non-Opt. LHS	Opt. LHS	Impr. Opt. LHS	Sobol	Halton
256	0.0346	0.182	2.9678	4.8593	0.0600	0.0438
512	0.0393	0.424	7.6848	12.2458	0.0640	0.0520
1024	0.0492	1.182	22.5293	37.7935	0.0754	0.0699
2048	0.0695	3.236	63.5179	115.1676	0.0952	0.1065

8 Results with meta-model

Settings of parameters of the Non-dominated Sorting Genetic Algorithm along with the Asymptotic Sampling methodology for reliability index prediction utilizing the Kriging meta-model are presented in Tab. 3. It is a question, whether to update the meta-model during

Tab. 3: Parameter settings for proposed methodology; all used symbols are explained in Sec. 2 in the last paragraph

NSGA parameters	
number of generations	50
number of individuals	20
crossover probability	1
mutation probability	1

AS parameters	
K	5
f_0	1
f_d	0.9
m	1024
N_0	10

the optimization or not. We have chosen the simplest method, first to train the meta-model and then, independently, run the optimization part with the trained meta-model.

There is also a problem of setting bounds for the DoE of the meta-model. Since the probability densities are unbounded, we cannot sample infinite space. We have selected square hypercube with coordinates $[\mu - 3 \cdot \sigma, \mu + 3 \cdot \sigma]$, where μ is the mean and σ a standard deviation of the given variable. Also note that we are starting from the DoE of 100 points.

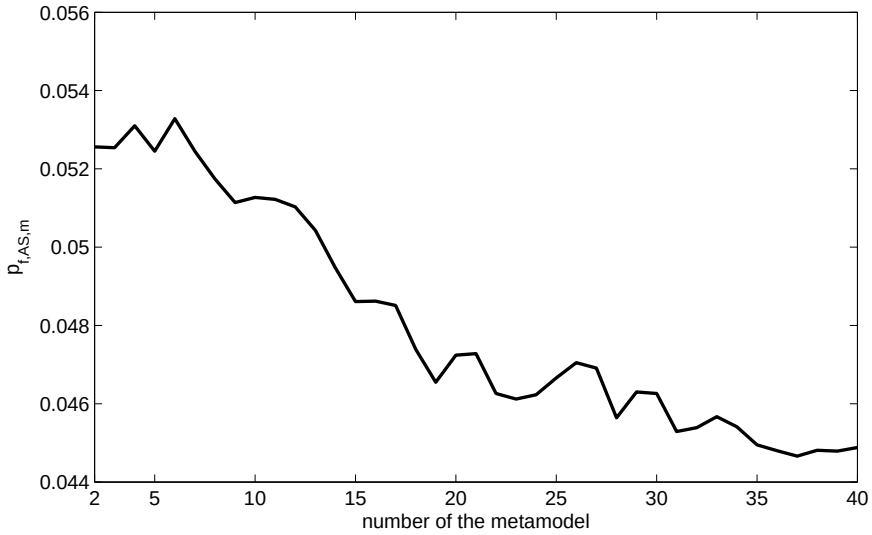

Fig. 6: Convergence of p_f of metamodel during its consecutive updating; the probability is computed by Asymptotic Sampling method; "precise" value computed with 10^6 Crude Monte Carlo samples is $p_f = 0.0432$ ($\beta = 1.7142$)

The quality of the meta-model is measured again by the probability of failure estimated by the Asymptotic Sampling method. Fig. 6 shows that after 40 iterations/updating of the original DoE, the probability of failure converges, i.e. differences among p_f's were smaller than 10^{-4} during the last five iterations. Note that approximately 220 points have been added by the updating procedure and that the final value is slightly over-estimated from the precise value computed by the Crude Monte Carlo method due to the low number of support points.

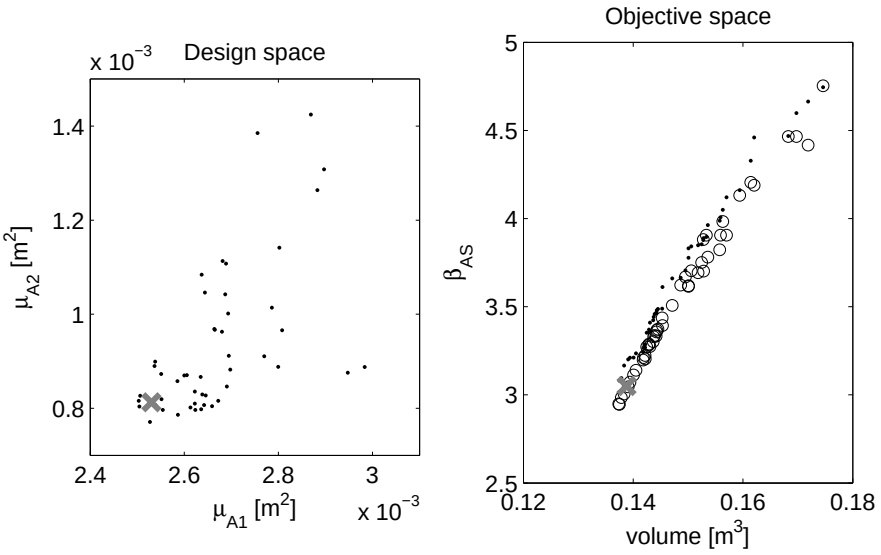

Fig. 7: The overall Pareto-set (left) together with the Pareto-front (right) is compared to the optimal solution presented in [3] (grey cross). Objective values obtained by the Asymptotic Sampling supported by the metamodel with β in range of 3 to 6 are represented by dots. This Pareto-front is recalculated by the Crude Monte Carlo with 10^6 samples and depicted by circles.

9 Conclusion

Fig. 7 reveal that the proposed methodology is, after several iterations, able to find the desired region. From the left part of the figure, the influence of both variables to the reliability index is also visible. Pareto optimal designs are formed by the variable A_2 approaching a value of $8 \cdot 10^{-4}$ m^2. The position, i.e. the resulting reliability index, is then dominantly influenced only by the A_1 variable.

The same figure also shows the obtained Pareto front after recalculation of the reliability indices by the CMC method with 10^6 samples. It is clearly visible that the Asymptotic Sampling often overestimates the true value of the index β. This can be attributed to the low number of support points as well as their uniform distribution. More advanced approach is presented in [14], which will be the goal of our future research.

Acknowledgements

This research was supported from the Czech Scientific Foundation through the project GAČR P105/12/1146.

Literature

[1] C. Bucher. Asymptotic sampling for high-dimensional reliability analysis. *Probabilistic Engineering Mechanics*, 24(4), 2009, p. 504–510

[2] K. Deb, S. Agrawal, A. Pratap, and T. Meyarivan. A fast elitist non-dominated sorting genetic algorithm for multi-objective optimization: NSGA-II. *IEEE Transactions on Evolutionary Computation*, 6(2), 2000, p. 849–858

[3] V. Dubourg. *Adaptive surrogate models for reliability analysis and reliability-based design optimization*. PhD thesis, Blaise Pascal University – Clermont II, France, 2011

[4] D.R. Jones. A taxonomy of global optimization methods based on response surfaces. *Journal of Global Optimization*, 21, 2001, p. 345–383

[5] F. Jurecka. *Robust Design Optimization Based on Metamodeling Techniques*. PhD thesis, Technische Univesität München, 2007

[6] Z. Kang. *Robust Design Optimization of Structures under Uncertainties*. PhD thesis, Univesität Stuttgart, 2005

[7] J.S. Lee, T.S. Cho, J. Lee, M.K. Jang, T.K. Jang, Dongkyung Nam, and Cheol Hoon Park. A stochastic search approach for the multidimensional largest empty sphere problem. *Citeseer*, 2004

[8] S.H. Lee and B.M. Kwak. Reliability based design optimization using response surface augmented moment method, 2005

[9] S.H. Lee and B.M. Kwak. Response surface augmented moment method for efficient reliability analysis. *Structural Safety*, 28(3), 2006, p. 261–272

[10] S.N. Lophaven, H.B. Nielsen, and J. Sondergaard. Aspects of the Matlab toolbox Dace. Technical Report IMM-REP-2002-13, Informatics and Mathematical Modelling, Technical University of Danemark, 2002

[11] E. Myšáková and M. Lepš. Comparison of Maximin LHS Design Strategies. In *Proceedings of the 3rd Conference Nano and Macro Mechanics NMM 2012*, pages 163–170. CTU in Prague, 2012

[12] J. Sacks, W.J. Welch, T.J. Mitchell, and H.P. Wynn. Design and analysis of computer experiments. *Statistical Science*, 4(4), 1989, p. 409–435

[13] K. Sastry and D. Goldberg. *Search Methodologies*, chapter Genetic Algorithms, pages 97–125. Springer, 2005

[14] M.T. Sichani, S.R.K. Nielsen, and C. Bucher. Applications of asymptotic sampling on high dimensional structural dynamic problems. *Structural Safety*, 33(4–5), 2011, p. 305–316

[15] B. Sudret. *Uncertainty propagation and sensitivity analysis in mechanical models – Contributions to structural reliability and stochastic spectral methods*, Habilitation à diriger des recherches, Universitè Blaise Pascal, Clermont-Ferrand, France, 2007

[16] M. Valtrová. Computation aspects of Kriging in chosen engineering problems. Master's thesis, CULS Prague, 2009

Recent advances in seismic fragility estimation

Dirk Proske[1], Davide Kurmann[1] and Jan Červenka[2]
[1]Axpo Power AG, Baden, Switzerland
[2]Cervenka Consulting, Prague, Czech Republic

Abstract: Seismic load bearing capacity of structures can be presented in terms of fragilities and HCLPF-values respectively. These values are computed based on the dynamic properties of the structures as well as on the hazard described as hazard curve and uniform hazard spectra (UHS) respectively. Improved HCLPF-values of structures can be achieved by means of highly sophisticated non-linear structural and dynamic models. Furthermore the UHS can be applied in a more sophisticated way as Conditional Spectra or Conditional Mean Spectra. Using such procedures the numerical characteristic seismic load capacity of structures can be increased further. However in both cases, besides this positive effect, the computation efforts also grow heavily.

Keywords: Seismic Fragility, Uniform Hazard Spectra (UHS), Conditional Spectra (CS), Conditional Mean Spectra (CMS), Incremental Dynamic Analysis (IDA), Pushover-Curve

1 Introduction

Seismic loadings are common in regions with high and moderate seismicity. They endanger the critical infrastructures, such as bridges and buildings, and the lives of humans. Therefore new structures in such regions are designed for seismic loadings. However for existing structures, the proof of the required seismic load bearing capacity can become very challenging.

In this paper the proof of the seismic load bearing capacity is done in terms of fragilities and especially in terms of HCLPF-values. The original concept of seismic fragilities has been introduced some decades ago. However observations of reinforced concrete structures during earthquakes have indicated that the seismic load bearing capacity may be higher than estimated by traditional fragilities. Advances of the concept in recent years have been developed and yield to, depending on the individual structure, a significant higher numerical seismic loading capacity. These advanced concepts will be introduced in this paper.

The paper is divided into the following parts: First in Sec. 2 the concept of seismic fragilities is introduced. Subsequently in Sec. 3 advanced structural models and dynamical models are discussed. In Sec. 4 the differences between the concept of UHS and the concept of Conditional Spectra is outlined. Finally some results are presented and discussed.

2 Seismic fragilities

The current safety concept in structural engineering is based on a probabilistic and statistic approach. Whereas other mathematical methods exist to deal with uncertainty (PROSKE [1]), stochasticity as umbrella term of probabilistic and statistic means is the mathematical tool most widely used, best understood and with the greatest variety of tools. However, the direct application of a full probabilistic analysis is limited to special cases, since modeling, computation and reporting are extremely time consuming. Simulations may run over weeks or even months, although major progress has been made in the last years, both computationally and methodically. Such computation times are not acceptable in engineering business. However, if certain assumptions about the outcome of probabilistic computations are made, the required computation time can be significantly decreased. Fragilities belong to this group of simplified probabilistic analyses.

In general, fragilities are functions of the probability of failure of a certain structure depending on the intensity of the loading. For seismic fragilities the intensity of the loading is represented by the intensity of the earthquake. We have used the peak ground acceleration value as anchor point for the earthquake intensity scale. Other spectral acceleration values may be used as alternative anchor points.

The removal of the loading from the full probabilistic analysis can be seen as a first step of simplification. The next step is an assumption about the function type of the fragility. Usually here only a limited number of probability functions are considered, such as lognormal distribution (EPRI [2]), normal distribution or Weibull distribution (Eurocode 1). With the selection of the probability function based on recommendation documents, the need to prove this function in the specific case is eased. Some researchers assume that it is extremely difficult, if not impossible to prove the validity of a probability distribution. Indeed it requires high sample sizes or high simulation efforts when looking at the correct representation of the distribution tails. In contrast, by selecting a normal or lognormal distribution, the probability function and the fragility respectively can be fully developed by using only two supporting points. Since the supporting points do not have to be located in regions of extreme low or extreme high probabilities of failure, there is no need to carry out probabilistic computations in these regions. For sampling based probabilistic techniques this is an overwhelming advantage.

Current studies have shown again (ZENTNER et al. [3]) that the assumption yields reasonably accurate results. Therefore the following probability function and fragility respectively will be used within this study:

$$P_{f/a} = \Phi\left(\frac{\ln(a / A_m}{\beta}\right) \tag{1}$$

with P as probability of failure as function of the seismic intensity a, whereas a is spectral acceleration of an anchor point of the uniform hazard curve (we have used the PGA-value), Φ as Gauss-distribution (normal distribution), A_m as value of the spectral acceleration yielding a median failure probability (50 % fractile) and β as parameter of uncertainty (standard deviation). Furthermore, the uncertainty parameter is divided into aleatoric and epistemic uncertainty. The aleatoric uncertainty is the immanent uncertainty of the material and loading. In contrast, the epistemic uncertainty considers the limitation of knowledge.

Whereas the epistemic uncertainty can be lowered by additional data, the aleatoric uncertainty is immutable.

It is common to consider the aleatoric uncertainty as a random variable, whereas the epistemic uncertainty is considered as uncertainty of the statistical parameters, usually known as confidence intervals. This yields the function corridor shown in Fig. 1. The complete probability function and fragility respectively with explicit consideration of the types of uncertainty is

$$P_{f/a} = \Phi\left(\frac{\ln(a/A_m) + \beta_U \Phi^{-1}(Q)}{\beta_R}\right) \tag{2}$$

with β_R as aleatoric uncertainty (standard deviation), β_U as epistemic uncertainty (standard deviation) and Φ^{-1} as inverse Gauss distribution. Furthermore often the composite-uncertainty is used, which is defined as:

$$\beta_C = \sqrt{\beta_U^2 + \beta_R^2} \tag{3}$$

An important point on the fragility curve is the HCLPF-value (High Confidence of Low Probability of Failure). This value can be directly related to the semi-probabilistic codes of practice. Modern codes of practice use so-called characteristic material values. The HCLPF value is defined as the 5 % fractile value with 95 % confidence interval. It is interesting to note, that with the application of nonlinear methods also structural characteristic values and safety factors have been developed (ČERVENKA ET AL. [4]), which can be interpreted as the HCLPF-value. Since maintenance of the distinction of the uncertainty parameters throughout the analysis is very difficult, the HCLPF-value is often defined as the 1 % fractile value of the fragility function assuming, that the confidence interval will be covered by the adjustment from the 5 % to the 1 % fractile value. This gives the HCLPF-value with

$$HCLPF = \frac{A_m}{\exp(2.33 \cdot \beta_c)} \tag{4}$$

The unit of the HCLPF-value, but also of the A_m value and the uncertainty parameters depends on the selection of the earthquake intensity parameter. We have used the acceleration unit *g*.

For the computation of the fragility curve a sufficient structural and dynamical model is required.

3 Deterministic static and dynamic model

Usually structures experience a highly non-linear behavior during extreme loadings, such as seismic loading. This non-linear behavior can be considered in terms of a pushover-analysis. With such an analysis, the entire force and deformation capabilities of the structure can be determined as well as the energy dissipation capabilities. In general, a pushover-curve is a force-deformation-function for a structure regarding a one-sided horizontal loading (FEM 356 [5], MESKOURIS ET AL. [6]).

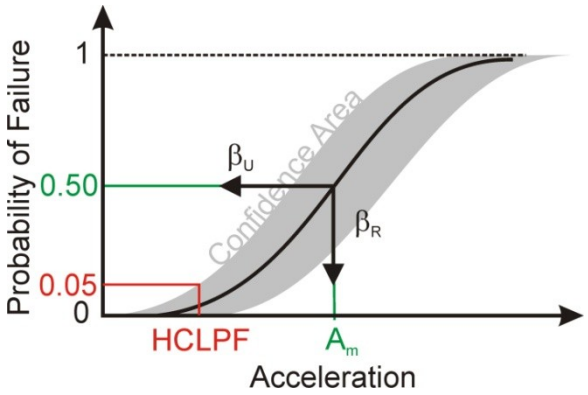

Fig. 1: Seismic fragility: terms

A pushover-analysis carried out with the program ATENA yields to maximal ultimate loads, since it considers all important concrete failure mechanisms such as concrete cracking, crushing, reinforcement yielding or rupture (ČERVENKA & PAPPANIKOLAOU [7], ČERVENKA ET AL. [8]). However, computation times for pushover-curves with ATENA can become quite extensive, for example up to one day.

Fig. 2 shows an obtained pushover-curve (taken from [9]). The considerable ductility of the structure becomes clearly recognizable in this figure.

This pushover-curve does not yet consider any dynamic properties. The curve is independent from the specific seismic dynamic loading and therefore it can be used even under changing seismic loading spectra. In contrast to the pushover-analysis, the following steps are highly dependent upon the specific seismic loading.

Usually the seismic hazard is given as a uniform hazard spectrum (UHS) for a certain ground level and a certain return period of the value (Fig. 3). In general, the uniform hazard spectrum gives the spectral acceleration over the frequency range.

The uniform hazard spectrum can be either taken from codes, as usually done for common building structures, or experts provide them. An example of the provision by experts is the PEGASOS Project, presented by RENAULT [10].

In a first step, for the given uniform hazard spectra acceleration time histories were taken from real earthquake databases and adjusted. Details about this time histories are given later. Based on this spectra-compatible acceleration time histories a dynamic soil-structure interaction (SSI) analysis was carried out using the program SASSI (APA CONSULTING [11]). Fig. 4 shows such a floor response spectrum. Furthermore, the SSI considers random input variables and provides statistical information about the results.

The SSI gives the fundamental frequency of the structure and the modal parameter such as mass and damping considering the coupled system (soil-structure) (SADEGH-AZAR & HARTMANN [12]). The damping considers material damping of the structure, material damping of the ground (strain-dependent damping) and emission damping of the ground (foundation and light embedment). To consider the uncertainty of the different types of damping, variations were included in the analysis. Furthermore the SSI provided the effective height and the participation factors needed to adapt the pushover results. With this information we are able to construct a representative oscillator with the dynamic properties of the full structure. So far the pushover curve considers only monotonic increased loads.

However for the non-linear dynamic analysis cyclic structural behavior has to be considered. Therefore in the next step a representative oscillator model is expanded including a hysteresis functions.

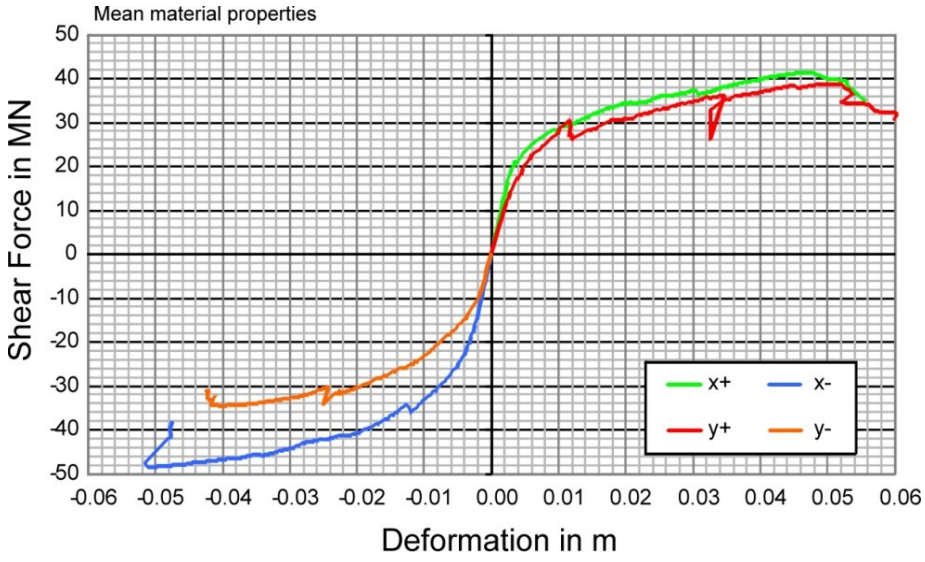

Fig. 2: Pushover-curve based on mean material properties

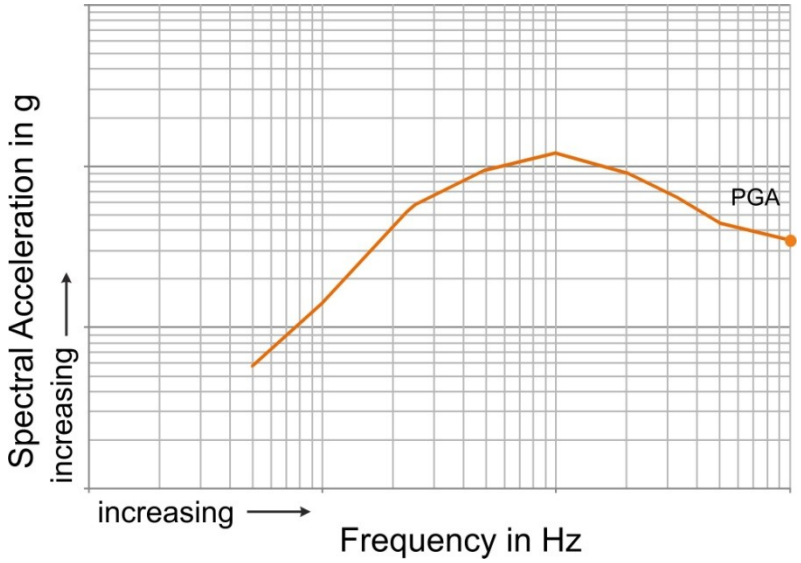

Fig. 3: Uniform hazard spectrum (PGA: Peak Ground Acceleration)

There exist different theoretical hysteresis models, such as hybrid models, Modified-Takeda or the Origin-Centered. The methods and their application are illustrated in KURMANN [13]. It should be noted, that this models still include a noticeable conservatism (BIMSCHAS & DAZIO [14]). Finally a function for the force drop has to be defined. This model and the hysteresis model have to be incorporated into the representative oscillator.

Fig. 5 shows the force-deformation-function of the representative oscillator for monotone increasing ductility demand (PROSKE, KURMANN & CERVENKA [9]).

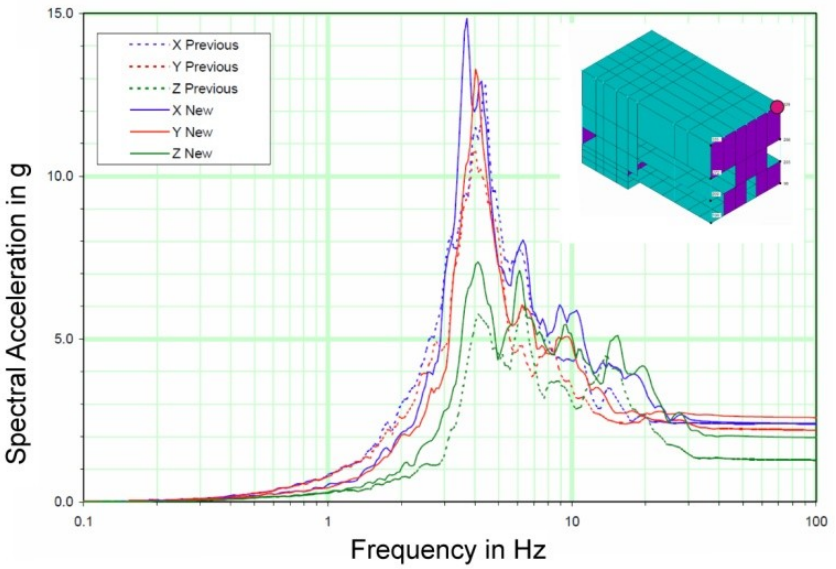

Fig. 4: Floor response spectra in the upper part of the building

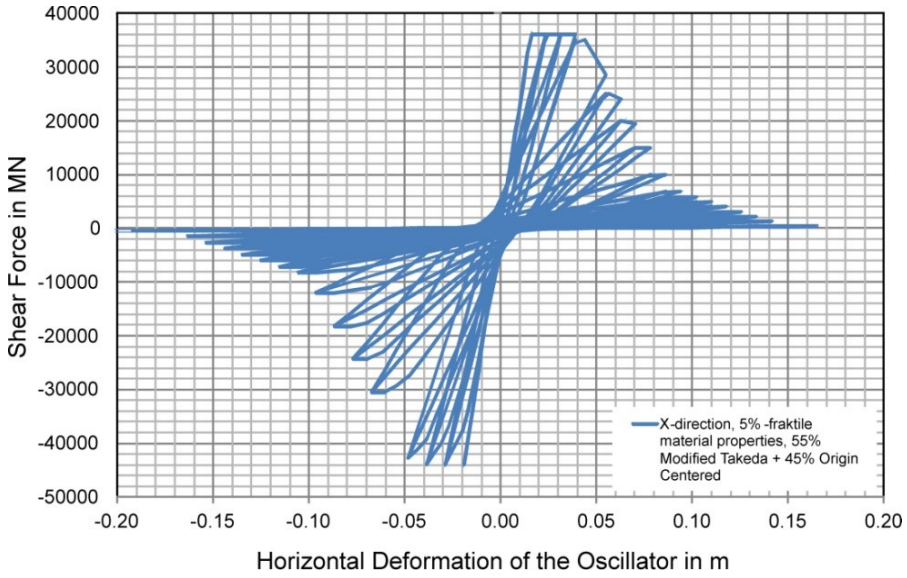

Fig. 5: Hysteresis in *x*-direction using the 5 % fractile value of material properties

In the next step, the representative oscillator is exposed to 30 acceleration time histories based on real earthquake measurements (Fig. 6). These 30 curves are selected and modified to meet the uniform hazard spectrum over a great frequency range. However, here again can be a reason found for a significant conservatism in the computation. The uniform hazard curve considers high spectral acceleration of the entire frequency range. However not a single earthquake will cover the entire broad band UHS. This effect will be discussed in Sec. 4.

Applying and scaling the acceleration time histories, to consider the different earthquake intensities, the ductility demand of the structure for different anchor accelerations can be computed. Since the acceleration time histories are incrementally scaled up, this computation is called Incremental Dynamic Analysis (IDA).

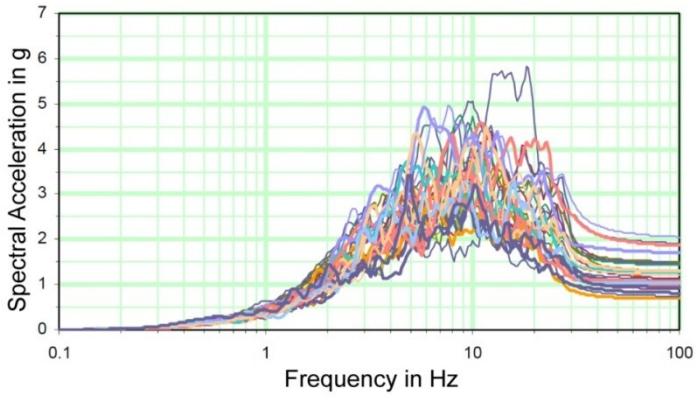

Fig. 6: Individual spectra of the different Acceleration-Time-Functions

Since the analysis was not only carried out using mean material properties but also characteristic material properties and furthermore using the 30 time histories, also the uncertainty is considered in the analysis. The uncertainty of exceeding the maximum acceptable ductility is given in terms of β_R and β_U.

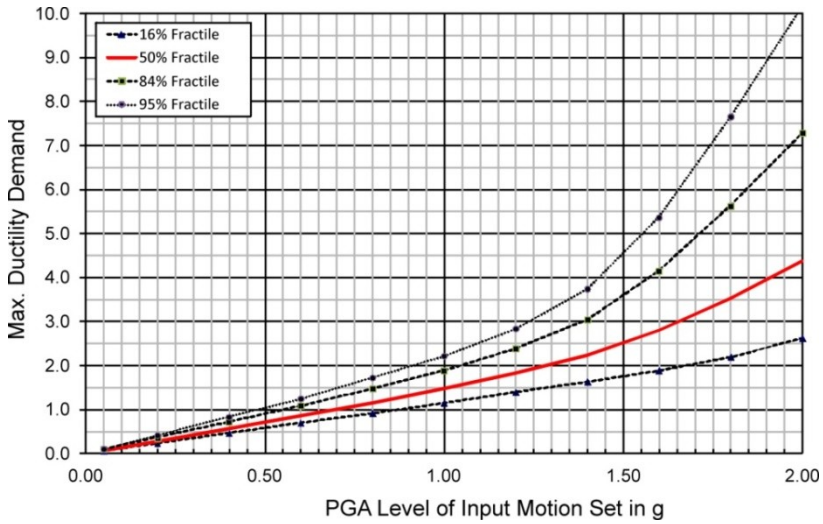

Fig. 7: Incremental dynamic analysis for representative oscillator with characteristic material values

Since the entire analysis was carried out for different material properties and different time histories, both central tendency estimators as well as uncertainty estimators were computed. With this data the fragility can be constructed.

In general, applying such an advanced approach, the HCLPF-value as anchor point of the fragility can increase by a factor of 2 compared to former analysis.

4 Application of UHS versus CS/CMS

Besides the advances in the modeling of structures by using highly non-linear static models, by consideration of hysteresis curves and force drops, advances can also be reached by the application of Conditional Spectra instead of Uniform Hazard Spectra (UHS) (BAKER ET AL. [18]). In general, the UHS consider the maximum median or mean spectral acceleration for all possible frequencies based on a wide range of earthquakes. However in reality,

certain time histories during an earthquake are possible, which do not cover the entire UHS. In other terms, the maximum median or mean spectral accelerations are not found over the full frequency range, but rather at some frequency range parts. That means the UHS overestimates the spectral accelerations at certain regions of frequencies. This numerical conservatism can be used, if the UHS is disaggregated to certain earthquake distances and intensities (Fig. 8).

However that yields to higher numerical requirements since many different Conditional Spectra have to be created. An alternative, sometimes found in Structural Engineering, are Conditional Mean Spectra (BAKER & CORNELL [19], [20]), where not all the frequency points are covered, but usually only two or three points of the UHS (Fig. 9). In this case, only two- or three-times the computational effort is required. The Conditional Mean Spectra can then be the basis for time acceleration histories and can be applied in the same procedure as shown in Sec. 3. The results of this double or triple computation do not have to be added, but rather the maximum loading or the minimum HCLPF-value has to be chosen.

Comparing the results between UHS based acceleration time histories and CS or CMS based time histories, it yields to increased HCLPF-values, probably in the range of 20 % to 30 % (RENAULT & KURMANN [15]).

5 Results

Reinforced concrete structures designed in former decades may not meet current seismic requirements. On the other hand, applying new structural methods, it may be shown, that seismic load bearing behavior of older structures still performs very well under extreme seismic loadings. Using latest non-linear modeling and consideration of hysteresis approaches, the characteristic loading can be increased by 100 % (PROSKE ET AL. [9]).

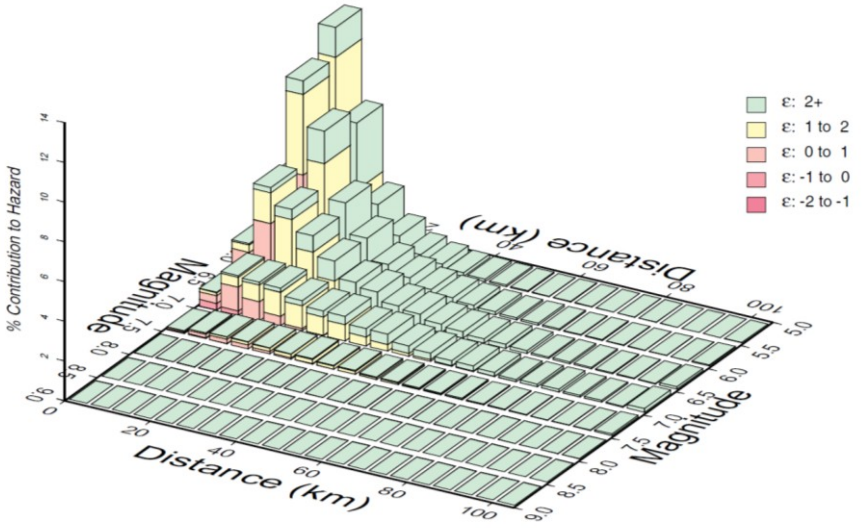

Fig. 8: Disaggregation of hazard curve

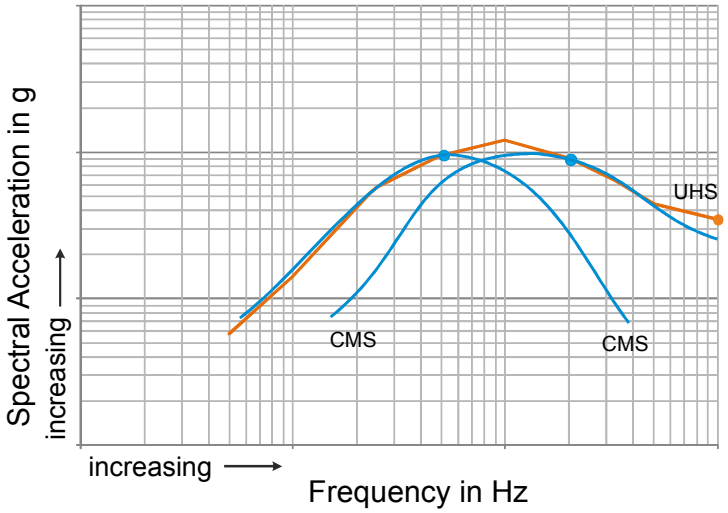

Fig. 9: Development of Conditional Mean Spectra.

On the other hand, applying advanced hazard estimations, such as Conditional Spectra and Conditional Mean Spectra, the HCLPF-value can be additionally increased by 20 to 30 % (RENAULT & KURMANN [15]).

It can be summarized, by using advanced techniques the numerical seismic load bearing capacity of existing concrete or masonry structures can be significantly increased. Therefore it is strongly recommended to engineers to apply such techniques, where the proofs cannot be carried out using traditional or code based techniques.

Literature

[1] Proske, D. Zur Zukunft der Sicherheitskonzepte im Bauwesen, *Bautechnik* 88(4) (2011), p. 217–224

[2] EPRI. *Methodology for developing seismic fragilities*, prepared by J. R. Benjamin and Associates, Inc and RPK Structural Mechanics Consulting, TR-103959, Project 2722-23, 1994

[3] Zentner, I., Nadjarian, A., Humbert, N. & Viallet, E. Estimation of fragility curves for seismic probabilistic risk assess-ment by means of numerical experiments. C.-A. Graubner, H. Schmidt & D. Proske (Eds.): *6th International Probabilistic Workshop*, 26–27 November 2008, Darmstadt, Germany 2008, Technische Universität Darmstadt, 2008, p. 305–316

[4] Cervenka, J., Cervenka, V., Pukl., R & Janda, Z. Assessment of remaining structural capacity by computer simulation. *Tailor Made Concrete Structures* – Walraven & Stoelhorst (eds), London: Taylor & Francis Group, 2008, p. 665-671. ISBN 978-0-415-47535-8

[5] FEMA 356. *Prestandard and commentary for the seismic rehabilitation of buildings*. Federal Emergency Management Agency, American Society of Civil Engineers, Reston, Virginia, 2000

[6] Meskouris, K., Hinzen, K.-G., Butenweg, C., Mistler, M. *Bauwerke und Erdbeben: Grundlagen-Anwendung–Beispiele*. Vieweg + Teubner Verlag; 2. Auflage, 2007

[7] Cervenka, J., Pappanikolaou, V. Three dimensional combined fracture-plastic material model for concrete. *International Journal of Plasticity* 24(12) (2008), p. 2192–2220

[8] Cervenka, J., Jendele, L., Cervenka, V. *ATENA Program documentation*. Cervenka Consulting, 2010

[9] Proske, D., Kurmann, D., Cervenka, J. Seismische Tragfähigkeit eines Stahlbetonbauwerkes. *Beton und Stahlbetonbau* 8 (2013)

[10] Renault, P. PEGASOS Refinement Project: New Findings and Challenges from a PSHA for Swiss Nuclear Power Plants. In: Dutta, B. K., Singh, R. K. & Durgaprasad, O. V. (editors), *SMIRT 21 - International Conference on Structural Mechanics in Reactor Technology*, New Delhi, India, 2011

[11] APA Consulting. Development of Acceleration Time Histories for the Intermediate PRP Uniform Hazard Spectra Walnut Creek. 2011

[12] Sadegh-Azar, H., Hartmann, H.-G. Grundlagen der seismischen Auslegung von Kernkraftwerken und Einfluss der Boden-Bauwerk Wechselwirkung. *Bauingenieur* 86(3) (2011), p. S3–S10

[13] Kurmann, D. *Seismic Analysis of Existing Bridges with Detailing Deficiencies*. ROSE School Master Thesis, Istituto Universitario di Studi Superiori di Pavia, Università degli Studi di Pavia, 2009

[14] Bimschas, M. & Dazio, A. Large Scale Quasi-Static Cy-clic Tests of Existing Bridge Piers. *14th World Conference on Earthquake Engineering,* Beijing, China, 2008

[15] Renault, P., Kurmann, D. Comparision of Uniform Hazard Spectra and Conditional Spectra Approach in the Framework of Fragility Curve Development. Smirt-22, San Francisco, August 2013

[16] Carr, A. J. RUAUMOKO-Volume 2; *User Manual for the 2D-Version, Ruaumoko 2D*. Department of Civil Engineering, University of Canterbury, Christchurch, New Zealand, 2004

[17] Yanev, P.I., Yanev, A.J. Earthquake Engineering Lessons for Nuclear Power Plant Structures, Systems, and Components from Fukushima and Onagawa. *8th Nuclear Plants current Issues Symposium*, 23–25.1.2013. Orland, Florida, US, 2013

[18] Baker, J.W. 2013. http://www.stanford.edu/~bakerjw/publications.html

[19] Baker, J.W., Cornell, C.A. Spectral shape, epsilon and record selection. *Earthquake Engineering and Structural Dynamics* 35 (2006), p. 1077–1095

[20] Baker, J.W., Cornell, C.A. *Vector-Valued Ground Motion Intensity Measures for Probabilistic Seismic Demand Analysis*. PEER Report No. 2006/08, 2006

Probability of log jams at bridges

Dirk Proske, Andreas Vögeli
Axpo Power AG, Baden, Switzerland

Abstract: Flooding is not necessarily caused by pure water flow, but can also be related to debris and log jams. Both causes changes of the flow river profile and therefore to different flowing conditions. This paper discusses the probability of a log jam at a certain bridge by considering the amount of dead wood, estimating the number and size of woods and then the probability of a log jam at the bridge. Furthermore the paper discusses several structural rules to prevent log jams at bridges.

Keywords: log jam, probability, bridge

1 Introduction

Floods endanger tangible assets and lives of humans in regions exposed to this hazard. Floods can be caused by extreme weather conditions, such as heavy rain or wind, or by impulse waves.

Examples of heavy floods with major loss of human lives are the tsunami events 2004 in Southeast Asia with about 250 000 casualties and the tsunami event 2011 in Japan with about 15 000 casualties. Flooding examples related to human infrastructure are the Vajont disaster in Italy 1963 with about 2 000 casualties and the failure of the Banqiao Dam 1975 with about 85 000 direct casualties and further 145 000 casualties related to hunger and disease [1]. All this tragic disasters are related to impulse waves.

However, flood events can also be related to changes of flow regimes. Log jams and debris flows belong to this group. Under log jams the partially or fully closure of the river flow cross section caused by deadwood is understood [2]. Another definition considers log jams as natural barrier in a flowing river cross section made of deadwood, which causes a temporal retention [3].

Log jams can reach extreme volumes and can cause extreme damages, especially at dams. Fig. 1 shows the Swiss gravity dam Palagnedra, which experienced a heavy log jam 1978. About 25 000 m^3 deadwood were washed up, closing the flooding overran and eroded the abutment [5].

Examples for log jams at bridges in Switzerland are given in [5]. In some cases, bridges were destroyed. Fig. 2 shows an example from Austria [6].

Fig. 1: Log Jam at the Palagnedra Dam in Switzerland 1978 [4],[5]

Fig. 2: Log jam at the state road in Hintereggerbach [6]

2 Design criteria for bridges

Bridges have to be designed to avoid log jams. There exist several design documents giving recommendations. For example, [7] and [8] recommend, that the freeboard of bridges should not be lower than 0.5 m. [9] gives a bridge clearance of 1.5 to 2 m related to the design flood. [10],[12] do not only give values for clearance, it is furthermore suggested:

- vouted bridges are recommended, with maximum clearance in the middle,
- no piers in the river cross section, if possible,
- clearance of 1 m,
- the abutments should not confine the river cross section more than 20 %,
- the bridge span should be more the twice the maximum length of the expected tree,
- the clearance should reach 1.7 of the expected rootstock.

Also [11] recommends vouted bridges with maximum clearance in the middle of the river. However, the application of these rules does not fully prevent log jams. In certain cases it is interesting to estimate the remaining probability of log jams at the individual bridge.

3 Probability of a log jam at a bridge

3.1 Introduction

The estimation of a log jam at a bridge can be carried out in different computational steps:

- estimation of deadwood volume,
- retention factors at further hydraulic structures,
- estimation of deadwood tree length,
- probability of a log jam of a single tree,
- probability of a full log jam.

Each of these steps can include either simplified models or extreme detailed and complex models. In many cases the simple empirical models are used since detailed models may lack the required input data.

Furthermore some of the parameters include uncertainties and can therefore be considered as random variables. This yields to a convolution integral resulting in the probability of a log jam.

3.2 Deadwood Volume Estimation

The probability of a log jam and a drift accumulation at a bridge depends heavily on the amount and the properties of the deadwood volume transported with the river and reaching the bridge or a dam. To estimate such a volume, one has to consider the properties of the catchment area in terms of forest resources, forest properties, ground properties, slopes and flow properties. Fig. 3 gives an overview of a detailed deadwood activation system. Simplified empirical models to estimate the deadwood volume are for example given in RICKENMANN [14]. We have used a model given by Rickenmann.

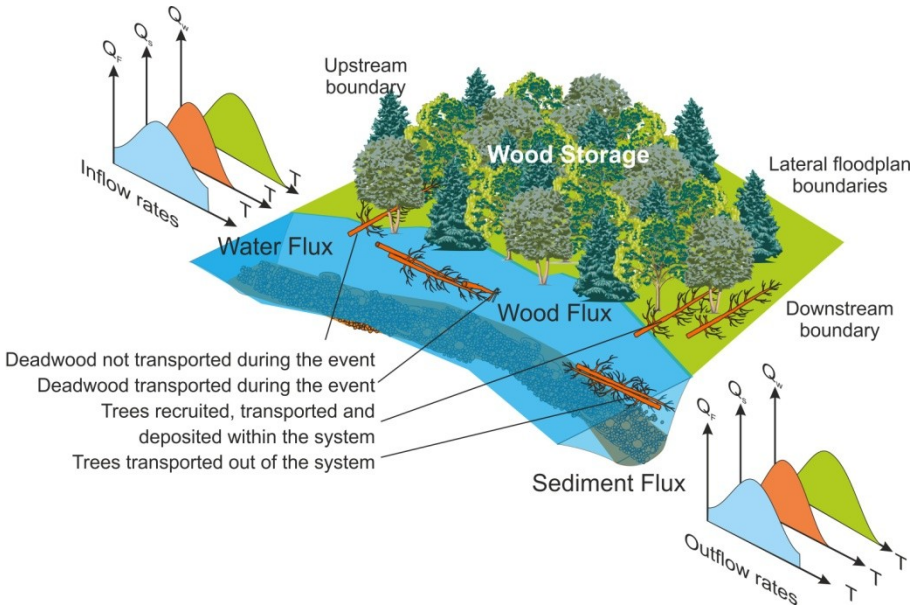

Fig. 3: Wood, sediment and water fluxes and system dynamics [17]

3.3 Retention factors

However the transported deadwood volume is not constant over the river length. Hydraulic structures, such as weirs, or shallow river parts may retention parts of the deadwood volume. Fig. 4 shows the content of deadwood in the Reuss in the 2005 flood in Switzerland [19]. MOULIN ET AL. gives the distribution over the river Roanoke River [21].

We have mainly used a retention probability factor based on the length of the trees in the deadwood and based on the distance to the investigated structure, such as:

$$P_R(A) = 1 - \frac{2.5}{l} \tag{1}$$

with $P_R(A)$ as retention probability for a tree with the length l in the catchment area A.

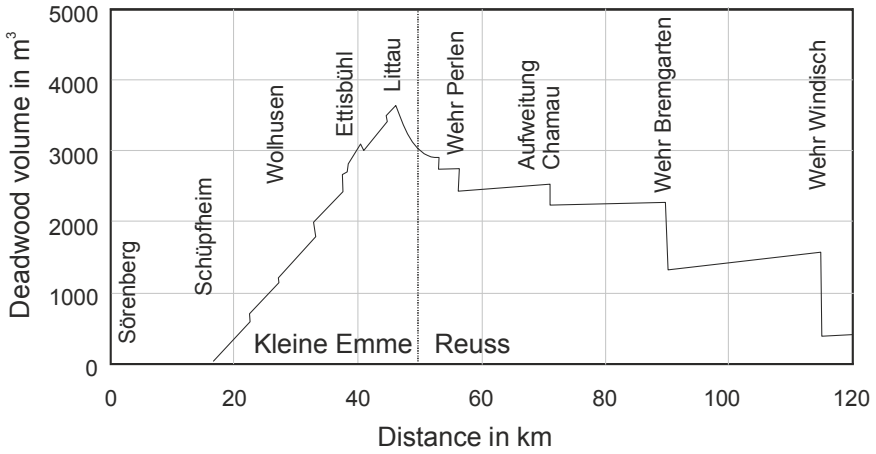

Fig. 4: Deadwood volume during the flooding of the Reuss 2005 [19]

3.4 Deadwood tree length

After estimation of the deadwood volume or the mass, properties of the deadwood, such as the tree length, are investigated. The tree length is also important for the retention factor. Fig. 5 shows for example the distribution of the tree length in deadwood found 2005 in Switzerland at the River Reuss [18]. However usually the deadwood found is distinguished regarding the accumulation procedure. Furthermore for the log jam probability usually only large trees are of interested. Therefore in our case we have used a truncated exponential distribution for the tree length with minimum 8 m length.

3.5 Probability at Bridge

If the deadwood reaches a weir or a bridge, it may accumulate at the bridge with a certain probability. There have been experimental research investigations [16],[22],[23] carried out to estimate the probability of single trees and rootstocks depending on the bridge type, but also for weirs [20]. For example for truss bridges the probability is much higher than for other bridges. The probability also depends on the Froude Number and on the properties the trees and rootstocks. Fig. 6 shows an example. Here h is the water level, H is the height of the bottom side of the structure, B is the span of the bridge and L is the length of

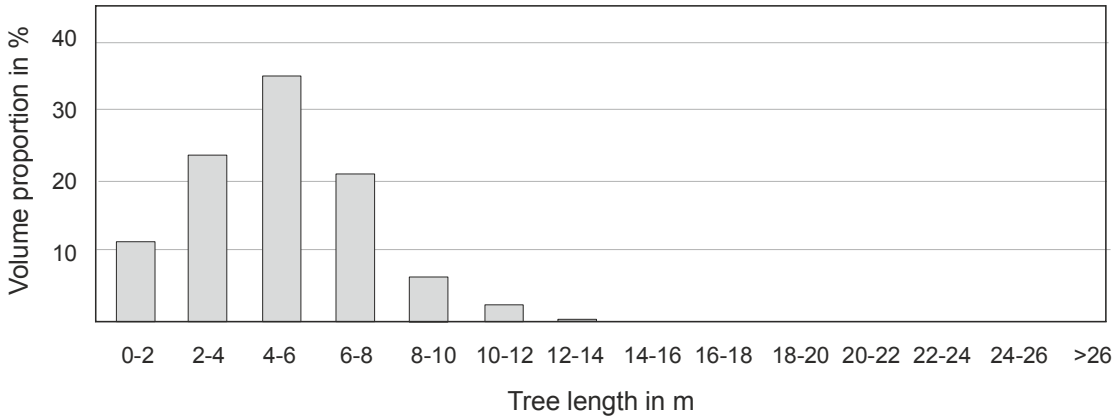

Fig. 5: Length distribution of trees in deadwood related to the deadwood volume [18]

the tree. Based on such diagrams the probability of the blocking of one single tree at a bridge can be estimated. Based on this number the growth of the log jam will be computed.

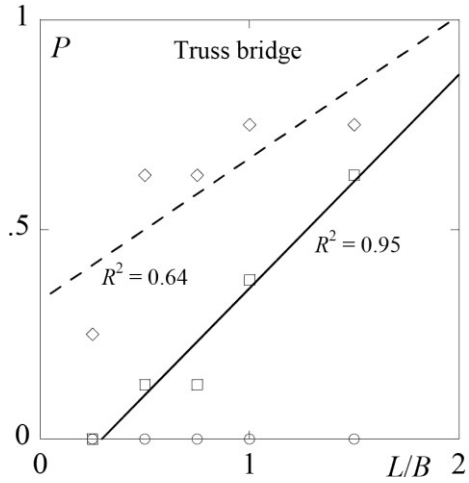

Fig. 6: Blocking probability P versus L/B (single logs) for $F = 0.8$, $h/H = 0.90$ (○, - · -), 1.00 (□,——), and 1.07 (, - - -) for a truss bridges [16]

4 Example

The investigated bridge is a three span vouted prestessed concrete bridge (Fig. 7). The middle span reaches nearly 45 m and the outer spans have about 32 m each. The bridge is constructed as double webbed T-beam. The bridge has been designed for seismic horizontal loading and is therefore able to bear certain horizontal loads.

The river is usually 6.4 m deep. The maximum clearance of the vouted bridge is about 2 m. Therefore the bridge complies with current requirements. However in case of 500 year flood the clearance at the piers becomes zero, the clearance in the middle becomes zero in case of the 10 000 year flood. Since the middle of the bridge is clearly above ground, also the surroundings will be flooded.

Since the probability that the handrail is reached only during floods with extreme low probability, also the probability of the log jam is extremely low. Furthermore the condi-

tional probability that a full close of the river cross section occurs by log jam occurs is extremely low (< 10^{-7} ... 10^{-5} per flooding) (see Fig. 8).

This can be easily shown by the deadwood volume required. For example, with a span of about 100 m and a height including full log jam, we assume a required deadwood volume of 100 m × 8 m × 8 m = 6400 m^3, which is extreme large volume (see Fig. 4).

Since the bridge does not cross the river rectangular, also deadwood will concentrate in the acute angle, therefore keeping the middle of the river free.

Furthermore the ratio of bridge span to tree length is extremely large, this furthermore confirms the low probability.

Fig. 7: Picture of the investigated bridge

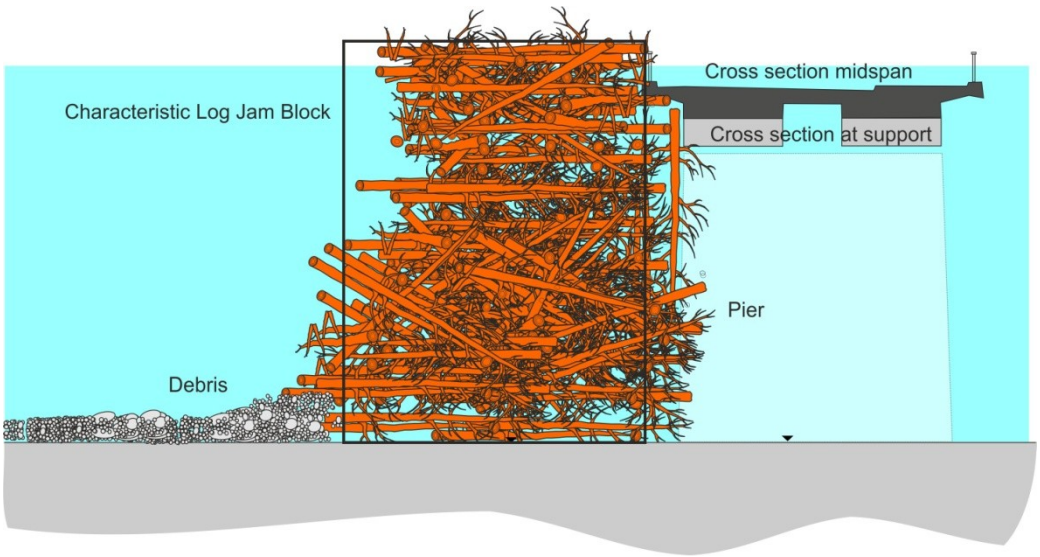

Fig. 8: Log jam model for the bridge

5 Results

In this paper we have presented a procedure to estimate the probability of a log jam at a bridge. Considering the development of deadwood in the catchment of the river, the properties of the deadwood in terms of number of trees, geometry of trees, the retention of the trees over the course of the river, the probability of log jam of an single tree at the bridge and then the probability of log jam causing a complete closure of the river cross section we received a conditional probability. This probability has to be multiplied by the probability of the related flood yielding the total probability.

This low value computed is not surprising since the bridge is not located at a torrent, but rather at a low gradient river. Therefore the flow velocity and deadwood content even in extreme floods is low.

Literature

[1] Proske, D. *Catalogue of risks*. Berlin, Heidelberg: Springer, 2008

[2] Lindner, J. „Beseitigung von Verklausungen“ Erfahrungen – Hochwassereinsatz, Bezirks-Feuerwehrkommando PERG. 2002. http://bfw.ac.at/ort1/Vortraege_als_pdf/verklausung/Lindner_Verklausung.pdf

[3] Amt der Tiroler Landesregierung, Landesbaudirektion, Abteilung Wasserwirtschaft: Fließgewässeratlas Tirol – Handbuch, Innsbruck, 2002

[4] Boes, R. Wasserbau, Konstruktionsbeispiele Wehr & Tosbecken, ETH Zürich, 2011

[5] Rickli,Chr. & Bucher, H. Einfluss ufernaher Bestockungen auf das Schwemmholzvorkommen in Wildbächen, WSL-Projektbericht vom 22.12.06 zuhanden des Bundesamtes für Umwelt BAFU, Sektion Schutzwald und Naturgefahren

[6] Hübl, J., Eisl, J., Hohl, D., Kogelnig, B., Mühlböck, F. Ereignisdokumentation und Ereignisanalyse Wölzerbach; IAN Report 143, Band 1: Ereignisdokumentation, Institut für Alpine Naturgefahren, Universität für Bodenkultur − Wien, 2011

[7] Landestalsperrenverwaltung des Freistaates, Talsperrenmeisterei Zwickauer Mulde/Weiße Elster: SachsenGefahrenkarten - Gefahr durch Überschwemmung im Bereich der Gemeinde: Schlema mit den Ortslagen Wildbach, Niederschlema; erstellt durch: Ingenieurgemeinschaft H.P.Gauff Ingenieure GmbH & Co. KG

[8] Sereinig, N., Schober, S. Gefahrenzonenausweisung Szenarien, Bundeswasserbauverwaltung vertreten durch das Amt der Kärntner Landesregierung, Abteilung 18 - Schutzwasserwirtschaft, Klagenfurt, Februar 2012

[9] Bundesamt für Energie, Sektion Talsperren: Sicherheit der Stauanlagen – Basisdokument zum Nachweis der Hochwassersicherheit. Juni 2008

[10] Interpraevent. Wildholz – Praxisleitfaden, Schriftenreihe 1, HB 2, Klagenfurt, 2011

[11] DVWK – Merkblatt „Flussdeiche“ (Heft 210/1986)/Lebensministerium.at: Freibord - Überströmstrecken. Leitfaden zur Festlegung des erforderlichen Freibordes anhand projektspezifischer Rahmenbedingungen einschließlich der Kriterien für die Anordnung von Überströmstrecken, FASSUNG 2006

[12] Lange, D., Bezzola, G. R. Schwemmholz - Probleme und Lösungsansätze, Versuchsanstalt für Wasserbau Hydrologie und Glaziologie der Eidgenössischen Technischen Hochschule Zürich, Mitteilungen 188, Zürich, 2006

[13] Hunzinger, L., Zarn, B., Bezzola, G. R. Beurteilung der Wirkung von Schutzmassnahmen gegen Naturgefahren als Grundlage für ihre Berücksichtigung in der Raumplanung, TEIL F: FLÜSSE, Nationale Plattform Naturgefahren PLANAT, 2008

[14] Rickenmann, D. Schwemmholz und Hochwasser. *Wasser, Energie, Luft* 89(5/6) (1997), p. 115–119

[15] Overney, O., Bezzola, R. G. Schwemmholz: Strategien und Perspektiven. in Minor, H.-E.: Neue Anforderungen an den Wasserbau, Versuchsanstalt für Wasserbau, Hydrologie und Glaziologie der Eidgenössischen Technischen Hochschule Zürich, Mitteilungen 207, Zürich, 2008

[16] Schmocker, L. & Hager, W. H. Drift accumulation at river bridges, River Flow 2010 - Dittrich, Koll, Aberle & Geisenhainer (eds) - © 2010 Bundesanstalt für Wasserbau

[17] Mazzorana, B. Woody Debris Recruitment Prediction Methods and Transport Analysis. *PhD Thesis*, Institute of Mountain Risk Engineering, University of Natural Resources and Applied Life Sciences, Vienna, 2009

[18] Waldner, P., Köchli, D., Usbeck, T., Schmocker, L., Sutter, F., Rickli, C., Rickenmann, D., Lange, D., Hilker, N., Wirsch, A., Siegrist, R., Hug, C., Kaennel, M. Schwemmholz des Hochwassers 2005, Schlussbericht des WSL-Teilprojekts Schwemmholz der Ereignisanalyse BAFU/WSL des Hochwassers 2005, WSL, Birmensdorf, 2005

[19] Zumsteg, M. Hochwassermanagement im Reusstal, Departement Bau, Verkehr und Umwelt des Kantons Aargau. 2007. http://www.ag.ch/alg/shared/dokumente/pdf/bremgarten_19.09.2007_zumsteg.pdf

[20] Hartlieb, A. Modellversuche zur Verklausung von Hochwasserentlastungsanlagen mit Schwemmholz. *WasserWirtschaft* 6 (2012), p. 15–19

[21] Moulin, B., Schenk, E. R., Hupp, C. R. Distribution and characterization of in-channel large wood in relation to geomorphic patterns on a low-gradient river. Earth Surf. Process. *Landforms* 36 (2011), p. 1137–1151

[22] Gantenbein, S. Verklausungsprozesse-Experimentelle Untersuchungen. Diplomarbeit, VAW-ETH Zürich, 2001

[23] Gems, B. Entwicklung eines integrativen Konzeptes zur Modellierung hochwasserrelevanter Prozesse und Bewertung der Wirkung von Hochwasserschutzmassnahmen in alpinen Talschaften. Forum Umwelttechnik und Wasserbau, Band 13, innsbruck university press, 2012

Probabilistic description of the *S–N* field of concrete using Weibull and Gumbel fatigue software

Constanze Przybilla[1], Stanislav Seitl[2], Zbyněk Keršner[3], Alfonso Fernández-Canteli[1]
[1]Dep. of Construction and Manufacturing Engineering, Faculty of Engineering, University of Oviedo, Campus de Gijón, 33203 Gijón
[2]Institute of Physics of Materials, Academy of Sciences of the Czech Republic, Brno
[3]Brno University of Technology, Faculty of Civil Engineering, Brno
przybillaconstanze@uniovi.es, seitl@ipm.cz, kersner.z@fce.vutbr.cz, afc@uniovi.es

Abstract: While the problem of deciding which statistical model is the "true one" in fatigue studies has occupied investigators for many years, only the analysis of the lower tail of the fatigue lifetime distribution, i.e. the distribution of minima values, is relevant for design purposes. Accordingly, in this work a probabilistic fatigue model for analysis of the S–N field is suggested after justification of Weibull or Gumbel domains of attraction, and the consequences of its extension to other cases are discussed. Finally, the *ProFatigue* software is applied for assessment of selected concrete fatigue data.

Keywords: Weibull and Gumbel distribution, probabilistic *S–N* field, software

1 Introduction

Four parameters can be considered as being significant in the analysis of the fatigue phenomenon, namely, crack size, driving force (as for instance, stress range, strain range, *J*-integral, etc.), fatigue lifetime (as the number of cycles to failure, see SURESH [11]) and probability of failure. In the different conventional fatigue approaches (stress based, strain based and fracture mechanics approach, characterized, respectively, by the *S–N* field, ε–*N* field and crack growth rate curve, as well as the Kitagawa–Takahashi (KT) diagram improved as El-Haddad equation) some of those determining parameters in fatigue are neglected or not explicitly considered. Thus, in the *S–N* field, usually, only driving force and number of cycles are considered implicitly as a mean or median value *S–N* curve, whereas only in the best case percentiles curves are also defined. The crack size is, therefore, out of consideration. The same holds for the ε–*N* field. In the crack growth curve, the driving force and crack size are pooled together as the stress intensity factor range, whereas the rate of the crack size with respect to the number of cycles forms the other variable. The same as in the crack growth curves, where driving force, crack size and number of cycles to failure are implied, no consideration of the probability of failure is made.

Finally, in the KT diagram, the endurance limit or, more precisely, the fatigue limit associated to a certain limit number of cycles, is given as a function of the crack size. Again, probabilistic considerations are missed.

This analysis presents two models including three of the four parameters mentioned before by a probabilistic description of the *S–N* field this being representative of the whole fatigue approaches. The application of the described process is shown on the *S–N* data for a material on cement base. The problematic of fatigue of cement based composites is now one of the most relevant areas of study, see LEE AND BARR [6], SEITL ET AL. [8, 9, 10] and PRYL ET AL. [7].

2 The probabilistic model

The Weibull regression model proposed by CASTILLO AND FERNÁNDEZ-CANTELI [3] is based on physical and statistical assumptions. In particular, the probability distributions present in the Wöhler field, i.e. the probability distribution $P_f(\Delta\sigma|N)$ of $\Delta\sigma$ for constant N and the probability distribution $P_f(N|\Delta\sigma)$ of N for constant values of stress must be compatible so that the values of the failure probability for every combination of $\Delta\sigma$ and N must be equal for $P_f(\Delta\sigma|N)$ and $P_f(N|\Delta\sigma)$. The model describes the Wöhler field in a probabilistic way by means of percentile curves, which are associated to different initial crack sizes, for the moment unknown, and computes the failure probability $P_f(N,\Delta\sigma)$ for a combination of stress range $\Delta\sigma$ and number of cycles N by

$$P_f(N,\Delta\sigma) = 1 - \exp\left[-\left(\frac{(\ln N - B)(\ln \Delta\sigma - C) - \lambda}{\delta}\right)^{\beta}\right], \tag{1}$$

where

B is a threshold value of lifetime,

$\exp(C)$ the endurance limit for $N \to \infty$,

λ, δ and β the location, scale and shape Weibull parameters.

Fig. 1 gives an example of the model depicting the *S–N* field on the left and the normalized variable on the right. A detailed description of the model can be found in CASTILLO AND FERNÁNDEZ-CANTELI [3].

The percentile curves are hyperbolas sharing the asymptotes $\ln N = B$ and $\ln \Delta\sigma = C$, whereas the zero percentile curve represents the minimum possible required number of cycles to achieve failure for different values of $\ln \Delta\sigma$. The probability of failure of an element subject to a stress range $\Delta\sigma$ during N cycles, depends only on the normalizing variable $V = (\ln N - B)\ (\ln \Delta\sigma - C)$, which allows the model parameters being estimated in a two-step method: firstly, B and C, then the other three parameters of the normalized Weibull distribution using a standard procedure. The statistical normalization proves to be a suitable procedure. As soon as B and C are known, the whole *S–N* field reduces to a unique statistical distribution opening interesting perspectives for the consideration of the

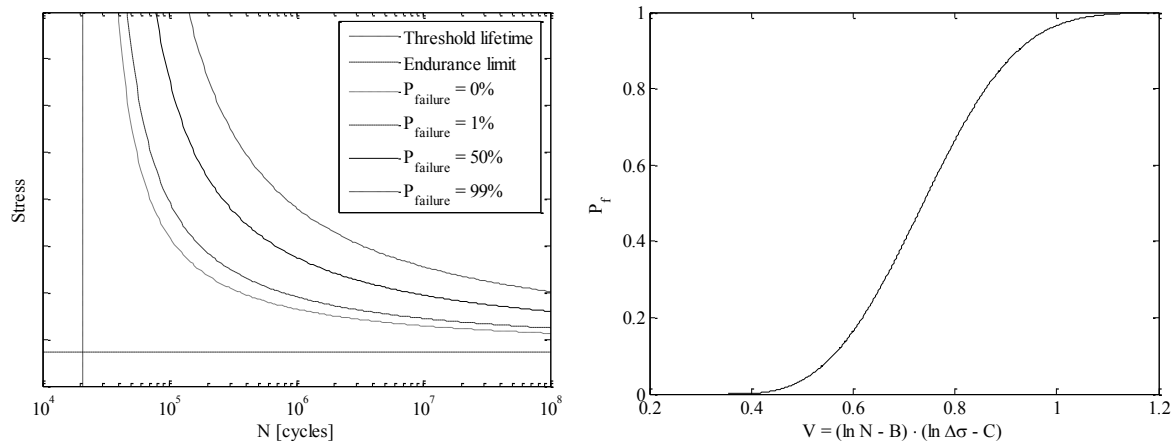

Fig. 1: *S–N* field and normalized variable *V*

damage accumulation by predicting lifetime under varying loading. Thus, the model parameters are estimated with higher reliability. Run-outs are considered in the parameter evaluation.

Once the five parameters are estimated, the analytical expression of the whole *S–N* field is known. This enables a probabilistic prediction of the fatigue failure under constant amplitude loading to be achieved.

Compared to conventional ones, the proposed model proves to provide higher reliability and capability to reproduce the whole Wöhler field as the up-and-down method or the Basquin model having been satisfactorily applied to a number of different materials and situations, including size effect, sensitivity analysis and extrapolation for very high number of cycles, as reported in previous works of the authors CASTILLO ET AL. [3, 4]. Besides, it provides knowledge that facilitates optimizing planning of testing programs by means of an adequate testing strategy. Its inability to reproduce adequately the low-cycle fatigue (LCF) region is a serious limitation of the model that is now being investigated (see FERNÁNDEZ-CANTELI ET AL. [5]).

If the lower bound of the results, represented by the location parameter in the Weibull model, can be relaxed a Gumbel model can be assumed as a limiting case of the Weibull model, which depends only on four parameters taking the form:

$$P_f(N,\Delta\sigma) = 1 - \exp\left[-\exp\left(\frac{(\ln N - B)(\ln \Delta\sigma - C) - \lambda}{\delta}\right)\right]. \tag{2}$$

This allows avoiding the always compromising task of assuming a lower bound associated to zero probability of failure. When the value of the Weibull shape parameter is greater than, say, 6, the assumption of the Gumbel model is fully justified based on the practical coincidence of the data evaluation for both probability distributions, at least up to fairly low probabilities of failure (CASTILLO [2]).

3 Experimental fatigue data of concrete

The data for analysis was taken from an experimental program that was done during the solution of the project of Czech Science Foundation P104/11/0833, see SEITL ET AL. [10] and PRYL ET AL [7]. This paper continues and develops the previous study of the co-authors SEITL ET AL. [8, 9]. For the present analysis the material labeled C210909 was selected and the controlled mix proportion is shown in Tab. 1. All specimens considered were tested in a standard laboratory environment at controlled values for temperature and relative humidity of 22 ± 2 °C and 50%, respectively. Three-point bending tests on concrete beams with a notch of depth a_n and width b_n were carried out. Beams 100 × 100 × 400 mm (see Fig. 2) were made from the C210909 concrete. Fatigue testing was conducted under load control (constant-amplitude cyclic loading tests). A stress ratio $R = \sigma_{max}/\sigma_{min} = 0.1$ was selected, where σ_{max} and σ_{min} refer to the maximum and minimum load during each cycle. In this way, the stresses generated are considered to be representative of beams under dead loads, and permanent contact is guaranteed at the supports. The load frequency used for all repeated-load tests was approximately 10 Hz. The respective fatigue lifetimes to failure were recorded.

Tab. 1: Composition of C210909 concrete mixture

Component	Dosage [kg/m^3]
Cement CEM I 42.5	770
Metakaolin Metaver I	32
PCC superplasticizer	8
Water	250
Sand 0/4 mm	1250
Fibres – 25 mm length	2.5

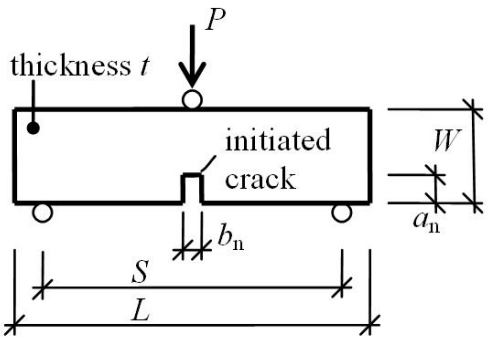

Fig. 2: Schematic of three-point bend (3PB) specimen geometry

4 Probabilistic evaluation of the fatigue data

The probabilistic fatigue model described in section 2 was applied to the experimental fatigue data of plain concrete The *ProFatigue* software, developed as collaboration between the University of Oviedo, University of Cantabria, both Spain, and the Swiss Federal Testing and research Laboratories, Empa-Dübendorf, Switzerland, was used in the assessment. *ProFatigue*, which is available without charge from the authors, estimates the model parameters fitting the experimental fatigue data, whereas run-outs, i.e. experiments being stopped before failure occurred, can be included into the analysis and their expected lifetime is estimated. Parameter estimates for the Weibull model are $B = 0.00$ (1 cycle), $C = 0.87$ (2.39 MPa), $\beta = 15.20$, $\delta = 5.18$ and $\lambda = 0.01$. The high value of the shape parameter β points out that the distribution function tends to be a Gumbel distribution. For the Gumbel model the parameter estimates are $B = 0.00$ (1 cycle), $C = 0.87$ (2.39 MPa), $\delta = 0.33$ and $\lambda = 5.21$, thus having the same values of B and C as the Weibull model. Whereas for the Weibull model the values exp(B) and exp(C) present a vertical asymptote

for lifetime and a horizontal asymptote for stress, respectively, for the Gumbel model the parameters B and C are only used to define the normalized variable V, but below $\exp(C)$ fracture could still occur, even though with a very low probability. Fig. 3 shows the experimental fatigue data and the S–N fields corresponding to each fatigue model by means of percentiles, representing failure probabilities of 0.01%, 5%, 50%, and 95%. The percentiles curves for the Weibull model are represented with continuous lines while the percentile curves for the Gumbel model are represented with dashed lines. As can be observed from Fig. 3 the two models are almost identical for failure probabilities between 5 and 95% whereas some difference is observable at $P_f = 1\%$ which becomes larger as such low failure probabilities as 0.01% are approached. In this "tail" region of low failure probabilities for the tested material the Gumbel distribution leads to a more conservative estimate, predicting lower lifetime at constant stresses than the Weibull model.

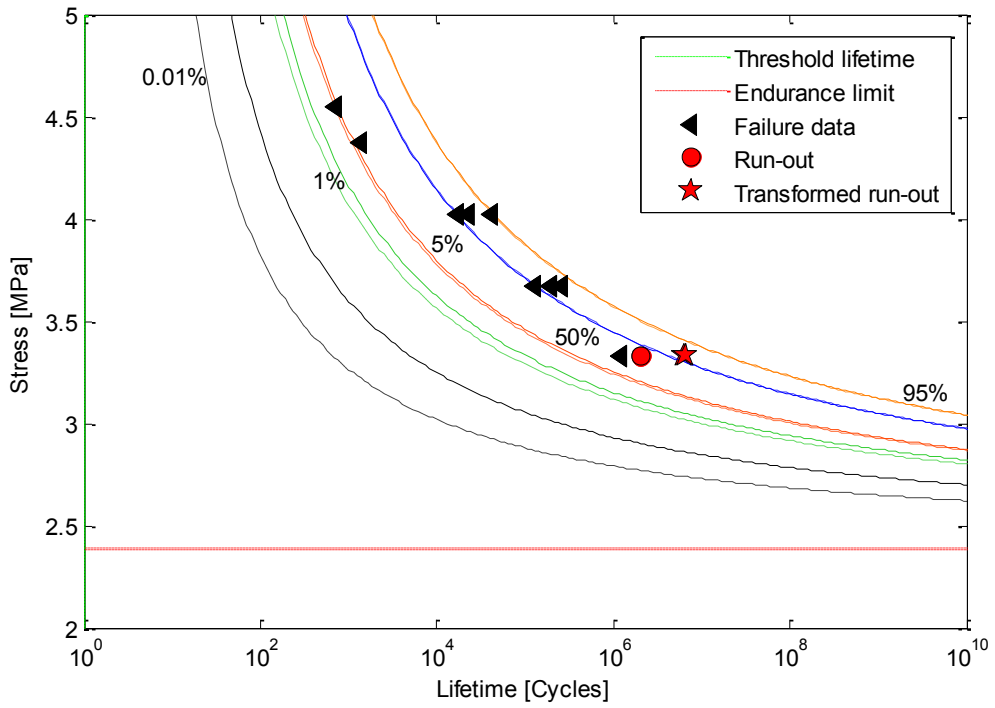

Fig. 3: S–N field for concrete represented by percentile curves (continuous lines: Weibull model; dashed lines: Gumbel model; x% indicate failure probability)

5 Discussion

In principle, the Weibull model, based on the weakest link assumption associated to a unique growing master crack (that interpreted as the weakest link, typical for metals) up to failure, should be put into question in the case of fatigue analysis of plain concrete. Instead, generalized microcracking as a spread damage extended over the whole specimen bulk must be considered for modelling. Accordingly, an alternative distribution, such as Normal or log-Normal ones, is more likely to represent the fatigue failure process, as being dependent of a high number of factors or simultaneous multiple growing cracks leading to failure. Nevertheless, the analysis of the limit behaviour of the lower tail of the distribution, being of interest for practical purposes, should follow under the assumption of a

Gumbel distribution, since the domain of attraction for minima for both, Normal and log-Normal distributions, is Gumbel (see Castillo [2]). The Weibull distribution could be a possible alternative as the domain of attraction for minima for other common distributions such as Exponential, Gamma, Pareto and Rayleigh, while the third alternative limit distribution, that of Fréchet, must be discarded due to its special boundary conditions. Incidentally, in the standard version both the Normal and log-Normal distributions are not able to reproduce the effect of scale so that an extended version should be considered (see [1]). Consequently, the S–N field was determined for the sample using first the Weibull model, then the Gumbel model for comparison of the results.

6 Conclusions

A Weibull and a Gumbel-type probabilistic fatigue model have been applied to experimental data of plain concrete using the *ProFatigue* software. The *S–N* fields, consisting of curves of constant failure probability, computed by both models fit the fatigue data well. While for low failure probabilities the predicted percentile curves by both models differ, they practically coincide for probabilities of failure over 5%. Thus, it has been demonstrated that those probabilistic models are suitable for the assessment of fatigue data of concrete. Furthermore these models, under assumptions of weakest-link principle and statistical independence, are able to consider the size effect, i.e. the influence of decreasing lifetime and decreasing scatter for larger specimens.

Acknowledgment

The work has been elaborated in support of grant project number M100411204, P104/11/0833 from the Czech Science Foundation and project number SV-PA-11-012 of the Dept. of Education and Sciences of the Asturian Regional Government.

Literature

[1] Castillo E. , Fernández Canteli A., Mora E., Ascorbe A. Length on the fatigue resistance of tendons in stayed cable bridges (in Spanish), *Anales de Ingeniería Mecánica*, 2:383–389, 1984.

[2] Castillo E. *Extreme Value Theory in Engineering*, Academic Press, 1988.

[3] Castillo, E., Fernández-Canteli, A., *A Unified Statistical Methodology for Modeling Fatigue Damage*, Springer, 2009.

[4] Fernández-Canteli, A. Castillo, E., López-Aenlle, M., Seitl, S. Using statistical compatibility to derive advanced probabilistic fatigue models, *Procedia Engineering*, 2 (2010), p. 1131–1140.

[5] Fernández-Canteli, A.; Przybilla, C.; Correia, J.; de Jesus, A. & Castillo, E. Extending the Applicability of Probabilistic S-N Models to the LCF Region Using Energetic Damage Parameters, *XVI International Colloquium "Mechanical Fatigue of Metals"* Brno, Czech Republic, September 24–26, 2012.

[6] Lee, M.K. & Barr, B.I.G. An overview of the fatigue behaviour of plain and fibre reinforced concrete. *Cement & Concrete Composites*, Vol. 26, (2004), p. 299–305.

[7] Pryl, D., Mikolášková, J., Pukl, R. Modeling Fatigue Damage of Concrete, *Key Engineering Materials*, (2014) Vols. 577–578, p. 385–388.

[8] Seitl, S., Bílek, V., Keršner, Z., Veselý, J. Cement based composites for thin building elements: Fracture and fatigue parameters, *Procedia Engineering*, Volume 2, Issue 1, (2010), p. 911–916.

[9] Seitl, S., Keršner, Z., Bílek, V., Knésl, Z. Fatigue parameters of cement-based composites with various types of fiber, *Key Engineering Materials*, Vols. 417-418, (2010), p. 129–132.

[10] Seitl, S., Šimonová, H., Keršner, Z., Fernández-Canteli, A. Evaluation of concrete fatigue measurement using standard and non-linear regression model, *Applied Mechanics and Materials*, Vols. 121–126, (2012), p. 2726–2729.

[11] Suresh, S. *Fatigue of materials*. Cambridge University Press, Cambridge, 1998.

The new method in acceptance of lower quality concrete based on the Dempster-Shafer theory

Izabela Skrzypczak
Department of Geodesy and Geotechnics, Rzeszow University of Technology, Poland
izas@prz.edu.pl

Abstract: The uncertainties in acceptance of lower quality concrete influencing the risk of contractors are complex and difficult. As a mathematical instrument, the Dempster-Shafer theory gives a great advantage in the expression and combination of these uncertainties. In paper an innovative method for evaluation of lower quality concrete, based on the Dempster-Shafer theory, has been proposed in order to improve the accuracy of risk determination. In case of the quality control of concrete this application allows to link information data concerning both contracting parties. And so the D-S theory enables to take the rational decision including business of both − the producer and the client, when e.g. a batch of concrete was produced about a bad quality. The result shows that the quality assessment method based on the Dempster-Shafer theory is feasible, effective and the most reasonable.

Keywords: concrete, quality, Dempster-Shafer theory, risk

1 Introduction

Statistical conformity criteria, applied in compliance control of concrete, are of the following type:

- in case of continuous production of concrete for sample size $n \geq 15$:

$$\overline{x} \geq f_{ck} + 1.48 S_n \,,\; x_{\min} \geq f_{ck} - 4 \text{ MPa} \tag{1}$$

- in case of initial production for $n = 3$:

$$\overline{x} \geq f_{ck} + 4 \text{ MPa} \,,\; x_{\min} \geq f_{ck} - 4 \text{ MPa} \tag{2}$$

These criteria are recommended in PN-EN-206 [1]. Compliance criteria should fulfil three major requirements [2, 6, 7, 8]:

- bigger sample size n should correspond with lower probability of acceptance of bad quality lot and higher probability of acceptance of good quality lot;
- among lots of good quality the conformity criteria should privilege those with lower variability;

- the probability of acceptance of bad quality lot should not be higher than a predefined value;
- the requirement of minimum values is critical only for very high values of standard deviation and they may lead to production with too high values of the client risk.

Risk in conformity control of concrete should be balanced between two sides involved: the producer and the client. Hence, the usefulness of statistical criteria for small sample size is questioned. In order to solve this problem, evidence theory of Dempster-Shafer is applied to realize the information fusion of parameters in conformity control of concrete.

2 Basic assumptions of Dempster-Shafer (D-S) theory

In the D-S theory, the set of all possible outcomes in a random experiments is called the frame of discernment (FOD), usually denoted by θ. The 2^{θ} subsets of θ are called propositions and probability masses are assigned to propositions, i.e., to subsets of θ. The interpretation given to the probability mass assigned to a subset of θ is that the mass is free to move to any element of the subset. Under this interpretation, the probability mass assigned to θ represents ignorance, since this mass may move to any element of the entire FOD. When a source of evidence assigns probability masses to the propositions represented by subsets of θ, the resulting function is called a basic probability assignment (bpa). Formally, a bpa is function m: $2^{\theta} \rightarrow [0,1]$, where:

$$m(\theta) = 0; \qquad \sum_{A \in 2^{\theta}} m(A) = 1 \tag{3}$$

Subsets of θ that are assigned non zero probability mass are said to be focal elements of m. The core of m is the union of its focal elements. A belief function, *Bel(A)*, over θ is defined by:

$$Bel(A) = \sum_{B \subseteq A} m(B) \quad A, B \in 2^{\theta} \tag{4}$$

Assuming that belief function $Bel(A)_1$, $Bel(A)_2, \ldots, Bel(A)_n$ are assigned to independent sources of evidence in same frame of discernment (i.e., 2^{θ}), and the relevant basic probability assignment is $m_1, m_2, ., m_n$, then according to Dempster's rule of combination, the new belief function $Bel(A)$ and basic probability assignment $m(A)$ may be yielded via:

$$Bel(A) = \left(((Bel_1 \oplus Bel_2) \oplus Bel_3) \oplus ...\right) \oplus Bel_n \tag{5}$$

$$m^k(A) = \frac{\sum_{A_i \cap B_j = C} m^{k-1}(A_i) m_k(B_j)}{1 - \sum_{A_i \cap B_j = \Phi} m^{k-1}(A_i) m_k(B_j)} \tag{6}$$

The formula is commonly called Dempster's orthogonal sum. Here, we use the notation $\oplus$ to represent the combination.

If there is a pose/identity hypothesis, assume that the hypotheses A supporting by each source is respectively $m_1(A)$, $m_2(A)$,..., $m_n(A)$, and the hypotheses A refusing by the each source is respectively $m_1(\theta)$, $m_2(\theta)$,..., $m_n(\theta)$, where [9]:

$$\begin{aligned} m_1(\theta) &= 1 - m_1(A), \\ m_2(\theta) &= 1 - m_2(A), \\ &\ldots\ldots\ldots\ldots\ldots\ldots\ldots \\ m_n(\theta) &= 1 - m_n(A), \end{aligned} \tag{7}$$

We have combination rule:

$$m^k(A) = \frac{\sum_{A_i \cap B_j = C} m^{k-1}(A_i) m_k(B_j)}{1 - \sum_{A_i \cap B_j = \Phi} m^{k-1}(A_i) m_k(B_j)} = \tag{8}$$

$$= \frac{1}{1-\theta}\left[m^{k-1}(A) m_k(A) + m^{k-1}(A) m_k(\theta) + m^{k-1}(\theta) m_k(\theta) \right] = \tag{9}$$

$$= m^{k-1}(A) + m^{k-1}(\theta) m_k(A) = \tag{10}$$

$$= 1 - \prod_{i=1}^{k-1} m_i(\theta) + \left[1 - m_k(\theta)\right] \prod_{i=1}^{k-1} m_i(\theta) = \tag{11}$$

$$= 1 - \prod_{i=1}^{k} m_i(\theta) \tag{12}$$

More about the Dempster-Shafer theory can be found in [3, 4, 5].

According to the results from the acceptance of bad quality of concrete, the probability of a bad quality concrete are summarized. Probability assignment with the Dempster-Shafer is given out with use of the experience and opinions of some experts, representing all contractors' interests. This value determines the probability for the both − a producer and a client. The calculation of combination rule of producers risk and clients risk is also advanced with using the D-S method. The analysis and calculations show that principle of data fusion is very useful for information process in concretes production.

2.1 Examples

Example 1

Bad quality concrete lot was found during the quality control of a ready-mix concrete plant. Two sides − the producer and the client − are interested and they have identified probabilities particular actions:

The frame of discernment is defined as follows: Θ = {Repeated control, Reduction in price, Rejection of a lot, Repair or strengthening, Catastrophic event}.

Tab. 1: The probabilities for particular decision specified by the producer and the client

States	Producer $p_i(P)$	Client $p_i(C)$
1 − Repeated control	0.74	0.00
2 − Reduction in price	0.20	0.95
3 − Rejection of a lot	0.05	0.00
4 − Repair or strengthening	0.00	0.0495
5 − Catastrophic event	0.00	0.0001

The first step in the calculation is the data combination. Multiplication of probability values of all possible events are presented in Tab. 2.

Tab. 2: Partial results – data combination

Producer / **Client**		$p_1(P)$	$p_2(P)$	$p_3(P)$	$p_4(P)$	$p_5(P)$	$p(\theta)$
		0.75	0.20	0.035	0.00	0.01	0.005
$p_1(C)$	0.00	0	0	0	0	0	0
$p_2(C)$	0.95	0.7125	0.19	0.03325	0	0.0095	0.00475
$p_3(C)$	0.00	0	0	0	0	0	0
$p_4(C)$	0.0495	0.037125	0.0099	0.0017325	0	0.000495	0.0002475
$p_5(C)$	0.0001	0.000075	0.00002	0.0000035	0	0.000001	0.0000005
$p(\theta)$	0.0004	0.0003	0.00008	0.000014	0	0.000004	0.000002

In accordance with the denominator of the Eq. (8), degree of conflict and normalization factor has been calculated:

$$K = 0.805 \qquad \text{and} \qquad 1 - K = 1 - 0.805 = 0.195$$

Tab. 3 contains the new values of probability for particular decisions, obtained with help of the Dempster combination rule, having regard to the both stakeholders (knowledge derived from the client and the producer).The table also contains the final results of the calculated values of belief function (9) and plausibility function (13) for possible events.

Tab. 3: Final results − belief function and plausibility function

Producer/Client	$m_i(P\_C)$	$Bel(P\_C)$	$Pl(P\_C)$	$U_i(P\_C)$
Repeated control – m_1	0.0015	0.0015	0.00151	[0.0015; 0.00151]
Reduction in price – m_2	0.9971	0.9971	0.99711	[0.9971; 0.99711]
Rejection of a lot – m_3	0.00007	0.00007	0.00008	[0.00007; 0.00008]
Repair or strengthening – m_4	0.0013	0.0013	0.00131	[0.0013; 0.00131]
Catastrophic event – m_5	0.00005	0.00005	0.00006	[0.00005; 0.00006]
Θ	0.00001	1.0000	1.000	[1.000; 1.000]
	$\sum = 1.000$			

The upper bound of plausibility is defined as the summation of basic probability assignment of the sets of the particular decision. The plausibility function can be related to belief function trough a function called doubt, which is defined as the compliment of belief

$$Pl(P\_C) = 1 - Bel(\neg(P\_C)) \tag{13}$$

$$Pl(P\_C) = 1 - doubt(P\_C) \tag{14}$$

The belief interval (U_i) represents a range in which true probability may lie. It can be determined by subtracting belief from plausibility. The narrow uncertainty band represents more precise probabilities. If $U_i(P\_C)$ has an interval [0, 1], it means that no information is available, but if the interval is [1, 1], it means that (P_C) has been completely confirmed by $m_i(P\_C)$.

Using the Dempster-Shafer theory at decision making, when verified batch of concrete is of bad quality, the price reduction is the best solution that takes into account the interests of the producer as well as the client.

Although the producer has identified probability for price reduction as 0.20, and the client as 0.85, this decision on the price reduction is the most certain. The truth of this hypothesis is represented by the interval [0.9971; 0.99711].

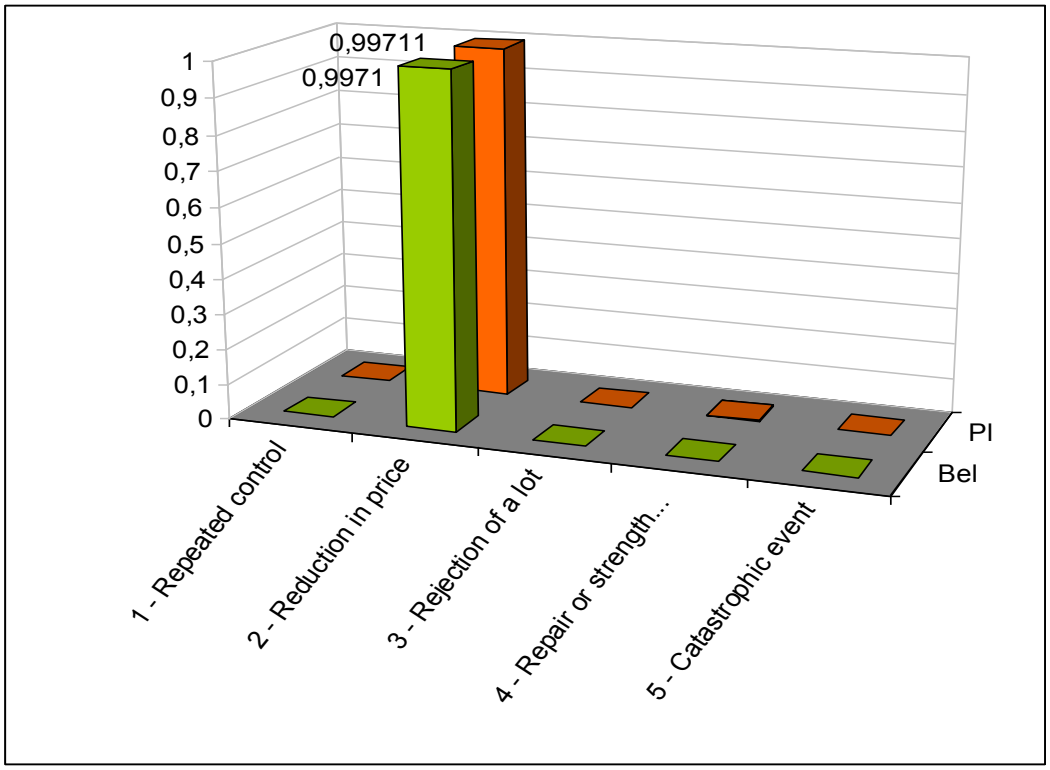

Fig. 1: The belief function and the plausibility function of particular decisions

In the case of growing number of conditions related with the possible decisions, the difference between *Pl* and *Bel* for a verified hypothesis will decrease.

Example 2

Risk of producer and client of a preferred decision (using the combination rules):

This example refers to application of belief functions to determine the probability for the producer and the client in case of acceptance of bad quality concrete lot. These values are calculated according to the formula (12) with use of the combination rules.

Tab. 4: The probabilities defined for the producer and the client in case of acceptance of bad quality lot

Producer $p_i(P)$	Client $p_i(C)$
1 – Repeated control – 0.75	----------
2 – Reduction in price – 0.20	2 – Reduction in price – 0.95
3 – Rejection of a lot – 0.05	----------
	4 – Repair or strengthening – 0.499
	5 – Catastrophic event – 0.0001

Calculation of belief functions for the producer with the formula (12):

$$m_P(1) = 0.75 \qquad m_P^1(\theta) = 0.25$$

$$m_P(2) = 0.20 \qquad m_P^2(\theta) = 0.80$$

$$m_P(3) = 0.05 \qquad m_P^3(\theta) = 0.95$$

$$m_P = 1 - \{ m_P^1(\theta) \times m_P^2(\theta) \times m_P^3(\theta)\}$$

$$m_P = 1 - \{0.25 \times 0.80 \times 0.95\} = 0.81 = Bel(P)$$

Calculation of belief functions for the client with the formula (12):

$$m_C(2) = 0.95 \qquad m_C^2(\theta) = 0.05$$

$$m_C(4) = 0.0499 \qquad m_C^4(\theta) = 0.9501$$

$$m_C(5) = 0.0001 \qquad m_C^5(\theta) = 0.9999$$

$$m_2 = 1 - \{m_C^2(\theta) \times m_C^4(\theta) \times m_C^5(\theta)\}$$

$$m_C = 1 - \{0.05 \times 0.9501 \times 0.9999\} = 0.9525 = Bel(C)$$

In practice, an equal risk of client and producer are usually assumed 0.5 = 0.5 and probabilities of rejection and acceptance are usually assumed $\alpha = \beta = 0.05$. The risk balance index calculated using Eq. (12) is equal 0.9525, and significantly bigger risk is transferred to the client in comparison with a risk transferred to the producer 0.810.

In order to estimate the risk of the producer and the recipient the next step is to transform these values. Sum of them [3] must give value 1.000:

$$R_P = \frac{0.810}{0.810 + 0.9525} = 0.460$$

$$R_C = \frac{0.9525}{0.810 + 0.9525} = 0.540$$

$$R_P + R_C = 0.460 + 0.540 = 1.000$$

If a lot of bad quality concrete is accepted, the estimated risk identified with the probability of the client will be greater than the producer one (Fig. 2).

Obtained effects confirm the results presented in [2, 6, 7].

The general concept of statistical conformity criteria consistent with the semi probabilistic design method can have prejudicial effects to both sides involved in conformity control process, i.e. the producer and client.

From the foregoing analysis it is followed that in the case of conformity control all major types of adverse states (Repeated control, Reduction in price, Rejection of a lot, Repair or strengthening, Catastrophic event, etc.), with the corresponding probabilities of occurrence and consequence should be identified and considered in risk analysis.

A risk balance which expresses how the risk is divided into two sides involved is defined. A risk partition into the producer and the client may be a matter of the trade contract. The risk balance index is 0.5 (a risk is transferred fifty-fifty to both sides, the producer and the client).

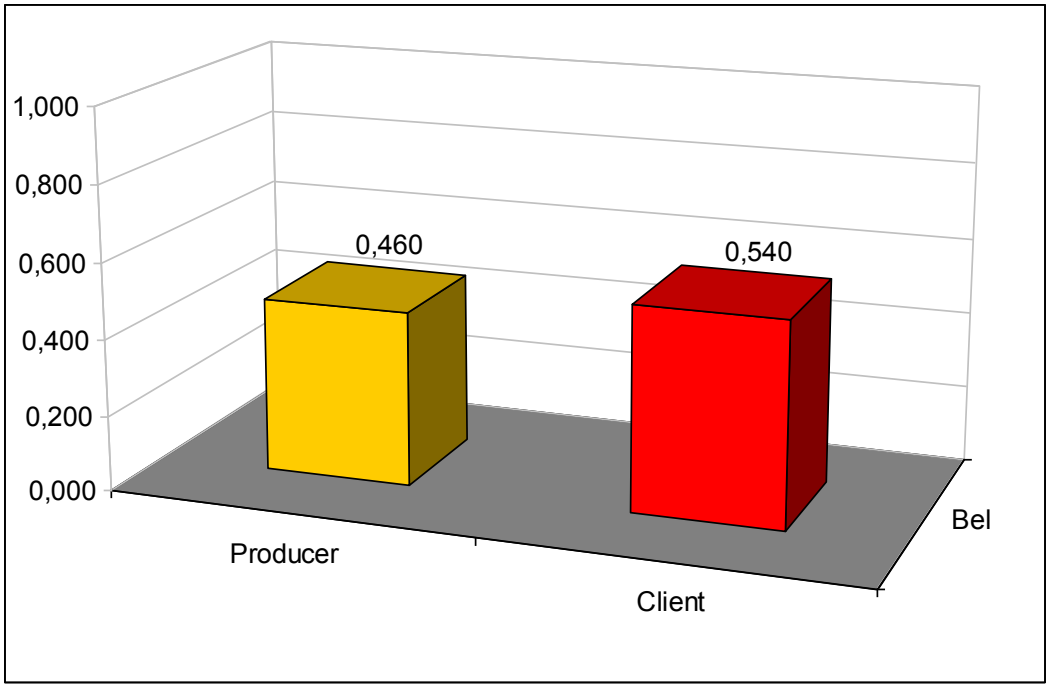

Fig. 2: The risk of producer and client

3 Results

The Dempster-Shafer theory can be very helpful at making a decision where one should take into account the knowledge coming from different sources.

This method enables to link the information from different sources, as well as can serve as the tool for the incomplete presentation of statistical knowledge. In case of the quality control of concrete this application allows to link information data concerning both contracting parties. And so the D-S theory enables to take the rational decision including business of both the producer and the client, when e.g. a batch of concrete was produced about the bad quality. Analyses conducted with the Dempster-Shafer method and fuzzy logic confirm that considerably the greater risk is standing on the side of the client in case of accepting a

lot about the lowered quality of 0.540. However, the risk suffered by the producer is relatively smaller 0.460.

Using the Dempster-Shafer theory at making a decision, when the verified quality of concrete is bad, reduced price is the best decision including business of both − the producer and the recipient. The truth of this hypothesis is represented by the period [0.9971; 0.99711].

4 Conclusions

The Dempster-Shafer theory, based on belief function and plausibility function of the bad quality concretes, determined according to data fusion technique experiments has been given to acceptance process. In practice the statistical methods of the concrete quality control are commonly applied. They take into account balancing of the risk of the producer and the client. Connecting the information, taking into account interests of the producer and the client can be useful at making a decision in case of the receipt of concrete of the bad quality. Application of the Dempster-Shafer theory in the acceptance of concrete enables to describe the risk of the producer and the client. He also enables to take the right decision at the acceptance of concrete of bad quality built by belief functions on the basis of the frame of discernment.

In order to solve the problem of acceptance of bad quality of concrete, evidence theory of Dampster-Shafer is applied to realize the information fusion of parameter in conformity control of concrete. According to the results from the acceptance of bad quality of concrete, the probability of a bad quality concrete are summarized. The weights of probabilities of producer and client are determined in more advanced way by using D-S method. The analysis and calculations show that principle of data fusion is useful for information process in concrete production.

Literature

[1] PN-EN 206-1: 2003, *Polish Standard, Concrete – Part 1: Specification, performance, production and conformity*, [in Polish]. PKN, Warszawa 2003

[2] Catarino, J.MR. *Statistical criteria for acceptance of materials performance of concrete standards ENV206*: *1993 and pr EN 206:1997*. 12th ERMCO Congress. Proceedings, Vol.1, Lisbon, June 1998

[3] Kłopotek, M.A. *Metody identyfikacji I interpretacje struktur rozkładów przekonań w teorii Demstera-Shafera*. Instytut Podstaw Informatyki PAN, W-wa 1998

[4] Kokos, D., Challa, S. *An Introduction to Bayesian and Dempster-Shafer Data Fusion*. Australian Government Department of Defence, DSTO-TR-1436, 2005

[5] Lentz, K., Ferson, S. *Combination of Evidence in Dempster-Shafer Theory*. SAND 2002-0835, April 2002

[6] Wolinski, S. Conformity control of concrete strength based on the risk assessment. *Zeszyty Naukowe Politechniki Rzeszowskiej* 53 (2009), p. 163–169

[7] Wolinski, S. *Statystyczne i rozmyte kryteria zgodności wytrzymałości betonu na ściskanie*. Problemy naukowo-badawcze konstrukcji z betonu, Monografia 247, Kraków: Politechnika Krakowska, 1999, p. 51–57

[8] Taerwe, L. Evaluation of compound compliance criteria for concrete strength. *RILEM, Materials and Structures* 21 (1988), p. 13–20

[9] Yan, X.P., Xie, Y.B., Xiao, H.L. *Application of Dempster-Shafer theory to oil monitoring*. http://www.plant-maintenance.com/articles/Dempster-Shafer.shtml

The statistical analysis of design methods efficiency in determining shear capacity of reinforced concrete beams

Marta Słowik, Magdalena Rogalska
Faculty of Civil Engineering and Architecture, Lublin University of Technology, Lublin, Poland
m.slowik@pollub.pl, m.rogalska@o2.pl

Abstract: The paper deals with shear capacity of concrete beams reinforced longitudinally but without transverse reinforcement. The objective of the paper is to analyze the efficiency of design methods proposed in different codes. In particular, three models are considered: the ACI 318 shear design model, the equation by Eurocode 2 and the new design procedure from Model Code 2010. The relationships between design shear resistance obtained from these three codes and compressive strength of concrete are compared with experimental results. On the basis of this comparison the conclusions are drawn according to the fit between the design methods and the test data.

Keywords: reinforced concrete beams, shear capacity, concrete strength, statistical analysis, standard code, efficiency of design methods

1 Introduction

Different models are used to describe shear failure and different methods are provided in codes to determine shear capacity of reinforced concrete members. The dimensioning rules from AMERICAN CONCRETE INSTITUTE DESIGN CODE ACI 318 [1], EUROPEAN STANDARD EUROCODE 2 [4], and INTERNATIONAL FEDERATION FOR STRUCTURAL CONCRETE *FIB* MODEL CODE 2010 [9] according to design shear resistance of longitudinally reinforced concrete beams without shear reinforcement are presented in the paper.

Since the shear failure mechanism of concrete beams depends on many parameters, it is not easy to accurately evaluate the shear resistance of beams. As a result, the rules for estimating the shear capacity of flexural concrete members with longitudinal reinforcement and without transverse reinforcement given in design codes differ significantly.

The tensile strength of concrete is the main parameter which influences the shear capacity of concrete beams. Other parameters which also influence shear resistance are the ratio of longitudinal reinforcement, the shear span-to-depth ratio, $a/d = M_u/(V_u d)$, and the size of a member. As the concrete tensile strength is of paramount importance it is included in shear design models. Most codes, however, evaluate shear capacity while assuming an empirical

tensile-compressive relationship. For example, in Eurocode 2 the tensile strength f_{ct} is proportional to $\sqrt[3]{f_c}$ (f_c – compressive concrete strength), in ACI 318 the tensile strength is expressed as $f_{ct} = 0.556\sqrt{f_c}$, whereas NEVILLE [10] suggested the following rule for splitting tensile strength $f_{ct} = 0.3\sqrt[3]{f_c^2}$.

In order to analyze the efficiency of design methods for shear capacity, a statistical analysis was performed. In this analysis the results of calculated shear resistance of the member without shear reinforcement were compared with the test data.

2 Shear design methods

2.1 Eurocode 2

In the EUROPEAN STANDARD EN 1992-1-1:2004 [4], which is the basic code for designing concrete structures in Poland and several European countries, the design method for shear was developed from the truss model.

The design value for the shear resistance in members not requiring design shear reinforcement is given by:

$$V_c = \left[C_{Rd,c} k \left(100 \rho_l f_c\right)^{\frac{1}{3}} + 0.15\sigma_{cp} \right] b_w d \geq \left(v_{\min} + 0.15\sigma_{cp}\right) b_w d \tag{1}$$

where:

f_c – compressive strength of concrete in MPa,

b_w – smallest width of the cross section in the tension area in mm,

d – effective depth of the cross section in mm,

ρ_l – ratio of tensile reinforcement $\rho_l \geq 0.02$,

$k = 1 + \sqrt{\dfrac{200}{d}} \leq 2$,

$\sigma_{cp} = \dfrac{N_{Ed}}{A_c} \leq 0{,}2 f_{cd}$ – stress caused by axial force in MPa,

$v_{\min} = 0.035 k^{\frac{3}{2}} f_{ck}^{\frac{1}{2}}$,

$C_{Rd,c} = 0.18 / \gamma_c$,

γ_c – safety coefficient for concrete.

2.2 ACI 318

The equations provided in ACI 318 [1] were developed in the middle of 20th century on the basis of several experiments obtained for example by KANI [8, 9].

According to ACI 318, shear resistance attributed to the concrete can be calculated from the Eq. (2):

$$V_c = \left(0.16\sqrt{f_c} + 17\rho \frac{V_u d}{M_u} \right) b_w d \;\le\; 0.29\sqrt{f_c} b_w d \tag{2}$$

where:

V_c in N,

f_c – compressive strength of concrete in MPa,

ρ – ratio of longitudinal reinforcement ($A_s/b_w d$),

V_u – shear force in cross section considered in N,

M_u – bending moment in cross section considered in Nmm,

d – effective depth of cross section in mm,

b_w – width of cross section in mm.

2.3 Model Code 2010

In *FIB* MODEL CODE 2010 [9] a new approach for calculating the shear resistance attributed to concrete of reinforced concrete beams without shear reinforcement is proposed. To design a member in a complex loading state or to asses a structure more elaborately, a level III approximation should be used. The equations of the Level III were derived from the Modified Compression Field Theory (MCFT). This theory was proposed by VECCHIO AND COLLINS [15,16].

The design shear resistance of longitudinally reinforced concrete beams without shear reinforcement can be taken as:

$$V_c = k_v \frac{\sqrt{f_c}}{\gamma_c} z b_w \tag{3}$$

where: f_c – compressive strength of concrete in MPa,

γ_c – safety coefficient for concrete,

z – the effective shear depth.

The value of $\sqrt{f_c}$ shall not be taken as greater than 8 MPa.

The Eq. (3) can be used with:

$$k_v = \frac{0.4}{(1+1500\varepsilon_x)} \cdot \frac{1300}{(1000+0.7k_{dg}z)} \tag{4}$$

$$\varepsilon_x = \frac{M_{Ed}/z + V_{Ed} + 0.5N_{Ed} - A_p f_{po}}{2(E_s A_s + E_p A_p)} \tag{5}$$

where: z in mm,

E_s, A_s − elastic modulus and cross section of reinforcing bars,

E_p, A_p − elastic modulus and cross section of presstresing tendons,

$k_{dg} = \frac{48}{16+d_g} \geq 1.15$

d_g − aggregate diameter in mm.

The variable ε_x represents the average longitudinal strain at the mid-depth of the member.

3 Experimental data

For statistical analysis of the efficiency of design methods, the design shear capacity was confronted with experimental results. The analysis was carried out for members made of normal strength concrete of compressive strength from 10 to 40 MPa. The comparison was based on the database of two different experiments: the test performed by DESAI [3] and some tests from the experimental investigation performed by PERERA AND MUTSUYOSHI [11]. The test data were chosen in such a way that the only changing parameter was the properties of concrete, while other parameters were the same or similar. All beams had the same cross section 0.2 × 0.3 m. All beams were tested in three point bending test and the shear span-to-depth ratio was 3.6. The beams had longitudinal steel bars of typical reinforcement ratio 1.8 % in Desai test and 3.0 % in Perera and Mutsuyoshi test. In both experiment the aggregate size did not exceed 20 mm.

In the experiments different concrete mixtures were used: typical portland cement concrete PC1 from Desai test and PC2 from Perera and Mutsuyoshi test; portland cement concrete with limestone filer PL; portland cement concrete with pulverized fuel ash PF; portland cement concrete with ground granulated blast furnace slag PG.

All considered beams failed suddenly in shear soon after the appearance of diagonal cracks. The character of failure confirmed that the shear failure was due to principle tensile stress. The obtained test results according to concrete strength are presented in Fig. 1.

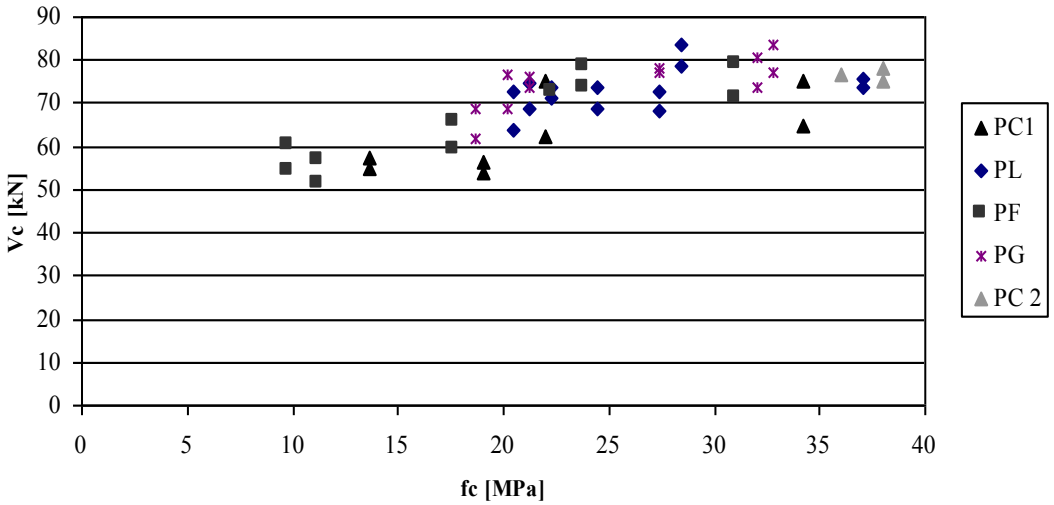

Fig. 1: Shear capacity versus concrete compressive strength

4 Statistical analysis

The statistical analysis was carried out in two steps: the prediction of dependent variable v_u and the comparison of the obtained regression equation with the design formulas. The StatSoft's Statistica programme was used for prognostic calculations. Two methods were used: the Multiple Regression MR [9, 14] and the Generalized Additive Models GAM [5]. The partial autocorrelation function and the autocorrelation function of the residual number [2] of different models were used in statistical analysis.

4.1 Prediction for dependent variable v_u

4.1.1 Data analysis

Data analysis was performed to study the distribution character of the following variables: compressive concrete strength, f_c,, ultimate shear stress from test, $v_u = V_c/b_w d$, calculated shear stress on the basis of ACI 318, v_u^{ACI}, calculated shear stress on the basis of Eurocode 2, v_u^{EC2}, calculated shear stress on the basis of Model Code 2010, v_u^{MC}.

The Shapiro-Wilk normality test was applied to the analysis [13]. On the basis of summary statistics performed for every variable, the coefficient W was determined and then compared to critical value $W_{critical} = 0.945$ (for number of observation $N = 45$ and level of confidence $\alpha = 0.05$). It appeared that two variables v_u ($W = 0.939 < W_{critical} = 0.945$) and v_u^{MC} ($W = 0.938 < W_{critical} = 0.945$) did not have a normal distribution. It was concluded that the multiple regression method could not be successfully used. It was necessary to apply a more advanced method.

4.1.2 Regression analysis

During the regression analysis, the ultimate shear stress v_u was the dependent variable and the concrete compressive strength f_c, as the independent variable, was taken in the form of

different functions: f_c, $\sqrt{f_c}$, $\sqrt[3]{f_c}$, $\ln(f_c)$, $1/f_c$, f_c^2, f_c^3, f_c^4, f_c^5, f_c^6, f_c^7, f_c^8, f_c^9, f_c^{10}. Looking for the best fit between the regression function and the test data v_u, the Multiple Regression Method and the Generalized Additive Method were used. A mean absolute percentage error MAPE was calculated from the formula (6):

$$MAPE = \frac{1}{T-n} \sum_{i=T-n}^{T} \frac{\left|Y_i - Y_{ip}\right|}{Y_i} \tag{6}$$

where:

T –calculation and forecast periods total number,

n – forecast periods number,

Y_i – the actual value of the variable in the period i,

Y_{ip} – the predicted value of the variable in the period i.

First, the Multiple Regression Method MR1 was applied. In this method the dependent variable v_u was analyzed and the independent variable of compression strength was taken as the function $\sqrt[3]{f_c}$ and then $\sqrt{f_c}$. These functions were chosen because the design shear strength in considered codes depends on them. The obtained results are presented below as: regression equation coefficients (Tabs. 1 and 2), regression equation (Eqs. 7 and 8), line plot of variables v_u and applied models (Figs. 2 and 3), partial autocorrelation function and autocorrelation function of the residual number (Figs. 4 and 5), the mean absolute percentage error.

Tab. 1: Regression summary for dependent variable: v_u ($\sqrt[3]{f_c}$)

$N = 45$	Regression Summary for Dependent Variable: v_u $R = 0.99914664$, $R^2 = 0.99829401$, Adjusted $R^2 = 0.99825433$ F(1.43) = 25162, $p < 0.0000$ Std. Error of estimate: 0.00663					
	b*	Std. Err. of b*	b	Std. Err. of b	t(43)	p-value
Intercept			−2.50783	0.024120	−103.974	0.00000
$\sqrt[3]{f_c}$	0.999147	0.006299	3.49515	0.022034	158.626	0.00000

Tab. 2: Regression summary for dependent variable: v_u ($\sqrt{f_c}$)

$N = 45$	Regression Summary for Dependent Variable: v_u $R = 0.74561578$, $R^2 = 0.55594289$, Adjusted $R^2 = 0.54561598$ F(1.43) = 53.834, $p < 0.00000$ Std. Error of estimate: 0.10700					
	b*	Std. Err. of b*	b	Std. Err. of b	t(43)	p
Intercept			0.573762	0.102275	5.609997	0.000001
$\sqrt{f_c}$	0.745616	0.101621	0.155049	0.021132	7.337192	0.000000

$$\mathrm{MR1}(v_u; \sqrt[3]{f_c}) = -2.50783 + 3.49515 \sqrt[3]{f_c} \tag{7}$$

$$\mathrm{MR2}(v_u; \sqrt{f_c}) = 0.573762 + 0.155049 \sqrt{f_c} \tag{8}$$

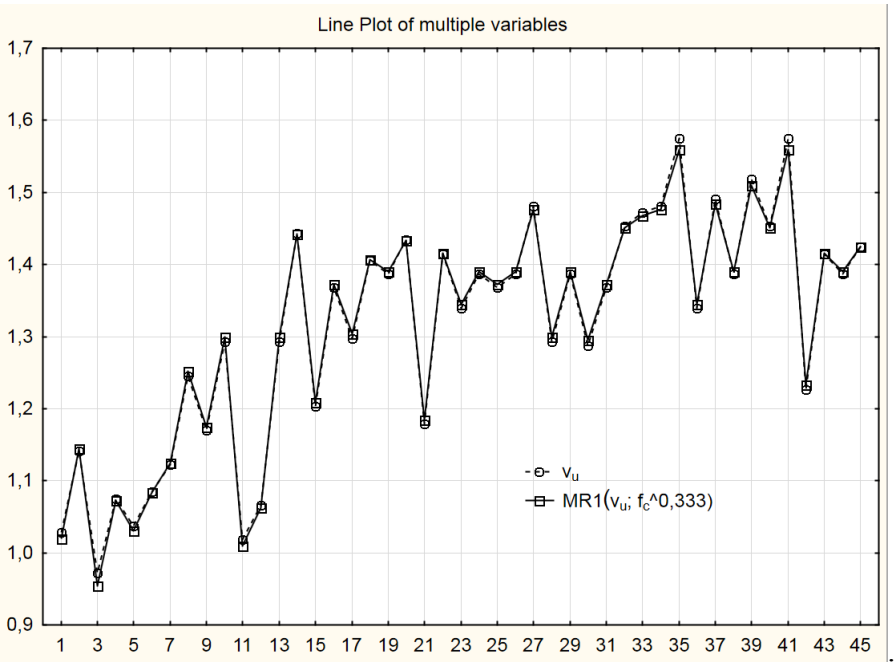

Fig. 2: Line plot of variables v_u and $\mathrm{MR1}(v_u; \sqrt[3]{f_c})$ – a very good fit

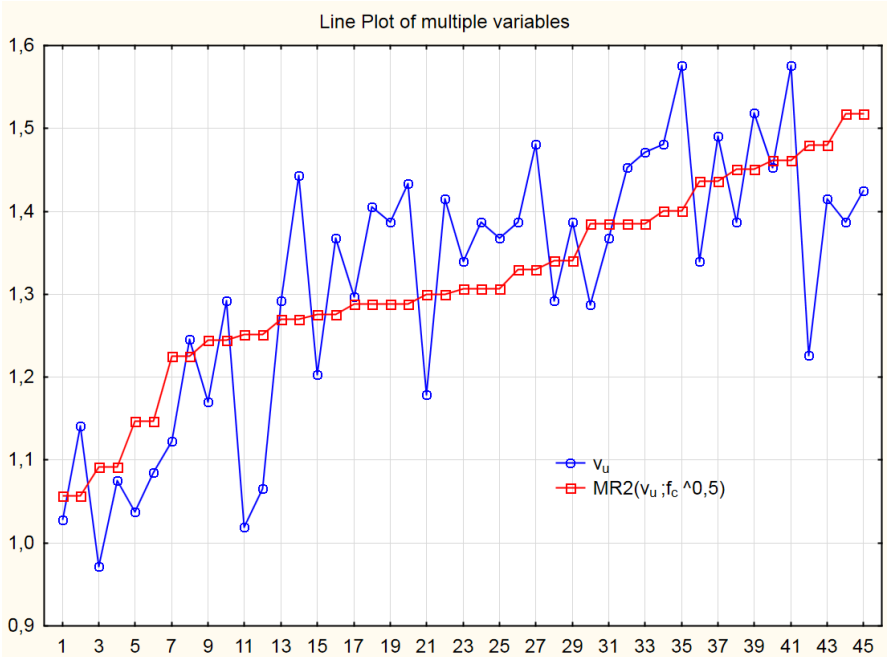

Fig. 3: Line plot of variables v_u and $\mathrm{MR2}(v_u; \sqrt{f_c})$ – a middle fit

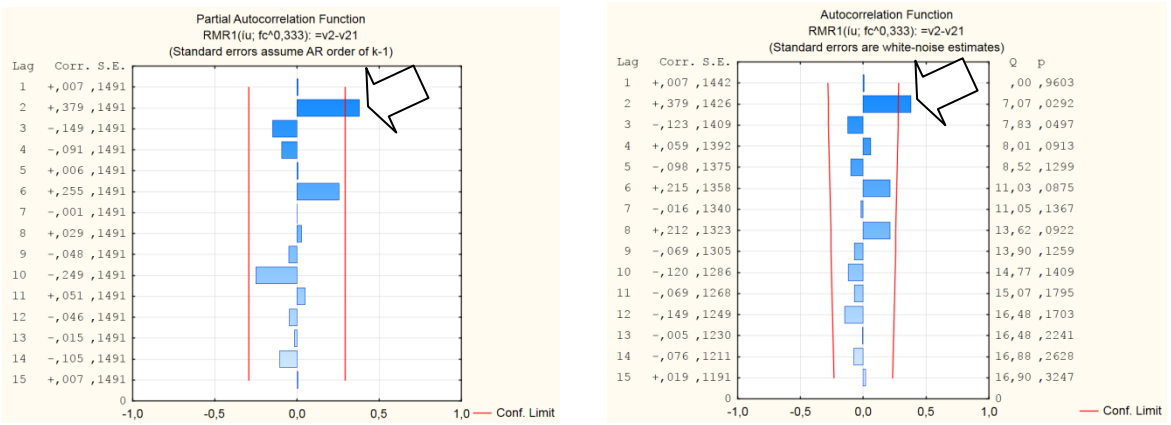

Fig. 4: The residual number RMR1($v_u; \sqrt[3]{f_c}$) of partial autocorrelation function and auto-correlation function − RMR1($v_u; \sqrt[3]{f_c}$) is not white noise $MAPE = 0.408556$ % for $N = 45$

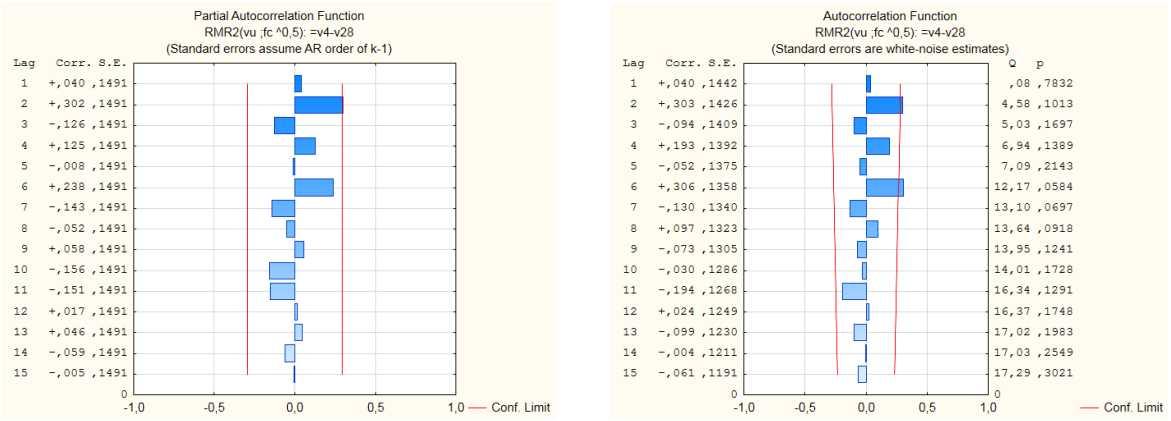

Fig. 5: The residual number RMR2($v_u; \sqrt{f_c}$) of partial autocorrelation function and auto-correlation function – RMR2($v_u; \sqrt{f_c}$) is not white noise $MAPE = 6.929256$ % for $N = 45$

The Eq. (7) **is not a regression equation** because the residual number RMR1($v_u; \sqrt[3]{f_c}$) is not a white noise. A very good line plot fit of variables v_u and MR1, a very small mean absolute percentage error $MAPE = 0.408556$ % (perfect fit) and a very high adjusted $R^2 = 0.99825433$ are not sufficient factors to consider the equation MR1 as a regression equation.

The Eq. (8) **is not a regression equation** because the residual number RMR2($v_u; \sqrt{f_c}$) is not a white noise. A middle line plot fit of variables v_u and MR2, a middle mean absolute percentage error $MAPE = 6.929256$ % and a low adjusted $R^2 = 0.54561598$ are the factors which do not allowed to consider the equation MR2 as the regression equation.

In the next step the Generalized Additive Method GAM was used. In this method the dependent variable v_u was analyzed with regard to different functions of compressive strength: $\sqrt{f_c}$, $\sqrt[3]{f_c}$, f_c^2, f_c^3, f_c^4, f_c^5. The obtained results are presented below as: regression equation coefficients (Tab. 3), regression equation (Eq. 9), line plot of variables v_u and

applied models (Fig. 6), the partial autocorrelation function and autocorrelation function of the residual number of models (Fig. 7), the mean absolute percentage error.

Tab. 3: The list of regression equation coefficients – distribution: Gamma; link function: Log

	Fit summary Response: v_u Distribution: Gamma; link function: Log		
	Variable index	Degr. of freedom	GAM coef.
Intcpt.	0	1.000000	0.00000
$\sqrt{f_c}$	1	4.002432	−1.91852
$\sqrt[3]{f_c}$	2	4.001182	2.83856
f_c^2	3	4.001834	0.13130
f_c^3	4	3.999337	−0.02204
f_c^4	5	3.999161	0.00207
f_c^5	6	4.000788	−0.00012
f_c^6	7	4.000846	0.00000
f_c^7	8	4.003390	−0.00000
f_c^8	9	4.000112	0.00000
f_c^9	10	4.001686	−0.00000
f_c^{10}	11	4.001100	−0.00000

$$\mathrm{GAM1}(v_u; \sqrt{f_c}, \sqrt[3]{f_c}, f_c^2, f_c^3, f_c^4, f_c^5) = \exp(-1.91852\sqrt{f_c} + 2.83856\sqrt[3]{f_c} + \\ + 0.1313\ f_c^2 - 0.02204\, f_c^3 + 0.00207\ f_c^4 - 0.00012\, f_c^5) \tag{9}$$

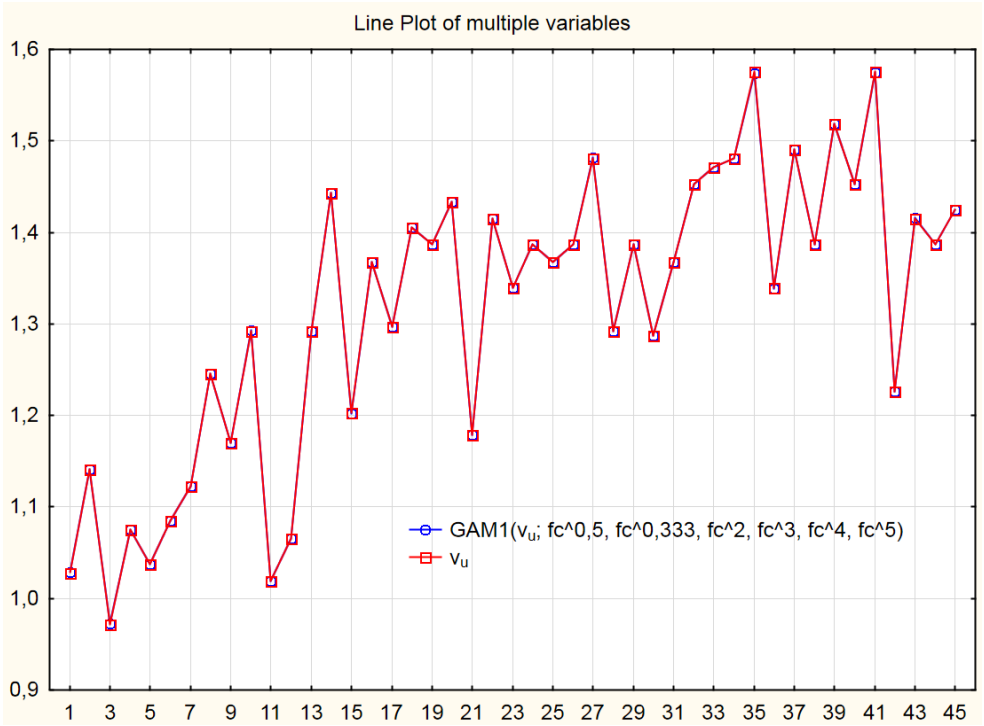

Fig. 6: Line plot of variables v_u and $\mathrm{GAM1}(v_u; \sqrt{f_c}, \sqrt[3]{f_c}, f_c^2, f_c^3, f_c^4, f_c^5)$ – excellent fit

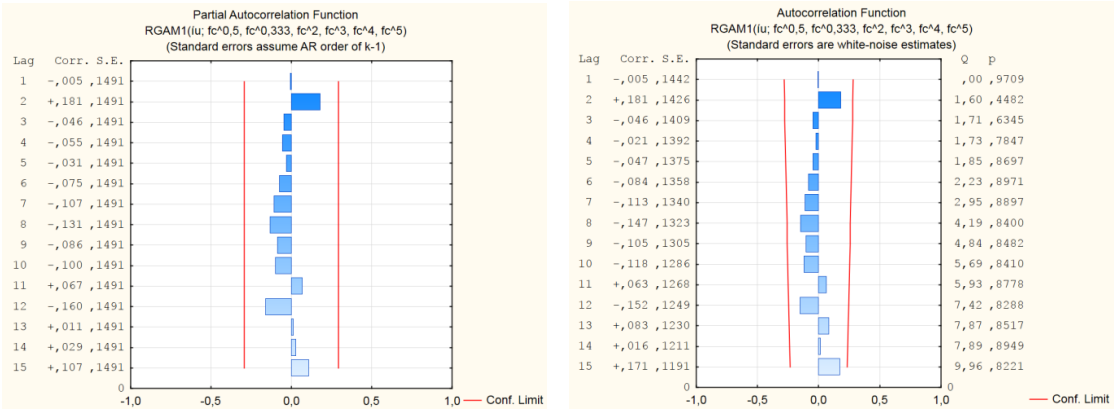

Fig. 7: The residual number RGAM1(v_u; $\sqrt{f_c}$, $\sqrt[3]{f_c}$, f_c^2 , f_c^3 , f_c^4 , f_c^5) of partial autocorrelation function and autocorrelation function – RGAM1 is white noise $MAPE = 0.018715$ % for $N = 45$

The Eq. (9) **is a regression equation.** The residual number RGAM1 is a white noise. An excellent line plot fit of variables v_u and GAM1, a very small mean absolute percentage error $MAPE = 0.018715$ % (very good fit) were obtained. This equation was applied to the next step of statistical analysis in which the test data were compared with the design values.

4.2 Comparative statistical analysis

The comparative statistical analysis considered determining the efficiency of design methods given in different codes according to the ultimate shear stress.

The t-test for independent samples was performed [12]. It was noticed that t-values for all variables (see Tab. 4) were greater than the normal t-value equalling 1.662354 for the degree of freedom $df = 88$ and probability $p = 0.95$. The conclusion was that the variables were independent and that they could be compared.

Tab. 4: T-test for independent samples

Group 1 vs. Group 2	T-test for independent samples Note: Variables were treated as independent samples				
	Mean Group 1	Mean Group 2	t-value	*df*	*p*
GAM1(v_u; $\sqrt{f_c}$, $\sqrt[3]{f_c}$, f_c^2 , f_c^3 , f_c^4 , f_c^5) vs. v_u^{EC2}	1.314982	1.151979	5.41470	88	0.000001
GAM1(v_u; $\sqrt{f_c}$, $\sqrt[3]{f_c}$, f_c^2 , f_c^3 , f_c^4 , f_c^5) vs. v_u^{MC}	1.314982	1.075845	8.39372	88	0.000000
GAM1(v_u; $\sqrt{f_c}$, $\sqrt[3]{f_c}$, f_c^2 , f_c^3 , f_c^4 , f_c^5) vs. v_u^{ACI}	1.314982	0.849898	15.58048	88	0.000000

To study if there is any significant difference between the obtained test results $v_u = V_c/b_w d$ and the calculated values: v_u^{ACI}, v_u^{EC2}, v_u^{MC}, the obtained regression function was compared

to the theoretical ones plotted for design formulas from different codes. This comparison is presented in Fig. 8.

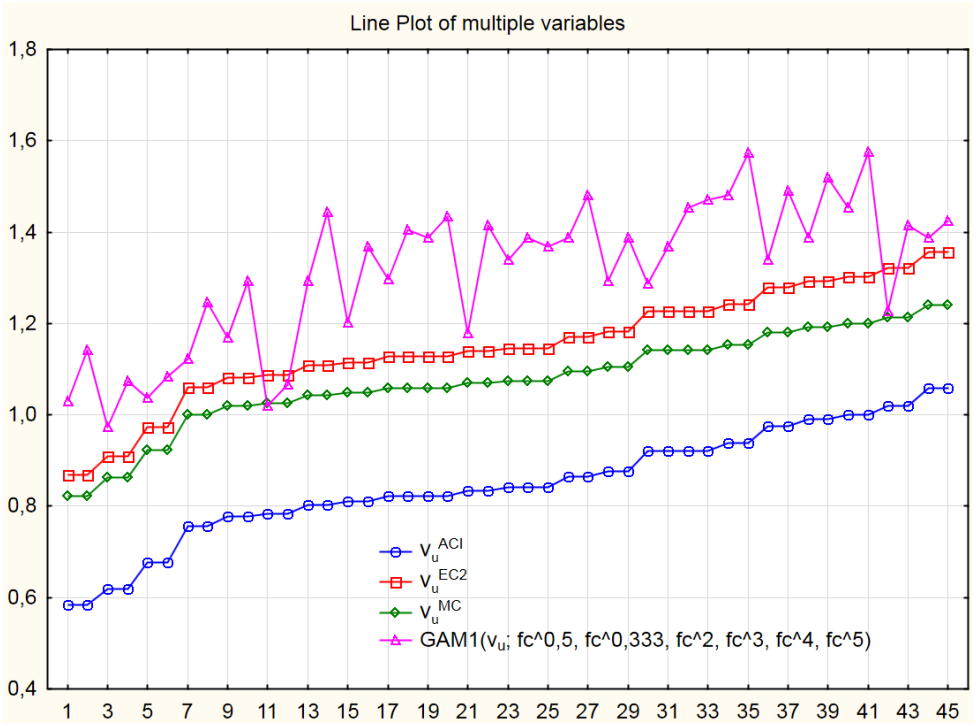

Fig. 8: Line plot of multiple variables

The mean absolute percentage error *MAPE* was calculated from Eq. (6) to estimate the difference between the observed experimental data and the theoretical values. When comparing the regression equation (Eq. 9) with the formulas from different codes the following values of *MAPE* were obtained:

- for Eurocode 2: *MAPE* = 12.7 %
- for Model Code 2010: *MAPE* = 17.7 %
- for ACI 318: *MAPE* = 35.0 %

5 Conclusions

When estimating the shear resistance of longitudinally reinforced concrete members without shear reinforcement, the design formulas from different codes, presented in the paper, differ with respect to their form and tensile-compressive concrete strength relations used in them. Due to the simplicity of design methods the tensile-compression relations such as $f_{ct} \to \sqrt[3]{f_c}$, $f_{ct} \to \sqrt{f_c}$ are commonly used. The performed statistical study has shown that the regression equation for selected experimental observations cannot be successfully built on the basis of them. Much more complex equations are needed to give a good correlation with experimental data, for example the Eq. (9).

The comparison of the obtained regression equation (Eq. 9) with the design formulas from the considered codes shows that the smallest value of the mean absolute percentage error was obtained for the formula from Eurocode 2. Yet, when considering the safety of shear

capacity calculations, the Model Code formula seems to be the best one, as it is the nearest to the regression function and at the same time always below it.

It must be noticed that the performed statistical analysis was made for normal strength concrete of compressive strength not exceeding 40 MPa. Further analysis should be performed for design method efficiency in determining shear resistance of reinforced concrete beams made of high strength concrete.

Literature

[1] ACI Committee 318, Building Code Requirements for Structural Concrete (ACI 318-02) and Commentary (ACI 318R-02). *American Concrete Institute*, 2002

[2] Box, G.E.P., Pierce, D.A. Distribution of residual autocorrelations in autoregressive-integrated moving average time series models. *Journal of the American Statistical Association* 65 (1970), p. 1509–1526

[3] Desai S. Influence of Constituents of Concrete on Its Tensile Strength and Shear Carrying Capacity. *Magazine of Concrete Research* 55(1) (2003), p. 77–84

[4] EN 1992-1-1:2004, Eurocode 2: Design of concrete structures. Part 1: General rules and rules for buildings. *European Committee for Standardization*, 2004

[5] Hastie, T.J., Tibshirani, R.J. *Genaralized additive models*. London: Chapman Hall, Chapter 9, 1990

[6] Kani, G.N.J. Basic Facts Concerning Shear Failure. *Journal of ACI,* June 1966

[7] Kani, G.N.J. The Riddle of Shear Failure and Its Solution. *Journal of ACI*, April 1964

[8] Kot, S., Jakubowski, J., Sokołowski, A. *Statystyka*. DIFIN, 2011 Model Code 2010, First complete draft. *fib* Bulletin 56(2) 2010

[9] Model Code 2010, First complete draft. *fib* Bulletin 56(2) 2010

[10] Nevill, A.M. *Właściwości betonu*. Polski Cement Sp. z o. o., Kraków, 2000

[11] Perera, S.V.T. Mutsuyoshi, H. Shear Behavior of Reinforced High-Strength Concrete Beams. *ACI Structural Journal* 110(1) (2013), p. 43–52

[12] Raju, T.N. William Sealy Gosset and William A. Silverman: two "students" of science. *Pediatrics* 116 (3) (2005), p. 732–735

[13] Shapiro, S.S., Wilk, M.B. An analysis of variance test for normality (complete samples), *Biometrika*, 52(3,4) (1965), p. 591–611

[14] Stanisz, A. *Przystępny kurs statystyki z zastosowaniem STATISTICA PL na przykładach z medycyny*. StatSoft Polska Sp. z o.o., Kraków, 2006

[15] Veccio, F.J., Collins, M.P. The modified compression field theory for reinforced concrete elements subjected to shear. *Journal of ACI* 83(2) (1986), p. 219–231

[16] Veccio, F.J., Collins, M.P. Predicting the response of reinforced concrete beams subjected to shear using the modified compression field theory. *Journal of ACI* 85(4) (1988), p. 256–268

Ultimate capacity increase and reliability assessment of reinforced concrete bridge

Ondřej Slowik[1], Drahomír Novák[1], Radomír Pukl[2]
[1] Institute of Structural Mechanics, Faculty of Civil Engineerinng,
Brno University of Technology,
[2] Červenka Consulting, Ltd
slowikO@study.fce.vutbr.cz, novak.d@fce.vutbr.cz, radomir.pukl@cervenka.cz

Abstract: The paper is focused on optimization of ultimate capacity increase of reinforced concrete bridge. Strengthening is proposed by concreting above of the bridge deck on both sides of the deck. Two parameters are optimized: Height of concrete layer and the quality of concrete used. Ultimate capacity is determined by software tools of nonlinear fracture mechanics, the optimization is performed by pseudo-stochastic optimization approach based on Latin Hypercube Sampling. Resulting alternative of ultimate capacity increase is assessed fully probabilistically.

Keywords: Reliability, Strengthening, Optimization, Concrete bridges, Nonlinear analysis, Simulation

1 Introduction

Over the last few decades, there has been a rapid increase in the volume and weight of heavy vehicles using national road networks. Many road bridges which were built to previous design standards are not able to cope with the current traffic requirements and require either weight restriction, strengthening or even total replacement. This trend can be observed worldwide. Many roads, which were originally built for light traffic, are being used by heavy vehicles that were not envisaged during the original design. Some of bridges are deficient because their load-carrying capacity is inadequate for today's traffic. Ultimate capacity increase of such bridges is needed. The problem involves many uncertainties in material, geometry, loading and degradation phenomena and therefore the concept of reliability theory has to be applied and usually leads to the most economic solution [1].

The aim of the paper is to study and evaluate the existing reinforced concrete slab bridge behavior before and after strengthening [5]. Strengthening parameters are optimized using pseudo-optimization method. The bridge is calculated by the nonlinear finite element fracture mechanics [2]. As many uncertainties are involved in the problem, a statistical approach was used to assess the influence of uncertainties on structural response (load-carrying capacity), [4]. It is based on a randomization of nonlinear finite element analysis

of concrete structures using advanced statistical and reliability techniques. An increase of reliability after strengthening can be then assessed.

2 Bridge and optimization task

Existing short-span reinforced concrete bridge is subjected to rehabilitation, Fig. 1. The aim is to strengthen the bridge by concreting of the layers above the slab deck on the both sides. The aim of the optimization is to find the most suitable (from the perspective of low cost and sufficient ultimate capacity) combination of height of concreting h and the quality of concrete used. The function of concrete cost vs. concrete grade was considered.

Fig. 1: Bridge under rehabilitation

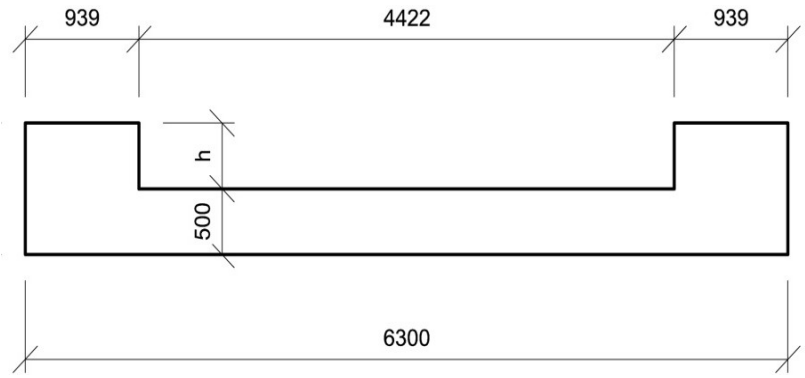

Fig. 2: Cross-section of the bridge (in mm)

These optimization constraints were considered: Bridge must safely carry loading from self-weight and live load – continuous loading corresponding to 6 cars of weight 7 tons. It corresponds to support reaction R_{cn} = 315 kN. Therefore first constraint is introduced as:

$$R_{cc} \geq R_{cs} + R_{cn} = R_{cs} + 315\ , \tag{1}$$

where R_{cc} is total value of support reaction at the ultimate state (peak of load-deflection diagram), R_{cs} is a part of support reaction corresponding to self-weight and R_{cn} is part of support reaction corresponding to live load. The left side is obtained from computational model and the right side represents prescribed values. Next constraints define maximal acceptable cost C [CZK] the height of concrete layer h [m]:

$$C \leq 350000;\ h \in (0; 0{,}5)\ . \tag{2}$$

3 Results

3.1 Optimization

A stochastic pseudo-optimization was based on 30 generated alternatives of bridge structure with different height of concreting layer h and the quality of concrete. For optimization, all related random variable were considered having rectangular distribution. As concrete quality has been considered by 4 variables (modulus of elasticity E, compressive strength f_c, tensile strength f_t and fracture energy G_f), also suitable statistical correlation was necessary to consider. The ranges of variables for optimization:

$$\begin{aligned} h &\in (0; 0.5)\ [\mathrm{m}]\ , \\ f_c &\in (-50;\ -8)\ [\mathrm{MPa}]\ , \\ f_t\ &\in (1.3; 3.5)\ [\mathrm{MPa}]\ , \\ G_f\ &\in (50; 150)\ [\mathrm{Jm}^{-2}]\ , \\ E\ &\in (26000; 35000)\ [\mathrm{MPa}]\ . \end{aligned} \tag{3}$$

ATENA computational model and corresponding crack patterns are shown in Fig. 3.

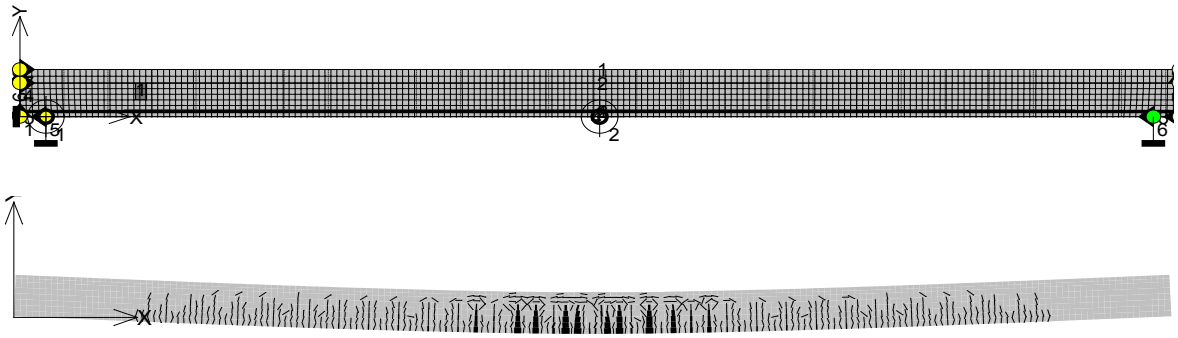

Fig. 3: Finite element mesh and bending cracks

The optimal values of parameters were determined by stochastic pseudo-optimization based on 30 virtual simulations. For practical design it was necessary to use the concrete grade as close as possible to optimal solution – concrete compressive strength 45.1 MPa. The closest concrete grade is C40/50 with unit cost 2495 CZK/m^3. The height of concreting layer was rounded off to h = 100 mm. Resulting corresponding cost is 7302 CZK, and all optimization constraints are satisfied. Note, that not all 30 samples satisfied optimization constraints, these samples were excluded.

3.2 Reliability

Final reliability assessment was performed – calculation of reliability index for stages before and after strengthening for different levels of mean value of loading (μE), Fig. 4. Coefficient of variation 0.15 was considered for live load. Software FReET was used to calculate mean value and standard deviation of load capacity. Based on these values were calculated reliability index β and the failure probability for the interval of mean value of

live load (μE) 0.4 to 0.8 MN. Random variables for concrete and steel reinforcement, and statistical correlations were considered from available sources, including [3], and they are summarized in Tab. 1.

Tab. 1: Basic random variables

Concrete:	Variable	Symbol	Unit	PDF	Mean value	COV
	Tensile modulus	E_c	MPa	Normal	3.56E+04	0.1
	Poisson number	υ	-	Log-normal	0.2	0.05
	Compressive strength	f_c	MPa	Log-normal	−3.83E+01	0.1
	Tensile strength	f_t	MPa	Weibull	3.04E+00	0.1
	Fracture energy	G_f	N/m	Weibull	7.59E−05	0.2
	Strain on the compressive strength in uniaxial compression test	ε_c	-	Log-normal	−2.15E−03	0.15
	Reduction of compressive strength		-	Rectangular	0.8	0.06
	Critical compressive strain	w_b	m	Log-normal	−5.00E−04	0.1
	Specific weight of the material	ρ	MN/m^3	Log-normal	2.30E−02	0.1
Steel:	Variable	Symbol	Unit	PDF	Mean value	COV
	Yield strength	f_y	MPa	Log-normal	500	0.05

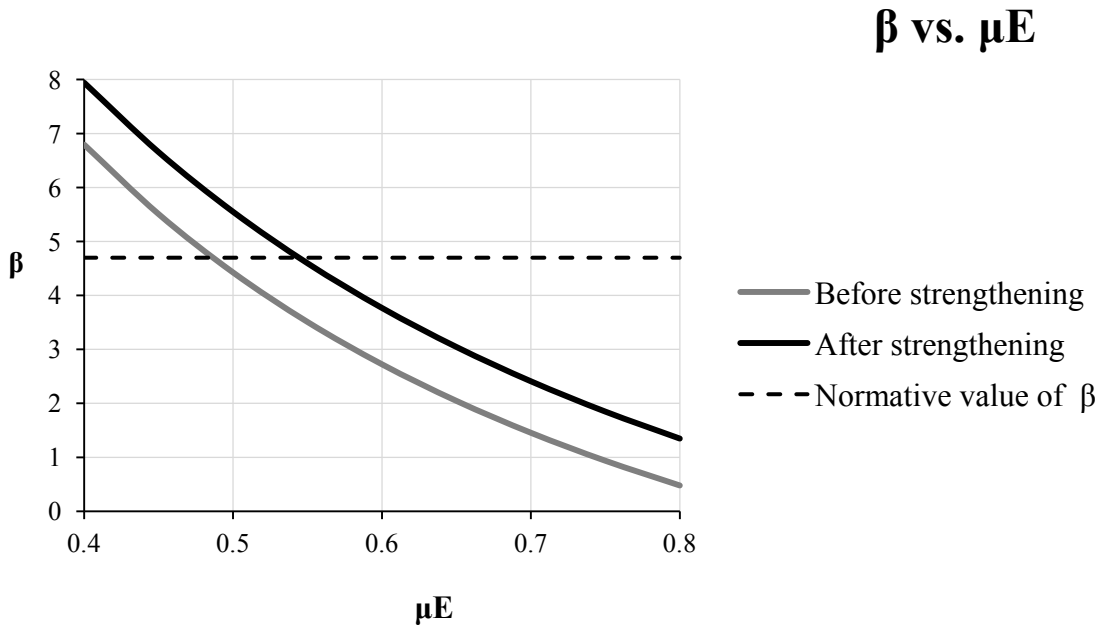

Fig. 4: Reliability index vs. load

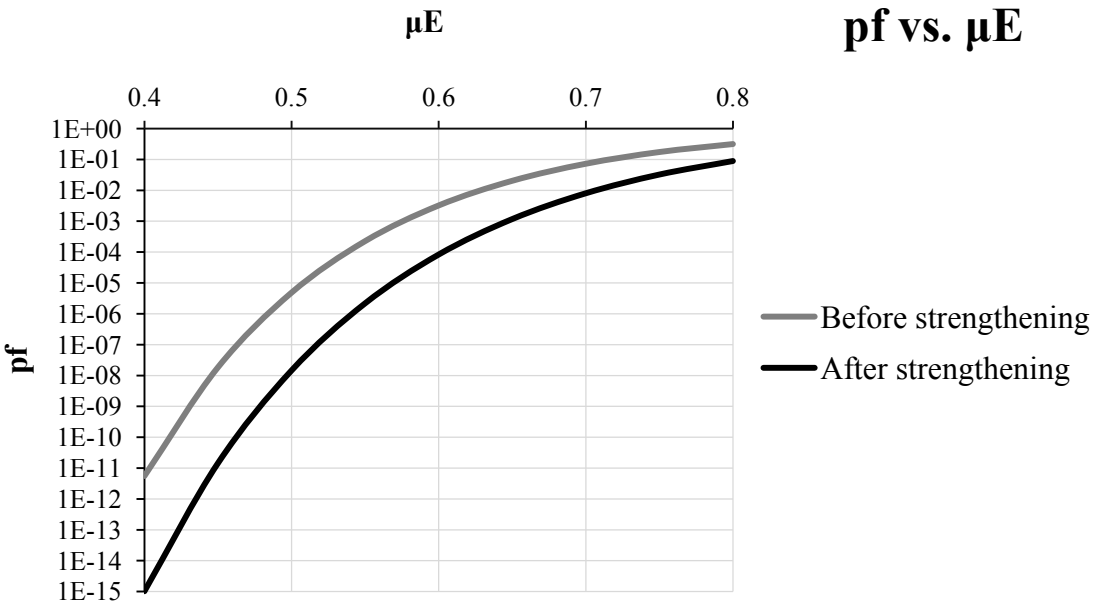

Fig. 5: Probability of failure vs. load

Fig. 4 and Fig. 5 shows, that reliability index increased after strengthening and probability of failure is reduced compared to the original state.

4 Conclusions

The paper shows the possibility of stochastic pseudo-optimization for strengthening of particular concrete bridge. Probabilistic assessment to calculate reliability follows the optimization process. Both steps use the same software tools which combine nonlinear finite element simulation and probabilistic simulation of Monte Carlo type. These tools can be routinely applied for any concrete structure optimization.

Acknowledgement

The presented research is funded by research project No. TA01011019 of Technological Agency of Czech Republic "SimSoft" and by the Czech science foundation project No. P104-13-03662S "FRAPA". Authors gratefully acknowledge this support.

Literature

[1] Enevoldsen, I. Practical implementation of probability based assessment methods for bridges. *Structure and Infrastructure Engineering* 7(7-8) (2011), p. 535–549

[2] Červenka, V., Jendele, L. and Červenka, J. *ATENA Program Documentation – Part 1: Theory.* Czech Republic, Prague: Cervenka Consulting, 2007

[3] Joint Committee on Structural Safety: Probabilistic Model Code, Part 3: Material Properties. 2000. http://www.jcss.byg.dtu.dk

[4] Novák, D., Vořechovský, M. and Rusina, R. *FReET v.1.5 – program documentation. User's and Theory Guides*. Czech Republic, Brno/Červenka Consulting, 2012. http://www.freet.cz

[5] Slowik, O. *Optimization of concrete structures using stochastic methods of optimization.* Bachelor thesis, Institute of Structural Mechanics, Faculty of civil Engineering, Brno University of Technology (in Czech), 2012

Reliability based optimization of concrete structural components

Charl Francois Smit, Celeste Barnardo-Viljoen
Department of Structural Engineering, University of Stellenbosch, Stellenbosch
15372383@sun.ac.za, cbarnardo@sun.ac.za

Abstract: Standards define target reliability levels that govern the safety of designed structures. These target levels should be around an economic optimum for the class of structure under consideration. However, society may have safety requirements in excess of that required to achieve an economic optimum. The LQI criterion can be used to determine society's willingness to invest in safety, thereby defining a minimum acceptable safety- or reliability level. This paper determines economically optimised target reliability levels for class 2 concrete structures in South Africa, over a range of typical input parameters. RACKWITZ'S (2000) [13] approach is used here, adjusted for the South African context. The structure is described using a simple limit state function, defined as the difference between load and resistance, with resistance a function of a global safety parameter. Various case studies are conducted using South African costs and a South African discount rate in the objective function for economic optimisation. The results of the case studies are compared to the generic approach used by RACKWITZ (2000) [13]. Situations where the minimum required reliability would exceed the economically optimum reliability level are discussed. Obtained values are compared to current South African target levels of reliability and recommendations are made.

Keywords: SVSL, SWTP, optimum safety, consequence estimation, sustainable discounting, LQI, work time fraction, target reliability index

1 A generic approach to reliability optimization

1.1 The objective function

Target reliability indices determine the safety of structures, but how safe is safe enough? The target safety can be determined by calculating the optimum safety of structures by weighing the costs of increasing safety against the consequences of failure.

The objective function used to determine the optimum safety is derived by Rackwitz (2002) [12] based on renewal theory:

$$Z(p) = B - C(p) - A(p) - D(p) - U(p) \tag{1}$$

B is the benefit of the existing structure, $C(p)$ is the cost of construction of the structure, $A(p)$ is the obsolescence cost, $D(p)$ is the cost of ultimate failure and $U(p)$ is cost of serviceability failure. The parameter p is the central safety factor defined in Sec. 1.2. In this study the serviceability cost is removed from the objective function due its relatively insignificant effect on the optimum safety of the structure as shown by RACKWITZ (2000) [13].

The construction cost can be broken down into two components:

$$C(p) = C_0 + C_1 p \tag{2}$$

Parameter C_1 is the cost of increasing the safety of the structure, while C_0 denotes all the other construction costs. The obsolescence cost and failure cost must be discounted to the starting time of project by a discount rate γ to be comparable to the construction cost. The discount rate could either be chosen by a private owner, if the optimization is done for a privately owned infrastructure, or be equivalent to the public discount rate if the optimization is done for the public. For obsolescence cost it is assumed that the structure is systematically renewed with obsolescence rate ω:

$$A(p) = (C_0 + C_1 p)\frac{w}{\gamma} \tag{3}$$

The damage cost is given according to RACKWITZ (2000) [13] and assuming that the demolition cost is independent of parameter p:

$$D(p) = (C(p) + H_f + H_m)\frac{\lambda p_f(p)}{\gamma} \tag{4}$$

In Eq. (4), λ is the intensity of a random process, $p_f(p)$ is the probability of failure, H_f is the cost of lost lives due to structural failure and H_m is the other direct and indirect cost due to structural failure. The cost component H_f depends on the number of lost lives due to structural failure (N_{lol}) and the life compensation cost here chosen as SVSL (Societal Value of a Statistical Life). Parameter H_m includes costs such as economic losses, environmental costs, lost of content costs and costs due to injuries as a result of structural failure. The optimum safety is determined by taking the minimum of the following objective function, which excludes all terms independent of the central safety factor p:

$$C_{tot}(p) = -C_1 p - (C_1 p)\frac{w}{\gamma} - (C(p) + N_{lol} \times SVSL + H_m)\frac{\lambda p_f(p)}{\gamma} \tag{5}$$

RACKWITZ (2000) [13] assumed that most structures can be accurately represented by a simple limit state function with resistance (R), central safety factor p and load effect (E). The probability of failure is obtained from the following limit state function assuming statistical distributions as defined in Tab. 1.

$$G = R \times p - E \tag{6}$$

Tab. 1: Random variables *R* and *E*

Parameter	Description	Statistical Distribution	Mean	Standard Deviation
R	Resistance	LN	1**p*	VR**p*
E	Load Effect	LN	1	VS

1.2 The relationship between optimum safety and risk related parameters

In a study conducted by FISCHER ET AL. (2012) [6] the same generic approach used by RACKWITZ (2000) [13] was used. However FISCHER ET AL. showed that there is a relationship between the optimum probability of failure and a parameter *K* depending on the coefficients of variance of the load effect and the resistance. Parameter *K* was defined as all the costs in the objective function excluding the failure cost, divided by the failure cost. *K* is defined as:

$$K = \frac{C_1(\omega+\gamma)}{(C_0+C_1+H_m+N_{lol}\times SVSL)\lambda} \tag{7}$$

Fig. 1 shows the optimum reliability for South African structures, found using the approach detailed in Sec. 1.1, with South African values assigned to the different cost components and discount rate. With SVSL = R3 752 257, N_{lol} = 0.1/m^2, H_m = 0, C_0 = R8000/m^2, λ = 1, ω = 0.02, γ = 0.024 and C_1 and the coefficients variance (VR & VS) varied between reasonable bounds to produce the relationship between the optimum probability of failure and parameter *K*. The calculation of SVSL and γ are discussed in Sec. 3.

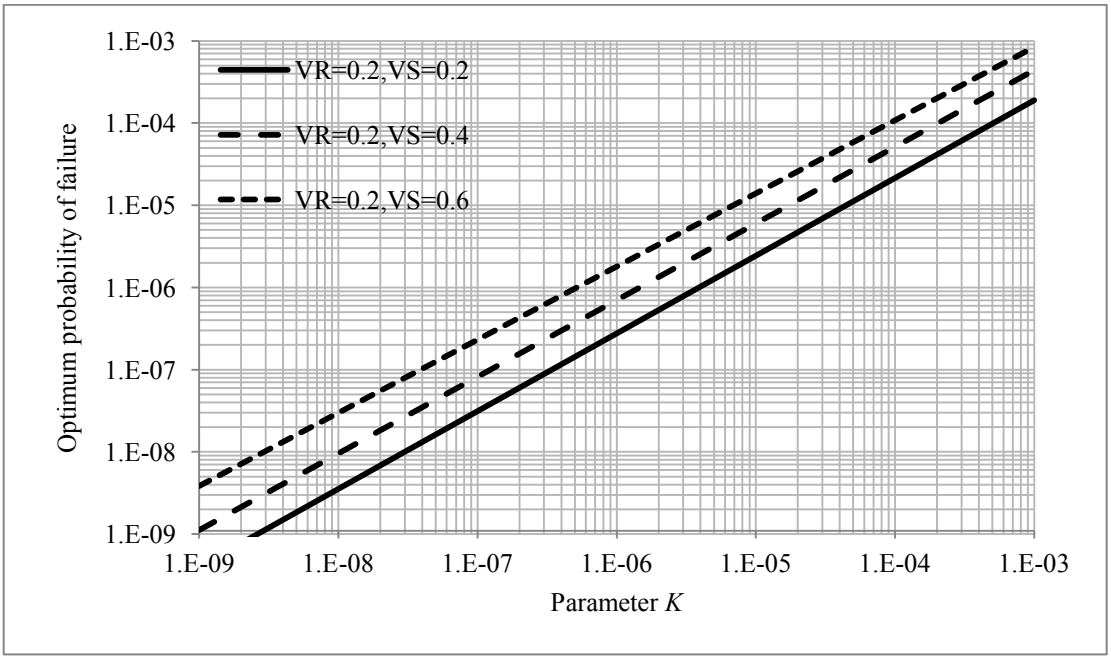

Fig. 1: Optimum probability of failure against increasing parameter *K*

In the following section the simple limit state function (Eq. 6) is improved upon for the specific case of concrete slabs.

2 Case studies

2.1 General approach

Three different types of slabs namely flat slabs, one-way spanning slabs and two way spanning slabs are considered here as a case study. Span lengths between 5 m and 10 m were considered, with the limit state function according to the failure mode under consideration. The different random variables that enter the limit state functions are detailed in Tab. 3. Calculation of the number of fatalities (N_{lol}) is described in Sec. 4. Due to lack of information the probability of escape P(Q) used to determine N_{lol} is assumed between a best case scenario and a worst case scenario, shown in Tab. 2.

Tab. 2: Summary of case studies

Slab Type	Mode of Failure	Best Case P(Q)	Worst Case P(Q)	Population at Risk
One-way	Flexure	0.65	0.2	$0.1/m^2$
Two-way	Flexure	0.65	0.3	$0.1/m^2$
Flat Slab	Flexure	0.5	0.1	$0.1/m^2$

The highest probability of escape was assigned to two-way spanning slabs as these structural components have various alternative load paths and is thus the most robust. The worst probability of escape was assumed for a flat slab, as it is the least robust. The following table gives a summary of all the random variables used for this study, obtained from the JCSS codes part 1, 2 and 3:

Tab. 3: Random variables of case studies

Description	Type of Statistical Distribution	Mean	Standard Deviation	Skewness	Λ	Units
Model uncertainty factor for resistance	Lognormal	1.2	0.18	0.45	NA	NA
Yield strength of reinforcement	Lognormal	510000000	30000000	0.18	NA	Pa
Area of reinforcement	Deterministic	Variable X p	NA	NA	NA	m^2
Height of slab	Normal	0.3	0.01	0	NA	m
Cover of concrete +16/2mm	Gamma	0.033	0.005	0.3	NA	m
Model uncertainty factor for load	Lognormal	1	0.2	0.6	NA	NA
Long-term load	Gamma	500	900	3.6	0.2	Pa
Short-term load	Gumbel	200	566	1.14	1	Pa
Density of concrete	Normal	24000	960	0	NA	N/m^3
Length *y*	Deterministic	5	NA	NA	NA	m
Strength of concrete	Lognormal	39062500	7031250	0.54	NA	Pa

The area of reinforcement is determined by solving the following equation:

$$E(G) = 0 \tag{8}$$

Here $E(G)$ is the expected value of the limit state function. The cost of increasing safety is determined by using simplified curtailment rules obtained from Robberts ET AL. (2010) [16] based on the South African codes and using typical cost of reinforcement of R9000/ton. For all case studies a C_0 of R8000/m^2 and a H_m of R12000/m^2 was assumed. All cost are normalised by taking them as per unit of collapsed floor area.

2.2 Results and discussion

A total of 54 data points were generated by considering different span lengths and probabilities of escape. Fig. 2 shows the results of the optimization for flexural failure in slabs:

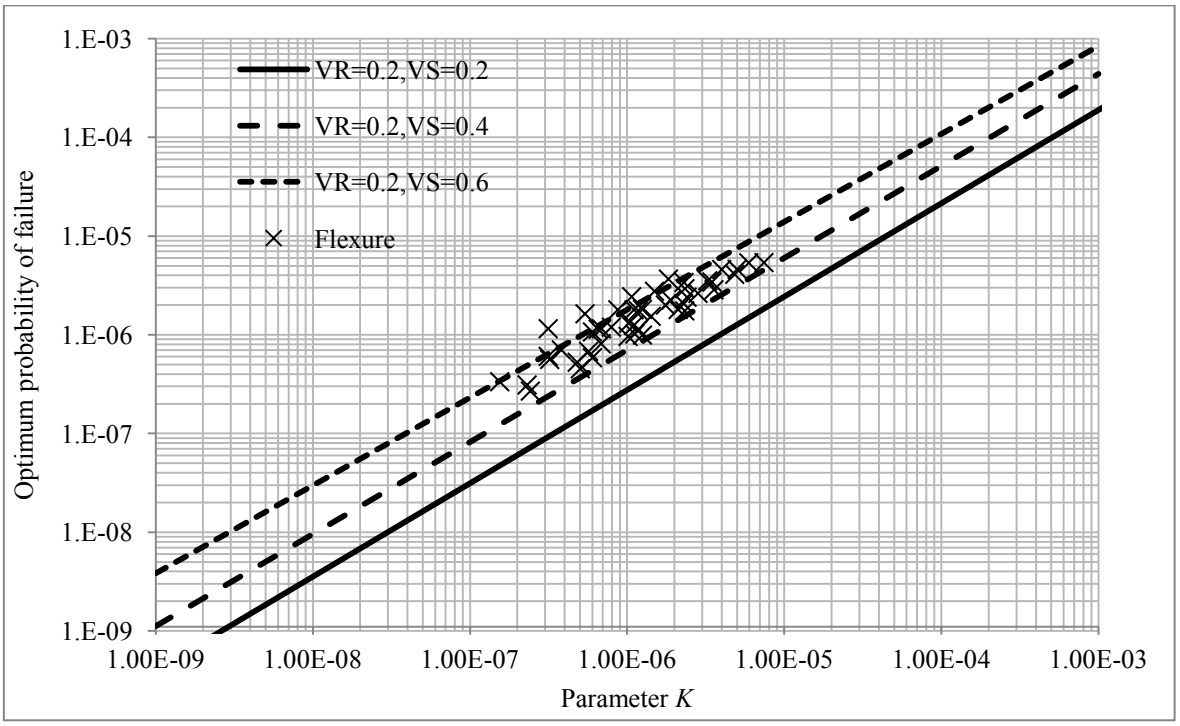

Fig. 2: Optimum probability of failure against increasing parameter K

It is observed that the results from slabs in flexure compare well with the generic trend lines previously generated. Note that changes in span length imply changes in the variance of resistance and loads. Typically the relative cost of increasing safety increases as the span of the slab is increased. Thus the effective coefficient of variance of the slab decreases with increasing length. Furthermore the standard deviation of the load effect depends on the size of the loading area, which increases with increased span length, decreasing the standard deviation. However the mean of the load remains the same, thus the coefficient of variances decreases.

Tab. 5 shows the mean target reliability indices obtained for slabs in flexure and for punching shear respectively, based on a 50 year reference period.

Tab. 4: Optimum target reliability indices for slabs

Mode of failure	β target	
	Mean	Range
Slabs in flexure	3.76	3.42−4.24

The current South African concrete design standard recommends target reliability indices of 3.0 and 4.0 respectively for RC2 structures and brittle failure modes, based on a 50 year reference period. The results indicate that the target reliability index for ductile failure is too low and needs to be increased. Furthermore the results compare well with the European target reliability index of 3.8 for RC2 structures.

3 Deriving life saving & life compensation costs for South Africa

3.1 Formulation of SWTP and SVSL

The Life Quality Index (LQI) is widely used as a measure of society's well-being. It was defined by NATHWANI ET AL. (1997) [10] as:

$$L = g^q e_0 \qquad q = \frac{1}{\beta}\frac{w}{1-w} \tag{9}$$

The term g is the GDP per capita, e_0 is the life expectancy at birth and w is the work time fraction is defined as total time spent working over total available time. The LQI criterion requires that if some decision in a risk related project results in a marginal change in g and l, the LQI should as a minimum requirement remain the same. From this statement RACKWITZ (2008) [14] showed that the life saving cost (SWTP) is derived and formulated as follows:

$$dg \geq \frac{g}{q}\frac{de}{e} = SWTP \tag{10}$$

An assumption associated with the failure of typical concrete structures falling under RC2 is made that the risk is distributed evenly between all the age groups, thus a delta mortality reduction scheme is used for this particular study which is:

$$C_\Delta(a,n,\delta,\rho) = \int_0^{a_u} \frac{\int_a^{a_u}(t-a)exp\left[-\left(\int_a^t (\mu(\tau)+\rho(\tau))\mathrm{d}\tau + \delta(t-a)\right)\right]\mathrm{d}t}{\int_a^{a_u} exp\left[-\left(\int_a^t(\mu(\tau)+\rho(\tau))\mathrm{d}\tau + \delta(t-a)\right)\right]\mathrm{d}t} h(a,n)\mathrm{d}a \tag{11}$$

$$SWTP = \frac{g}{q}C_\Delta \tag{12}$$

The demographic constant is depended on the mortality rate (μ), the average growth rate of the population under consideration (n) and the two components of a sustainable discount rate, namely the pure time preference rate (p) and the economic growth rate (δ). The pure time preference rate was assumed constant over all age groups for this study.

RACKWITZ (2006) [15] shows how SVSL (Societal Value of a Statistical Life) is derived by using a utility function with only monetary units and with mathematical manipulations combining it with life expectancy to form:

$$SVSL = \frac{g}{q}\bar{\mathrm{E}}(a, n, \delta, \rho) \tag{13}$$

Where $\bar{\mathrm{E}}$ is the age-averaged, discounted life expectancy and SVSL should be interpreted as a *compensation* cost, while SWTP is a life *saving* cost.

3.2 Sustainable discounting

In order to conduct a benefit/cost analysis a long term sustainable discount rate must be used to convert all costs occurring at different time intervals to present values. The classical Ramseyan formulation of optimal stable growth in perfect markets is as follows:

$$\gamma = p + \varepsilon\delta \tag{14}$$

In this formulation ε is the elasticity of consumption and is shown by RACKWITZ (2008) [14] to be equal to $1 - q$. The economic growth rate (δ) can be calculated as follows:

$$\ln\left(\frac{g1992}{g1870}\right)/(1992 - 1870) \tag{15}$$

In this formulation g is defined as the real GDP per capita for a specific year.

However the difficulty comes in computing the time preference rate as it is a purely psychological phenomenon where people discount the value of something simply because it will be received in the future and not now. Reasons for this phenomenon are the fact that humans won't live forever and due to impatience and economic myopia.

KULA (1984) [8] conducted a study where the social time preference rates (STPR) for Canada and the USA were calculated. KULA (1984) [8] also derived a formulation for the societal time preference rate based on the assumption that people discount future utilities simply because they may not be alive to enjoy it. The formulation of STPR is as follows:

$$STPR = (1 + g)^e\left(\frac{1}{\pi}\right) - 1 \tag{16}$$

In Eq. 16 g is the growth rate of consumption, e is the elasticity of marginal utility and π is the probability of an average individual being alive. Using the above formulation STPR is calculated as 2.3% for South Africa.

Many have criticised the classical Ramseyan approach based on ethical intergenerational grounds due to the fact that the generations not yet born are negatively affected by a high discount rate. A more ethically defensible approach is to use the generation adjusted discounting model which discounts the living generation by $\rho + \varepsilon\delta$ and discounts the generation not yet born by $\varepsilon\delta$. (RACKWITZ 2008) [14]. Using the following equation which is an accurate approximation of the generation adjusted discounting model:

$$\gamma \approx \varepsilon\delta + pexp[-am] \tag{17}$$

In this equation a is a suitably chosen constant. Using $1 - q = 0.8$, $\rho = 2.3\%$, $\delta = 1.52\%$, $a = -0.013$ and $t = 50$ years γ is calculated as 2.4%.

3.3 The work time fraction

The work time fraction is a measure of society's preferences. A society with a relatively high work time fraction places more emphasis on obtaining or maintaining wealth where a society with a relatively low work time fraction places more emphasis on the enjoyment of life. Thus a society with a high work time fraction prefers to invest less in to safety than a society with a low work time fraction.

RACKWITZ (2008) [14] proposed a formulation of the work time fraction as follows:

$$w = \frac{labour\ force}{Population} \times \frac{yearly\ worked\ hours}{365.24} \times \frac{9}{8} \tag{18}$$

This formulation includes the unemployed who wants to work, but cannot find work, assuming that they would approximately work the same amount of yearly hours as the currently employed.

A study by BUDLENDER (2000) [1] to determine how South Africans spend their time was conducted with three rounds namely February, June and October of the year 2000. The study covered nine provinces and covered all settlement types − formal urban, informal urban, commercial farms and rural settlements. The results were obtained by using 24-hour diaries updated every half an hour, revealing that employed women spend an average of 19% of their day time working while men spend an average of 24.5% working.

The number of men and women making up the labour force was used to calculate a weighted average time an employed South African spends working. This amounts to 22.0% of their total time or 1928 hours per year. This compares well with yearly working hours for other countries composed by RACKWITZ (2008) [14]. For example in the year 1996 Australia had a yearly worked hours of 1875 and the USA has a yearly working hours of 1950. Using Eq. (18), a labour force of 17482000, a population of 50586757 and yearly working hours of 1928 South Africa's work time fraction was calculated as 0.086. This is a surprisingly low w, given South Africa's relatively low GDP.

RACKWITZ (2008) [14] expects that countries with a low GDP per capita will have a higher w than countries with higher GDP per capita as people in poorer countries would prefer more work to increase their personal wealth, although exceptions may exist. A multinational study conducted by RACKWITZ (2008) [14] of predominantly European countries showed a mean work time fraction of 0.106. This is significantly higher than the work time fraction obtained for South Africa, which is surprising given South Africa's relatively low GDP per capita of about R58000 (roughly 7000 US$ (2012)). Fig. 3 shows the results of a comparative study between the work time fractions of African vs. European countries.

An assumed yearly worked hours of 2000 was assigned to each African country and an assumed yearly worked hours of 1600 was assigned to each European country which compares well with data compiled by RACKWITZ (2008) [14].

The result depicted in Fig. 3 is unexpected on two accounts. Firstly, even though all of the African countries have a lower GDP per capita than the European countries their work time

fractions are lower. This is contrary to the theory that a relatively low GDP per capita will result in a high work time fraction. However, the low life expectancy of these countries causes their ratio of labour force to total population to be significantly lower than what is the case for European countries. For example, only 57% of Nigeria's population is over 15, compared to 87% in Germany. As a result the potential labour force relative to population size is far smaller in African countries compared to Europe, as can be seen in Tab. 6 (European countries have a mean labour force over total population of 49%, LABOURISTA [5]). I.e. even though a typical individual in one of these societies may work long hours while part of the active labour force, their short life expectancy causes the average work time spent over a lifetime to be low.

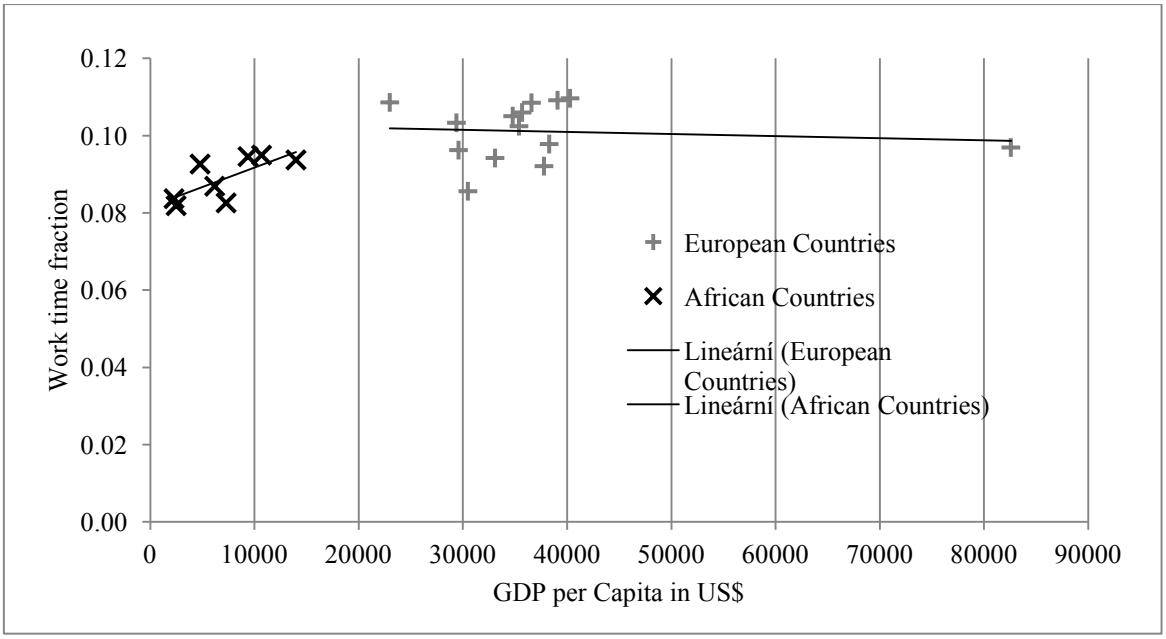

Fig. 3: Work time fraction for various African & European countries

Tab. 5: Work time fractions for various African Countries

Country	(1) GDP per capita (PPP) US$ (2010)	(2) Population (a)	(3) Labour force (b)	(4) Labour force/Population	(5) w(2000ywh)
Algeria	7300	36485830	11727130	32.1%	0.083
Angola	8200	20162520	7611537	37.8%	0.097
Egypt	6200	83958370	28396610	33.8%	0.087
Libya	14000	6469497	2359688	36.5%	0.094
Morocco	4800	32598540	11754700	36.1%	0.093
Nigeria	2500	166629400	53095240	31.9%	0.082
South Africa	10700	50738260	18752530	37%	0.095
Sudan	2300	45722080	14891270	32.6%	0.084
Tunisia	9400	10704950	3939954	36.8%	0.095
Mean	7150	50385494	16947629	34.9%	0.090
Standard dev.	4074			2.3%	0.006

1) Obtained from OECD[11] (2010) in US$

2) Obtained from Labourista [5]

3) Obtained from Labourista [5]

4) Labour force as % of Total Population

5) Work time Fraction assuming 2000 yearly working hours

Secondly, while the work time fraction of the European countries decreases with increasing GDP, as expected, it increases with increasing GDP for the African countries, which was unexpected. This is likely another symptom of the root cause discussed above: In these countries an increase in GDP is strongly linked to an increase in life expectancy, which in turn increase the labour force ratio and w. As a result the potential labour force relative to population size is far smaller in African countries. This property can be seen on Tab. 6.

3.4 Sensitivity of the optimum reliability

The computed values for SVSL as well as the assumed number of fatalities in case of failure will influence the estimate of optimum reliability. This section investigates these influences.

SVSL and SWTP was calculated as R3 752 257 and R3 078 640 respectively for South Africa using $\beta = 0.45$, g = R36 769 (62% of GDP according to [3]), $w = 0.086$, $C_\Delta = 17.55$ and $\bar{E} = 21.39$.

However, using a w of 0.125 as estimated by RACKWITZ (2000) [14] the SVSL and SWTP becomes R2 093 057 and R2 628 273. The effect of the two work time fractions on the optimum safety is tested by using a generic approach to produce the following graph by varying the cost of increasing safety and using the two different life compensation cost.

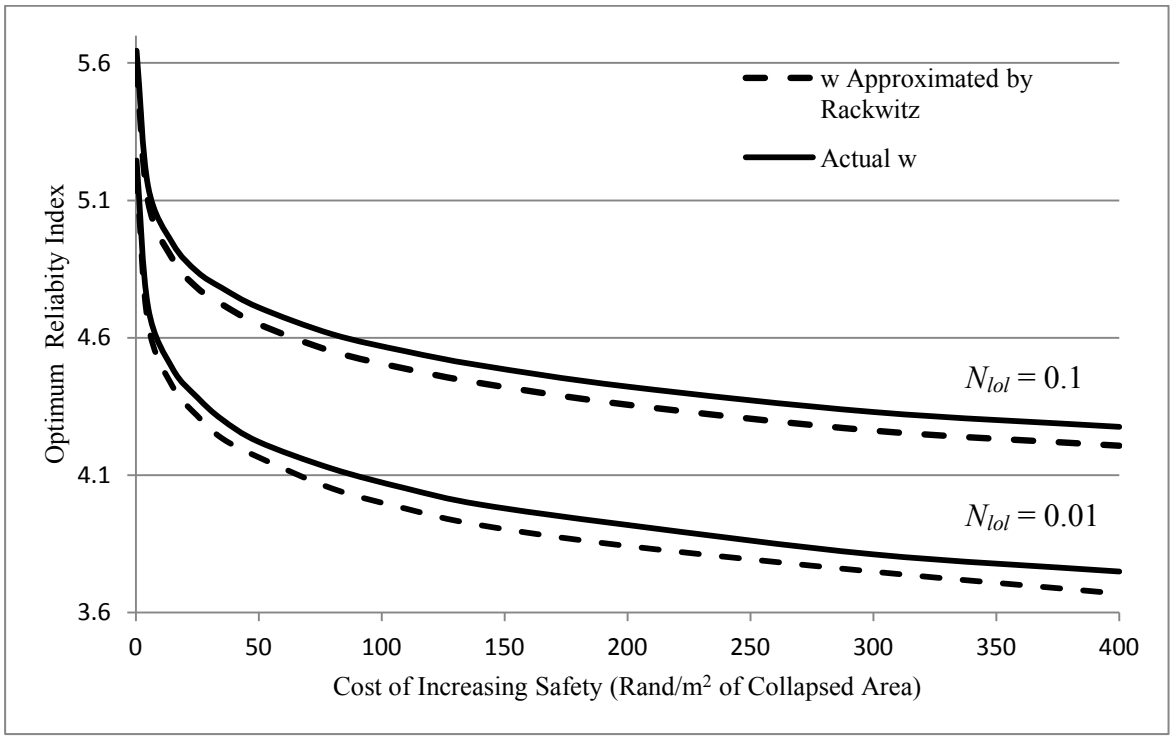

Fig. 4: Target reliability indices against changing cost of increasing safety

Even though the SVSL related to the two work time fractions differ by a factor of more than 1.5, the relative differences between the target reliability indices are small. In contrast, the assumed number of fatalities in case of failure has a significant influence on the optimum reliability. When the costs of safety approaches zero the optimum reliability indices exponentially increase, as expected.

3.5 When is minimum safety safer than optimum safety?

The minimum reliability level derived from the LQI criterion should be chosen as the target reliability when the optimum reliability is less than the minimum reliability. However a study conducted by FISCHER ET AL. (2012) [7] showed that if the optimization is done for the public (discount rate = $\rho + \varepsilon\delta$) the optimum safety is *always* larger than the minimum safety if the life compensation cost (SVSL) is *larger* than the life saving cost (SWTP). RACKWITZ (2006) [14] noted that the ratio of SVSL over SWTP was not constant. This property implied that there could possibly be a situation where SWTP was larger than SVSL. Both the formulations of SWTP and SVSL have q and g as parameters, thus the ratio of SWTP and SVSL is only depended on the age-averaged life expectancy and the demographic constant. These two parameters are dependent on the same three parameters (discount rate, mortality rate and population growth rate). The population distribution (depended on population growth rate) has no effect on the ratio as the age averaging component of SVSL and SWTP cancels out.

Three different countries were chosen to study the impact of these various parameters on the $\bar{E}/C_{\Delta}$ ratio. The countries were Japan, Australia and South Africa. Out of these three countries South Africa has the highest age dependent mortality rate while Japan and Australia have almost identical mortality rates. All life tables and population growth rates were obtained from WHO [17] 2006 data. The following graph shows the results of the study:

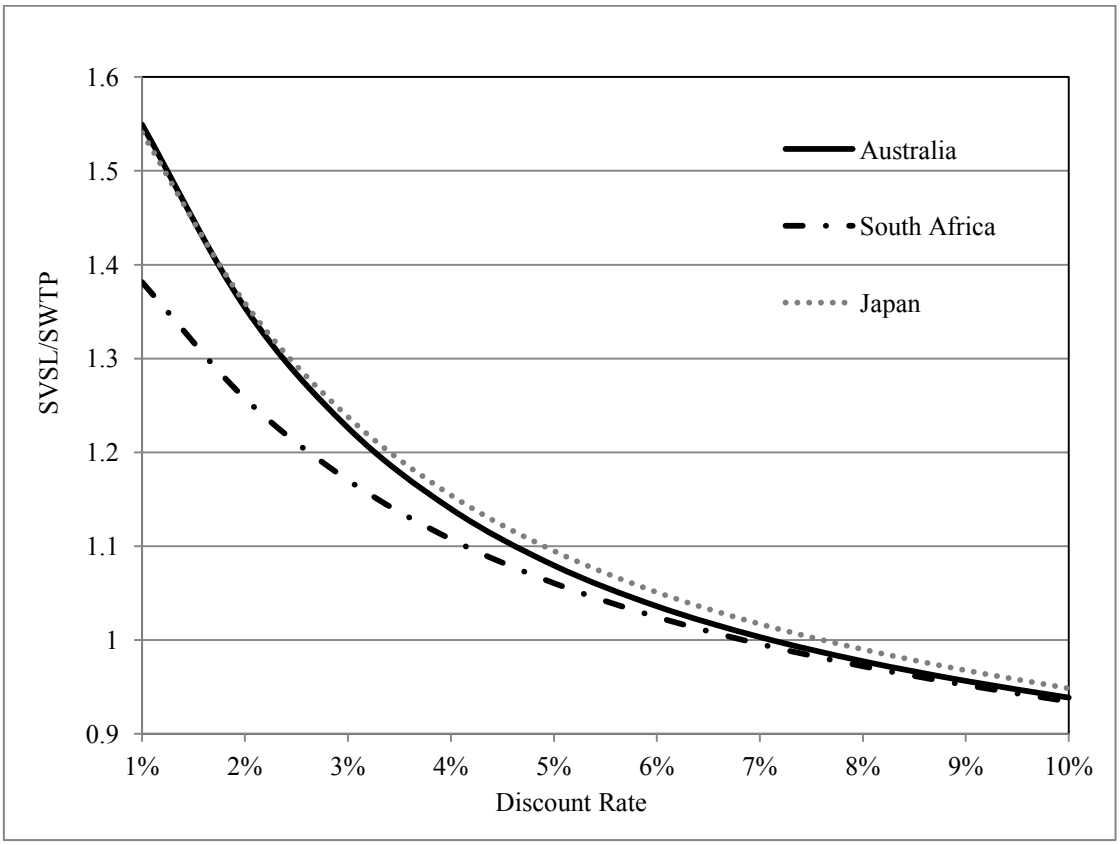

Fig. 5: SVSL/SWTP against increasing discount rate

An observation is made that at low discount rates South Africa has the lowest SVSL/SWTP ratio as a result of the relatively high mortality rate. However as the discount

rate is increased the differences between the SVSL/SWTP ratios for the three countries decreases. A conclusion is made that SVSL can only be larger than SWTP at discount rates larger than 7%. Optimisation done on behalf of the public would usually imply a discount rate significantly lower than this.

4 Fatality estimation due to structural collapse

Fatality estimation is crucial to structural optimization as the life compensation costs generally dominate the consequences costs. LENTZ ET AL. (2004) [9] estimates the number of fatalities as follows:

$$N_{LOL|F} = N_{par}\big(1 - P(Q)\big).k \tag{19}$$

In this formulation N_{par} is the population at risk, $P(Q)$ is the probability of escape and k is the probability of dying if a person fails to escape. Tab. 7 and 8 were obtained from historical data from various structural failures due to earthquakes in various regions [2]. Number 1 in Tab. 7 is used in combination with number 4 in Tab. 8 to determine k. In Tab. 7, M3 is the $1 - P(Q)$ and M1 and M2 is related to N_{par}.

Tab. 6: Immediate injuries at collapse (COBURN ET AL. (1992) [2])

M4 Estimated Injury Distributions at Collapse (% of M3)		
Triage Injury Category	Masonry	RC
1) Dead or Unsaveable	20	40
2) Life threatening cases needing immediate medical attention	30	10
3) Injury requiring hospital treatment	30	40
4) Light injury not necessitating hospitalization	20	10

Tab. 7: Post event casualty estimation of living trapped victims (COBURN ET AL. (1992) [2])

M5 (as % of M3 − M4) Living victims trapped in collapsed buildings that subsequently die		
Situation	Masonry	RC
1) Community incapacitated by high casualty rate:	95	-
2) Community capable of organising rescue activities:	60	90
3) Community + emergency squads after 12 hours	50	80
4) Community + emergency squads + SAR experts after 36 Hours	45	70

5 Conclusions

The results of the study cases suggest that the target reliability indices set by the current South African codes are too low. The optimum reliabilities calculated in this study compares well with the current target reliabilities set by the Euro Code for RC2 structures.

The discount rate calculated for South Africa is small compared to other discount rates in literature. This is due to the relatively low pure time preference rate of South Africa which

is only 2.3% compared to Kula's results for the USA and Canada which was 5.3% and 5.2%.

Fischer's observation that for a limit state function having a lognormal distribution representing both the resistance and load effect a relationship exists between parameter K and target probability of failure is also observed in this paper. The study cases reveal that the effective variance of the limit state function is depended on the length of the member under consideration.

The calculated yearly worked hours of an average South African compares well with results from literature. However it was shown that the preference for work is not only depended on the magnitude of the GDP of a country, but sensitive to the population distribution of a country. The work time fraction for African countries is low due to their low life expectancy, but increase with increasing GDP due to related increased life expectancy.

For public structures the optimum reliability would be larger than the minimum target reliability if SVSL is larger than SWTP. This paper showed that SWTP becomes larger than SVSL for discount rates in excess of 7%, which is typically not the case.

Literature

[1] Budlender D, Chobokohane N, Mpetsheni Y. How South Africans Spend their Time. Available from http://unstats.un.org/unsd/demographic/sconcerns/tuse/Country/SouthAfrica/sourcezaf00c.pdf, 2000

[2] Coburn, A., Spence, R. J., & Pomonis, A. Factors determining human casualty levels in earthquakes: Mortality prediction in building collapse. *Proceedings of the First International Forum on Earthquake-Related Casualties.* Madrid: Reston, VA, U.S. Geological Survey, 1992.

[3] Department of National Treasury. Budget Summary. Available from: http://www.treasury.gov.za: , 2012

[4] Dunne P, Edkins B. The Demand for Food in South Africa. *Proceedings of the Economics Society South Africa Conference*, Durban, South Africa, 2005

[5] EAPEP 1990-2020. Available from: http://laborsta.ilo.org

[6] Fischer K, Barnardo-Viljoen C, Faber M.H. Deriving Target Reliabilities from LQI. *LQI Symposium in Kgs. Lyngby, Denmark*. Conducted by the JCSS, 2012

[7] Fischer K, Faber M.H. The LQI Acceptance Criterion and Human Compensation Cost for Monetary Optimization − A Discussion Note. *LQI Symposium in Kgs. Lyngby, Denmark*. Conducted by the JCSS, 2012

[8] Kula E. Derivation of the Time Preference Rates for the United States and Canada. *The Quarterly Journal of Economics*, Vol 99, No 4, 1984, p. 873−882,

[9] Lentz A, Rackwitz R. (2004) Loss of Life Modelling in Risk Acceptance Criteria. Available from Probabilistic safety assessment and management (PSAM), Vol. 4, p. 1924−1929.

[10] Nathwani J.S., Lind NC, Pandey MD. *Affordable Safety by Choice: The Life Quality Method*. Institute for Risk Research, University of Waterloo, Canada, 1997

[11] OECD Statistics. Available from: http://stats.oecd.org/

[12] Rackwitz R. Optimization and Risk and Acceptability Based on the Life Quality Index. *Structural Safety*, 2002, p. 297−331,

[13] Rackwitz R. Optimization − The basis of Code-Making and Reliability Verification. *Structural Safety*, 2000, p. 27−60,

[14] Rackwitz R. Philosophy behind the Life Quality Index and Empirical Verification. Joint Committee of Structural Safety (JCSS). Available from www.jcss.com, 2008

[15] Rackwitz R. The effect of Discounting, Different Mortality Reduction Schemes and Predictive Cohort Life Tables on Risk Acceptability Criteria. *Structural Safety*, 2006, p. 469−484,

[16] Robberts, J.M & Marshall, V. *Analysis and design of concrete structures*. Pretoria: University of Pretoria, 2010

[17] World Health Organization Available from: http://www.who.int/research/en/

Adjustment of tunnel lining design life based on nominal safety in LRFD

Panagiotis Spyridis[1], Alexios E. Tamparopoulos[2]
[1] Dr. Sauer & Partners Ltd., London;
[2] University of Natural Resources and Life Sciences, Vienna
pspyridis@dr-sauer.com, alexios.tamparopoulos@boku.ac.at

Abstract: The year 2013 finds the London Underground (the first metro worldwide) and the Thames Tunnel (the first tunnel underneath a navigable river) celebrating their 150th and 170th anniversary of operation, respectively. Once more with these occasions, one comes to appreciate the vast socioeconomic significance of such structures and moreover the necessity for sustainable infrastructure with particularly pronounced life-cycle requirements, which in several cases may exceed the service life attained through Eurocode provisions. A methodology to adjust the design service life of a tunnel lining is demonstrated through an engineered scaling of the involved Ultimate Limit State (ULS) load/resistance safety factors. This is achieved on the basis of the reliability level prescribed to the structure at the very beginning of its lifetime (during design), while some assumptions are verified through probabilistic simulations. Furthermore, this is discussed in consistency with the reliability concepts indicated in Eurocode 0 “Basis of Design”.

Keywords: codes of practice, tunnelling, service life, structural reliability

1 Introduction

Service life of significant infrastructure in the UK is typically required to reach 120 years [1], [2]. At the same time, Eurocodes are established as a design standard in the UK, the current provisions of which cover a service life of 50 years as a standard. This critical limitation may compromise the design efficiency in large infrastructure projects. In an antithesis, temporary works needed to serve for a limited timeframe (e.g. not more than 10 years) and may become particularly complicated and over-dimensioned if the Eurocode service life provisions are adhered to. In general, non-typical life-cycle requirements can pose a main concern among the engineering society nowadays and a core element in the design of new infrastructure projects.

Tunnels can typically comprise such large scale infrastructure projects, where a requirement for an increased service life is present. In order to meet such requirements – except

for a sophisticated design detailing, advanced material and construction quality, and a well specified structure monitoring plan, (e.g. as described in [3]–[6]) – the appropriate adjustment of safety factors is necessary. Paradigms of non-standard service life are discussed in [7], [8] and have been seen inter alia in the Brenner Base tunnel (200 years), the Koralm tunnel (150 years), or the Niagara tunnels (90 years).

The service life of a structure may be expressed in conjunction to its time-dependent performance level and be processed in the reliability discipline, as discussed in [9] and as integrated in codified performance based assessments [10]. In EUROCODE 0, "Basis of Design" [11] a structure's service life is defined as the *"assumed period for which a structure or part of it is to be used for its intended purpose with anticipated maintenance but without major repair being necessary"*. The structure's service life ends when the minimum acceptable (terminal) target reliability β_{TARGET} is reached. It should be highlighted that a key aspect of designing for long, non-standard service lives is a life-cycle engineering based maintenance/intervention plan, while deterioration models with and without maintenance can be considered. Structural deterioration in terms of reliability development for a service life of 50 and 120 years is exemplarily illustrated in Fig. 1.

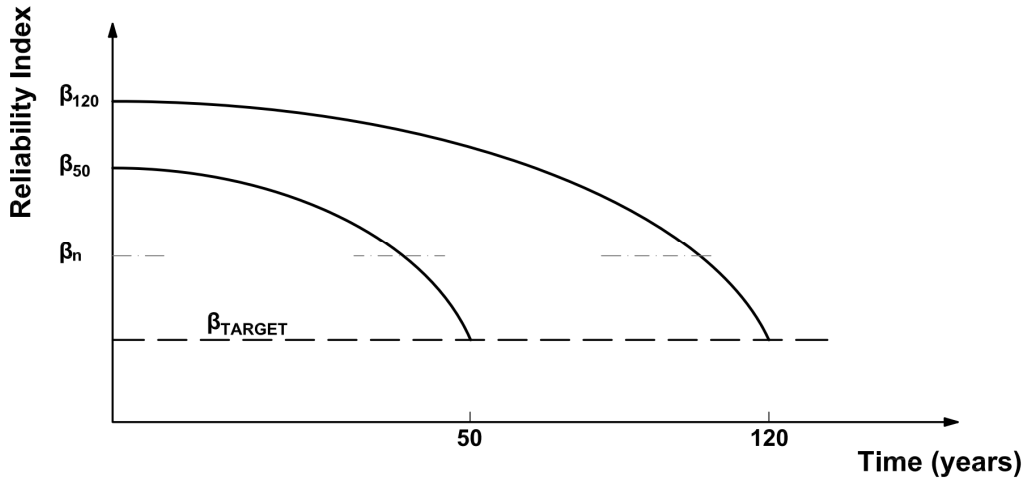

Fig. 1: Exemplary reliability-based service life model

The present paper discusses the adjustment of a tunnel lining's service life through an engineered scaling of the involved partial safety factors, though remaining in consistency with the reliability concepts indicated in EUROCODE 0 [11]. This is achieved through considerations of the reliability level inherited to the structure during design. Firstly, the paper recalls basic statistical elements in order to form a theoretical background of the discussed methodology, including measures of reliability, the nominal safety factor, and the influence of reliability measures in the assessments. At a second stage, the uncertainty of loading and resistance in tunnels is quantified (variation's coefficient) and validated through reliability-based assessments and Probabilistic Finite Elements Analyses (P-FEA) for representative Sprayed Concrete lining (SCL) tunnel structures. This design concept is then presented in a combination with special SCL design assumptions indicating the load sharing between the primary and secondary tunnel SCL support in SCL schemes and the primary lining degradation in long term situations.

1.1 Probability based assessments

In the procedure below, a design safety concept (e.g. an appropriate set of safety factors, or a relevant life-cycle assessment) is adopted and justified to be in line with typical project design standards. This concept is still consistent with the project and structural elements' service life, while the applied safety factors should reflect the intended service life of a structure. Simultaneously, the end of service life is represented by a time-dependent target reliability index (Cornell – β) as per the Annex C of EUROCODE 0 [11]. The action (S) and resistance (R) probability distributions are assumed independent and normally distributed, and the limit state function is determined as $Z = R - S$ (see Fig. 2). In this context, the notion of a structure's *nominal safety* is used (safety with respect to the characteristic values), defined through the nominal safety factor:

$$\gamma_{nom} = \frac{R_{ck}}{S_{ck}} \tag{1}$$

with

R_{ck} characteristic resistance value
S_{ck} load characteristic value

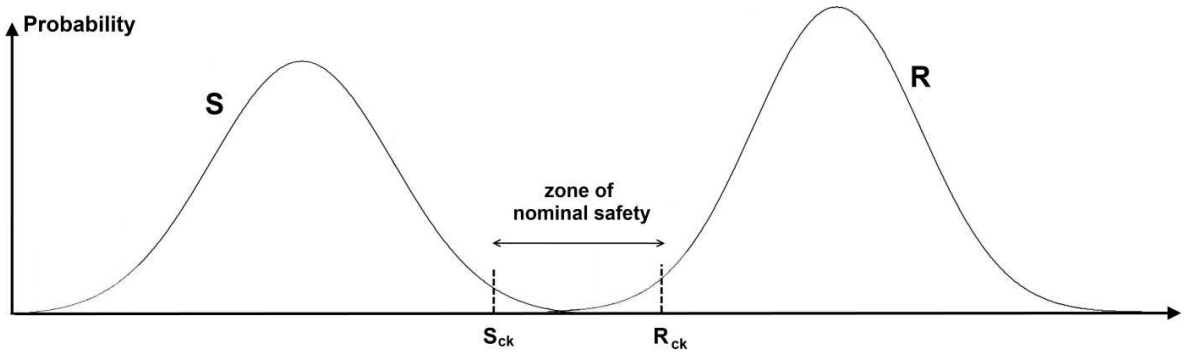

Fig. 2: Representation of resistance and loads of a structure, and the nominal structural safety

Assuming that a structure is at tha limit state of equilibrium between design load S_d and design resistance R_d:

$$R_d = S_d \Leftrightarrow \frac{R_{ck}}{\gamma_R} = S_{ck} \cdot \gamma_S \tag{2}$$

with

R_d design resistance,
S_d design load,
γ_i partial safety factor,
$_{R,\,S}$ indices of resistance and load parameters, respectively.

The structure's nominal (or global) safety factor γ_{nom} can be expressed as

$$\gamma_{nom} = \gamma_S \cdot \gamma_R \tag{3}$$

Cornell's reliability index β can be defined as:

$$\beta = \frac{\mu_R - \mu_S}{\sqrt{\sigma_R^2 + \sigma_S^2}} \tag{4}$$

with

μ_i mean value,

σ_i standard deviation,

or through:

$$\Phi(-\beta) = p_f \tag{5}$$

with

Φ cumulative distribution function of the standardised Normal distribution,

p_f failure probability per annum.

Based on Eq. (5), and assuming that the failure events per year are statistically independent, the values of β_n for different reference periods can be calculated solving the equation (see also the sketch in Fig. 1):

$$\Phi(\beta_n) = \left[\Phi(\beta_1)\right]^n \tag{6}$$

Besides, the characteristic values of resistance and load respectively may be calculated through [12]:

$$R_{ck} = \mu_R \cdot (1 - k \cdot \upsilon_R) \tag{7.1}$$

$$S_{ck} = \mu_S \cdot (1 + k \cdot \upsilon_S) \tag{7.2}$$

with

υ_i coefficient of variation, $\upsilon_i = \sigma_i/\mu_i$

k characteristic value factor accounting for the required statistical confidence and the sample size

Based on the Eqs. (4), (7.1), (7.2), the nominal safety factors γ_{nom} of the structure may be expressed through the equation

$$\gamma_{nom} = \frac{1 - k \cdot \upsilon_R}{1 + k \cdot \upsilon_S} \cdot \frac{1 + \beta \cdot \sqrt{\upsilon_R^2 + \upsilon_S^2 - \beta^2 \cdot \upsilon_R^2 \cdot \upsilon_S^2}}{1 - \beta^2 \cdot \upsilon_R^2} \tag{8}$$

As seen in Eq. (8), the nominal safety factor is related to three main items:

- k, the characteristic value factor (also referred to as fractile coefficient)
- The reliability index β

- The uncertainties in the design parameters, reflected by variation coefficients for the resistance (material) and load parameters.

Eurocode 0 distinguishes between three Reliability Classes (RC) of structures, corresponding to increasing significance (an identical classification has been implemented in the UK). For RC-3 a reliability index of $\beta = 5.2$ is required at year 1 of the structure's life. Besides, the nominal safety factor according to Eq. (3) becomes $\gamma_{nom} = 1.5 \cdot 1.35 = 2.03$. Then taking $k = 1.64$ ("for infinite trials"), and assuming $\upsilon_R = \upsilon_S = \upsilon$, a variation coefficient of approximately $\upsilon = 0.13$ is estimated by solving Eq. (8). As also shown in the following, these variation coefficient values may be of strong influence to the calculations, and are further investigated and validated independently through a probabilistic FE analysis and a reliability-based back analysis of the EUROCODE 2 [12] provisions for the actions and the resistance side respectively. At this point it should also be noted that mainly dead loads are considered in the present study, as live loads (e.g. traffic) have much lower, essentially negligible effects.

2 Probability-based verification

2.1 Variation coefficient for loads through probabilistic FE analyses

In order to assess a range of the loads that may act in a lining, a set of probabilistic FE analyses were performed by a combination of the Phase2 – Rocscience FE program and the Point Estimate Method (PEM) for sampling [14], which has been shown to be well applicable in real life tunnelling problems [16]. In particular, the PEM is a practice – oriented sampling method that constructs a sample for each input stochastic variable by the definition of its mean value and standard deviation, i.e. two points: $\mu_{\underline{X}} \pm \sigma_{\underline{X}}$ (see Fig. 3). The advantage of this method is that it requires a low number of simulations, while the input is within the capacities of routine geotechnical investigations, or even engineering judgements of a upper-bound / best-estimate / worst-credible range of soil parameters (e.g. "the shear strength of this soil at this depth is a hundred plus-minus 50 kPa"). For all its simplicity, this method uses a small amount of information to construct the probability distributions of samples and deliver results. So, in certain circumstances it may be overtaken in accuracy by more advanced non-deterministic FE methods (e.g. Monte Carlo). However in the present case of the assessment of coefficients of variation, the PEM lies per definition within the scope of the problem.

Two tunnel cross sections were elaborated through 2D plane-strain non-linear FE analyses. The first cross section simulates an ovoid tunnel ("Tun_", Fig. 4) excavated in a Top-Heading, Bench, Invert sequence, with a thickness of 350 mm for both the primary and the secondary lining. The other is an elongated cavern ("Cav_", Fig. 5), also excavated in a Top-Heading, Bench, Invert sequence, but with two side-drifts. In this cavern the primary and the secondary linings are 500mm and 400mm thick respectively. Both geometries are adapted by models prepared by the author in the Cat. 3 independent design checks of Crossrail SCL structures and both tunnels are assumed to be located within a London Clay stratum. The geological model and the range of parameters used have been selected based on an extensive survey of available geotechnical information on major recent SCL projects

[17]−[21] and have been juxtaposed to other relevant publications [22], [23], so they represent typical tunnelling conditions in London Clay in Central London.

The numerical models implemented non-linear Mohr-Coulomb plasticity with a graded mesh of 6-noded triangular solid material elements and Timoshenko-beam elements to model the ground and the liners respectively. The procedure included an undrained analysis in the construction phase followed by a switch to drained parameters with pore water pressure for the long term condition after installation of the secondary lining. In the undrained part, the soil was considered to be effectively watertight because of London Clay's very low permeability, which blocks the pore-water flow in short term. In that case, a total stress analysis is carried out with the undrained shear strength parameters to simulate this short term behaviour of the soil. In drained analyses the soil is considered to be permeable; therefore, the excess pore water is able to dissipate as expected to happen in the long term in London Clay. In this situation, an effective stress analysis is switched in the model with the drained strength parameters to simulate the long term behaviour of the system. The primary and the secondary lining were assumed fully bonded (composite action). A surface surcharge of 75 kN/m^2 was also applied.

In order to simulate the stress relief and 3D arching effects during excavation, a relaxation factor was applied in order to simulate the soil deformation prior to advance and installation of the lining at each excavation step. This has been realised through the stiffness reduction method, i.e. the soil within excavation zone was assigned lower elastic parameters (Young's modulus, Poisson's ratio) and the ground was allowed to deform to a new equilibrium before the lining installation. The relaxation factor was estimated to be 75% based on axisymmetric FE calculations carried out in the framework of relevant projects [20], [21], while accurate methodologies and an extensive description of the theoretical background of this modelling approach is given in [24], and [25].

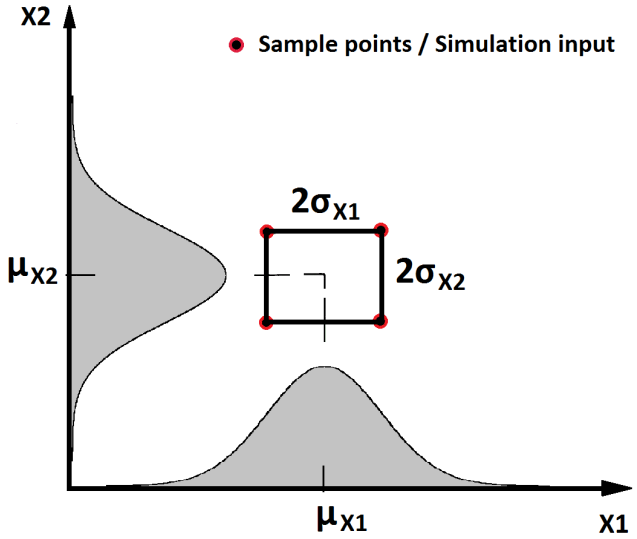

Fig. 3: Representation of the point estimate sampling method for the elementary case of two random variables

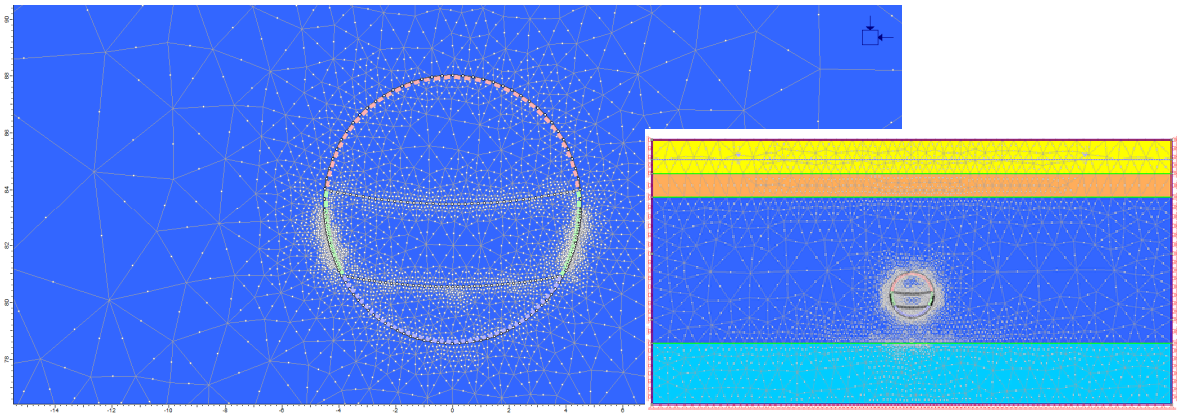

Fig. 4: Overview of ovoid tunnel model (Tun_): Cross section geometry and geological model; tunnel size is 9 × 9.5 m, depth to tunnel axis is 31 m

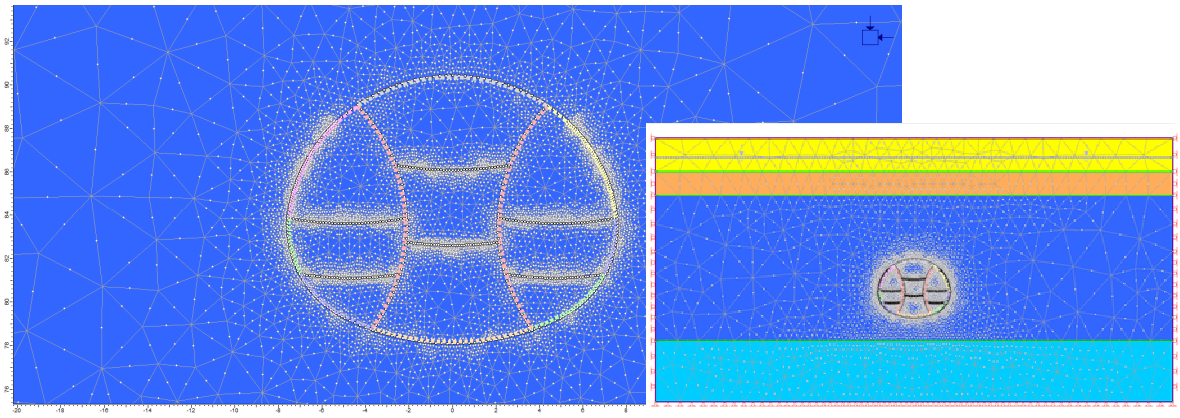

Fig. 5: Overview of cavern model (Cav_): Cross section geometry and geological model; tunnel size is 15 × 12.5 m, depth to tunnel axis is 30.5 m

In this context, the London Clay parameters (averaged from the A3 and A2 formations) have been processed probabilistically at two levels: (a) with variation of the lateral pressure coefficient K_0 and the soil's Young's modulus (_EK_0), and (b) with additional variation of the undrained shear strength (_$EK_0\tau_u$). This total four full probabilistic FE analyses sets (Tun_EK_0, Tun_$EK_0\tau_u$, Cav_EK_0, and Cav_$EK_0\tau_u$) provides an envelope of expected variation coefficients for the loads on the linings. The input parameters are given in Tab. 1, together with the variability of soil parameters for London Clay. The range of the non-deterministic variables reflects a 95% confidence. An overview of the main results for the primary linings (i.e. the lining most affected by the soil parameter variations) of the analyses is provided below in Figs. 6 and 7 and Tab. 2. Based on these analyses it is made evident that the variation coefficient of the hoop forces in primary linings lie on average in the range of $v_{l,S}$ = 0.10 to $v_{l,S}$ = 0.16 (reaching a maximum of 0.20 at the tunnel invert), while the variation coefficient of the hoop forces in secondary linings were substantially lower, as they mainly depend on the (deterministic) pore water pressure. Hence, the original assessment of v_S (= v_R) = 0.13 is proven to be a relevant value.

Tab. 1: Input for the FE models, including the stochastic variation for London Clay

SOIL PROPERTIES		Made ground	River Deposits	London Clay (at tunnel axis)	Lambeth Group
Stratification (thickness)	[m]	3	5	31	> 13
Undr. Young's modulus	[MPa]	10	50	100–300	> 200
Drained Young's modulus	[MPa]	-	-	75–225	>150
Undrained Poisson's ratio	[-]	0.20	0.25	0.45	0.45
Drained Poisson's ratio	[-]	-	-	0.20	0.2
Undrained Friction Angle	[°]	25	40	~ 0	~ 0
Drained Friction Angle	[°]	-	-	22–28	27
Undrained Shear Strength	[kPa]	~ 0	~ 0	100–300	≥ 200
Cohesion	[kPa]	~ 0	~ 0	10	10
Unit Weight	[kN/m^3]	18	20	20	21
K_0 coefficient	[-]	0.5	0.6	0.9–0.3	1.2

Tab. 2: Mean values and variation from the probabilistic FE analyses (averaged)

Model	Hoop Force − Mean value [kN]	Hoop Force − Coef. of Variation [-]
Tun_EK_0	964	0.159
Tun_$EK_0\tau_u$	927	0.162
Cav_EK_0	1 710	0.103
Cav_$EK_0\tau_u$	1 747	0.095

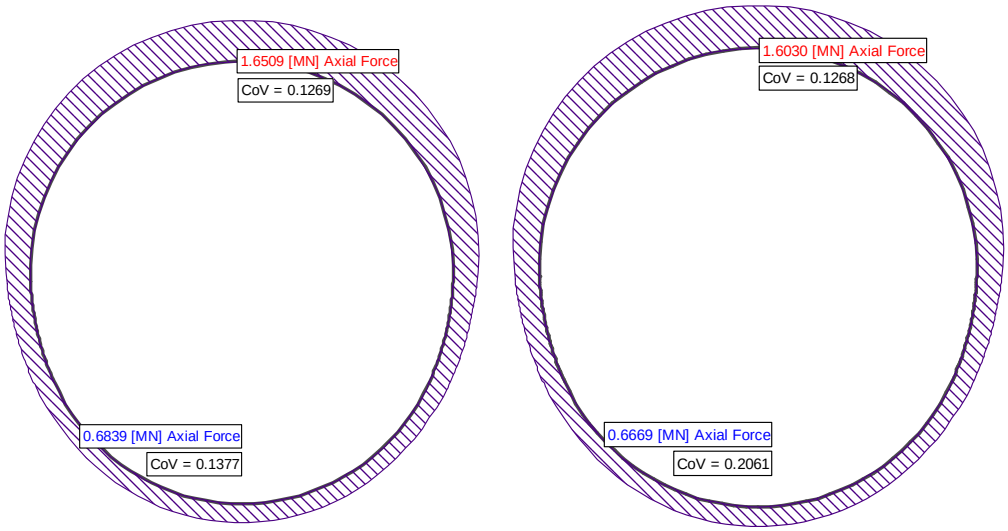

Fig. 6: Average results, and indicative coefficients of variation, for the primary lining hoop forces of the models Tun_EK$_0$ (left) and Tun_EK$_0\tau_u$ (right)

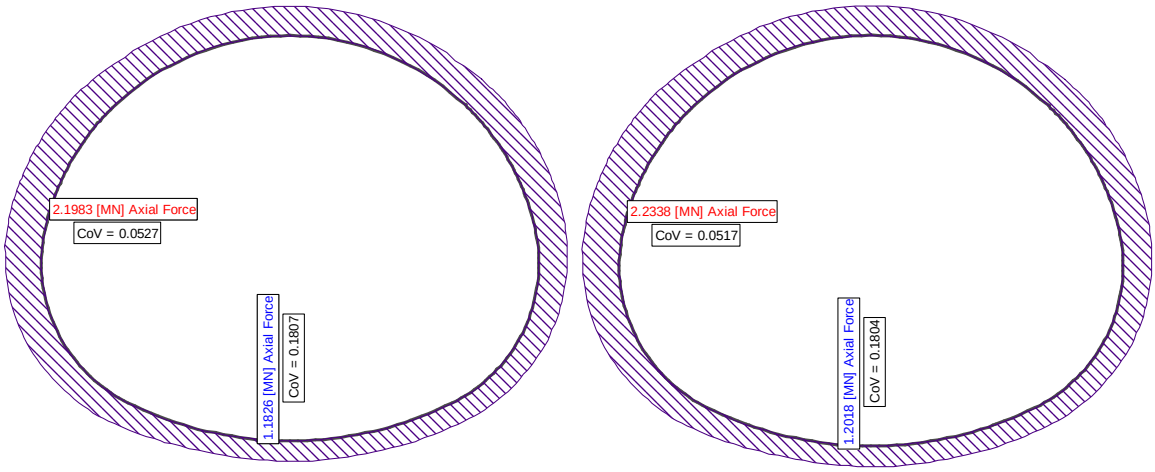

Fig. 7: Average results and indicative coefficients of variation, for the primary lining hoop forces of the models Cav_EK$_0$ (up) and Cav_EK$_0\tau_u$ (down)

2.2 Variation coefficient of concrete's resistance in accordance to EC2

According to EUROCODE 2 [12] for normal strength concrete, the relationship between the mean compressive strength value f_{cm} and the characteristic value f_{ck} is expressed by Eq. (9). Then according to Eq. (7.1) with $k = 1.64$, and for concrete classes between C25/30 to C45/55, the variation coefficient of concrete's compressive resistance is estimated to be in the range of $\upsilon_{c,R} = 0.09$ to $\upsilon_{c,R} = 0.15$ and the original estimate of υ_R (= υ_S) = 0.13 again lies within this reasonable range.

$$f_{ck} = f_{cm} - 8 \text{ MPa} \tag{9}$$

3 Adjustment of safety factors

As currently applied in the Eurocode, a 50 year design service life for the RC3 category of structures is achieved with a reliability index at the end of the design service life equal to $\beta = 4.3$. Back calculating Eq. (6) and for different Design Service Life Categories (DSLC's), the following reliability indices need to be prescribed at the design, i.e. at the beginning of the structures life (year 1):

- for $\beta_{120} = 4.3$, then $\beta_1 = 5.26$
- for $\beta_{50} = 4.3$, then $\beta_1 = 5.10$
- for $\beta_{10} = 4.3$, then $\beta_1 = 4.79$.

Consequently, nominal safety factors for DSLC-1 (10 years) and DSLC-2 (120 years) are back-calculated through Eq. (8) and are provided as design guidance in Tab. 3. The nominal safety factors for a design life on 1 year only, i.e. for $\beta_1 = 4.3$, is also included. These values are envisaged to apply only for structural concrete under dead-load conditions. Tab. 3 shows the estimated nominal safety factor ($\gamma_{nom} = \gamma_S \cdot \gamma_R$) for $\upsilon_R = \upsilon_S = 0.13$.

It should be noted that, as recommended in [11], it is seen as generally more practical to adjust the system's reliability through adjustments of the load safety factors instead of material safety factors. Hence, the values of Tab. 3 may be divided by $\gamma_R = 1.50$ (= γ_c for concrete: this is possible since only concrete is used in the structure, and only short-term transient or persistent situations are examined, so no creep is assumed to develop) in order to obtain a load safety factor and apply it in the design load calculation.

Tab. 3: Pursued nominal safety factors acc. to Eq. 8 ($k = 1.64$; $\upsilon_R = \upsilon_S = 0.13$)

Indicative Service life	γ_{nom} (ULS)	γ_R	γ_S
1 year	1.63	1.50	1.09
10 years	1.89	1.50	1.27
50 years	2.12	1.50	1.41
120 years	2.25	1.50	1.50

4 Application on the design of SCL tunnel structures

In SCL tunnels, primary (or initial) support is provided mainly by sprayed concrete. The design of the primary support and in particular the sprayed concrete lining is governed by requirements in terms of expected ground loads and permissible deformations. The secondary (or permanent) lining may generally be formed from cast in-situ or sprayed, reinforced or unreinforced concrete in order to resist all long term loadings and to provide the desirable finishing for operational reasons. The permanent lining is generally formed after movements of the ground/primary lining have effectively ceased or stabilised. Consequently, it typically comes under load due to long term pore water pressure changes in the surrounding ground and if/when the primary lining deteriorates and loses part or its entire load carrying capacity. Special design assumptions can indicate the load sharing between the two linings (primary and secondary) in the long term. Depending on the interface between the primary and secondary lining (sheet or sprayed waterproofing membrane, addi-

tional smoothing layers, contact grouting), and the structural characteristics of the linings (e.g. deteriorated properties of the primary lining due to environment aggressivity, or relative stiffness of the support layers) a level of load transfer to both the primary and secondary lining may be assumed in the long term.

Based on the service life and safety factor considerations above, two schemes of loading assumptions on the primary and secondary supports are given in Tab. 4. If the primary lining is assumed to participate in the long term load bearing behaviour of the tunnel structure, its integrity needs to be verified as a structure with 120 years lifetime and the respective safety factor. Noteworthy is that an alternative design assumption may be that part of the primary lining deteriorates and is neglected on the long term, while the intact part of it may contribute to the tunnel's load bearing behaviour (a similar approach has been considered for the London Crossrail SCL structures). In that case the remaining intact part should be designed with the safety factor associated to the designated design life of 120 years. On the other side, if the entire sprayed concrete layer is assumed to deteriorate, a lower safety factor (e.g. for 1 or 10 year service life) is suggested for the primary support design.

Tab. 4: Design assumptions with differentiating safety factors between the short term (assumed 10 years) and long term (assumed 120 years)

Support system in the long term	Design Assumption
Primary lining and secondary lining combined.	Both support systems are designed for 120 year lifetime. Both the primary and secondary lining are designed with a nominal safety factor of $\gamma_{nom} = 2.25$ ($\gamma_R = \gamma_S = 1.50$).
Part of primary lining and secondary lining combined.	The primary lining is partially degraded in the long term. If applicable, the sacrificial primary lining is designed with a nominal safety factor of $\gamma_{nom} = 1.90$ ($\gamma_R = 1.50$, $\gamma_S = 1.27$). The remaining primary and the secondary lining are designed with a nominal safety factor of $\gamma_{nom} = 2.25$ ($\gamma_R = \gamma_S = 1.50$).
Secondary lining.	Primary Lining is designed for a short service life and secondary lining is designed for 120 year lifetime; the primary lining is fully degraded in the long term, i.e. the primary lining is designed for a short service life with a nominal safety factor of $\gamma_{nom} = 1.90$ ($\gamma_R = 1.50$, $\gamma_S = 1.27$), and the secondary lining is designed with a nominal safety factor of $\gamma_{nom} = 2.25$ ($\gamma_R = \gamma_S = 1.50$).

5 Conclusions

A need for increased service life of large infrastructure projects – as for example tunnelling projects – is discerned, while particularly for the UK a service life demand of 120 years often appears. Besides, Eurocodes which have been recently introduced, cover a service life of 50 years as a standard. Therefore, when it comes to large infrastructure projects (e.g. Category 3 structures) adjustments of the codified design may be required. At the same time, temporary works or primary linings (which often form a large portion of the project's required resources and budget) could prove to be over-dimensioned for a 50-year target

service life, since the service life of such elements could be actually limited to only a few years. A relevant concern emerges when it comes to design assumptions with combined long-term action of the primary and secondary lining, which extends to various load sharing and degradation assumptions.

Based on the study reported herein a methodology is unfolded, in order to design the service life of tunnel linings per each assumption, with an appropriate adjustment of the respective safety factors in an LRFD framework.

With the assumptions and calculations presented herein, the design of a tunnel structure for a service life of 120 years can assign a safety factor of 1.5 for dead loads on concrete linings. Under the same conditions and for a temporary tunnel structure with a service life of less than 10 years the safety factor for dead loads may be 1.27. The concrete material safety factor (1.50) should be maintained.

Applicability of the main assessment concept is not excluded from other types of tunnel structures and it can serve as guidance for similar design adjustments for various types of structures in the UK with increased design service life demands.

Literature

[1] BSi (British Standards Institute). NA to BS EN 1990:2002+A1:2005: UK National Annex for Eurocode. Basis of structural design. BSi, London, 2004

[2] DfT (Department for Transport) – Highways Agency. Interim Advice Note 95/07. DfT, 2007. www.dft.gov.uk/ha/standards/ians/ (accessed on 04.02.2013)

[3] Budelmann, H., Holst, A., Wachsmann, A. Durability related life-cycle assessment of concrete structures: Mechanisms, models, implementation. In: Strauss, A., Frangopol, D.M., Bergmeister, K. (eds.). *Life-Cycle and Sustainability of Civil Infrastructure Systems*. London: Taylor & Francis Group, 2013

[4] Yuan, Y., Bai, Y., Liu, J. Assessment service state of tunnel structure. *Tunnelling and Underground Space Technology* 27(1) (2012), p. 72–85

[5] Schiessl, P., Gehlen, C., Kapteina, G. Assessment and service life updating of existing tunnels. In *First International Symposium: Safe & Reliable Tunnels*. Prague: ITA-AITES, 2004

[6] Kasper, T., Edvardsen, C., Wittneben, G., Neumann, D. Lining design for the district heating tunnel in Copenhagen with steel fibre reinforced concrete segments. *Tunnelling and Underground Space Technology* 23(5) (2008), p. 574–587

[7] BTS, ICE (British Tunnelling Society, Institution of Civil Engineers). *Tunnel Lining Design Guide*. London: Thomas Telford, 2004

[8] Bergmeister, K. Life-cycle design for the world's longest tunnel project. In: Strauss, A., Frangopol, D.M., Bergmeister, K. (eds.). *Life-Cycle and Sustainability of Civil Infrastructure Systems*. London: Taylor & Francis Group, 2013

[9] Frangopol, D.M., Kallen, M.J., van Noortwijk, J.M. Probabilistic models for life-cycle performance of deteriorating structures: review and future directions. *Progress in Structural Engineering and Materials* 6(4) (2004), p. 197–212

[10] fib (The International Federation for Structural Concrete). *fib - Bulletin N° 65: Model Code 2010 − Final draft, Volume 1*. Lausanne: fib, 2012

[11] CEN (European Committee for Standardization). EN 1992-2002: *Eurocode 0, "Basis of Design"*. Brussels, Belgium: CEN, 2002

[12] Ditlevsen, O. and Madsen, H.O. *Structural Reliability Methods.* Lyngby: Technical University of Denmark, 2007

[13] CEN (European Committee for Standardization). *EN 1992-1-1: Eurocode 2, "Design of concrete structures − Part 1: General rules and rules for buildings*." Brussels: CEN, 2002

[14] Ang, A.H.S., Tang, W.H. *Probability Concepts in Engineering*, 2edn. New York: Wiley, 2007

[15] Rosenblueth, E. Point estimates for probability moments. *Proc. Nat. Acad. Sci.* USA 72(10) (1975), p. 3812–3814

[16] Nasekhian, A., Schweiger, H., Marcher, T. Point Estimate Method vs. Random Set – A case study in Tunnelling. In Huber, Moormann & Proske (eds.) *Proceedings 10th International Probabilistic Workshop*. 2012, p. 243–256

[17] London Underground. *Tottenham Court Road Station Upgrade, Geotechnical interpretative report.* London, 2007

[18] Tubes Lines Ltd. *Green Park Station step-free access. Geotechnical interpretative report.* London, 2009

[19] Crossrail C121 *Non Linear Numerical Modelling Parameters – Rev 2.* London, 2011

[20] Dr. Sauer and Partners Ltd. *Crossrail C121 – Independent Check Work Plan – Whitechapel Station.* London, 2011

[21] Dr. Sauer and Partners Ltd. *Crossrail C121 – Independent Check Work Plan – Fisher Street Shaft.* London, 2012

[22] Hight, D. W., Gasparre, A., Nishimura, S., Minh, N. A., Jardine, R. J., Coop, M. R. Characteristics of the London Clay from the Terminal 5 site at Heathrow Airport. *Géotechnique* 57(1) (2007), p. 3–18

[23] Bond, A., Harris, A. *Decoding Eurocode 7*. London: Taylor & Francis, 2008

[24] Möller, S. "Tunnel induced settlements and structural forces in linings" *Universitat Stuttgart, Mitteilung* 54 (2006)

[25] Moedlhammer, H. *Numerical Methods for Tunnelling using ABAQUS and Investigation of Long-Time-Effects of the Shotcrete Shell and its Impact on the Combined Support System.* 2010 Marshall Plan Scholarship Paper, University of Leoben, 2010

Calcium hydroxide ($Ca(OH)_2$) as a component of scaled deposits in tunnel drainage systems

Michael Stur [a], Franz Ottner [a], Tobias Schachinger [b], Karin Wriessnig [a]

[a]Institute of Applied Geology, University of Natural Resources and Applied Life Sciences, Vienna
[b]ÖBB-Infrastruktur AG, GB Engineering services, OE Tunneling, Vienna
michael.stur@boku.ac.at

Abstract: Due to problems with scaled deposits in the drainage system of the Lainzer Tunnel studies were carried out to understand and to reduce this problem. Scaled deposits are precipitations of dissolved compounds, usually calcium carbonate, in drainage systems. They are triggered by changes in chemical equilibria and they result in a complicated and expensive maintenance of drainage pipes. The main aim of the studies was trying to understand how the scaled deposits are formed in the drainage pipes of the Lainzer Tunnel. For this reason samples from different parts of the Lainzer Tunnel were analyzed in order to gain an overview of the mineral composition of the scaled deposits. The drainage water regime in the Lainzer Tunnel was investigated too. The data were compared with samples from other tunnels and literature. Surprisingly, it was verified that besides of calcium carbonate also calcium hydroxide ($Ca(OH)_2$) can precipitate in drainage pipes in the form of scaled deposits. This is described in the following paper. In 15 samples of scaled deposits calcium hydroxide was detected. Up to today this compound has never been detected in this setting.

Keywords: Calcium hydroxide, portlandite, scaled deposits, encrustations, sinter formation, drainage system, tunnel, aqueous solutions, concrete, elution

1 Introduction

Drainage systems in tunnels are used to reduce groundwater pressure on the tunnel lining and to drain off water. Due to the use of shotcrete and other cementeous support elements and

the chemical composition of the groundwater, drainage water contains many dissolved components like calcium, magnesium, silicium, etc. The precipitation of dissolved components in drainage systems, triggered by changes in chemical equlibria, are called scaled deposits, encrustations or sinter formation. Until 2011 the general opinion was that only calcium carbonate and magnesium hydroxide precipitate in the drainage systems of tunnels as scaled deposits BENEDIX, GAMISCH AND GIRMSCHEID, DIETZEL ET.AL, RINDER ET.AL and VDZ [1, 4, 8, 14, 17].

If the drainage system is clogged by scaled deposits, it is possible that groundwater pressure on the tunnel structure increases. This can cause damages on the tunnel structure, especially on the inner lining.

In 2010 and 2011 problems arising from scaled deposits of drainage pipes in the Lainzer Tunnel (Vienna, Austria) were investigated in order to evaluate possible mitigation strategies.

Sometimes it is tried to use solid or liquid "hardness stabilizators" either to reduce or to avoid scaled deposits or to change the texture of the scaled deposits built by calcium carbonate DOTZLER ET. AL, GALLI, GAMISCH AND GIRMSCHEID and KLEIN ET. AL [5, 7, 8, 10].

In the Lainzer Tunnel for example polyaspartic acid $(C_4H_5NO_3)_n$ was used as crystallization inhibitor.

A sketch of the investigated area is shown in Fig. 1.

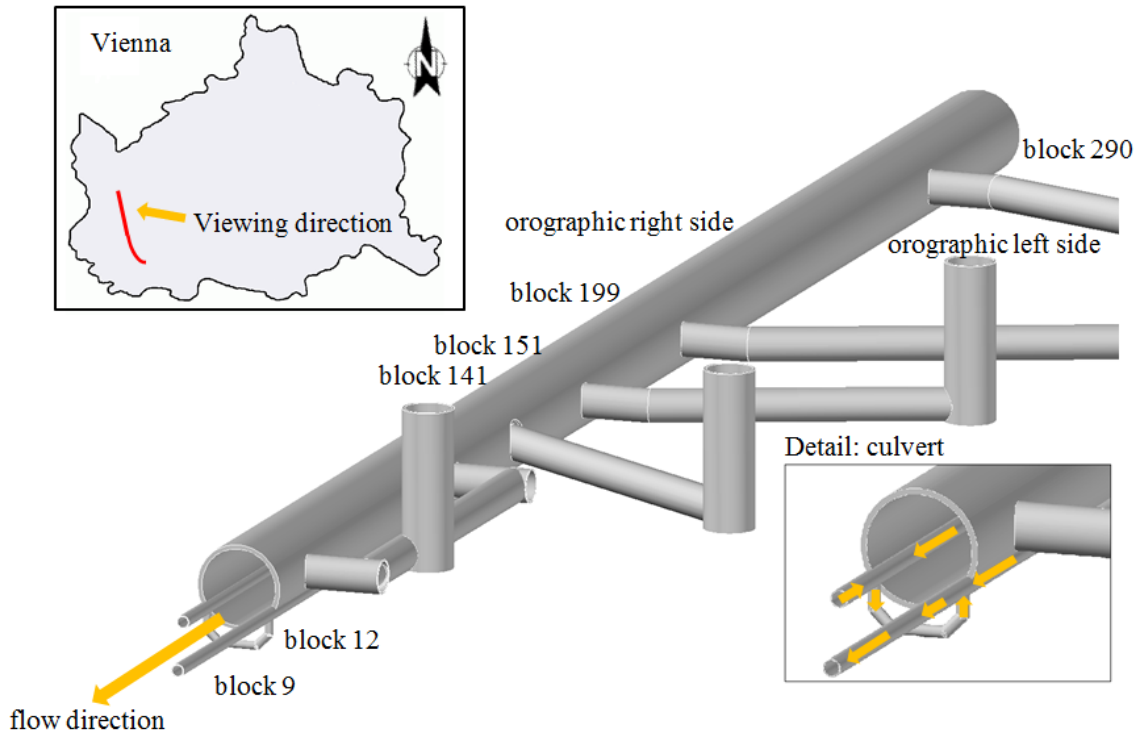

Fig. 1: Sketch of the investigated area of the Lainzer Tunnel in the south eastern part of Vienna and a scheme of the tunnel; the emergency exits are situated orographically left

Samples from different sites in the Lainzer Tunnel and from other tunnels were periodically examined (Fig. 2). The results of the analyses were compared and evaluated.

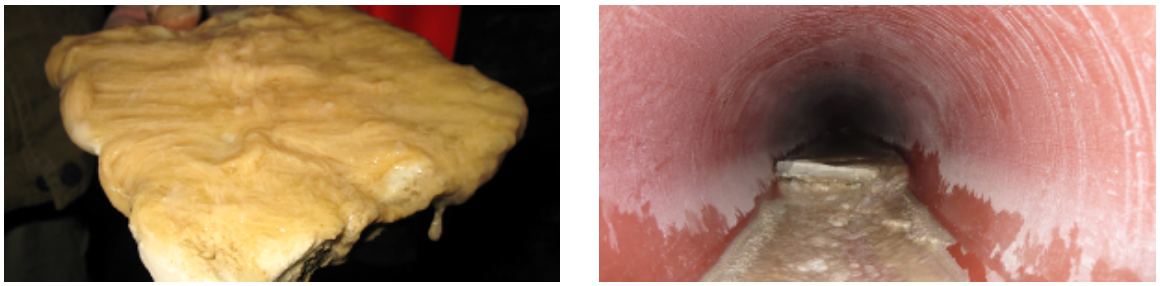

(a) A sample of scaled deposits with a layer of algae (Sample Nr. 10.905)

(b) Not removable very hard scaled deposits

Fig. 2: Samples of scaled deposits from the Lainzer Tunnel; both contain calcium carbonate and calcium hydroxide STUR [16]

The following aspects had to be considered too:

- structural engineering: information about the different support elements and the used concrete;
- concrete chemistry: depending on the used concrete the groundwater is influenced by the concrete in a very local area;
- geology: the Lainzer Tunnel is situated in the Flysch zone; generally these rocks are rich in calcium carbonate;
- hydrogeology: depending on the geology the groundwater in these rocks is rich in calcium carbonate;
- actual construction time for different parts of the tunnel works.

Methods used to identify the mineral composition of the samples of the scaled deposits were PXRD, STA and FT-IR. The drainage water samples were analyzed by ICP-OES and IC to gather information about the water chemistry. Additionally temperature, electrical conductivity and pH-value were determined.

The authors use the denomination “mineral” for not naturally developed compounds like calcium carbonate, calcium hydroxide and magnesium hydroxide to simplify the depictions in these paper.

These investigations in the Lainzer Tunnel prove that scaled deposits can also be formed by calcium hydroxide. In the knowledge of the authors calcium hydroxide was not mentioned before in this context.

2 Material and methods

2.1 Material – “primary” and “secondary” monitoring network

For these investigations

- 49 solid samples from the Lainzer Tunnel,
- 19 solid samples from the other tunnels (Wienerwald Tunnel, Tunnel St. Marx and City Tunnel Waidhofen/Ybbs),
- 65 water samples from the Lainzer Tunnel,
- 13 water samples from three other tunnels (Wienerwald Tunnel, Tunnel St. Marx and City Tunnel Waidhofen/Ybbs) and
- 16 water samples from eluting experiments in the laboratory of the BOKU

were analyzed.

The "primary" monitoring network was used to gain general information (such as mineralogy of the scaled deposits, main cations and anions, pH and electrical conductivity) on the scaled deposits and the drainage water regime and to define relevant zones for long term measurements (= the secondary monitoring network) in the Lainzer Tunnel. In this first campaign 26 water samples and 26 samples of scaled deposits were taken. Samples were taken especially from intersections between drainage pipes (especially at the crossings of the main tunnel with emergency exits), changes of the flow direction and overflowing structures. Information from the staff about existing problems when cleaning the drainages was used too. The Lainzer Tunnel was put into operation during the long term investigations. For this reason access was not always possible to every area of the system, therefore the selection of points for long term measurements also depended on the possibility of access.

Water samples from different groundwater gauging stations along the tunnel axis also were taken to compare the chemistry of the groundwater and the tunnel drainage water. Due to the little natural groundwater flow it was not possible to take fresh groundwater. Only moldy water which was not representative for the groundwater regime could be taken.

The main results of these investigations were

- spots with samples with pH $>$12.0
- detection of samples containing calcium hydroxide in form of scaled deposits
- electrical conductivities $>$3000 μS/cm and
- relevant spots regarding fluid hydraulics

Using this information a "secondary" monitoring network for long term measurements consisting of eleven measuring and sampling spots was defined. Some analyses (temperature and electrical conductivity) were done in situ in the tunnel, the other ones (water chemistry, PXRD, STA, etc) in the laboratory.

Additionally, investigations to elute shotcrete with different compositions were done in the laboratory to simulate the eluting rate in relation to the age of the shotcrete.

2.2 Methods

2.2.1 Solid samples

All solids collected from the Lainzer Tunnel (Vienna), Tunnel St. Marx (Vienna), Wienerwald Tunnel (Lower Austria) and City Tunnel Waidhofen/Ybbs (Lower Austria) were analyzed by powder X-ray diffraction (PXRD). Depending on the result of the PXRD some samples were also analyzed by infrared-spectroscopy (FT-IR), and simultaneous thermoanalysis (STA). The carbonate content was determined with the Scheibler method according to ÖNORM L1084.

Following methods were used:

- PXRD: X'Pert Pro PANalytical with theta-theta geometry using CuKα-radiation (45 kV, 40 mA) in the range of 2 ° and 70 ° 2 Θ (PAN-alytical B.V.; AA Almelo; The Netherlands);
- FT-IR: Pellets of 300 mg potassium bromide and 1 mg sample were measured with a Perkin Elmer Spectrum 1000 (Perkin Elmer Vertriebs GmbH; Brunn am Gebirge; Austria);
- STA: 50 mg milled ground sample was heated up to 1000 °C with a gradient of 10 °C/min with a STA 409 PC (Erich NETZSCH GmbH and Co. Holding KG; Selb; Germany);
- Carbonate content after Scheibler: according to ÖNORM L1084.

2.2.2 Water samples

All water samples collected from the Lainzer Tunnel (Vienna), Tunnel St. Marx (Vienna) Wienerwald Tunnel (Lower Austria) and City Tunnel Waidhofen/Ybbs (Lower Austria) were analyzed by different methods, like inductively coupled plasma optical emission spectrometry (ICP-OES), ion chromatography (IC), hardness tests, etc.

Temperature and electrical conductivity tests of the samples from the secondary monitoring network were recorded in situ in the tunnel. pH, cations (Al^{3+}, Ca^{2+}, Fe^{3+}, K^{+}, Mg^{2+}, Mn^{3+}, Na^{+}), anions ($SO_4{}^{2-}$, $PO_4{}^{3-}$, Cl^{-}, F^{-}, $NO_3{}^{-}$), total hardness, carbonate hardness, TC (total carbon), NPOC (non purgeable organic carbon) and TIC (total inorganic carbon), and m- and p-value were determined in the laboratory. Statistical analyses (MANOVA – multivariate analysis of variance) with SPSS were done additionally.

Following methods were used:

- Electrical conductivity and temperature: Multi 350i and VARIO Cond (WTW Wissenschaftlich Technische Werkstätten GmbH; Weilheim Germany);
- pH: WTW pH 196 (WTW);

- IC: ICS 900 (Dionex; Thermo Fisher Scientific wissenschaftliche Geräte GmbH; Vienna; Austria);
- ICP-OES: Optima 3000 XL (Perkin Elmer Vertriebs GmbH; Brunn am Gebirge; Austria);
- TC, TIC and NPOC: TOC-L (Shimadzu Österreich; Vienna; Austria);
- Total hardness: titration test (Total hardness test; titration with dropping bottle; Merck KGaA; Darmstadt; Germany);
- Carbonate hardness and m-value: titration test with methylorange and 0,1 M HCl;
- P-value (acidity to pH $= 8.2$): titration tests with phenolphthalein (2 g in 50 ml ethanol) and 0.1 M HCl;
- MANOVA: multivariate analysis of variance ($\alpha = 5\%$; $n = 2$; $N = 39$; Scheffé-test as posthoc test): SPSS 15.0.

3 Results

The data from the secondary monitoring network are shown in Tab. 1, 2 and 3. The data for Fe^{3+}, Mn^{3+}, $PO_4{}^{3-}$; F^- NPOC and TIC are not shown in Tab. 2 and 3.

3.1 Solid samples

Sixty-eight samples of scaled deposits and further 34 solid samples (concrete, rock material, material from eluting experiments; not shown in Tab. 3) were analyzed. Calcium carbonate is the main constituent in most of the samples. In 15 samples of scaled deposits calcium hydroxide $Ca(OH)_2$ was detected. These findings were verified, checked by PXRD and also confirmed by STA and IR-spectroscopy.

The structure of the samples of the scaled deposits is very variable:

The thickness of the scaled deposits in the drainage pipes varies between some mm up to about 15 cm and more. Most of the samples of the scaled deposits have differently coloured layers in the range of white-yellowish to dark-brown.

In some samples layers are not visible. Most of the samples do not show calcium carbonate crystals at macroscopic scale, only a few samples show calcium carbonate crystals up to a size of some mm (Fig. 4).

Some samples of the scaled deposits are fine-grained and soft, other ones are very hard (up to the Mohs hardness of 4) with a plain surface.

The macroscopically visible porosity of the hard samples varies from no porosity to minor porosity. The samples of the scaled deposits containing calcium hydroxide are very hard, not layered and coloured white to white-gray.

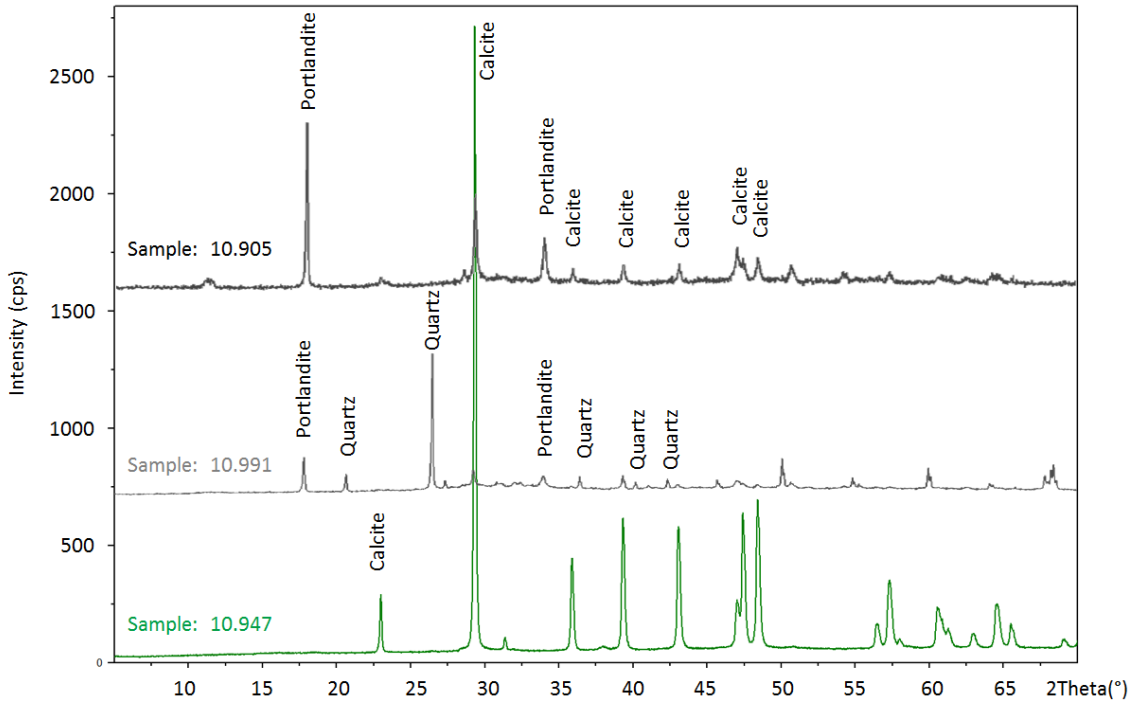

Fig. 3: X-Ray diffractograms of three samples of scaled deposits; 10.947 (calcium carbonate), 10.199 (calcium carbonate, calcium hydroxide and quartz) and 10.905 (calcium hydroxide and calcium carbonate)

Tab. 1: Semi-quantitative PXRD-analysis of the solid samples STUR [16]

ID [1]	Block Nr. and side	Ca	Po	Qz	Do	ID	Block Nr. and side	Ca	Po	Qz	Do
sample from the 22nd of October 2010 - LT						samples from the 10th of March 2011 - LT					
10.905	12/right	XX	X			11.208	199/left	X	X	X	X
						11.209	97/left	XXX			
sample from the 1st of December 2010 - LT						11.210	4/left	XXX		X	XX
10.947	199/left	XXX				11.211	4/left	XXX			
samples from the 2nd of December 2010 - LT						sample from the 6th of Mai 2011 - LT					
10.951	199/left	XXX				11.322	199/left	XXX			
10.952	147/left	XXX									
10.953	147/left	XXX	X	XX		samples from the 16th of Mai 2011 - LT					
10.954	147/left	XX	X	XXX		11.356	4/basin	XXX			
10.955	147/left	XXX	X			11.357	4/basin	XXX			
10.956	199/left	XXX		X							
10.957	197/left	X	X	X	XX	samples from the 27th of Mai 2011 - LT					
10.958	197/left	XXX	X			11.408	290/left	XXX			
10.959	197/left	XXX	X			11.409	290/right	XXX			
10.960	197/left	XXX	X			11.410	12/right	XXX			
10.961	197/left	XX	*			11.411	4/basin	XXX			
10.962	197/left	XX	XX	XXX		11.412	4/basin	XX		*	*
10.990	247/left	XX	XXX	XX							
10.991	247/left	XX	XXX	XXX		additional samples from other tunnels					
10.992	247/left	X	*	X		Tunnel St. Marx (Vienna)					
10.993	247/left	XXX				11.323	ic 37	XXX			

sequel next page

Tab. 1 – sequel

ID	Block Nr. and side	Ca	Po	Qz	Do	ID	Block Nr. and side	Ca	Po	Qz	Do
10.994	12/right	X	X			11.324	ic 40	XXX			
10.995	12/left	XXX				11.325	ic 47	XXX			
10.996	12/left	XXX	*								
10.997	12/left	XXX					City Tunnel Waidhofen/Ybbs				
10.998	12/left	XXX					(Lower Austria)				
10.999	12/left	XXX				11.776	114/right	XX	X	X	X
11.000	12/right	XXX	X	XX		11.777	114/left	XX	X	X	XX
11.001	12/right	XXX	*			11.778	GA3-1	XX	XX	X	
11.002	12/right	XXX				11.779	GA3-2	XXX			
11.003	12/right	XXX				11.780	ee	XXX			
						11.781	oird	XX		X	XXX
	samples from the 10th of March 2011 - LT					11.782	oird	XXX			
11.199	247/left	X	X	X		11.783	oird	XXX		X	
11.200	247/left	X									
11.201	247/left	XXX		X			Wienerwald Ttunnel				
11.202	197/left	X		XXX			(Lower Austria)				
11.203	197/left	X		X	XXX	11.784	43/left	XXX			
11.204	197/left	XXX				11.785	43/left	XXX			
11.205	199/left	XXX				11.786	50/right	XX			
						11.787	72/right	XX		XX	X
	samples from the 10th of March 2011 - LT					11.788	73/right	XX			
11.206	199/left	XX				11.789	73/right	XX			
11.207	199/left	XXX									

ID: sample number; LT: Lainzer Tunnel; XXX: mineral is the main constituent of the sample; XX: mineral is between main and minor constituent of the sample; X: mineral is a minor constituent of the sample; *: traces (< 1 mass-%) of the mineral were detected; Ca: Calcium carbonate; Po: Calcium hydroxide; Qz: Quartz; Do: Dolomite; ee: emergency exit; ic: inspection chamber; oird: outlet into runoff ditch

Fig. 4: A scaled deposit sample (10.957); two different layers: upper dark layer (1) – calcium carbonate, lower bright layer (2) – calcium carbonate with calcium hydroxide STUR [16]

The peaks in a diffractogram (for e.g. Fig. 3) represent the reflections of the X-ray beam

by the different crystal structures of the minerals. The position and relative intensities of the peaks are like fingerprints of minerals. Higher peaks, i.e. higher intensities of reflection (vertical ordinate), mean higher amounts of the detected mineral in the sample.

Three groups of scaled deposits with different mineralogical compositions were identified (Fig. 3). The first group consists mainly of calcium hydroxide. The highest amount of calcium hydroxide was found in sample 10.905. The second group, such as sample 10.991, consists mainly of quartz and calcium carbonate and has a small amount of calcium hydroxide. The third group (most commonly found), represented by sample 10.947, contains pure precipitated crystallized calcium carbonate with more or less other minerals mentioned in Tab. 1.

3.2 Water samples – physical parameters and chemistry

3.2.1 Temperature

The water temperature increases in both drainages downstream between 1.5 and 3.0 °C from block 290 to 9.

3.2.2 Electrical Conductivity and pH

The electrical conductivity varies between 902 and 4670 μS/cm. The electrical conductivity maximum of water in the main drainages was measured in block 290 in both drainages where the right drainage peaked at 4450 μS/cm. In addition an increase in electrical conductivity in the short drainage in block 12 was detected. The pH was also very high (up to 12.95) in the left drainage in block 290. The electrical conductivity as well as the pH decreased (down to 8.54) from block 290 to block 9.

3.2.3 Total hardness, carbonate hardness and p-value

Total hardness showed no detectable trend. In some samples the carbonate hardness was higher than the total hardness.

The carbonate hardness of water from the right drainage is nearly constant, one exception is block 290 where it is very high. Compared to the right drainage, the water of the left drainage shows an increase in carbonate hardness from block 290 to block 9.

Very high p-values were detected in block 290. They decreased between block 290 and 151 from 16.6 mM/l to values about 0.2 mM/l. During the further flow path along the tunnel drainage system the p-value is constant, but shows a correlation with the pH.

3.2.4 Anions and cations

Traces of Al^{3+} were detected only in the samples of December 2010.

In block 290 a very high concentration of Ca^{2+} and K^+ was measured. During the further flow path along the tunnel drainage system the amount of Ca^{2+} and K^+ seems to be constant (Tab. 2).

Mg^{2+} was not found in samples of block 290, but it was detected after the first 1400 m in both drainages. The concentration of $SO_4{}^{2-}$ shows a different trend. The amounts of $SO_4{}^{2-}$ and TC increase from block 290 to 9 in both drainages.

The concentration of Cl^- in the drainage water decreases linearly with an increase of the flow rate in the tunnel. In block 290 a very high amount of Cl^- was detected. The content of $NO_3{}^-$ could be an indicator for dissolved polyaspartic acid.

Tab. 2: Parameters of the water samples taken in the secondary monitoring network of the Lainzer Tunnel STUR [16]

ID	Block Nr. and side	Add. Info	Temp. [°C]	Cond. [μS/cm]	pH	Total hardness °dH	Carbonate hardness °dH	p-value [mM/l]
			samples from the 15th of December 2010					
1	290/right	md	10.5	4450.0	12.4	13.4	45.0	4.0
2	151/right	md	11.1	969.0	9.1	11.5	17.0	0.3
3	19/right	md	11.9	1002.0	9.2	10.8	17.0	0.5
4	12/right	md	12.1	1004.0	9.0	8.8	17.0	0.6
5	12/right	Culvert In	12.1	1007.0	9.4	12.8	22.0	0.0
6	12/right	md short	11.9	1061.0	8.9	11.8	21.0	2.6
7	290/left	md	11.0	2630.0	13.0	13.4	21.0	3.0
8	147/left	md	10.9	988.0	9.8	5.0	15.0	0.4
9	12/left	md	11.6	1008.0	9.6	6.4	12.0	0.5
10	12/left	Culvert out	12.3	1012.0	8.5	11.2	19.0	0.5
11	9left	md	11.7	1005.0	9.41	6.6	18.0	0.5
			samples from the 10th of March 2011					
12	290/right	md	8.8	2130.0	11.8	20.0	23.0	16.6
13	151/right	md	10.0	946.0	8.4	15.0	22.0	0.2
14	19/right	md	11.2	987.0	9.9	15.2	21.0	0.2
15	12/right	md	11.2	979.0	9.0	15.0	22.0	0.0
16	12/right	Culvert In	11.2	977.0	9.0	14.2	21.0	0.0
17	12/right	md short	11.8	1150.0	11.3	16.4	9.1	2.6
18	290/left	md	8.5	2000.0	11.9	16.0	15.0	3.1
19	147/left	md	9.8	933.0	9.0	10.0	18.0	0.6
20	12/left	md	10.5	948.0	8.9	13.4	19.0	0.1
21	12/left	Culvert out	11.2	979.0	9.0	11.6	19.0	0.1
22	9left	md	10.6	955.0	8.94	10.6	43.0	0.8
			samples from the 6th of Mai 2011					
23	199/left	sd ee ic W	10.7	984.0	9.3	12.2	6.4	0.2
24	199/left	md	9.9	902.0	8.47	12.8	26.8	0.4
25	199/left	sd ee ic E	10.6	1084.0	8.7	5.6	9.3	0.5
26	147/left	sd ee ic W	11.1	1949.0	10.2	4.4	10.4	0.6
27	147/left	sd ee ic E	11.4	4670.0	12.4	11.8	26.7	16.8
28	99/left	sd ee ic E	11.6	1000.0	8.5	16.0	8.7	0.5

sequel next page

Tab. 2 – sequel

ID	Block Nr. and side	Add. Info	Temp. [°C]	Cond. [μS/cm]	pH	Total hardness °dH	Carbonate hardness °dH	p-value [mM/l]
			samples from the 27th of Mai 2011					
29	290/right	md	10.2	1675.0	12.0	16.0	14.6	0.4
30	151/right	md	11.2	976.0	8.4	17.2	21.0	0.1
31	19/right	md	11.7	998.0	8.8	17.2	20.8	0.2
32	12/right	md	11.4	1011.0	8.9	17.0	21.9	0.2
33	12/right	Culvert In	11.4	1001.0	8.9	17.2	20.1	0.3
34	12/right	md short	12.0	1708.0	11.9	9.2	10.9	1.2
35	290/left	md	10.9	1919.0	12.0	13.6	10.9	0.3
36	147/left	md	11.0	976.0	8.4	17.6	17.9	0.4
37	12/left	md	11.6	982.0	8.8	15.0	18.5	0.3
38	12/left	Culvert out	11.6	1008.0	8.9	19.8	21.3	0.2
39	9left	md	11.5	987.0	8.8	15.6	21.7	0.3

md: main drainage; sd: side drainage; ee: emergency exit; ic: inspection chamber; E: east; W: west; Block distance: 12 m (290 Blocks = 3480 m); 1°dH Carbonate hardness = 61.1 ppm HCO_3

Tab. 3: Water chemistry of the samples from the Lainzer Tunnel STUR [16]

ID	Al^{3+} [mM/l]	Ca^{2+} [mM/l]	K^{+} [mM/l]	Mg^{2+} [mM/l]	Na^{+} [mM/l]	$SO_4{}^{2-}$ [mM/l]	Cl^{-} [mM/l]	$NO_3{}^{-}$ [mM/l]	TC [mM/l]
				samples from the 15th of December 2010					
1	13.49	6.39	3.56	nbb.	4.67	0.33	2.49	bld	2.53
2	0.88	0.77	1.06	1.15	4.39	1.37	0.82	0.12	6.14
3	1.07	0.87	1.09	1.12	4.74	1.33	0.77	0.13	6.62
4	1.17	0.93	1.15	1.09	4.71	1.41	0.88	0.15	7.81
5	1.00	0.93	1.19	1.10	4.79	1.45	0.91	0.08	7.39
6	0.63	0.43	1.56	bld	bld	1.53	1.36	0.08	3.62
7	1.70	2.93	2.05	bld	5.22	0.85	5.83	bld	1.59
8	1.31	0.20	1.22	0.50	5.68	1.07	2.07	0.17	4.82
9	1.30	0.45	1.20	0.66	5.41	1.22	2.12	0.19	5.35
10	1.24	0.93	1.19	1.08	4.96	1.31	0.89	0.11	8.28
11	1.82	0.64	1.25	0.73	5.19	1.10	1.45	0.10	6.04
				samples from the 10th of March 2011					
12	bld	3.60	1.10	nbb.	1.83	0.42	1.66	0.01	0.52
13	bld	0.75	0.49	0.78	2.88	0.77	0.60	0.04	3.75
14	bld	0.83	0.87	1.27	4.90	0.78	1.02	0.07	3.55
15	bld	0.74	0.95	1.31	5.28	0.72	1.07	0.08	3.21
16	bld	0.70	0.81	1.11	4.36	1.08	0.89	0.06	4.34
17	bld	0.76	0.73	0.83	3.95	0.75	0.76	0.06	3.37
18	bld	2.60	1.05	bld	3.34	0.48	5.10	0.02	0.39
19	bld	0.65	0.56	0.57	4.08	0.87	1.48	0.05	4.81

sequel next page

Tab. 3 – sequel

ID	Al^{3+} [mM/l]	Ca^{2+} [mM/l]	K^+ [mM/l]	Mg^{2+} [mM/l]	Na^+ [mM/l]	$SO_4{}^{2-}$ [mM/l]	Cl^- [mM/l]	$NO_3{}^-$ [mM/l]	TC [mM/l]
20	bld	0.22	0.57	1.01	3.76	1.32	1.46	0.10	6.11
21	bld	0.40	0.58	0.71	2.98	1.22	0.64	0.07	4.47
22	bld	0.39	0.65	0.82	3.85	0.64	1.28	0.09	2.98
				samples from the 6th of Mai 2011					
23	bld	0.84	0.72	0.64	4.32	0.98	2.69	0.21	5.29
24	bld	0.81	0.66	0.87	3.65	1.25	1.32	0.09	6.68
25	bld	0.57	0.31	0.30	7.27	0.79	2.62	0.07	8.33
26	0.00	0.14	7.05	0.01	10.17	1.90	5.60	0.64	6.80
27	0.00	0.05	9.88	bld	16.18	1.71	4.95	bld	8.77
28	bld	1.55	0.46	1.45	4.38	1.41	1.51	0.04	7.57
				samples from the 27th of May 2011					
29	bld	0.15	1.50	bld	2.20	0.83	2.03	0.01	0.41
30	bld	1.07	0.61	1.34	4.44	1.55	0.74	0.06	8.02
31	bld	0.95	0.69	1.35	5.04	1.66	0.81	0.08	7.68
32	bld	1.49	0.75	1.57	6.01	1.62	0.79	0.08	7.65
33	bld	1.27	0.80	1.33	5.00	1.65	0.84	0.09	7.50
34	bld	0.07	2.92	0.98	2.82	1.51	3.39	0.01	0.48
35	bld	0.68	1.24	bld	4.69	0.95	6.14	0.01	0.35
36	bld	1.19	0.60	0.75	4.52	1.15	1.61	0.08	7.10
37	bld	1.34	0.66	0.83	4.09	1.23	1.71	0.09	7.07
38	bld	0.73	0.75	1.30	4.79	1.62	0.81	0.08	7.57
39	bld	1.27	0.70	1.27	5.88	1.41	1.48	0.08	6.97

bld: below limit of determination

3.3 Results of the multivariate analysis of variance – MANOVA

Multivariate analyses of variance were done with the data of Tab. 2 and 3. Shown are only the most significant results of the MANOVA. The distance of 500 m is used for the samples from the 6th of May 2011.

Tab. 4: Multivariate analysis of variance – Ca^{2+}, Mg^{2+} and $SO_4{}^{2-}$

			Subcategory	
	Distance	N	1	2
	Ca^{2+} in mM/l			
Scheffé	500	6	0.66	
	147	3	0.68	
	12	15	0.76	0.76

sequel next page

Tab. 4 – sequel

			Subcategory	
	Distance	N	1	2
	9	3	0.77	0.77
	151	3	0.87	0.87
	19	3	0.88	0.88
	290	6		2.72
	Significance		1.00	0.05
	Mg^{2+} in mM/l			
Scheffé	290	6	0.00	
	500	6	0.54	0.54
	147	3	0.61	0.61
	9	3	0.94	0.94
	12	15	0.99	0.99
	151	3		1.09
	19	6		1.25
	Significance		0.09	0.40
	pH-value			
Scheffé	151	3	8.6	
	9	3	9.0	
	147	3	9.1	
	19	3	9.3	9.3
	12	15	9.3	9.3
	500	6	9.6	9.6
	290	6		12.2
	Significance		1.0	0.071

4 Interpretation of the water chemistry and the MANOVA

The temperature of the drainage water increases downstream from block 290 to 9 as a result of the contact of the water with the warmer atmosphere in the tunnel during the discharge.

Fig. 5 a shows the electrical conductivity, pH and temperature of all water samples from both sides of the Lainzer Tunnel. The lineup of these three parameters shows that there are no correlations.

The high carbonate hardness describes indirectly a very high buffering capacity at pH $= 4.3$ of the drainage water, which means that these samples contain a high amount of dissolved hydrogen carbonate ions (HCO_3^- – analogue Eq. 2 in Sec. 5) – as a result of contact with cementeous material.

During the flow downstream from block 290 to 9 the concentration of the ions in the water samples changes. The multivariate analysis of variance shows, that:

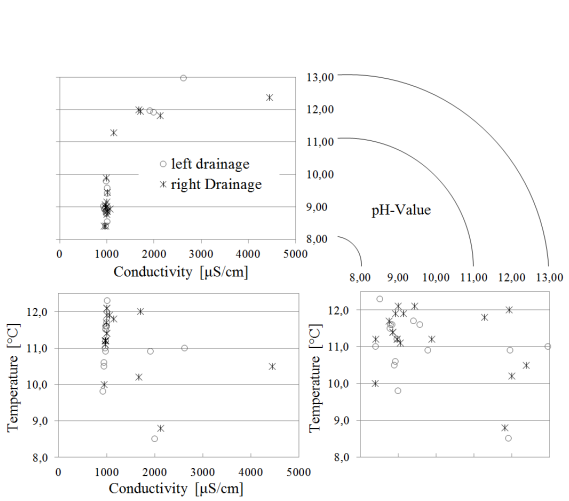

(a) Direct comparison of physical parameters of all water samples from both sides of the Lainzer Tunnel

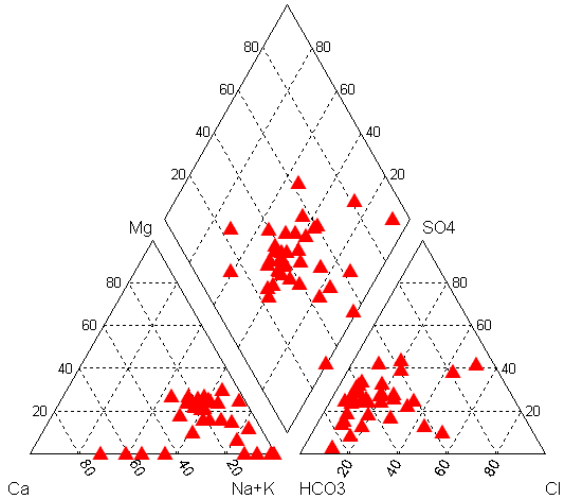

(b) Piper-Plot of the samples of the Lainzer Tunnel (2^{nd} measuring network)

Fig. 5: Chemical comparison of the water samples of the Lainzer Tunnel using the parameters pH, temperature and electrical conductivity (a) and Mg^{2+}, Ca^{2+}, Na^{+}+K^{+}, $HCO_3{}^{-}$, Cl^{-} and $SO_4{}^{2-}$ (b) STUR [16]

- for the variables temperature, total hardness, Al^{3+}, $SO_4{}^{2-}$ and TC the factor "date" is significant;
- for the variables temperature, electrical conductivity, pH, Ca^{2+}, Mg^{2+}, Cl^{-}, $SO_4{}^{2-}$ and TC the factor "distance" is significant;
- only for the variable Ca^{2+} an interaction between the factors "distance" and "date" is significant.

There are no clearly identifiable trends in the concentrations of the ions between block 290 and block 9. Of course there are changes in the concentrations, but no identifiable trends.

The disappearance of Al^{3+} might be a result of the elution of Al^{3+} from the accelerating admixture. CHABOT AND REHBOCK-SANDER [2] wrote that Na-Al-carbonates were eluted from the accelerating admixture. A correlation or reaction of Al^{3+} with dissolved calcium hydroxide was not detected.

The comparison of the most relevant cations (Ca^{2+}, Mg^{2+}, Na^{+}, K^{+}) and anions (Cl^{-}, $SO_4{}^{2-}$ and $HCO_3{}^{-}$) presented in Fig. 5b shows, that it is not possible to detect a correlation between the different ions.

5 Discussion

Regarding existing literature, usually calcium carbonate seems to precipitate in tunnel drainage systems. This process is controlled by several factors, mainly changes in the carbonate balance, water temperature and fluid hydraulics.

Mainly two equations describe the precipitation of $CaCO_3$ and different steps are necessary to dissolve and precipitate Ca-bonds (Eqs. 1 and 2). This means, if the origin of the scaled deposits in tunnel drainage systems is thought to be groundwater rich in dissolved calcium carbonate, the process is described as follows:

$$CaCO_{3,solid} + CO_2 + H_2O \rightleftharpoons Ca^{2+} + 2C_3{}^{2-} + 2H^+ \tag{1}$$

$$CO_2 + H_2O \rightleftharpoons H_2CO_3 \rightleftharpoons H^+ + HCO_3^- \rightleftharpoons 2H^+ + CO_3^{2-} \tag{2}$$

Both equations are strongly pH-dependent and reversible and are mostly used to describe the precipitation of calcium carbonate.

If it is assumed, that the source of calcium are cementeous support elements, such as shotcrete, anchor mortar, etc., the process is described as follows:

$$Ca(OH)_{2,aq} \rightleftharpoons Ca^{2+} + 2OH^- \tag{3}$$

$$Ca(OH)_{2,aq} + CO_2 \rightleftharpoons CaCO_{3,solid} + H_2O \tag{4}$$

Portland cement clinker is produced by burning (at about 1450 °C) a mix of mainly calcium carbonate, for example limestone or chalk, and an aluminosilicate-rich rock, for example clay or shale. During the reaction of the clinker with the batching water so called calcium silicate hydrate phases (CSH-phases) are built in the cement matrix. These phases are studied well in the cement chemistry BENEDIX, ISOPESCU ET.AL and VDZ [1, 9, 17].

Calcium hydroxide is generated out of the calcium silicate hydrate phases and is enclosed in the pore solutions of the concrete, causing very high pH (because of the high concentration of OH-Ions) in the cement matrix. Thus it is responsible for protecting the reinforcement steel in the reinforced concrete from corrosion VDZ [17]. Calcium hydroxide in the pore solution of the concrete always stays in an equilibrium to the calcium silicate hydrate phases. This means that if the pore solution is saturated with calcium hydroxide, the disintegration of the CSH-phases stops.

This pore solution seems to be a long term source for calcium hydroxide, when the permeating groundwater elutes calcium hydroxide and takes it as an aqueous solution to the drainage pipes. That means that – as long as calcium hydroxide is available – the contact of groundwater with concrete results in a solution of calcium hydroxide, a high concentration of OH-ions in the aqueous solution and thus in very high pH.

The ratio of the Ca^{2+}-sources probably varies, depending on the age of the tunnel (the older the tunnel the less seems to be the leaching of the cementeous support elements) and the chemistry of the surrounding groundwater.

Additionally BENEDIX, CHABOT AND REHBOCK-SANDER, DIETZEL ET.AL, MONTES-HERNANDEZ ET.AL, REARDON AND FAGAN and VDZ [1, 2, 4, 11, 12, 17] described very

high pH above 12 in the drainage systems due to the contact of water with the CSH-phases of the cement.

GAMISCH AND GIRMSCHEID [8] mentioned a so called "calcium hydroxide equilibrium" in aqueous solutions. A calcium hydroxide saturated water in a stable equilibrium has a pH $= 13.05$ and a total dissolved Ca^{2+} of 16.76 mM/l (T = 8 °C and a ionic strength I = 0.01 of the solution). They wrote that only calcium carbonate precipitates from calcium hydroxide saturated water. The amount of precipitated $CaCO_3$ is influenced by the pH-value of the water and the dissolving rate of carbon dioxide. The amount of precipitated $CaCO_3$ in combination with an enrichment of carbon dioxide is higher between pH 13.05 and pH 10.39 than below pH 10.39. Thus, regarding the mentioned calcium hydroxide equilibrium the dissolution of carbon dioxide is responsible for the formation of calcium carbonate scaled deposits between pH 13.05 and 10.39.

REARDON AND FAGAN [12] noted, that calcium hydroxide as a main constituent of the pore solution in the cement matrix is not stable in typical environments of normal aqueous solutions like groundwater.

That means, that literature and reports about scaled deposits in the drainage system of tunnels only deal with the precipitation of calcium carbonate and rarely magnesium hydroxide.

According to the literature, the precipitation of calcium hydroxide from an aqueous solution in solid form, as it was detected by the authors, seems to be very unlikely because calcium hydroxide is not stable in typical environments of normal aqueous solutions.

To the authors' opinion, there could be three possible explanations, how calcium hydroxide is formed as a precipitation in tunnel drainage pipes.

- **The "wash-out-effect":**

  The first theory is that there is something like a "wash-out-effect". Immediate contact of groundwater with the young concrete maybe washes out the calcium hydroxide saturated pore solution. In the pore solution calcium hydroxide particles precipitate immediately, and are transported as a suspension to the drainage pipes where they are deposited as scaled deposits, together with calcium carbonate. The upper layer of the hardened deposited calcium hydroxide is in contact with the drainage water, being enriched in CO_2 during the further construction time of the tunnel. The reaction with carbon dioxide leads to the carbonatization of the calcium hydroxide ($Ca(OH)_2$) of the upper layer. So this upper layer of calcium carbonate acts as a protection for the lower parts of the scaled deposits containing calcium hydroxide.

  The layer structures of some samples of scaled deposits (Fig. 4) might confirm this theory. The upper dark layer had contact with carbon dioxide, thus it consists of calcium carbonate. The brighter layer was calcium carbonate with calcium hydroxide as a minor constituent of the sample as a result of less contact with carbon dioxide. Some smaller samples of scaled deposits were also taken from similar spots like the sample 10.957. All other smaller samples from this location did not have any traces of calcium hydroxide. Thus it is possible, that the carbonatization of calcium hydroxide to calcium carbonate in these samples was already finished.

- **Dissolved carbon dioxide:**

  The second theory is, that there is too little dissolved carbon dioxide in the drainage water to fit Eq. 4 (reaction of carbon dioxide with calcium hydroxide). Especially during the early stages of construction time of a tunnel, the elution of calcium hydroxide out of the cementeous support elements seems to be high, therefore there could be an environment where there is too much solved calcium hydroxide in the drainage water compared to the available carbon dioxide. Then, under special conditions not only calcium carbonate, but also calcium hydroxide precipitates out of the drainage water in form of scaled deposits.

  During the further construction time the chemistry of the drainage water changes, as mentioned before, it seems that the leaching of cementeous support elements is reduced with the age of the tunnel. The available amount of CO_2 stays the same compared to the decreasing amount of calcium hydroxide. At some point there is enough CO_2 to fulfil Eq. 4, and thus just calcium carbonate precipitates.

  DUCHESNE AND REARDON [6] point out that calcium hydroxide dissolves better at lower temperatures. That means, that higher temperatures lead to an increase of degasing CO_2 and with it to a deficit of dissolved carbon dioxide.

  VDZ [17] calculated that water with a temperature of 20°C dissolves 215.95 mM/l of calcium hydroxide ($Ca(OH)_2$) while the dissolving rate decreases with increasing temperature. REGNAULT ET.AL and ROQUE ET.AL [13, 15] proved this theory experimentally. The temperature in the Lainzer Tunnel increases in both drainages during the discharge from block 290 to 9, and calcium hydroxide was found only downstream after an increase of temperature.

  At higher temperatures less carbon dioxide is dissolved in the water resulting in less calcium hydroxide being transformed into calcium carbonate.

- **Reaction with magnesium hydroxide:**

  The third theory, for small amounts of calcium hydroxide precipitated as scaled deposits in tunnel drainage systems might be a reaction of brucite ($Mg(OH)_2$) with the dissolved Ca^{2+}. DIETZEL ET. AL and RINDER ET.AL [3, 4, 14] noted that magnesium hydroxide (brucite) can be precipitated as scaled deposits in the drainage systems of tunnels. Magnesium hydroxide was not found in the Lainzer Tunnel, but an exchange of anions in form of a substitution of the magnesium by the calcium might be possible.

  This theory of the exchange of ions is described in Eq. 5.

$$Mg(OH)_2 + Ca^{2+} \rightleftharpoons Ca(OH)_2 + Mg^{2+} \tag{5}$$

6 Conclusions

It was verified for the first time that besides of calcium carbonate also calcium hydroxide ($Ca(OH)_2$) can precipitate in drainage pipes in the form of scaled deposits. At the moment

it is not clear, if the occurrence of this phenomenon happens more often. The possible time dependent changing mineralogy of the scaled deposits might be the reason that calcium hydroxide was not detected earlier.

Mostly investigations and measurements are initiated years after construction of the tunnel as a reaction to maintenance problems caused by scaled deposits. In case of the Lainzer Tunnel (Vienna) and the City Tunnel Waidhofen/Ybbs (Lower Austria) investigations were started much earlier and so it was possible to detect calcium hydroxide ($Ca(OH)_2$) precipitated in the form of scaled deposits in tunnel drainage systems.

Calcium hydroxide maybe shows other characteristics regarding the possibility of removal from the drainages. Some known strategies to mitigate the precipitation of dissolved calcium carbonate or for the curing process of scaled deposits are used.

In the Lainzer Tunnel the crystallization inhibitor polyaspartic acid was used in the primary drainage system. Polyaspartic acid should change the texture and the hardness of the precipitated calcium carbonate. Calcium hydroxide maybe shows other characteristics regarding the possibility of removal from the drainages, in the Lainzer Tunnel scaled deposits containing $Ca(OH)_2$ were very hard and thus it was not possible to remove them in different locations in the drainage system.

For optimal maintenance in the future further investigations are necessary. Without any doubt there are several questions that have to be answered, especially why and when calcium hydroxide ($Ca(OH)_2$) precipitates as a component of scaled deposits in tunnel drainage systems and if the known mitigation strategies also work for calcium hydroxide.

Acknowledgements

This research was supported by Austrian Federal Railways, GB Engineering services, OE Tunneling. We thank Johannes Tintner for assistance in statistical tasks and Stephanie Neuhuber for her comments. Special thanks are given to the anonymous reviewers for careful reviewing and important contributions to the improvement of this paper.

Literature

[1] Benedix R. *Bauchemie*. Stuttgart: B. G. Teubner Verlag / GWV Fachverlag GmbH, 2006

[2] Chabot J. D., Rehbock-Sander M. Entwässerung bergmännischer Tunnel – neue Tendenzen. *Schweizer Ingenieur und Architekt* 12 (2000), p. 243–249

[3] Dietzel M., Rinder T., Leis A., Reichl P., Sellner P., Draschitz C., Plank G., Klammer D., Schöfer H. Koralm Tunnel as a Case Study for Sinter Formation in Drainage Systems – Precipitation Mechanisms and Retaliatory Action. *Geomechanik und Tunnelbau* 1(4) (2008), p. 271–278

[4] Dietzel M., Rinder T., Niedermayr A., Mittermayr F., Leis A., Klammer D., Köhler S., Reichl P. Ursachen und Mechanismen der Versinterung von Tunneldrainagen. *Berg- und Hüttenmännische Monatshefte* 10(153) (2008), p. 369–372

[5] Dotzler B., Meinlschmidt A., Roschig F.H., Wüstefeld D. Härtestabilisation von Bergwässern. *Eisenbahningenieur* 7(54) (2003)

[6] Duchesne R., Reardon E.J. Measurement and prediction of portlandite solubility in alkali solutions. *Cement and Concrete Research* 25(5) (1995), p. 1043–1053

[7] Galli M. Härtestabilisierung in kalkführenden Entwässerungen. *Schweizer Ingenieur und Architekt*. 12 (2000), p. 249–253

[8] Gamisch T., Girmscheid G. *Versinterungsprobleme in Bauwerksentwässerungen*. Berlin: Beuth, 2007

[9] Isopescu R., Mihai M., Capat C., Olaru A., Mateescu C., Dumitrescu O., Ion U. Modelling of Calcium Carbonate Synthesis by Gas-Liquit reaction Using CO_2 from Flue Gases. *Associazione Italiana Di Ingegneria Chimica*, 2011

[10] Klein T., Mitschker A., Moritz R.J. Zur Hydrolyse von Polysuccinimid und dessen Wirkung gegen Tunnelversinterung *Wasserwirtschaft*, 4 (2004), p. 32–37

[11] Montes-Hernandez G., Daval D., Chiaric R., Renard F. Growth of Nanosized Calcite through Gas-Solid Carbonation of Nanosized Portlandite under Anisorbaric Conditions. *Crystal Growth and Design*, 10 (2010), p. 4823–4830

[12] Reardon E.J., Fagan R. The calcite/portlandite phase boundary: enhanced calcite solubility at high pH. *Applied Geochemistry* 15 (2000), p. 327–335

[13] Regnault R., Lagneau V., Scheider H. Experimental measurement of portlandite carbonation kinetics with supercritical CO_2. *Chemical Geology* 256 (2009), p. 113–121

[14] Rinder T., Dietzel M., Leis A. Calcium carbonate scaling under alkaline conditions – Case studies and hydrochemical modelling. *Applied Geochemistry*, 35 (2013), p. 132–141

[15] Roque J., Molera J., Vendrell-Saz M., Salvad N. Crystal size distributions of induced calcium carbonate crystals in polyaspartic acid and Mytilus edulis acidic organic proteins aqueous solutions. *Journal of Crytsal Growth* 262 (2004), p. 543–553

[16] Stur M. *Versinterungsproblematik in Tunneldrainagen*. Master thesis, University of Natural Resources and Applied Life Sciences, Vienna, 2012

[17] VDZ. *Hydratation des Zements und Gefüge des Zementsteins*. Technical report, Verein Deutsche Zementindustrie, Düsseldorf, 2011

Optimum target reliability for bridges considering emergency situations

Miroslav Sýkora [1], Milan Holický [1], Roman Lenner [2], Pavel Maňas [3]
[1] Klokner Institute, Czech Technical University in Prague, Prague
[2] Institute of Structural Engineering, University of Bundeswehr, Munich
[3] Faculty of Military Technology, University of Defence, Brno
miroslav.sykora@klok.cvut.cz, milan.holicky@klok.cvut.cz,
roman.lenner@unibw.de, pavel.manas@unob.cz

Abstract: Specification of the target reliability levels is one of the key issues of the assessment of existing structures in emergency situations. International standards ISO 13822 and ISO 2394 indicate procedures for specification of the target reliability levels by optimisation of the total cost. In the submitted study these approaches in conjunction with the human safety criteria are applied to estimate the target reliability levels of existing bridges considering an emergency situation. Obtained target reliabilities range in most cases from 2.0 up to 3.5 and are significantly lower than those applied in the design of new structures.

Keywords: emergency situation, failure consequences, human safety, optimization, target reliability

1 Introduction

The target reliability levels recommended in various national and international documents for new and existing structures are inconsistent in terms of the recommended values and the criteria according to which appropriate values are to be selected. According to HOLICKY [4] almost no recommendations are available for temporary structures and this holds likewise for structures under temporary conditions including emergency situations.

This study aims to develop a general procedure for the assessment of target reliabilities of structures during emergency situations. According to the definition of the Ministry of Interior of the Czech Republic an emergency situation is considered here to be the situation caused by the threat of an origin of or as a consequence of an extraordinary event that is managed in a standard way by cooperation of the emergency services of the Integrated Rescue System, national security system, system of the protection of economy, defence etc. together with relevant authorities in the framework of their competences and common procedures, without the declaration of crisis states. Extraordinary events can be caused by natural disasters, accidents, threat to a critical infrastructure, diseases, threat to the internal

security of the state and economics. In this study a particular focus is put on road bridges exposed to loads due to passages of heavy military and civilian traffic.

Target reliabilities related to emergency situations can be required for:

1. Design of new bridges considering possible occurrence of the emergency situation (with considerations of low occurrence probability of the situation, potentially high consequences of bridge failure and relatively low costs of safety measures − increases of structural resistance),
2. Assessment of temporary bridges (special-purpose structures erected due to the emergency situations, with a given resistance and high costs of safety measures),
3. Assessment of existing bridges when immediate decisions on permissions for crossing of heavy freights are needed (bridge resistance cannot be readily increased).

This study focuses on the third case only. Some modifications would be needed to adjust the proposed technique for the first two cases.

Hereafter an emergency situation is assumed to last few days or weeks. Note that applications of the proposed technique are in principle not constrained by the duration of the emergency situation and even purpose of the structure. Though adjustments might be needed e.g. for assessment of civilian buildings or industrial structures under emergency situations of longer durations.

2 Reliability assessment of existing bridges

It is widely recognised that the reliability assessment of existing bridges differs from design of new structures in a number of aspects including:

- Increased safety levels usually involving more costs for existing bridges than for new bridges.
- The remaining working life of existing bridges often different from the standard design working life of 100 years assumed for new bridges.
- Information on actual structural conditions that may be available for assessment (inspections, tests, measurements).

The first aspect is of particular interest since it might be difficult or even impossible to strengthen a bridge during a short time period of the emergency situation. On the contrary the second and third aspect may apply in the assessment under persistent design situations as the emergency situation is inherently of a shorter duration in comparison with service life of bridges. Moreover, in the emergency situation it is often impossible to obtain detailed information concerning the bridge conditions by means of inspections and testing.

At present, existing bridges are mostly verified using simplified deterministic procedures based on the partial factor method commonly applied in design of new bridges. Such assessments are often conservative and may lead to expensive upgrades. More realistic verification of actual performance of existing bridges can be achieved by probabilistic methods when uncertainties of basic variables are described by appropriate probabilistic models.

Specification of the target reliability levels is required for the probabilistic assessment of existing bridges. In addition, the target reliabilities can be used to modify the partial factors used in a deterministic assessment. VROUWENVELDER AND SCHOLTEN [15] and SYKORA AND HOLICKY [13] recognised that it would be uneconomical to specify for all existing buildings and bridges the same reliability levels as for new structures. This is also demonstrated by the present practice in Canada, the Netherlands and USA, where the target reliability indices for existing structures decrease by about 0.5−1.7 compared with indices for new structures, see CASAS AND WISNIEWSKI [2] and MALJAARS ET AL. [8].

In the probabilistic framework the target reliability levels should be compared with "nominal" structural reliabilities resulting from randomness of basic variables (resistance and load effect variables, model uncertainties) rather than from actual failure frequencies that are dominantly affected by human errors, MELCHERS [9] and VROUWENVELDER ET AL. [17].

3 Target reliability levels in codes

The target reliability levels recommended in EN 1990:2002 *Eurocode − Basis of structural design* are primarily intended for design of new bridges; reliability classes are associated with consequences of failure. More detailed classification is given in ISO 2394:1998 *General principles on reliability for structures* where relative costs of safety measures are also taken into account. The target reliability levels provided in both documents are partly based on calibrations to previous practice and should be considered as indicative only.

ISO 13822:2010 *Bases for design of structures − Assessment of existing structures* indicates a possibility to specify the target reliability levels for existing bridges by optimisation of the total cost related to an assumed remaining working life. This approach in conjunction with the criteria for safety of people in accordance with ISO 2394 is further developed here.

EN 1990 recommends the target reliability index for two reference periods (1 and 50 years), see Tab. 1. These target reliabilities are intended to be primarily used in design of new structures.

Tab. 1: Reliability classification for different reference periods according to EN 1990

Reliability class	Failure consequences	β (1 y.)	β (50 y.)	Examples
RC3	high	5.2	4.3	bridges, public buildings
RC2	medium	4.7	3.8	residences, offices
RC1	low	4.2	3.3	agricultural buildings

The couples of β-values given in Tab. 1 for each reliability class correspond approximately to the same reliability level. For a bridge of RC2, the reliability index $\beta = 3.8$ should be thus used provided that probabilistic models of basic variables are related to the reference period of 50 years. The same reliability level should be reached when $\beta = 4.7$ is applied using the theoretical models for one year. Note that the couples of β-values correspond to the same reliability level only when failure probabilities in individual time intervals (basic reference periods for variable loads) are independent. VROUWENVELDER [16] indicated that

the EN 1990 target reliability index $\beta = 3.8$ could better be interpreted as corresponding to 4.5 per year as complete independency of resistance and loads in subsequent years is not realistic.

Considering a reference period t_{ref}, it might be understood from EN 1990 that the related reliability level can be derived as follows:

$$\beta_{tref} = \Phi^{-1}\{[\Phi(\beta_1)]^{tref}\} \quad (1)$$

with

β_1 target reliability index taken from Tab. 1 for a relevant reliability class and the reference period $t_{ref} = 1$ year,

Φ, Φ^{-1} cumulative distribution function of the standardised normal variable and its inverse function.

However, this concept seems to be hardly applicable for the emergency situations where the reference period can be very small and reliability level excessively increases (for instance $\beta \approx 5.5$ should be considered for $t_{ref} = 1/52$ year = 1 week and RC2).

A more detailed recommendation is provided by ISO 2394 where the target reliability index is given for the working life and related not only to the consequences but also to the relative costs of safety measures (Tab. 2). The target reliability might thus be selected independently of the reference period (duration of the emergency situation) which seems to be a more appropriate approach than that provided by EN 1990. VROUWENVELDER [16] observed that, using Tab. 2, for existing structures the target level usually decreases as it takes more effort to increase the reliability level. So for similar new and existing structures, e.g. moderate costs of safety measures can be considered at a design stage while high costs may apply when assessing the existing structure.

Tab. 2: Target reliability index (life-time, examples) in accordance with ISO 2394

Relative costs of safety measures	Failure consequences:	small	some	moderate	great
High		0	1.5	2.3	3.1
Moderate		1.3	2.3	3.1	3.8
Low		2.3	3.1	3.8	4.3

Similar recommendation is provided by the Probabilistic Model Code of the Joint Committee on Structural Safety (JCSS) [6]. Recommended target reliability indices are also related to both the consequences and to the relative costs of safety measures, however for the reference period of one year. These recommendations also seem to be less suitable for emergency situations.

ISO 13822 indicates four target reliability levels for different consequences of failure (the ultimate limit states):

- Small consequences: 2.3,
- Some: 3.1,
- Moderate: 3.8,
- High: 4.3.

The related reference period is "a minimum standard period for safety (e.g. 50 years)".

In general ISO 2394 seems to provide the most appropriate reliability differentiation for existing bridges in emergency situations since costs of safety measures are taken into account and the reliability levels are associated with a working life (duration of the emergency situation here).

The following additional notes are made concerning available approaches to the target reliabilities:

1. Costs of safety measures might be perceived as an unacceptable factor for the target reliability particularly of new structures.
2. Several empirical models for the assessment of target reliabilities have been proposed in previous studies; SYKORA AND HOLICKY [12] provided a brief overview.

4 Basis of cost optimisation

Lower target reliability levels can be used if justified on the basis of social, cultural, economical, and sustainable considerations as indicated in ISO 13822. ISO 2394 shows that the target level of reliability should depend on a balance between the consequences of failure and the costs of safety measures. From an economic point of view the objective is to minimize the total structural cost.

ANG AND DE LEON [1] and ONOUFRIOU AND FRANGOPOL [10] indicated that the expected total costs C_{tot} may be generally considered as the sum of the expected costs of inspections, maintenance, upgrades and costs related to failure of a bridge. The objective is to optimise relevant decision parameters *d,* represented by factors affecting the resistance, serviceability, durability, maintenance, inspection, upgrade strategies, etc. In the present study the decision parameter is assumed to concern mainly the immediate upgrade while inspection, maintenance and future repair or upgrade strategies are influenced marginally. This may be a reasonable assumption in many practical cases. Implications for the assessment in emergency situations will be clarified in the following.

An upgrade of the bridge, immediately undertaken during the emergency situation, may in general lead to the following costs:

- Cost C_0 independent of the decision parameter - economic losses and potential societal consequences (injuries or fatalities) caused by temporary bridge closure in the emergency situation due to upgrade works,
- Marginal cost C_m per unit of the decision parameter.

Estimation of the cost C_0 may be a difficult task and expert judgements may be necessary. However, it is further assumed that the upgrade costs C_0 and C_m can be reasonably estimated.

The main reason for the existence of civil infrastructures is the public interest. Therefore, all related societal aspects should be considered when assessing the failure consequences C_f. Depending on a bridge concerned, failure may be associated with the following consequences:

- Potential societal consequences directly caused by the failure (collapse),

- Cost of repair or replacement,
- Economic losses and potential societal consequences caused by temporary bridge closure in the emergency situation due to upgrade works; these may also include potential losses due to damage on detour routes,
- Possible other consequences such as unfavourable environmental or psychological effects.

Estimation of the failure cost is a very important, but likely the most difficult step in the cost optimisation. It is important to include not only direct consequences of failure (those resulting from the failures of individual components), but also indirect consequences (related to a loss of the functionality of a whole bridge). Background information for consequence analysis is provided by IMAM AND CHRYSSANTHOPOULOS [5] and by outcomes of the SeRoN project focused on security of road transport network, seron-project.eu.

In cost optimisations discounting is commonly applied to express the upgrade and failure costs on a common basis, HOLICKY [4]. Apparently such considerations are not needed in the case of emergency situations of short-term durations.

Based on these assumptions, the expected total costs can be expressed as follows:

$$\text{In case of upgrade: } C_{tot}(d) = C_0 + C_m\, d + C_f\, p_f(d) \tag{2a}$$

$$\text{No upgrade (accepting a present state): } C_{tot} = C_f\, p_f(d_0) \tag{2b}$$

with

$p_f(\cdot)$ failure probability related to a reference period,
d_0 value of the decision parameter before an upgrade.

From equation (2a), the optimum value of the decision parameter d_{opt} (optimum upgrade strategy) can be assessed:

$$\text{minimum}_d\, C_{tot}(d) = C_{tot}(d_{opt}) \tag{3}$$

From an economic point of view, no upgrade is undertaken when the total cost according to Eq. (2b) is less than the total cost of the optimum upgrade. It follows from Eqs. (2a) and (3) that d_{opt} is independent of C_0.

5 Target reliabilities based on cost minimisation

The optimum upgrade strategy should aim at the target reliability corresponding to d_{opt}, $\beta_{up} = -\Phi^{-1}[p_f(d_{opt})]$. However, the total costs given in Eqs. (2b) and (3) should be compared to decide whether to upgrade the bridge or not. The limiting value d_{0lim} of the decision parameter before the upgrade is then found as follows:

$$p_f(d_{0lim}) = C_0/C_f + C_m\, d_{opt}/C_f + p_f(d_{opt}) \tag{4}$$

For $d_0 < d_{0lim}$ the reliability level of an existing bridge is too low, failure consequences become high and the decision is to upgrade the bridge as the optimum upgrade strategy yields a lower total cost. For $d_0 > d_{0lim}$ the present state is accepted from an economic point of view since no upgrade strategy leads to a lower total cost than costs expected when no

upgrade is taken. The minimum reliability index β_0 below which the bridge is unreliable and should be upgraded then corresponds to $d_{0\text{lim}}$, $\beta_0 = -\Phi^{-1}[p_f(d_{0\text{lim}})]$.

Realistically assuming $C_f >> C_m$ d_{opt} for important bridges in emergency situations, the minimum reliability index β_0 becomes:

$$\beta_0 \approx -\Phi^{-1}[C_0/C_f + p_f(d_{opt})] \tag{5}$$

Assessment of the optimum repair strategy (d_{opt}) requires a case-specific approach and detailed information on this is beyond the scope of this paper. However, it can be often assumed that the failure probability $p_f(d_{0\text{lim}})$ will mostly be governed by the ratio C_0/C_f for emergency situations where C_0 may become comparable with C_f. The evaluation of $p_f(d_{opt})$ is then of lower importance.

To simplify the present analysis, results obtained by SYKORA AND HOLICKY [13] are adopted and failure probabilities related to optimum upgrade strategies are considered as follows:

- Failure consequences small/some: $p_f(d_{opt}) \approx 0.03$ ($\beta(d_{opt}) \approx 1.9$),
- Medium: $p_f(d_{opt}) \approx 0.008$ ($\beta(d_{opt}) \approx 2.4$),
- High: $p_f(d_{opt}) \approx 0.003$ ($\beta(d_{opt}) \approx 2.8$).

Fig. 1 indicates variation of the minimum reliability index β_0 with the cost ratio C_0/C_f. The cost ratio is apparently a significantly influencing factor. It appears that for:

- $C_0/C_f < 0.001$ the minimum reliability index is about 2.4 for CC2 and 2.7 for CC3,
- $C_0/C_f > 0.01$ the minimum reliability index drops below two which is the reliability level commonly considered for the Serviceability limit states.

It is interesting to note that for high relative costs of safety measures, ISO 2394 (Tab. 2) indicates $\beta = 2.3$ and 3.1 for moderate and great failure consequences, respectively.

6 Requirements on human safety

The cost optimisation is commonly perceived to aim at finding the optimum decision from the perspective of an owner of the bridge. However, society commonly establishes limits at human safety. General guidelines for the assessment of the target reliabilities with respect to human safety are provided in ISO 2394. In principle structural design and assessment of existing bridges are not distinguished.

ISO 2394 states that structural reliability is important first and foremost if people may be killed or sustain injuries as a result of the collapse. An acceptable maximum value for the failure probability might be found from a comparison of risks resulting from other activities. Taking the overall individual lethal accident rate of 10^{-4} per year as a reference, values in the range of 10^{-6}–10^{-5} seem reasonable for structures in persistent design situations [11, 13].

However, in emergency situations higher risks may be acceptable since they may be compensated by mitigation of consequences in endangered areas. Therefore, a tentative value

of 10^{-3} per year is considered hereafter that may be associated with uncommon accidents, MELCHERS [9]. Further specification of this value is, however, needed.

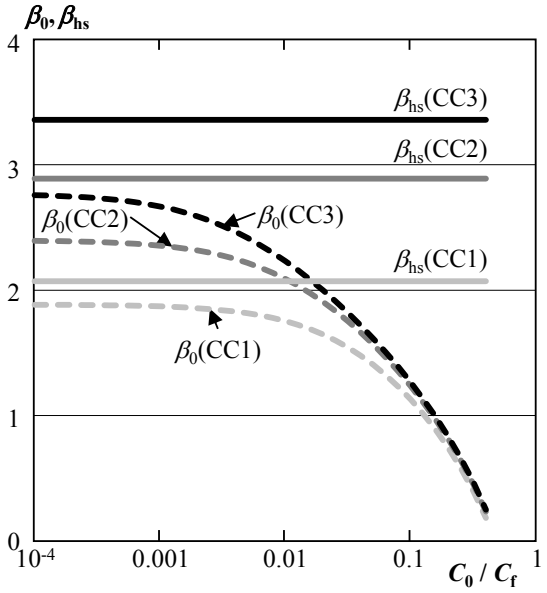

Fig. 1: Variation of the target reliability indices based on the economic (β_0) and human safety (β_{hs}) criteria with the cost ratio C_0/C_f for the different consequence classes

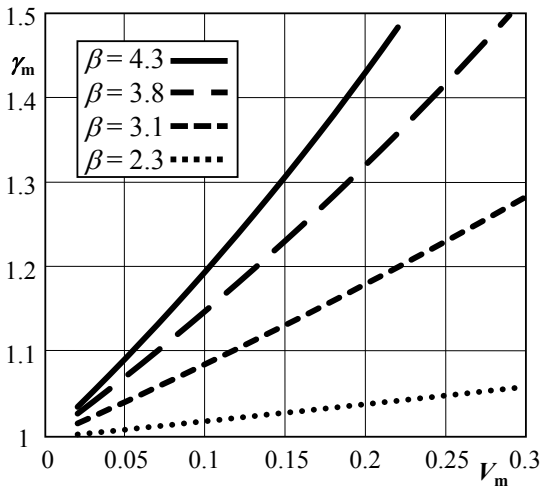

Fig. 2: Variation of the partial factor γ_m with the coefficient of variation V_m for $\beta = 2.3$, 3.1, 3.8 or 4.3 (adopted from CASPEELE ET AL. [3])

The concept of individual risk provided in ISO 2394 then yields the following relationship between the target failure probability $p_{ft,hs}$ and the conditional probability of casualty p_1, given the structural failure in emergency situation:

$$p_{ft,hs} \leq 10^{-3}/p_1 \tag{6}$$

With respect to the loss of human life, EN 1990 distinguishes among low, medium, or high consequences (Consequence Classes CC1-CC3, respectively). The Consequence Classes may be associated with the Reliability Classes indicated in Tab. 1 Based on a literature review SYKORA ET AL. [14]considered the following conditional probabilities for assessment of bridges:

- $p_1 = 0.05$ for CC3,
- $p_1 = 0.01$ for CC2,
- $p_1 = 0.001$ for CC1.

For an emergency situation, the target failure probabilities of a structural member, related to a reference period t_{ref} (duration of the emergency situation << 1 year), become from Eq. (6) (with t_{ref} in years):

$$\text{CC1: } p_{ft,hs} \leq t_{ref}\text{; CC2: } p_{ft,hs} \leq 0.1t_{ref}\text{, CC3: } p_{ft,hs} \leq 0.02t_{ref}, \tag{7}$$

Fig. 1 indicates the target reliability index β_{hs} (obtained from Eq. (5) and (7)) for the different consequence classes. The human safety criterion is apparently dominating the target reliability over the minimum reliability level based on the cost ratio C_0/C_f.

However, it is questionable whether the target level should be selected on the basis of the human safety criterion since it regards only safety of users of a bridge and does not consider losses related to temporary bridge closure (cost C_0). The decision depends on case-specific conditions and in general should aim at balancing risks of users and risks of people endangered when the crossing of heavy freights is not allowed.

Note that besides the individual risk concept, ISO 2394 indicates that in many cases authorities explicitly want to avoid accidents where large numbers of people may be killed and proposes an additional societal risk criterion based on a so-called $F{-}N$ curve, ISO 13824:2009 *General principles on risk assessment of systems involving structures*. However, application of this criterion requires a case-specific approach and it is out of the scope of this paper to provide a general guidance in this regard. Moreover, SYKORA AND HOLICKY [13] showed that the individual risk criterion is dominating over the societal criterion except failures with vast collapsed areas. Therefore, the societal risk criterion is not considered in this study.

7 Example of application

Application of the derived target reliabilities in conjunction with the partial factor method (EN 1990) is illustrated by a simple example. It is assumed that:

1. An excessively heavy freight of well-defined weight is to be transported over a reinforced concrete bridge during an emergency situation (duration of one week).
2. The bridge is classified in CC 2.
3. Considering economic and societal consequences, the cost ratio C_0/C_f is estimated to be 0.01.
4. It is impossible to conduct measurements and tests on the structure.

Two alternatives are foreseen:

- Human safety is not endangered when the transport is not allowed. The cost C_0 thus includes economic losses only. Human safety (safety of a driver) included in the consequences of bridge failure is considered and β_{hs} is dominating the target level; then $\beta = \beta_{hs} = 2.9$ follows from Fig. 1.
- Human safety is endangered when the transport is not allowed. The cost C_0 thus includes societal consequences and the target reliability is assessed on the basis of the minimum level β_0; $\beta = \beta_0 = 2.1$ follows from Fig. 1.

For the assessment the partial factors for material properties are needed. The partial factor of a material property γ_M can be obtained as a product of (see CASPEELE ET AL. [3]):

$$\gamma_M = \gamma_{Rd}\gamma_m = \gamma_{Rd1}\gamma_{Rd2}\gamma_m \tag{8}$$

with

γ_{Rd1} partial factor accounting for model uncertainty,
γ_{Rd2} partial factor accounting for geometrical uncertainties,
γ_m reliability-based partial factor accounting for variability of the material and statistical uncertainty.

Referring to CASPEELE ET AL. [3] the following uncertainty factors can be recommended:

- $\gamma_{Rd1} = 1.05$ for concrete strength and $\gamma_{Rd1} = 1.025$ for reinforcement,
- $\gamma_{Rd2} = 1.05$ for geometrical uncertainties of the concrete section size or reinforcement position when measurements are not available.

Variation of the partial factor γ_m with the coefficient of variation of the material property V_m is shown in Fig. 2 for selected target reliabilities. Considering common values $V_c = 0.15$ and $V_s = 0.05$ the following partial factors are obtained:

$$\begin{aligned} \text{for } \beta = 2.9&: \gamma_C = 1.05 \times 1.05 \times 1.11 = 1.22;\ \gamma_S = 1.025 \times 1.05 \times 1.03 = 1.11 \\ \text{for } \beta = 2.1&: \gamma_C = 1.05 \times 1.05 \times 1.0 = 1.10;\ \gamma_S = 1.025 \times 1.05 \times 1.0 = 1.08 \end{aligned} \quad (9)$$

In a similar way the partial factors for permanent loads can be obtained [3] and for load effect due to heavy transport [7].

8 Conclusions

The target reliability levels recommended in various standards for new and existing structures are inconsistent; almost no recommendations are available for structures under temporary conditions including emergency situations. Target reliabilities related to emergency situations can be required for (1) design of new bridges considering possible occurrence of the emergency situation, (2) assessment of temporary bridges or (3) assessment of existing bridges when immediate decisions on permissions for the crossings of heavy freights are needed. Concerning the third case the following conclusions can be made:

- It is uneconomical to require that existing bridges comply with the target reliability levels for new bridges; lower target reliability levels can be justified by social, cultural, economic, and sustainability considerations.
- Decisions in the assessment can result in the acceptance of an actual state or in the upgrade of a bridge; in principle two target reliability levels are needed - the minimum level below which the bridge is unreliable and should be upgraded (β_0), and the level indicating the optimum upgrade strategy (β_{up}).
- In particular situations it needs to be clarified whether the minimum levels of human safety should be considered.
- Critical issue in the assessment of the minimum reliability level β_0 is estimation of the cost ratio of upgrade and failure consequences (C_0/C_f).
- For $C_0/C_f > 0.01$ the reliability level β_0 drops below two which is the reliability level commonly considered for the Serviceability Limit States.
- Human safety criterion leads to target reliabilities in the range from 2.0 to 3.5.

Acknowledgements

The study is based on outcomes of the research projects VG20122015089 supported by the Ministry of the Interior of the Czech Republic and P105/12/0589 supported by the Czech Science Foundation.

Literature

[1] Ang, A.H.S., De Leon, D. Determination of optimal target reliabilities for design and upgrading of structures. *Structural Safety* 19 (1997), p. 91–103

[2] Casas, J.R., Wisniewski, D. Safety requirements and probabilistic models of resistance in the assessment of existing railway bridges. *Structure and Infrastructure Engineering* 9 (2013), p. 529–545

[3] Caspeele, R., Allaix, D.L., Steenbergen, R.D.J.M., Sykora, M. On a partial factor approach for existing concrete structures: the Design Value Approach and Adjusted Partial Factor Method (accepted for publication). *Structural Engineering International* (2013)

[4] Holicky, M. Optimisation of the target reliability for temporary structures. *Civil Engineering and Environmental Systems* (2012), p. 1–10

[5] Imam, B.M., Chryssanthopoulos, M.K. Causes and Consequences of Metallic Bridge Failures. *Structural Engineering International* 22 (2012), p. 93–98

[6] JCSS *JCSS Probabilistic Model Code.* Zurich: Joint Committee on Structural Safety, 2001 <www.jcss.byg.dtu.dk>

[7] Lenner, R., Sykora, M., Keuser, M. Partial factors for military loads on bridges. In: Krivanek, V.; Stefek, A. (eds.): *Proc. ICMT'13, Brno, 22-23 May 2013.* Brno: University of Defence, 2013, p. 409–418

[8] Maljaars, J., Steenbergen, R., Abspoel, L., Kolstein, H. Safety Assessment of Existing Highway Bridges and Viaducts. *Structural Engineering International* 22 (2012), p. 112–120

[9] Melchers, R.E. *Structural Reliability Analysis and Prediction.* Chichester, England: John Wiley & Sons Ltd., 2001

[10] Onoufriou, T., Frangopol, D.M. Reliability-based inspection optimization of complex structures: a brief retrospective. *Computers & Structures* 80 (2002), p. 1133–1144

[11] Steenbergen, R.D.J.M., Vrouwenvelder, A.C.W.M. Safety philosophy for existing structures and partial factors for traffic loads on bridges. *Heron* 55 (2010), p. 123–139

[12] Sykora, M., Holicky, M., Markova, J. Target reliability levels for assessment of existing structures. In: Faber, M. H.; Köhler, J.; Nishijima, K. (eds.): *Proc. ICASP11, ETH Zurich, 1-4 August 2011.* Leiden: CRC Press/Balkema, 2011, p. 1048–1056

[13] Sykora, M., Holicky, M. Target reliability levels for the assessment of existing structures – case study. In: Strauss, A.; Bergmeister, K.; Frangopol, D.M. (eds.): *Proc. IALCCE 2012, Vienna, 3 - 6 October 2012.* Leiden: CRC Press/Balkema, 2012, p. 813–820

[14] Sykora, M., Holicky, M., Manas, P. Target Reliability for Bridges in Emergency Situations. In: Krivanek, V.; Stefek, A. (eds.): *Proc. ICMT'13, Brno, 22-23 May 2013.* Brno: University of Defence, 2013, p. 371–382

[15] Vrouwenvelder, A.C.W.M., Scholten, N. Assessment Criteria for Existing Structures. *Structural Engineering International* 20 (2010), p. 62–65

[16] Vrouwenvelder, A.C.W.M. Developments towards full probabilistic design codes. *Structural Safety* 24 (2002), p. 417–432

[17] Vrouwenvelder, T., Leira, B.J., Sykora, M. Modelling of Hazards. *Structural Engineering International* 22 (2012), p. 73–78

Probabilistic load bearing capacity assessment of post-tensioned composite bridge

Martina Šomodíková, Jiří Doležel, David Lehký
Institute of Structural Mechanics, Brno University of Technology, Brno
somodikova.m@fce.vutbr.cz, dolezel.j@fce.vutbr.cz, lehky.d@fce.vutbr.cz

Abstract: With respect to the current state of existing bridges an importance of load bearing capacity and reliability evaluation is growing up. As a case study an existing single-span road bridge made of post-tensioned concrete MPD4 girders was used. The paper deals with determination of load-bearing capacity which is performed using nonlinear FEM computational model and regarding the random properties of load and material parameters the fully probabilistic approach is used. Owing to the type of the bridge, the values of individual load bearing capacities are assessed with respect to the ultimate limit state, as well as the serviceability limit states.

Keywords: bridges, load bearing capacity, MPD girder, probabilistic nonlinear analysis, reliability assessment

1 Introduction

Currently, there are more than 17400 bridges on the Czech highways and roads (January 2013 [10]). However, supporting structures of almost 3000 of them are in poor or emergency condition. A large number of deteriorating bridges needs to be reconstructed necessarily, nevertheless, because of insufficient financial support of reconstructions on the part of the state funds the capacity of such bridges is often being reduced with respect to their current state and other safety, serviceability and durability requirements, whereas the geometric properties, loading and material characteristics are considered according to the original bridge documentation and/or performed bridge inspection.

The current Standards for the load bearing capacity assessment are mostly applied using linear solution and deterministic approach when the uncertainties of input parameters are taken into account using partial safety factors. Alternatively, nonlinear solution can be used and the global safety factors assessed according to appropriate Standard. An application of these methods ensures that the safety and reliability of the structure reach the target level. However, probabilistic methods and the theory of structural reliability provide more accurate analysis of verification of existing bridges. For example, ENEVOLDSEN [6] has demonstrated that more thorough probabilistic analysis of bridge structures at their critical limit states leads to higher load bearing capacities and the structures did indeed have the load bearing capacity to remain in service without strengthening or rehabilitation. Conse-

quently, using probabilistic methods have also been demonstrated to provide significant cost savings to bridge owners whilst required safety of the structure was not compromised and a more realistic safety assessment was performed.

1.1 Load bearing capacity

In the Czech Republic load bearing capacity of new and existing road bridges is assessed according to the Czech technical Standard ČSN 73 6222 [2]. Before the determination of load bearing capacity, a bridge inspection must be carried out and consequently, a real condition of the structure must be taken into account. If the load bearing capacity of concrete bridges is assessed with respect to the ultimate as well as the serviceability limit states, then the limit states of decompression (for prestressed concrete bridges) and the crack width (for prestressed and reinforced concrete bridges) should be verified.

In most cases three basic types of load bearing capacity are investigated:

- *Normal load bearing capacity* (V_n) – is the maximum immediate total weight of one vehicle. Vehicles of such weight can cross a bridge in an arbitrary number and with no transport limitation.
- *Reserved load bearing capacity* (V_r) – is the maximum immediate total weight of a vehicle which can cross a bridge separately, but with no further transport limitation.
- *Exceptional load bearing capacity* (V_e) – is the maximum immediate total weight of a vehicle or a heavy haul trailer which can cross a bridge only separately from further traffic and with other limitations (e.g. prescribed path and velocity, etc.).

Dynamic effects of the traffic load are incorporated into load bearing capacity assessment using dynamic coefficient δ, by which the static effects of a corresponding load are multiplied. For detailed information about loading schemes and the other requirements for determination of individual load bearing capacities see [2].

1.2 Target reliability level

When using probabilistic methods, a procedure of load bearing capacity assessment of existing bridges is as follows. The first step of the process involves deterministic assessment to identify the critical limit state. Next, required reliability level is defined. The minimum safety requirements, in terms of target reliability index, β_t, are specified by appropriate Standards [5],[12]. The safety index, β, is formally defined in terms of the probability of failure, p_f, as:

$$\beta = -\Phi^{-1}\left(p_f\right), \tag{1}$$

where $\Phi^{-1}(\cdot)$ is the inverse function of the standardized normal distribution.

Values of target reliability index, β_t, and corresponding probability of failure, p_f, that are for selected limit states presented in Tab. 1, can be specified in more details depending on the estimated residual lifetime of a bridge, on the consequences of damage, or considering the economic, social and ecological consequences.

Tab. 1: Target values of reliability index

Limit states	β_t	p_f	Note
Serviceability limit states:			
- reversible	0.0	-	
- irreversible – small consequence of damage	1.3	9.7×10^{-2}	
- irreversible – medium consequence of damage	1.5	6.7×10^{-2}	
- irreversible – high consequence of damage	2.3	1.1×10^{-2}	
Ultimate limit states:			
- very small consequence of damage	2.3	1.1×10^{-2}	Bridges on roads with minimal usage
- small consequence of damage	3.1	9.7×10^{-4}	Short-span bridges on the roads of the 2nd and the 3rd class
- medium consequence of damage	3.8	7.2×10^{-5}	Common bridge types
- high consequence of damage	4.3	8.5×10^{-6}	Long-span bridges, bridges on highways and speedways

Very small, small, medium and high consequences of damage are distinguished with respect to possible losses of human lives. Additionally, the required value of reliability can be prescribed for the whole structure or for its individual supporting member.

Next step of the process of assessing load bearing capacity is the stochastic modelling of basic variables such as material parameters, self-weight and other loads, also including traffic load, or model uncertainties. Here, the information from bridge inspection should be included. These provide further knowledge of the analysed structure, thereby the uncertainties are reduced. After the description of input variables by statistical parameters and the theoretical models of probability distribution function with respect to all information and other recommendations, the reliability index or the failure probability is calculated using probabilistic methods. Conversion between β and p_f was mentioned above in Eq. (1). Computed value of reliability index, β, is then compared with the target reliability index, β_t, and the load bearing capacity is assessed. When $\beta > \beta_t$, the value of particular load bearing capacity may be increased, on the contrary, load bearing capacity is reduced when $\beta < \beta_t$. Regarding the keeping all defined requirements for safety and reliability of the structure, the final value of load bearing capacity is assessed from the condition $\beta \approx \beta_t$. Sensitivity analysis of input variables can be also helpful for improvement of model.

2 Load bearing capacity assessment of analysed bridge

As an example a single-span post-tensioned composite bridge, crossing a single-track railway on the road I/55 near the village Uherský Ostroh, was analysed. The bridge design was performed in 1957, but the original documentation is not available. Based on the diagnostic survey from 2007, the bridge is made of twelve precast post-tensioned concrete MPD3 (outer) and MPD4 (intermediate) type girders, which were used from 1955 for construction of slab bridges up to a clear span of 18 m. Each of MPD4 girders was composed of six segments that are connected to each other by the transverse joints. The bridge composition is obvious from Fig. 1. According to bridge inspection, the values of normal and reserved load bearing capacities are 25 tonnes and 48 tonnes, respectively.

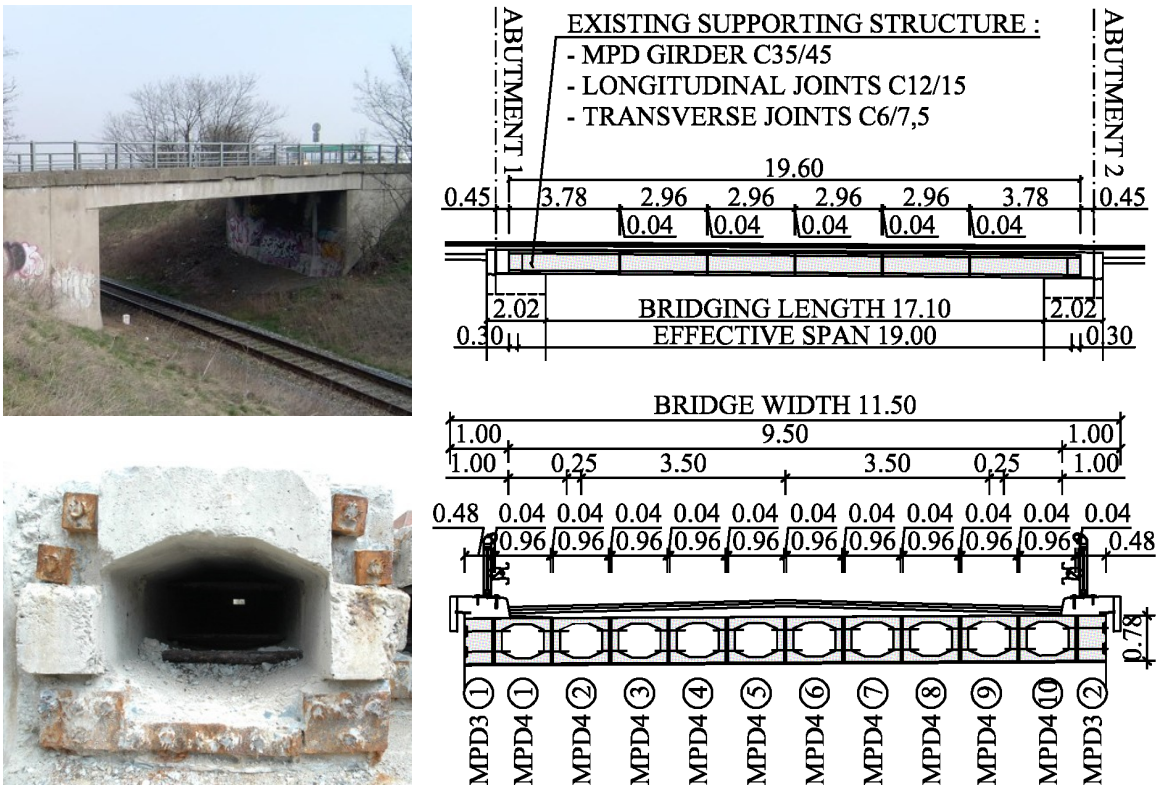

Fig. 1: Longitudinal and transversal section of analysed bridge

As has already been noted, probabilistic methods provide more accurate verification of existing structures and more realistic safety assessment is performed. Therefore, the load bearing capacity was assessed using fully probabilistic approach and regarding the current state of analysed bridge the ultimate limit states as well as the serviceability limit states were investigated. In connection with type of the bridge, the limit state of decompression and limit state of cracking were verified as well. Fully probabilistic analysis was carried out using SARA Studio [11] – a software tool which controls the communication between ATENA (ČERVENKA ET AL. [1]) – a software developed for nonlinear modelling of concrete and reinforced concrete structures using finite element method – and a multipurpose probabilistic software FReET (NOVÁK ET AL. [9]) for statistical, sensitivity and reliability analysis of engineering problems, allowing to simulate their uncertainties at random variables level.

2.1 Numerical FEM model

Numerical model in its simplified form was created in ATENA 2D software. For concrete, 3D Non Linear Cementitious 2 material model was used (for more details see [1]). Prestressing tendons and shear reinforcement were modelled as discrete and smeared reinforcement, respectively, by means of bilinear stress-strain diagram with hardening.

The following load cases were modelled: dead load of the structure, longitudinal prestressing, secondary dead load and traffic load. The loading schemes applied here for determination of individual types of load bearing capacities are depicted in Fig. 2. These were used in accordance with current Czech technical Standards. Load was applied by the increment of forces up to reaching the investigated limit state. Nonlinear solution was performed using the combination of standard Newton-Raphson and Arc Length methods.

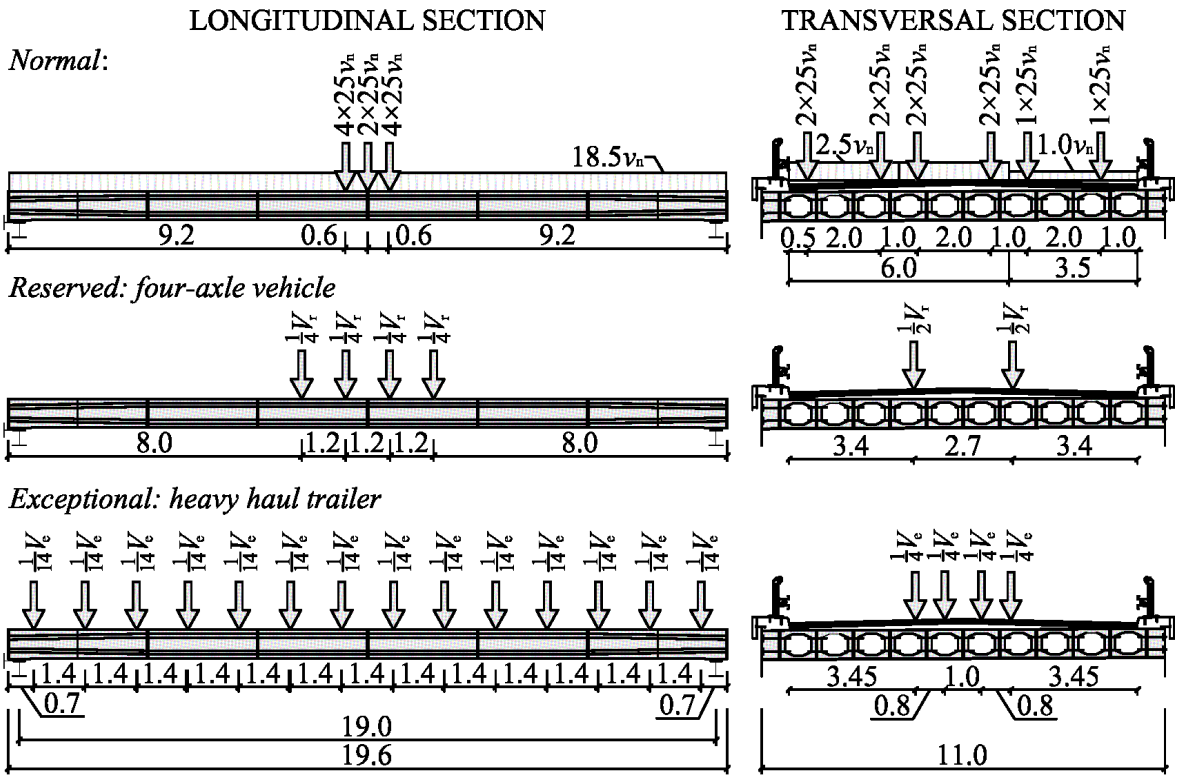

Fig. 2: Loading schemes for assessment of individual load bearing capacities

2.2 Stochastic modelling of input variables

Stochastic parameters of random input variables were defined using software FReET according to JCSS [7] and TP 224 [12] recommendations and these were updated based on the material parameters testing according to diagnostic survey. Concrete of segments was classified as C35/45 and concrete of joints only as C6/7.5 because of high variability in diagnostic measurements of cubic compressive strength. However, the average value of measured cubic compressive strengths was more than 40 MPa. Since the strength of transverse joints has a significant effect on the capacity of the bridge, especially with respect to the ultimate limit state, parameters of transverse joints were defined using the mean value of compressive strength equal to 36 MPa as well as reduced value of 22.5 MPa, which better corresponds to the results obtained from diagnostic survey. Definitions of random input variables are summarized in Tab. 2, parameters of concrete of transverse joints with reduced strength are listed in parentheses.

Alongside concrete and reinforcement material parameters, the dead load of the structure and the weight of road layers were also randomized, see concrete mass density and secondary dead load, respectively, in Tab. 2. Values of prestressing force were defined by their mean values with respect to short-term as well as long-term losses of initial tension according to ČSN EN 1992-1-1. Considering their substantial effect on global level of load bearing capacity at the serviceability limit states, applied stochastic model was also defined fully in agreement with JCSS recommendations. Finally, traffic load for determination of normal, reserved and exceptional load bearing capacities was defined using deterministic values of load according to valid loading schemes introduced in current Standards.

Tab. 2: Definition of input parameters for load bearing capacity assessment

Variable	Symbol	Unit	Probability distribution	Mean value	CoV
Concrete of segments:					
Elastic modulus	E_c	[GPa]	Lognormal (2 par)	37.20	0.10
Tensile strength	f_t	[MPa]	Weibull min (2 par)	3.301	0.15
Compressive strength	f_c	[MPa]	Lognormal (2 par)	43.35	0.08
Specific fracture energy	G_f	[N/m]	Weibull min (2 par)	82.51	0.15
Mass density	ρ	[kN/m^3]	Normal	23.80	0.04
Concrete of transverse joints:					
Elastic modulus	E_c	[GPa]	Lognormal (2 par)	34.03 (26.81)	0.15
Tensile strength	f_t	[MPa]	Weibull min (2 par)	2.807 (1.913)	0.35
Compressive strength	f_c	[MPa]	Triangular	36.00 (22.50)	0.25
Specific fracture energy	G_f	[N/m]	Weibull min (2 par)	70.18 (47.82)	0.25
Mass density	ρ	[kN/m^3]	Normal	23.80 (23.80)	0.04
Shear reinforcement:					
Elastic modulus	E	[GPa]	Lognormal (2 par)	200.0	0.07
Yield strength	f_y	[MPa]	Lognormal (2 par)	465.1	0.07
Ultimate strength	f_u	[MPa]	Lognormal (2 par)	581.4	0.07
Limit strain	ε_{lim}	[-]	Normal	0.050	0.07
Prestressing tendons:					
Elastic modulus	E	[GPa]	Normal	190.0	0.03
Yield strength	$f_{y,p}$	[MPa]	Normal	1248	0.03
Ultimate strength	$f_{u,p}$	[MPa]	Normal	1716	0.03
Limit strain	ε_{lim}	[-]	Normal	0.050	0.07
Prestressing force	P	[MN]	Normal	P_{mean}	0.09
Other:					
Secondary dead load	g_1	[kN/m]	Normal	65.55	0.05
Normal, reserved and exceptional load bearing capacity schemes	V_n	[t]	Deterministic	V_n	-
	V_r	[t]	Deterministic	V_r	-
	V_e	[t]	Deterministic	V_e	-

Note:Values in parentheses represent parameters with reduced strength of transverse joints

Statistical correlation between material parameters of concrete of segments and transverse joints, prestressing tendons and concrete reinforcement was also considered and imposed using a simulated annealing approach (VOŘECHOVSKÝ & NOVÁK [13]). Correlation matrices (see Fig. 3) were defined with respect to formerly performed tests and recommendations of JCSS.

	E_c	f_t	f_c	G_f	ρ
E_c	1	0	0.3	0	0
f_t	0	1	0.4	0.8	0
f_c	0.3	0.4	1	0	0
G_f	0	0.8	0	1	0

(a) Concrete of segments and transverse joints

	f_y	f_u	ε_{lim}	E
f_y	1	0.9	0.5	1
f_u	0.9	1	0.5	0
ε_{lim}	0.5	0.5	1	0
E	1	0	0	1

(b) Prestressing tendons and shear reinforcement

Fig. 3: Correlation matrices of material parameters

2.3 Probabilistic reliability analysis

First, load bearing capacity of one MPD4 girder was determined and subsequently the global assessment of the load bearing capacity of the structure as a whole was performed. Normal, reserved and exceptional load bearing capacities were assessed with respect to the target reliability level, corresponding to an investigated limit state and defined by target reliability index, β_t (see Tab. 1). For analysed bridge, its values were assigned as follows: $\beta_t = 3.8$ for ultimate limit state, and $\beta_t = 0$ for serviceability limit states (limit state of decompression and limit state of cracking). Reliability analysis was performed using 32 virtual simulations of structural response using Latin Hypercube Sampling method (MCKAY ET AL. [8]) and Cornell reliability index was used with respect to relatively small number of simulations. Results obtained from the fully probabilistic analysis were compared with the values of individual capacities, computed according to current Standards [2],[3],[4].

2.3.1 Ultimate (ULS) and serviceability (SLS) limit states

As has been mentioned before, load bearing capacity assessment was performed in two levels – at the level of an individual MPD4 girder and at the level of the whole bridge. In both cases, fully probabilistic nonlinear FEM analysis was carried out.

At first, attention will be focused on the intermediate beam specified above as MPD4-5 (see the transversal section of analysed bridge in Fig. 1). The beam was statically evaluated in the form of bending moments. Bending moments caused by applied loads, corresponding to individual loading schemes, were compared with moments of resistance at all investigated limit states. Results from the local fully probabilistic analysis are being marked by FP_LOC in following figures. In the second case, global probabilistic nonlinear analysis of the whole bridge was carried out. Applied load was increasing in successive steps up to reaching the particular limit state. Final values of carrying-capacity were statistically evaluated and subsequently the values of individual types of load bearing capacity were obtained (in figures being marked by FP_GLOB). The same way as in the case of local evaluation, the target reliability level of global analysis was kept according to prescribed requirements (see above).

Load bearing capacity and reliability analysis of MPD4-5 girder was also performed using deterministic approach according to current Standards – results in figures being marked as DET – and results from local as well as global evaluation of analysed bridge were compared with these. Comparison of results of mentioned computational alternatives was also performed with the values of load bearing capacities, that were determined according to Standardized document (being marked as SD) and from the inspection of the bridge (marked as INSP). Summary of results is given in Fig. 4.

It is obvious, that the values of the load bearing capacities obtained from the global analysis at the ultimate limit state are approximately twice higher than these obtained in compliance with limit state of cracking or decompression. This means, that serviceability limit states are critical for the determination of load bearing capacity of analysed structure. Because investigated bridge is a prestressed one, the greatest significance should be focused on limit state of cracking, because eventual corrosion of tendons due to potential penetration of atmospheric oxygen or chloride ingress by cracks could have a critical influence on the structure functionality. Further, it has been demonstrated that the probabilistic approach is less conservative and leads to slightly higher capacities than the deterministic one.

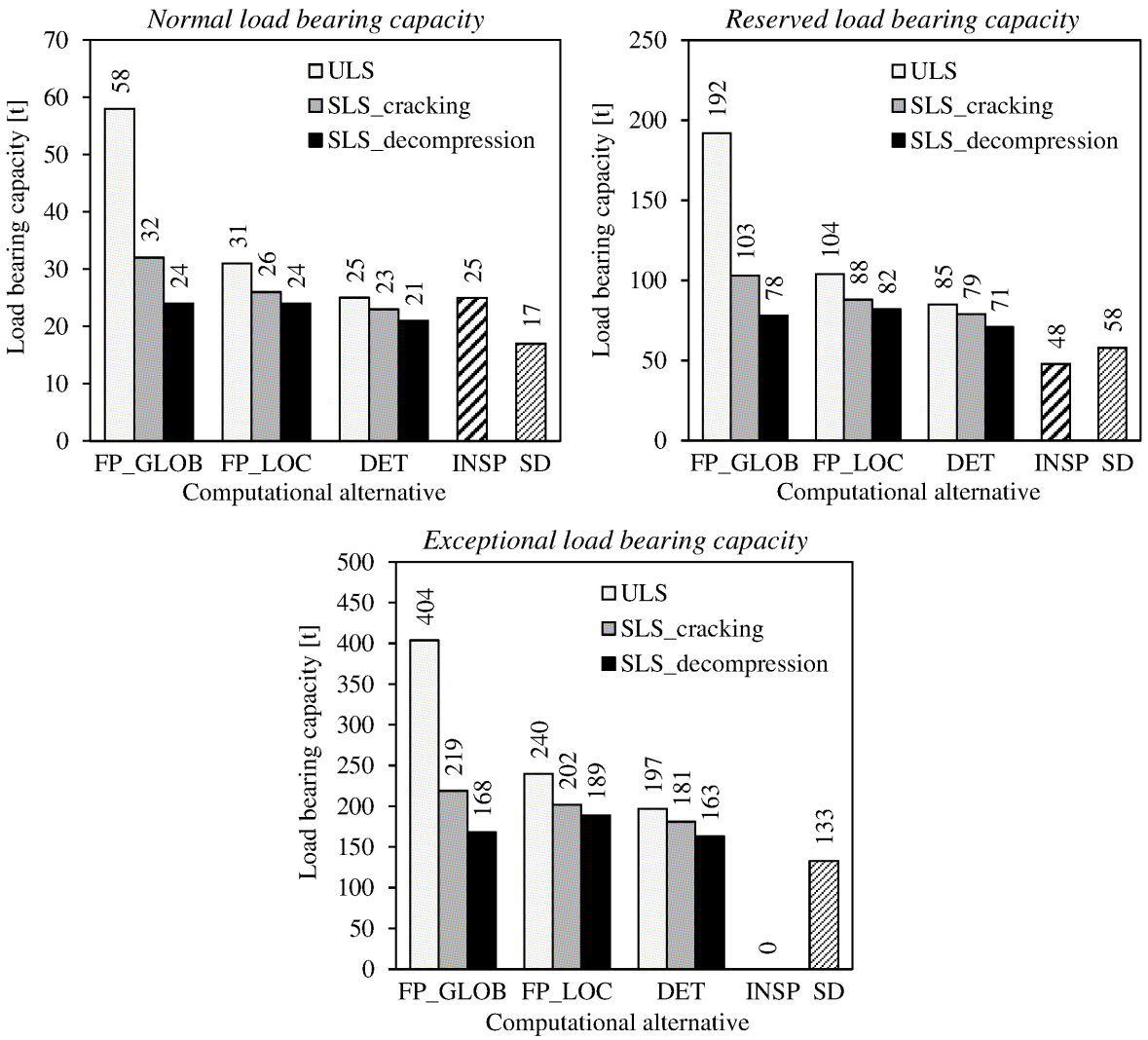

Fig. 4: Comparison of results of all computational alternatives

Considering the strong effect of material parameters of transverse joints on the values of load bearing capacities especially at ultimate limit state, and with respect to high variability of cubic compressive strength obtained from measurements within diagnostic survey, the concrete strength of transverse joints was reduced (see values in parentheses in Tab. 2). These parameters better correspond to the concrete classification in the framework of diagnostics, when the concrete of transverse joints was classified as C6/7.5. Fully probabilistic nonlinear FEM analysis was carried out once more and updated values of individual load bearing capacities were computed at the global level of analysed bridge. Their final values are shown in Fig. 5.

As can be seen, updated values of load bearing capacities at ultimate limit state have dramatically decreased in comparison with those in Fig. 4. However, a good compliance with the values defined according to diagnostic survey and Standardized document has been demonstrated. Slightly greater difference is only obvious in the case of reserved load bearing capacity, which is caused by neglect of vehicle's critical position in transverse direction. It was assumed that the four-axle vehicle for reserved load bearing capacity assessment crosses the bridge in its axis as well as in the case of heavy haul trailer for determination of exceptional load bearing capacity.

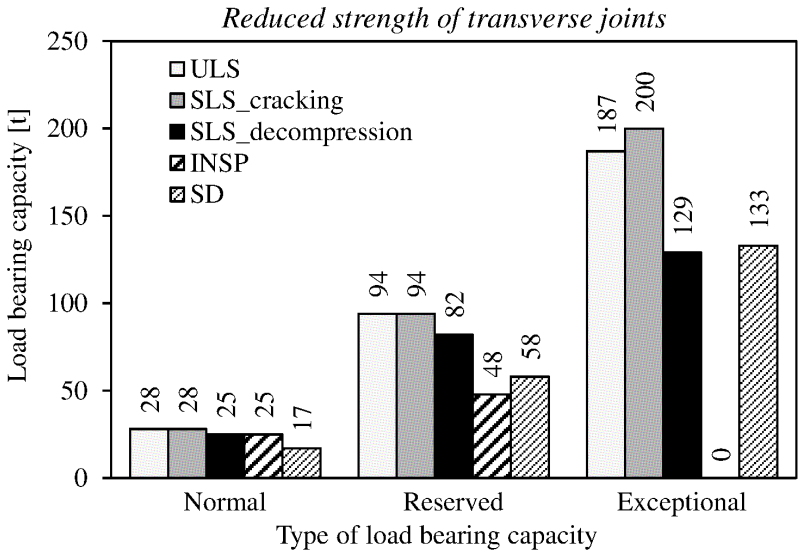

Fig. 5: Comparison of results of all computational alternatives for global analysis with reduced concrete strength of transverse joints

3 Summary

The aim of this contribution was to outline the possibility of load bearing capacity assessment of existing road bridges using computational tools of advanced nonlinear mechanics and probabilistic methods. This methodology, which can be generally used, was applied to a slab composite bridge made of post-tensioned MPD3 and MPD4 girders. Design of the bridge was most likely realized in 1957. Therefore, the analysis of individual types of load bearing capacity was performed with respect to type and current state of the bridge and, considering the random properties of material parameters, the fully probabilistic approach was used. Within the verification of bridge capacities, the ultimate limit states as well as the serviceability limit states were investigated. In connection with unguaranteed strength of concrete among particular segments of MPD girders, load bearing capacity was further assessed in terms of different material parameters of concrete of transverse joints.

Probabilistic methods in combination with nonlinear FEM analysis represent an effective and practical tool in cases of evaluation of load bearing capacity and reliability of existing structures. It has been demonstrated that probabilistic approach is less conservative and leads to higher capacities than the deterministic one, which is mostly applied using current Standards, whilst required safety of the structure was not compromised. The direct application of probabilistic methods can serve to gaining valuable information for decision making about maintenance, repairs and to a certain extent it can also help for efficient treatment of financial sources allocated for maintenance of road-traffic infrastructure.

Acknowledgement

The authors thank for the financial support from project of the specific university research at Brno University of Technology, registered under the number FAST-S-13-2017, and from project No. 13-03662S provided by the Grant Agency of the Czech Republic.

Literature

[1] Červenka, V., Jendele, L., Červenka, J. *ATENA Program Documentation – Part 1: Theory*. Prague: Cervenka Consulting, 2012. Available from: http://www.cervenka.cz/assets/files/atena-pdf/ATENA_Theory.pdf

[2] ČSN 73 6222. *Load bearing capacity of road bridges*. Praha: Úřad pro technickou normalizaci, metrologii a státní zkušebnictví, 2009

[3] ČSN EN 1992-1-1. *Eurocode 2: Design of concrete structures – Part 1-1: General rules and rules for buildings*. Praha: Český normalizační institut, 2006

[4] ČSN EN 1992-2. *Eurocode 2: Design of concrete structures – Part 2: Concrete bridges – Design and detailing rules*. Praha: Český normalizační institut, 2007

[5] ČSN ISO 13822. *Bases for design of structures – Assessment of existing structures*. Praha: Český normalizační institut, 2005

[6] Enevoldsen, I. Practical implementation of probability based assessment methods for bridges. *Structure and Infrastructure Engineering* 7(7–8) (2011), p. 535–549

[7] Joint Committee on Structural Safety. *Probabilistic Model Code* [online]. Last updated 25.1.2013 [cit. 2013-05-29]. ISBN 978-3-909386-79-6. Available from: http://www.jcss.byg.dtu.dk/Publications/Probabilistic_Model_Code.aspx

[8] McKay, M. D., Beckman, R. J., Conover, W. J. Comparison of Three Methods for Selecting Values of Input Variables in the Analysis of Output from a Computer Code. *Technometrics* 21(2) (1979), p. 239–245

[9] Novák, D., Vořechovský, M., Rusina, R. *FReET v. 1.5 – program documentation. User's and Theory Guides*. Brno: Cervenka Consulting, 2013. http://www.freet.cz

[10] Přehledy z informačního systému o silniční a dálniční síti ČR. *Ředitelství silnic a dálnic ČR* [online]. © 2012 [cit. 2013-05-29]. Available from: http://www.rsd.cz/sdb_intranet/sdb/download/prehledy_2013_1_cr.pdf

[11] *SARA – Structural Analysis and Reliability Assessment: User's manual*. Version 2.0.1.1. Prague: Cervenka Consulting, 2003

[12] TP 224. *Ověřování existujících betonových mostů pozemních komunikací*. Praha: Ministerstvo dopravy, Odbor silniční infrastruktury, 2010

[13] Vořechovský, M., Novák, D. Correlation control in small-sample Monte Carlo type simulations I: A simulated annealing approach. *Probabilistic Engineering Mechanics* 24(3) (2009), p. 452–462

Asserting failure probability associated with degradation of concrete structures

Břetislav Teplý, Dita Vořechovská
Institute of Structural Engineering, Faculty of Civil Engineering,
Brno University of Technology, Brno
teply.b@fce.vutbr.cz, vorechovska.d@fce.vutbr.cz

Abstract: With regard to performance based design, together with sustainability and environmentally friendly policies, the probability of failure is an important indicator in design or assessment of concrete structures. The present contribution deals with three areas: the assessment of time-dependent reliability level, life cycle costing and the quantification of risk; all are covered with regard to concrete structures. The attention is focused to steel corrosion as it is one of the most usual deterioration attacking reinforced concrete structures.

Keywords: degradation, life cycle costing, reinforced concrete structures, durability limit states

1 Introduction

In the context of performance-based approaches, time is the decisive parameter and the durability issues connected with time and the consequences for reliability are pronounced. The reliability aspect is significant in service life, inspection and maintenance planning, decisions about making repairs and life cycle costing. Thus, both durability and reliability rank amongst the most decisive structural performance characteristics. This is also reflected e.g. in recent standardization activities ([1] and [2]). Both these documents advocate probabilistic approaches and the utilization of mathematical models, and in this way the enhancement of the assessment of structures for durability – i.e. a time-dependent limit state approach.

The ability to make a reliable comparison of the life-cycle costs for different construction, technological and material scenarios brings the necessary clarity to the decision-making process. Therefore, the most important topics are e.g. the probabilistic vulnerability assessment of civil infrastructure systems, life cycle costing (LCC), life cycle assessment (LCA) and life cycle management (LCM). Generally, cost-benefit issues are considered ([3] and [4]) together with sustainability and environmentally friendly policies. With regard to these areas, it is evident the probability of failure may be utilised for different purposes; in the present contribution three areas are dealt with:

(i) the assessment of time-dependant reliability level;

(ii) the LCC issue, and

(iii) the quantification of risk.

The goal of this paper is to briefly describe these items with regard to concrete structures and to show some applications. The text may serve for the purpose of instructing students and/or for the dissemination of this part of probability theory and its utilization by practicing engineers.

2 Concrete structures

2.1 Reliability and durability

The term 'target reliability level' refers to an acceptable failure probability corresponding to a specified reference period. The well known general definition of structural reliability is introduced e.g. in [5] and [2]. The verification of a structure with respect to its reliability, i.e. to a particular limit state (LS), is carried out via estimation of the probability of the occurrence of failure in a specified reference period. In other words, the aim of reliability analysis is the estimation of unreliability using a probability measure called the theoretical failure probability P_f, defined as:

$$P_f = P\left(R \le S\right) < P_d \tag{1}$$

S is the effect of an action and R is the resistance; both are random variables (or, in a more general sense, random fields). P_d is the design (acceptable, target) probability value; Eq. (1) expresses the general limit condition for both the ultimate and serviceability limit states (ULS and SLS).

The index of reliability β is alternatively utilized instead of P_f in practice; the target value then becomes β_d. The formula for the transformation reads:

$$\beta = -\Phi^{-1}\left(P_f\right) \tag{2}$$

where $\Phi(.)$ is the standard normal probability distribution function. Generally, both S and R may change in the course of time and hence P_f and β are time dependent. This should be stressed especially in the context of limit states associated with durability ([1] and [2]). Thus, for the reliability assessment of newly designed as well as existing structures the full probabilistic safety format has to be *employed*. The considerable uncertainties associated with e.g. parameters governing deterioration processes highlight the need for the use of this approach.

Durability and its reliability implications need to be addressed during the design process due to their pronounced economic and sustainability impacts; the agreement or decision of the client should be a fundamental part of that process. This is not yet a view commonly held by engineers, even though these ideas are clearly expressed in Section 3 of the [2]: *"Specifying performance requirements and the associated constraints of service life and reliability creates an initial bridge between the needs of the stakeholders and the design or the assessment. … The specified (design) service life or the residual service life are related to the required service life as given by the stakeholders and to other implications of the*

service criteria agreement e.g. with regard to structural analysis, maintenance and quality management".

Focusing on concrete structures and their durability performance, limit states can also be alternatively expressed by means of the service life format as:

$$P_f = P(t_S \le t_D) \le P_d \tag{3}$$

where t_D is the design life; the service life t_S can be determined as the sum of two service life predictors (periods):

$$t_S = t_i + t_p \tag{4}$$

In Eq. (4), t_i is the time at which the initiation of reinforcement corrosion takes place and t_p is the part of the service life after corrosion initiation – the propagation period. Frequently, the initiation period only serves as the decisive limit state. The direct consequence of passing this limit state is that possible future measures needed to repair the structure become more expensive.

2.2 Durability Limit States

Concerning reinforcement *corrosion* as one of the main stressors, appropriate limit states (i) − (vii) may be distinguished:

a) For limit states associated with the initiation period – the principal factors causing depassivation of reinforcement in concrete are carbonation and chloride ingress. Then:

   (i) The variables in Eq. (1) for the case of concrete carbonation may be interpreted as follows: R is concrete cover thickness and S is the actual (modelled) depth of carbonation at time t_D.

   (ii) In the case of chloride ingress, it is the critical concentration of Cl^- which leads to steel depassivation, and S is the actual concentration of Cl^- in contact with the reinforcement in the concrete at time t_D.

b) For limit states associated with the propagation period – the volume expansion of rust products develops tensile stresses in the surrounding concrete, leading to concrete cracking (mainly affecting the concrete cover). In such cases, the following LS can be recognised:

   (iii) R in Eq. (1) represents the critical tensile stress that initiates a crack in concrete at the interface with a reinforcing bar. S is the actual tensile stress in concrete at design service life t_D;

   (iv) Alternatively, R is the critical crack width at the concrete surface and S is the crack width at the concrete surface generated by reinforcement corrosion at time t_D.

   (v) When the progress of corrosion and consequently the opening of cracks continue, a network of cracks is propagated that possibly reaches the surface of the concrete cover. Together with cracks arising due to mechanical loading [6], a crack network may form and lead to the separation of concrete ele-

ments. Such delamination is a complex effect depending on e.g. the diameters of reinforcing bars, their location, concrete quality, coarse aggregate size, cover, the type and amount of loading, and the configuration of the structure. The limit state condition may contain for example the actual distance between cracks and the tolerated distance or the actual area of the reinforcement that is naked and the allowed one.

(vi) Given a decrease in the effective reinforcement cross-section due to corrosion and excessive deformation, loss of bearing capacity and finally the collapse of the member/structure in question may occur. In this situation, R is the actual (modelled) reinforcement cross-sectional area at time t_D and S is the minimum acceptable reinforcement cross-sectional area with regard to either an SLS or a ULS.

(vii) Finally, some changes will occur in the characteristics of the bond between steel and concrete due to corrosion. This may lead either to an excessive deflection of the structure or to a loss of structural strength. The former appears to be a more critical effect [7]. The bond may be modelled by using the time function of bond stress against to slip affected by the degree of reinforcement corrosion. The limit state condition may be defined using the actual bond between the steel and concrete and the minimum required bond.

LS (i) and (ii) are commonly regarded as belonging to the SLS category; the remaining LS listed above are either SLS or ULS depending on the impact on the structure's performance. Being random quantities, the relevant values of variables S and R used in Eq. (1) have to be assessed through the utilization of a suitable degradation model or by field or laboratory investigations. In the former case, effective probabilistic software tools should be utilized.

2.3 Example

It appears that predictive probabilistic models are needed to estimate how resistance, loads and safety levels will change over time. The software package FReET-D (a specialized module of FReET software at www.freet.cz) can be used efficiently. Models for carbonation, chloride ingress, reinforcement corrosion, sulphide, acid and frost attacks are provided. Some applications are described e.g. in [8].

A parametric study based on the following limit state condition has been extracted from [9] and is described below:

$$P_f(t_D) = P\left\{w_{cr} - w_a\left(t_D\right) \le 0\right\} \le P_d \tag{5}$$

where w_{cr} is the limit value of a crack width equal to 0.3 mm – one of the essential limits for the serviceability assessment of corrosion-affected RC structures recommended in CEN [10]. The actual corrosion-induced crack width w_a over time is computed according to an analytical model implemented in FReET-D and adopted from [11]. In this example, time t_D represents the propagation period only; to perform a service life prediction, the appropriate initiation period must be added.

All input information is listed in Tab. 1. Note that the adopted concrete is approximately of class C35/40, which is relevant e.g. to exposition class XD3 according to [10].

Fig. 1 shows the reliability index β vs. concrete cover for three different propagation time values; the limit value of $\beta = 1.5$ prescribed typically for SLS is also shown in the figure. It appears that e.g. for $t_D = 25$ years the cover should be greater than 50 mm to satisfy the serviceability requirements; for $t_D = 15$ years, 30 mm of cover would be satisfactory.

3 Life Cycle Costing

It should be noted that reliability level, limit state definition, target service life and cost-saving results are mutually related – some elements of whole life costs and benefits are service life dependent. These are especially:

(a) operating costs,

(b) maintenance costs, and

(c) repair and/or degraded element replacement costs (including any possible loss due to the discontinuation of operations).

Tab. 1: Input parameters for crack width analysis

Input parameter	Unit	Distribution	Mean/COV
Initial bar diameter	mm	Normal	20/0.02
Porous zone thickness	mm	Deterministic	0.0125
Concrete cover	mm	Deterministic	30-70
Time of exposure	years	Deterministic	15, 20, 25
Current density	μA/cm^2	Normal	1.5/0.2
Specific gravity of rust	kg/m^3	Normal	3600/0.02
Specific gravity of steel	kg/m^3	Normal	7850/0.01
Ratio of steel to rust molecular weight	-	Deterministic	0.57
Tensile strength of concrete	MPa	Lognormal (2 par)	3.3/0.12
Modulus of elasticity of concrete	GPa	Lognormal (2 par)	27/0.08
Poisson ratio of concrete	-	Deterministic	0.18
Creep coefficient	-	Deterministic	2
Material constant	-	Deterministic	1
Uncertainty factor of model	-	Lognormal (2 par)	1/0.15

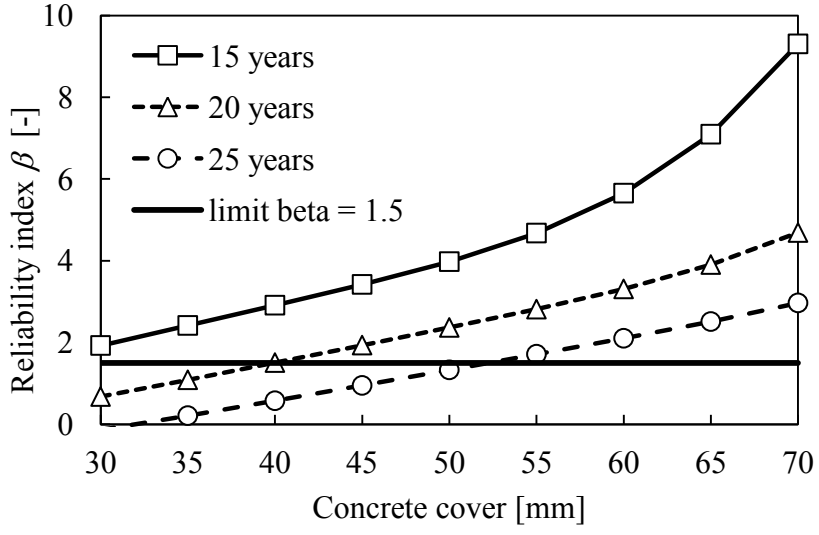

Fig. 1: Reliability index β after 15, 20 and 25 years of steel corrosion development (Eq. 5).

Typically, the effects listed in (c) can appear *with a certain probability* associated with the relevant limit state, i.e. with the probability of failure. This should be taken into account when making decisions about the optimization of costs and benefits. When doing this and when assessing some design variants, the parts of the costs in question are "weighted" by the probability:

$$C_{i,w} = P_f C_i \tag{6}$$

In the case of concrete structures, P_f is analyzed for the relevant limit state – see Section 2.2.

The level of reliability in the context of durability should be left to the client's decision together with the definition of a target service life, creating in this way a necessary background for the making of critical decisions (e.g. financial optimisation) – see e.g. [2] and [12].

4 Quantified risk utilization

Probabilistic risk and hazard assessment are increasingly being used in decision making for a wide range of applications. In certain situations, the evaluation of hazard scenarios and the associated risk analysis are based on structural lifetime considerations. In its *quantified form*, the risk R is defined as

$$R = P_f C \tag{7}$$

with P_f standing for probability of failure (accident, limit state) and C for the consequences associated with the negative event in question.

The value of quantified risk may be effectively utilized in risk management policies while, e.g.:

(a) Comparing the risk of analyzed LS appearance for several material or construction variants.

(b) Allocating R – contractual risk transfer as a form of risk management involves the allocation or distribution of the risks inherent to a construction project between or among contracting parties.

(c) Making decisions or assessing construction or material variants with regard to costs, schedules, quality or other factors.

In practice, the quantified form of the risk R is used only seldom; the authors believe the above activities can be enhanced in this respect. Again, FReET can be used; in case (a), P_f is analyzed for a relevant limit state of concrete structures – see the list in Section 2.2.

5 Conclusions

The role of probability values in different areas of structural engineering is described. Firstly, for safety management, i.e. for the assessment of time-dependent reliability level in the form of the probability of failure (which is an obvious and well known role). Secondly, in life cycle management, i.e. for life cycle costing purposes – the making of critical decisions considering financial optimisation. Finally, in risk management, i.e. for the quantification of risk. In the last two cases the demand of probability measure is not common, although it can have positive effects.

Acknowledgement

Financial support from a Brno University of Technology specific university research project, registered under the number FAST-S-13-2017, is gratefully acknowledged.

Literature

[1] ISO 13823. General Principles in the Design of Structures for Durability. ISO, 2008

[2] FIB. *fib Final Model Code*. *fib* Bulletins No. 65 and 66, Lausanne, Switzerland, 2012

[3] Frangopol, D.M., Saydam, D., Kim, S. Maintenance, management, life-cycle design and performance of structures and infrastructure: a brief review. *Structure and Infrastructure Engineering* 8 (2012), p. 1−25

[4] Thoft-Christensen, P. Infrastructure and life-cycle cost-benefit analysis. *Structure and Infrastructure Engineering* 8 (2012), p. 507−516

[5] ISO 2394. General principles on reliability for structures. ISO, 1998

[6] Miyazato, S., Otsuki, N. Steel Corrosion Induced by Chloride or Carbonation in Mortar with Bending Cracks or Joints. *Journal of Advanced Concrete Technology*, 8 (2010), p. 135−144

[7] Zhang, R., Castel, A., Francois, R. Serviceability Limit State criteria based on steel-concrete bond loss for corroded reinforced concrete in chloride environment. *Materials and Structures* 42 (2009), p. 1407−1421

[8] Vořechovská, D., Chromá, M., Podroužek, J., Rovnaníková, P., Teplý, B. Modelling of Chloride Concentration Effect on Reinforcement Corrosion. *Computer-Aided Civil and Infrastructure Engineering* 24 (2009), p. 446−458

[9] Teplý, B., Vořechovská, D. Reinforcement corrosion: Limit states, reliability and modelling. *Journal of Advanced Concrete Technology* 10 (2012), p. 353−362

[10] CEN. *General rules and rules for buildings*. EN 1992-1-1 Design of concrete structures, Part 1-1, Eurocode 2, 2003

[11] Li, C.Q., Melchers, R.E., Zheng, J.J. An analytical model for corrosion induced crack width in reinforced concrete structures. *ACI Structural Journal*, 103 (2006), p. 479−482

[12] Teplý, B. Durability, reliability, sustainability and client's decision. In: *CEBS 07 Prague Conference*, Prague, Vol. 1, 2007, p. 430−436

A Bayesian probabilistic method for radionuclide releases status estimation in nuclear accident scenario

Pierre Tricard, Sheng Fang, Jianlong Wang, Hong Li, Jiejuan Tong, Jun Zhao
Institute of Nuclear and New Energy Technology, Tsinghua University, Beijing
pierre.tricard@gmail.com

Abstract: The radionuclide release source estimation is the key issue of nuclear power plant safety status assessment. Due to the unavailability of thermal-hydraulic monitoring data, the release source status may only be obtained by inversing the radionuclide transportation process based on environmental monitoring data. To accomplish this task, a Bayesian probabilistic method was proposed in this study. This method reformulates the inverse problem of release estimation using the Ensemble Kalman Filter. The release status of the source is obtained by maximizing the a posteriori probability through recursive optimization procedure. The radionuclide transportation model and practical imperfectness of measurement were considered and integrated into the probabilistic estimation. The proposed method was verified using the twin experiment. The experiment results demonstrate that the proposed method can simultaneously provide most probable release and reduces the statistic fluctuations in measurements and the estimate matches the true release status well.

Keywords: source estimation, data assimilation, radionuclides, atmospheric dispersion

1 Introduction

The potential radioactive nuclides release in nuclear power plant accident is a primary concern of the safety of nuclear energy. Such radionuclide release information is also crucial for determining the emergency response after accident and minimizing its consequences. One promising way to access this information is to estimate the radionuclides release status by Bayesian probability method using off-site radiation monitoring data.

In recent years, many Bayesian techniques have been developed for this topic, such as the Kalman Filter (MA ET AL. [7]) or Monte Carlo algorithm (BERGIN ET AL. [2]). These techniques, also known as data assimilation methods, exploit the stochastic information behind monitoring data and estimate the release status based on appropriate stochastic process modeling and air dispersion modeling.

In previous studies, Gaussian models are often used to solve this problem since it only has limited inherent parameters and are very fast to compute which meet the requirement of

fast emergency response well. For instance, Gaussian plume model has been used by DREWS AT AL. [3] with an Extended Kalman filter, and by JEONG ET AL. [5] with an adaptive neuro-fuzzy inference system for source term estimation. Some other air dispersion models have also been implemented including Monte Carlo dispersion model (ZHENG ET AL. [13]) which is more precise for the case that terrain and climatic conditions are very irregular. However, these models are highly dependent on parameterization, and are computationally intensive, which might fail to provide timely source term information for emergency response.

In this paper, a source term estimation method that is based on the ensemble Kalman filter and a Gaussian puff model called RIMPUFF (developed by the Risø DTU National Laboratory [11]), was proposed for simultaneously estimation of the release rate and height of the radioactive emission in different atmospheric condition. Several types of accidental radionuclides release profiles and corresponding measurements were simulated, furthermore, a perturbation representing the captors sensitivity was added to the measurements. Non-constant releases were tested. A sensitivity study was also conducted to assess the influence of some important parameters such as meteorological condition, frequency of iterations and the release rate slope. The results show that the method can provide precise and robust estimation in most situations, including highly nonlinear release profiles.

2 Ensemble Kalman Filter

The Ensemble Kalman Filter (EnKF) is a Monte Carlo implementation of the Bayesian update problem: given the density probability of the state vector of the modeled system and associated measurements, the algorithm is used to obtain an estimation of the state vector. It is similar to the Kalman Filter, it assumes that all the probability density functions are Gaussian, however, it does not compute the covariance matrix. The EnKF represents the distribution of the system using a random sample (or ensemble), thus, the covariance matrix is replaced by the sample covariance which makes the algorithm more stable for high dimensional systems. Each element of this sample can be seen as a particle of the Particle Filter. The version of the Ensemble Kalman filter used in this study is based on the algorithm of GILLIJNS ET AL. [4].

Let $x = (a_1, a_2, ..., a_n)^T$ be the state vector we need to estimate given a p-dimensional series of observations $z = (z_1, z_2, ..., z_p)^T$. The ensemble $X_k = (x_k^1, x_k^2, ..., x_k^q)$, q being the sampling number, is created by the following relation:

$$\forall i \quad x_k^i = f(x_{k-1}^i) + w_k^i \tag{1}$$

with

w^i a perturbation,

f the relation that represents the time evolution of the state vector.

We can compute the forecast measurements ensemble $Y_k = (y_k^1, y_k^2, ..., y_k^q)$:

$$y_k^i = h(x_k^i) \tag{2}$$

with

h the relation between the state vector and the measurements.

We create then the error ensembles:

$$E_k^a = (x_k^1 - \bar{x}_k, x_k^2 - \bar{x}_k, ..., x_k^q - \bar{x}_k) \tag{3}$$

$$E_k^d = (y_k^1 - \bar{y}_k, y_k^2 - \bar{y}_k, ..., y_k^q - \bar{y}_k) \tag{4}$$

with

$\bar{x}_k$ the mean value of the ensemble X_k,

$\bar{y}_k$ the mean value of the ensemble Y_k.

Then, we approximate the error covariance matrices:

$$\hat{P}_k^{ad} = E_k^a \times (E_k^d)^T / (q-1) \tag{5}$$

$$\hat{P}_k^{dd} = E_k^d \times (E_k^d)^T / (q-1) \tag{6}$$

We can now compute the Kalman gain, and use it to correct the estimation of the state vector:

$$K_k = \hat{P}_k^{ad} \times (\hat{P}_k^{dd})^{-1} \tag{7}$$

$$X_{k+1} = X_k + K_k \left((z_k, ..., z_k) - Y_k \right) \tag{8}$$

$$x_{k+1}^{est} = \frac{1}{q} \sum_i x_{k+1}^i \tag{9}$$

In the Eg. (8), the matrix $(z_k, ..., z_k)$ is a $p \times q$ matrix in order to match with Y_k.

In our study, the state vector is composed of the release rate and the release height, the monitoring data vector is composed of the measurements gathered by all the captors. The evolution of the state vector is a random walk process, a classical method for source estimation, and the relation between the state vector and the measurements is the RIMPUFF model that is described below.

3 RIMPUFF model

RIMPUFF (Risø Mesoscale Puff) is a mesoscale atmospheric dispersion model designed for calculating the concentration and dose resulting from the dispersion of airborne materials (THYKIER-NIELSEN ET AL. [11]). Since this model can cope well with inhomogeneous terrain and meteorological situations, it has been often used for source estimation in accidental materials release. This model simulates the airborne materials emission by using a

succession of Gaussian shaped puffs that are released at a fixed rate. The amount of airborne materials allocated to each puff is the amount of particles that have been emitted between two successive puffs emissions. The model can be applied to both homogeneous and inhomogeneous terrain with moderate topography on a horizontal scale of up to 50 km (THYKIER-NIELSEN ET AL. [11]). The strong point of this model is that it is more reliable to estimate the release rate average value, especially if the rate is not constant.

For each grid point (x,y,z), the radionuclides concentration at time t is the superposition of all the puffs emitted:

$$C(x,y,z) = \sum_{i=1}^{N_{puff}} \frac{Q(i)\Delta t}{(2\pi)^{\frac{3}{2}}\sigma_{xy}^2(i)\sigma_z(i)} \exp\left(-\frac{1}{2}\frac{\left(x-x_c(i)\right)^2}{\sigma_{xy}^2(i)} - \frac{1}{2}\frac{\left(y-y_c(i)\right)^2}{\sigma_{xy}^2(i)}\right) \left[\exp\left(-\frac{1}{2}\frac{\left(z-z_c(i)\right)^2}{\sigma_z^2(i)}\right) + \exp\left(-\frac{1}{2}\frac{\left(2z_{inv}-z_c(i)\right)^2}{\sigma_z^2(i)}\right)\right] \tag{10}$$

with

$Q(i)$ the emission rate of the i^{th} puff,

Δt the time elapsed between two successive puff releases,

$\left(x_c(i), y_c(i), z_c(i)\right)$ the coordinates of the i^{th} puff center,

$\sigma_{xy}(i), \sigma_z(i)$ the puff dispersion parameters in horizontal and vertical direction,

z_{inv} the height of the inversion lid,

N_{puff} the number of emitted puffs at time t.

A puff can be visualized as a kind of spherical or ellipsoidal cloud, a body of air and suspended released material. The size of a single puff is determined by the dispersion parameters. Each puff is advected with the local wind speed at its center, which changes its size and position. The puffs are usually overlapped with each other and form different status of air dispersion.

The dispersion parameters are calculated using the Karlsruhe-Jülich law. The $\sigma_{xy}(i), \sigma_z(i)$ values are functions of the downwind distance x (in meters):

$$\sigma_{xy} = p_{xy} x^{q_{xy}} \tag{11}$$

$$\sigma_z = p_z x^{q_z} \tag{12}$$

with

p_{xy}, q_{xy}, p_z, q_z air dispersion coefficients that depend on the Pasquill-Gifford stability class and the release height.

4 Implementation

The accidental release was simulated in a field of 5 km × 2 km whose each grid cell size was 10 m × 10 m. A puff is released every 200 seconds from the source point (0,0,50). Every release was simulated for two hours, time during the data assimilation method will try to estimate the source parameters, release rate and height.

The radioactivity field below has been computed for a C atmospheric stability class, a wind speed of 2 m/s and a 1000 Bq/s release rate after 1 hour of emission.

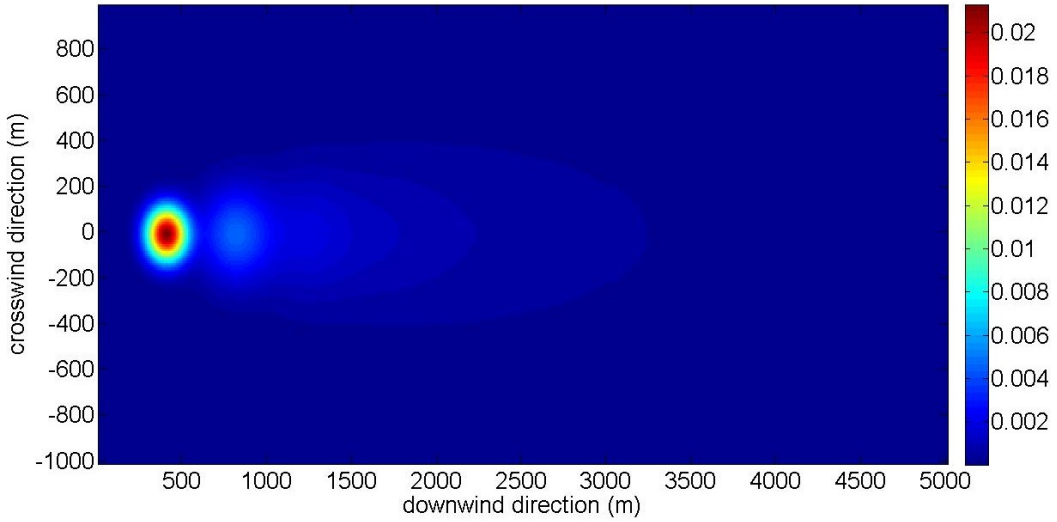

Fig. 1: Ground radioactivity after one hour release

3 rows of captors was set to simulate the radiation monitoring data. The first row was set at 200 m from the release point, and was composed of 2 captors 200 m far from each other. The second row was set at 600 m from the release point, and was composed of 2 captors 400 m far from each other. Finally, the last row was set at 1 km from the release point and is composed of 2 captors 600 m far from each other. In order to simulate the uncertainties related to the quality of the captors, a Gaussian white noise was added to the measurements.

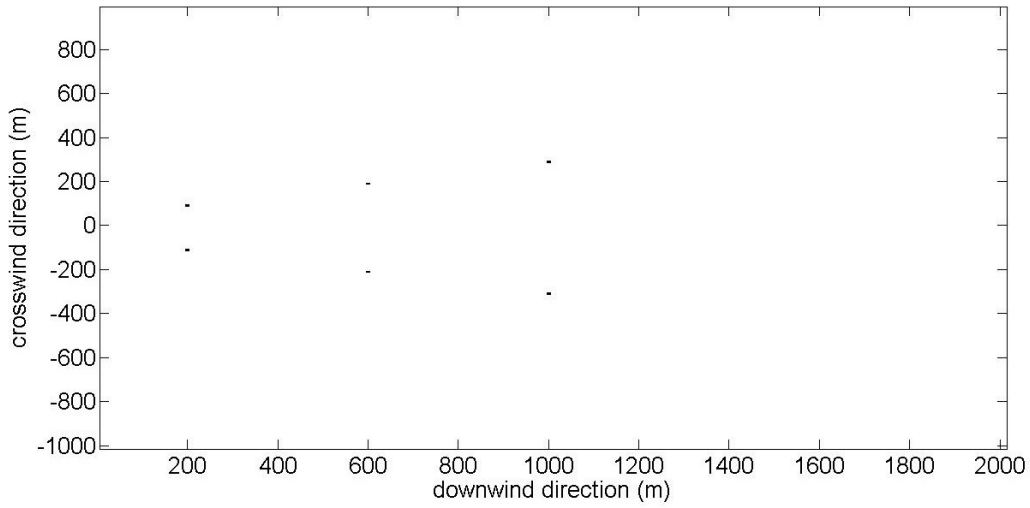

Fig. 2: Captors network for the experiment

The state vector was composed of several emission rates whose puff is in the range of the captor. We set this range from 10 m (because the model has some problems near the source emission point) to 2000 m, which was 1000 m from the last captor. It is assumed that a puff does not make substantial contribution to a captor if the distance between them is more than 1 km. The feasibility of ensemble Kalman filter was demonstrated with four kinds of release profiles:

The constant release:

$$q(t) = q_0 \tag{13}$$

The ramp profile:

$$q(t) = \begin{cases} 0 & t < t_0 \\ c(t - t_0) & t > t_0 \end{cases} \tag{14}$$

with

t_0 the time of the accident,

c the ramp coefficient.

The logarithm profile:

$$q(t) = \begin{cases} 0 & t < t_0 \\ Q_0 \ln(1 + \dfrac{t - t_0}{\tau}) & t > t_0 \end{cases} \tag{15}$$

with

t_0 the time of the accident,

Q_0 a coefficient that characterizes the amplitude of the profile

τ a coefficient that characterizes the evolution of the profile.

The inverse profile:

$$q(t) = \begin{cases} 0 & t < t_0 \\ Q_0 \dfrac{t - t_0}{t - t_0 + \tau} & t > t_0 \end{cases} \tag{16}$$

with

t_0 the time of the accident,

Q_0 the saturation value of the emission rate,

τ a coefficient that characterizes the evolution of the profile.

The last three profiles have a delay t_0 in order to simulate a sudden accident in the power plant. The ramp profile is simpler and enables to assess the effect of the ramp slope on the estimation; the logarithm profile and inverse profile are more complex and realistic.

Experimental conditions are summarized in the following table.

Tab. 1: Conditions for experimental setup

Parameters	Value
Time between two successive puffs Δt	200 s
Emission height	50 m
Atmospheric stability	C class
Wind speed	2 m/s in the x direction
Height of the inversion lid	1000 m
Duration of the experiment	2 h
Number of iterations	One every 30 s
Measurements perturbation	10^{-6} Bq/m^3
Release rate initial guess	700 Bq/s
Release height	80 m
Release height sample standard deviation	1 m
Measurements sample standard deviation	10^{-4} Bq/m^3

5 Results and discussion

5.1 Constant release

An emission of a constant release whose rate is equal to 1000 Bq/s was simulated. The initial guess was set to 700 Bq/s and 80 m. Fig. 3 shows that the estimation is fast and accurate. Indeed, after 700 s (about 12 minutes), the estimation error is already less than 10% for both of the parameters.

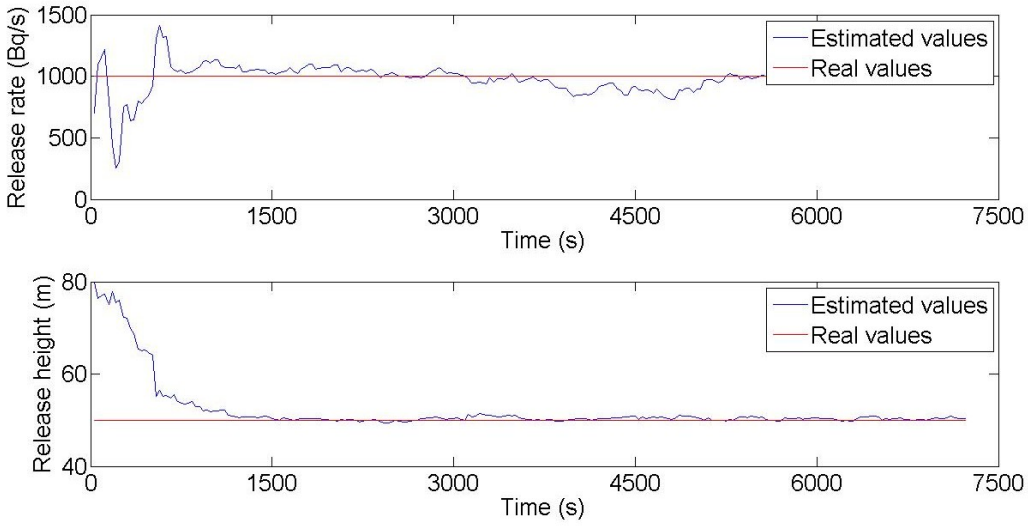

Fig. 3: Constant release estimation

5.2 Non-constant release

5.2.1 Ramp profile

The EnKF was also utilized to estimate the release rate which does not remain constant. In this part, the accidental release is supposed to happen 400 s after the beginning of the experiment. The first case is a ramp with a coefficient of $1 Bq/s^{-2}$ (see the Eq. 14). We set the initial guesses to 700 Bq/s and 80 m. We can see on the Fig. 4 that the EnKF deals well with this situation. The average error for the release rate is less than 10%, and the estimation error for the release height is around 2% after 2 h. It is interesting now to assess if it can be as efficient with non-linear release profiles.

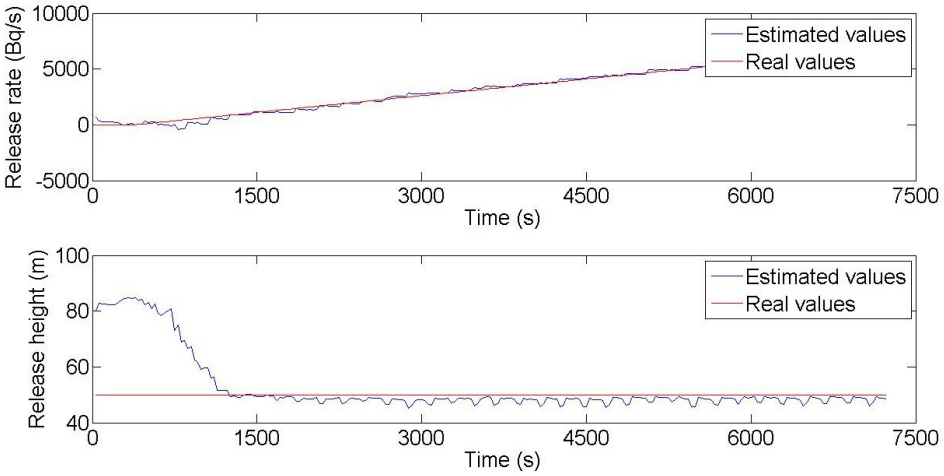

Fig. 4: Ramp profile release estimation

5.2.2 Logarithm profile

The logarithm profile is more close to a real accidental release. The characteristics of this emission are fixed to $Q_0 = 500$ Bq/s and $\tau = 100$ s (see the Eq. 15). The initial guesses are set to 0 Bq/s and 80 m. The results are shown on Fig. 5. The estimation is pretty accurate, even at the beginning of the accident. The average error for the estimation of the release rate is less than 7%, and the error for the estimation of the release height is less than 1% after 2 h. Thus, the Ensemble Kalman filter deals well with logarithm release rates.

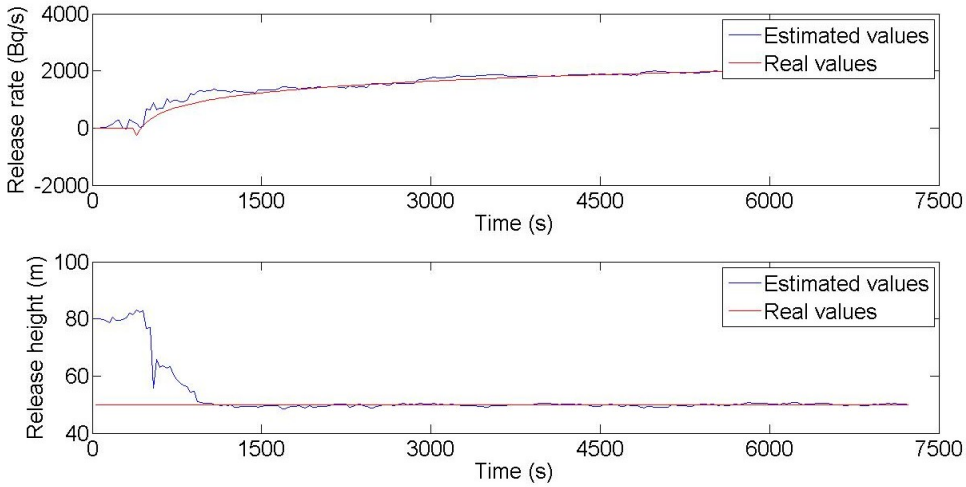

Fig. 5: Logarithm profile release estimation

5.2.3 Inverse profile

An inverse profile can simulate the sudden rise of release rate of emission. The characteristics of this emission are fixed to $Q_0 = 1000$ Bq/s and $\tau = 1000$ s (see the Eq. 16). The initial guesses are fixed to 0 Bq/s and 80 m. The results are satisfying. Indeed, the average estimation error is around 10% for the release rate and the estimation error for the release height is less than 2% after 2 h.

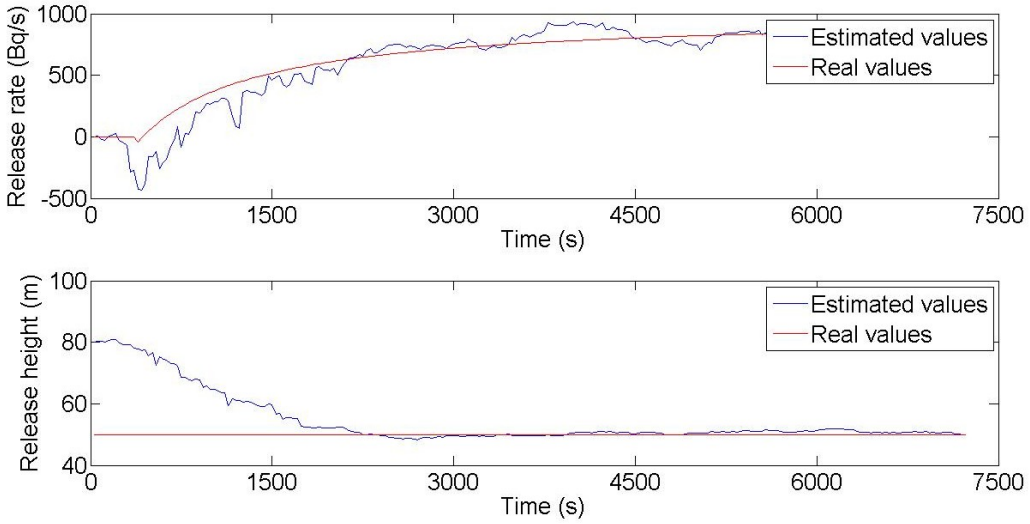

Fig. 6: Inverse profile release estimation

As a result, the EnKF shows promising results to estimate on-line the release rate and height for many kinds of releases, whether it is constant, non-constant, non-linear… We shall test its robustness in the next part by conducting a sensitivity study.

5.3 Sensitivity study

The influence of the following three important parameters were assessed in this study: the number of iterations, the meteorological conditions (atmospheric stability class) and the slope of the release rate. In all those cases, only the parameter that we want to test the influence changes, the others are fixed as in the experiment in Sec. 5.1.

5.3.1 Influence of the number of iterations

The Tab. 2 shows the results of three experiments where the value of the number of iterations has been changed.

Tab. 2:

Number of iterations	Real values	Estimated values
1 every 5 seconds	q = 1000 Bq/s, h = 50 m	q_{est} = 846 Bq/s, h = 49.8 m
1 every 30 seconds	q = 1000 Bq/s, h = 50 m	q_{est} = 992 Bq/s, h = 50.0 m
1 every 2 minutes	q = 1000 Bq/s, h = 50 m	q_{est} = 979 Bq/s, h = 50.7 m

To conclude, the number of iterations has an influence on the estimation. The results are less precise if the iteration frequency is very high or very low. The results are very satisfying when the iteration period is between 10 s and 1 minute.

5.3.2 Influence of meteorological conditions

The Tab. 3 presents the results of three experiments which show the influence of the stability class. The A stability class represents extremely unstable conditions, the C stability class represents slightly unstable conditions, and the E stability class represents slightly stable conditions.

Tab. 3:

Atmospheric stability class	Real values	Estimated values after 2 h
A	q = 1000 Bq/s, h = 50 m	q_{est} = 950 Bq/s, h = 50.0 m
C	q = 1000 Bq/s, h = 50 m	q_{est} = 987 Bq/s, h = 50.5 m
E	q = 1000 Bq/s, h = 50 m	q_{est} = 1023 Bq/s, h = 51.0 m

Therefore, the estimation is more accurate for more stable atmospheric conditions. Furthermore, the estimation in very unstable conditions takes longer to be accurate. Indeed, for the stability class A, it takes 176 iterations (4280 s) to reach an estimation error lower than 10%, whereas it only takes 42 iterations (1260 s) to reach an estimation error lower than 10% for the stability class E.

5.3.3 Influence of the slopes

The influence of the slope is related to the standard deviation of the random walk process. Indeed, if the slope is very high, it means that the release rate is increasing very quickly, thus the standard deviation of the random walk process has to be very high to make a good estimation.

Tab. 4:

Slope steepness	Random walk process standard deviation	Average error of the release rate estimation	Estimated release height after 2 h
1 Bq/s^{-2}	100 Bq/s	13%	48.8 m
10 Bq/s^{-2}	100 Bq/s	8.2%	48 m
100 Bq/s^{-2}	100 Bq/s	227%	5x10^{3} m
100 Bq/s^{-2}	1000 Bq/s	15%	46 m
1000 Bq/s^{-2}	1000 Bq/s	10^{7}%	109 m
1000 Bq/s^{-2}	10000 Bq/s	11%	46 m

Therefore, when an accident occurs, it is important to have access to some information in order to fix a random walk process appropriate to the situation.

6 Conclusion

The purpose of this study was to assess if the Ensemble Kalman Filter was suited for online estimation of two parameters, the release rate and release height in case of accidental radioactive emission. This twin experiment shows promising results. Indeed, the EnKF manages to estimate in a short amount of time those two parameters, the estimation error is usually less than 10%. Moreover, it deals well with non-constant releases, whether the pro-

file is linear or non-linear. However, the major drawback of this method is the difficulty to parameter the standard deviation of the random walk process to create the sample. This value has to be of the same magnitude than the release rate. A possibility is to use some on-site information or the first measurements in order to give a relevant value to this parameter. Nonetheless, this method shows promising results for practical usage and should be tested in a real on-site experiment.

Literature

[1] Astrup, P., Turcanu, C., Puch, R.O., Rojas Palma, C., Mikkelsen, T. *Data assimilation in the early phase: Kalman filtering RIMPUFF*. Risø-R-1466(EN), 2004

[2] Bergin, M.S., Milford, J.B. Application of Bayesian Monte Carlo analysis to a Lagrangian photochemical air quality model. *Atmospheric Environment* 34 (1999), p. 781–792

[3] Drews, M., Lauritzen, B., Madsen, H., Smith, J.Q. Kalman filtration of radiation monitoring data from atmospheric dispersion of radioactive materials. *Radiation Protection Dosimetry* 111(3) (2004), p. 257–269

[4] Gillijns, S., Barrero Mendoza, O., Chandrasekar, J., De Moor, B.L.R., Bernstein, D.S., Ridley, A. What Is the Ensemble Kalman Filter and How Well Does it Work? *Proceedings of the 2006 American Control Conference*. 2006

[5] Jeong, H.J., Han, M.H., Hwang, W.T., Kim, E.H. Application of data assimilation to improve the forecasting capability of an atmospheric dispersion model for a radioactive plume. *Annals of Nuclear Energy* 35 (2007), p. 838–844

[6] Krystaa, M., Bocquet, M., Sportisse, B., Isnard, O. Data assimilation for short-range dispersion of radionuclides: An application to wind tunnel data. *Atmospheric Environment* 40 (2006), p. 7267–7279

[7] Ma, Y., Wang, D. *Inversion Method of Source Term in Nuclear Accident based on Gaussian Puff Model*. ICONE 19, 2011

[8] Mandel, J. *A Brief Tutorial on the Ensemble Kalman Filter*. UCDHSC/CCM Report No. 242, 2007

[9] Quélo, D., Sportisse, B., Isnard, O. Data assimilation for short range atmospheric dispersion of radionuclides: a case study of second-order sensitivity. *Journal of Environmental Radioactivity* 84 (2005), p. 393–408

[10] Shankar Rao, K. Source estimation methods for atmospheric dispersion. *Atmospheric Environment* 41 (2007), p. 6964–6973

[11] Thykier-Nielsen, S., Deme, S., Mikkelsen, T. *Description of the Atmospheric Dispersion Module RIMPUFF*. RODOS (WG2)-TN(98)-02, 1999

[12] Zheng, D.Q., Leung, J.K.C., Lee, B.Y. An ensemble Kalman filter for atmospheric data assimilation: Application to wind tunnel data. *Atmospheric Environment* 44 (2010), p. 1699–1705

[13] Zheng, D.Q., Leung, J.K.C., Lee, B.Y. Online update of model state and parameters of a Monte Carlo atmospheric dispersion model by using ensemble Kalman filter. *Atmospheric Environment* 43 (2009), p. 2005–2011

Structural reliability quantification and cost-based design optimization of concrete elements subjected to fire

Ruben Van Coile, Robby Caspeele, Luc Taerwe
Magnel Laboratory for Concrete Research, Faculty of Engineering and Architecture, Ghent University, Ghent
ruben.vancoile@ugent.be, robby.caspeele@ugent.be, luc.taerwe@ugent.be

Abstract: Fire is one of the most severe loads for concrete structures. Consequently, fire resistance is an important consideration during design. However, current design practice is generally governed by prescriptive design rules which are based on experience and do not explicitly take into account e.g. the damage costs due to a fire-induced failure and the probability of fire ignition and successful fire suppression. A more rational approach would be to take into account the characteristics of the structure and to determine the economic optimum fire safety design. As an example, the methodology is applied for determining the economic optimum concrete cover of a simply supported concrete slab, considering a more refined structural reliability calculation based on a mixed-lognormal modelling of the bending resistance.

Keywords:cost optimization, fire, concrete cover, concrete slab

1 Introduction

Structural fire safety is a topic of general concern. However, current design rules and common practice focus on meeting prescriptive requirements which are based on experience and do not necessarily correspond with the optimum investment in structural fire safety. A more rational approach would be to consider the specific characteristics of the structure and its intended use, and to determine the economic optimum fire safety design. This optimum is obtained by minimizing the total costs, explicitly taking into account e.g. the fire ignition frequency, the probability of successful fire suppression, the probability of structural failure in case of fire and the damage costs due to a fire-induced failure. Consequently, this type of optimization balances up-front investments in additional safety with the expected benefits from loss-prevention.

2 Cost-optimization of structural elements

The cost-optimization of structural elements can be based on the utility function $Y(p)$ as proposed by ROSENBLUETH AND MENDOZA [13] and elaborated by RACKWITZ [11]:

$$Y(p) = B(p) - C(p) - D(p) \tag{1}$$

with

p an optimization design parameter

$B(p)$ the benefit function

$C(p)$ the initial cost of construction

$D(p)$ the costs due to failure

Maximizing $Y(p)$, an optimum utility is achieved which balances current investments with the expected future benefits from loss prevention. Therefore, all future costs and benefits should be discounted. In accordance with[11], a continuous discounting function is used relating a future monetary sum $A(t)$ to its value at the time of construction $A(0)$:

$$A(0) = A(t)\exp(-\gamma t) \tag{2}$$

with

γ the continuous discount rate

t the time (in years)

The theoretical optimum is determined by assuming a systematic replacement after failure and an indefinite lifetime of the structure. While greatly simplifying the calculations, the indefinite lifetime does not constitute a problem for most situations as the discounting function (2) ensures that the results are not significantly affect by long-term costs.

The benefit function $B(p)$ is related to a benefit rate b which can be assumed constant and independent of the occurrence of failures if the reconstruction time is small compared to the time between failures. Considering a systematic replacement after failure, $B(p)$ can be written as:

$$B(p) = \int_0^\infty b\exp(-\gamma t)\,\mathrm{d}t = \frac{b}{\gamma} \tag{3}$$

The construction cost $C(p)$ can be considered to be composed of a cost C_0 independent of the design parameter p and a cost C_1 which is function of p:

$$C(p) = C_0 + C_1(p) = C_0\left(1 + \varepsilon(p)\right) \tag{4}$$

with

ε the ratio of $C_1(p)$ to C_0

The failure cost $D(p)$ is composed of the cost of reconstruction and the external damages due to failure. These external damages incorporate both human casualties and indirect costs such as business interruptions and social distress experienced by people affected by

the failure. A theoretical study of failure costs was made by KANDA and SHAH [8]. Based on past experience from earthquakes and learned guesses the ratio ξ of the costs due to a single failure to the initial construction cost $C(p)$ was found to be in the range of 2 for private houses, 7 for tall office buildings and over 2000 for nuclear power plants. Assessing the monetary value of human life and indirect costs falls outside the scope of this paper and hence optimum solutions will be calculated as a function of this cost ratio ξ. Considering systematic replacement after failure, $D(p)$ can be written as:

$$D(p) = \xi C_0 \left(1+\varepsilon(p)\right) \sum_{n=1}^{\infty} \int_0^{\infty} \exp(-\gamma t) f_n(t,p)\,\mathrm{d}t \tag{5}$$

with

$f_n(t,p)$ the probability density function (PDF) describing the time to the n^{th} failure

Using Laplace transform and the convolution theorem, Eq. (5) simplifies to:

$$D(p) = \xi C_0 \left(1+\varepsilon(p)\right) \sum_{n=1}^{\infty} \left[f^*(\gamma,p) \right]^n = \xi C_0 \left(1+\varepsilon(p)\right) \frac{f^*(\gamma,p)}{1-f^*(\gamma,p)} \tag{6}$$

with

$f^*(\gamma,p)$ the Laplace transform of the PDF of the time to first fire-induced failure

Considering Eqs. (3)−(6), Eq. (1) can be written as:

$$Y(p) = \frac{b}{\gamma} - C_0 \left(1+\varepsilon(p)\right) \left(1+\xi \frac{f^*(\gamma,p)}{1-f^*(\gamma,p)} \right) \tag{7}$$

As the optimum design corresponds with the maximum of $Y(p)$, this design solution is obtained when the derivative of Y is equal to zero:

$$\frac{\mathrm{d}Y(p)}{\mathrm{d}p} = \frac{\mathrm{d}}{\mathrm{d}p} \left[C_0 \left(1+\varepsilon(p)\right) \left(1+\xi \frac{f^*(\gamma,p)}{1-f^*(\gamma,p)} \right) \right] = 0 \tag{8}$$

3 PDF of the time to first fire-induced structural failure

Evaluating the optimization criterion (8) requires calculating the Laplace transform of the probability density function (PDF) describing the time to the first fire-induced failure:

$$f^*(\gamma,p) = \int_0^{\infty} \exp(-\gamma t) f_1(t,p)\,\mathrm{d}t \tag{9}$$

with

$f_1(t,p)$ the PDF of the time to first fire-induced failure

The probability density function of the time to first fire-induced structural failure $f_1(t,p)$ depends on the fire ignition frequency, the probability of successful fire suppression and the probability of structural failure in case of a fully-developed fire.

3.1 The time to the first fully-developed fire

If fire ignitions are assumed independent, the time between fire ignitions T_{ig} can be modelled by an exponential distribution with parameter λ equal to the yearly probability of fire ignition p_1. Consequently, the time to the k^{th} fire ignition can be modelled by a Gamma distribution:

$$f_{Tig,k}(t) = \frac{\lambda(\lambda t)^{k-1}\exp(-\lambda t)}{(k-1)!} \tag{10}$$

The first fully-developed fire occurs when a fire ignition coincides with a failure of fire suppression. This probability of fire suppression p_{sup} is modelled in accordance with ALBRECHT and HOSSER [1] as:

$$p_{\text{sup}} = (1 - p_2 p_3 p_4) \tag{11}$$

with

p_2 the failure probability of fire suppression by users of the building

p_3 the failure probability of early fire suppression by the fire brigade

p_4 the failure probability of the sprinkler system

For a building without sprinklers (i.e. $p_4 = 1$), p_{sup} can be taken as 0.9. This value corresponds with a common probability of fire suppression by the users ($p_2 = 0.5$ according to [1]) and a fire brigade intervention time of less than 15 minutes (i.e. $p_3 = 0.2$).

The probability that the k^{th} fire ignition results in the first fully developed fire is:

$$P_{fi,k} = (1 - p_{\text{sup}})\, p_{\text{sup}}^{k-1} \tag{12}$$

with

$P_{fi,k}$ the probability that k^{th} ignition results in the first fully-developed fire

Combining Eqs. (10) and (12), the PDF of the time to the first fully developed fire is given by an exponential distribution with parameter $(1 - p_{sup})\lambda$:

$$f_{T,fi}(t) = \sum_{k=1}^{\infty}(1 - p_{\text{sup}})\, p_{\text{sup}}^{k-1} \frac{\lambda(\lambda t)^{k-1}\exp(-\lambda t)}{(k-1)!} = (1 - p_{\text{sup}})\,\lambda \exp\left(-(1 - p_{\text{sup}})\lambda t\right) \tag{13}$$

3.2 The time to the first fire-induced structural failure

Given the occurrence of a fully-developed fire, the severity of the fire can be linked to an ISO 834 standard fire duration t_E by taking into account for example the fire load and ventilation characteristics of the structure [9]. Alternatively, the standard fire duration t_E can be taken from national legal requirements which prescribe the resistance to fire as a function of the dimensions and the usage of the structure. For example in the UK, values of t_E can be found in Approved Document B (Fire Safety) [10].

Subsequently, the probability of failure $P_{f,tE}$ in case of exposure to t_E minutes of the standard fire should be assessed, using for example the advanced calculation tool described by VAN COILE ET AL. [15]. This probability of failure will depend on the characteristics of the structure.

Knowing $P_{f,tE}$, the probability that the k^{th} fire ignition results in the first fire-induced structural failure can be calculated as:

$$P_{f,fi,k} = P_{f,tE}\left(1-p_{\text{sup}}\right)\left(1-P_{f,tE}\left(1-p_{\text{sup}}\right)\right)^{k-1} \tag{14}$$

with

$P_{f,fi,k}$ the probability that the k^{th} ignition results in the first structural failure

Eq. (14) has the same layout as Eq. (12). Consequently, the time to the first fire-induced structural failure is given by:

$$f_{T,f,fi}\left(t\right) = P_{f,tE}\left(1-p_{\text{sup}}\right)\lambda\exp\left(-P_{f,tE}\left(1-p_{\text{sup}}\right)\lambda t\right) = f_1\left(t,p\right) \tag{15}$$

where $P_{f,tE}$ is a function of the design parameter p.

3.3 Evaluating the Laplace transform and the optimization criterion

As the time to the first fire-induced structural failure is described by an exponential distribution, the Laplace transform (9) can be evaluated analytically:

$$\begin{aligned} f^*\left(\gamma,p\right) &= \int_0^\infty \exp\left(-\gamma t\right) P_{f,tE}\left(1-p_{\text{sup}}\right)\lambda\exp\left(-P_{f,tE}\left(1-p_{\text{sup}}\right)\lambda t\right)\mathrm{d}t = \\ &= \frac{P_{f,tE}\left(1-p_{\text{sup}}\right)\lambda}{\gamma + P_{f,tE}\left(1-p_{\text{sup}}\right)\lambda} \end{aligned} \tag{16}$$

This allows to elaborate the optimization criterion (8):

$$\frac{\mathrm{d}\varepsilon\left(p\right)}{\mathrm{d}p}\left(1+\xi\frac{P_{f,tE}\left(p\right)\left(1-p_{\text{sup}}\right)\lambda}{\gamma}\right)+\left(1+\varepsilon\left(p\right)\right)\frac{\xi}{\gamma}\left(1-p_{\text{sup}}\right)\lambda\frac{\mathrm{d}P_{f,tE}\left(p\right)}{\mathrm{d}p} = 0 \tag{17}$$

The derivative of $P_{f,tE}$ may be evaluated numerically.

4 Application example: simply supported solid slab

A simply supported solid slab with a thickness of 0.2 m and a free span of 6 m is load-bearing in one direction and carries an uniformly distributed permanent load g_k consisting of the self-weight of the slab, and a uniformly distributed variable load q_k of 3.8 kN/m². According to EN 1990 [2], the design value of the bending moment M_{Ed} induced by these loads equals 50.4 kNm. Consequently, the design value of the bending moment capacity M_{Rd} calculated in accordance EN 1992-1-1 [3] should be larger than or equal to 50.4 kNm.

As many publications emphasize the importance of the concrete cover for structural fire resistance, e.g. [16], choosing a large concrete cover may correspond with additional safety in case of fire. However, for a constant value of M_{Rd}, increasing the concrete cover necessitates the placement of additional reinforcement bars. Consequently, an economic optimum concrete cover may be determined for which the up-front investment in additional reinforcement is balanced with a reduction of the expected losses due to fire-induced failures.

The basic variables used for describing the slab are given in Tab. 1, as well as the associated probabilistic models. These models are chosen in accordance with the study performed by HOLICKY AND SYKORA [6] and HOLICKY ET AL. [7].

Tab. 1: Probabilistic models for the basic variables involved in the analysed concrete slab

Symbol	Name	Distribution	Mean μ	Standard dev. σ
M_{Rd} [kNm]	design value of the bending moment capacity in normal design conditions	DET	50.4	-
h [mm]	thickness	N	200	5
f_c [MPa]	20°C concrete compressive strength (f_{ck} = 30 MPa)	LN	42.9	6.4
f_y [MPa]	20°C reinforcement yield stress (f_{yk} = 500 MPa)	LN	581.4	40.7
c [mm]	concrete cover {min = $\mu - 3\sigma$; max = $\mu + 3\sigma$}	Beta	c_{nom}	5
A_s [mm²]	bottom reinforcement area per m ($\varnothing$ = 10 mm)	N	1.02 $A_{s,nom}$	$0.02\mu_{As}$
$k_{fc(\theta)}$ [-]	concrete compressive strength reduction factor at temperature θ (see also [16])	Beta	θ-dependent	θ-dependent
$k_{fy(\theta)}$ [-]	steel yield stress reduction factor at temperature θ (see also [16])	Beta	θ-dependent	θ-dependent
K_R[-]	model uncertainty of the resistance effect	LN	1.1	0.11
K_E[-]	model uncertainty of the load effect	LN	1	0.1

The nominal reinforcement area $A_{s,nom}$ is defined by:

$$A_{s,nom} = \frac{\pi \varnothing^2}{4} \cdot \frac{1000}{s} \tag{18}$$

with

s horizontal spacing of the reinforcement bars
$\varnothing$ reinforcement bar diameter (10 mm)

The parameter s is varied as a function of the concrete cover in order to maintain a constant design value for the bending moment capacity M_{Rd}.

4.1 The probability of structural failure $P_{f,tE}(p)$

The probability of structural failure associated with an ISO 834 duration of t_E minutes is related to the limit state function:

$$Z = K_R M_{R,fi,t} - K_E \left(M_Q + M_G \right) \tag{19}$$

with

$M_{R,fi,t}$ bending moment capacity at t minutes of ISO 834 duration
M_G bending moment induced by the permanent load
M_Q bending moment induced by the variable load

For M_G a normal distribution is assumed, while for M_Q a Gumbel distribution is considered [6]. The model uncertainties K_R and K_E are described by a lognormal distribution (Tab. 1). Traditionally, a lognormal distribution is also considered as appropriate for the stochastic representation of the resistance effect [14]. However, as elaborated in [16], the uncertainty with respect to the concrete cover necessitates that the bending moment capacity $M_{R,fi,t}$ of concrete slabs during fire is modelled by a mixed-lognormal distribution:

$$M_{R,fi,t} = \sum_i P\left[c_i\right] M_{R,fi,t}\left(c_i\right) \tag{20}$$

with

$P\left[c_i\right]$ the probability of a concrete cover in the range $c_i \pm \Delta c/2$
$M_{R,fi,t}\left(c_i\right)$ the lognormal distribution of $M_{R,fi,t}$ for a fixed concrete cover c_i
Δc the concrete cover interval width (1 mm)

Consequently, the probability of failure (i.e. $P[Z < 0]$) can be written as:

$$P\left[Z<0\right] = \sum_i P\left[c_i\right] P\left[K_R M_{R,fi,t}\left(c_i\right) - K_E\left(M_Q + M_G\right) < 0 \right] = \sum_i P\left[c_i\right] P_{f,t}\left(c_i\right) \tag{21}$$

with

$P_{f,t}\left(c_i\right)$ the probability of failure for a fixed concrete cover c_i

For each of the constituent functions with lognormal distributed $M_{R,fi,t}(c_i)$, a FORM analysis can be applied together with the Rackwitz-Fiessler theorem to determine the reliability

index $\beta_{fi,t}(c_i)$. This reliability index can be associated with the failure probability $P_{f,t}(c_i)$ through [2]:

$$P_{f,t}(c_i) = \Phi\left(-\beta_{fi,t}(c_i)\right) \tag{22}$$

with

$\Phi(.)$ the standardized cumulative normal distribution

Evaluating Eqs. (21) and (22) for the slab configuration of Tab. 1 allows to visualize the probability of failure as a function of the ISO 834 fire duration t_E for different values of the nominal concrete cover c_{nom} (Fig. 1).

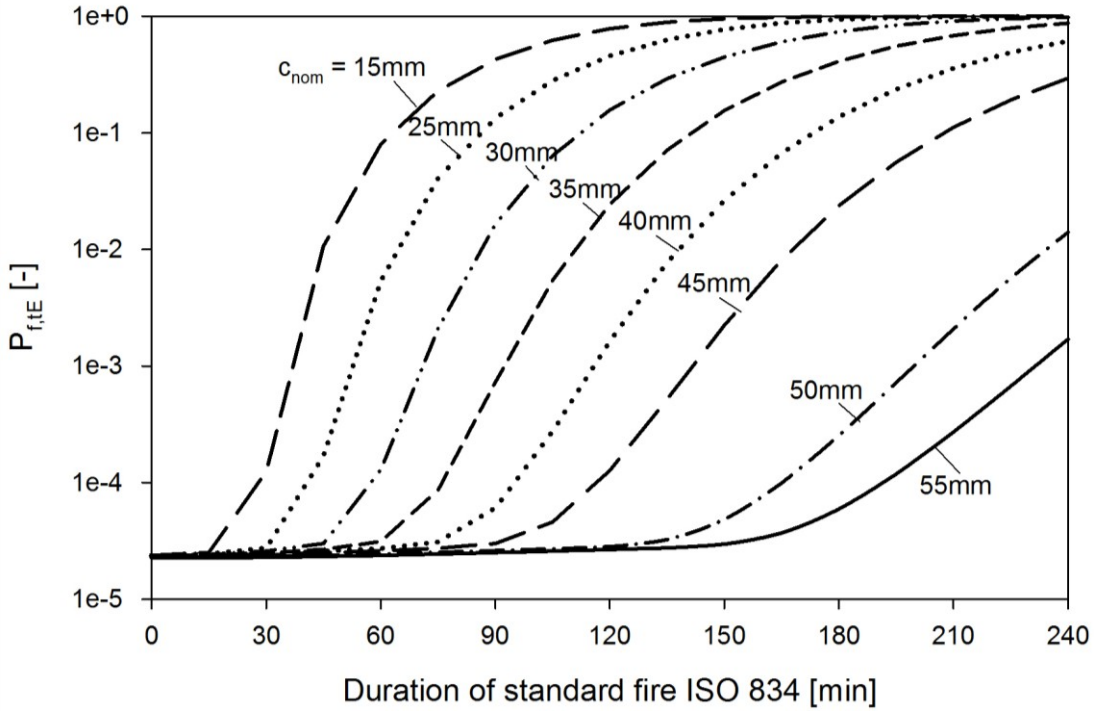

Fig. 1: Probability of failure for the example slab as a function of the ISO 834 exposure duration for different nominal concrete covers c

4.2 The ratio of additional investments in safety $\varepsilon(p)$

As defined above, $\varepsilon(p)$ is the ratio of the additional cost $C_1(p)$ associated with the design parameter p to the basic construction cost C_0. For the specific situation under consideration, the additional costs refer to the additional reinforcement bars necessary to compensate an increase in nominal concrete cover.

For the slab configuration of Tab. 1, Fig. 2 visualizes the relationship between an increase in concrete cover Δc and the corresponding increase in reinforcement area ΔA_s, with c_{ref} a reference concrete cover of 15 mm and $A_{s,ref}$ the associated reinforcement area (683 mm²). As illustrated in Fig. 2, the following linear approximation can be used:

$$\frac{\Delta A_s}{A_{s,ref}} \approx 0.11 \frac{\Delta c}{c_{ref}} = 0.11 \frac{c - c_{ref}}{c_{ref}} \tag{23}$$

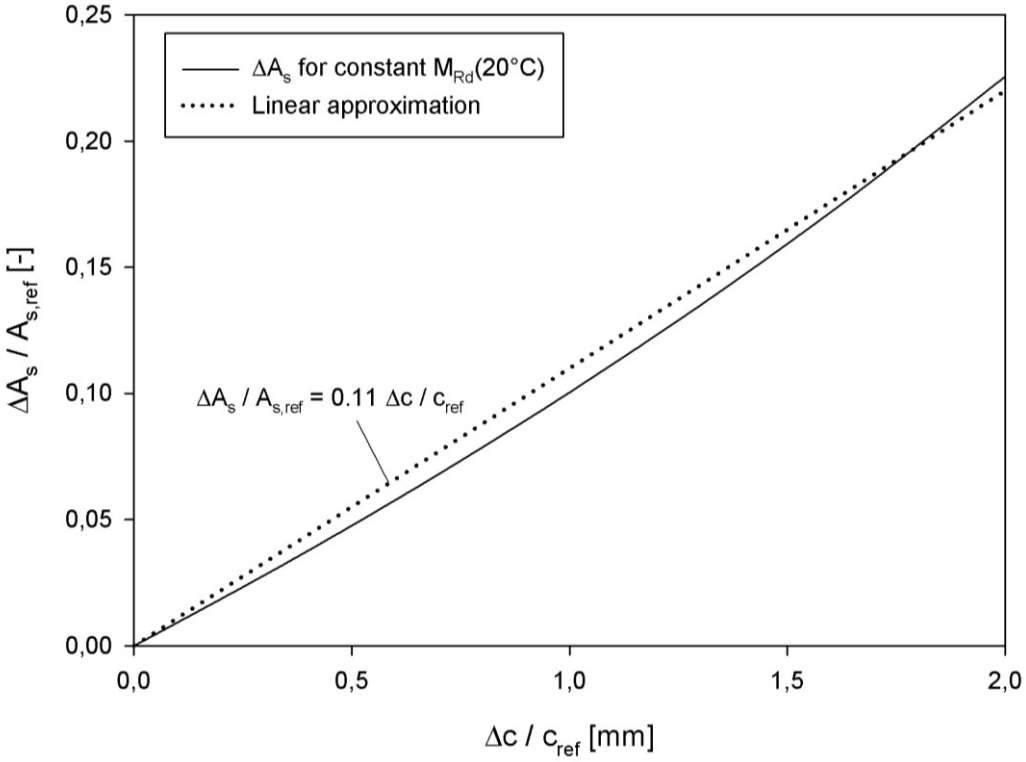

Fig. 2: Additional reinforcement area as a function of the increase in concrete cover

If the costs with respect to the additional reinforcement can be considered proportional with the reinforcement area, then:

$$\varepsilon(p) = \frac{C_1(p)}{C_0} = \frac{a \Delta A_s}{C_0} \frac{A_{s,ref}}{A_{s,ref}} = 0.11 \frac{a A_{sref}}{C_0} \frac{\Delta c}{c_{ref}} \tag{24}$$

with

a the proportionality constant

4.3 Evaluating the optimization criterion

Considering Eq. (24), the optimization criterion (17) can be evaluated as:

$$\begin{aligned} &0.11 \frac{A_{s,ref}}{C_0} \left(1 + \xi \frac{P_{f,tE}(p)\left(1 - p_{\text{sup}}\right)\lambda}{\gamma} \right) + \\ &+ \left(1 + 0.11 \frac{a A_{s,ref}}{C_0} \frac{\Delta c}{c_{ref}} \right) \frac{\xi}{\gamma} \left(1 - p_{\text{sup}}\right) \lambda \frac{\mathrm{d}P_{f,tE}(p)}{\mathrm{d}p} = 0 \end{aligned} \tag{25}$$

This optimization criterion gives the value of Δc which results in the lowest overall cost with respect to fire-induced structural failure. Fig. 3 visualizes this optimum nominal concrete cover c_{nom} for different ignition frequencies λ, as a function of the reinforcement cost ratio aA_{sref}/C_0. Other variables are taken for a high-rise office building: $t_E = 120$ minutes, $p_{sup} = 0.9$ and $\xi = 7$. Furthermore, the discount rate γ is assumed to be 0.03, as was used in [4] for optimizing the number of escape routes from road tunnels.

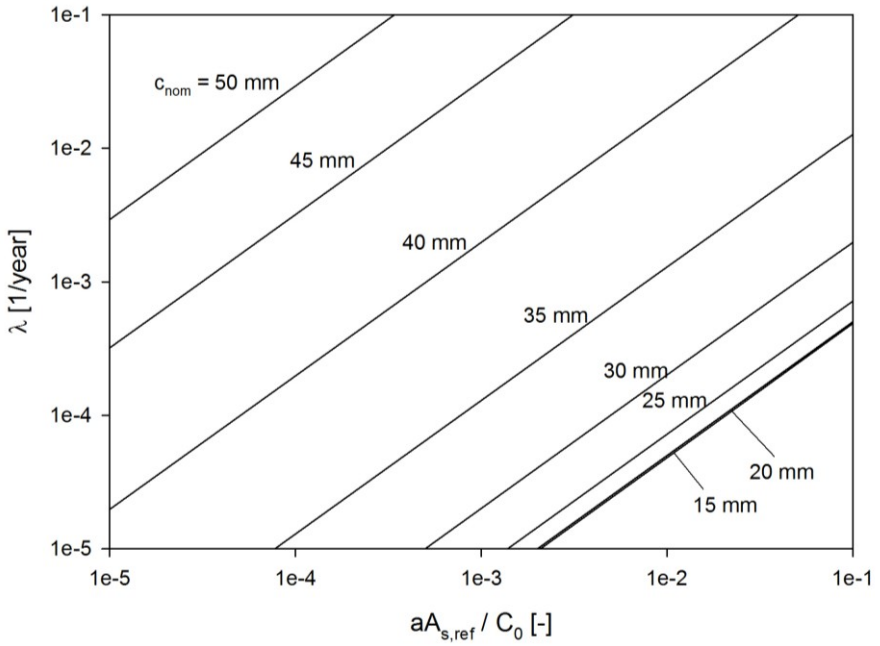

Fig. 3: Optimum concrete cover as a function of the reinforcement cost ratio and the fire ignition frequency λ, ($\xi = 7$, $p_{sup} = 0.9$, $\gamma = 0.03$, $t_E = 120$ minutes)

Fig. 3 illustrates how the fire ignition frequency can have an important influence on the optimum concrete cover. Similarly, the influence of the failure cost ratio ξ can be investigated. Assuming an ignition frequency of 2.5 10^{-3} per year for an office building, as indicated by RAHIKAINEN AND KESKI-RAHKONEN [12], the optimum concrete cover is given in Fig. 4 as a function of the reinforcement cost ratio for different values of ξ.

Fig. 4 indicates that a higher failure cost ratio ξ results in a larger optimum concrete cover. However, for large reinforcement cost ratio $aA_{s,ref}/C_0$, the optimum cover decreases.

Furthermore, there is no consensus considering the discount rate γ. The influence of the discount rate on the target reliability level for structures was investigated by HOLICKY in [5]. The effect of the discount rate on the optimum concrete cover for the slab configuration of Tab. 1 is investigated in Fig. 5.

It is concluded that the discount rate is an important parameter with respect to the cost-optimization of structural elements. As expected, a higher discount rate favours less up-front investment in safety, while a low discount rate corresponds a with higher concrete cover as the optimum design.

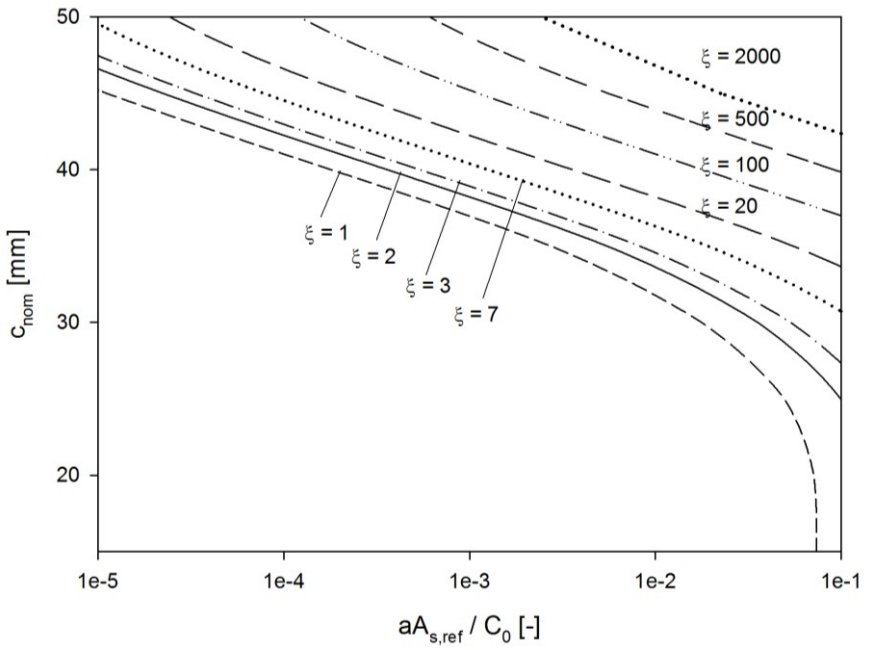

Fig. 4: Optimum concrete cover as a function of the reinforcement cost ratio and the failure cost ratio ξ, ($\lambda = 2.5\ 10^{-3}$ per year, $p_{sup} = 0.9$, $\gamma = 0.03$, $t_E = 120$ minutes)

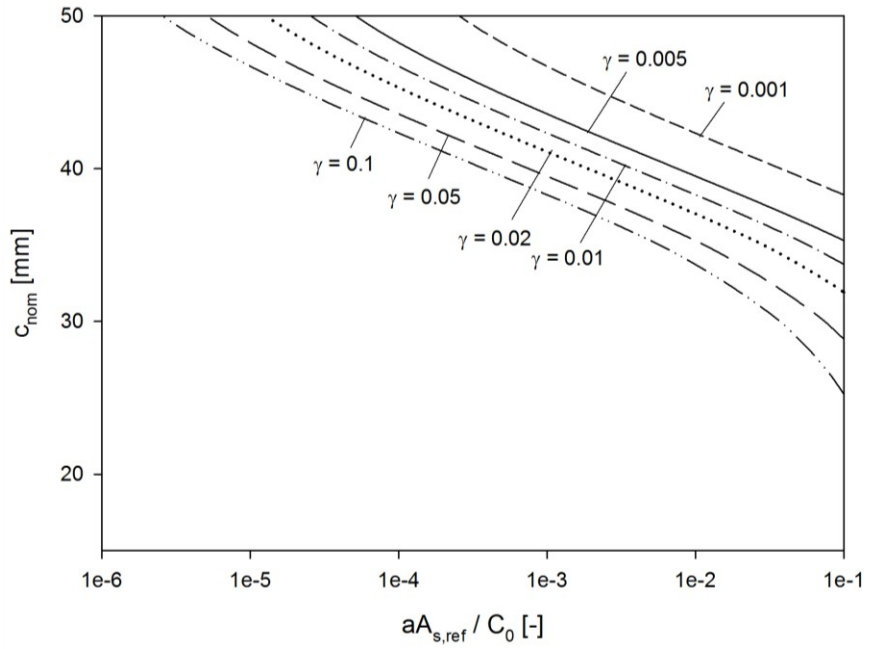

Fig. 5: Optimum concrete cover as a function of the reinforcement cost ratio and the discount rate γ, ($\xi = 7$, $\lambda = 2.5\ 10^{-3}$ per year, $p_{sup} = 0.9$, $\gamma = 0.03$, $t_E = 120$ minutes)

5 Conclusions

- Mathematical formulations for deriving optimum design solutions for structural elements exposed to fire are presented. The optimization balances up-front investments in structural safety with the expected benefits from loss prevention.

- As an example application, the economic optimum concrete cover is derived for a specific simply-supported concrete slab configuration as a function of the fire ignition frequency, the failure cost ratio and the cost of additional reinforcement. Parameter studies are presented demonstrating the effect of changes in key parameters on the optimum design solution.
- The derived formulations are generally applicable and can be used for other design problems as well, e.g. the optimum reinforcement ratio of a concrete column, or the optimum investment in fire suppression measures in a wooden building.

Literature

[1] Albrecht, C., Hosser, D. Risk-informed framework for performance-based structural fire protection according to the eurocode fire parts. *Proceedings of the 12th Interflam Conference*. 2010, p. 1031–1042

[2] CEN, EN 1990: *Basis of structural design*. European Standard, 2002

[3] CEN, EN 1992-1-1: *Design of concrete structures: Part 1-1: General rules and rules for buildings*. European Standard, 2004

[4] Holický, M. Probabilistic risk optimization of road tunnels. *Structural Safety* 31 (2009), p. 260–266

[5] Holický, M. Optimisation of the target reliability for temporary structures. *Civil Engineering and Environmental Systems* 30 (2013), p. 87–96

[6] Holický, M., Sýkora, M. Stochastic models in analysis of structural reliability. *Proceedings of the International Symposium on Stochastic Models in Reliability Engineering, Life Sciences and Operation Management*. 2010

[7] Holický, M., Retief, J.V., Dunaiski, P.E. The reliability basis of design for structural resistance. *Proceedings of the third International Conference on Structural Engineering Mechanics and Computation (SEMC)*. 2007

[8] Kanda, J., Shah, H. Engineering role in failure cost evaluation for buildings. *Structural Safety* 19 (1997), p. 79–90

[9] Kodur, V.K.R., Pakala, P., Dwaikat, M.B. Energy based equivalent approach for evaluating fire resistance of reinforced concrete beams. *Fire Safety Journal* 45 (2010), p. 211–220

[10] National Building Specification. *Approved Document B – Fire Safety: Volume 2 – Buildings other than dwellinghouses (2013 edition)*. 2013

[11] Rackwitz, R. Optimization – the basis of code-making and reliability verification. *Structural Safety* 22 (2000), p. 27–60

[12] Rahikainen, J., Keski-Rahkonen, O. Statistical Determination of Ignition Frequency of Structural Fires in Different Premises in Finland. *Fire Technology* 40 (2004), p. 335–353

[13] Rosenblueth, E., Mendoza, E. Reliability Optimization in Isostatic Structures. *Journal of the Engineering Mechanics Division* 97 (1971), p. 1625–1642

[14] Torrent, R.J. The log-normal distribution: a better fitness for the results of mechanical testing of materials. *Matériaux et Constructions* 11 (1978), p. 235–245

[15] Van Coile, R., Caspeele, R., Taerwe, L. Quantifying the structural safety of concrete slabs subjected to the ISO 834 standard fire curve using full-probabilistic FEM. *Proceedings of the 10th International Probabilistic Workshop*. 2012, p. 313–330

[16] Van Coile, R., Caspeele, R., Taerwe, L. The mixed lognormal distribution for a more precise assessment of the reliability of concrete slabs exposed to fire. *Proceedings of the European Safety and Reliability Conference (ESREL 2013)*. In press

TOPAAS – A method to quantify the probability of software failure

Sipke van Manen
Rijkswaterstaat, Ministry of Infrastructure and the Environment, the Netherlands
sipke.van.manen@rws.nl

Abstract: In the Netherlands law imposes quantitative probabilistic requirements on the probability of flooding of an area. The supervisor of the flooding protection system of a flood prone area is obliged to show that these probabilistic requirements are met. The protection system usually consists of dykes, dams, locks and storm surge barriers. The use of software in these systems is increasing and the probability of failure of a lock or movable flood barrier is determined not only by its hardware components, but increasingly more so by the software involved. Other areas where Quantitative Risk Assessment (QRA) is important are the road and waterway networks maintained by the Ministry of Infrastructure and the Environment. The availability of these networks is determined by capacity, maintenance and traffic management. The relation between costs of maintenance and traffic management on one hand and the availability of the network on the other becomes transparent with the use of QRA. Here too, the software of the systems (i.e. tunnels, movable bridges, sluices) is increasingly important and software failure frequently determines the availability of (parts of) the network. This evolvement makes it necessary to be able to quantify the probability of failure of software. Some accepted methods on quantification of software reliability exist, but none of them is generally applicable, as will be shown. A new model is proposed, based on critical software properties and expert opinion, bringing software into the QRA domain by introducing the probability of failure of software modules as basic events in a Fault Tree Analysis. The method is called TOPAAS: Task Oriented Probability of Abnormalities Analysis for Software. An example is given.

Keywords: software, probability, expert opinion, quality

1 Introduction

Software is becoming a more and more important component in many systems. Software failure turns out to be the origin of system failure in a growing number of cases and determines in an increasing way the reliability and availability of the system. This shows espe-

cially in cases where the software is little used, as is the case in safety-related systems. Due to the specific nature of software, i.e. lack of deterioration, systems that are frequently used soon become bug free and thus reliable.

Rijkswaterstaat uses QRA to develop and maintain its safety devises. These devices run from tunnel operating systems to decision support systems for storm surge barriers. The reason for Rijkswaterstaat to use QRA is twofold.

First, and most important, is transparency. QRA shows the weak spots in reliability or safety of the system and makes it possible to focus on these components. Optimization with regard to costs or other targets becomes possible. Transparency also facilitates communication with laymen, usually political decision makers.

The second advantage of QRA is that requirements can be specified in probabilistic terms. The flood protection system in the Netherlands is based on probabilistic requirements. But also tunnel safety is being bound by an acceptable probability of failure.

As software becomes increasingly important, it becomes increasingly important to be able to quantify its probability of failure in order to use this component probability in a QRA frame. This article shows a new method, called TOPAAS, by which an estimate of the probability of failure of a software module can be established.

The remainder of this paper describes why software failure differs from other types of component failures and evaluates current methods to quantify software reliability. Finally, TOPAAS is introduced and a simple example is given.

2 Specific properties of software

In general, the probability of failure of hardware components, like motors, pumps, valves, etc. is derived by either:

- history, compiled in databases,
- calculation, if a mathematical description of the physical behavior is available,
- expert opinion, if both methods mentioned above, fail.

The probability of failure of human actions is intensively studied in the last 40 years, with the SWAIN AND GUTTMAN [18] handbook as a very important landmark. Many methods and tools have been developed by which general accepted estimates of the probability of failure of human actions can be derived.

Software behavior is quite different from hardware or human behavior. Software failure is by definition systematic, caused by faults introduced during development (requirements definition, design and implementation). And if the fault is fixed properly it will never show up again. Physical processes like stress and wear are absent in the case of software. Software performs faultless in repeating tasks, but may fail in incidental tasks at a new, never before executed path, introduced by new input or by circumstances that have not yet occurred at previous runs of the software.

Although software failure is systematic in nature, random failure can be observed due to creation processes, leaving defects at unknown places, and environmental circumstances

causing unforeseen/untested input combinations. Therefore the probability of failure is a software property too and statistical analysis on this property is feasible, see e.g. [10].

To our knowledge there are (only) two well-known means to estimate the probability of failure of software:

- Reliability Growth Modeling
- Monte Carlo Simulation

Reliability Growth Modeling is based on the principle that the reliability of software grows every time a defect is found and properly corrected [13], [14]. When a significant number of defects over time is available, statistical models to quantify software reliability can be applied. Over the years, guidelines and tools have been developed to support the model selection and the mathematical processing of defect data [4]. However, if a rigorous defect prevention strategy is followed in the creation process, it is unlikely that operational tests will find enough defects to be able to apply a growth model accurately. And this is often the case when safety critical systems are developed.

Monte Carlo Simulation is based on random testing and comparing the results with predicted outcome. Tests are performed using randomly distributed input, according to the likelihood of their occurrence in real life. The estimate of the failure probability is calculated by the ratio of failed runs to total runs. With highly reliable software the amount of necessary total runs will increase rapidly. To show that the probability of failure is at most 10^{-6} (0.000001), at least 10^{7} (10,000,000) runs will have to be executed. And, next to the problem of execution time, the results will have to be checked by outcomes that have been established independently.

Both methods are hardly applicable on software that 1) is complex, 2) should be highly reliable and 3) is very rarely used. Typical the type of software that is used with safety critical systems, e.g. warning and operating systems in tunnels and decision support systems in storm surge barriers.

It should be mentioned that there are some well established methods, e.g. the prescription of IEC 61508 [**7**] and Formal Methods, that improve software quality substantially, but they do not provide and estimate of the probability of failure.

3 TOPAAS

As has been argued in the previous section, it is practically not feasible to estimate the probability of failure of software by either Reliability Growth Modeling or by Monte Carlo Simulation. A practical method means that it should always be possible to get a useful reliability number within a limited amount of time and effort, preferably before the system is accepted for production. It should be usable for products off the shelf as well as tailor-made systems. And the outcome should be repeatable.

In the following paragraphs a new method is proposed, based on a factor model emulating expert judgment of software reliability.

3.1 Expert opinion and Bayesian statistics

The use of the Bayesian probability concept is suggested. This notion expands the classical statistical notion of probability by adding that probability can also be a degree of belief of the observer. This approach is adopted extensively in practical science, see e.g. [6],[15], [1], and it is suggested to deal in this manner with the probability of failure of software.

The Bayesian probability notion gives us the opportunity to quantify the probability of failure of software by using expert estimates [3]. This approach is frequently used for assessing risk in environments that lack data or have no precedent, ranging from nuclear radiology [8] to food safety [19]. This concept is applied to assess the probability of failure of task execution on a software 'module'.

3.2 Definitions

The software of a system usually consists of components (i.e. modules, units, subroutines, etc) that have a specific function and perform a specific task in order to have the system perform its task. Good programming practice separates these functions. Some functions may directly affect the primary function of the system and failure of these functions may cause the system to fail. Other functions, e.g. printer software, may not be critical to the system.

It seems logic to model the failure of these separate functions, with specific tasks and programmed as components, as basic events in a QRA. Although definition of these components, called modules, still is somewhat ambiguous, in practice the following definition works well:

> A *software module* is a piece of software that is represented by a specific group of lines of source code (or its graphical equivalent) with the following properties:
>
> - A clear distinction with respect to other pieces of code and clear separated functionality provided by the module that is required by the system;
> - Observable behavior with specific qualities (like timeliness, reliability, etc.);
> - It is not useful or possible to make a further decomposition with respect to the QRA.

A single software module can perform one or more tasks in an overall mission, where the execution of a task is defined as:

> *Task execution* is an action of a module that is observable on the outside (on a technical level) with the property that it can be determined whether the action is correctly or incorrectly executed with respect to the overall mission of the system.

Given the definition of a software module and task execution the definition of failure is:

> *Failure of task execution* is the (too long) absence/delay of desired task execution, or the incorrect task execution, by a software module, with respect to the mission of the overall system.

Explicitly, this includes not showing any behavior (being 'frozen' or 'crashed'), showing 'spontaneous' behavior (generating events, consuming resources), exhibiting behavior outside the specifications and completing the required task execution too late.

3.3 The factor model

Direct use of experts can be a practical approach for a single assessment of (a piece of) software. But the choice and gathering of the experts, the tedious procedures to calibrate, collect and combine the expert opinions [3] makes the approach unpractical for larger amounts of assessments. Another disadvantage is the lack of transparency of the result.

In order to overcome these drawbacks, it is proposed to capture expert opinion into a factor model. Factors that influence software reliability have been determined in quite a few different studies ([20],[16],[12]). Also the importance of these factors with regard to the resulting reliability of software has been studied [11]. It is proposed to link the implicit expert knowledge to these factors and combine them through a mathematical model.

The general idea is simple. First the (most) important factors that determine software quality are established, assuming that quality correlates with probability of failure. Next, for each factor certain performance levels are decided: e.g. good, less good, average, below average and bad. Finally numbers are assigned to these levels, expressing both the importance of the factor involved as the impact of the level. And these numbers are chosen in such a way, that they directly contribute to the final result: the probability of failure of the software module.

Thus every relevant factor induces a quantified increase or decrease of the total failure probability. This is illustrated in Fig. 1, as example. The numbers either decrease (0.1, 0.3), increase (3, 10) or are indifferent (1) to the final resulting probability of failure.

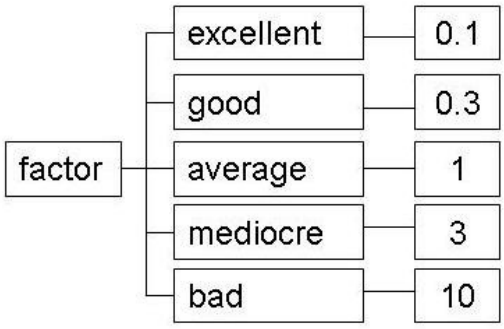

Fig. 1: Factor, levels and numbers

It is important to note that every answer directly influences the overall score; the weight of the factor involved is directly expressed by the magnitude of the score.

From a mathematical point of view, the factor model provides n factors F_i to determine failure probability by demand P:

$$P = P_B \times F_1 \times F_2 \times \cdots \times F_n \quad (1)$$

where

P	between 10^{-5} and 1 (and set to one of these boundaries if exceeded)
P_B	the base failure rate, being conservative, i.e. set to 1
F_i	the contribution of a specific factor. These factors are explicitly not independent.

It was consciously decided to start with the most conservative default for the base rate P_B, i.e. $P_B = 1$. Another starting point was that an unknown factor would not influence the final reliability outcome: if a factor is unknown then $F_i = 1$. This means that $F_i = 1$ is usually allocated to average performance, a performance that can be expected in general. These assumptions mean that, if all factors are unknown, the estimate of the software failure probability equals 1. And this implies that missing information will result in a conservative bias of the model, while adding information will improve the quality of the estimate and in most cases the software failure probability.

3.4 Identifying the factors considered

To identify the factors that experts implicitly use to estimate software reliability and their range, reliability and software experts were gathered both from industry and the academic world. To qualify, all experts involved had to have a field expertise with safety and mission critical software applications for over 10 years in various industrial sectors. A group of 11 experts finally decided that the following 15 aspects of software were the most important quality determining factors:

Software development process:

1. Software development process used that complies with the IEC 61508
2. The use of software inspections
3. The frequency and impact of design changes
4. The "Safety" culture within the development team
5. The experience and level of education of the development team (both in IT and in the specific domain)
6. The nature of collaboration between the development team and acquiring organization
7. The traceability of requirements
8. The test-techniques used and test coverage attained

Product characteristics:

9. The complexity of the decision logic of the task execution
10. The size of the decision logic of the task execution
11. The clarity and transparency of the architecture of the system
12. The amount of trust in the compiler

Execution environment:

13. Run-time environment
14. Availability of representative field data for the specific function
15. Availability of field monitoring

This list of aspects was cross-checked with papers that focused on expert opinion of factors that influenced software reliability ([20],[16],[12],[5],[9]). Some lists contain more details, but generally the same subjects are covered.

3.5 Quantification

The next challenge was the quantification of the influence on the probability of failure of the chosen factors, making the model a reliability prediction system (RPS). Although the work of SMIDTS AND LI ([11],[16],[12]) does provide a relative (numerical) ranking of the effect of measures on reliability, it does not provide the means of estimating the effect of a specific measure on the probability of failure.

For each factor a question and the possible answers were defined, usually consisting of ranges of possible values to a specific metric, making the model discrete, as shown in Fig. 1. Combination of expert opinion on every outcome of each possible answer of each factor resulted in a consistent set of numbers that represented the impact of that specific answer on the probability of failure. It was allowed that an answer could either increase or decrease the probability estimate.

Another assumption made by the experts involved, was that the lowest attainable level of software failure probability was chosen to be 10^{-5} per demand. The experts were not comfortable with lower estimates. This practice is also found in industry standards ([17] [7], and [2]) that use bands of software reliability with a 10^{-5} as best possible performance.

The resulting method was named TOPAAS (Task Oriented Probability of Abnormalities Analysis for Software).

3.6 Calibration

TOPAAS was tested and calibrated on 20 software modules: 7 so-called archetypes and 13 parts of real-life projects. The 7 archetypes were theoretical cases to explore the boundaries of the model, containing an intensively tested black box system, an unproven system from an immature supplier, etc. The real-life cases included systems from the field of avionics, railway safety, storm surge barriers, bridges and other safety/mission critical systems. Specific focus was on variation: the cases included a system developed under a SIL-4 regime [7], as well as extremely simple components that underwent a lot of testing and had a lot of representative field data.

The experts first estimated the probability of failure of the task execution by the software module directly. After that the probability of failure was estimated using the TOPAAS model and the outcome was compared to the experts estimate.

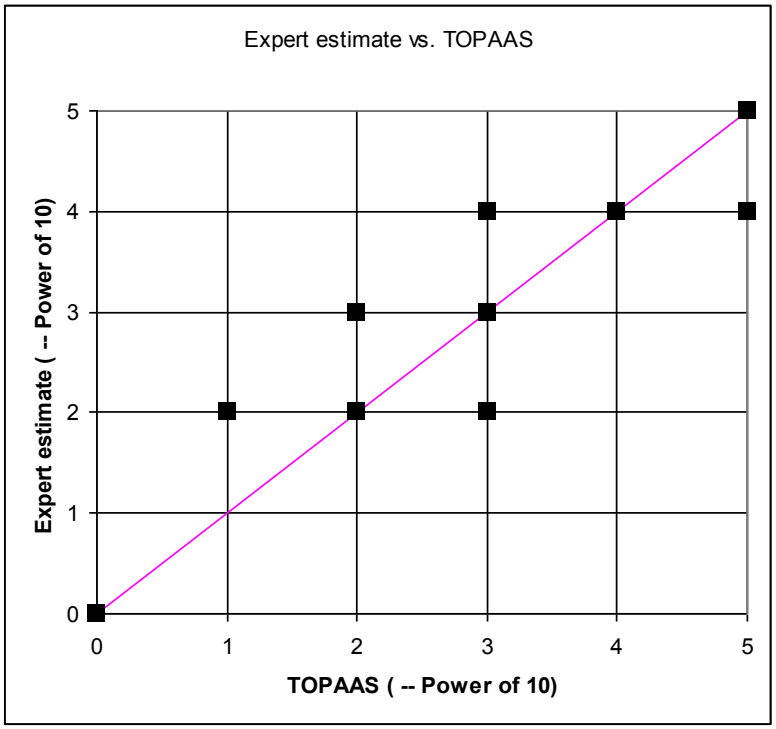

Fig. 2: Calibration results

The result is shown in Fig. 2. It shows the relation between the direct expert estimates (*y*-axis) versus the TOPAAS estimates (*x*-axis). Note that some points may contain several experiments. Both the combined expert opinions as the TOPAAS results have been rounded to natural powers of 10, in conservative direction. The conclusion is that the TOPAAS model reflects the expert perception of the probability of failure of the investigated software modules quite well.

4 Example

As an example, a standard software module is chosen that is sold as a component 'off-the-shelf': a valve control device, working on a dedicated PLC. Although many aspects (factors) are unknown, it still is very well possible to use TOPAAS. On the basis of the known factors, Tab. 1 is specified.

Only 6 aspects were well enough known to be used. The numbers in the rightmost column are a result of the chosen level at each aspect. Note that aspect no. 14, i.e. the availability of representative field data, is a much more important factor than the others.

The resulting probability of failure of this simple software module amounts to:

$$P = P_B \times F_1 \times F_2 \times \cdots \times F_n = 1 \times 0.3 \times 0.3 \times 0.3 \times 0.3 \times 0.5 \times 0.01 = 0.0000405 = 4.05 \cdot 10^{-5} \qquad (2)$$

The method prescribes to round the result in a conservative way to the next natural power of 10. The final estimate of the probability of failure of the software thus becomes 10^{-4} (0.0001). This small probability of failure is in full agreement with expert estimates of such a device.

Tab. 1:

Development process		
4	The "Safety" culture within the development team Choice: 3 Learning Organization Based on: the experienced delivery and installation procedures	0.3
5	The experience and level of education of the development team (both in IT and in the specific domain) Choice: 4 Demonstrable excellent knowledge and lots of experience of IT and of the specific domain Based on: reputation of the producing company, in combination with experience during delivery and installation	0.3
Product characteristics		
9	The complexity of the decision logic of the task execution Choice: 4 Decision logic and error recognition are very simple, McCabe Index smaller than 10 Based on: an estimate of the decision logic that was automated: the actions to be taken are extremely straight-forward.	0.3
10	The size of the decision logic of the task execution Choice: 5 LOC less than 1000 Based on: an estimate by function point analysis	0.3
Execution environment		
13	Run-time environment Choice: 4 Dedicated CPU and memory on no or trivial OS Based on: application runs on a dedicated PLC	0.5
14	Availability of representative field data for the specific function Choice: 4 Lots of representative field data present of identical or comparable applications Based on: the huge amount of the same valve controls, used in the gas and oil industry, in comparable circumstances	0.01

5 Conclusions and future work

It was argued that a factor model is the best attainable way to obtain an estimate for the probability of software failure. Other, statistical based methods are not feasible because of the huge test time needed. A factor model (TOPAAS) was presented that uses the knowledge of software experts. The result of the model is an estimate of the probability of software module failure by demand in safety-related systems.

A structured approach was followed to extract the expert knowledge to determine the relevant factors, the essential questions and scores on the possible answers. The result was calibrated on 20 software modules.

It is realized that the currently identified factors are a first start, hopefully opening a discussion on software reliability estimates. The current properties, measures and contributions determining the contribution of the chosen aspects to the software failure probability,

expressed by the factors F_i will be subject to change in the future, e.g. based on statistics, research results or better insights. A change of perception requires a recalibration of the TOPAAS model, which is not a trivial procedure and the way to deal with this has yet to be developed and implemented.

Literature

[1] Benjamin, J.R. and Cornell, C.A. *Probability, Statistics and Decision for Civil Engineers*. New York: McGraw-Hill, 1970

[2] CENELEC. *Railway applications - Communication, signalling and processing systems - Safety related electronic systems for signalling*. EN 50129, 2005

[3] Cooke, R.M. *Experts in Uncertainty*. New York: Oxford University Press, 1991

[4] Corro Ramos, I. *Statistical Procedures for Certification of Software Systems*. Eindhoven University of Technology Library, 2009

[5] Fenton, N.E. and Neil, M. A Critique of Software Defect Prediction Models. *IEEE Transactions on Software Engineering* 25(5) (1999)

[6] Finetti, B. de. Theory of Probability. *translation by A Machi and AFM Smith, 2 volumes,* New York: Wiley, 1974-5

[7] International Standard IEC 61508-1. *"Functional safety of electrical/electronic/programmable electronic safety-related systems – Part 1: General requirements"*. CEI/IEC 61508-1:2010, First Edition, 2010

[8] Jang, H., Ryu, H., Kim, J., Lee, J. and Cho, K. A Probabilistic Risk Assessment for Field Radiography Based on Expert Judgment and Opinion. *Progress in Nuclear Science and Technology* 1 (2011), p. 471–474

[9] Johnson, G., Lawrence, J.D. and Yu, X. *Conceptual Software Reliability Models for Nuclear Power Plant Safety Systems*. Lawrence Livermore National Laboratory, UCRL-ID-138577, 2000

[10] Jones, C. *Software Assessments, Benchmarks and Best Practices*. Addison-Wesley Professional, 2000. ISBN 978-0201485424

[11] Li, M. and Smidts, C. A Ranking of Software Engineering Measures Based on Expert Opinion. *IEEE Transactions on Software Engineering* 29(9) (2003)

[12] Li, M., Wei, Y., Desovski, D., Nejad, H., Ghose1, S., Cukic, B., Smidts, C. Validation of a Methodology for Assessing Software Reliability. *Proceedings of the 15th International Symposium on Software Reliability Engineering*. 2004

[13] Lyu, M.R. *Handbook of Software Reliability Engineering,* McGraw-Hill, 1996

[14] Ohba, M. *Software reliability analysis models*. Japan: IBM, 1984

[15] Savage, L.J. *The Foundations of Statistics*. New York: Wiley, 1954

[16] Smidts, C., Li, M. and Brill, R.W. Ranking Software Engineering Measures Related to Reliability Using Expert Opinion. *Proceedings of the 11th International Symposium on Software Reliability Engineering*. 2000

[17] SO/IEC 25010:2011 *Systems and software engineering – Systems and software Quality Requirements and Evaluation (SQuaRE) – System and software quality models*. 2011

[18] Swain, A.D. and Guttmann, H.E. *Handbook of Human Reliability Analysis with Emphasis on Nuclear Power Plant Applications*. Final report, Sandia National Laboratories, Albuquerque, 1983

[19] The European Food Authority. Opinion of the Scientific Panel on Animal Health and Welfare on a self mandate on the Framework for EFSA AHAW Risk Assessments. *The EFSA Journal* 550 (2007), p. 1–46

[20] Zhang, X. and Pham, H. An analysis of factors affecting software reliability. *The Journal of Systems and Software* 50 (2000), p. 43–56

Creep and shrinkage prediction models for concrete: uncertainty quantification

Roman Wendner[a], Mija H. Hubler[b], Zdeněk P. Bažant[b]
[a] Institute of Structural Engineering, University BOKU, Vienna
[b] Northwestern University, Evanston, IL, USA
roman.wendner@boku.ac.at, mija.hubler@gmail.com, z-bazant@northwestern.edu

Abstract: The accuracy of prediction models significantly influences the lifetime performance of engineering structures. For aging concrete structures, these are mainly deterioration models (chloride ingress, reinforcement corrosion, carbonation), as well as models for changes in material properties and long term deformations, such as creep and shrinkage (CS). Prediction models not only govern the inherent safety level in design but also represent key elements of any performance assessment. Although the numerical framework for the latter is well established, suitable stochastic models for many input parameters are still missing. A recently expanded database of laboratory CS tests as well as multi-decade bridge deflection data has now become available, making it possible to quantify the uncertainty of CS models embodied in the current design codes and standard recommendations. In this study, the stochastic models for the major input parameters are presented, the formulations of the new model B4, which represents a significant update and expansion of model B3 (1995 RILEM Recommendation), are introduced and applied to a case study in order to obtain sensitivity factors and prediction bounds.

Keywords: creep, shrinkage, concrete, multi-decade creep, prediction, database, B4, reliability analysis, sensitivity study

1 Introduction

The design of new and assessment of existing concrete structures require accurate prediction of the structural response under mechanical and environmental loads during construction as well as operation until the end of the intended service life. Bridges and other important structures are designed for a service life of at least 50 years, and for modern large bridges the required lifetimes are generally over 100 years. Such designs obviously require realistic multi-decade prediction models.

1.1 Database

Recently, it has become clear that the existing creep and shrinkage prediction models for the time-dependent behavior of concrete are highly inaccurate, especially for the desired multi-decade life spans. This insight was revealed in the deflection analysis of numerous large-span prestressed segmental bridges, beginning with the Koror-Babeldaob (KB) Bridge in Palau [12].

An extensive database should, in theory, reveal the correct functional form of the creep and shrinkage prediction equation if the appropriate full statistical analysis could be performed for all composition, environmental, and response variables. Unfortunately, such a database does not exist. Most laboratory data usable for model development, calibration, and validation are limited to less than 6 years in duration. Recently a database of both short term tests as well as multi-decade bridge observations has been completed [17]. With this new dataset it is not only possible to develop improved long term prediction formulations such as model B4 [10], but also perform statistical comparisons of parameters and of existing prediction equations to aid in the assessment of current and reliable designs of future concrete structures.

Furthermore, this extensive set of concrete test data can serve as the basis for the derivation of stochastic models for concrete composition and mechanical properties. In particular, for a given strength range and cement type, the functional dependency between the strength and elastic modulus, as well as the strength and composition parameters, can be identified and correlation fields can be developed.

1.2 Code provisions and recommendations

The internationally available literature contains many, more or less involved, theories and models that have been developed to predict shrinkage and creep. These are, among others, the micro-prestress solidification theory for creep [11], as well as models that can capture the chemical reactions involved in early age hydration, and predict the pore humidity development as influenced by diffusion and self-desiccation [15], causing drying shrinkage. Thus, from a scientific point of view, a very complex system of connected physical, chemical, and mechanical mechanism involving various length and time scales must be captured to obtain accurate predictions. This situation is further complicated by the inherent heterogeneity of the composite concrete material, which is composed of aggregates and cement paste. While basic principles such as mass balance or thermodynamics always need to be satisfied, for structural problems local phenomena that happen on smaller scales can be combined and considered only in their average effect on the larger scale. Similarly, very short early-age processes can be captured in their final effect only.

Engineering societies follow these simplifications in their models and recommendations, thus introducing a certain level of uncertainty. Some of the more widely used models in practice are the model of the AMERICAN CONCRETE INSTITUTE ACI-92 [21], the Eurocode model which is based on the *FIB* MODEL CODE 1990 [13] with its revision in 1999 [14], the new *FIB* MODEL CODE MODEL 2010 [20], and the model of the Japanese Society of Civil Engineers [1; 2]. Additionally, professional engineers and scientist have suggested models such as the Gardner-Lockman model GL2000 [16], and the B3 model [4; 5; 6; 7; 8], developed by Bažant and his co-workers and approved in 1995 as RILEM Recommendation.

While most creep prediction equations [13; 16; 21] approach a finite asymptote, the structural responses and theory reveal a non-zero terminal slope in the logarithmic time scale [9]. Another key weakness of the previous prediction equations is a scarcity of laboratory calibration data of the compositions of modern concretes (with admixtures) and for the full multi-decade prediction time range.

Limitations and drawbacks that all of these models except B3 have in common are the computationally intensive integral form [26] which, contrary to a rate form, cannot be applied under changing environmental conditions and is unfit for being applied together with nonlinear material models which account, e.g., for damage development and cracking of concrete or viscoplastic relaxation of prestressing steel. Further compromises with in accuracy and applicability result from the cross-sectional form in which an average shrinkage strain and compliance function value for the full cross-section needs to be determined.

1.3 Model B4

The new B4 prediction model surpasses the performance of the well-established model B3 and extends the range of applicability to modern concretes with admixtures. B4 captures the behavior of Portland cement concretes based on model parameters that are derived from the composition of the concrete and the environmental conditions. Further modifications include a recalibration for multi-decade behavior, the introduction of a split between autogenous shrinkage and drying shrinkage. In the service stress range (up to $0.4f_c'$) a linear dependence of creep strain on stress may be assumed as an acceptable approximation. This means that, for constant stress σ applied at age t',

$$\epsilon(t) = J(t,t')\sigma + \epsilon_{sh}(t,t_0) + \epsilon_{au}(t,t_0) \tag{1}$$

in which σ is the uniaxial stress. The stress-independent strain is split into the drying shrinkage, $\epsilon_{sh}(t,t')$, and autogenous shrinkage, $\epsilon_{au}(t,t_0)$. The compliance function, $J(t,t')$, as introduced in BAŽANT AND BAWEJA [6] is adopted without change. E_0 represents the asymptotic (truly instantaneous) elastic modulus, C_0 the basic creep compliance, and C_d the drying creep compliance;

$$J(t,t') = \tfrac{1}{E_0} + C_0(t,t') + C_d(t,t',t_0) \tag{2}$$

The prediction equations for E_0, C_0, and C_d have been adapted and recalibrated. The average shrinkage of a cross-section undergoing drying may be captured with the relation

$$\epsilon_{sh}(t,t_0) = -\epsilon_{sh,\infty}(t_0)k_h \tanh\sqrt{\tfrac{t-t_0}{\tau_{sh}}} \tag{3}$$

where $\epsilon_{sh}(t,t_0)$ is the evolution of drying shrinkage strains, $\epsilon_{sh,\infty}(t_0)$ is the final drying shrinkage as a function of the curing time t_0; k_h is a factor describing the dependence on environmental humidity, as published in [4]. The shrinkage halftime, τ_{sh}, is predicted based on a cement type and admixture dependent basic value, τ_0, modified for composition and effective diffusivity parameter, $k_s D$, where k_s is a shape parameter of the cross-section [4] and D is the effective thickness of cross section. The final shrinkage $\epsilon_{sh,\infty}(t_0)$ is determined accordingly. The influence of ageing and thus of the gain in stiffness, is accounted for (as originally proposed in [4], by the ratio between the 607-day modulus and the modulus at the end t_0 of curing;

The evolution of autogenous shrinkage $\epsilon_{au}(t)$ is, contrary to drying shrinkage, a function of the total time (or age) t [20], rather than the drying time, and can be described in logarithmic time by a sigmoid function of the shape

$$\epsilon_{au}(t) = \epsilon_{au0}(a/c, w/c)\left[1 + \left(\frac{\tau_{au}}{t}\right)^{\alpha}\right]^{-r_2} \quad (4)$$

with the basic value of the final autogenous shrinkage, ϵ_{au0}, and an empirical correction term for the composition. The rate of evolution of the autogenous shrinkage evolution is characterized by the autogenous shrinkage half-time τ_{au}, and affected by exponent r_2 of the time function and the water-cement ratio dependent exponent $\alpha(w/c)$. Alternative time functions such as the exponential form [3; 18; 20; 22; 23; 25], e.g., as proposed in the 2010 Model Code, were unable to represent the time evolution with sufficient accuracy and flexibility.

2 Uncertainty quantification

A proper understanding of the uncertainties involved in the modeling of creep and shrinkage is quintessential for safe and sustainable construction. The gap between the length of available laboratory data (<< 10 years) and typical design service lives of at least 50 years further aggravates the situation. As the first step, stochastic models for all the required input parameters as well as the correlation fields are needed to properly calibrate partial safety factors for creep and shrinkage, as well as to provide the basis for realistic probabilistic assessment of reliability. In the subsequent section, such stochastic models, derived from an extensive database of laboratory tests, will be presented. Stochastic models for environmental conditions, variability in the structural system and cross-section geometry will add the missing information to provide sensitivity factors between model inputs and creep shrinkage prediction and thus serve for the determination of reliability profiles in time.

2.1 Stochastic model

The broad scope of composition, mechanical, and environmental parameters characterizing each creep and shrinkage test in the database calls for the use of stochastic models. The parameters of highest interest are those already used in the existing prediction models: the water cement ratio (*w*/*c*), cement content (*c*), aggregate to cement ratio (*a*/*c*), 28 day Young's modulus (E_{28}), and the 28 day compressive strength (f_{28}). This parameter set has the dominant effect on the response of concrete as observed in tests. Stochastic models with log-normal marginal distributions were developed for each of these parameters in a subset of all shrinkage tests characterized by mid-range 28 day compressive strength values from 25 to 30 MPa. The results are tabulated in Tab. 1.

To develop a full stochastic framework for creep and shrinkage models, additional stochastic models are needed for all input parameters including the test setup parameters such as the test duration and loading time. These values have specified recommendations in testing guidelines and strong biases toward times that allow for workable consistencies of the mix. Fig. 1 lists the linear Pearson's correlation coefficients between the composition and 28-day measured strength and modulus. While the sign and relative magnitude of the composition correlations may be estimated from typical requirements for hydration and workability, these values reflect a set of representative distributions across a full spectrum of recent and older cements that may be used to capture standard relationships for design. As is typi-

cally assumed, the correlations also reflect a prominent correlation between the water cement ratio, the corresponding strength and Young's modulus.

Tab. 1: Stochastic Model

Variable	PDF	Mean	C.o.V.	Datasets
Cement Content c [kg]	LGN	377	0.39	1019
Water/Cement Ratio w/c	LGN	0.486	0.35	1101
Aggregate/Cement Ratio a/c	LGN	5.44	0.43	1056
Compressive Strength f_c [MPa]	LGN	27.4	0.04	617
Young's Modulus E_c [MPa]	LGN	28,773	0.12	622
Relative humidity h [-]	N	0.75	0.05	
Temperature T [°C]	N	20	0.05	

	w/c	a/c	c	f_{28}	E_{28}
w/c	1	0.83	−0.73	−0.19	0.34
a/c	-	1	−0.91	−0.13	0.38
c	-	-	1	0.30	−0.41
f_{28}	-	-	-	1	0.06
E_{28}	-	-	-	-	1

Fig. 1: Correlation matrix

2.2 Case study

Creep and shrinkage prediction is of particular importance for concrete structures with transitions in mechanical properties, moisture, or temperature. These conditions are created by concrete interactions with masonry or steel parts, particularly thick or slender structures, and high temperature applications. Aside from long-time deflections, creep causes prestress loss in concrete bridge structures and is critical for the safety analysis of nuclear reactor containments and vessels. As a simple case study that illustrates the sensitivity of the structural response to creep and shrinkage we may consider a composite concrete steel truss girder, as depicted in Fig. 2. The derived stochastic models (as listed in Tab. 1) are used to determine the scattering shrinkage strain and creep compliance predictions for the concrete slab. The environmental conditions, temperature T and relative humidity h, depend on the geographical zone and also the micro-climate. For the purpose of this investigation, a fictitious construction in central Europe is considered. The cross-section dimensions are considered as deterministic variables only in order to isolate the variability in the creep and shrinkage prediction. For the sake of simplicity it is further assumed that the concrete slab is solely loaded in compression and the steel tube in tension. Let us consider such a composite girder bending under a uniformly distributed load g = 30 kN/m as illustrated in Fig. 2 for analysis. The statically determined girder has a length L = 15.0 m, a concrete slab of thickness h_1 = 0.2 m and width w = 2.0 m. The distance between centroid of the steel pipe with d_i = 180 mm and d_0 = 220 mm and the bottom surface of the concrete slab h_2 = 0.60 m.

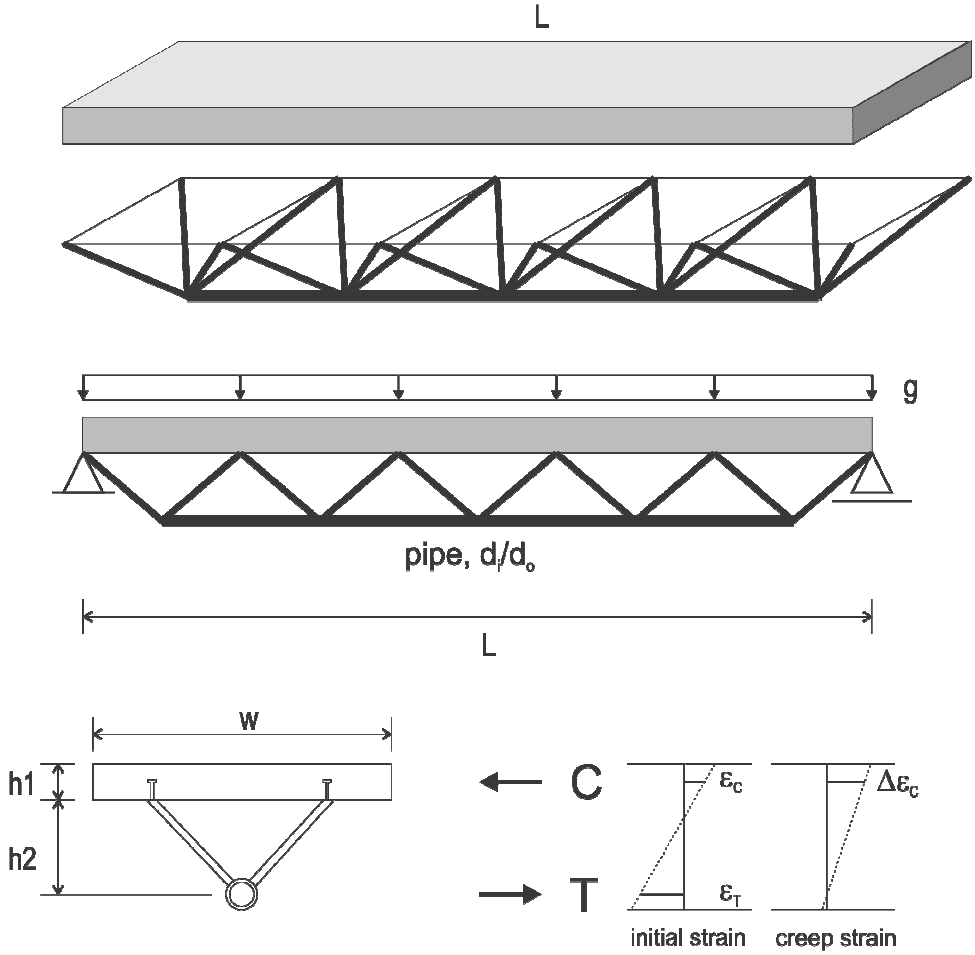

Fig. 2: Composite grider; concrete slab, I-beam and shear connectors under uniform load.

2.3 Methodology

After implementing the new formulations for model B4, a set of 100 realizations for the input variables were generated based on the formulated stochastic models. The concept of Latin Hypercube Sampling [19] allows to approximately capture the full characteristic of the input distributions including their tails. The intended correlations are ensured by simulated annealing [24].

The goal of this investigation are (a) the determination of scatter bands for structural response, which, in the next step, can serve for the calculation of reliability levels; and (b) the derivation of sensitivity factors between model input parameters and observed structural response. The latter provide an indication of the most critical quantities of the mix design.

2.4 Results and discussion

Assuming a concrete compressive strength f_{28} of 27.5 MPa, a Young's modulus E_{28} = 29962 MPa can be calculated. The properties of the steel pipe are assumed to be f_y = 235 MPa, and E_c = 200,000 MPa. The elastic centerpoint deflection of the assumed simplified model with rigid truss members then yields 19.4 mm. In comparison, the average additional creep deflection after 100 years amounts to 7.5 mm. In Fig. 3 the scatter bands for creep compliance and shrinkage strains are presented, based on the formulated

stochastic model. The additional longterm deflection due to the asymetric shortening of the girder (shrinkage and creep of the concrete slab) is presented in Fig. 4. The centerpoint deflection increases over a time period of 100 years by 25.225/19.4 = +130 % on average.

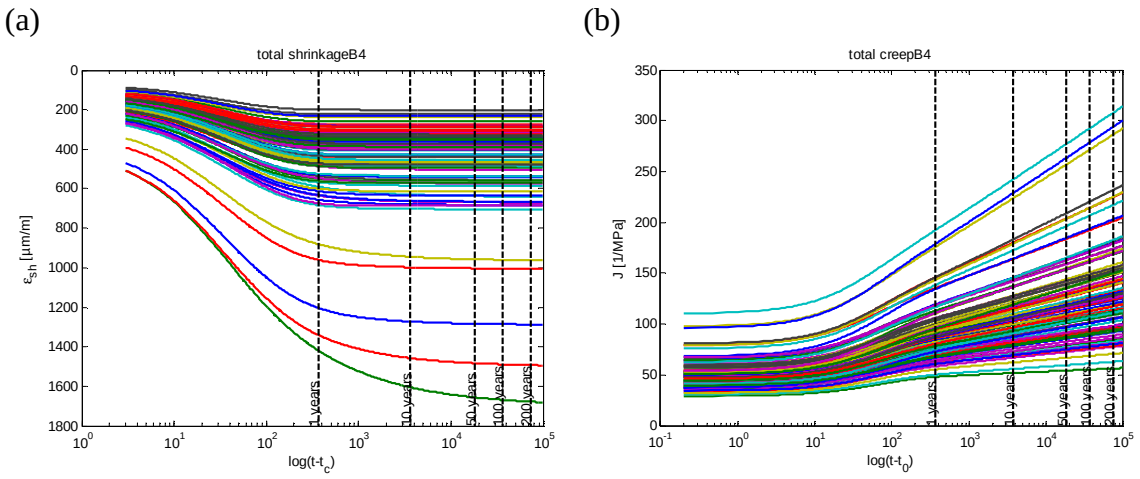

Fig. 3: Scatterband for (a) shrinkage, and (b) creep compliance

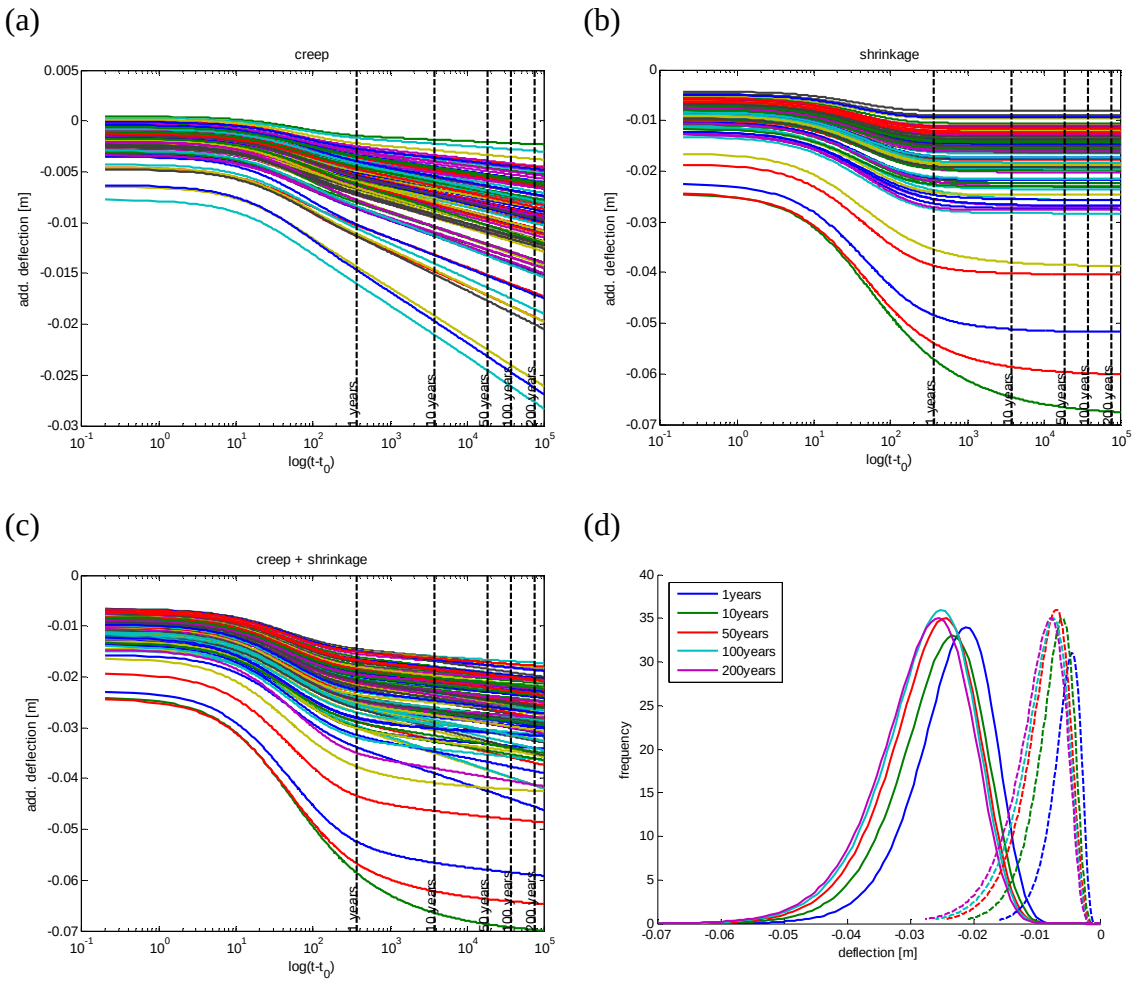

Fig. 4: Additional long-term deflections due to (a) creep, (b) shrinkage, (c) creep and shrinkage; (d) PDF of total (solid) and purely creep related (dashed) long-term deflections (exceeding the initial deformations) after 1, 10, 50, 100, 200 years

2.5 Conclusions

The new B4 model for creep and shrinkage of concrete, presented here, allows a more accurate prediction of long-term structural response. Based on a comprehensive database of laboratory tests it was possible to formulate a stochastic model for the composition and strength parameters. An associated case study shows that the expected scatter, compared to an assumed deterministic design strength, can be significant. In the chosen example the additional long-term deflection due to creep and shrinkage on average amounts to 130% of the initial deformation.

Acknowledgements

Financial support from the U.S. Department of Transportation, provided through Grant 20778 from the Infrastructure Technology Institute of Northwestern University, is gratefully appreciated. Further support was provided under U.S. National Foundation Grant CMMI-1153494 to Northwestern University. The first author is thankful Erwin-Schrödinger Scholarship J3619-N13 granted by the Austrian Science Fund (FWF).

Literature

[1] (JRA), J. R. A. Specifications for Highway Bridges with Commentary. Part III. Concrete, 2002
[2] (JSCE), J. S. o. C. E. Standard Specifications for Design and Construction of Concrete Structures. Part I, Design. (in Japanese), 1996
[3] Avoidance of thermal cracking in concrete at early age − recommendations, materials and structures. RILEM TC 119-TCE. 30**:** 451-64, 1997
[4] Bažant, Z. P. Creep and shrinkage prediction model for analysis and design of concrete structures − model B3. *Matériaux et constructions* 28(180): 357−365, 1995
[5] Bažant, Z. P. and Baweja, S. Justification and refinements of model B3 for concrete creep and shrinkage 1. statistics and sensitivity. *Materials and Structures* 28(7): 415−430, 1995
[6] Bažant, Z. P. and Baweja, S. Justification and refinements of model B3 for concrete creep and shrinkage 2. Updating and theoretical basis. *Materials and Structures* 28(8): 488−495, 1995
[7] Bažant, Z. P. and Baweja, S. Short form of creep and shrinkage prediction model B3 for structures of medium sensitivity. *Materials and Structures/Matériaux et Constructions* 29(194): 587−593, 1996
[8] Bažant, Z. P. and Baweja, S. Creep and shrinkage prediction model for analysis and design of concrete structures: Model B3. *Adam Neville Symposium: Creep and Shrinkage—Structural Design Effects*. A. Al-Manaseer. Farmington Hills, Michigan, ACI**:** 1−83, 2000
[9] Bažant, Z. P.; Hubler, M. H. and Yu, Q. Pervasiveness of excessive segmental bridge deflections: Wake-up call for creep. *ACI Structural Journal* 108(6): 766−774, 2011
[10] Bazant, Z. P.; Wendner, R. and Hubler, M. H. Model B4: Overview and development. *RILEM MAAS* (to be submitted), 2013
[11] Bazant, Z. P.; Xi, Y. and Baweja, S. Solidification theory and mechanisms of aging creep of concrete. *Proceedings of Engineering Mechanics* **2**: 1372-1375, 1995
[12] Bažant, Z. P.; Yu, Q.; Li, G.-H.; Klein, G. J. and Křístek, V. Excessive Deflections of Record-Span Prestressed Box Girder − Lessons learned from the collapse of the Koror-Babeldaob Bridge in Palau. *Concrete International* 32(6): 44−52, 2010
[13] CEB-FIP MODEL CODE 1990. Comitte Euro-International du Béton, 1993

[14] fib. Structural Concrete: Textbook on Behaviour, Design and Performance, Updated Knowledge of the CEB/FIP Model Code 1990. *Bulletin No. 2*. Lausanne, Fédération internationale du béton (FIB). 1**:** 35−52, 1999

[15] Garboczi, E.; Bullard, J.; Martys, N. and Terrill, J. The Virtual Cement and Concrete Testing Laboratory: Performance Prediction, Sustainability, and the CSHub. *NRMCA Concrete Sustainability Conference April 13−July 15, 2010*. Tempe, AZ, 2010

[16] Gardner, N. J. and Lockman, M. J. Design Provisions for Drying Shrinkage and Creep of Normal Strength Concrete. *ACI Materials Journal* 98(2): 159−167, 2001

[17] Hubler, M. H.; Wendner, R. and Bažant, Z. P. Extensive Concrete Creep and Shrinkage Database − Analysis and Recommendations for Testing and Reporting. *ACI Journal* (to be submitted), 2013

[18] Lee, K. M.; Lee, H. K.; Lee, S. H. and Kim, G. Y. Autogenous shrinkage of concrete containing granulated blast-furnace slag. *Cement and Concrete Research* 36(7): 1279−1285, 2006

[19] McKay, M. D.; Conover, W. J. and Beckman, R. J. A comparison of three methods for selecting values of input variables in the analysis of output from a computer code. *Technometrics* 21(2): 239−245, 1979

[20] Model Code 2010 − Final draft, Volume 1. *fib Bulletin 65*, fib**:** 350, 2012

[21] Prediction of Creep, Shrinkage, and Temperature Effects in Concrete Structures. *ACI Committee 209*, American Concrete Institute, Farmington Hills, MI. ACI 209R-92**:** 47, 1992

[22] *Structural concrete: textbook on behavior, design and performance,*. Sprint-Druck Stuttgart, 1999

[23] Tazawa, E. and Miyazawa, S. Influence of cement and admixture on autogenous shrinkage of cement paste. *Cement and Concrete Research* 25(2): 281−287, 1995

[24] Vořechovský, M. and Novák, D. Correlation control in small sample Monte Carlo type simulations. *A Simulated Annealing approach. Probabilistic Engineering Mechanics* 24(3): 452−462, 2009

[25] Yoo, S. W.; Kwon, S.-J. and Jung, S. H. Analysis technique for autogenous shrinkage in high performance concrete with mineral and chemical admixtures. *Construction and Building Materials* 34(0): 1−10, 2012

[26] Yu, Q.; Bazant, Z. P. and Wendner, R. Improved Algorithm for Efficient and Realistic Creep: Analysis of Large Creep-Sensitive Concrete Structures. *ACI Structural Journal* 109(5): 665−676, 2012

Simulation of random fields in structural design

Sebastian Wolff [a]

[a]DYNARDO Austria GmbH, Wagenseilgasse 14, 1120 Vienna, Austria
sebastian.wolff@dynardo.at

Abstract: Many physical quantities in structural design are fields being distributed on structures and being random processes. The physical structures are often represented by finite element models, the fields are random variables defined at each mesh node. The analysis of the autocovariance function of such discrete random fields and their reduction to a limited number of mode shapes allow engineers to eliminate noise and, further, to identify and to quantify important parameters that influence the random field. This article deals with the opposite, i.e. the simulation of random fields by taking into account constraints (eg. lower and upper bounds of a yield stress), arbitrary random distribution functions and a spatial correlation structure. The presented algorithm is illustrated using the software package *Statistics on Structures* applied to an industrial example.

Keywords: random fields, simulation, geometric deviation, modal reduction, spatial correlation

1 Introduction

Current developments in CAE often employ investigations on robustness, sensitivity or statistics of random effects on finite element structures. For example, an optimization must be accompanied by a robustness and reliability analysis. For this purpose, random influences are measured from experiments or are generated by Monte Carlo methods in conjunction with FEM simulation [2]. The performance of a structure is then assessed by statistical means [8]. Many processes involve random quantities being spatially distributed on the examined structure.

When utilizing random fields one is able to assess random effects as well as their localization. They provide several levels of insight: First, the distribution of scatter on the structure is

observed and hot spots are located. Next, random field data can be decomposed into scatter shapes, which can be ranked by their contribution to the total scatter. These shapes can be used to reduce the number of random variables (which may be very largely depending on the number of nodes and elements in the FEM mesh) and to reduce noise while only keeping the essential features of the random field.

DYNARDO [3] developed the software *Statistics on Structures* (SoS) which is capable of decomposing random fields into scatter shapes, analyzing random properties on FEM structures, locating "hot spots" of variation and investigating correlations. Aside the analysis of a given set of samples, engineers are also interested in generating random samples with a specified spatial correlation structure. For example, in sheet metal forming one often wants to generate random geometric imperfections (induced by the production process) and analyze the performance of the individual designs later on. This article deals with the simulation of pseudo-random fields focusing on very large structures. These simulations are usually restricted to small FEM meshes due to computer hardware limitations. Hence one needs to find suitable approximations which allow to generate random field samples with high numerical efficiency.

The article starts with an introduction to random fields and its Karhunen-Loeve expansion in section 2. Section 3 presents the brute force approach to simulation while section 4 enhances the procedure to very large meshes. Section 5 presents an industrial example illustrating the performance of the proposed methodology.

The author wants to point out that he originally used a different interpolation method for large scale FEM structures. During the review process, however, the reviewer proposed the usage of EOLE which turned out to outperform the original solution leading to major changes of the direction of this article, see section 4.1.

2 Random fields

Let us consider a scalar field which is defined by a real-valued function value H over an n-dimensional space, i.e.

$$H \,:\, \mathbb{R} \to \mathbb{R}^n \; \mathbf{x} \to z, \quad z \in \mathbb{R}, \, \mathbf{x} \in \mathbb{R}^n \tag{1}$$

In most structural applications this function is defined in three-dimensional space, i.e. $n = 3$. Let us assume that the field given through H usually varies smoothly in space whereby points being very close to each other have similar function values. If the field is influenced by random quantities, then one may measure different realizations of the same field, see figure 1. Therein, four random samples ω of the same scalar field H defined in one dimension x are illustrated. Two points in space are highlighted in the figure, for which one can compute statistical measures as if they are individual random variables. For example, one can compute the mean value function

$$\bar{H}(\mathbf{x}) = \mathbf{E}[H(\mathbf{x})] \tag{2}$$

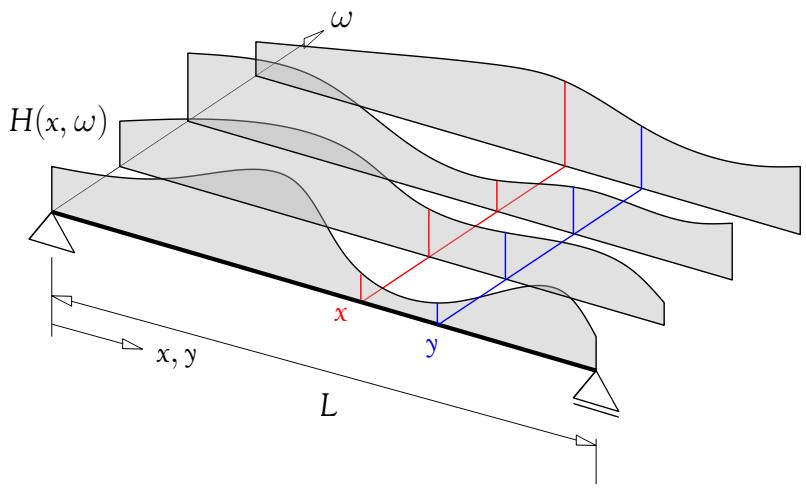

Fig. 1: Different realizations of a one-dimensional field. Source: [9]

One can further compute correlation measures for the field values at different coordinates, for example by the covariance between two points $\mathbf{x}$ and $\mathbf{y}$

$$C_{HH}(\mathbf{x},\mathbf{y}) = \mathbf{E}[\{H(\mathbf{x}) - \bar{H}(\mathbf{x})\}\{H(\mathbf{y}) - \bar{H}(\mathbf{y})\}] \tag{3}$$

with auto-covariance function C_{HH}.

The design space $\mathbf{x} \in \mathbb{R}^n$ is infinite large. In engineering applications one is interested in reducing the number of variables to a small finite number. A tool is to express the field H by a Fourier-type series expansion using deterministic basis functions ϕ_k and random coefficients c_k

$$H(\mathbf{x}) = \sum_{k=1}^{\infty} c_k \phi_k(\mathbf{x}), \quad c_k \in \mathbb{R},\ \phi_k \in \mathbb{R} \tag{4}$$

This transforms the field being originally expressed by the unknowns $\mathbf{x}$ to a space expressed by the unknowns $\mathbf{c}$. By truncating the series, a reduction of the number of variables can be achieved. The Karhunen-Loeve expansion states that an optimal choice of the basis functions is given by an eigenvalue ("spectral") decomposition of the auto-covariance function, i.e.

$$C_{HH} = \sum_{k=1}^{\infty} \lambda_k \phi_k(\mathbf{x})\phi_k(\mathbf{y}), \quad \int_{\mathbf{R}^n} C_{HH}(\mathbf{x},\mathbf{y})\phi_x(\mathbf{x})d\mathbf{x} = \lambda_k \phi_k(\mathbf{y}) \tag{5}$$

The obtained basis functions are orthogonal and the coefficients become uncorrelated.

When a scalar field is measured as a distribution on a FEM mesh (or on any other discrete space), the field H is represented by discrete values, i.e.

$$H_i = H(\mathbf{x}_i), \quad i = 1 \ldots N \tag{6}$$

In this case the spectral decomposition is given through

$$H_i - E(H_i) = \sum_{k=1}^{N} \phi_k(\mathbf{x}_i) c_k = \sum_{k=1}^{N} \phi_{ik} c_k \tag{7}$$

or in matrix-vector notation

$$\mathbf{H} = \Phi\mathbf{c} + \bar{\mathbf{H}} \tag{8}$$

Again, a significant reduction in the number of variables can be achieved when truncating the series after a few items. The field H being measured in terms of a large number of values H_i (usually in terms of single values per node or finite element) is expressed through a small number of coefficients c_k. The "scatter shapes" ϕ_{ik} define the transformation basis.

By reducing the number of random variables, one improves the statistical significance for a small sample size (eliminates noise), reduces the numerical effort in statistical analysis and may simplify the representation of input/output relations based on meta models. The basis functions should be orthogonal reducing the computational effort for the projection (reduction) and its inverse transformation. As a side effect the random coefficients are uncorrelated simplifying the digital simulation of random fields.

3 Simulation of random fields

For simplicity, the consideration is restricted to the following assumptions:

- The distribution type (with CDF $F(X_j)$) of individual points in the field is the same for all points j.
- The realization of a random variable may be bounded (due to restrictions in the production process).
- Inhomogenity is limited to different mean and standard deviation at individual field points.
- The spatial correlation is defined by autocorrelation functions, i.e. $C(d) = C_{HH}(\mathbf{x}, \mathbf{y})$ wherein $d = d(\mathbf{x}, \mathbf{y})$ denotes the distance between two points. (eg. through correlation length parameters).
- The spatial correlation is defined in standard-normal space.

3.1 Very small correlation length

If a very small correlation length is chosen, one can assemble a sparse correlation matrix using piecewise polynomial covariance functions [7], i.e.

$$C_{l,p}(d) = (1 - d/l)_+^p\,, \quad p > 2 \tag{9}$$

with correlation length l and polynomial order p. The covariance matrix Cov_{ij} defining the covariance between two mesh points $\mathbf{x}_i$ and $\mathbf{x}_j$ has compact support. The simulation then follows the steps:

1. Perform a decomposition of the covariance matrix $\mathbf{Cov} = \mathbf{L}\mathbf{L}^T$, eg. by a sparse Cholesky factorization.

2. Simulate N field vectors $\mathbf{u}_k$ of statistically independent standard-normal random variables, one number for each node.

3. Apply the correlation in standard normal space for each sample k: $\mathbf{z}_k = \mathbf{L}\mathbf{u}_k$.

4. Transform the correlated field samples into the space of the desired random field: $x_{k,i} = F^{(-1)}\left(N(z_{k,i})\right)$.

This procedure allows the generation of random field samples without approximation or loss of model information.

The major challenge is the numerical efficiency of the Cholesky factorization. In numerical tests using a mesh with only 33.000 nodes, a correlation length of 5% of the largest model dimension already leads to more than 1% non-zero elements in the covariance matrix. In turn the simulation took more than half an hour on a recent Intel i7 processor (using the Eigen sparse solver http://eigen.tuxfamily.org). In practice, in particular when simulating geometric imperfections, a correlation length of 20%–50% is often used making this approach unattractive for moderately large meshes and impossible for very large meshes.

3.2 Large correlation length

For a large characteristic length-scale one usually obtains a dense covariance matrix. A widely used covariance function is the squared exponential function, i.e.

$$C_l(d) = \exp\left(-\frac{d^2}{2l^2}\right) \tag{10}$$

with correlation length l. A spectral decomposition is used to factorize the covariance matrix by $\mathbf{Cov} = \Phi\text{diag}(\lambda_{ii})\Phi^T$ with eigenvalues λ_i and orthogonal eigenvectors $\Phi = [\phi_i]$. This decomposition is used to reduce the number of random variables. Given a moderately large correlation length, only a few (eg. 3-5) eigenvectors are required to represent more than 90% of the total variability.

The simulation then follows the steps:

1. Perform a decomposition of the covariance matrix $\mathbf{Cov} = \Phi\text{diag}(\lambda_{ii})\Phi^T$ and chose c basis vectors ϕ_i being associated with the largest eigenvalues.

2. Simulate N vectors $\mathbf{u}_k$ of statistically independent standard-normal random variables, each vector is of dimension c.

3. Apply the correlation in standard normal space for each sample k: $\mathbf{z}_k = \sum_i^c \sqrt{\lambda_i}\phi_i u_{k,i}$.

4. Transform the correlated field samples into the space of the desired random field: $x_{k,j} = F^{(-1)}\left(N(z_{k,j})\right)$.

A global error measure ϵ may be based on the total variability being explained by the selected eigenvalues, i.e.

$$\epsilon = 1 - \frac{\sum_{i=1} c\lambda_i}{\sum_{i=1} n\lambda_i} = 1 - \frac{1}{n}\sum_{i=1} c\lambda_i \tag{11}$$

wherein n is the number of discrete points.

This procedure allows the generation of random field samples with relatively large correlation length parameters. It is based on a model order reduction, i.e. only a portion of the desired variability can be retained. Furthermore, the covariance matrix is stored as a dense matrix. Hence, the size of the FEM mesh is effectively limited to ≈ 10.000 nodes.

4 Simulation of random fields on large scale structures

An enhancement of the strategy presented in 3.2 can be used to generate random field samples on very large FEM meshes. The idea is to select an appropriate subspace. The covariance matrix is created in this sub space, the same is true for the generation of spatially correlated standard normal variables. Then one must interpolate the missing field points in the original space based on the sub-space samples. This interpolation must be chosen in such a way that it optimally represents the statistical properties of the random distribution at the respective field points.

For the choice of the sub-space one may use a second mesh with small number of nodes approximating the fine original FEM mesh. Such a strategy requires the implementation of a mesh coarsening algorithm. Such an algorithm may be difficult to implement in practice, if sufficiently accurate coarsening is aimed at for a great variety of mesh topologies (bold vs. thin-walled structures, multiple finite element types - 1d, 2d, 3d, 2.5d, etc.).

In this article, a very simple and efficient strategy is used to select the sub-space: The node indices are randomly chosen from the original FEM mesh.

The simulation then follows the steps:

1. Randomly select M support points from the finite element mesh.

2. Assemble the covariance matrix for the selected sub-space.

3. Perform a decomposition of the covariance matrix $\mathbf{Cov} = \Phi \text{diag}(\lambda_{ii}) \Phi^T$ and chose c basis vectors ϕ_i.

4. Create basis vectors ψ_i by interpolating the values of $\sqrt{\lambda_i}\phi_i$ on the FEM mesh.

5. Simulate N vectors $\mathbf{u}_k$ of statistically independent standard-normal random variables, each vector is of dimension c.

6. Apply the correlation in standard normal space for each sample k: $\mathbf{z}_k = \sum_i^c \psi_i u_{k,i}$.

7. Transform the correlated field samples into the space of the desired random field: $x_{k,j} = F^{(-1)}\left(N(z_{k,j})\right)$.

4.1 Expansion Optimal Linear Estimation (EOLE)

An optimal representation of a stochastic field as a linear combination of a subset of its values was proposed by [4]. It is widely used when simulating random fields, see for example [6, 1] and the references therein. The method is called Expansion Optimal Linear Estimation (EOLE) and is an extension of Kriging. Kriging interpolates a random field based on samples being measured at a sub-set of mesh points. It then minimizes the variance of the interpolation error. When simulating random fields, one is interested in minimizing the variance of the error when representing the stochastic field by the Karhunen-Loeve expansion while only the base vectors are known at a sub-set of field nodes.

Assume that the sub-space is described by the field values

$$\mathbf{y}_k = \{z_{k,1}, \ldots, z_{k,M}\} = \{\sum_{i=1}^{c} \sqrt{\lambda_i}\phi_{i,1}u_{k,i}, \ldots, \sum_{i=1}^{c} \sqrt{\lambda_i}\phi_{i,M}u_{k,i}\} \tag{12}$$

Minimization of the variance between the target random field and its approximation under the constraint of equal mean values of both results in:

$$\psi_i = \mathbf{Cov}_{zy}^T \mathbf{Cov}_{yy}^{-1} \frac{\phi_i}{\sqrt{\lambda_i}} \tag{13}$$

with $\mathbf{Cov}_{yy}$ denoting the correlation matrix between the sub-space points and $\mathbf{Cov}_{zy}$ denoting the (rectangular) covariance matrix between the sub-space points and the nodes in full space. For the choice of an optimal number of required sub-space points per correlation length, one could further read [5].

4.2 Restoring statistical moments

The mean estimate $E(\hat{\mathbf{X}})$ of the generated random field samples $\mathbf{x}_k$ is unbiased, i.e. $E(\mathbf{X}) = E(\hat{\mathbf{X}})$. The variance, however, is bounded, i.e. $Var(\mathbf{X}) \geq Var(\hat{\mathbf{X}})$. This results directly by application of two smoothening filters, the modal reduction of the covariance matrix and the interpolation of the sub-space field samples. Both eliminate parts of the original variability which will not be present in the final samples.

In order to restore the desired variance, one may reintroduce the eliminated random parts of the solution in terms of white noise. To achieve this, statistically independent random numbers $e_{k,j}$ are generated for each sample and for each field point and added to the field sample vectors before the transformation into the target space takes place. The mean of these random numbers is zero while the standard deviation can be computed from

$$Z_j = Z_{j,approx} + Z_{j,error} \tag{14}$$

$$Var(Z_j) = E\left[\left(\sum_{j}^{c} \psi_j U_j + Z_{j,error}\right)^2\right] = 1 \tag{15}$$

$$\sigma_j^2 = 1 - \sum_{j}^{c} \psi_j^2 \tag{16}$$

Additionally to the steps in the previous section, one generates statistically independent standard-normal random numbers $e_{j,k}$ for each sample k and for each field point j. The field samples are then computed from $x_{k,j}^{corr} = F^{(-1)}\left(N\left(z_{k,j} + \sigma_j e_{j,k}\right)\right)$.

Furthermore, the vector σ provides a measure for the actual local error arising from the two steps of model order reduction. A global error can be obtained by relating the sum of the eigenvalues of the actual correlation matrix to the sum of the eigenvalues of the true correlation matrix. One first computes the eigenvalues κ_i of $\Psi\Psi^T$ (the nonzero eigenvalues of the matrix $\Psi^T\Psi$ are the same, but more efficient to compute). Then the global error is

$$\epsilon = 1 - \frac{1}{n}\sum_i \kappa_i \tag{17}$$

wherein n is the number of all discrete points.

5 Example

A simple structure from a sheet metal forming application serves as a numerical example. It is modelled by 4-node shell elements using 8786 finite element nodes. The maximum dimension is 540. The correlation length parameter is chosen to be 100 in standard normal space. The distribution of the considered field quantity (eg. a geometric deviation due to random process parameters) is a truncated Gaussian distribution with mean value 5, standard deviation 15, lower bound -20 and upper bound 30 - being equal at all nodes. The number of nodes is small enough to compute a reference solution based on the full model. The sub-space dimension is chosen to be small (between 50 and 1000 points). Then one may extrapolate the results to the large-scale case of > 50.000 nodes.

The correlation matrix is expanded using 20 eigenvectors representing $> 99.9\%$ variability in sub-space. Figure 2 shows the support point coordinates using different numbers of support points in sub-space. Figure 3 shows the first shapes ψ_i obtained from 50 support points. For comparison, figure 4 presents the same shapes if the correlation matrix is computed in full space. The MAC values comparing the full model with individual sub-space shapes are listed in table 1. The table also lists the global error and the average local error. The average local error is approximately the the square root of the global error norm obtained by the eigenvalues κ_i. The MAC values agree well even for very small sub-space dimensions. Figure 5 shows the corresponding local approximation errors of the spatial correlation. Surprisingly, the EOLE method approximates the problem very well even for a very small number of support points.

The local statistics is evaluated at all nodes, i.e. the mean value $\bar{X}$, the standard deviation σ_X and the 99% quantile value $F^{-1}(0.99) = 39.8952$ agree with the respective estimators of the simulated random numbers.

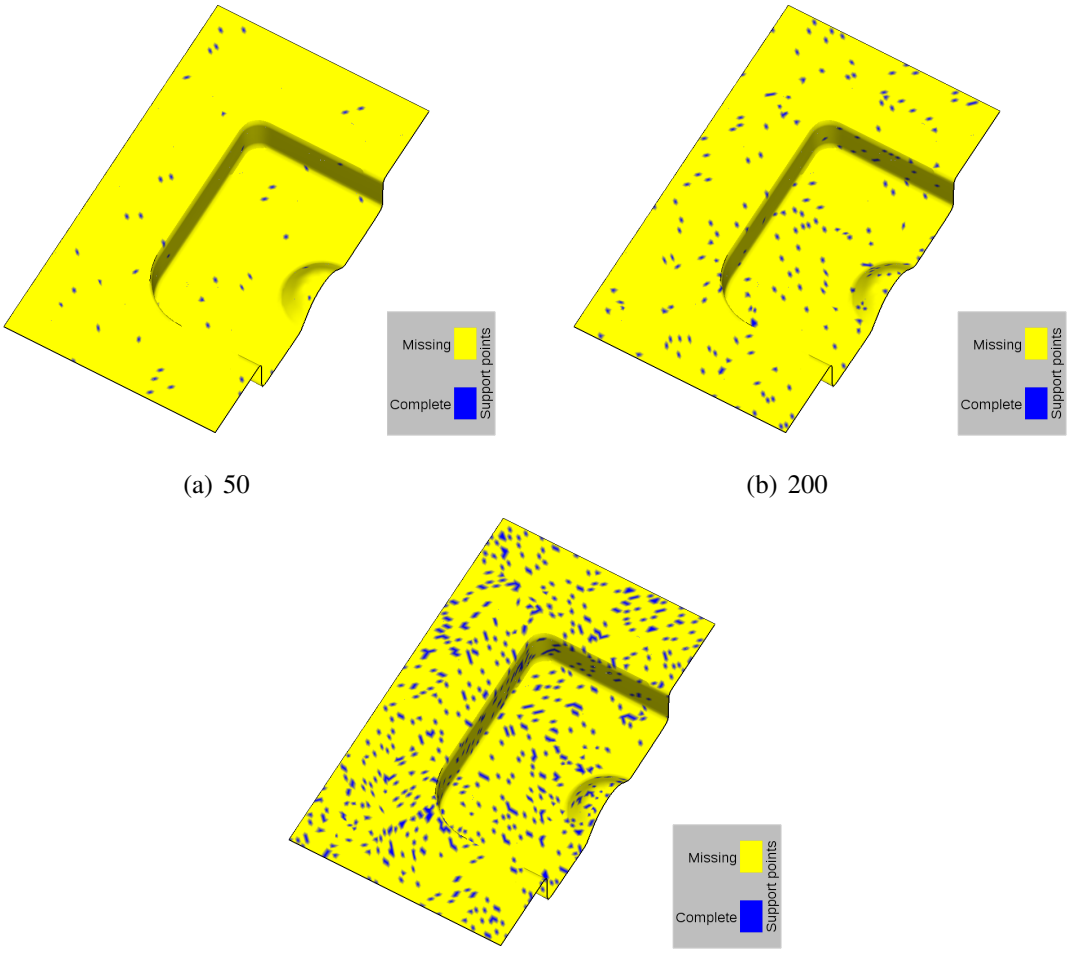

(a) 50 (b) 200

(c) 800

Fig. 2: Selected support point positions for different numbers of support points

Tab. 1: Errors and MAC values of various shapes (reference of comparison: full model) for different numbers of support points n.

n	global error	mean local error	MAC ψ_1	MAC ψ_2	MAC ψ_5	MAC ψ_{10}
50	0.055	0.185	0.999	0.999	0.949	0.393
100	0.027	0.151	0.999	0.999	0.999	0.986
200	0.024	0.145	0.999	0.999	0.999	0.999
400	0.023	0.141	0.999	0.999	0.999	0.999
800	0.022	0.140	1	1	0.999	0.999
8786	0.021	0.140	1	1	1	1

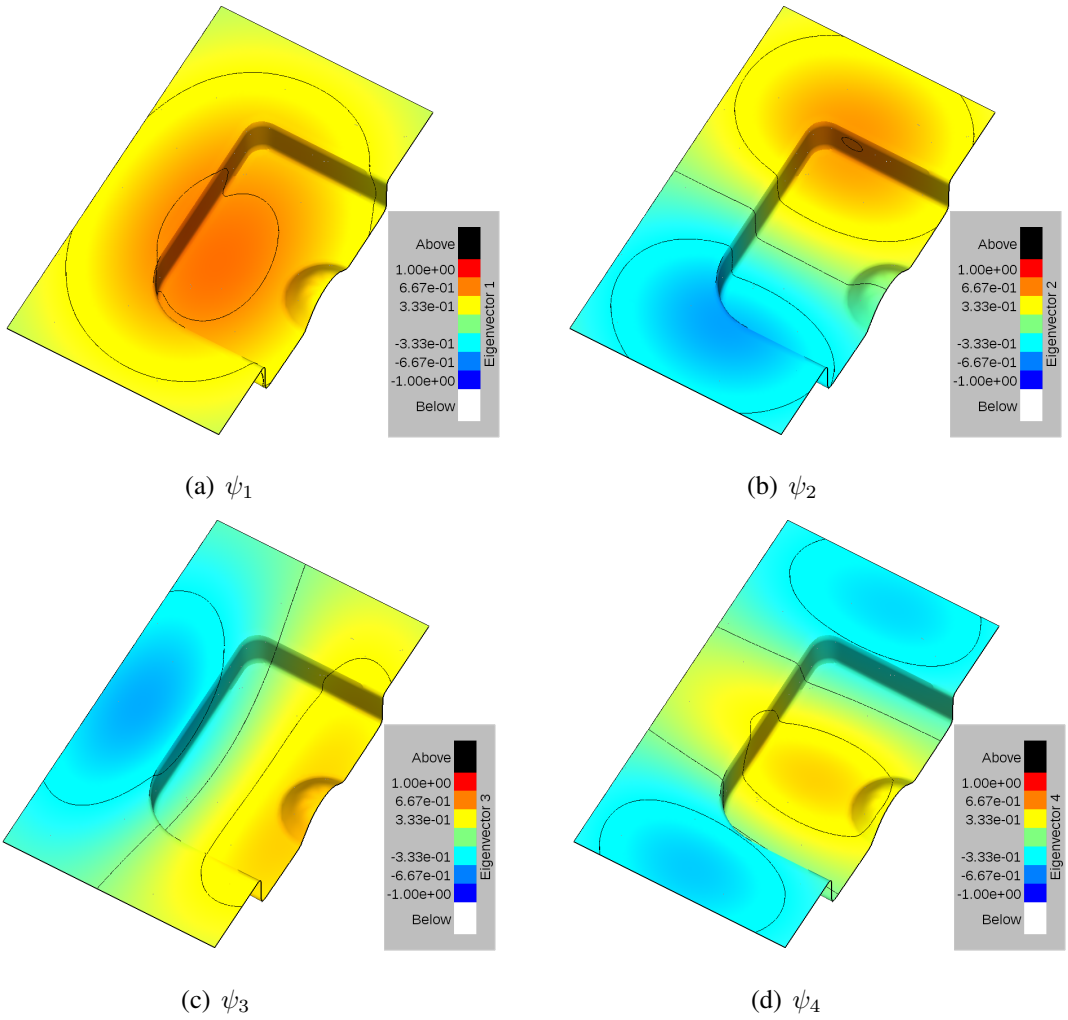

(a) ψ_1 (b) ψ_2

(c) ψ_3 (d) ψ_4

Fig. 3: First shapes ψ_k for 50 support points in sub-space

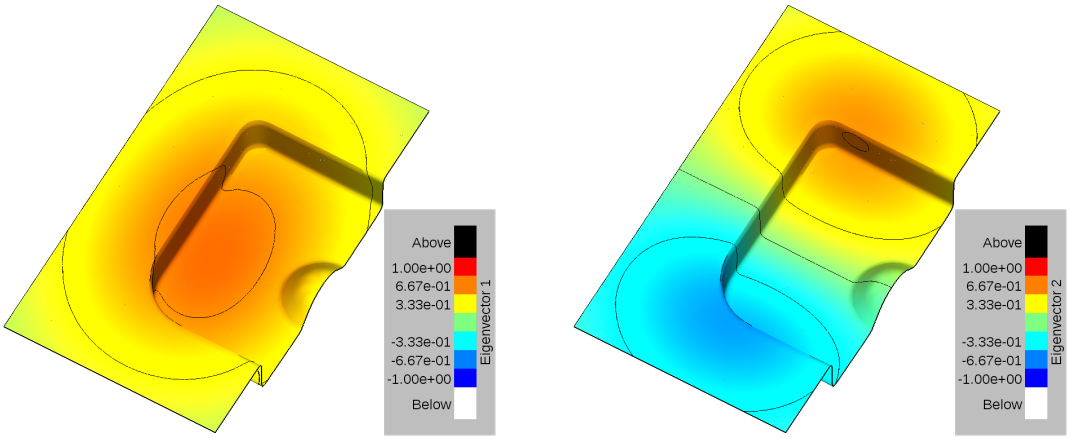

(a) ψ_1 (b) ψ_2

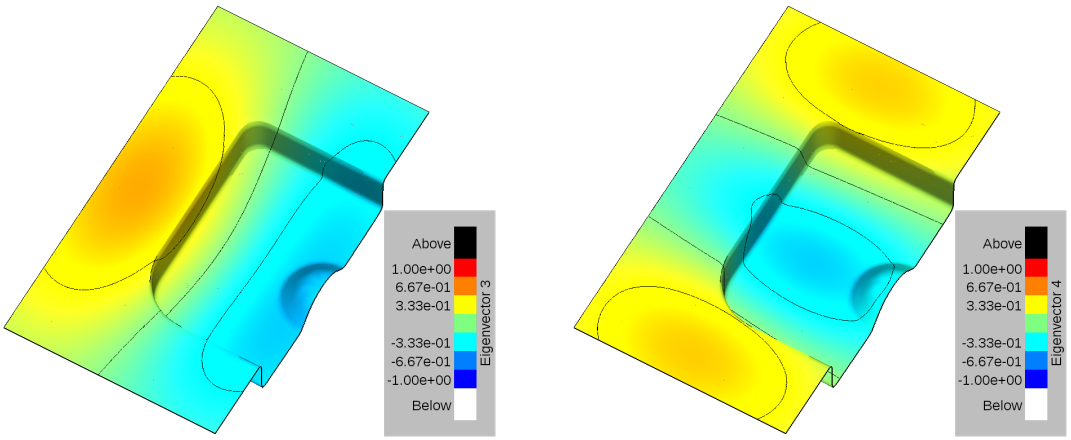

(c) ψ_3 (d) ψ_4

Fig. 4: First shapes ψ_k using the full model

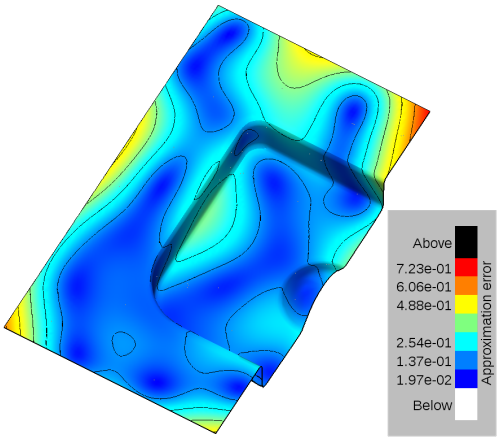

(a) 50

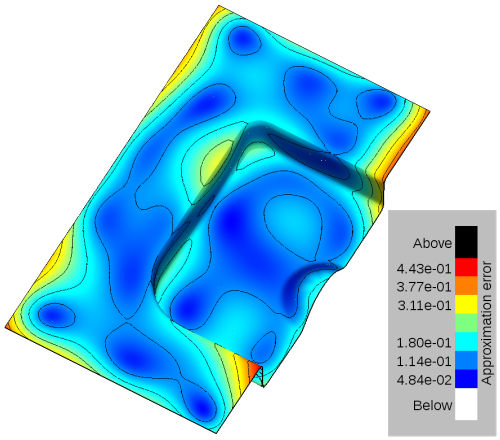

(b) 200

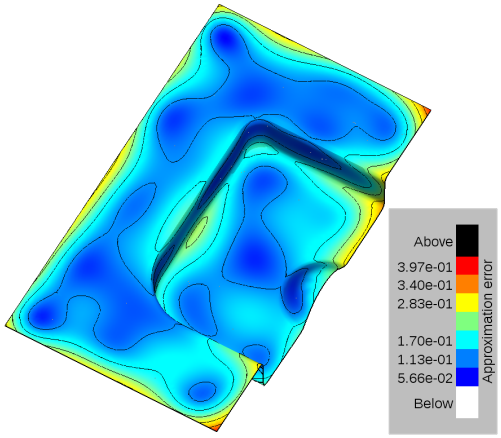

(c) 800

Fig. 5: Local approximation error for different numbers of support points

6 Conclusion

This article presented two strategies to simulate random fields on large finite element structures. The strategy for very small correlation length-scale parameters based on a sparse correlation matrix is not yet applicable in practice due to the missing availability of fast numerical linear algebra packages that provide access to the Cholesky factors of a sparse matrix. It is, however, possible to efficiently generate random fields with relatively large correlation length-scale parameters based on approximation methods. Herein, a spectral decomposition of the covariance matrix in a randomly selected sub-space and interpolation in full space using the EOLE method was studied. Errors due to the approximation can be easily quantified. The spatial correlation structure may be well represented even if only a very small number of support points is used. The presented algorithms will be soon available in the software *Statistics on Structures* by DYNARDO Austria GmbH.

Acknowledgement

This research was funded by DYNARDO Austria GmbH, project *Statistics on Structures*. I also want to thank Prof. Dr. Christian Bucher and Dr. Veit Bayer for their input during numerous discussions.

Furthermore, I want to thank the reviewer of this article who gave me the hint to the EOLE method.

Literature

[1] Diego Lorenzo Allaix and Vincenzo Ilario Carbone. Numerical discretization of stationary random processes. *Probabilistic Engineering Mechanics*, 25(3):332–347, 2010.

[2] Veit Bayer. Random fields in statistics on structure (SoS). In *Weimarer Optimierungs- und Stochastiktage 7.0*, Weimar, Germany, 2009. Dynardo GmbH.

[3] DYNARDO Austria GmbH. http://www.dynardo.at.

[4] Chun-Ching Li and A. Der Kiureghian. Optimal discretization of random fields. *Journal of Engineering Mechanics*, 119(6):1136–1154, 1993.

[5] Bruno Sudret and Armen Der Kiureghian. Stochastic finite element methods and reliability: a state-of-the-art report. Technical Report UCB/SEMM-2000/08, Dept. of Civil and Environmental Engineering, University of California, Berkeley, USA, 2000.

[6] Miroslav Vořechovský. Simulation of simply cross correlated random fields by series expansion methods. *Structural Safety*, 30(4):337–363, 2008.

[7] Holger Wendland. *Scattered data approximation*. Cambridge monographs on applied and computational mathematics. Cambridge University Press, Cambridge, 2005.

[8] Johannes Will and Christian Bucher. Statistical Measures for the CAE-based Robustness Evaluation. In *Weimarer Optimierungs- und Stochastiktage 3.0*, Weimar, Germany, 2006. Dynardo GmbH.

[9] Johannes Will, Christian Bucher, Markus Ganser, and Kathrin Grossenbacher. Berechnung und Visualisierung statistischer Mae auf FE-Strukturen fr Umformsimulationen. In *Weimarer Optimierungs- und Stochastiktage 2.0*, Weimar, Germany, 2005. Dynardo GmbH.

Comparison among the methodologies for seismic fragility evaluation

Sai Zhang, Jun Zhao, Jiejuan Tong
Institute of Nuclear and New Energy Institute, Tsinghua University, Beijing
zhangsai12@mails.tsinghua.edu.cn, zhaojun@tsinghua.edu.cn, tongjj@tsinghua.edu.cn

Abstract: The Fukushima accident in Japan evoked a global reconsideration on nuclear safety, especially under seismic conditions. A growing number of nuclear power plants in China are required to carry on Seismic Probability Risk Assessment (SPRA) or Seismic Margin Assessment (SMA) in order to define seismic capacity. The fragility analysis of key components and structures is essential to SPRA and SMA. In the analysis of fragility, fragility curve and HCLPF (High Confidence of Low Probability of Failures) are usually used to represent the seismic capacity of equipment or structures, which can be established using several methodologies, including probabilistic fragility analysis, conservative deterministic failure margin method (CDFM), test results, deterministic approach, generic fragility data, etc. In this paper, those approaches are discussed respectively in order to develop an overall comparison from several perspectives. Based on that, the paper will discuss the technology roadmap of development of general fragility analysis data base that is applicable to fragility analysis of nuclear power plants in China.

Keywords: seismic, fragility, HCLPF

1 Introduction

Seismic Probablistic Safety Assessment (SPSA) and Seismic Margin Assessment (SMA) are two effective approaches in providing individual plant examination under seismic circumstances. As a common essential part, fragility evaluation is of great significance for both SPSA and SMA. During the evaluation process, HCLPF (High Confidence, Low Probability of Failure) value is usually used as a fragility indicator for key structure or equipment. Its lower bound is also taken to represent a comprehensive seismic capacity at plant level.

This paper starts with an overview of previous activities. Related fragility studies have been conducted by Brookhaven National Laboratory (BNL), Electric Power Research In-

stitute (EPRI) and in AP1000 seismic margins evaluation. Research framework and results for each of them will be covered in Sec. 2.

Several common methodologies in fragility evaluation will be discussed in Sec. 3. Considering construction characteristics and data availability, HCLPF values can be established by a series of parallel methods, including probabilistic fragility analysis, conservative deterministic failure margin method (CDFM), test results, deterministic approach and generic fragility data. Corresponding general procedures will be respectively illustrated.

Based on the analysis in Sec. 2 and Sec. 3, practical application situation of five methodologies are going to be covered in Sec. 4, including an overall comparison. Finally, this section will also give guidance on technical feasibility study of generic fragility data base in Chinese nuclear power plants.

2 Overview of previous activities on seismic fragility evaluation

2.1 Brookhaven national laboratory

Sponsored by the U.S. Nuclear Regulatory Commission (NRC), BNL carried on a series of research on fragility level establishment for various nuclear power plant equipment classes in 1985. The research framework can be summarized as follows.

2.1.1 Data collection

After sufficient contacting and negotiating with both domestic and foreign institutions, BNL has collected over 70 seismic capacity test reports which records existing fragility data for some certain equipment classes. The report consists of equipment description, test input and test result, presented in the form of Test Response Spectrum (TRS, as Fig. 1 shows).

2.1.2 Fragility evaluation

As the variability in manufacturer, model and vibration test input, a large amount of response curves are obtained corresponding to various failure modes.

Each failure mode can be described by a set of curves. The lower bound of the curves can be used to represent the deterministic fragility level. Also, all the curves can be taken in a statistic way out of probabilistic method. Zero Period Acceleration (ZPA) and Average Spectral Acceleration (ASA) are two indicators in both deterministic and probabilistic terms. Based on a lognormal distribution, HCLPF value can be calculated by a function of median and composite standard deviation of both the indicators respectively.

BNL has emphasised in electrical equipment and published several reports presenting fragility study results of eighteen equipment classes, including switchgears, motor control centres, relays, etc.

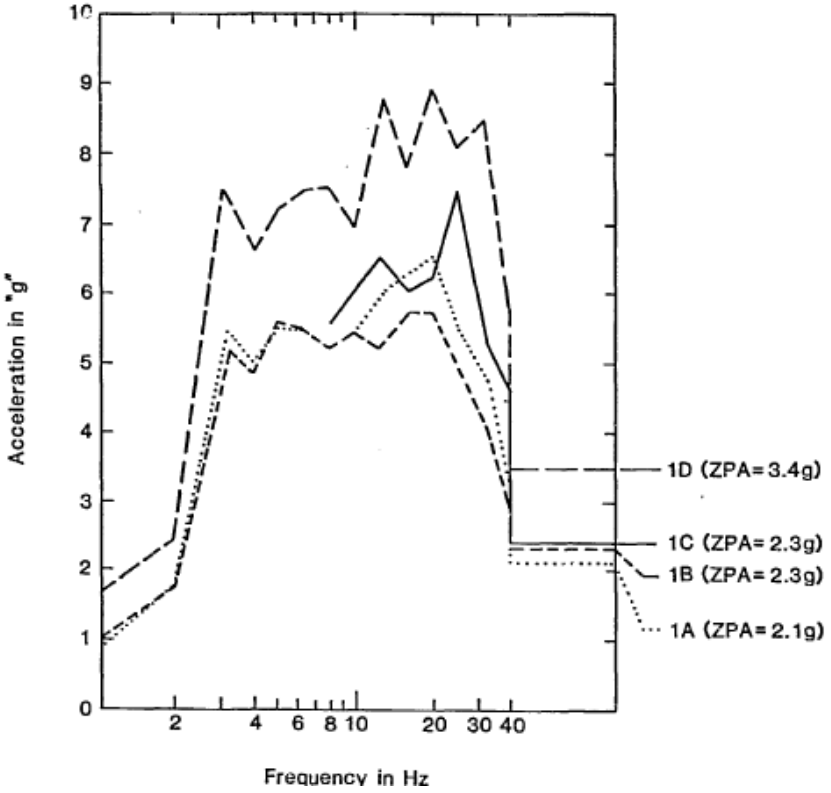

Fig. 1: A TRS example from report BNL-NUREG-37333

2.2 Electric power research institute

In 1994, EPRI accomplished fragility evaluation for structures, passive equipment and active equipment. Similar to BNL, EPRI applies both deterministic and probabilistic methodologies. However, instead of using existing data from test reports, EPRI conducted a full fragility analysis based on a number of fragility variables for some key components. Meanwhile, the majority of other structures or components obtain their fragility level through Conservative Deterministic Failure Margin (CDFM) with the use of finite element analysis.

2.3 AP1000

In AP1000 Seismic Margins Evaluation, a fragility analysis is utilized for essential structures and components. HCLPF value is again taken as the indicator of seismic capacity level. According to the construction characteristics and data available, HCLPF is established, consisting of as many as five parallel approaches, including probabilistic method, CDMF, test result, etc. It also published several tables summarizing HCLPF values for each structure or component, also pointing out the approach based on.

3 Seismic fragility evaluation methodologies

With the objective to estimate the capacity of given structure or equipment under seismic conditions, a lot of parallel fragility evaluation methodologies have been developed.

According to various construction characteristics and data availability, the methodologies can be used respectively or cooperatively at plant level. This section will discuss both their general procedures and key methodologies.

3.1 Probabilistic fragility analysis

3.1.1 General procedure

The HCLPF here is derived from a function of both median seismic capacity and composite standard deviation β_c. The median capacity is related to mean capacity by a function of β_c, as shown in Eq. (1).

$$Median\ Capacity = Mean\ Capacity \times f_1(\beta_c) \tag{1}$$

The mean capacity can be expressed by Eq. (2).

$$Mean\ Capacity = No\,min\,al\ Capacity \times \left(\prod [X_i]\right) \tag{2}$$

with

X_i i^{th} design mean margin factor.

The composite standard deviation β_c can be derived from Eq. (3),

$$\beta_c = \sqrt{\left[\sum (\beta_c)_i^2\right]}. \tag{3}$$

3.1.2 Key methodology

Unavoidable variability is identified while choosing numerous seismic margin factors, including variable strength factors, material, damping, ductility, analysis and modelling error, mode shapes, mode frequency variability, imperfections and soil structure interaction. Each factor is estimated in a statistic way, establishing a median and a composite standard deviation. For example, variable strength factors are given corresponding to different failure modes, as well as material properties.

Thus, the probabilistic methodology is reflected on the evaluation process of seismic margin factors. However, some deterministic strength factors with no variability in design have to be considered as well, in order to establish an accurate and proper median capacity. Their standard deviation values are taken zero when calculating β_c.

3.2 Conservative Deterministic Failure Margin method (CDMF)

Both CDMF and Probabilistic Fragility Method are similar in the general procedure. The key difference lies in the seismic margin factor selection and evaluation: factors in CDMF are determined values instead of a lognormal distribute in probabilistic methodology, calculated and established by Finite Element Analysis (FEA). Strength, inelastic energy absorption and damping are three common deterministic seismic factors. Then the HCLPF

capacities at plant level can be synthesised after computing margin factors with CDMF method for all the necessary structures and equipment.

3.3 Test results method

3.3.1 Key methodology

This methodology is often used when evaluating electrical equipment for their sufficient available existing data. Major reactor suppliers, testing laboratories and equipment manufacturers usually have conducted a series of seismic capacity tests. Identifying and collecting existing test data can be a convenient and accurate way for fragility evaluation, saving time and expenses on tests for various equipment classes.

3.3.2 General procedure

Test results are recorded in a form of Test Response Spectrum (TRS). Each failure mode is described by a group of response curves. As previously stated in 2.1.2, ZPA and ASA are two indicators for fragility level. Both deterministic and probabilistic methodology can be applied in Test Results Method.

In probabilistic terms, the median and composite standard deviations (β_c) of either ZPA or ASA are taken to derive corresponding HCLPF for a certain failure mode, as shown in Eq. (4) and (5).

$$HCLPF = Median \times f\left(\beta_c\right) \tag{4}$$

$$\beta_u^2 = \beta_c^2 - \beta_r^2 \tag{5}$$

with

β_c composite standard deviation

β_r randomness variation coefficient

β_u uncertainty variation coefficient

3.4 Deterministic approach

For certain structure or equipment whose seismic capacities are already available, changing load combination or environment may cause the HCLPF to vary correspondingly. Thus, a lower bound HCLPF under new circumstances is needed to be compared with primary seismic capacity. Deterministic approach is such a quick and direct way to verify if the supports can control the new HCLPF.

3.5 Generic fragility data

Generic Fragility Data Method is a supplementary one for the methodologies described above. It is usually used when information available is not enough to carry on HCLPF capacity analysis with any of the four methodologies.

4 Application and comparison among different fragility evaluation methodologies

4.1 Practical application situation summary

Base on fragility evaluation of BNL, EPRI and AP1000, application of different methodologies is summarized in Tab. 1a and Tab. 1b.

4.2 Comparison among different fragility evaluation methodologies

4.2.1 Circumstances without data available

Under the circumstances without available data, HCLPF values can be established by either probabilistic fragility analysis or conservative deterministic failure margin (CDFM) method. The former approach covers quite a large number of seismic margin factors, taking their condition-varying characteristic into account. HCLPF derived from both the medians and composite standard deviations of each margin factor is relatively accurate and comprehensive, regardless of a plenty of time spent on data collection and calculation. Thus, this method is usually used in some essential components or structure with a limited number. The latter approach has a more direct and deterministic way in choosing seismic margin factor. Strength, inelastic energy absorption and damping are three major concerns. Familiar to most engineers, CDFM is widely taken for structure seismic fragility evaluation.

PFA is a statistic way while CDFM is quite deterministic. Both approaches are convincingly accurate, whereas slight differences exist in selection under certain circumstances. The former approach is usually applied when margin factors tend to be a function of the failure mode. It covers a larger range of margin factors, including material allowable, analysis and modelling error. Also, PFA suits for those site-specific conditions, since it always takes soil structure interaction into account.

4.2.2 Circumstances with data available

Test Results Analysis saves a lot time and work in margin factor collection. However, in evaluating process with this method, one specimen in multiple test runs and uncertain in population may induce deviation. And the selection work for scale factors when standardizing all the curves of one failure mode still need further exploration.

Deterministic Approach tends to be used in verifying whether intrinsic seismic capacity could control the new HCLPF level under new loads or environment.

Generic Fragility Data Method is a supplementary measure when none of the four approaches works well. Based on previous data base, its general applicability is limited.

4.3 Technical feasibility study of generic fragility data base in Chinese nuclear power plants

Generic fragility data base usually consists of fragility test data, generic seismic qualification test data and earthquake experience data. As is synthesized from a large number of

Tab. 1a: Application of five parallel fragility evaluation methodologies (1)

	Probabilistic Fragility Analysis	CDFM	Generic Fragility Data
BNL	---	---	---
EPRI	Few key components	Most of the structure and components	---
AP1000	Steam generator supports Reactor pressure vessel supports Pressurizer supports Containment vessel Inner containment structure	Shield building roof	Reactor internals and core assembly Control rod drive mechanism Reactor coolant pump including supports Accumulator tank Main control room operation Piping, cable trays, valves, ceramic insulators

Tab. 1b: Application of five parallel fragility evaluation methodologies (2)

	Test Results		Deterministic Approach
	Deterministic	Probabilistic	
BNL	18 equipment classes most of which are electrical	18 equipment classes most of which are electrical	---
EPRI	---	---	---
AP1000	Some electric equipment	---	Polar crane Baffle plate supports Heat exchanger Core makeup tank Valves

tests based on sufficient equipment or structure categories, the generic fragility data base is quite representative and can reflect the realistic seismic capacity well.

Carrying out seismic fragility evaluation on all the components and structure could take a lot of work. Thus, generic data base can be used under two conditions.

On one hand, some certain component categories have high seismic capacity with low probability to be the critical parts under seismic conditions, according to previous documentation and experience. Generic data can be conservative enough to represent their realistic and plant-specific capacities. To minimize the effort on nonsignificant items and to save resources for more essential aspects, certain high seismic capacity component categories can be screened out using generic data.

On the other hand, common fragility evaluation methodologies, such as probabilistic and conservative methods, need a large amount of plant-specific or component-specific data. When data available is insufficient for such assessments, generic data can be taken as a substitute to represent and reflect the realistic capacity level.

A combination of plant-specific evaluation and generic data base can be a comprehensive way to carry on seismic fragility capacity evaluation in China. To make it more convincing, the evaluation results of some certain component categories using plant-specific methods can be used to compare with those in generic data base, demonstrating that use of such generic data is conservative.

5 Summary

Five parallel seismic fragility evaluation methodologies are concluded from previous work conducted by BNL, EPRI and AP1000. With different characteristics and application conditions, all the five approaches can be used respectively or cooperatively in nuclear power plant seismic fragility evaluation.

Literature

[1] Bandyopadhyay, K.K., Hofmayer, C.H. *Seismic Fragility of Nuclear Power Plant Components (Phase I)*. NUREG/CR-4659-Vol.1, 1986

[2] Bandyopadhyay, K.K., Hofmayer, C.H., Kassir, M.K., Pepper, S.E. *Seismic Fragility of Nuclear Power Plant Components (Phase II)*. NUREG/CR-4659-Vol.3, 1990

[3] Bandyopadhyay, K.K., Kana, D.D., Kennedy, R.P., Schiff, A.J. *An Evaluation of Methodology for Seismic Qualification of Equipment, Cable Trays, and Ducts in ALWR Plants by Use of Experience Data*. NUREG/CR-6464, 1997

[4] Electric Power Research Institute. *Methodology for Developing Seismic Fragilities*. Technical Report, TR-103959, 1994

[5] The American Society of Mechanical Engineers. *Standard for Level 1/ Large Early Release Frequency Probabilistic Risk Assessment for Nuclear Power Plant Applications*. ASME/ANS RA-Sa-2009, 2009

[6] Westinghouse. *AP1000 Probabilistic Risk Assessment*, 2003

Measurement redundancy incorporating measurement uncertainty

Thomas Zimmermann [a,b], Katharina Haider [a], Alfred Strauss [a]

[a]Institute for Structural Engineering, University of Natural Resources and Life Sciences, Vienna, Austria

[b]Faculty of Civil Engineering, Brno University of Technology, Brno, Czech Republic

zimmermann.thomas@boku.ac.at, katharina.haider@boku.ac.at, alfred.strauss@boku.ac.at

Abstract: Engineers are increasingly being asked to monitor or evaluate the efficiency and the performance of a structure for an assessment or for continuously monitoring. Therefore appropriate measurement devices have to be used. However, measurement data has to be accurate, which means that an objective method for assessing data quality and measurement uncertainty is needed. Results are often derived from the combination of values determined from a number of individual measurements. Those individual measurements can be a set of deterministic or stochastic values. Unfortunately, a realistic estimate of deviation/uncertainty cannot be achieved, although it is possible to estimate the potential size of a particular deviation or combination of deviations. Uncertainty analysis is a vital part of any experimental program or measurement system. Any experimental result will involve some level of uncertainty that may originate from causes such as the lack of accuracy in measurement equipment, random variation in the measurands, and approximations in data reduction relations. Those uncertainties can be caused by systematic deviations or random deviations in the measurement process. All these individual deviations eventually influence the final result. The aim of the paper is to show how uncertainties of measurement devices can be taken into consideration with respect to redundant measurement systems.

Keywords: measurement, uncertainty, deviation, redundant systems

1 Introduction

In recent years major advances have been accomplished in the design, modeling, analysis, monitoring, maintenance and rehabilitation of civil engineering structures. These developments are currently undergoing a transition towards a life-cycle and performance oriented design. Monitoring is a key factor in this process, while the term *monitoring* includes all types of acquisition, observation and supervision of an activity or a process [7, 14, 15]. Scientists and practitioners are interested in the investigations and the development of monitoring systems and approaches for the efficient incorporation of monitored information in the performance assessment of structures associated with the identification of defects and degradation processes [11, 17].

Therefore measurement begins with the definition of the measurand and the quantity intended to be measured. The specification of a measurand requieres the knowledge of the kind of quantity. Independently it must be taken into consideration that uncertainty is part of any experimental program or measurement system. In any experiment the researcher seeks to obtain numerical values for certain physical variables. These unknown variables are known as measurands. However obtained results of a physical quantity should be related to a quantitative indication of the quality of the result which can be further used to assess its reliability [9, 10]. Without any indication the obtained results of the measurement cannot be compared between each other or cannot be compared to any reference values. It is therefore necessary to evaluate both the obtained results of a measurement and the related uncertainty to each measurand.

Measurement uncertainty can be defined as the difference between the true value and the measured value of the quantity and can be expressed as follows:

$$E = M - T \tag{1}$$

Thereby E = deviation/uncertainty, M = a measured or observed value and T = actual value. Normally, the researcher can never really know the uncertainty of a measurement. He can only estimate the uncertainty interval of the measurement. Generally, uncertainties can be divided into two categories: fixed or systematic deviations and random deviations. Although both types of deviations falsify the validity of the data, their causes are different and therefore different actions must be taken to minimize them. Fixed or systematic deviations are consistent and repeatable deviations. If the same measurement is performed in the same way more than once, the fixed or systematic uncertainties will be the same each time. One example for the fixed uncertainty is the calibration process.

Random deviations are mostly caused by a lack of repeatability in the output of the measuring system. They can originate from the measuring system itself, from the experimental system, or from the environment. Random deviations can be minimized by eliminating uncontrolled variables or shielding or grounding the measuring system. All these individual deviations translate into uncertainty of the final result. Uncertainty analysis is performed during the design state of an experiment as well as after the data taking has been completed in order to demonstrate the validity of the results. Figure 1 shows possible components which causes sources of uncertainties.

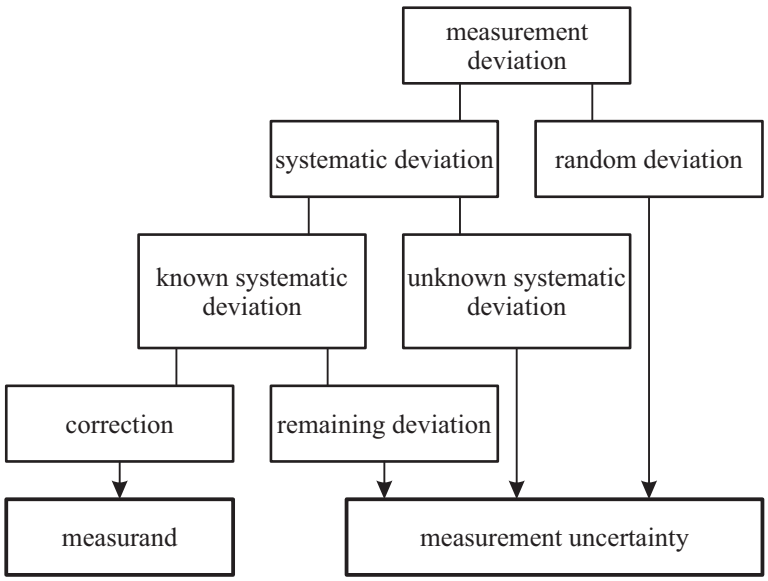

Fig. 1: Different possible components of uncertainty, [3]

2 Methodology of measurement

2.1 Monitoring systems

The configuration of a monitoring systems can be designed to be simple, using one measurement device to obtain data, or it can be sophisticated in order to gather additional information. Therefore the redundant configuration mentioned above can be used in order to incorporate different measurement devices or to obtain correlations and trends of measurements. Figure 2 shows a comparison of three different stages. Thereby (a) Level 1 is a simple monitoring layout to detect local and/or global maxima, (b) Level 2 is an advanced monitoring layout to detect beside local and/or global maxima also the gradient of the specific value, and (c) Level 3a and Level 3b are stochastically based layouts allowing correlation and sensitivity studies. In addition, monitoring layouts based on these levels can be seen as redundant systems if the individual measurement devices are independent from each other.

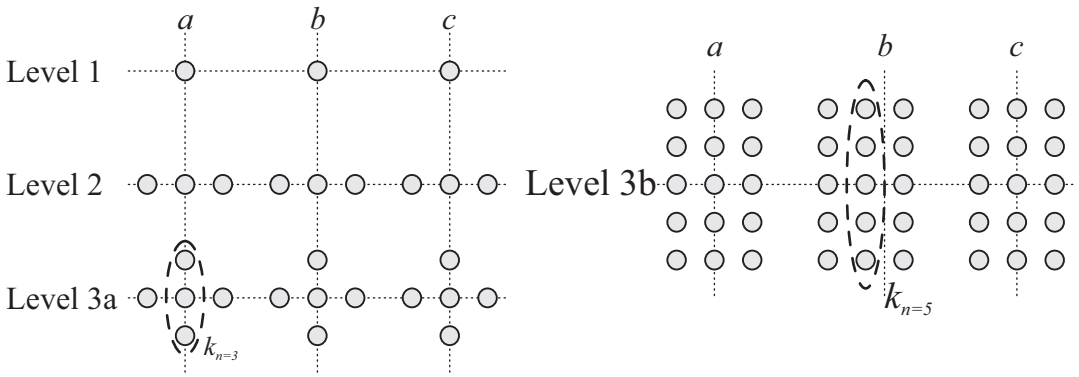

Fig. 2: Levels of monitoring configuration

2.2 Redundant systems

In engineering, redundancy is the duplication of critical components or functions of a system with the intention to increase reliability of the system. The two functions of redundancy are passive redundancy and active redundancy. Both functions prevent performance decline from exceeding specification limits without human intervention using extra capacity. Passive redundancy uses excess capacity to reduce the impact of component failures. One common form of passive redundancy is the extra strength of cabling and struts used in bridges. Active redundancy eliminates performance decline by monitoring performance of individual device, e.g. error detection and correction.
Additional information regarding monitoring, monitoring application and novel techniques can be found e.g. in [1, 2, 8, 13].

3 Measurement uncertainty

3.1 General

The general procedure for the evaluation of measurement uncertainty is documented in the Guide for the expression of uncertainty in measurement [6]. The following section provides an overview of the assessment.
In most cases a measurand Y is not measured directly, but determined from n other quantities using a functional relationship $Y = f(X_1, X_2, \ldots, X_n)$. If the measurement uncertainty is only depending on the sample size, an estimation function $\mu = \mu(X_1, \ldots, X_n)$ with respect to the variables of the samples $X_1, \ldots, X_n$ can be determined, [16]. The expected value of the random variable μ is mostly $E(\mu) = \bar{x}$ and it is:

$$P(\bar{x} - e < \mu < \bar{x} + e) = 1 - \alpha \tag{2}$$

The absolute error is equal to:

$$e = c_{1-\alpha/2}\sqrt{Var(\mu)} \tag{3}$$

hence:

$$P\left(\bar{x} - c_{1-\alpha/2}\sqrt{Var(\mu)} < \mu < \bar{x} + c_{1-\alpha/2}\sqrt{Var(\mu)}\right) = 1 - \alpha \tag{4}$$

Thereby $c_{1-\alpha/2}$ is depending on the type of the distribution of μ. The variance $Var(\mu)$ is depending on the sample size. In the case that the standard deviation is known a priori the random variable $(\bar{x} - \mu)/\sqrt{Var(\mu)}$ follows a normal distribution. With increasing sample size, this distribution is *narrower* and tend to the standard normal distribution. For the standard deviation, which corresponds to the sample error, the following applies:

$$\sqrt{Var(\mu)} = \frac{\sigma}{\sqrt{n}} \tag{5}$$

with $\sigma =$ standard deviation of the basic population and $n =$ sample size.

3.2 Uncertainty and extended uncertainty

In general, the standard deviation is unknown and must be estimated from the sample. Instead of the standard deviation σ of the basic population the standard deviation s of the sample is used. Hence the random variable $(\bar{x}-\mu)/\sqrt{Var(\mu)}$ is not normally distributed, especially when the sample size n is small. With a limited sample size and unknown standard deviation $c_{1-\alpha/2} = t_{1-\alpha/2}$ can be used. $t_{1-\alpha/2}$ corresponds to the $(1-\alpha/2)$–quantile of the t–student distribution with $n-1$ degrees of freedom. For the standard deviation of $\sqrt{Var(\mu)}$ the standard uncertainty is used. This result is analogous to Eq. 5:

$$\sqrt{Var(\mu)} = \frac{s}{\sqrt{n}} \tag{6}$$

with $s =$ standard deviation of the sample and $n =$ sample size.
In general, the uncertainty of a measurement is not only the standard uncertainty of the individual values, but is composed of a number of uncertainty contributions. This individual uncertainties u_i have to be combined linearly and possibly existing correlations have to be taken into consideration. In most cases, between the individual uncertainties no correlations are evident [3]. The combination of the individual uncertainties leads to the measurement uncertainty $u\,(y)$. If correlation is neglected it can be calculated by:

$$u\,(y)^2 = \sum_{i=1}^{n} \left(\frac{\partial f}{\partial x_i}\right)^2 \cdot u\,(x_i)^2 \tag{7}$$

However, if a correlation between the individual variables is present, for determining the measurement uncertainty eq. 7 extends to:

$$u\,(y)^2 = \sum_{i=1}^{n} \left(\frac{\partial f}{\partial x_i}\right)^2 u\,(x_i)^2 + 2\sum_{i=1}^{n-1}\sum_{k=i+1}^{n} \left(\frac{\partial f}{\partial x_i}\right)\left(\frac{\partial f}{\partial x_k}\right) \cdot u\,(x_i, x_k) \tag{8}$$

$$\text{with} \quad u\,(x_i, x_k) = r\,(x_i, x_k) \cdot u\,(x_i) \cdot u\,(x_k)$$

Thereby $r\,(x_i, x_k) =$ correlations coefficient and $u\,(x_i, x_k) =$ covariance of input variable. The correlation coefficient is in the interval $r\,(x_i, x_k) = \langle -1, 1\rangle$.
The measurement uncertainty is subsequently transferred to the extended uncertainty.

$$U\,(y) = k \cdot u\,(y) \tag{9}$$

with $k =$ extension factor. The extended uncertainty is chosen to delineate an area of which can be expected to contain the true value of the result with a given probability. The exact choice of the extension factor requires knowledge of the distribution function of the measured values. However, usually this information isn't quite often present. According to [6] a value between 2 and 3 should be chosen for k. If no comprehensible reasons for another choice are available. It is recommended to use a value of $k = 2$. This corresponds very roughly to a confidence interval of 95 % [3]. Instead of the recommended value of the extension factor the 5 %–fractile of a non-central t–student distribution can be used. Details of the distribution can be found e.g. in [4, 12].

3.3 Redundancy and Uncertainty

In order to obtain reliable data during a monitoring campaign and to combine the obtained data in order to perform error compensation it is necessary to use several measurement devices. Figure 3 shows exemplary the determination of the position of a point, using different measurement devices $M_1, M_2, \ldots, M_n$.

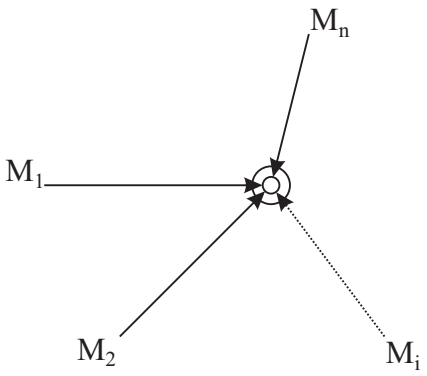

Fig. 3: Determination of the position of a point with different measurement devices

In case of measuring the position of the point several times with each measurement device the mean value for each device can be evaluated and by using e.g. least square method error compensation can be done. The accuracy will increase as the number of measurements and measurement devices will increase. This improvement of the measurand takes place only if measurement uncertainty is neglected. On the one side the standard uncertainty according to eq. 6 decreases if available data increases, but on the other side the cumulative uncertainty according to eq. 7 increases with the increasing amount of available data. Hence the final uncertainty of the measurement, which is the amount of standard uncertainty and systematic and random deviation, do not monotonically decrease. At a certain amount of incorporated measurement devices the final uncertainty increases, see figure 4.

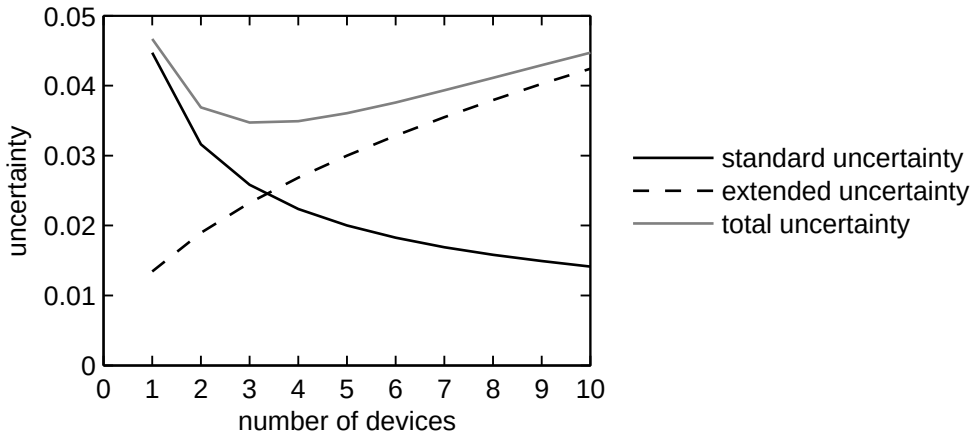

Fig. 4: Devolution of different uncertainty quantities

Figure 4 shows the different uncertainty quantities as well as the total uncertainty exemplary if ten independent measurement devices are used within a measurement campaign.

Each measurement is done five times and it is assumed that all devices are related with the same systematic and random deviation respectively. The extended uncertainty was calculated according to eq. 9 by using an extension factor of $k = 2$. For this example the lowest uncertainty amount arises if three or four independent devices are used to obtain monitoring data.

3.4 Accuracy, trueness and precision

In addition to the uncertainty mentioned before also the accuracy should be taken into consideration. The terms accuracy, trueness and precision are defined in the standard ISO 3534 [5]. They can be used to characterize a measurement procedure with respect to the associated uncertainty. Thereby accuracy characterizes the closeness of agreement between a measurement result and the true value of a measurand. If several results are available e.g. due to redundant systems or different devices to obtain the same measurand, accuracy may be divided into trueness (right/wrong) and precision. The closeness between the mean value and the true value are accounted by the trueness. The closeness of agreement between the individual values (scattering) are accounted by the precision. The different possible combinations resulting from true or wrong, precise or imprecise are shown in figure 5.

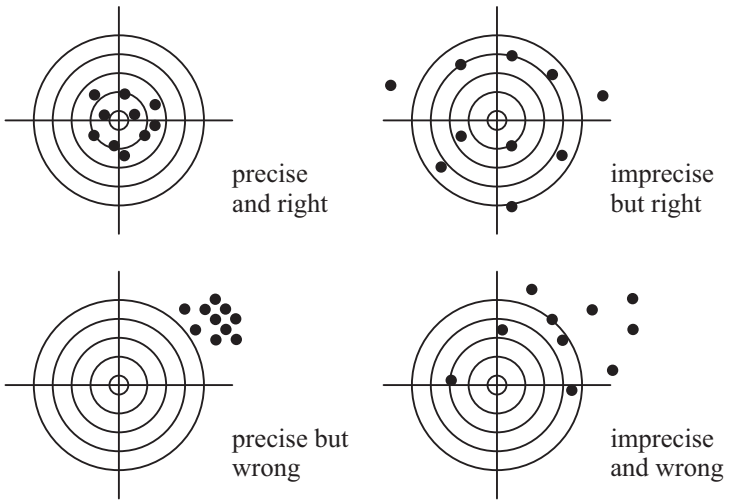

Fig. 5: Illustration of trueness and precision, [3]

4 Conclusions

Any experimental result will involve some level of uncertainty that may originate from causes such as the lack of accuracy in measurement equipment and random or systematic deviations in the measurands. All these aspects should be taken into consideration for the evaluation of monitoring data and further numerical assessment. For the evaluation of the measurement uncertainty the individual deviations (systematic and random) have to be quantified and taken into consideration also a likely to be present correlation of the measurands

have to be considered. Finally the observance of uncertainty influences the monitoring layout, especially in case of redundant monitoring systems. The reason therefore arises due to the fact that an increasing number of independent measurement devices do not steadily decrease the measurement uncertainty. Uncertainty analysis is a vital part of any monitoring campaign or experimental program.

5 Acknowledgment

The support of the investigations by the project CZ.1.07/2.3.00/30.0005 of Brno University of Technology is gratefully acknowledged.

Literature

[1] K. Bergmeister and et al. *Monitoring and safety evaluation of existing concrete structures*. fib Bulletin No. 22, 2003.

[2] J.M.W Brownjohn. Structural health monitoring of civil infrastructure. *Philosophical Transactions of the Royal Society A: Mathematical,Physical and Engineering Sciences*, 365(1851):589–622, 2007.

[3] Eurolab. Leitfaden zur ermittlung von messunsicherheiten bei quantitativen prfergebnissen. Technical Report 2/2006, eurolab Deutschland, 2006.

[4] Catherine Forbes, Merran Evans, Nicholas Hastings, and Brian Peacock. *Statistical Distributions*, chapter Student's t (Noncentral) Distribution. John Wiley & Sons, Inc., Hoboken, NJ, USA., 4 edition, 2010.

[5] ISO3534. Statistics - vocabulary and symbols - part 1: General statistical terms and terms used in probability, 2009.

[6] JCGM. Evaluation of measurement data - guide to the expression of uncertainty in measurement. Technical report, Joint Committee for Guides in Metrology (JCGM), 2008.

[7] S. Kim and D.M. Frangopol. Optimal planning of structural performance monitoring based on reliability assessment. *Probabilistic Engineering Mechanics*, 25(1):86–98, 2010.

[8] A. Krawtschuk, A. Strauss, K. Haider, T. Zimmermann, and K. Bergmeister. Novel monitoring techniques for abutment free bridge structures. *Beton- und Stahlbetonbau*, 107(12):824–835, 2012.

[9] T.B. Messervy, D.M. Frangopol, and S. Casciati. Application of statistics of extremes to the reliability assessment of monitored highway bridges. *Structure and Infrastructure Engineering*, 7:87–99, 2010.

[10] D. Novak and R. Pukl. Simulation of random behavior of engineering structures: From parameters identification to reliability assessment. In *Proceedings of the 3rd International Symposium on Life-Cycle Civil Engineering, IALCCE 2012*, pages 2267–2272, 2012.

[11] D. Novak, B. Teply, R. Pukl, and A. Strauss. Reliability assessment of concrete bridges. In *Proceedings of the Sixth International Conference on Bridge Maintenance, Safety and Management, IABMAS 2012*, pages 654–659, 2012.

[12] D.B. Owen. *Handbook of Statistical Tables*. Addison-Wesley Publishing Company, Inc., 1962.

[13] A. Strauss, D.M. Frangopol, and S. Kim. Monitoring based structural performance assessment. In *Proceedings of the 1st International Symposium on Life-Cycle Civil Engineering, IALCCE 2008*, pages 649–654, 2008.

[14] A. Strauss, D.M. Frangopol, and S. Kim. Statistical, probabilistic and decision analysis aspects related to the efficient use of structural monitoring systems. *Beton- und Stahlbetonbau*, 103:23–28, 2008.

[15] A. Strauss, D.M. Frangopol, and S. Kim. Use of monitoring extreme data for the performance prediction of structures: Bayesian updating. *Engineering Structures*, 30(12):3654–3666, 2008.

[16] Ronald E. Walpole, Raymond H. Myers, Sharon L. Myers, and Keying Ye. *Probability & Statistics for Engineers & Scientists*. ISBN: 0-13-204767-5. Pearson Education, Inc., Upper Saddle River, NJ, 8. edition, 2007.

[17] T. Zimmermann, A. Strauss, and K. Haider. Determination of material parameters of concrete for non-linear modeling. *Advanced Materials Research*, 651:321–324, 2013.

Material properties of early aged concrete

Thomas Zimmermann [a,b], Katharina Haider [a], Alfred Strauss [a], Konrad Bergmeister [a]

[a]Institute for Structural Engineering, University of Natural Resources and Life Sciences, Vienna, Austria

[b]Faculty of Civil Engineering, Brno University of Technology, Brno, Czech Republic

zimmermann.thomas@boku.ac.at, katharina.haider@boku.ac.at, alfred.strauss@boku.ac.at

Abstract: Within this paper an experimental investigation of basic material parameters as well as fracture mechanical properties for early aged concrete is presented. In total two different concrete types – C40/50 and C50/60 – have been investigated. In particular material parameters are experimentally obtained after 1 day and 7 days cure time and further on after 28 days and 126 days. The results of this investigation serve as a basis for further numerical assessment with respect to (a) time-variant changes of the individual properties, (b) non-linear finite element analysis and (c) definition of suitable stochastic models. An additional target was to capture the effects of testing procedure on the mechanical properties. The associated knowledge of these material parameters is an important issue for a realistic reliability assessment during the construction of a structure.

Keywords: concrete, fracture mechanical parameters

1 Introduction

The reliability approach, based on the principles of probability and statistics, provides a rational basis for the quantitative modeling of uncertainty and the analysis of its effects on the performance and safety of engineering systems. However, the implementation of the reliability approach in engineering practice is not simple or straightforward. Major developments have been and are required, in order to render the approach more acceptable to the practicing professional. Stochastic models for material characterized in the new code specifications are primarily required in order to make the reliability approach more practice-oriented and usable [9, 10, 11].

Uncertainties can be captured by probabilistic methods which allow the incorporation of geometrical as well as material uncertainties. This is done at the time of construction and during the entire life-cycle of a structure in form of probability density functions (PDFs) and/or cumulative distributions. Probabilistic methods are generally based on advanced Monte Carlo simulation techniques. The probability of failure p_f and the reliability index β may be calculated from the total number of simulations and the number of cases where a defined limit value is exceeded [1, 7, 14, 15]. Such advanced Monte Carlo simulation techniques, as well as the First Order Reliability Method or the Second Order Reliability Method, both simplified analytical tools, provide the means for probabilistic reliability assessment and life-cycle analysis of new and existing structures with acceptable computing complexity and within a reasonable computing time. The scattering input quantities, like compressive strength f_c or tensile strength f_{ct} for the probabilistic assessment, must be defined based on literature or on experimental investigations [8, 13, 16].
Therefore, this contribution focuses on the characterization of stochastic mechanical properties of specified concrete classes, based on comprehensive experimental tests to obtain basic material parameter as well as fracture mechanical parameters. An additional target was to capture time dependent effects for the investigated stochastic models and the effects of testing procedures on the mechanical properties of interest. The knowledge associated with stochastic material parameters is an important issue for the realistic reliability assessment of the performance of structures or structural elements.

2 Experimental Program

In general, the properties of concrete are characterized via the compressive strength according to EN 12390-3, the exposure classes and the slump value. Nevertheless, the realistic modeling of structures requires the incorporation of (a) nonlinear effects in the analysis and material properties of concrete (usually called fracture mechanical parameters), which can be captured e.g. by a variable modulus of elasticity E_c, the tensile strength f_{ct}, and the fracture energy G_f, and (b) of uncertainties in material and geometrical properties caused by nature, manufacturing processes and curing among others. These requirements and the new characterized concrete classes in the Eurocode concept gave rise to the experimental investigations. To obtain material properties laboratory tests on two different concrete types were carried out. The test program involved the determination of compressive strength, modulus of elasticity, tensile strength and fracture energy. In particular the two tested concerts are C50/60 and C40/50 according to EN 206-1 [4]. For the first strength class additionally tests were carried out on concrete with steel fibers. Table 1 shows the mixture for these different concrete types.
In particular, the standardized compressive test, the standardized three–point bending test of notched specimens and the wedge splitting test were applied in the course of the investigations. The experiments allowed a partially redundant determination of the material properties mentioned above and consequently an effective comparison and a verification of testing procedures.

Tab. 1: Concrete mixture

	unit	I: C50/60 B4	II: C40/50 B4	III: C50/60 B4-SF
Aggregate 0/4 edge	kg	101.85	61.00	99.54
Aggregate 0/4 round	kg	849.17	567.61	845.76
Aggregate 4/8 round	kg	370.79	242.61	373.71
Aggregate 8/16 round	kg	550.64	364.66	-
Aggregate 8/16 edge	kg	-	-	535.61
Water content	kg	181	130	159
Cement CEM 52.5 R	kg	464.90	308.89	459.36
Sky 657	kg	6.67	4.32	6.45
Sky 911	kg	-	-	0.92
steel fibers	kg/m^3	-	-	25 – 40
w/c	-	0.39	0.42	0.35

The tests to obtain the relevant parameters of the different concrete strength classes have been carried out after different curing times, see table 2. Thereby CT = compressive test, 3PBT = three–point bending test and WST = wedge splitting test.

Tab. 2: Testing program

	I: C50/60 B4			II: C40/50 B4			III: C50/60 B4-SF	
days	CT	3PBT	WST	CT	3PBT	WST	3PBT	WST
1	-	7	7	-	-	-	-	-
7	7	7	-	-	7	-	-	-
28	7	7	7	7	7	7	7	7
126	7	7	7	-	7	10	7	7

2.1 Compressive tests

Compression tests according to EN 12390-3 [2] were carried out in order to determine the basic material parameters like compressive strength f_c and modulus of elasticity E_c. Test cubes had dimensions of 150 $\times$ 150 $\times$ 150 mm and were loaded with a gradual increase of the stress level until the maximum load was reached and the specimen failed.

2.2 Three–point bending tests

Three–point bending tests according to EN 12390-5 [3] were carried out in order to determine the tensile strength f_{ct}. The nominal size of the specimens was 100 $\times$ 100 $\times$ 400 mm, the depth of the central edge notch was about 1/3 of the depth of the specimen, and the loaded span was equal to 300 mm. Figure 1a shows the test configuration.

2.3 Wedge splitting tests

For the characterization of the non-linear parameter G_f = fracture energy the testing procedure according to ON B 3592 [12] was used . Figure 1b illustrates the principle of the wedge splitting method for uniaxial loading.
A starter notch is cut into the rectangular groove of the specimen. The load transmission pieces (comprising rollers or roller bearings) are inserted into this groove. Afterward the slender wedge is laid into the groove. The force in vertical direction P_v from the testing machine is transmitted via the load transmission pieces onto the wedge, leading to the splitting of the specimen. The friction between wedge and force transmission pieces is negligible and the horizontal splitting force P_h can be determined by means of a simple calculation by taking the wedge angle θ into consideration:

$$P_h = P_v / (2 \cdot \tan\theta) \tag{1}$$

Figure 1c shows a detailed sketch of the wedge and the acting forces during the wedge splitting test.

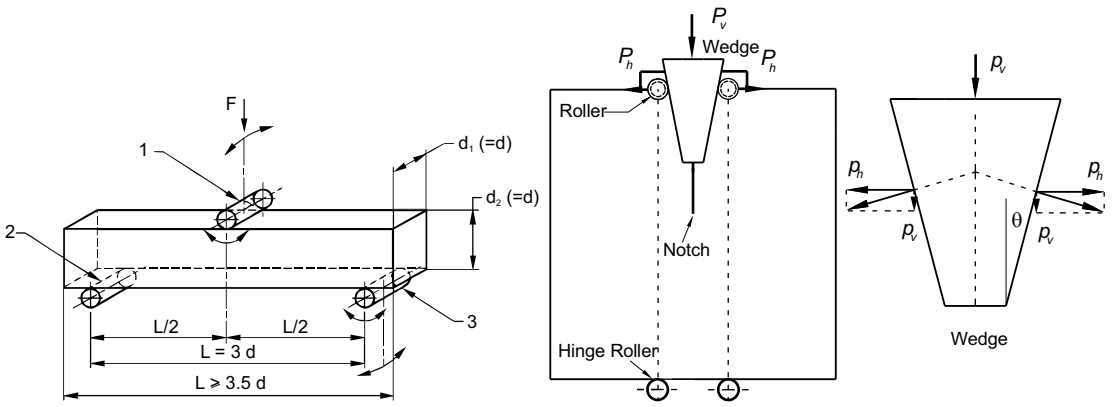

(a) three–point bending test (b) wedge splitting test (c) wedge

Fig. 1: Schematic test setup for three–point bending and for wedge splitting test

3 Results

From basic compressive tests the compressive strength f_c and the modulus of elasticity E_c are evaluated separately for each concrete class. The obtained data from three–point bending tests are used to determine the tensile strength f_{ct}. Based on the data from wedge splitting tests the fracture energy G_f is calculated by using eq. 2.

$$G_f = W / (D - N) \cdot B \qquad \text{with} \quad W = \int_0^{d_{h,max}} P_h \cdot \mathrm{d}d_h \tag{2}$$

thereby W = total work of the area under the load–deflection curve, D = effective depth of the crack, N = notch length, B = thickness of the specimen and d_h = horizontal crack

opening.
Currently the evaluation of the experimentally obtained data is only available for the concrete strength class I: C50/60 B4. The tests were performed after 1 day, 7 days and 28 days. Table 3 summarizes the results of this strength class.

Tab. 3: Mean values and coefficient of variation of experimentally obtained results

days	f_{cm} MPa	cov -	E_c MPa	cov -	G_f N/m	cov -
1	-	-	-	-	207	0.22
7	72.63	0.039	52300	0.070	-	-
28	85.74	0.022	50300	0.068	90	0.15

For the obtained values of concrete strength class I: C50/60 B4 the strength development over time is compared to the empirical function according to *ceb-fib* Model Code 90 [5]. Figure 2 shows the individual values of compressive strength after 7 days and after 28 days. In addition the time depending function according to eq. 3 for the assessment of compressive strength is shown.

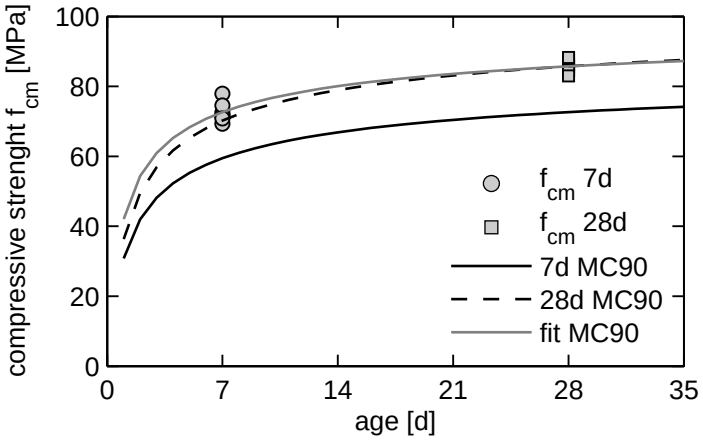

Fig. 2: Time depending development of compressive strength

$$f_{cm}(t) = \beta_{cc}(t) \cdot f_{cm} \qquad \text{with} \quad \beta_{cc}(t) = \exp\left\{ s \left[1 - \left(\frac{28}{t/t_1} \right)^{0.5} \right] \right\} \tag{3}$$

thereby $f_{cm}(t)$ = compressive strength after t days, f_{cm} = compressive strength after 28 days, t_1 = reference age (1 day), $\beta_{cc}(t)$ = coefficient for time depending gradient and s = coefficient for the type of cement [6].
Only considering the 7 days strength data for the prediction of strength development doesn't add up to an acceptable agreement between obtained values and eq. 3. On the contrary, a rather acceptable prediction can be achieved by considering the values of strength after 28 days. In both cases the coefficient $s = 0.200$, according to [6]. However, if this coefficient is adjusted to $s = 0.166$ an accurate agreement between both, 7 days and 28 days, strength

data, based on mean values can be achieved for the prediction of compressive strength development.

4 Conclusions and Outlook

In order to determine experimentally the basic material parameters as well as fracture mechanical properties two different concrete types have been investigated. The basic material parameters like compressive strength and modulus of elasticity have been assigned by compressive tests according to EN 12390. For the characterization of the stochastic concrete properties for non-linear modeling purposes the wedge splitting test method according to according to ON B 3592 has been used.
After the laboratory tests the compressive strength f_c and the modulus of elasticity E_c have been evaluated separately for each concrete strength class. Within this investigation the statistically descriptive parameters have been calculated.
Obtained data can be used to define appropriate probabilistic models. These models can serve as a basis for a further reliability assessment to calculate reliability index β and probability of failure p_f respectively.
The time-variant changes of the concrete properties, e.g. for the compressive strength can be described in an accurate way by using the empirical function according to *ceb-fib* Model Code 90 and furthermore it can be used for life-cycle assessment.

5 Acknowledgment

For the preparation of the specimens the authors thank the company Oberndorfer. The support of the investigations by the project CZ.1.07/2.3.00/30.0005 of Brno University of Technology is gratefully acknowledged. Additionally the support from project FRAPA, No. P104-13-03662S, of the Grant Agency of Czech Republic is acknowledged.

Literature

[1] A.H.-S. Ang and W.H. Tang. *Probability Concepts in Engineering Planning*. Wiley & Sons, Inc., 2 edition, 2007.

[2] EN12390-3. Testing of hardened concrete – part 3: Compressive strength of test specimens, 2009.

[3] EN12390-5. Testing of hardened concrete – part 5: Flexural strength of test specimens, 2009.

[4] EN206-1. Concrete – part 1: Specification, performance, production and conformity, 2005.

[5] fib. *CEB-FIP Model Code 90*. Thomas Telford Services Ltd, 1993.

[6] Peter Grübl, Helmut Weigler, and Sieghart Karl. *Beton: Arten, Herstellung und Eigenschaften*. Ernst & Sohn, 2. edition, 2001.

[7] A. Krawtschuk, A. Strauss, K. Haider, T. Zimmermann, and K. Bergmeister. Novel monitoring techniques for abutment free bridge structures. *Beton- und Stahlbetonbau*, 107(12):824–835, 2012.

[8] A. Krawtschuk, T. Zimmermann, and K. Haider. Determination of mechanical and temperature induced deflection based on monitoring data for assessing the load factor. In *Proceedings of the 3rd International Symposium on Life-Cycle Civil Engineering, IALCCE 2012*, pages 2161–2167, 2012.

[9] D. Lehky and D. Novak. Solving inverse structural reliability problem using artificial neural networks and small-sample simulation. *Advances in Structural Engineering*, 15(11):1911–1920, 2012.

[10] D. Novak and R. Pukl. Simulation of random behavior of engineering structures: From parameters identification to reliability assessment. In *Proceedings of the 3rd International Symposium on Life-Cycle Civil Engineering, IALCCE 2012*, pages 2267–2272, 2012.

[11] D. Novak, B. Teply, R. Pukl, and A. Strauss. Reliability assessment of concrete bridges. In *Proceedings of the Sixth International Conference on Bridge Maintenance, Safety and Management, IABMAS 2012*, pages 654–659, 2012.

[12] ON-B3592. Determination of cut-through-tensile splitting strength and specific fracture energy of building materials, combinations of building materials and composites – wedge splitting method, 2011.

[13] M. Sejnoha, M. Broucek, E. Novotna, Z. Kersner, D. Lehky, and P. Frantik. Fracture properties of cement and alkali activated fly ash based concrete with application to segmental tunnel lining. *Advances in Engineering Software*, 2013. Article in Press.

[14] A. Strauss, D.M. Frangopol, and S. Kim. Monitoring based structural performance assessment. In *Proceedings of the 1st International Symposium on Life-Cycle Civil Engineering, IALCCE 2008*, pages 649–654, 2008.

[15] M. Vorechovsky and D. Novak. Correlation control in small-sample monte carlo type simulations i: A simulated annealing approach. *Probabilistic Engineering Mechanics*, 24:452–462, 2009.

[16] T. Zimmermann, A. Strauss, and K. Haider. Determination of material parameters of concrete for non-linear modeling. *Advanced Materials Research*, 651:321–324, 2013.

List of Probabilistic Symposiums in this Series

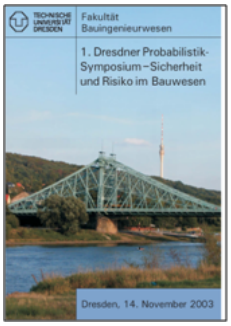

Dirk Proske & Manfred Curbach (Eds.),
1. Dresdner Probabilistik-Symposium –
– Sicherheit und Risiko im Bauwesen,
14 November 2003, Dresden, Germany,
TU Dresden, 2003,
ISBN-10 3-00-019234-4, ISBN-13 978-3-00-019234-0 (2. Auflage 2006)

Dirk Proske & Manfred Curbach (Eds.),
2. Dresdner Probabilistik-Symposium –
– Sicherheit und Risiko im Bauwesen,
12 November 2004, Dresden, Germany,
TU Dresden, 2004,
ISBN-10 3-00-019235-2, ISBN-13 978-3-00-019235-7 (2. Auflage 2006)

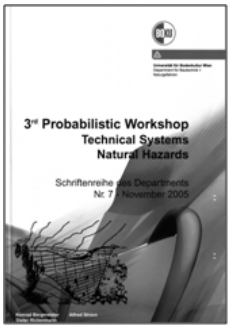

Konrad Bergmeister, Alfred Strauss & Dieter Rickenmann (Eds.),
3rd Probabilistic Workshop – Technical Systems, Natural Hazards,
12–13 October 2005, Vienna, Austria,
University of Natural Resources and Life Sciences, Vienna, 2005

Dirk Proske, Milad Mehdianpour & Lucjan Gucma (Eds.),
4th International Probabilistic Symposium,
12–13 October 2006, Berlin, Germany,
BAM (Federal Institute for Materials Research and Testing),
Universität für Bodenkultur, Bundesanstalt für Materialforschung
und -prüfung, Maritime University of Szczecin,
Berlin • Wien • Szczecin, 2006,
ISBN-10 3-00-019232-8, ISBN-13 978-3-00-019232-6

Luc Taerwe & Dirk Proske (Eds.),
5th International Probabilistic Workshop,
28–29 November 2007, Ghent, Belgium,
Published by ACCO, Ghent, 2007,
ISBN 978-3-00-022030-2

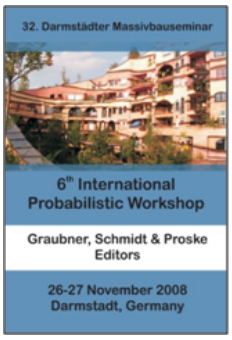

Carl-Alexander Graubner, Holger Schmidt & Dirk Proske (Eds.),
6th International Probabilistic Workshop,
26–27 November 2008, Darmstadt, Germany,
Technische Universität Darmstadt, 2008,
ISBN 978-3-00-025050-7

Pieter van Gelder, Dirk Proske & Han Vrijling (Eds.),
7th International Probabilistic Workshop,
25–26 November 2009, Delft, The Netherlands,
TU Delft, 2009,
ISBN 978-3-00-025048-4

Pieter van Gelder, Lucjan Gucma & Dirk Proske (Eds.),
8th International Probabilistic Workshop,
18–19 November 2010, Szczecin, Poland,
Maritime University of Szczecin, Akademia Morska, 2010,
ISBN 978-83-89901-49-1

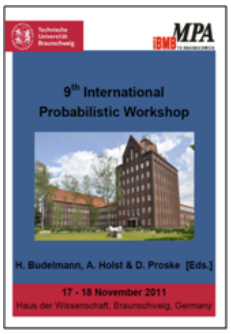

Harald Budelmann, Alexander Holst & Dirk Proske (Eds.),
9th International Probabilistic Workshop,
17–18 November 2011, Braunschweig, Germany,
Technische Universität Carolo-Wilhelmina zu Braunschweig, 2011,
ISBN 978-3-89288-201-5

Christian Moormann, Maximilian Huber & Dirk Proske (Eds.),
10th International Probabilistic Workshop,
15–16 November 2012, Stuttgart, Germany,
Institut für Geotechnik der Universität Stuttgart, 2012,
ISBN 978-3-921837-67-2